"Supramolecular interactions for controlling the structure, self-organization and dynamics of stimuli-responsive polymeric systems"

Brassinne, Jérémy

Abstract

In the last years, the advent of supramolecular chemistry has provided chemists with new possibilities to synthesize complex structures and dynamic materials by self-assembly. By virtue of their properties, metal–ligand interactions are particularly promising for the synthesis of supramolecular polymers and the construction of “smart” materials with self-restructuring abilities. Among them, supramolecular gels constitute a very interesting sub-class because of numerous applications in various fields. In this frame, the goal of this thesis is to gain an unprecedented control over the structure, self-organization and molecular dynamics of polymeric gels by exploiting a novel combination of classical macromolecular architectures and supramolecular interactions of the metal–ligand type. The first goal of this thesis relies on the synthesis of well-defined copolymers, functionalized with a ligand of interest. These building blocks will then be used in the design of supramolecular ...

Document type : *Thèse (Dissertation)*

UCL
Université
catholique
de Louvain

Université catholique de Louvain
Institute of Condensed Matter and Nanosciences
Division of Bio and Soft Matter

Supramolecular Interactions for Controlling the Structure, Self-Organization and Dynamics of Stimuli-Responsive Polymeric Systems

Brassinne Jérémy

Supervisor: Professor J.-F. Gohy
Co-supervisor: Professor C.-A. Fustin

Thesis submitted in fulfilment of
the degree of Doctor in Sciences

Louvain-la-Neuve 2015

UCL
Université
catholique
de Louvain

Université catholique de Louvain
Institute of Condensed Matter and Nanosciences
Division of Bio and Soft Matter

Supramolecular Interactions for Controlling the Structure, Self-Organization and Dynamics of Stimuli-Responsive Polymeric Systems

Brassinne Jérémy

Committee members:

Prof. J.-F. Gohy, supervisor
Prof. C.-A. Fustin, co-supervisor
Prof. C. Bailly (UCL)
Prof. L. Bouteiller (UPMC)
Prof. E. van Ruymbeke (UCL)
Prof. D. Vlassopoulos (FORTH)
Prof. J. Devaux (UCL), president

Thesis submitted in fulfilment of
the degree of Doctor in Sciences

Louvain-la-Neuve 2015

À mes parents et grands-parents...

REMERCIEMENTS

Par les quelques lignes qui suivent, je tiens à remercier toutes les personnes qui, d'une manière ou d'une autre, ont contribué à l'aboutissement de cette thèse. Leur soutien, gentillesse, et attention tout au long de ces années sont autant d'engagements que j'ai tenus à honorer à travers la réalisation de ce travail de recherche doctorale.

Tout d'abord, mes plus vifs remerciements vont à mes deux copromoteurs, Prof. Jean-François Gohy et Prof. Charles-André Fustin, qui m'ont chaleureusement accueilli au sein du Groupe de Recherche en Chimie Macromoléculaire. La complémentarité de leur aide a soigneusement encadré et dirigé la réalisation de ce travail, depuis son origine jusqu'à son épanouissement. Leurs enseignements et leur guidance ont été les facteurs déterminants et stimulants dans la progression et la réussite de cette recherche.

Par son charisme et son enthousiasme communicatif, le Prof. Gohy a pu susciter, puis transmettre l'intérêt et l'impact positif d'un tel projet. Il m'a accordé sa confiance en me laissant une grande liberté de pensées et d'action, tout en me faisant part de ses avis, conseils et suggestions. Je lui suis reconnaissant de m'avoir laissé organiser un environnement de travail riche, stimulant et nouvellement rénové. En outre, je tiens à le remercier tout particulièrement pour m'avoir donné l'opportunité de présenter mes résultats de recherche lors de nombreuses conférences nationales et internationales.

Comme un véritable privilège, j'ai pu bénéficier d'un double en-

cadrement académique particulièrement enrichissant et précieux pour l'accomplissement de cette recherche scientifique. C'est pourquoi je tiens à témoigner autant de reconnaissance et de sympathie à l'égard de Prof. Fustin. Sa rigueur intellectuelle et son côté perfectionniste sont entrés en résonance avec mes convictions scientifiques, contribuant ainsi profondément à la qualité de ce travail. Je tiens à le remercier chaleureusement pour son implication primordiale et la grande disponibilité qu'il a manifesté à mon égard.

Mes remerciements sont ensuite destinés à ma famille et proches pour les encouragements et l'attention qu'ils m'ont témoignés déjà bien avant et tout au long de mes études. Mes pensées les plus chères vont à mes parents et grand-parents qui ont tant contribué à ma réussite. Leur éducation et leur soutien indéfectible ont su me donner le gout du travail et de la persévérance qui m'a mené à rédiger ces quelques lignes aujourd'hui. Pour l'appui qu'ils n'ont cessé de m'apporter, je leur adresse toute mon affection et leur dédie ce travail afin qu'ils y trouvent toute ma reconnaissance.

Je tiens également à exprimer ma gratitude aux membres de mon jury, les Professeurs Jacques Devaux, Christian Bailly, Laurent Bouteiller, Evelyne van Ruymbeke et Dimitris Vlassopoulos, pour avoir accepté de juger ce travail et pour l'intérêt qu'ils ont porté à celui-ci. Ils ont pris le temps de lire attentivement ce manuscrit, et le soin d'y accompagner les commentaires judicieux et pertinents qui ont contribué au raffinement de celui-ci. Je remercie particulièrement Prof. van Ruymbeke pour toutes les discussions et réflexions que nous avons partagées, ainsi que pour m'avoir introduit au sein du réseau Supolen. Je joins à ma reconnaissance le Professeur Benjamin Elias pour m'avoir accompagné, avec Prof. Bailly, en tant que membre de mon comité d'encadrement.

Je souhaite maintenant saluer et souligner l'importance de personnes qui ont, par leur implication directe ou indirecte, influé sur la réalisation de cet ouvrage.

À bien des égards, les personnalités qui m'ont précédé sur ce chemin m'ont aidé à établir l'itinéraire d'une recherche universitaire avancée. Comme un héritage, ils ont transmis le savoir et les connaissances accumulées tout au long de leur voyage, afin que leurs successeurs les utilisent pour paver leur route. Pour leur instruction et leur aide en synthèse, assemblage et caractérisation, je tiens à complimenter gracieuse-

ment Dr. Clément Mugemana, Dr. Sandie Piogé, Dr. Florian Jochum et Dr. Dietmar Auhl. Par amitié, je tiens également à honorer Dr. Jean-Marc Schumers, Dr. Alexandru Vlad, Dr. Shabbair Mohammad, Dr. Aurélie Laquièvre, Dr. Bhavesh Bharatiya, Dr. Nisar Ahamed, Dr. Cé Guinto Gamys, Dr. Anne Van Quaethem et Dr. Guillaume De Bo, en leur souhaitant une carrière fructueuse, riche en défis et en accomplissements.

J'adresse encore plus de reconnaissance et d'amitié aux personnes que j'ai eu le plaisir de côtoyer tout au long de mon cheminement universitaire et garderai de bons souvenirs des moments passés avec eux, en particulier, Dr. Olivier Bertrand, pour ses nombreux conseils et avis, Julien Rolland, pour son accompagnement et ses enseignements, Jean-Pierre Bourgeois, pour sa bonne humeur quotidienne, Guillaume Hauffman, pour sa complicité amicale, Elio Poggi, pour sa perspicacité détachée, Roland Duchêne, pour son assiduité et sa sympathie, Bruno Ernould, pour ses considérations techniques, et Dr. Claire Guerlain, pour sa gentillesse. Avec sincérité, je dois souligner la contribution décisive de Julien Rolland, véritable charnière inter-générationnelle dans notre initiation au voyage. Pour leur implication respective dans la synthèse des copolymères séquencés, l'analyse calorimétrique, et l'imagerie par AFM, je tiens aussi à remercier chaleureusement Arnaud Stevens et, une seconde fois, Jean-Pierre et Elio.

À la croisée de chemins, les travaux menés au cours de cette thèse ont été enrichis par des collaborations passionnantes de diverses origines. Ils ont également été l'opportunité de voir progresser bon nombre de stagiaires et mémorant(e)s dont les qualités sont sources de motivation essentielles. À la nouvelle génération de jeunes doctorants, Emanuele Simonini, Flanco Zhuge, Vusala Ibrahimova, Fadoi Boujioui, Louis Sieuw, Guillaume Dolphijn, j'encourage à beaucoup de réflexion, rigueur et persévérance au travail. Aussi, je les félicite d'avance et leur souhaite beaucoup de réussite dans les épreuves qui les attendent. Parmi eux, je tiens à inspirer Flanco, ses innombrables qualités faisant de lui le candidat idéal pour reprendre le flambeau hérité de mes prédécesseurs.

Bien sur, cette thèse n'aurait pu voir le jour sans soutien financier nécessaire. Il me fut accordé par l'Université catholique de Louvain (UCL) et le Fonds pour la Formation à la Recherche dans l'Industrie et dans l'Agriculture (FRIA), que je remercie très sincèrement.

Dernièrement, j'aimerais exprimer toute ma gratitude à tous les Professeurs, étudiants, doctorants, post-doctorants, secrétaires et techniciens rencontrés pendant mes cinq années d'étude et quatre années de thèse à l'UCL. Que ces quelques mots soient pour toutes ces personnes l'expression de ma sincère gratitude et profonde estime. Merci!

ABSTRACT

In the last years, the advent of supramolecular chemistry has provided chemists with new possibilities to synthesize complex structures and dynamic materials by self-assembly. By virtue of their properties, metal–ligand interactions are particularly promising for the synthesis of supramolecular polymers and the construction of "smart" materials with self-restructuring abilities. Among them, supramolecular gels constitute a very interesting sub-class because of numerous applications in various fields. In this frame, the goal of this thesis is to gain an unprecedented control over the structure, self-organization and molecular dynamics of polymeric gels by exploiting a novel combination of classical macromolecular architectures and supramolecular interactions of the metal–ligand type.

The first goal of this thesis relies on the synthesis of well-defined copolymers, functionalized with a ligand of interest. These building blocks will then be used in the design of supramolecular materials with responsive properties. Precisely, the coordination of metal to ligands will be used to link micellar objects, obtained by the self-assembly of covalent block copolymers. The rheological behaviour of the accordingly obtained materials will be thoroughly characterized in order to establish relationships between their structure, dynamics and mechanical properties. The present thesis aims at studying in details the response of these systems to external stimuli. These stimuli-responsive properties will be inherent to the supramolecular materials and further obtained by using stimuli-responsive polymer sequences as building blocks.

FOREWORD

This dissertation aims to rationalize the thoughts and efforts put into a 4-years project called a Doctoral thesis. Presenting the author's research and findings, this document supports his candidature for the academic degree of Doctor of Sciences. In so doing, the manuscript has been divided into five parts, consisting of chapters, and structured as follow:

1. *Introductory background*, hosting the research significance;
2. *Objectives and strategy*, explaining goals and methodology;
3. *State of the art*, reviewing relevant literature around the issue;
4. *Results and discussion*, analyzing and discussing the findings;
5. *Concluding remarks*, outlining the breakthroughs and scopes.

Given its multidisciplinary topic, the research project has the potential to raise interest from scientists belonging to well-distinct disciplinary communities, including but not limited to polymer chemistry and physics, supramolecular chemistry, and material science and engineering. According to individual predispositions, each reader might feel the need to go through, or come back to, one or different chapters constituting the *Introductory background*.

In *Objectives and strategy*, a theoretical approach is developed to address the goal of this thesis project. Hence, the methodology provides design guidelines that constitute the basis of the current research. In addition, the same approach justifies the data collection and analysis being used in this project.

Prior getting into the heart of the matter, it is commonly admitted to establish a *State of the art* to situate the present work among anterior studies. As such, this part aims to establish the novelty and relevance of the present work. In addition, the literature review reminds the reader that this fairly modest contribution is in fact part of a whole. In turn, this much more complex ensemble constitutes the actual progress in the broad field of exact sciences.

The *Results and discussion* constitutes the most important part of a thesis, bringing into light the research findings and outcomes. The latter are discussed in the context of the literature review and theoretical considerations. One more time, the reader should keep in mind that those findings result from a synergy through instrumental mastering, coordinated effort and collective reflection.

Some *Concluding remarks* logically close the manuscript, integrating the major breakthroughs of the project. If the primary goal of this thesis is to extend our fundamental understanding in the research field, such a work may also orient toward advanced developments. In line, last elements include implications and potential application, as well as recommendations, forecasting future trends, and the need for further research.

TABLE OF CONTENTS

LIST OF SYMBOLS

A	pre-exponential factor
C	concentration
C^*	overlap concentration
D	diffusion coefficient
D_e	Deborah number
E_a	activation energy
G	shear modulus
G'	storage modulus
G''	loss modulus
I	intensity
I_{X}	integration
K	binding constant
M	molar mass
N	number
R	radius
R_c	radius of core
R_g	radius of gyration
R_h	hydrodynamic radius
R_m	micelle radius
T	torque
T°	temperature
T_θ°	theta temperature

T_g°	glass transition temperature
T_m°	melting temperature
T_{gel}°	gelation temperature
W_e	Weissenberg number
Y	tensile modulus
Z	aggregation number
ΔH	enthalpy change
$\bar{M}_n$	number average molar mass
$\bar{M}_w$	weight average molar mass
$\bar{M}_z$	z average molar mass
β	overall binding constant
χ	polymer–solvent interaction parameter
δ	phase lag
δ_{X}	chemical shift
$\mathrm{d}Q/\,\mathrm{d}t$	heat flow
$\mathrm{d}T^\circ/\,\mathrm{d}t$	heating rate
$\dot{\gamma}$	shear rate
η	dynamic viscosity
γ	strain
γ^c	yield strain
γ_0	strain amplitude
λ	wavelength
ν	kinematic viscosity
ω	angular frequency
ϕ	weight-to-volume fraction
ρ	density
σ	stress
σ^c	yield stress
σ_0	stress amplitude
τ	relaxation time
$Đ$	dispersity
θ	angular displacement
ε	molar absorptivity
φ	volume fraction
ϑ	initiator efficiency

ξ	relaxation rate
c	conversion
f	frequency
k	rate constant
k_B	Boltzmann's constant
t	time
t_{exp}	experiment time scale

LIST OF ACRONYMS

AFM	atomic force microscopy
AIBN	2,2'-azobis(isobutyronitrile)
AMU	atomic mass unit
ATRP	atom transfer radical polymerization
CMC	critical micelle concentration
CPAD	4-cyano-4-(phenylcarbonothioylthio)pentanoic acid
CRP	controlled radical polymerization
CTA	chain transfer agent
CuAAC	copper(I)-catalysed azide–alkyne cycloaddition
DCM	dichloromethane
DDMAT	*S*-dodecyl-*S'*-(α, α'-dimethyl-α''-acetic acid) trithiocarbonate
DLS	dynamic light scattering
DMAEMA	2-(dimethylamino)ethyl methacrylate
DMF	*N,N*-dimethylformamide
DMSO	dimethyl sulfoxide
DNA	deoxyribonucleic acid
DP	degree of polymerization
DRI	differential refractive index
DSC	differential scanning calorimetry
EDCI	*N*-(3-dimethyl-aminopropyl)-*N'*-ethylcarbodiimide
ESI	electrospray ionization

ET	electron tomography
HOBT	1-hydroxybenzotriazole
I	initiator
LAOS	large amplitude oscillatory shear
LCST	lower critical solution temperature
LVR	linear viscoelastic regime
MALDI	matrix-assisted laser desorption ionization
MS	mass spectroscopy
MSP	metallo-supramolecular polymer
MSPG	metallo-supramolecular polymer gel
NIPAAm	*N*-isopropylacrylamide
NLVR	non-linear viscoelastic regime
NMP	nitroxide mediated polymerization
NMR	nuclear magnetic resonance
PDMAEMA	poly(2-(dimethylamino)ethyl methacrylate)
PEG	poly(ethylene glycol)
PNIPAAm	poly(*N*-isopropylacrylamide)
PS	polystyrene
PTC	phase transfer catalyst
RAFT	reversible addition–fragmentation chain transfer
S	styrene
SEC	size exclusion chromatography
SEM	scanning electron microscopy
SLS	static light scattering
TEM	transition electron microscopy
TMS	tetramethylsilane
tpy	2,2':6',2"-terpyridine
UCST	upper critical solution temperature
UV-Vis	ultraviolet–visible

Part I

Introductory background

CHAPTER 1

POLYMER ARCHITECTURES, SYNTHETIC DESIGN AND SOLUTION BEHAVIOUR

Abstract

In this opening chapter, some fundamentals on polymer chemistry and physics are reminded. First, definitions and core concepts are exposed, highlighting the richness of macromolecular structures that can be encountered in this field. Then, the different synthetic routes toward polymer materials are presented with a particular attention on living and controlled polymerizations. Finally, the solution behaviour of polymers is discussed, with emphasis on the self-assembly of block copolymers and responsiveness of stimuli-sensitive sequences.

1.1 Definitions and concepts

1.1.1 Polymer

In daily life and popular beliefs, it is common to equate polymer with plastic. However, polymer and plastic are in fact two well-distinct things! Indeed, a plastic, from the Greek "*plastikós*" meaning *shapeable*, designates a type of material, whereas a polymer is a very large molecule.[1,2] The word polymer also founds its etymology from the Greek "*pollus*" meaning *many*, and "*meros*" meaning *part*, thus designating a molecule made up by the repetition of a large number of simpler structural units called a *mer* (Figure 1.1).[2,3] Also, the words polymer and macromolecule are used interchangeably, although the latter strictly defines the molecules of which the former is composed. Practically, polymers are prepared by joining a large number of small molecules called *monomers*.[3]

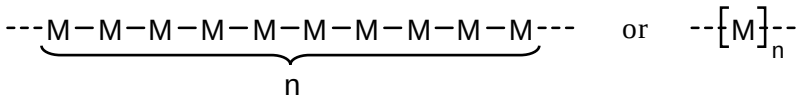

Figure 1.1 – Schematic representation of a macromolecule.

The number of repeating units generally varied from hundreds to thousands of mers, depending on the molar mass of the polymer that may extend to several millions. For low-molecular-weight polymers, no firm lower limit of molar mass can be defined. Strictly, a relatively small molecule composed of only a few mer units might also be called a polymer.[3] However, the term polymer is generally accepted to imply molecules of large size that have the possibility to entangle. Accordingly, the lower-molecular-weight products with relatively small number of structural units should preferably be called *oligomers* (from the Greek "*oligo*" meaning *few*) to distinguish them from polymers.[2,3]

Many of the physical properties of polymers are simply a consequence of their large size.[1] Generally speaking, a species is called polymeric if materials made from it have significant mechanical strength and oligomeric if such articles are not strong enough to be practically useful.[3] Hence, a gradual transition is observed in the physical properties of simple hydrocarbon chains, revealing the effect of the number of

repeating units (Table 1.1).[1]

Table 1.1 – Molar mass and physical state of linear hydrocarbons.[1]

Name	Formula	Molar mass [g/mol]	Physical state
methane	CH_4	16	gas
butane	CH_3-$(CH_2)_2$-CH_3	58	gas
octane	CH_3-$(CH_2)_6$-CH_3	114	liquid
oligomer	CH_3-$(CH_2)_{20}$-CH_3	450	semi-solid
polyethylene	CH_3-$(CH_2)_{2000}$-CH_3	420,030	solid

1.1.2 Monomers

Monomers are generally simple organic molecules, less often inorganic (siloxanes, phosphazenes),[4,5] from which the polymer is made.[6] It is the presence of multiple bonds, active functional groups or strained rings, in case of cyclic monomers, that acts as the driving force to add one monomer molecule upon the other, by a process known as polymerization, to create a macromolecule.[3] As a consequence, the structure of the repeating unit of a polymer is essentially that or closely related to that of the monomer molecule.[6]

Molecules suitable for the formation of macromolecules must be at least bifunctional, *i.e.*, they contains reactive group(s) can give rise to the formation of two linkages, in the intended reaction. In this respect, linear macromolecules result from the coupling of bifunctional monomers with each other or with other bifunctional molecules. In contrast, branched or cross-linked polymers are formed when tri- or poly-functional compounds are involved (see below).

1.1.3 Polymerization degree, molar mass and chain ends

The degree of polymerization (DP) refers to the number of repeating units that constitute a polymer chain. The subscript n used in formulas to illustrate the structural periodicity for polymers, represents this DP.[3,6] The relationship between degree of polymerization and molar

mass M of the same macromolecule is given by, where M_0 is the molar mass of the repeating unit:

$$M = \mathrm{DP} \cdot M_0 \tag{1.1}$$

In literature, the term "molecular weight" is still widely used instead of "molar mass" though it can be somewhat misleading. Strictly, molecular weight is a dimensionless quantity defined by ratios of the masses of the particular atoms to 1/12 of the mass of the most abundant carbon isotope atom $^{12}C_6$ (12 AMU, where 1 AMU equals 1.6604×10^{-24} g). On the other hand, the molar mass of a substance is the mass of one mole of this substance and usually is quoted in units of g/mol. Thus, a molecular weight of 100,000 is equivalent to a molar mass of 100,000 g/mol.[3,6]

In reality, nearly all polymers are a mixture of molecules with a different degree of polymerization, *i.e.*, of different sizes. This polydispersity is exceptionally absent in some synthetic oligomers and some polymers of biological origin such as proteins or nucleic acids. In this respect, monodisperse polymers refer to those with a unique molecular weight. Synthetic polymers are usually polydisperse and are characterized by a distribution of molar masses.[7,8]

Considering a polymer sample consisting of n_i chains of degree of polymerization i and molar mass M_i, the number-, weight-, and z-average molar masses of the considered sample, respectively $\bar{M}_n$, $\bar{M}_w$, and $\bar{M}_z$, are defined as:

$$\bar{M}_n = \frac{\sum_{i=1}^{\infty} (n_i \cdot M_i)}{\sum_{i=1}^{\infty} n_i}, \quad \bar{M}_w = \frac{\sum_{i=1}^{\infty} (n_i \cdot {M_i}^2)}{\sum_{i=1}^{\infty} (n_i \cdot M_i)}, \quad \bar{M}_z = \frac{\sum_{i=1}^{\infty} (n_i \cdot {M_i}^3)}{\sum_{i=1}^{\infty} (n_i \cdot {M_i}^2)} \tag{1.2}$$

In the number average, each polymer chain is counted equally regardless of its length. In the weight average, a longer chain is counted with a greater proportion. In the z average, this proportion is further increased.[7,8] For a perfectly monodisperse polymer, $\bar{M}_n = \bar{M}_w = \bar{M}_z$. Otherwise, $\bar{M}_n < \bar{M}_w < \bar{M}_z$. The ratio of $\bar{M}_w$ to $\bar{M}_n$ is often used to express how polydisperse the polymer sample is. The ratio is called

dispersity, abbreviated as $Đ$:

$$Đ = \frac{\bar{M}_w}{\bar{M}_n} = \frac{\sum_{i=1}^{\infty} n_i \times \sum_{i=1}^{\infty} (n_i \cdot {M_i}^2)}{\left(\sum_{i=1}^{\infty} (n_i \cdot M_i)\right)^2} \tag{1.3}$$

Common techniques used in the determination of $\bar{M}_n$ are osmometry, tonometry, size exclusion chromatography (SEC), and end-group titration.[9–12] Estimation of $\bar{M}_w$ is achieved by light scattering and chromatographic techniques.[9–11]

Nowadays, mass spectroscopy has been increasingly applied to the analysis of the molar mass distribution of polymers, notably due to its ability to resolve complex systems (Figure 1.2).[13] Although the resolution is poorer than that of mass spectrometry by orders of magnitude, size exclusion chromatography has been the mainstay in the analysis of the molecular weight distribution.[7]

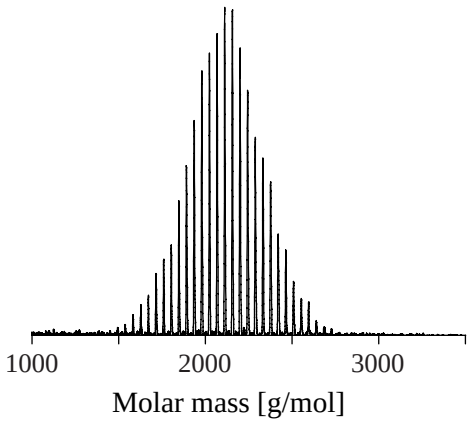

Figure 1.2 – Mass spectrum of a poly(ethylene glycol) ($\bar{M}_n = 2000\,\mathrm{g/mol}$) obtained in matrix-assisted laser desorption ionization (MALDI) coupled with time-of-flight mass analyzer.[14]

In none of the above examples of structural representation of polymers the end groups, *i.e.*, the group of atoms located at the extremities of the chain, have been shown. This is partly because the exact nature

of those groups is often unknown. Also, the same groups constitute an insignificant fraction of the mass of high molecular weight polymer, thus having generally negligible effect on polymer properties.[3,6] Nevertheless, the controlled introduction of functional groups as chain ends of a polymer, therefore termed as *telechelic*, is of great interest as the latter are precursors of higher architectures.[15–17]

1.1.4 Structure and topology

Polymers can be classified in three major structural categories according to the shape of constitutive macromolecular chains: linear, branched and cross-linked polymers.[3,6,18] However, it is common practice to subdivide those categories and hence differentiate further linear, cyclic, branched, hyper-branched, cross-linked, dendritic, comb- or star-shaped polymer conformations (Figure 1.3).[19]

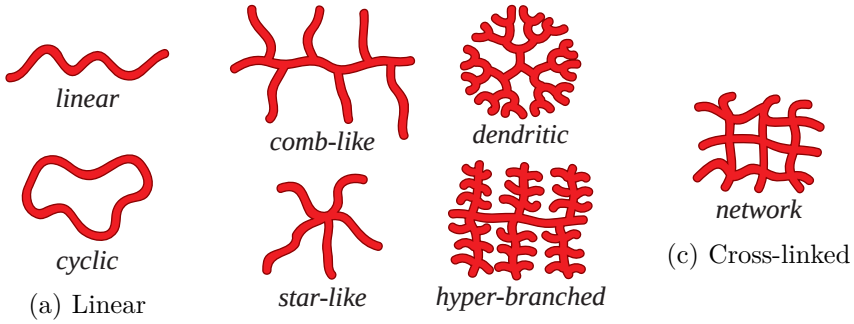

(a) Linear (b) Branched (c) Cross-linked

Figure 1.3 – Overview of macromolecular architectures.

Linear polymers are composed of monomer units linked only to two others, thus forming a continuous chain. The latter is thus strictly built from bifunctional monomers.[18] Although generally free, the chain extremities can however be attached, which is characteristic of cyclic polymers, or macrocycles.[20] Examples of natural macrocycles include plasmids, *i.e.*, small DNA molecule that can be found in primitive microorganisms, whereas synthetic analogues are synthetically challenging targets.[20,21]

If a few points of tri- or poly-functionality are introduced (either in-

tentionally or through side reactions) at random locations along linear chains, branched polymers result. [18,22,23] Therefore, branched polystyrene can be easily obtained by adding small quantities of divinyl benzene during the polymerization of styrene. Also, branching may result from intra-molecular chain transfer during the polymerization process. Branching has generally tremendous effect on the properties of polymers through geometric effects. [8,24,25]

Branching in polymers can be of different types: either short or long, regularly or randomly distributed, forming a comb or star... A particular interest is devoted to macromolecules where branching points are repeated in profusion but in regular, successive layers to form a fractal. These particular assemblies are qualified as dendritic, or simply called dendrimers. [26] Hyperbranched polymers are similar to dendrimers but less perfect, thus showing various topologies. Once again, we can point the tendency of chemists to artificially reproduce structures that have been found in nature for millennia and that consist of amylopectin and proteoglycan.

As the length and frequency of the branches on polymer chains increases, the probability of connecting them together increases, resulting in the formation of an interconnected branched polymer, or network. For example, a cross-linked network structure will develop, instead of a branched structure, if styrene is copolymerized with higher concentrations of divinyl benzene. The three-dimensional structure of the network implies that all chains are finally connected together to form one tremendous molecule, of virtually infinite mass. With the formation of network structure, polymers acquire greater rigidity, dimensional stability, and resistance to heat and chemicals. [3,6] This particular stability has been known for several years, while the vulcanization of natural rubber, or polyisoprene, with sulphur has been used to mechanically reinforce the material. [27]

1.1.5 Homopolymers and copolymers

As suggested above, a poly-functional monomer can be intentionally added to a polymerization mixture to introduce branching or bridges into a macromolecular architecture. Thus, polymer chains can be made from different monomeric species. When only one species of monomer is used to build a macromolecule, the product is called *homopolymer*, neglecting

minor irregularities like chain ends. The word homopolymer is often used more broadly to describe polymers whose structure can be represented by repetition of a single type of monomer unit which may contain one or more species of monomer unit. Therefore, macromolecules alternating two types of monomers, *e.g.*, poly(ethylene terephthalate), also fall under the homopolymer denotation.[2,3,6]

Formally denoting polymers derived from two or more chemically distinct monomers, the term *copolymer* is more commonly used to describe macromolecules containing more that one type of monomer units.[2] Are distinguished: *bipolymer*, a polymer derived from two monomer species; *terpolymer*, a polymer derived from three monomer species...[2] Depending on the particular arrangement of repeating units along the chain, several categories of copolymers are further distinguished (Figure 1.4): statistical copolymers, whose different units are randomly distributed along the chain; alternating copolymers, whose two monomers alternate in a regular fashion along the chain; gradient copolymers, whose chain composition gradually change from one type of unit to the other; and block copolymers, composed of two (diblock) or more (triblock, tetrablock...) uninterrupted sequences of each monomer in the chain.[2,3,6,28]

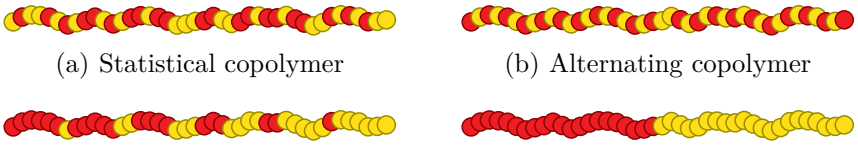

(a) Statistical copolymer (b) Alternating copolymer

(c) Gradient copolymer (d) Block copolymer

Figure 1.4 – Representations of the different categories of copolymers.

Depending on the structural arrangement of the units along the chains, copolymers show different physical properties. In particular, random or alternating copolymers exhibit average properties compared to homopolymers from which they derive. For example, a statistical copolymer derived from two or more comonomers will be characterized by a unique glass transition temperature, *i.e.*, temperature below which the translational modes of motion of chain backbone segments are effectively freezing out.[29] This intermediate value can be evaluated from the glass transition temperatures of the corresponding homopolymers, averaged

by the weight fraction of each monomer in the copolymer. On the other hand, segmented copolymers combine the properties of the different corresponding homopolymers in an additive way, thus constituting one of the most studied class of copolymers for many years.[8,30,31] Indeed, their constitutive blocks are generally immiscible, which leads to a microphasic separation within the material.

1.2 Polymer synthesis

Polymerisation reactions can be classified in various ways. Classically, polymerization reactions have been differentiated into two categories according to the mechanism by which the chains grow: chain-growth polymerizations; and step-growth polymerizations.[1,3,18]

1.2.1 Step-growth polymerizations

Step-growth polymerizations proceed by stepwise reactions between functional groups of reactants. The reaction leads successively from monomer to dimer, trimer, tetramer, pentamer, and so on.[3,18,32,33] Then, the same reaction occurs at random between the intermediates and the monomer as well as among the oligomeric intermediates until a large macromolecule is finally formed:

$$\text{monomer} + \text{monomer} \rightarrow \text{dimer} \tag{1.4}$$

$$\text{dimer} + \text{monomer} \rightarrow \text{trimer} \tag{1.5}$$

$$\text{trimer} + \text{monomer} \rightarrow \text{tetramer} \tag{1.6}$$

$$\text{n-mer} + \text{monomer} \rightarrow \text{(n+1)mer} \tag{1.7}$$

$$\text{n-mer} + \text{m-mer} \rightarrow \text{(n+m)mer} \tag{1.8}$$

Depending on the concentration of reacting species, the kinetics will favour the addition of a monomeric or oligomeric unit. Consequently, the average molecular weight of the growing chains builds up slowly in the early stage of the polymerization process. In turn, high molecular-weight polymer chains are formed only when the monomer conversion (c) is higher than 98 % (Figure 1.5). Therefore, long polymer chains can

only be obtained when high-purity reagents are present in stoichiometry amount. [3,32,33]

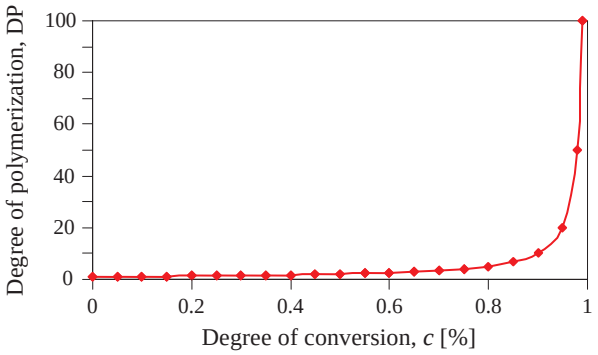

Figure 1.5 – Relationship between the degree of polymerization and monomer conversion in step-growth polymerization.

As a general rule, the step-growth polymerization involves polycondensation, which explains why both terms are often used synonymously. Indeed, the step-growth processes lead to the formation of small molecules such as water, hence the term condensation reactions. [3,34] Monomers that undergo a step-growth polymerization must at least contain two reactive functional groups, several leading to the formation of branching or cross-linking. The most common system involves the polymerization of two difunctional monomers, both antagonist functional groups being either carried by a single entity or, more often, by two different entities. [33,34]

1.2.2 Chain-growth polymerizations

Chain-growth polymerizations involve the sequential step-wise addition of monomers to a growing chain. Usually, the monomer is unsaturated, almost always a derivative of ethylene, and most commonly vinylic, that is mono-substituted. [35] Ring-opening polymerizations also exhibit many features of chain-growth polymerization, but may also show some characteristic of step-growth polymerizations. [20,36] In both cases, the polymerization process is thermodynamically driven, either via the formation of simple bonds from weaker unsaturations, or via ring opening of strained cycles.

Chain polymerization involves three basic processes: chain *initiation*, *propagation*, and *termination*. A fourth process, chain *transfer*, may also be involved, but it may be regarded as a combination of chain termination and chain initiation. Chain initiation occurs by a reaction between the monomer molecule and a reactive species (I*), like a free radical, an anion, or a cation (Equation 1.9).[3] The latter is generated by the dissociation or decomposition of a relatively unstable material called *initiator*. According to the nature of the reactive species, the chain polymerization processes are called free-radical polymerization,[35,37–39] anionic polymerization,[39–43] or cationic polymerization.[39,44]

Once initiated, chain-growth polymerization propagates via transfer of the reactive centre from the growing chain to the added monomer (Equation 1.10) If the active site is transferred to another molecule than a monomer (solvent, polymer chain, *etc.*), the growth of the chain stops but the propagation may continue elsewhere due to the transfer until another process destroys the reactive centre, resulting in growth termination (Equation 1.11). There may be several termination reactions depending on the type of reactive site and the polymerization conditions. Common terminations include recombination or disproportionation of free radicals, transfer reactions toward stable centre carriers...[3]

$$\mathrm{I^* + M \rightarrow I\text{–}M^*} \tag{1.9}$$

$$\mathrm{I\text{–}M_n^* + M \rightarrow I\text{–}M_{n+1}^*} \tag{1.10}$$

$$\mathrm{I\text{–}M_n^* \rightarrow I\text{–}M_n} \tag{1.11}$$

Chain-growth polymerization may also be driven by coordination of monomers to an organometallic active site, generally via unsaturated bonds. This process is referred as coordination polymerization, which include Ziegler–Natta and ring opening metathesis polymerizations.[39,45–47]

1.2.2.1 Living and controlled polymerizations

The term living polymer was suggested by M. Szwarc to qualify the products of the anionic polymerization of styrene initiated by electron transfer in tetrahydrofuran.[48]. In this context, the adjective *living* de-

notes the ability of a polymer chain to further add monomer after the initial batch has been consumed. This implies that the polymer chains do not undergo irreversible chain breaking reactions. Hence, living polymerizations are defined as polymerizations from which chain transfer and termination are absent.[40] In many cases, the rate of chain initiation is fast compared with the rate of chain propagation, so that the number of growing chain is essentially constant throughout the polymerization. In turn, such a process should lead to a very narrow Poisson molecular weight distribution, hence characterized by low dispersity:[39,40,42]

$$Đ \approx 1 + \frac{1}{\mathrm{DP}} \tag{1.12}$$

When the absence of chain transfer and termination reactions is coupled with fast initiation process, a linear increase in the degree of polymerization with monomer conversion is expected (Figure 1.6) Consequently, the average degree of polymerization of macromolecular chains can be evaluated from the ratio of concentrations of reacted monomer to introduced initiator:[32,39]

$$\mathrm{DP} = c \cdot \frac{[\mathrm{M}]_0}{[\mathrm{I}]_0} \tag{1.13}$$

The feature of livingness was also discovered in cationic polymerization.[44] However, free-radical polymerizations have no living character because of the multiple recombination and transfer reactions of free radicals. Although favoured at high concentration in free radicals, these side reactions can be minimized by reversibly scavenging free radicals in the form of inactive, called dormant, species to keep radical concentration low and hence control the polymerization. In this respect, the term controlled polymerization can be defined as a synthetic method to prepare polymers, which are well-defined with respect to topology, terminal functionality, composition, and arrangement of comonomers, and which have a degree of polymerization predetermined by equation 1.13, but not necessarily a narrow dispersity. Strictly, a living polymerization is thus not always controlled and a controlled polymerization is not always living.[39]

Almost all new controlled/living systems have one common feature, which is the coexistence of active and inactive species, being in a dy-

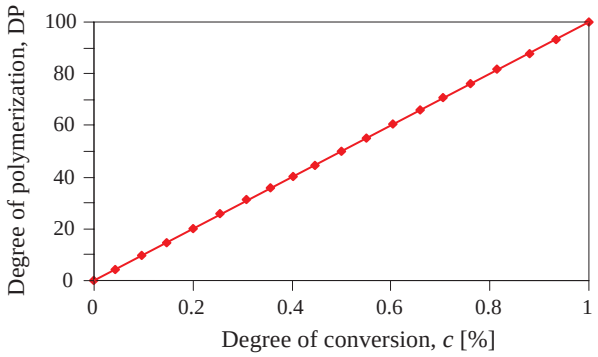

Figure 1.6 – Relationship between the degree of polymerization and monomer conversion in chain-growth polymerization.

namic equilibrium, either via reversible deactivation processes (equation 1.14) or via reversible degenerative transfer (Equation 1.15).[39]

$$\sim\sim\sim M_n^* + D \leftrightharpoons \sim\sim\sim M_n\text{–}D \tag{1.14}$$

$$\sim\sim\sim M_n^* + \sim\sim\sim M_m \leftrightharpoons \sim\sim\sim M_n + \sim\sim\sim M_m^* \tag{1.15}$$

Reversible deactivation is a process where active species are in a dynamic equilibrium with inactive dormant, typically covalent species, formed by reaction with a deactivator (D). This balance may be spontaneous, as in nitroxide mediated radical polymerization (NMP),[49] or catalysed, as in atom transfer radical polymerization (ATRP).[50,51] The first process involves permanent nitroxide radicals (NO*) as deactivator, which reversibly associate to free radicals (Figure 1.7 (a)). The second process involves transition metal complexes (Mt) that proceed to an inner sphere electron transfer with the active radical centre (Figure 1.7 (b)), associated with the migration of a ligand (X), often an halogen or pseudo-halogen, from its coordination sphere towards the chain end.[39]

Reversible transfer is a bimolecular reaction between a dormant and an active polymer chain, which leads to a direct exchange of activity between two chain ends. This degenerative process is coordinated at the molecular level by a chain transfer agent (CTA). A typical example is the reversible addition–fragmentation chain transfer (RAFT) polymerization (Figure 1.7 (c)).[39,52–54]

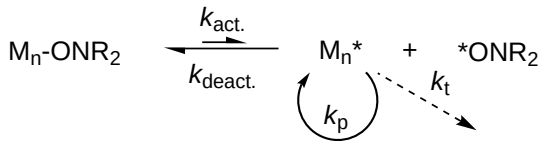

(a) Nitroxide mediated polymerization

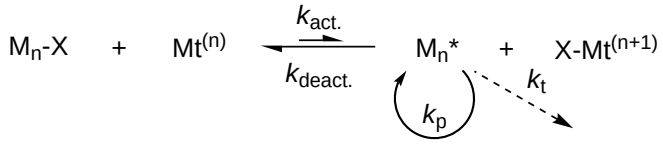

(b) Atom transfer radical polymerization

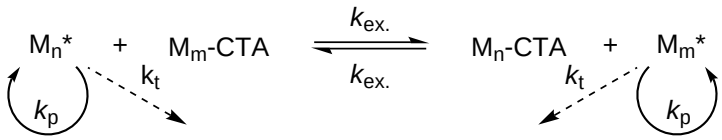

(c) Reversible addition–fragmentation chain transfer

Figure 1.7 – Controlled radical polymerization processes.[50]

In the last years, the advent of controlled radical polymerization (CRP) has provided a welcome alternative to ionic living polymerizations, whose effectiveness is counterbalanced by a particularly difficult implementation, the limited number of polymerizable monomers and the stringent conditions required for the survival of active sites. As shown in Table 1.2, each of the controlled radical polymerization methods has advantages as well as limitations. Among the different CRP techniques, the RAFT process is characterized by its versatility with respect to monomer choice and the absence of catalyst. In addition, RAFT offers the possibility of direct functionalization by the use of functional chain transfer agents. However, RAFT polymerization rely on a radical source, which may decrease end functionality as part of the chains are directly initiated by the primary radical.[37]

1.2.2.2 RAFT polymerizations

Historically, reversible addition–fragmentation chain transfer polymerization is one of the most recent controlled radical polymerizations

Table 1.2 – Comparison of NMP, ATRP, and RAFT processes.[37]

Features	NMP	ATRP	RAFT
Monomers	styrenes, (meth)acrylates, acrylamides	all activated vinylic monomers	nearly all monomers
Temperature	elevated ($> 120\,℃$)	large range ($-30\,℃$-$150\,℃$)	room to elevated
Chain end	alkoxyamine	(pseudo)halide	thiocarbonyl
Oxygen	sensitive	some tolerance	sensitive
Additives	free nitroxide	transition metal	radical initiator

(1998). This technique relies on thiocarbonyl compounds as RAFT agents to establish a subtle balance between the active and dormant forms, via reversible degenerative transfer (Figure 1.8). In this equilibrium, the initiating or propagating radical adds to the sulphur of the thiocarbonyl centre to produce an intermediate carbon-centred radical. This stabilized radical can then undergo β-scission, either to reform the propagating radical or to liberate a new carbon-centred radical. The R group of the CTA is chosen so that it undergoes β-scission from the RAFT-adduct radical in preference to the propagating species, but is still capable of re-initiating polymerization. In this way, the initial RAFT agent is rapidly converted to the macro-CTA, which ensures a fast initiation through the establishment of a degenerative equilibrium.[52–54]

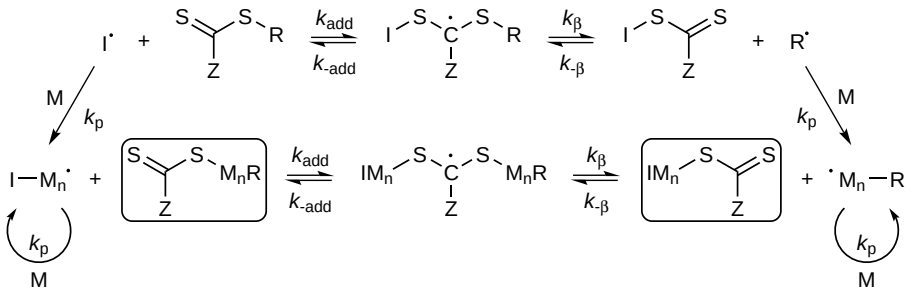

Figure 1.8 – RAFT polymerization mechanism.[52]

To achieve control over the polymerization process, a delicate balance of the rates of these various reactions is required, so as to ensure that the dormant species is orders of magnitude greater in concentration than the active species, but the exchange between the two forms is rapid. Thus, the reactivity of the RAFT agent must be tailored to match the reactivity and stability of the polymeric propagating radical.[52] In this regard, the structure of stabilizing Z group might be properly chosen in order to favour (OR or NH_2) or disfavour (CN, Ph or CF_3) the fragmentation of the adduct. Also, several groups (SR and modified OR/NH_2) constitute an intermediate category for which the effects on the fragmentation equilibrium are moderate.[39]

Despite all the advantages of RAFT, this technique relies, as mentioned above, on a conventional radical initiator to initiate the polymerization process. Part of macromolecular chains is thus initiated directly and therefore has no functional R group at chain extremity. Fortunately, the proportion of chains initiated by the primary radicals originating from the dissociation of the initiator remains relatively low considering the CTA-to-initiator ratios usually involved.

1.3 Polymer solutions

In the solid state, polymer molecules pack the space with little voids either in a regular array (crystalline polymers), or at random (amorphous polymers). In this configuration, the macromolecules are in close contact with each other. In solutions, in contrast, each polymer molecule is surrounded by solvent molecules. In this dispersed state, their physical properties differ markedly from those of the bulk material. Due to their large size, many of those properties are however common to all polymer molecules.[7]

1.3.1 Chain conformation

In solution, a polymer chain is changing its shape incessantly, an instantaneous shape being called a conformation. Each possible chain conformation has a certain probability, or statistical weight, due to purely entropic effect. Whereas a fully stretched conformation is highly unlikely, chains are rather crumpled and take a random coil conformation.

A linear flexible homopolymer chain can be modelled as a random walk trajectory normally distributed in the three dimensions, which defines a Gaussian chain.[7,55]

The dimension of the random walk chain is classically measured by the root-mean-square radius of gyration, R_g, or simply radius of gyration. Its square is the second moment around the centre of mass of the chain. The latter is defined as the mean square of the distance between the segments, r_i, and the centre of mass, r_c of the chain (Figure 1.9 (a)):

$$R_g{}^2 = \left\langle \frac{1}{N} \cdot \sum_{i=1}^{N} (r_i - r_c)^2 \right\rangle \tag{1.16}$$

Roughly, the polymer chain occupies the space of a sphere of radius R_g that can be experimentally evaluated by static light scattering (SLS) technique. This radius can be further defined for any chain architecture including non-linear chains such as branched polymers, providing a universal measure for the chain dimension.[7,55,56] An apparent radius of gyration can also be defined for segmented copolymers, where conformations may drastically differ from normal distribution. Indeed, they can adopt a segregated conformation where the chemically different blocks occupy distinct regions in space due to the unfavourable thermodynamic interactions between the dissimilar segments. Also, block copolymer chains in solution can consist of mutually interpenetrating random coils, which leads to more extended conformations.[31]

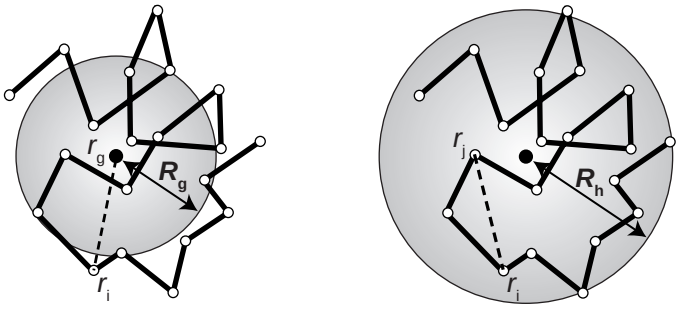

(a) Radius of gyration (b) Hydrodynamic radius

Figure 1.9 – Radius of gyration (a) and hydrodynamic radius (b) of a random coil polymer.[7]

Another often used measure of the chain dimension is the hydrodynamic radius, which roughly corresponds to the radius of the chain as it migrates through a solution. In turn, it gives a measure of the friction received by each segment from the solvent and is commonly evaluated by dynamic light scattering (DLS) technique. The inverse of the hydrodynamic radius is given as the average of the reciprocal of the distance between two segments of the chain (Figure 1.9 (b)):[7,55,56]

$$\frac{1}{R_h} = \left\langle \frac{1}{|r_i - r_j|} \right\rangle \tag{1.17}$$

Like substances spreading throughout accessible volume, polymer chains in solution change their positions all the time by diffusion. This phenomenon is made possible by microscopic motions of parts of the chain, which accompany motions of adjacent segments in the same direction. Solvent molecules collide randomly with particles to change their trajectory and velocity, resulting in a random stochastic motion activated by thermal energy, called Brownian motion. The latter is characteristic of the polymer conformation (R_h) and accelerates at higher temperatures, in less viscous solvents.[7,55,56]

In solution, each linear polymer chain occupies, in crude approximation, the space of a sphere of a linear dimension of R_g. At low concentration, C, these spheres are well separated from each other and behave more or less independently. This situation corresponds to the dilute regime, as illustrated in Figure 1.10 (a). As the concentration increases, they become congested and eventually touch each other, the whole volume of the solution being packed with these spheres. As the concentration further increases, chains overlap and ultimately entangle if they are long enough (Figure 1.10 (c)). In this semi-dilute regime, the interactions between the chains are strong and their mobility is greatly reduced. The lower limit of the semi-dilute range is defined as the overlap concentration, C^*, which is classically encountered for a weight-to-volume fraction in polymer, ϕ, at around 1 % w/v. At a higher concentration, the solution enters a so-called concentrated regime in which each segment of the polymer chain does not have sufficient space available. At the upper limit of the semi-dilute range, the weight-to-volume fraction in polymer is typically between 20 and 30 % w/v.[7,55]

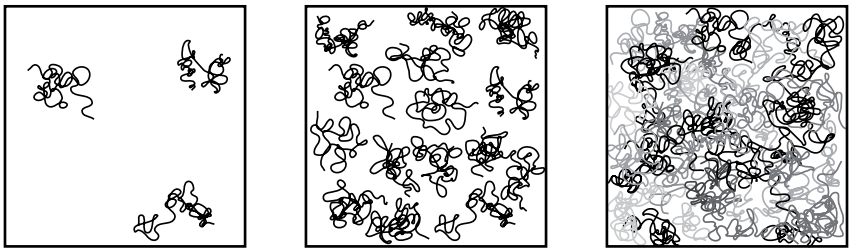

(a) $C << C^*$ (b) $C \approx C^*$ (c) $C >> C^*$

Figure 1.10 – Concentration regimes for solutions of linear flexible polymers: dilute solution (a), solution at the overlap concentration (b) and semi-dilute solution (c).[7,55]

1.3.2 Solvent quality

For a given polymer, there are solvents that dissolve the polymer well, said "good solvents", and others that do not dissolve the polymer, said "non-solvents". A good solvent will interact in a strong manner with the polymer, replacing the secondary interactions between chains by chain–solvent interactions. In contrast, poor or non-solvents only lead to weak interactions, which are not sufficient to overcome the interactions between chains. Practically, this results in the aggregation of the chains and precipitation of the polymer in the considered solvent.[7] Strictly, cross-linked polymers remain insoluble but can swell in good solvents to form gels, which can be defined as semi-solid systems consisting of a three-dimensional network in which a liquid is trapped.[2] In this regard, the degree of swelling can be used as an indication of the solvent quality.[18]

Dissolution of a polymer into a solvent is governed by the second law of thermodynamics, *i.e.*, an overall increase in entropy of the system. Thermodynamics of dilute polymer solutions is described by Flory–Huggins solution theory.[57,58] To measure the quality of a solvent toward a given polymer, this theory defines an interaction parameter, denoted χ, as the enthalpy (energy) change associated with the solvation of polymer chains reduced by the thermal activation energy. This parameter thus depends on the nature of both polymer and solvent, as well on temperature. On one hand, a positive χ denotes that the polymer-solvent contacts are less favoured compared with the polymer–polymer

and solvent–solvent contacts. On the other hand, a negative χ means that polymer–solvent contacts are preferred, promoting solvation of the polymer. The solvent and temperature (T_θ°) conditions for which the interaction parameter is zero are called "*theta*" conditions.[7]

Mixing two pure compounds always leads to a less ordered state in solution, which in turn increase the entropy of the system. Due to their high molar masses, the entropy of mixing is small for polymer solutions, especially at low concentrations. To a certain extent, the favourable entropy of mixing is able to compensate an unfavourable enthalpy of mixing ($\chi \gg 0$). Therefore, below a critical value of the Flory–Huggins parameter, χ_c, the dissolution is favourable and the resulting solution is stable, whatever the composition, φ, of the mixture. Above this value, there is a concentration range for which the system is unstable, bordered on each side, strictly speaking, by a region where the solution is metastable (Figure 1.11).[7]

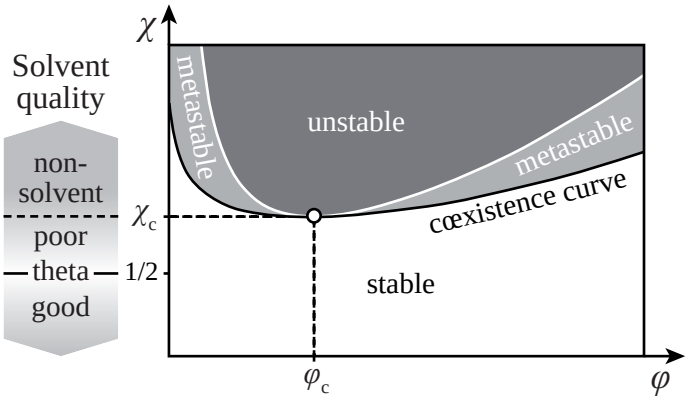

Figure 1.11 – Phase diagram for a polymer–solvent binary mixture.[7]

The critical value of the interaction parameter decreases with increasing molar mass, approaching a value of $\chi_c = 1/2$ for chains of infinite length. Intuitively, the solubility of polymers decreases with their size. Given the finite length of macromolecular chains, the quality of a solvent for a given polymer can be defined according to the value of the Flory–Huggins parameter: a solvent characterized by a χ value smaller than 1/2, including negative values, is called a good solvent; a solvent with $\chi > 1/2$ is qualified as a poor solvent; as χ further increases above χ_c, the solvent becomes unable to dissolve the polymer and is called a

non-solvent.[7]

The quality of a solvent for a given polymer can be altered by changing the temperature. In this respect, increasing temperature generally enhances the solubility of the polymer ($\Leftrightarrow \chi$ decreases). For a given composition, phase separation may occur within the system when temperature falls below a critical value. The temperature at the onset of phase separation is called the critical temperature, T_c°, and can defined for each system composition, φ, which enables to draw a coexistence curve on a temperature–composition diagram (Figure 1.12 (a)). The critical temperature at the highest point on the coexistence curve is referred to as the upper critical solution temperature (UCST). Above this temperature, the mixture forms a single phase whatever its composition. When cooled to temperatures below the coexistence curve, the solution separates into two phases, each being uniform but having different compositions.[7]

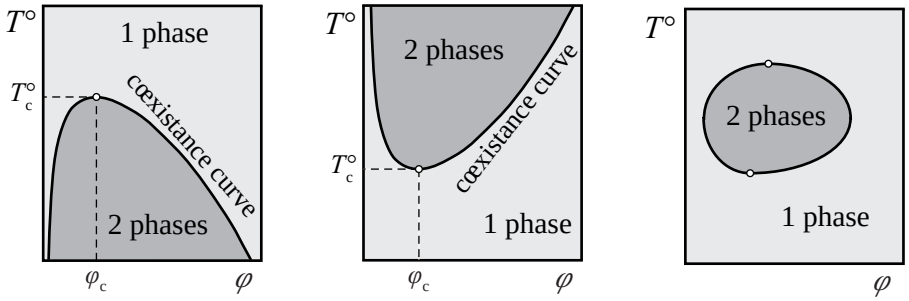

(a) UCST (b) LCST (c) UCST & LCST

Figure 1.12 – Phase diagram for polymer–solvent systems showing UCST (a), LCST (b) and both (c) type behaviours.[7]

In some cases, the phase diagram is inverted, *i.e.*, the solubility decreases ($\Leftrightarrow \chi$ increases) upon temperature rises. For a given composition, phase separation may occur within the system when temperature increases above a critical value. The critical temperature below which the mixture forms a single phase whatever its composition is referred to as the lower critical solution temperature, abbreviated LCST (Figure1.12 (b)).[7] A polymer soluble in water due to hydrogen bonding usually has an LCST-type phase diagram because the hydrogen bonds are disrupted at higher temperatures.

Polymer solutions may exhibit a variety of other coexistence behaviour, and the critical curves may possess multiple extrema. In particular, it may happen that a polymer solution shows a combination of both UCST and LCST (Figure 1.12 (c)). Phase behaviours in those systems may be such that an intermediate region is immiscible, as in the case with a closed-loop phase diagram, or miscible, when two parabolic coexistence curves are present.[7] The phase behaviours of some common polymer–solvent mixtures are given in Table 1.3.

Table 1.3 – Phase behaviour of some common polymer–solvent mixtures.[59,60]

Polymer	Solvent	Temperature	Type
polyethylene	anisole	$\sim 95\,^{\circ}\mathrm{C}$	UCST
poly(2-ethyl-2-oxazoline)	water	$\sim 62\,^{\circ}\mathrm{C}$	LCST
poly(*N*-isopropylacrylamide)	water	$\sim 32\,^{\circ}\mathrm{C}$	LCST
poly(methacrylamide)	water	$\sim 57\,^{\circ}\mathrm{C}$	UCST
poly(methyl methacrylate)	*n*-butanol	$\sim 80\,^{\circ}\mathrm{C}$	UCST
polystyrene	cyclohexane	$\sim 25\,^{\circ}\mathrm{C}$	UCST

The construction of phase diagrams is commonly achieved by cloud point measurements, via, *e.g.*, turbidimetry. Precisely, solutions at different concentrations are prepared and brought into a single phase, either by heating or cooling. The homogeneous solutions are then slowly cooled or heated, depending on the type of behaviour. As the temperature crosses the coexistence curve, the solution becomes turbid, indicating microscopic heterogeneity. The turbidity of the solution is due to scattering of light by a difference in the refractive index between the two phases. By connecting the cloud points measured for solutions of different concentrations, the coexistence curve and hence the phase diagram can be constructed.[7] After a sufficiently long time, the polymer–solvent system ultimately separates into two macroscopic phases, each of which being uniform.

1.3.3 Copolymer solutions

In a solvent, the phase behaviour of copolymers is controlled by the interaction between the small chain segments and the solvent molecules

as well as the interaction between the segments themselves. Hence, the design of copolymers, *i.e.*, composition and architecture, strongly impacts the chain behaviour in solution. In contrast to homopolymer solutions, quality of the solvent has to be defined in regard to the different monomer units, which may greatly vary according to their chemical nature. In this respect, non-selective solvents are those that are thermodynamically good for all parts of the macromolecule, which ensure solubility. On the other hand, non-solvents cause the aggregation of the chains and precipitation of the entire polymer. Also, the different parts of the macromolecules may develop contrasting affinity in regard to a given solvent or mixture of solvents. In this regard, solvophilicity or, on the opposite, solvophobicity measures respectively the affinity, and lack of affinity, of a particular sequence for a specific solvent. In aqueous solution, the terms hydrophilicity–hydrophobicity are commonly used to highlight the nature of the solvating media. In this continuity, *amphiphile* is a term describing a substance made up of monomer units containing groups that are solvophilic and others that are solvophobic with respect to a given solvent. [31,61]

In random or alternating copolymers, the distribution of groups, may they be solvophobic or solvophilic, leads to an average solvent quality in regard to the chain. Consequently, the lack of affinity for one unit may be sufficient to force the entire chain to shrink or collapse, as illustrated in Figure 1.13 (a). In other architectures including segmented and grafted copolymers, the chemically different blocks occupy distinct regions along the chain. In analogy to their bulk behaviour, those copolymers also self-assemble in block-selective solvents, which solubilize one but not the other block, forming colloidal-size particles called *micelles* (Figure 1.13 (b) and (c)). From a morphological point of view, those nano-structures consist of a more or less swollen core resulting from the aggregation of the solvophobic blocks surrounded by a corona formed by the solvophilic blocks. [30,62–68]

A deep analogy can be made between the associative behaviour of the simplest diblock copolymer into micelles and the situation observed for classical low molar mass surfactants that contain both hydrophilic groups (heads) and hydrophobic groups (tails). Accordingly, a critical micelle concentration (CMC) can be defined for block copolymer micelles, at which the first micelle forms in a given solvent. As the concentration of copolymer chains increases in the solution, more micelles are

formed while the concentration of non-associated chains, called *unimers*, remains constant to the CMC value.[30,64,69] Compared to classical surfactants, CMC values are much lower in the case of block copolymer macro-surfactants, which motivates their use as, *e.g.*, nano-containers for drug delivery.[70–73]

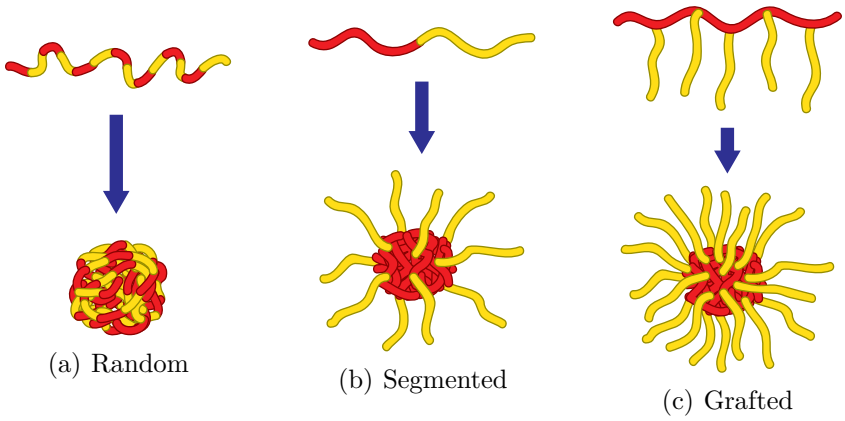

Figure 1.13 – Phase behaviour of various amphiphilic copolymer architectures in a selective solvent.

The micellization process is characterized by the aggregation of an average number (Gaussian distribution) of block copolymer chains into micelles, which defines the aggregation number Z.[64] For amphiphilic diblock copolymers, this number generally ranges from a few tens to thousands and depends on the length of both blocks. Empirically, the aggregation number is roughly correlated to the degree of polymerization of the insoluble block, but decreases with the length of the soluble block.[65,74]

The size of the micellar core is characterized by its radius, R_c, while the overall radius of the polymeric micelle is defined as R_m. The latter depends on the length of each constituting segment, and usually ranges from 10 to 100 nm, similar to that of viruses and lipoproteins. Other ways of defining the overall dimension of a micelle are the radius of gyration, R_g, and the hydrodynamic radius, R_h, as defined above. The core size is determined by the number and length of solvophobic segments that aggregate to form the micellar object.[62,64]

As illustrated in Figure 1.14 (a), dimensions of micellar objects are

experimentally evaluated by scattering methods, including but not limited to static and dynamic light scattering, and small angle X-ray and neutron scattering (SAXS and SANS). While giving a representative overview of the sample, scattering data are often fitted to a model, which can be problematic in the analysis of samples containing multiple or unknown structures. In complement, microscopy techniques allow observing differences in individual particles via direct imaging (Figure 1.14 (b)). In counterpart, the analysis of a representative number of particles is time consuming, which generally results in poor statistics. [68,75]

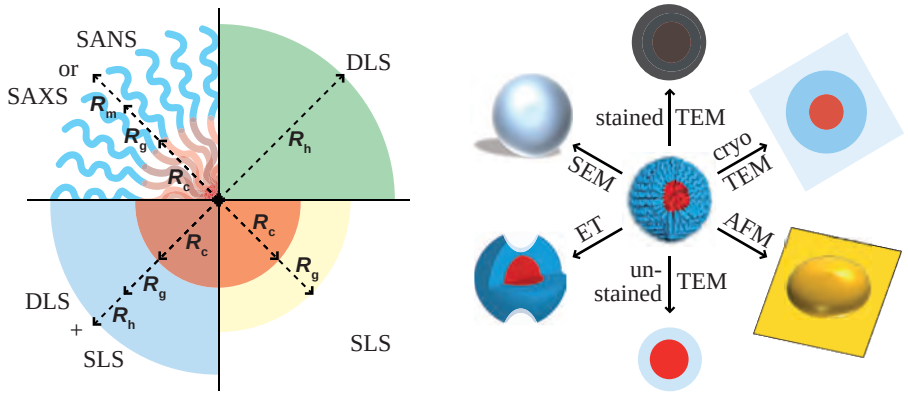

(a) Size of micelle (b) Imaging of micelle

Figure 1.14 – Schematics showing the size information and image obtained by different scattering and microscopy techniques for a spherical polymer micelle. [75]

Like surfactants, amphiphilic block copolymers aggregate to produce nano-objects of various morphologies like spheres, cylinders or vesicles. [66,69,76] Especially if the soluble segment is predominant, a diblock copolymer usually forms spherical micelles. As the length of the solvophobic block increases relative to the solvophilic block, cylindrical micelles or vesicles might be obtained. [65,67,77,78] Whereas the solvophobic parts become packed together, the solvophilic segments interact preferentially with solvent molecules than with each other, leading to short range repulsion between adjacent coronal chains. The delicate balance between solvophobic and solvophilic interactions gives rise to an optimal surface area at the core–corona interface, which in turn drives the

formation of nano-structures.[66,77,79,80]

More exotic micelles with shapes differing from spheres or coexistence of multiple morphologies in solution can also be observed depending on the preparation conditions, *i.e.*, concentration,[81] solvent,[82] or additives.[83,84] Indeed, these unusual micelles are frequently observed when nano-particles are kinetically trapped into a metastable state (kinetic control).[80,82,85] Even if the resulting structures are rather aggregates than true associates, the term non-equilibrium micelles has been commonly accepted. With time, dynamics of micelles potentially leads to rearrangement of the structure to the most stable morphology (thermodynamic control). In parallel, non-equilibrium micellar structures can be converted into stable, said equilibrium, micelles by heating, changing solvent quality or adding a plasticizer.[80,86–89]

The dynamics of micellar systems is relevant at several levels that are the micellization, *i.e.*, the formation of micelles, and micellar exchange or hybridation, *i.e.*, the establishment of an equilibrium. The kinetics for block copolymers is analogous to surfactants and controlled by two mechanisms that consist in exchange of unimers, *i.e.*, single chains, and slower fusion/fission of whole micellar species.[88,90,91] Both mechanisms are very sensitive to the copolymer structure, to the molecular weight and composition.[68,88] For small deviations from equilibrium, hybridation occurs mainly via step-wise association/dissociation of a single unimer at a time, according to the Aniansson–Wall mechanism (Figure 1.15).[92–94] Being apparently a distinct concern, the local dynamics of chain segments in the core or in the corona of the micelles can be thus linked to some extent to the hybridation mechanisms.

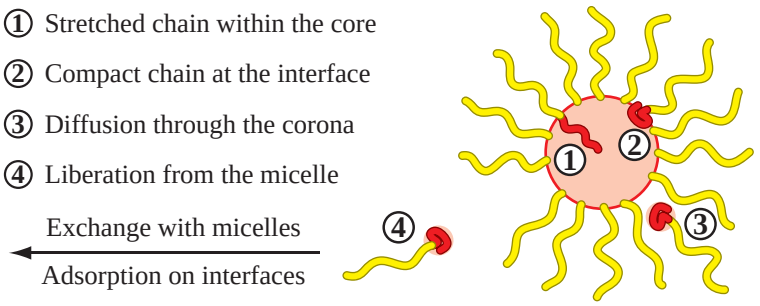

Figure 1.15 – Schematic representation of the escape of a unimer from a polymeric micelle.

In comparison with low molecular weight surfactant micelles, the exchange kinetics of polymeric micelles proceed on time scales drastically longer than for ordinary surfactant micelles, which are in the order of the microsecond/millisecond range. In comparison, dynamics of block copolymer micelles may stretch over a wide time window virtually ranging from infinity to hours/minutes. The reason for the slow kinetics is generally attributed to the strong incompatibility between the insoluble polymer block and the solvent.[69,88,90] Hybridation kinetics are usually studied by disrupting an equilibrium system and following its relaxation. Typically, the system is disequilibrated by a laser-induced temperature jump, and the relaxation process is monitored by light scattering or fluorescence measurements.[95,96] Other techniques consist in following the steady-state exchange of labelled copolymer chains between micelles via, *e.g.*, fluorescence spectroscopy.[97–99]

Dynamics of block copolymer micelles can be tuned over time scale via numerous parameters. Intuitively, longer insoluble blocks and less swollen cores slow down the expulsion of the chains. The mobility of the chains in the core also strongly depends on the glass transition temperature of the core-forming block. In this respect, micelles having glassy cores, such as polystyrene, are generally kinetically frozen, and show absent to very slow unimer exchange.[98,99] In addition to temperature, the exchange kinetic can be accelerated using several cosolvents and surfactants, which reduce the interfacial tension between the solvophobic group and the solvent. In parallel, the length and steric hindrance of the soluble block also plays a role, since the probability that unimers return to the core, instead of diffusing into the solution, is related to the time they need to diffuse through the micellar corona.[69,88,90,91]

1.3.4 Stimuli-responsive polymers

Stimuli-responsive polymers are polymers that undergo reversible or irreversible changes in their physico-chemical properties in response to external changes in environmental conditions.[100–102] Stimuli-responsive polymers have been coined differently such as intelligent, smart, stimuli or environmentally sensitive polymers.[100] Such polymers are widely found in living systems to sustain life and maintain biological functions. Indeed, proteins, polysaccharides and nucleic acids constitute typical stimuli-responsive biopolymers that change in their environment. In-

spired by Nature, synthetic polymer systems with very similar attributes have been developed towards tailored assemblies and interfaces with specific functions and structures (Figure 1.16).[103]

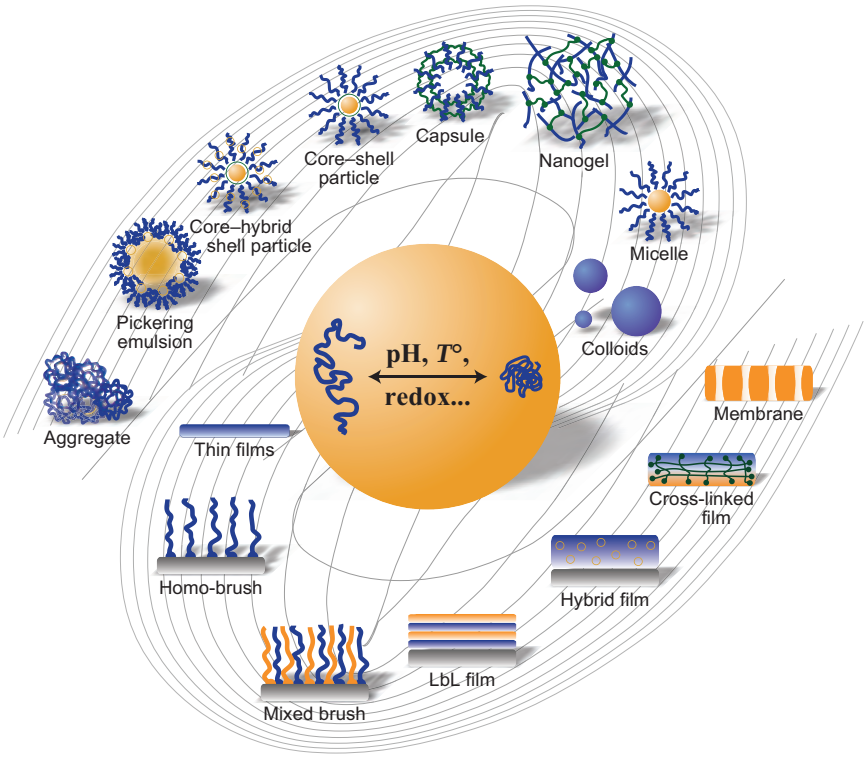

Figure 1.16 – "Galaxy" of nano-structured stimuli-responsive polymer materials.[103]

The basic operating principle of a stimuli-responsive polymer consists in the recognition of a stimulus as a signal, the evaluation of its magnitude, and finally a conformational and/or physico-chemical changes in direct response.[62,100,103] Indeed, stimuli-sensitive polymers generally incorporate functional groups that are amenable to a change in character, *e.g.*, charge, polarity and solvency. For example, water soluble thermo-responsive homopolymers have a repeating unit that contains both hydrophilic and hydrophobic moieties. As functional groups are multiplied along the polymer chain, the relative changes in chemical structure will be amplified synergistically, leading to dramatic transformations in conformational/physico-chemical properties.[104]

Many different stimuli have been employed to induce response in polymeric systems. These stimuli can be classified as physical, chemical or biological. Typical chemical stimuli are pH and redox changes, ionic strength variation and addition of specific analytes, external additives or any other chemical agents. The most common physical stimuli are temperature changes, light irradiation, electric, magnetic or acoustic field variations and mechanical force. More recently, biochemical stimuli have been recognized as a third category, which involves the responses to antigens, enzymes, ligands or other biochemical agents. Some systems combine two or more stimuli-responsive mechanisms in so-called multi-responsive polymers. For instance, temperature-sensitive polymers may also respond to pH changes. On the other hand, two or more signals could be simultaneously applied in order to induce response in one polymer systems.[62,100,101,105]

Smart polymers respond to stimuli in bulk, film, particle, solution or gel, and lead to modifications in surface characteristics, solubility, shape, formation of a molecular assembly, a sol-to-gel transition... Typically, the response of a polymer in solution is a change in its individual chain size, secondary structure, and/or solubility by changing the degree of intermolecular associations, *i.e.*, polymer–polymer and polymer–solvent (Figure 1.17). In most cases, the formation or destruction of secondary forces (hydrogen bonding, hydrophobic effects, electrostatic interactions, *etc.*), simple reactions (acid–base, redox, *etc.*) of moieties linked to the polymer backbone, and/or osmotic pressure differences are responsible for a coil-to-globule transition. Another type of response is due to dramatic alterations in the polymeric structure, such as degradation of polymers upon the application of a specific stimulus by bond breakage in the polymer backbone or at pendant cross-linking groups.[62,100,102,104]

The changes in physico-chemical properties of stimuli-responsive polymers enable the creation a large variety of smart devices with tailorable function and novel features, such as sensors, actuators and controlled release systems. Nowadays, recent advances in the design of stimuli-responsive polymers have created opportunities for broad applications in the area of materials science (Figure 1.16). Application of smart materials include but are not limited to responsive interfaces that are functionally similar to natural surfaces; controlled drug-delivery and release of therapeutics; coatings that are capable of interacting with and responding to their environment; engineered tissues that actuate and mimic the

action of muscles; and thin films and particles that are capable of sensing and/or separate very small concentrations of analytes. [101–103,106]

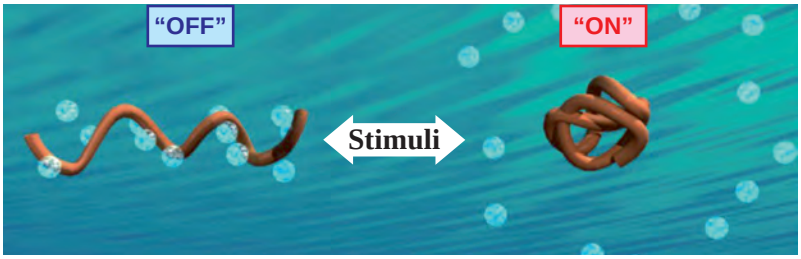

(a) Homopolymer in solution

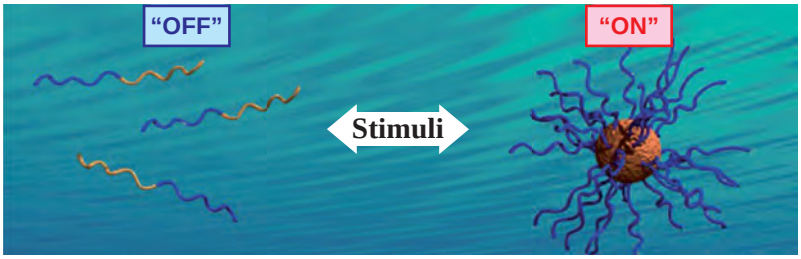

(b) Block copolymer in solution

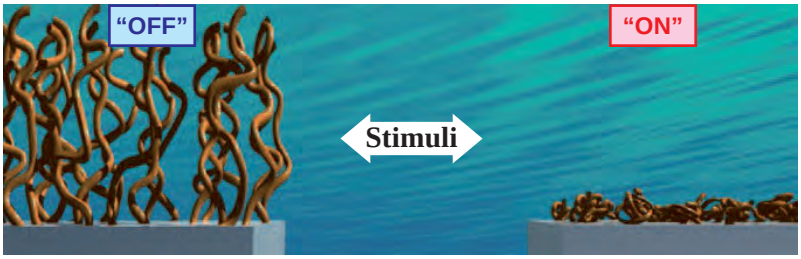

(c) Polymer brush in solution

Figure 1.17 – Schematic illustrations of stimuli-responsive phase transition behaviour of different polymer architectures in solution. [107]

1.4 Summary

Through this chapter, some fundamentals on polymer chemistry and physics were reminded. At first, the concept of macromolecules was

developed in terms of degree of polymerization, dipersity, monomer arrangement and chain topology, thereby highlighting the richness of structures that can be encountered in this field. Then, the different methods of living and controlled polymerizations were presented, with a particular attention on the reversible addition–fragmentation chain transfer process. Finally, the behaviour of polymer chains in solution was described, with emphasis on block copolymer self-assembly and stimuli-responsive polymer sequences.

Bibliography

[1] Painter, P. C. *Essentials of polymer science and engineering*, 1st ed.; DEStech Publications: Lancaster, 2008; pp xviii, 525.

[2] Gooch, J. W. *Encyclopedic dictionary of polymers*; Springer: New York, 2007; pp xxviii, 1237.

[3] Chanda, M. *Advanced polymer chemistry: A problem solving guide*; Marcel Dekker: New York, 2000; pp xiii, 852.

[4] Archer, R. D. *Inorganic and organometallic polymers*; Wiley: New York, 2001; p 264.

[5] Mark, J. E.; Allcock, H. R.; West, R. *Inorganic polymers*, 2nd ed.; Oxford University Press: Oxford, 2005; pp xiv, 338.

[6] Chanda, M. *Introduction to polymer science and chemistry: A problem solving approach*; CRC Press: Boca Raton, 2006; pp xviii, 640.

[7] Teraoka, I. *Polymer solutions: An introduction to physical properties*; Wiley: New York, 2002; pp xv, 338.

[8] Bueche, F. *Physical properties of polymers*; Wiley-Interscience: Huntington, 1962; pp x, 354.

[9] Cebe, P.; Hsiao, B. S.; Lohse, D. J. *Scattering from polymers: Characterization by X-rays, neutrons, and light*; ACS Symp. Ser.; American Chemical Society: Washington, 1999; pp xii, 558.

[10] Crompton, T. R. *Characterisation of polymers*; Smithers Rapra: Shawbury, 2008; p 2 v.

[11] Cheremisinoff, N. P. *Polymer characterization: Laboratory techniques and analysis*; Noyes Publications: Westwood, 1996; pp xi, 251.

[12] Bovey, F. A.; Mirau, P. A. *NMR of polymers*; Academic Press: San Diego, 1996; pp x, 459.

[13] Montaudo, G.; Lattimer, R. *Mass spectrometry of polymers*; CRC Press: Boca Raton, Fl., 2001; pp xi, 546.

[14] Matsuyama, S.; Nakahara, H.; Takeuchi, K.; Nagahata, R.; Kinugasa, S.; Teraoka, I. *Polym. J.* **2000**, *32*, 249–254.

[15] Uraneck, C.; Hsieh, H.; Buck, O. *J. Polym. Sci.* **1960**, *46*, 535–539.

[16] Tezuka, Y. *Prog. Polym. Sci.* **1992**, *17*, 471–514.

[17] Jerome, R.; Henrioulle-Granville, M.; Boutevin, B.; Robin, J. J. *Prog. Polym. Sci.* **1991**, *16*, 837–906.
[18] Rosen, S. L. *Fundamental principles of polymeric materials*, 2nd ed.; Wiley: New York ; Chichester, 1993; pp xvi, 420.
[19] Braun, D. *Polymer synthesis: Ttheory and practice. Fundamentals, methods, experiments*, 4th ed.; Springer: Berlin, 2005; pp xviii, 385.
[20] Semlyen, J. A. *Cyclic polymers*, 2nd ed.; Kluwer Academic: Dordrecht ; London, 2000; pp xx, 790.
[21] Davis, F.; Higson, S. *Macrocycles: Construction, chemistry and nanotechnology applications*; Wiley: Chichester, 2011; pp xii, 596.
[22] Roovers, J.; Charleux, B. *Branched polymers I*; Springer: Berlin ; London, 1999; pp viii, 242.
[23] Roovers, J.; Burchard, W. *Branched polymers II*; Springer: Berlin ; London, 1999; pp viii, 271.
[24] Meyer, T.; Keurentjes, J. *Handbook of polymer reaction engineering*; Wiley-VCH: Weinheim, 2005; pp xxxv, 1102.
[25] Riande, E. *Polymer viscoelasticity: Stress and strain in practice*; Marcel Dekker: New York, 2000; pp xv, 879.
[26] Frechet, J. M. J.; Tomalia, D. A. *Dendrimers and other dendritic polymers*; Wiley: Chichester, 2001; pp xxxix, 647.
[27] Porter, M. In *Organic Chemistry of Sulfur*; Oae, S., Ed.; Springer, 1977; Chapter 3, pp 71–118.
[28] Sperling, L. H. *Introduction to physical polymer science*, 4th ed.; Wiley: New York, 2006; pp xxx, 845.
[29] Hiemenz, P. C. *Polymer chemistry: The basic concepts*; M. Dekker: New York, 1984; pp xi, 722.
[30] Hamley, I. W. *Developments in block copolymer science and technology*; Wiley: Chichester, 2004; pp ix, 367.
[31] Hadjichristidis, N.; Pispas, S.; Floudas, G. *Block copolymers: Synthetic strategies, physical properties, and applications*; Wiley: New York, 2003; pp xx, 440.
[32] Odian, G. *Principles of polymerization*, 4th ed.; Wiley: Hoboken, 2004; pp xxi, 812.
[33] Rogers, M. E.; Long, T. E. *Synthetic methods in step-growth polymers*; Wiley-Interscience: Hoboken, 2003; pp xi, 605.
[34] Davis, F. J. *Polymer chemistry: A practical approach*; Oxford University Press: Oxford, 2004; pp xviii, 248.
[35] Mishra, M. K.; Yagci, Y.; Mishra, M. K. H. o. r. v. p. *Handbook of vinyl polymers: Radical polymerization, process, and technology*, 2nd ed.; CRC: New York, 2009; p 763.
[36] Dubois, P.; Coulembier, O.; Raquez, J.-M. *Handbook of ring-opening polymerization*; Wiley-VCH: Weinheim, 2009; pp xviii, 408.
[37] Matyjaszewski, K.; Davis, T. P. *Handbook of radical polymerization*; Wiley-Interscience: Hoboken, 2002; pp xii, 920.

[38] Buback, M.; Herk, A. v. *Radical polymerization: Kinetics and mechanism*; Wiley-VCH: Weinheim, 2007; pp x, 258.
[39] Muller, A. H. E.; Matyjaszewski, K. *Controlled and living polymerizations: Methods and materials*; Wiley-VCH: Weinheim, 2009; pp xxi, 612.
[40] Szwarc, M. *Living polymers and mechanisms of anionic polymerization*; Adv. Polym. Sci.; Springer-Verlag: Berlin, 1983; Vol. 49; p 187.
[41] Young, R.; Quirk, R.; Fetters, L.; Luston, J.; Vass, F. *Anionic Polymerization*; Adv. Polym. Sci.; Springer: Berlin Heidelberg, 1984; Vol. 56; p 133.
[42] Baskaran, D.; Muller, A. H. E. *Prog. Polym. Sci.* **2007**, *32*, 173–219.
[43] Bielawski, C. W.; Grubbs, R. H. *Prog. Polym. Sci.* **2007**, *32*, 1–29.
[44] Matyjaszewski, K. *Cationic polymerizations: Mechanisms, synthesis, and applications*; Dekker: New York, 1996; pp x, 768.
[45] Ivin, K. J.; Mol, J. C. *Olefin metathesis and metathesis polymerization*; Academic: London, 1997; pp xvi, 472.
[46] Kuran, W. *Principles of coordination polymerisation: Heterogeneous and homogeneous catalysis in polymer chemistry - Polymerisation of hydrocarbon, heterocyclic, and heterounsaturated monomers*; Wiley: Chichester, 2001; pp xxi, 522.
[47] Leibfarth, F. A.; Lohmeijer, B. G. G.; Nederberg, F.; Pratt, R. C.; Logan, J. W.; Waymouth, R. M.; Hedrick, J. L. *Abstr. Pap. Am. Chem. Soc.* **2007**, *233*, –.
[48] Szwarc, M.; Levy, M.; Milkovich, R. *J. Am. Chem. Soc.* **1956**, *78*, 2656–2657.
[49] Hawker, C. J.; Bosman, A. W.; Harth, E. *Chem. Rev.* **2001**, *101*, 3661–3688.
[50] Matyjaszewski, K. *Controlled/living radical polymerization: Progress in ATRP*; ACS Symp. Ser.; American Chemical Society: Washington DC, 2009; pp xii, 423.
[51] Matyjaszewski, K.; Xia, J. H. *Chem. Rev.* **2001**, *101*, 2921–2990.
[52] Barner-Kowollik, C. *Handbook of RAFT polymerization*; Wiley-VCH: Weinheim, 2008; pp xi, 543.
[53] Perrier, S.; Takolpuckdee, P. *J. Polym. Sci., Part A: Polym. Chem.* **2005**, *43*, 5347–5393.
[54] Keddie, D. J. *Chem. Soc. Rev.* **2014**, *43*, 496–505.
[55] Strobl, G. R. *The physics of polymers: Concepts for understanding their structures and behavior*, 3rd ed.; Springer: Berlin, 2007; pp xiii, 518.
[56] Des Cloizeaux, J.; Jannink, G. *Polymers in solution: Their modelling and structure*; Oxford science publications; Clarendon Press: Oxford ; New York, 2010; pp xlvi, 896.
[57] Flory, P. J. *J. Chem. Phys.* **1942**, *10*, 51–61.
[58] Flory, P. *Principles of polymer chemistry*; Cornell University Press: New York, 1953; pp xvi, 672.
[59] Roy, D.; Brooks, W. L. A.; Sumerlin, B. S. *Chem. Soc. Rev.* **2013**, *42*,

7214–7243.
[60] Wohlfarth, C. In *Polymer Solutions*; Lechner, M. D., Arndt, K. F., Eds.; Landolt-Börnstein - Group VIII Advanced Materials and Technologies; Springer Berlin Heidelberg, 2009; Vol. 6D1; Chapter 609, pp 3041–3045.
[61] Jones, R. G.; Ober, C. K.; Hodge, P.; Kratochvíl, P.; Moad, G.; Vert, M. *Pure Appl. Chem.* **2012**, *85*, 463–492.
[62] Lazzari, M.; Liu, G.; Lecommandoux, S. *Block copolymers in nanoscience*; Wiley-VCH: Weinheim, 2006; pp xix, 428.
[63] Abetz, V. *Block copolymers. Vol. 1*; Springer: Berlin ; London, 2005; pp x, 238.
[64] Abetz, V. *Block copolymers. Vol. 2*; Springer: Berlin ; London, 2005; pp x, 249.
[65] Forster, S.; Plantenberg, T. *Angew. Chem. Int. Ed.* **2002**, *41*, 689–714.
[66] Rodriguez-Hernandez, J.; Checot, F.; Gnanou, Y.; Lecommandoux, S. *Prog. Polym. Sci.* **2005**, *30*, 691–724.
[67] Mai, Y.; Eisenberg, A. *Chem. Soc. Rev.* **2012**, *41*, 5969–5985.
[68] Riess, G. *Prog. Polym. Sci.* **2003**, *28*, 1107–1170.
[69] Alexandridis, P.; Lindman, B. *Amphiphilic block copolymers: Self-assembly and applications*; Elsevier: Amsterdam ; Oxford, 2000; pp xii, 435.
[70] Harada, A.; Kataoka, K. *Prog. Polym. Sci.* **2006**, *31*, 949–982.
[71] Ottenbrite, R. M.; Kim, S. W. *Polymeric drugs and drug delivery systems*; Technomic: Lancaster, 2001; pp xiv, 313.
[72] Chilkoti, A.; Dreher, M. R.; Meyer, D. E.; Raucher, D. *Adv. Drug Delivery Rev.* **2002**, *54*, 613–630.
[73] Kataoka, K.; Harada, A.; Nagasaki, Y. *Adv. Drug Delivery Rev.* **2001**, *47*, 113–131.
[74] Lee, Y. S. *Self-assembly and nanotechnology: A force balance approach*; Wiley-Blackwell: Oxford, 2008; pp xvi, 344.
[75] Patterson, J. P.; Robin, M. P.; Chassenieux, C.; Colombani, O.; O'Reilly, R. K. *Chem. Soc. Rev.* **2014**, *43*, 2412–2425.
[76] Holmberg, K. *Surfactants and polymers in aqueous solution*, 2nd ed.; Wiley: New York ; Chichester, 2002; pp xvi, 545.
[77] Blanazs, A.; Armes, S. P.; Ryan, A. J. *Macromol. Rapid Commun.* **2009**, *30*, 267–277.
[78] Letchford, K.; Burt, H. *Eur. J. Pharm. Biopharm.* **2007**, *65*, 259–269.
[79] Smart, T.; Lomas, H.; Massignani, M.; Flores-Merino, M. V.; Perez, L. R.; Battaglia, G. *Nano Today* **2008**, *3*, 38–46.
[80] Giacomelli, C.; Schmidt, V.; Aissou, K.; Borsali, R. *Langmuir* **2010**, *26*, 15734–15744.
[81] Forster, S.; Berton, B.; Hentze, H. P.; Kramer, E.; Antonietti, M.; Lindner, P. *Macromolecules* **2001**, *34*, 4610–4623.
[82] Discher, D. E.; Eisenberg, A. *Science* **2002**, *297*, 967–973.
[83] Dan, N.; Shimoni, K.; Pata, V.; Danino, D. *Langmuir* **2006**, *22*, 9860–

9865.
[84] Aswal, V. K.; Wagh, A. G.; Kammel, M. *J. Phys.: Condens. Matter* **2007**, *19*, 1–9.
[85] Cameron, N. S.; Corbierre, M. K.; Eisenberg, A. *Can. J. Chem.* **1999**, *77*, 1311–1326.
[86] Hlavata, D.; Stejskal, J.; Plestil, J.; Konak, C.; Kratochvil, P.; Helmstedt, M.; Mio, H.; Laggner, P. *Polymer* **1996**, *37*, 799–805.
[87] Stejskal, J.; Hlavata, D.; Sikora, A.; Konak, C.; Plestil, J.; Kratochvil, P. *Polymer* **1992**, *33*, 3675–3685.
[88] Denkova, A.; Mendes, E.; Coppens, M. *Soft Matter* **2010**, *6*, 2351–2357.
[89] Van Stam, J.; Creutz, S.; De Schryver, F.; Jérôme, R. *Macromolecules* **2000**, *33*, 6388–6395.
[90] Lund, R.; Willner, L.; Richter, D.; Dormidontova, E. E. *Macromolecules* **2006**, *39*, 4566–4575.
[91] Nicolai, T.; Colombani, O.; Chassenieux, C. *Soft Matter* **2010**, *6*, 3111–3118.
[92] Aniansson, E.; Wall, S. N. *J. Phys. Chem.* **1974**, *78*, 1024–1030.
[93] Aniansson, E. G.; Wall, S. *J. Phys. Chem.* **1975**, *79*, 857–858.
[94] Aniansson, E.; Wall, S.; Almgren, M.; Hoffmann, H.; Kielmann, I.; Ulbricht, W.; Zana, R.; Lang, J.; Tondre, C. *J. Phys. Chem.* **1976**, *80*, 905–922.
[95] Rharbi, Y.; Winnik, M. A. *J. Phys. Chem. B* **2003**, *107*, 1491–1501.
[96] Faetibold, E.; Waton, G. *Langmuir* **1995**, *11*, 1972–1979.
[97] Creutz, S.; van Stam, J.; Antoun, S.; De Schryver, F. C.; Jerome, R. *Macromolecules* **1997**, *30*, 4078–4083.
[98] Wang, Y.; Balaji, R.; Quirk, R. P.; Mattice, W. L. *Polym. Bull.* **1992**, *28*, 333–338.
[99] Wang, Y.; Kausch, C.; Chun, M.; Quirk, R.; Mattice, W. *Macromolecules* **1995**, *28*, 904–911.
[100] Gil, E.; Hudson, S. *Prog. Polym. Sci.* **2004**, *29*, 1173–1222.
[101] Hu, J.; Liu, S. *Macromolecules* **2010**, *43*, 8315–8330.
[102] Jeong, B.; Gutowska, A. *Trends Biotechnol.* **2002**, *20*, 360–360.
[103] Stuart, M. A. C.; Huck, W. T.; Genzer, J.; Muller, M.; Ober, C.; Stamm, M.; Sukhorukov, G. B.; Szleifer, I.; Tsukruk, V. V.; Urban, M. *Nat. Mater.* **2010**, *9*, 101–113.
[104] Cabane, E.; Zhang, X.; Langowska, K.; Palivan, C. G.; Meier, W. *Biointerphases* **2012**, *7*, 1–27.
[105] Jochum, F. D.; Theato, P. *Chem. Soc. Rev.* **2013**, *42*, 7468–7483.
[106] Dai, L. *Intelligent macromolecules for smart devices*; Engineering materials and processes; Springer: New York, 2003; pp xvi, 496.
[107] Ebara, M. *Smart biomaterials*; Springer: Tokyo, 2014; pp x, 373.

CHAPTER 2

SUPRAMOLECULAR ASSEMBLY: TOWARD SELF-ASSEMBLED MATERIALS

Abstract

Inspired by Nature, supramolecular design emerged as an unprecedented tool toward functional and adaptive architectures. This chemistry is based on the non-covalent association of chemical entities, using weak interactions as molecular glue. The latter include but are not limited to ionic interactions, H-bonds, metal–ligand coordination, and π-stacking. In turn, these interactions have been explored in the development of materials showing stimuli-responsiveness, improved processing, and self-healing abilities. In this context, supramolecular polymers have attracted considerable attention since they exhibit distinct advantages over covalent counterparts.

2.1 Definitions and concepts

Introduced by the Nobel Prize J.-M. Lehn,[1,2] supramolecular chemistry, defined as "chemistry of inter-molecular bonds and molecular assemblies"[2] or more colloquially as "chemistry beyond the molecule",[3,4] has been established as a major field in chemical sciences.[5–8] Lying beyond the classical molecular chemistry, supramolecular chemistry relies on inter-molecular interactions, *i.e.*, non-covalent associations of chemical entities.[1–4,9,10] Since those secondary interactions are usually weaker than primary covalent bonds, they are dynamically more flexible and kinetically more labile,[11,12] which generates a binding equilibrium between molecular species and confers adaptive properties to the supramolecular assembly.[13,14]

Other definitions include concepts such as "the chemistry of non-covalent bonds" and "non-molecular chemistry".[8] Originally supramolecular chemistry was defined in terms of the non-covalent interaction between a "host" and a "guest" molecule.[8] Hence, other terms like "inclusion phenomena", "host–guest chemistry" or "molecular recognition" are used interchangeably with supramolecular chemistry.[15] It can also be described as "Lego® chemistry" in which each brick represents a molecular building block that are held together by intermolecular interactions, of a reversible nature, to form a supramolecular aggregate.[16] These intermolecular bonds include electrostatic interactions,[17,18] hydrogen bonding,[19–21] π-π stacking,[22] metal–ligand coordination,[23–27] and solvophobic effects.[28–32]

Supramolecular chemistry can be split into two broad categories; host–guest chemistry and self-assembly. The difference between these two areas is a matter of shape and size. If one molecule is significantly larger than another and can wrap around the latter, it is termed the *host* and the smaller substrate is its *guest*, which becomes enveloped by the host (Figure 2.1 (a)). Precisely, the host component is defined as an organic molecule or ion whose binding sites converge in the complex. On the other hand, the guest component is any molecule or ion whose binding sites diverge in the complex. A binding site is a region of the host or guest that is of the correct size, geometry and chemical nature to interact with the other species, and gives the selectivity of the interaction.[6,8,16,33,34]

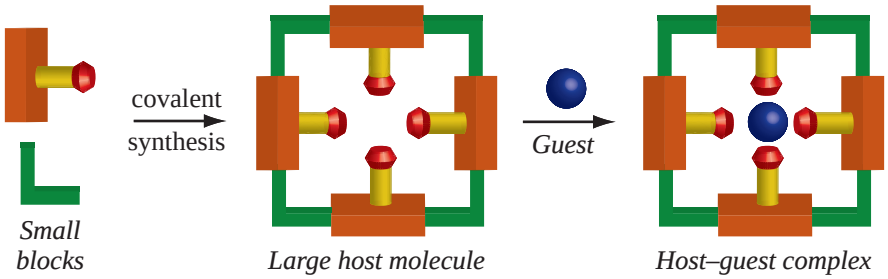

(a) Host–guest complexes

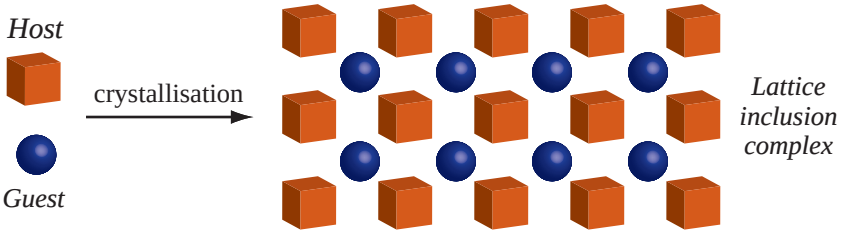

(b) Lattice inclusion compound

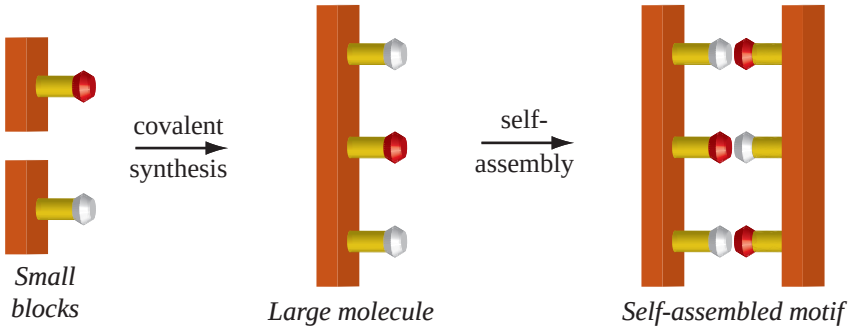

(c) Self-complementary assembly

Figure 2.1 – Construction of supramolecular systems from molecular building blocks.[16]

Host–guest complexes include biological systems, such as enzymes and their substrates, with enzymes being the host and substrates being the guest. In coordination chemistry, metal–ligand complexes can be seen as host–guest species, where large ligands can act as hosts for smaller metal cations. When possessing a permanent cavity that contains specific binding sites, such ligands act as a host both in solution and in the solid state. On the other hand, the class of solid state inclusion

complexes only exhibits host–guest behaviour as crystalline solids. In this compounds, the guest is bound within a cavity that is formed as a result of a hole in the packing of the host lattice (Figure 2.1 (b)). [6,8,16,33,34]

Where there is no significant size difference and no species is acting as a host for another, the non-covalent joining of two or more molecules is termed self-assembly. Strictly speaking, self-assembly is a dynamic equilibrium between two or more molecular species to produce an aggregate whose structure depends only on the information contained within the chemical building blocks (Figure 2.1 (c)). In that case, the selectivity of the association process arises from the complementarity of self-assembling species in term of position and number of binding sites. While occurring spontaneously, the self-assembly process may be influenced, in solution, by solvation or templation effects or, in the solid state, by nucleation and crystallisation. In nature, deoxyribonucleic acid (DNA) constitutes the most inspiriting biological structure, made up from the self-assembly of two strands via hydrogen bonds and aromatic stacking interactions to form the famous double helical structure. [6,8,16,33,34]

2.2 Binding equilibrium

The binding of a guest by a host species, or the association of two or more species by non-covalent bonds, is an equilibrium process (equation 2.1). The thermodynamic stability of a host–guest complex under specific conditions, *i.e.*, solvent and temperature, is gauged by the binding constant, K. The latter is also known by the terms formation constant, association constant, or stability constant as it provides a quantitative representation of the degree of association between species. [8,15,16]

$$\mathrm{Host} + \mathrm{Guest} \underset{k_{dissociation}}{\overset{k_{association}}{\rightleftharpoons}} \mathrm{Host{-}Guest} \tag{2.1}$$

Binding constants are expressed as the ratio between complex association and dissociation rate, which can be related to the concentrations of each species at thermodynamic equilibrium through the relationship:

$$K = \frac{k_{association}}{k_{dissociation}} = \frac{[\mathrm{host{-}guest}]}{[\mathrm{host}] \cdot [\mathrm{guest}]} \tag{2.2}$$

Frequently, host–guest complexes do not form exclusively in a straightforward 1:1 ratio. In such cases, there is more than one binding constant as subsequent guests bind to the host or inversely. Multiple equilibria of this type are described by stepwise binding constants for each guest as it binds, and an overall binding constant for the final complex which is termed beta, β.[8,16] For a 2:1 host–guest complex:

$$\mathrm{G} + \mathrm{H} \underset{k_{-1}}{\overset{k_1}{\rightleftharpoons}} \mathrm{HG} \text{ , with } K_1 = \frac{k_1}{k_{-1}} = \frac{[\mathrm{HG}]}{[\mathrm{G}] \cdot [\mathrm{H}]} \tag{2.3}$$

$$\mathrm{HG} + \mathrm{H} \underset{k_{-2}}{\overset{k_2}{\rightleftharpoons}} \mathrm{H_2G} \text{ , with } K_2 = \frac{k_2}{k_{-2}} = \frac{[\mathrm{H_2G}]}{[\mathrm{HG}] \cdot [\mathrm{H}]} \tag{2.4}$$

$$\mathrm{G} + 2\mathrm{H} \underset{k_{-2}}{\overset{k_2}{\rightleftharpoons}} \mathrm{H_2G} \text{ , with } \beta = K_1 \cdot K_2 = \frac{[\mathrm{H_2G}]}{[\mathrm{G}] \cdot [\mathrm{H}]^2} \tag{2.5}$$

In value, binding constants can range from near zero (no affinity) to very large (perfect affinity), which can be assessed theoretically. In real systems, the equilibrium is however subjected to environmental influences like, *e.g.*, competing interactions from other potential guests and the surrounding (solvation, ion pairing, crystal lattice, *etc.*). In particular, solvent molecules greatly outnumber the amount of host and guest, therefore having a pronounced effect upon the association dynamics and energetics. Indeed, many interactions with solvent molecules must be broken in order for binding to occur, which has both enthalpic and entropic consequences on the equilibrium.[8,16]

Practically, binding constants are thus calculated from experimental data that provide information about the position of the equilibrium under specific conditions. In this regard, potentiometric or nuclear magnetic resonance (NMR) monitored titrations, and ultraviolet–visible (UV-Vis) or fluorescence spectroscopy constitute the most common techniques in the determination of binding constants.[15,35] In parallel, the relative binding strength of host–guest complexes can also be addressed by more exotic techniques, *e.g.*, using variable laser intensities in matrix-assisted laser desorption/ionization mass spectrometry.[35,36] Behind, measurement of the binding strength of host–guest interaction at the single-molecule level remains a daunting challenge.[37–39]

2.3 Supramolecular interactions

Non-covalent bindings represent the energies that hold supramolecular species together. Concretely, the term "non-covalent" encompasses a wide range of attractions and repulsions that are summarised in Figure 2.2. They are labile in essence and hence individually weak compared to covalent interactions, which can range between *ca.* 150 to 450 kJ/mol for single bonds. On the other side, non-covalent interactions range from

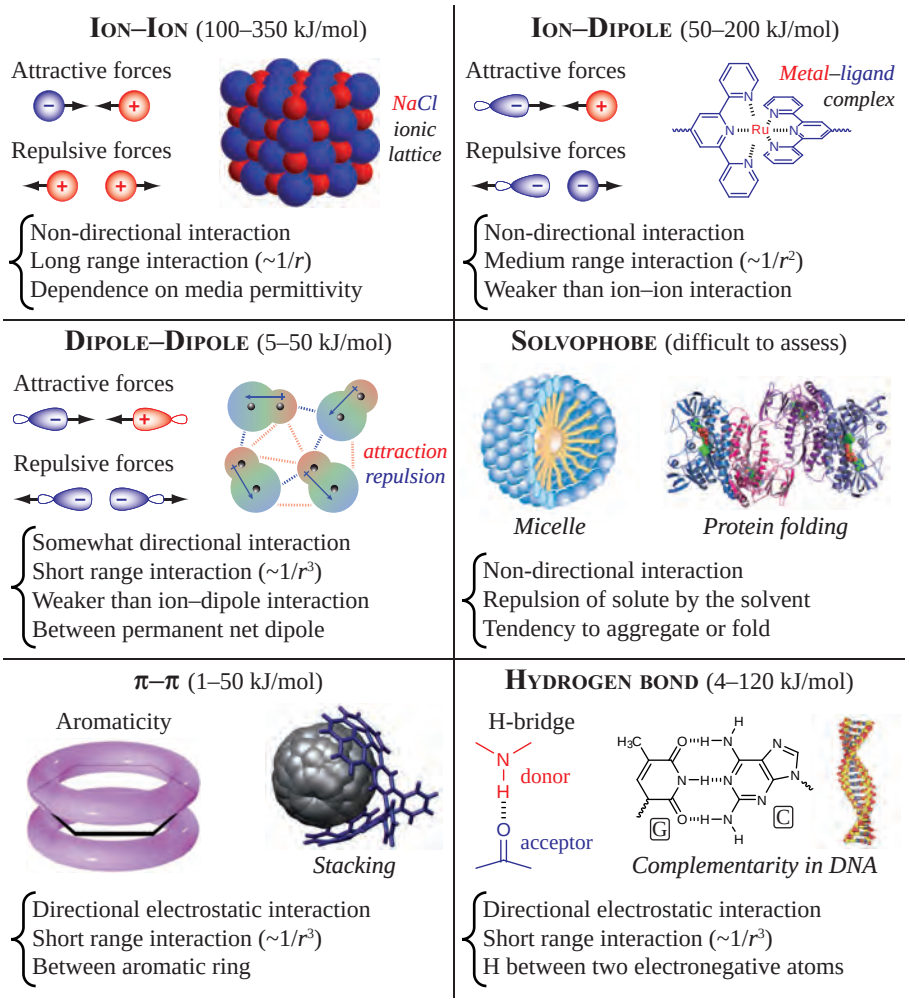

Figure 2.2 – Illustration showing non-covalent interactions commonly involved in supramolecular chemistry and their strength. [40]

very weak, *ca.* only a few kJ/mol for van der Waals force, to 350 kJ/mol for strong ion–ion interactions. However, when these interactions are used collectively in sufficient number, they can generate highly stable assemblies, their interplay governing the shape and function of the final assembly.[16,40]

2.3.1 Electrostatic interactions

Ionic and polar bonds can be split into three main categories that are ion–ion, ion–dipole, and dipole–dipole interactions. All are based on the electrostatic attraction and repulsion between respectively opposite and like charges. These charges may be inherent to species (ions), or virtually born from their electronic distribution (dipole, quadrupole, *etc.*).[16] The strength of these interactions follows Coulomb's law, decreasing with the distance between the charges. The strength of the electrostatic force is however directly proportional to the magnitudes of charges. Hence, binding energies decrease with the involvement of a dipole, quadrupole (...) as interactional partner. Consequently, only ionic bonding is comparable in strength to covalent bonding (100 to 350 kJ/mol). In turn, ion–dipole interactions are stronger than dipole–dipole associations (50–200 and 5–50 kJ/mol, respectively) as ions have a higher charge density than dipoles.[8]

Ion–ion interactions are non-directional in nature, meaning that the interaction can occur in any orientation. They can nevertheless result in highly directional self-assembled structures like crystal for example, showing uniform structure due to the periodicity of the assembly (Figure 2.3 (a)). Ion–dipole and dipole–dipole interactions, however, have orientation-dependant aspects requiring two or more entities to be arranged such that the interactions occur in the optimal direction. Due to the relative rigidity of directional interactions, only mutually complementary species are able to form supramolecular aggregates, whereas non-directional bonds can stabilise a wide range of molecular pairings. Despite providing the weakest association, dipole–dipole interactions are thus useful for bringing species into alignment, as it requires specific orientation of interacting entities. This type of interactions is also encountered in a certain number of solvent like, *e.g.*, acetone (Figure 2.3 (c)).[8,16]

The binding of an ion with a polar molecule, such as water, is an

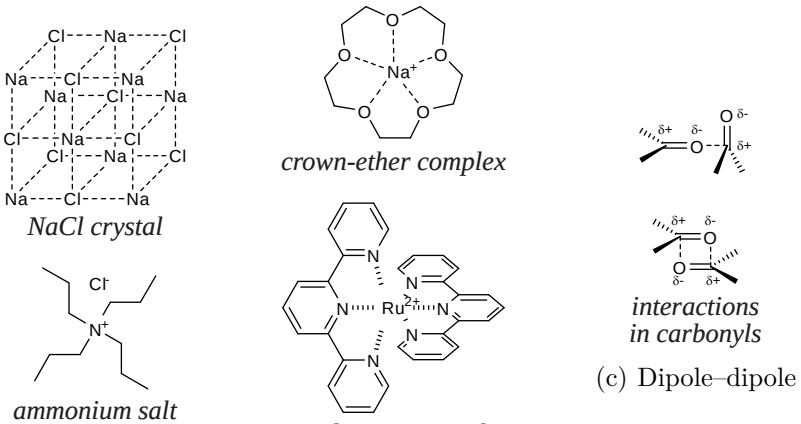

(a) Ion–ion (b) Ion–dipole (c) Dipole–dipole

Figure 2.3 – Examples of electrostatic interactions.

example of ion–dipole interaction, which can be observed in both solid state and solution. A supramolecular analogue is found in the structure of alkali cations complexes with macrocyclic ethers, known as crown ethers (Figure 2.3 (b)). Finally, ion–dipole interactions also include dipolar interactions, also known as dative or coordination bonds, where both electrons in the bond originate from the same atoms.[8,16] Such interactions are mostly electrostatic in nature in the case of the interactions of low-polarisable metal cations and hard bases. Nevertheless, other coordination bonds often used in self-assembly may show a significant covalent component, which blurs the distinction between molecular and supramolecular species.[41]

2.3.2 Hydrogen bonding

Because of its strength and highly directional nature, the hydrogen bond is arguably the most important non-covalent interaction. It represents a special kind of dipole–dipole interaction between a proton donor (D) and a proton acceptor (A). Donors are groups with a hydrogen atom attached to an electronegative atom, usually nitrogen or oxygen, therefore forming a dipole with the hydrogen atom carrying a small positive charge. Acceptors are dipoles with electron-withdrawing atoms by which the positively charged hydrogen atom can interact, for example,

carbonyl moieties.[16,19,42]

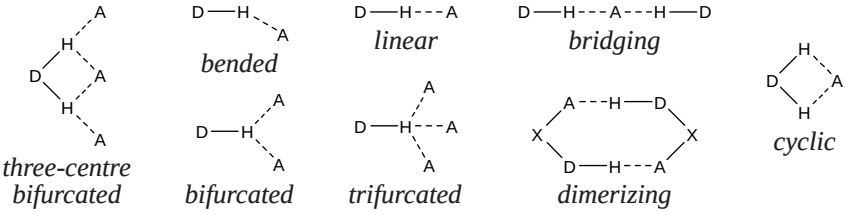

Figure 2.4 – Common arrangements of hydrogen bond types.[42]

The strength, length and nature of hydrogen bonds vary between systems and are correlated with the electronegativity of the atom to which the hydrogen is attached, along with the H-bond geometry (Figure 2.4). In this respect, the interaction can be divided into three broad categories that are summarized in Table 2.1. A strong interaction, like in HF_2^- ion, is somewhat similar in character to a covalent bond, whereby the hydrogen atom adopts a central position between donor and acceptor atoms. Moderate-strength H bonds are formed between neutral donor and acceptor via electron lone pairs, like in the dimerization of carboxylic acids. As a characteristic, moderate interactions do not have a linear geometry but are rather slightly bent. Weak hydrogen bonds are even less linear and in some cases can form perpendicular interactions, which are encountered for certain interactions between benzene rings. As a general rule, the strength of hydrogen interactions classically ranges from 4 to 120 kJ/mol, with the vast majority being under 60 kJ/mol, which depends on proton acidity.[8,16,42]

Table 2.1 – Hydrogen bond interactions and their properties.[8,16]

Properties \ Interactions	Strong	Moderate	Weak
Bond character D—H$\cdots$A	mainly covalent	mainly electrostatic	purely electrostatic
Bond energy [kJ/mol]	60 – 120	15 – 60	< 15
H$\cdots$A bond length [Å]	1.2 – 1.5	1.5 – 2.2	2.2 – 3.2
D—A bond length [Å]	2.2 – 2.5	2.5 – 3.2	3.2 – 4.0
Bond angle [°]	175 – 180	130 – 180	90 – 150

In daily life, hydrogen bonds ensure the cohesion in major biological building blocks whose best example is that of DNA double helix. Hydrogen bonds also explain the particular cohesion of certain liquid, like water, which allows the development of life on Earth. In addition, the high degree of directionality of hydrogen bonding interactions, together with the rich source (amino acids, carbohydrates and nucleobases) and specific alignment of hydrogen bond donors and acceptors, have proved to be a fruitful asset for the design of supramolecular systems.[16,42]

2.3.3 Pi stacking

Pi-stacking refers to interactions implying π-systems, *i.e.*, that possess electrons involved in covalent chemical bond formed by lateral overlap between atomic orbitals. Such interactions are commonly observed in crystal structures of aromatic molecules or in the layered structure of graphite. Those aromatic systems can be regarded as a positively charged framework of σ-bonds, *i.e.*, resulting from the front overlap of orbitals, sandwiched between two negatively charged π-electron clouds (Figure 2.5). In Nature, stacking plays a role in stabilising the recombinant tobacco mosaic virus rod scaffold and the DNA double helix shape through vertical base-pair interactions, being thus further involved in the intercalation of drugs.[8,16,42]

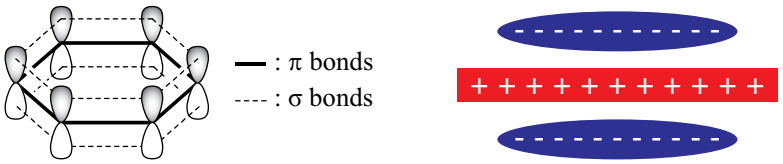

(a) Orbital description (b) Polar description

Figure 2.5 – Different descriptions of aromatic rings.

In supramolecular systems, three main categories of π-interactions can be found namely anion–π, cation–π and π–π interactions. Even if the interaction of an anion with π-electron density should intuitively be repulsive, aromatic rings may show some affinity, especially for small halides (Figure 2.6 (a)). Indeed, the possibility for an electrostatic attraction always exists due to charge difference between anions and overall neutral aromatic rings.[8,43]

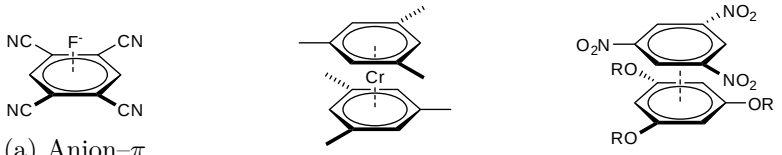

(a) Anion–π (b) Cation–π (c) π–π

Figure 2.6 – Examples of the three main categories of π interactions.

Cation–π interactions are common in the field of organometallic chemistry, whereby olefinic groups are bound to transition metal ions, like in metallocenes (Figure 2.6 (b)). In such complexes, the bonding is however relatively strong and can be regarded as covalent, since intimately related with the overlap of partially occupied orbitals of the metals. On the other hand, alkaline and alkaline earth cations form weaker interactions with unsaturated systems, typically the interaction of potassium cations with benzene, whose binding energy ranges between 5 and 80 kJ/mol.[8,16,42,43]

(a) Edge-to-face (b) Face-to-face

Figure 2.7 – Two main geometries for π–π interactions.

π–π interactions, sometimes called aromatic stacking, occur between aromatic rings, often in situations where one is relatively electron poor and the other is electron rich (Figure 2.6 (c)). Although a wide variety of intermediate geometries are known, two main types of π–π interaction are distinguished (Figure 2.7). In edge-to-face configuration, a hydrogen atom from one ring interacts in a perpendicular orientation with respect to the other ring centre. This configuration arises from the attraction between the π-electron cloud of one conjugated ring and the σ-framework of a neighbour, and is responsible for the packing in crystal structures of many small aromatic hydrocarbons. In face-to-face configuration, parallel ring-systems are generally offset due to repulsion between π-electron clouds, and the centre of one ring interacts with the corner of another. This configuration is encountered in graphite and also between electron-rich and electron-poor substituted aromatic rings,

namely arene–arene interaction.[8,16,42,43]

2.3.4 Solvophobic effects

Solvophobic effects arise from the exclusion of groups or molecules differing from the solvent in polarity. This phenomenon is typically obvious in the immiscibility of several liquids. In biological systems, hydrophobic effects play a crucial role in the formation of phospholipid bilayer cell walls and the maintenance of protein and polynucleotide structure.[40] Since solvent molecules preferentially interact with each other in those systems, the segregated situation is energetically more favourable than the hole created by the incompatible solute. In this respect, solvophobic effects can be split into two energetic components, namely an enthalpic solvophobic effect and an entropic solvophobic effect.[8,16]

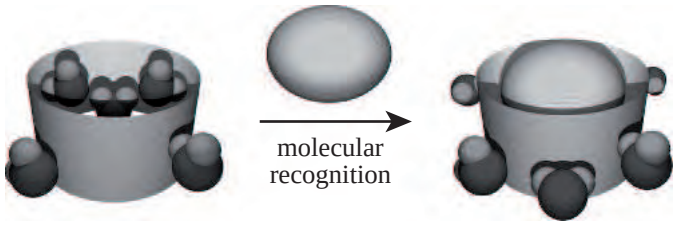

(a) Enthalpic solvophobic effect

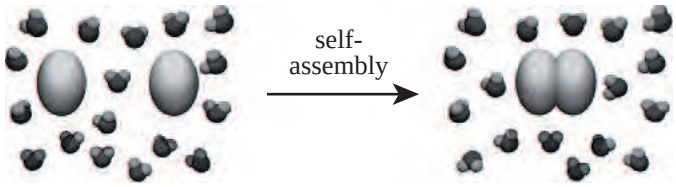

(b) Entropic solvophobic effect

Figure 2.8 – Energetic components of the solvophobic interactions.[16]

Enthalpic solvophobic interactions occur when a guest replaces solvent molecules within a solvophobic cavity (Figure 2.8 (a)). The energy in the system is high since the host does not interact strongly with the solvent molecules. When the latter are replaced by the guest, the system energy is lowered by the interaction of the guest with the host cavity. In addition, an entropic factor also contributes to this process since the

solvent molecules, initially ordered within the cavity, become disordered when leaving. [16,30]

Entropic solvophobic interactions appear when two or more solvophobic molecules combine to form a supramolecular complex, which creates a hole in the solvent. In turn, this results in less disruption (one hole in the solvent phase instead of multiple holes) and hence an entropic gain. Accordingly, the overall free energy of the system is lowered. [16,29,44] This effect is very important in biological systems in the creation and maintenance of the macromolecular structure and supramolecular assemblies of the living cell. Other examples are found in the formation of amphiphilic structures such as micelles, where amphiphiles assemble in spherical geometries, and lipid bilayers where the heads meet end-to-end. [28,32,44]

2.4 Supramolecular materials

Using small molecules as basic building blocks and the different non-covalent interactions as molecular glue, chemists are now exploring self-assembly and molecular recognition as alternatives to the classical methods of synthetic chemistry. Indeed, this new approach allows approaching complex structures having nanometer to millimeter dimensions that would otherwise be difficult, or impossible, to prepare by traditional techniques. In counterpart, supramolecular assemblies, be they static or dynamic, are encountered at all length scales in nature and technology. Commonly, self-assembly processes can be classified based on the size/nature of the building units, as with the level at which the self-assembly occurs (Figure 2.9). [45–47]

In nature, biological molecules such as polysaccharides or polypeptides may, under proper conditions, form supramolecular structures of great complexity via association of complementarity groups. Synthetic systems rely, for their part, on the ability of chemists to design molecules incorporating those complementary features. Obviously, direct control over self-assembled systems is not always possible, because it can rearrange to form the thermodynamically most stable supramolecular structure. Indeed, the bonds that combine the components are usually required to be stable but kinetically labile, so that the most favourable structure is formed quickly. However, it is possible to guide self-assembled

systems, taking rational strategic decisions so that the different constitutive elements of the system interact correctly with each other. [12,16]

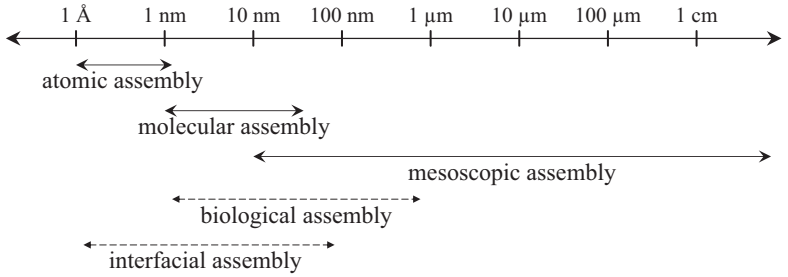

Figure 2.9 – Classification of self-assemblies based on their size and nature. [46]

The dynamics and thermo-mechanical reversibility of non-covalent interactions have been explored toward supramolecular materials with adaptive environment-dependent properties, improved processing, and intrinsic self-restructuring abilities (Figure 2.10). The responsiveness of such materials is derived from the possibility to impact the dynamic equilibrium inherent in the system with environmental stimuli like *e.g.*, temperature, chemical, pressure, light... [48] Dynamic and adaptive properties also enhance material processing by reducing potential manufacturing defects, which further extends their lifetime and promotes recycling. Under specific conditions, those supramolecular materials are ultimately able to restore their structural integrity and function after failure and damage, which defined self-healing attributes. [49–52]

Along with other significant developments in the field of supramolecular chemistry, supramolecular polymerizations were introduced as the assembly processes of step-growth supramolecular polymers, as distinction from the classical covalent polymerization leading to molecular polymers. [53–57] In these supramolecular assemblies, non-covalent interactions are part of the polymeric backbone, resulting in aggregates that often possess polymer-like properties. Assuming the absence of any kinetic traps, *e.g.*, crystallisation, main-chain supramolecular polymers exist as a dynamic equilibrium between monomeric, oligomeric, and polymeric species (Figure 2.11). In such dynamic systems, the formation of macrocycles and the presence of ring–chain or ring–ring equilibria constitute the other key consideration, impacting the size of polymeric aggregates

that can be obtained.[53,56,58]

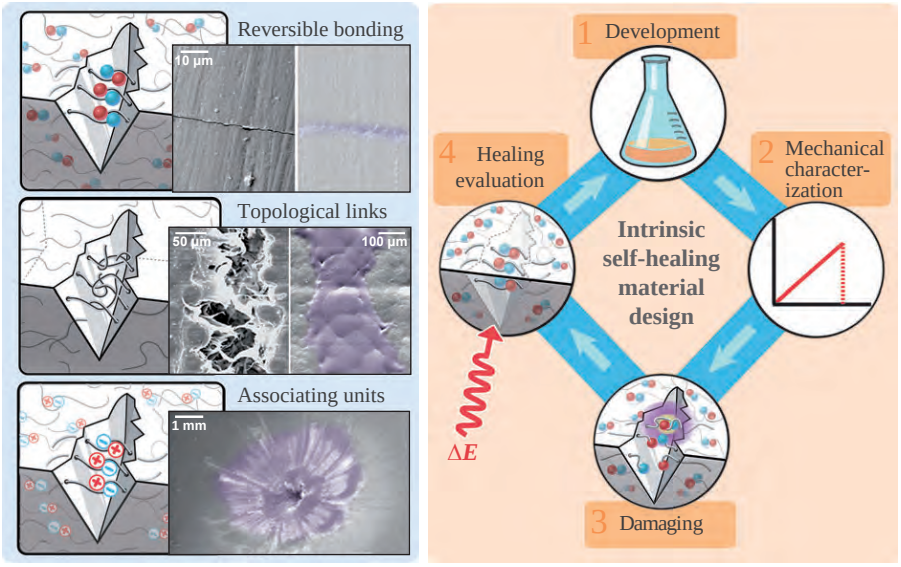

(a) Main schemes (b) Design strategy

Figure 2.10 – Achieving reparation and design strategy of intrinsic self-healing materials.[59]

For polymers that are formed by the reversible association of bifunctional monomers, the average degree of polymerization is determined by the strength of the end groups interaction and by the concentration in associating species.[60] Any environmental factor or stimulus that can influence the strength of the non-covalent association, and hence the binding between the (macro)monomer units, will shift the monomer/oligomer/polymer equilibrium, dramatically impacting the material properties. Being difficult to assess quantitatively, the distribution of macrocycles versus linear chains further depends on several factors including monomer shape, length and flexibility.[53,56,58]

In parallel to the development of synthetic routes toward complementary[20,61] and recognition motifs,[62,63] combining macromolecular and supramolecular chemistry has risen as a powerful approach toward polymeric architectures with adaptable and responsive properties.[48] Among them, supramolecular networks, where cross-linking is provided through ionic interaction,[64–68] π–π stacking,[69–73] hydrogen

bonding,[74–81] metal–ligand coordination,[82–90] solvophobic effect,[91–99] host–guest complexation,[100–110] or an orthogonal combination of those secondary interactions,[111–123] attracted specific attention[124,125]. Indeed, such networks reveal mechanical properties typical for rubbery materials but, unlike conventional rubber, they exhibit unprecedented self-healing abilities.[52,126–128]

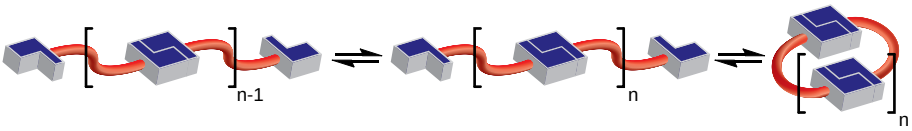

Figure 2.11 – Dynamic equilibrium in supramolecular polymers.

At the basis of supramolecular polymer networks, lie macromolecular building blocks that have been designed to carry functional groups. The latter can be of various nature and act as stickers, or "sticky points", for transient network formation, enabling connection and reconnection (Figure 2.12).[127,129] The strength and dynamics of sticky associations, *i.e.*, the time by which the supramolecular moieties dissociate and recombine, constitute relevant issues for their use in self-healing polymers. In addition, dynamics of individual polymer chains must be sufficient to enable a certain mobility of the supramolecular groups and hence heal damaged site. A characteristic feature of supramolecular polymer networks is thus that their dynamics is governed by at least two characteristic time scales: the one of formation and breakage of temporary inter-chain associations; the other for the relaxation of chains or chain segments as captured by classical polymer physics.[127,130]

According to the position of the associating units, two main classes of building block can be distinguished: main-chain functionalized polymers that incorporate associating groups in the polymer backbone (Figure 2.12 (d));[56,131] and side-chain functionalized polymers that bear pendant stickers along the main-chain (Figure 2.12 (b)).[132] In addition, telechelics constitute a particular subclass of main-chain polymers that possess functional groups located at each ends.[133–135]

Even if they constitute one of the most studied categories of polymers, telechelics are essentially used as precursors of higher linear assemblies, via head-to-tail associations. Indeed, a physical network can only be obtained from linear telechelics when the stoichiometry of the

end-association is higher than two, which mainly characterizes non-directional, *e.g.*, ionic [64] or solvophobic, [136] assemblies (Figure 2.12 (a)). Hence, telechelic star polymers have risen as promising precursors of supramolecular materials with potential model structure [88–90,137]. Indeed, they allow network formation with close to regular spacing of cross-linking, assuming that the different arms of the star are of comparable lengths (Figure 2.12 (c)). However, varying the functionality of such systems typically requires a control over the number of star branches, which can be synthetically challenging or restricted.

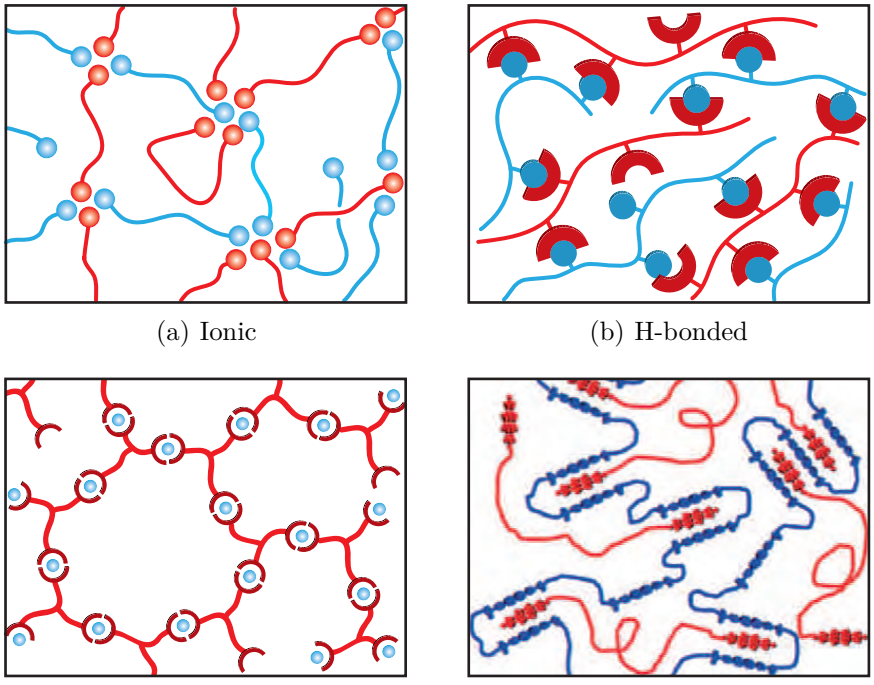

(a) Ionic (b) H-bonded

(c) Coordination (d) π-stacked

Figure 2.12 – Different types of supramolecular polymer networks.

2.5 Summary

To summarize, supramolecular chemistry was introduced with the concepts of self-assembly, molecular recognition, and host–guest associ-

ation. The main forces responsible for the supramolecular organization were reviewed that are electrostatic interactions, hydrogen bonding, π-stacking, and solvophobic effects. Then, the interest of developing materials using these dynamic reversible interactions was presented, highlighting the adaptive properties and self-healing abilities that may result from the supramolecular organization. In this respect, two main classes of macromolecular building block were distinguished that are the main-chain functionalized polymers, and side-chain functionalized polymers, with telechelics as a particular subclass.

Bibliography

[1] Lehn, J. M. *Struct. Bonding* **1973**, *16*, 1–69.
[2] Lehn, J. M. *Pure Appl. Chem.* **1978**, *50*, 871–892.
[3] Lehn, J. M. *Angew. Chem. Int. Ed.* **1988**, *27*, 89–112.
[4] Lehn, J. M. *Science* **1993**, *260*, 1762–1763.
[5] Lehn, J. M. *Chem. Soc. Rev.* **2007**, *36*, 151–160.
[6] Lehn, J. M. *Supramolecular chemistry: Concepts and perspectives*; VCH: Weinheim, 1995; pp x, 271.
[7] Dodziuk, H. *Introduction to supramolecular chemistry*; Kluwer Academic Publishers: Dordrecht, 2002; pp xii, 350.
[8] Steed, J. W.; Atwood, J. L. *Supramolecular chemistry*, 2nd ed.; Wiley: Oxford, 2009; pp xxvi, 970.
[9] Lehn, J. M. *Science* **1985**, *227*, 849–856.
[10] Lehn, J. M. *Science* **2002**, *295*, 2400–2403.
[11] Goshe, A.; Crowley, J.; Bosnich, B. *Helv. Chim. Acta* **2001**, *84*, 2971–2985.
[12] Goshe, A. J.; Steele, I. M.; Ceccarelli, C.; Rheingold, A. L.; Bosnich, B. *Proc. Natl. Acad. Sci. U. S. A.* **2002**, *99*, 4823–4829.
[13] Bohne, C. *Chem. Soc. Rev.* **2014**, *43*, 4037–4050.
[14] Li, W.; Kim, Y.; Li, J.; Lee, M. *Soft Matter* **2014**, *10*, 5231–5242.
[15] Cragg, P. J. *A practical guide to supramolecular chemistry*; Wiley: Chichester, 2005; pp x, 203.
[16] Steed, J. W.; Turner, D. R.; Wallace, K. J. *Core concepts in supramolecular chemistry and nanochemistry*; Wiley: Hoboken, N.J., 2007; pp xii, 307.
[17] Faul, C. F.; Antonietti, M. *Adv. Mater.* **2003**, *15*, 673–683.
[18] Grohn, F. *Macromol. Chem. Phys.* **2008**, *209*, 2295–2301.
[19] Mingos, D. M. P. *Supramolecular assembly via hydrogen bonds*; Springer: Berlin ; London, 2004; p 2 v.
[20] Baruah, P. K.; Khan, S. *RSC Advances* **2013**, *3*, 21202–21217.

[21] Davis, J. T.; Spada, G. P. *Chem. Soc. Rev.* **2007**, *36*, 296–313.
[22] Hoeben, F. J. M.; Jonkheijm, P.; Meijer, E. W.; Schenning, A. P. H. J. *Chem. Rev.* **2005**, *105*, 1491–1546.
[23] Lawrance, G. *Introduction to coordination chemistry*; Wiley: Chichester, 2009; pp xiii, 290.
[24] Lusby, P. J. *Annu. Rep. R. Soc. Chem. Sect. A: Inorg. Chem.* **2010**, *106*, 319–339.
[25] Costisor, O.; Linert, W. *Rev. Inorg. Chem.* **2003**, *23*, 289–338.
[26] Yan, Y.; Huang, J. B. *Coord. Chem. Rev.* **2010**, *254*, 1072–1080.
[27] Barman, S.; Garg, J. A.; Blacque, O.; Venkatesan, K.; Berke, H. *Chem. Commun.* **2012**, *48*, 11127–11129.
[28] Tanford, C. *The hydrophobic effect: Formation of micelles and biological membranes*; Wiley: New York, 1973; pp viii, 200.
[29] Chandler, D. *Nature* **2005**, *437*, 640–647.
[30] Biedermann, F.; Nau, W. M.; Schneider, H.-J. *Angew. Chem. Int. Ed.* **2014**, *53*, 11158–11171.
[31] Pratt, L. R.; Pohorille, A. *Chem. Rev.* **2002**, *102*, 2671–2691.
[32] Sorrenti, A.; Illa, O.; Ortuno, R. M. *Chem. Soc. Rev.* **2013**, *42*, 8200–8219.
[33] Ariga, K.; Kunitake, T. *Supramolecular chemistry - Fundamentals and applications*; Springer: Berlin, 2006; pp ix, 208.
[34] Gale, P. A. *Philos. Trans. R. Soc. London, A* **2000**, *358*, 431–453.
[35] Schalley, C. A. *Analytical methods in supramolecular chemistry*; Wiley-VCH: Weinheim, 2007; pp xvi, 484.
[36] Meier, M. A. R.; Lohmeijer, B. G. G.; Schubert, U. S. *J. Mass Spectrom.* **2003**, *38*, 510–516.
[37] Kudera, M.; Eschbaumer, C.; Gaub, H. E.; Schubert, U. S. *Adv. Funct. Mater.* **2003**, *13*, 615–620.
[38] Kersey, F.; Yount, W.; Craig, S. *J. Am. Chem. Soc.* **2006**, *128*, 3886–3887.
[39] Hao, X.; Zhu, N.; Gschneidtner, T.; Jonsson, E. .; Zhang, J.; Moth-Poulsen, K.; Wang, H.; Thygesen, K. S.; Jacobsen, K. W.; Ulstrup, J.; Chi, Q. *Nat. Commun.* **2013**, *4*.
[40] Mendes, A. C.; Baran, E. T.; Reis, R. L.; Azevedo, H. S. *Wiley Interdiscip. Rev. Nanomed. Nanobiotechnol.* **2013**, *5*, 582–612.
[41] Kurth, D. G. *Sci. Technol. Adv. Mat.* **2008**, *9*.
[42] Lindoy, L. F.; Atkinson, I. M. *Self-assembly in supramolecular systems*; Royal Society of Chemistry: Cambridge, 2000; pp ix, 224.
[43] Astruc, D. *Modern arene chemistry*; Wiley-VCH: Weinheim ; Cambridge, 2002; pp xviii, 617.
[44] Maibaum, L.; Aaron, R.; Chandler, D. *J. Phys. Chem. B* **2004**, *108*, 6778–6781.
[45] Whitesides, G. M.; Grzybowski, B. *Science* **2002**, *295*, 2418–2421.
[46] Lee, Y. S. *Self-assembly and nanotechnology: A force balance approach*;

Wiley-Blackwell: Oxford, 2008; pp xvi, 344.
[47] Reinhoudt, D. N. *Supramolecular materials and technologies*; Wiley: Chichester, 1999; pp viii, 309.
[48] Yan, X.; Wang, F.; Zheng, B.; Huang, F. *Chem. Soc. Rev.* **2012**, *41*, 6042–6065.
[49] Ghosh, S. K. *Self-healing materials: Fundamentals, design strategies, and applications*; Wiley-VCH: Weinheim, 2009; pp xiv, 291.
[50] Zwaag, S. v. d.; Schmets, A. J. M. *Self healing materials : An alternative approach to 20 centuries of materials science*; Springer: Dordrecht, 2007; pp xii, 385.
[51] Syrett, J.; Becer, C.; Haddleton, D. *Polym. Chem.* **2010**, *1*, 978–987.
[52] Yang, Y.; Urban, M. W. *Chem. Soc. Rev.* **2013**, *42*, 7446–7467.
[53] De Greef, T. F.; Smulders, M. M.; Wolffs, M.; Schenning, A. P.; Sijbesma, R. P.; Meijer, E. *Chem. Rev.* **2009**, *109*, 5687–5754.
[54] Ciferri, A. *Macromol. Rapid Commun.* **2002**, *23*, 511–529.
[55] Ciferri, A. *J. Macromol. Sci., Polym. Rev.* **2003**, *43*, 271–322.
[56] Fox, J. D.; Rowan, S. J. *Macromolecules* **2009**, *42*, 6823–6835.
[57] Kulkarni, C.; Balasubramanian, S.; George, S. J. *ChemPhysChem* **2013**, *14*, 661–673.
[58] Brunsveld, L.; Folmer, B. J. B.; Meijer, E. W.; Sijbesma, R. P. *Chem. Rev.* **2001**, *101*, 4071–4097.
[59] Blaiszik, B. J.; Kramer, S. L. B.; Olugebefola, S. C.; Moore, J. S.; Sottos, N. R.; White, S. R. *Annu. Rev. Mater. Res.* **2010**, *40*, 179–211.
[60] Xu, J.; Fogleman, E. A.; Craig, S. L. *Macromolecules* **2004**, *37*, 1863–1870.
[61] Schmuck, C.; Wienand, W. *Angew. Chem. Int. Ed.* **2001**, *40*, 4363–4369.
[62] Hu, J.; Liu, S. *Acc. Chem. Res.* **2014**, *47*, 2084–2095.
[63] Dong, S.; Zheng, B.; Wang, F.; Huang, F. *Acc. Chem. Res.* **2014**, *47*, 1982–1994.
[64] Hunt, J.; Feldman, K.; Lynd, N.; Deek, J.; Campos, L.; Spruell, J.; Hernandez, B.; Kramer, E.; Hawker, C. *Adv. Mater.* **2011**, *23*, 2327–2331.
[65] Lin, X.; Navailles, L.; Nallet, F.; Grinstaff, M. W. *Macromolecules* **2012**, *45*, 9500–9506.
[66] Berger, J.; Reist, M.; Mayer, J.; Felt, O.; Peppas, N.; Gurny, R. *Eur. J. Pharm. Biopharm.* **2004**, *57*, 19–34.
[67] Hayashi, M.; Noro, A.; Matsushita, Y. *J. Polym. Sci., Part B: Polym. Phys.* **2014**, *52*, 755–764.
[68] Wei, H.; Du, S.; Liu, Y.; Zhao, H.; Chen, C.; Li, Z.; Lin, J.; Zhang, Y.; Zhang, J.; Wan, X. *Chem. Commun.* **2014**, *50*, 1447–1450.
[69] Burattini, S.; Colquhoun, H. M.; Fox, J. D.; Friedmann, D.; Greenland, B. W.; Harris, P. J. F.; Hayes, W.; Mackay, M. E.; Rowan, S. J. *Chem. Commun.* **2009**, *45*, 6717–6719.
[70] Ajayaghosh, A.; Praveen, V. *Acc. Chem. Res.* **2007**, *40*, 644–656.

[71] Babu, S.; Praveen, V.; Prasanthkumar, S.; Ajayaghosh, A. *Chem. Eur. J.* **2008**, *14*, 9577–9584.
[72] Burattini, S.; Colquhoun, H.; Greenland, B.; Hayes, W. *Faraday Discuss.* **2009**, *143*, 251–264.
[73] Hart, L. R.; Hunter, J. H.; Nguyen, N. A.; Harries, J. L.; Greenland, B. W.; Mackay, M. E.; Colquhoun, H. M.; Hayes, W. *Polym. Chem.* **2014**, *5*, 3680–3688.
[74] Cordier, P.; Tournilhac, F.; Soulie-Ziakovic, C.; Leibler, L. *Nature* **2008**, *451*, 977–980.
[75] Nair, K.; Breedveld, V.; Weck, M. *Macromolecules* **2008**, *41*, 3429–3438.
[76] Noro, A.; Hayashi, M.; Ohshika, A.; Matsushita, Y. *Soft Matter* **2011**, *7*, 1667–1670.
[77] Lange, R.; Van Gurp, M.; Meijer, E. *J. Polym. Sci., Part A: Polym. Chem.* **1999**, *37*, 3657–3670.
[78] Lei, Y.; Lodge, T. P. *Soft Matter* **2012**, *8*, 2110–2120.
[79] Kieltyka, R. E.; Pape, A. C. H.; Albertazzi, L.; Nakano, Y.; Bastings, M. M. C.; Voets, I. K.; Dankers, P. Y. W.; Meijer, E. W. *J. Am. Chem. Soc.* **2013**, *135*, 11159–11164.
[80] Guo, M.; Pitet, L. M.; Wyss, H. M.; Vos, M.; Dankers, P. Y. W.; Meijer, E. W. *J. Am. Chem. Soc.* **2014**, *136*, 6969–6977.
[81] Lin, Y.; Li, G. *J. Mater. Chem. B* **2014**, *2*, 6878–6885.
[82] Beck, J. B.; Rowan, S. J. *J. Am. Chem. Soc.* **2003**, *125*, 13922–13923.
[83] Piepenbrock, M. O. M.; Lloyd, G. O.; Clarke, N.; Steed, J. W. *Chem. Rev.* **2010**, *110*, 1960–2004.
[84] Kimura, M.; Nakagawa, Y.; Adachi, N.; Tatewaki, Y.; Fukawa, T.; Shirai, H. *Chem. Lett.* **2009**, *38*, 382–383.
[85] Vermonden, T.; van Steenbergen, M.; Besseling, N.; Marcelis, A.; Hennink, W.; Sudhölter, E.; Stuart, M. *J. Am. Chem. Soc.* **2004**, *126*, 15802–15808.
[86] Kersey, F. R.; Loveless, D. M.; Craig, S. L. *J. R. Soc. Interface* **2007**, *4*, 373–380.
[87] Peng, F.; Li, G.; Liu, X.; Wu, S.; Tong, Z. *J. Am. Chem. Soc.* **2008**, *130*, 16166–16167.
[88] Rossow, T.; Habicht, A.; Seiffert, S. *Macromolecules* **2014**, *47*, 6473–6482.
[89] Rossow, T.; Seiffert, S. *Polym. Chem.* **2014**, *5*, 3018–3029.
[90] Ueki, T.; Takasaki, Y.; Bundo, K.; Ueno, T.; Sakai, T.; Akagi, Y.; Yoshida, R. *Soft Matter* **2014**, *10*, 1349–1355.
[91] Krieg, E.; Shirman, E.; Weissman, H.; Shimoni, E.; Wolf, S. G.; Pinkas, I.; Rybtchinski, B. *J. Am. Chem. Soc.* **2009**, *131*, 14365–14373.
[92] Hietala, S.; Strandman, S.; Jarvi, P.; Torkkeli, M.; Jankova, K.; Hvilsted, S.; Tenhu, H. *Macromolecules* **2009**, *42*, 1726–1732.
[93] Crichton, M. A.; Bhatia, S. R. *Langmuir* **2005**, *21*, 10028–10031.
[94] Derici, L.; Ledger, S.; Mai, S. M.; Booth, C.; Hamley, I. W.; Peder-

sen, J. S. *Phys. Chem. Chem. Phys.* **1999**, *1*, 2773–2785.
[95] Castelletto, V.; Hamley, I. W.; Waigh, T. A. *J. Chem. Phys.* **2004**, *121*, 11474–11480.
[96] Tanaka, F. *J. Non-Cryst. Solids* **2002**, *307*, 688–697.
[97] Willet, N.; Gohy, J.-F.; Lei, L. C.; Heinrich, M.; Auvray, L.; Varshney, S.; Jerome, R.; Leyh, B. *Angew. Chem. Int. Ed.* **2007**, *46*, 7988–7992.
[98] Schmalz, A.; Schmalz, H.; Muller, A. H. E. *Soft Matter* **2012**, *8*, 9436–9445.
[99] Zhou, C.; Hillmyer, M. A.; Lodge, T. P. *J. Am. Chem. Soc.* **2012**, *134*, 10365–10368.
[100] Li, L.; Guo, X.; Fu, L.; Prud'homme, R.; Lincoln, S. *Langmuir* **2008**, *24*, 8290–8296.
[101] Li, L.; Guo, X.; Wang, J.; Liu, P.; Prud'homme, R. K.; May, B. L.; Lincoln, S. F. *Macromolecules* **2008**, *41*, 8677–8681.
[102] Wang, J.; Pham, D.-T.; Guo, X.; Li, L.; Lincoln, S. F.; Luo, Z.; Ke, H.; Zheng, L.; Prud'homme, R. K. *Ind. Eng. Chem. Res.* **2009**, *49*, 609–612.
[103] Guo, M. Y.; Jiang, M.; Pispas, S.; Yu, W.; Zhou, C. X. *Macromolecules* **2008**, *41*, 9744–9749.
[104] Appel, E. A.; Biedermann, F.; Rauwald, U.; Jones, S. T.; Zayed, J. M.; Scherman, O. A. *J. Am. Chem. Soc.* **2010**, *132*, 14251–14260.
[105] Guo, X.; Wang, J.; Li, L.; Pham, D.; Clements, P.; Lincoln, S.; May, B.; Chen, Q.; Zheng, L.; Prud'homme, R. *Macromol. Rapid Commun.* **2010**, *31*, 300–304.
[106] Nakahata, M.; Takashima, Y.; Yamaguchi, H.; Harada, A. *Nat. Commun.* **2011**, *2*, 511.
[107] Zhang, M.; Xu, D.; Yan, X.; Chen, J.; Dong, S.; Zheng, B.; Huang, F. *Angew. Chem. Int. Ed.* **2012**, *51*, 7011–7015.
[108] Zhou, L.; Li, J.; Luo, Q.; Zhu, J.; Zou, H.; Gao, Y.; Wang, L.; Xu, J.; Dong, Z.; Liu, J. *Soft Matter* **2013**, *9*, 4635–4641.
[109] Li, S.; Lu, H.-Y.; Shen, Y.; Chen, C.-F. *Macromol. Chem. Phys.* **2013**, *214*, 1596–1601.
[110] Zeng, F.; Han, Y.; Yan, Z.-C.; Liu, C.-Y.; Chen, C.-F. *Polymer* **2013**, *54*, 6929–6935.
[111] Burattini, S.; Greenland, B. W.; Merino, D. H.; Weng, W. G.; Seppala, J.; Colquhoun, H. M.; Hayes, W.; Mackay, M. E.; Hamley, I. W.; Rowan, S. J. *J. Am. Chem. Soc.* **2010**, *132*, 12051–12058.
[112] Hofmeier, H.; Hoogenboom, R.; Wouters, M. E. L.; Schubert, U. S. *J. Am. Chem. Soc.* **2005**, *127*, 2913–2921.
[113] Brassinne, J.; Stevens, A. M.; Van Ruymbeke, E.; Gohy, J.-F.; Fustin, C.-A. *Macromolecules* **2013**, *46*, 9134–9143.
[114] Brassinne, J.; Gohy, J.-F.; Fustin, C.-A. *Macromolecules* **2014**, *47*, 4514–4524.
[115] Yan, X.; Xu, D.; Chi, X.; Chen, J.; Dong, S.; Ding, X.; Yu, Y.; Huang, F. *Adv. Mater.* **2012**, *24*, 362–369.

[116] Nair, K. P.; Breedveld, V.; Weck, M. *Macromolecules* **2011**, *44*, 3346–3357.
[117] Ziessel, R.; Pickaert, G.; Camerel, F.; Donnio, B.; Guillon, D.; Cesario, M.; Prangé, T. *J. Am. Chem. Soc.* **2004**, *126*, 12403–12413.
[118] Rossow, T.; Hackelbusch, S.; van Assenbergh, P.; Seiffert, S. *Polym. Chem.* **2013**, *4*, 2515–2527.
[119] Weng, W.; Fang, X.; Zhang, H.; Peng, H.; Lin, Y.; Chen, Y. *Eur. Polym. J.* **2013**, *49*, 4062–4071.
[120] Yan, X.; Xu, D.; Chen, J.; Zhang, M.; Hu, B.; Yu, Y.; Huang, F. *Polym. Chem.* **2013**, *4*, 3312–3322.
[121] Hackelbusch, S.; Rossow, T.; Becker, H.; Seiffert, S. *Macromolecules* **2014**, *47*, 4028–4036.
[122] Hu, X.-Y.; Xiao, T.; Lin, C.; Huang, F.; Wang, L. *Acc. Chem. Res.* **2014**, *47*, 2041–2051.
[123] Zhan, J.; Zhang, M.; Zhou, M.; Liu, B.; Chen, D.; Liu, Y.; Chen, Q.; Qiu, H.; Yin, S. *Macromol. Rapid Commun.* **2014**, *35*, 1424–1429.
[124] Noro, A.; Hayashi, M.; Matsushita, Y. *Soft Matter* **2012**, *8*, 2416–2429.
[125] Sun, Z.; Huang, Q.; He, T.; Li, Z.; Zhang, Y.; Yi, L. *ChemPhysChem* **2014**, *15*, 2421–2430.
[126] Bosman, A.; Sijbesma, R.; Meijer, E. *Mater. Today* **2004**, *7*, 34–39.
[127] Herbst, F.; Döhler, D.; Michael, P.; Binder, W. H. *Macromol. Rapid Commun.* **2013**, *34*, 203–220.
[128] Hart, L. R.; Harries, J. L.; Greenland, B. W.; Colquhoun, H. M.; Hayes, W. *Polym. Chem.* **2013**, *4*, 4860–4870.
[129] Binder, W. H. *Self-healing polymers: From principles to applications*; Wiley-VCH, 2013; pp xix, 425.
[130] Seiffert, S.; Sprakel, J. *Chem. Soc. Rev.* **2012**, *41*, 909–930.
[131] Yang, S. K.; Ambade, A. V.; Weck, M. *Chem. Soc. Rev.* **2011**, *40*, 129–137.
[132] Pollino, J.; Weck, M. *Chem. Soc. Rev.* **2005**, *34*, 193–207.
[133] Uraneck, C.; Hsieh, H.; Buck, O. *J. Polym. Sci.* **1960**, *46*, 535–539.
[134] Tezuka, Y. *Prog. Polym. Sci.* **1992**, *17*, 471–514.
[135] Jerome, R.; Henrioulle-Granville, M.; Boutevin, B.; Robin, J. J. *Prog. Polym. Sci.* **1991**, *16*, 837–906.
[136] Rubinstein, M.; Dobrynin, A. *Trends Polym. Sci.* **1997**, *5*, 181–186.
[137] Asoh, T.-A.; Yoshitake, H.; Takano, Y.; Kikuchi, A. *Macromol. Chem. Phys.* **2013**, *214*, 2534–2539.

CHAPTER 3

RHEOLOGY OF MATTER – SOLID, LIQUID OR VISCOELASTIC MATERIALS?

Abstract

The chapter closing the introductory part aims to develop some basics of rheology. This science studies the deformation and flow of the matter. In this respect, three different rheological behaviours are distinguished according to the response of the matter to an applied stress. At first, the ideal behaviours of elastic solids and viscous fluids are presented, following a mathematical approach. The intermediate category of viscoelastic material is finally discussed, with emphasis on polymers. Those particular materials involve time dependent phenomena, which are rationalized on the basis of fundamental rheological models.

3.1 Definitions and concepts

The term *rheology*, derived from the Greek "*rheos*" meaning *something flowing*, was proposed by Bingham in 1929 and is defined as the study of the deformation and flow of matter.[1,2] The response of materials to an applied stress is relevant of the different state of the matter. That response may be irreversible viscous flow, reversible elastic deformation, or a combination of the two.[3] Hence, fluids, *i.e.*, gases and liquids, will flow when a force is applied, while solids will deform by a fixed amount and we expect them to regain their shape when the force is removed.[4]

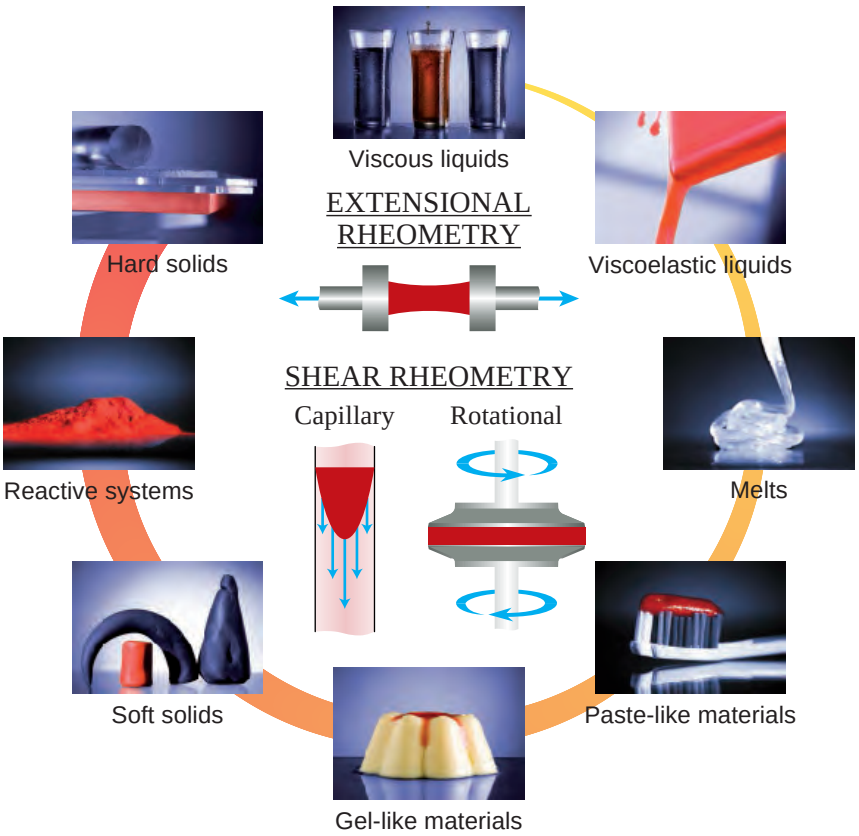

Figure 3.1 – Different rheometer instruments for material testing.

Most of the polymeric materials usually exhibit viscoelastic behaviour

during flow. In other words, they not only show viscous behaviour but also elastic behaviour in the liquid state.[5] Hence, rheology is a science that mainly deals with the deformation and flow of polymeric materials. Since there are a variety of polymeric materials, polymer rheology can be further classified into different categories, according to the nature of these materials, each exhibiting their own unique rheological characteristics: the rheology of homogeneous polymers, the rheology of polymer blends, the rheology of polymers composites, the rheology of block copolymers... [5]

Finding its etymology from the same origin, rheometry refers to the experimental quantification of rheological properties of materials.[1] For elastic or highly viscous materials, this quantification is generally achieved with a device called a rheometer. For relatively low viscosity liquids, a viscometer may be sufficient.[6] Control over rheological properties is essential for the manufacture and handling of numerous materials and products. Hence, rheology has earned a prominent place in food, cosmetic, rubber, plastic, paint, inks and many more industries (Figure 3.1).[3]

3.2 Stress and strain

When a stress is imposed to a material, it undergoes a deformation that is a change in shape or dimension.[1] The deformation is usually expressed in terms of extension undergone by the material, λ, as resulting from the application of mechanical force.[4] The stress, σ, is simply defined as the force divided by the area over which it is applied, thus expressed in N/m^2 or Pa. Following this idea, pressure is a compressive bulk stress (σ_c). When hanging a weight on a wire, an extensional stress (σ_e) is imposed. Finally, shear stress (σ_s) is applied when gumming a sheet of paper.[4]

Experimentally, most of the rheometers are based on the measure of material extension induced by the application of mechanical stress. This extension is commonly expressed in relative to the unit of length over which the deformation occurs, *i.e.*, volume, length, or other measurement, depending on the nature of the stress. In order to make calculations tractable, the strain, γ, is defined as the relative displacement from the rest position. This quantity is thereby dimensionless and

usually expressed as a percentage.[3,4]

The relationship between the applied stress and the resulting strain is intimately related to the chemical and physical structure of the material. In this respect, two limit and one intermediate classes of materials can be distinguished: the elastic solids, the viscous fluids and the viscoelastic liquids or solids.

3.3 Elastic solids

An ideal elastic solid is a material able to store all deformation energy, which in turn allows recovery of the original shape when the stress is released. Under low deformation, materials such as metals or ceramics are nearly ideal elastic solids and show almost no flow or viscous component. By definition, elasticity is the reversible stress–strain behaviour by which a body resists and recovers from deformation produced by a force. This behaviour is exhibited by rubber-like materials in a unique and extremely important manner. Unlike metals or glasses, they can undergo very large deformations without rupture and then can come back to their original shape.[3]

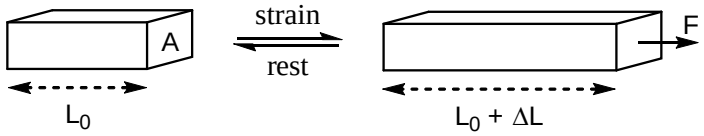

Figure 3.2 – Extensional deformation of an elastic material, of dimension A x L, in response to an applied force F.

As illustrated in Figure 3.2, the application of a tensile stress to a material will result in a corresponding extensional deformation. For uniaxial extension, stress is expressed as the imposed force, F, per unit cross-sectional area, A, of the material:[7,8]

$$\sigma_e(t) = \frac{F(t)}{A} \tag{3.1}$$

The uniaxial extension is expressed according to the length dimension of the material under rest, L_0, and stress condition, $L_0 + \Delta L$, by:[7–9]

$$\lambda_e(t) = \frac{L_0 + \Delta L(t)}{L_0} \tag{3.2}$$

Finally, the tensile strain is defined as the lengthening by unit of original length:[7–9]

$$\gamma_e(t) = \frac{\Delta L(t)}{L_0} = \lambda_e(t) - 1 \tag{3.3}$$

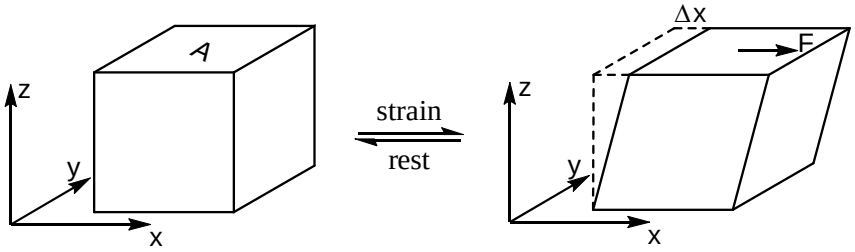

Figure 3.3 – Shear deformation of an elastic material, of dimension $x - y - z$, in response to a constant force, F.

The second type of deformation is illustrated in Figure 3.3 and is called simple shear. Here, the application of a tangential force results in shearing displacement. In that case, shear stress and strain can be defined similarly according to the dimensions of the material:[7–9]

$$\sigma_s(t) = \frac{F(t)}{A} = \frac{F(t)}{x \cdot y} \tag{3.4}$$

$$\gamma_s(t) = \frac{\Delta x(t)}{z} \tag{3.5}$$

Under low strain uniaxial deformation, the mechanical behaviour of ideal elastic solids is, like ideal springs, described by Hooke's law. A solid is said Hookean provided that stress varies linearly with strain, the proportionality being given by the tensile or Young's modulus, Y:[7–9]

$$\sigma_e(t) = Y \cdot \gamma_e(t) \tag{3.6}$$

The same linearity is valid in the case of shearing, where the proportionality is given by a different elastic modulus, G, called shear modulus: [7–9]

$$\sigma_s(t) = G \cdot \gamma_s(t) \tag{3.7}$$

The Hooke's law implies that instantaneous deformation follows the application of force to ideal elastic solids. Because the deformation energy is stored elastically, those materials recover their original shape as soon as stress is removed. Therefore, the elastic strain is said instantaneous and recoverable. In other word, the elastic strain follows, in phase, the mechanical stress applied to the Hookean solid (Figure 3.4). [4,10]

Table 3.1 – Moduli of elasticity for common materials.

Material	Tensile modulus, Y [GPa]	Shear modulus, G [GPa]
Diamond	$\sim$ 1,200	$\sim$ 475
Steel	190 – 210	75 – 80
Copper	110 – 120	40 – 47
Aluminium	70 – 79	26 – 30
Glass	48 – 83	19 – 35
Lead	17 – 19	12 – 14
Concrete	16 – 18	6 – 8
Fir wood	11 – 13	5 – 7
Nylon	2 – 4	0.6 – 1.6
Polyethylene	0.7 – 1.4	0.2 – 0.5
Rubber	0.1 – 0.6	0.03 – 0.2

At high stresses and strains, a limit of linearity can be reached beyond which Hooke's law is no longer valid. For example, strain hardening, *i.e.*, an increasing modulus with increasing strain, is normally observed with polymeric networks up to fracture. On the other hand, strain softening, *i.e.*, a decreasing modulus with increasing strain, is observed with some metals and colloids until yield is observed. [4]

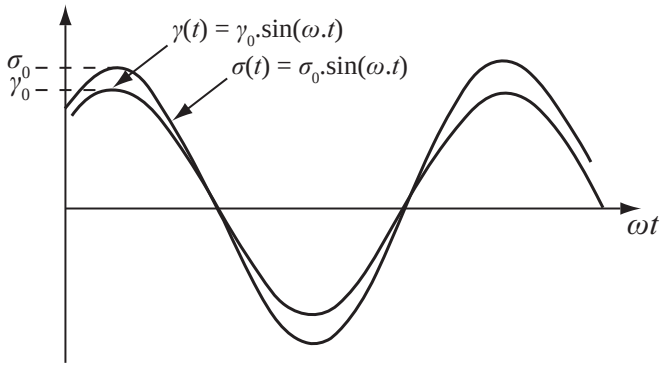

Figure 3.4 – Phase between oscillating strain resulting from the application of oscillating stress to a Hookean solid.

3.4 Viscous fluids

When a fluid system is studied by the application of a tensile or shear stress, motion is produced until the stress is removed.[4] When this force is applied tangentially, shear stress produces a sliding of one infinitesimal layer over another, resulting in a stack-of-cards type of flow (Figure 3.5).[3]

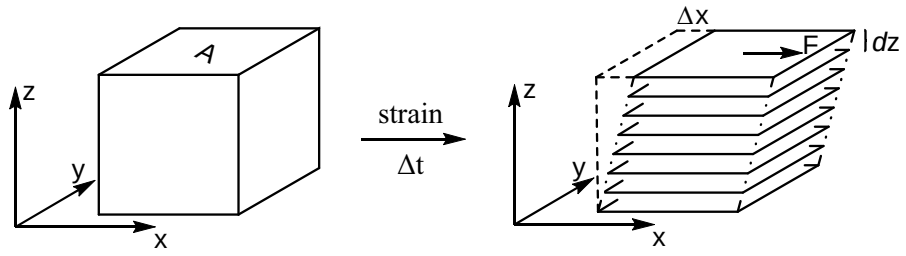

Figure 3.5 – Shear deformation of a viscous material, of dimension $x - y - z$, in response to a constant force, F, applied during a given time interval, Δt.

As for elastic solids, the stress is defined as the ratio of the force to the area of the surface where the latter is applied. Assuming a constant shear stress:[4]

$$\sigma_s = \frac{F}{A} = \frac{F}{x \cdot y} \tag{3.8}$$

By applying constant shear stress on the upper surface of the fluid, the latter will move at a constant velocity, v. Assuming there is no slip at the surface of the fluid, a continuous change in velocity will appear across the small gap, z, to zero at the lower surface. The displacement, Δx, produced within a given time interval, Δt, can be expressed in term of shear strain:[4]

$$\Delta\gamma_s = \frac{\Delta x}{z} = \frac{v \cdot \Delta t}{z} \tag{3.9}$$

If the force applied to the surface of the fluid is not constant during the time interval Δt, the displacement is decomposed into infinitesimal motion dx. The instantaneous shear stress and strain are respectively defined in regard to the instantaneous force and displacement, as follow:[4]

$$\sigma_s(t) = \frac{F(t)}{x \cdot y} \quad , \quad d\gamma_s(t) = \frac{v \cdot dt}{z} \quad \text{, with} \quad v(t) = \frac{dx}{dt} \tag{3.10}$$

Usually, the instant strain is reported per time unit, from which the shear rate, or velocity gradient, is derived:[4]

$$\dot{\gamma}_s = \frac{d\gamma_s(t)}{dt} = \frac{v}{z} \tag{3.11}$$

If the velocity profile of the different layers of fluid is not linear, the shear rate varies across the gap and must be written:[4]

$$\dot{\gamma}_s = \frac{dv}{dz} \tag{3.12}$$

When the plot of shear stress versus shear rate is linear, the fluid behaviour is simple and follows the Newton's law. Such a fluid is said Newtonian and the coefficient of viscosity, η, being the proportionality constant between shear rate and stress:[3,4]

$$\sigma(t) = \eta \cdot \dot{\gamma}(t) \tag{3.13}$$

By definition, the dynamic viscosity of a fluid, η, is a measure of its resistance to gradual deformation by shear stress or tensile stress. By relating the dynamic viscosity to the density of the fluid, ρ, the kinematic viscosity, ν, can be defined:[4]

$$\nu = \frac{\eta}{\rho} \tag{3.14}$$

Table 3.2 – Dynamic and kinematic viscosities of common fluids.

Fluid	Dynamic viscosity [Pa·s]	Kinematic viscosity [m^2/s]
Air	1.8×10^{-5}	1.6×10^{-5}
Water	1×10^{-3}	1×10^{-6}
Olive oil	8.4×10^{-2}	9.2×10^{-5}
Glycerol	1.5	1.2×10^{-3}
Honey	6	4.3×10^{-3}
Molten glass	10^1 – 10^3	5×10^{-3} – 10^{-1}
Asphalt	10^4 – 10^5	10^1 – 10^2
Earth's mantle	$\sim 10^{21}$	$\sim 2 \times 10^{17}$

Newtonian fluids are materials that dissipate the energy deformation during their flow. As a consequence, the viscous fluid remains in its deformed state when stress is released. Therefore, the viscous strain is said unrecoverable. This deformation is determined by integrating the stress imposed during a finite time interval:[4,10]

$$\gamma(\Delta t) = \frac{1}{\eta} \int_0^{\Delta t} \sigma(t) \cdot dt \tag{3.15}$$

In a way, the Newtonian fluid remembers all mechanical constraints that were imposed in the past. Indeed, the resulting deformation depends on all the values taken by the stress during the considered time interval ($\Leftrightarrow \sigma(t) = \sigma_0$). If the imposed stress is constant around a given value, σ_0, the fluid will flow indefinitely and the strain will increase

linearly with time:[4,10]

$$\gamma(\Delta t) = \frac{1}{\eta}\int_0^{\Delta t} \sigma_0 \cdot dt = \frac{\sigma_0}{\eta} \cdot \Delta t = \gamma_0 \cdot \Delta t \tag{3.16}$$

If the fluid is now subjected to a sinusoidal stress ($\Leftrightarrow \sigma(t) = \sigma_0 \cdot \cos(\omega t)$), *i.e.*, oscillating in time at a certain angular frequency, ω, the deformation will be out of phase by a quarter period (Figure 3.6):[4,10]

$$\gamma(\Delta t) = \frac{1}{\eta}\int_0^{\Delta t} \sigma_0 \cdot \cos(\omega t) \cdot dt = \frac{\sigma_0}{\eta \cdot \omega} \cdot \sin(\omega \Delta t) = \gamma_0 \cdot \sin(\omega \Delta t) \tag{3.17}$$

The original exposition of Newton's law states that the ratio of the stress to the shear rate, *i.e.*, the fluid viscosity, is a constant. This statement is in fact only true for ideal or Newtonian fluids. It fits water, solvents, and many diluted polymer solutions over a wide strain rate range. On the other hand, the viscosities of many liquids are not independent of shear rate. These non-Newtonian liquids may be classified according to their viscosity behaviour as a function of shear rate (Figure 3.7).[3]

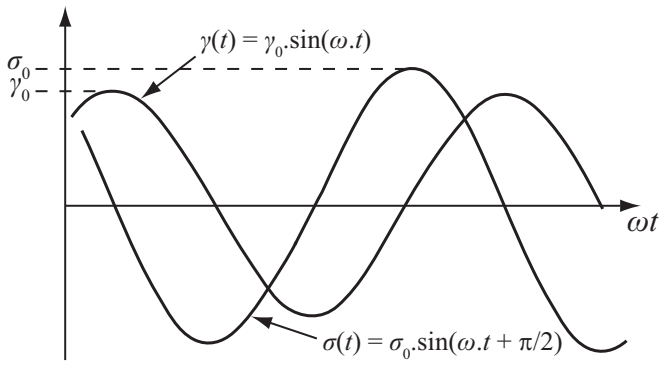

Figure 3.6 – Phase between oscillating strain resulting from the application of oscillating stress to a Newtonian fluid.

Many fluids exhibit shear thinning, *i.e.*, their viscosity decreases with shear rate, and are said pseudoplastic. They include dilute suspensions of solid particles or deformable vesicles (such as blood), polymer dilute

solutions and melts, lava, inks or paints.[3,4] Other fluids exhibit the opposite behaviour, *i.e.*, their viscosity increases as a function of the shear rate. Those materials resist to quick motion and are qualified as shear thickening or dilatant fluids. This less common behaviour is encountered for concentrated colloidal suspensions (such as starch solutions), or wet sand.[3,4]

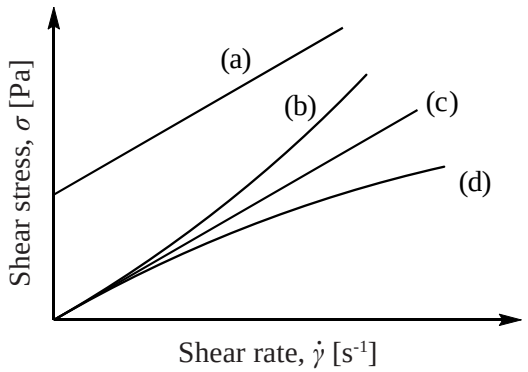

Figure 3.7 – Flow curves for different types of flow behaviour: plastic (a), shear thickening (b), newtonian (c), and shear thinning (d).[3]

To model the behaviour of many non-Newtonian fluids, a power law has been proposed. It holds for many solutions and can describe Newtonian, shear thinning, and shear thickening behaviour, depending on the power factor, also called the flow behaviour index. For a Newtonian fluid, this index is equal to 1 and the equation reduces to the Newtonian model. If the power factor less than 1, the fluid is shear thinning; if it is greater than 1, the fluid is shear thickening. In turn, the value of this index is a measure of the degree of shear thinning or shear thickening:[3,4]

$$\sigma(t) = k \cdot \dot{\gamma}^n(t) \tag{3.18}$$

Finally, some fluids at rest appear to behave like rigid bodies until the shear stress exceeds a certain value, called the yield stress, after which they flow readily. Those materials are called Bingham or plastic fluids, common examples being toothpaste and ketchup, which will not be extruded until a certain pressure is applied to the tube. Also, this behaviour is encountered for a number of dispersions, including some pigment pastes. Above the yield stress, Bingham model predicts

constant viscosity that can be determined from the slope beyond the intercept of the shear stress *vs* shear rate plot.[3,4]

3.5 Viscoelastic materials

A major non-Newtonian behaviour present in particular systems is viscoelasticity, also known as anelasticity. By definition, viscoelasticity is the property of materials which exhibit both elastic and viscous response when undergoing deformation. Indeed, these substances are capable to recover but also to creep after a strain due to the application of a stress. Viscoelastic materials are thus characterized by an intermediate behaviour lying somewhere between Hookean solid and Newtonian fluid, which depends on both duration and amplitude of deformation.[2,7,9,10]

Viscoelastic materials are classically dispersions like, *e.g.*, polymer or clay. At rest, they form a network by virtue of intermolecular forces or interparticle associations, which limits the movement of network elements, and gives the substance a solid behaviour. When external forces overcome the cohesive strength of the network, the constitutive elements are forced to flow, as illustrated in Figure 3.8. The plasticity threshold beyond which the material flows is called the yield point, which can be defined in terms of stress, σ^c, or strain, γ^c.[2,7,9,10]

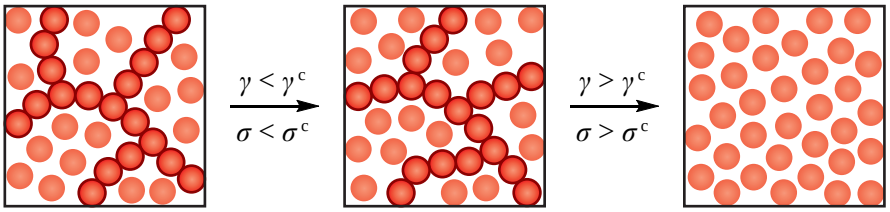

Figure 3.8 – Yielding of micro-structures in a colloidal dispersion in response to mechanical stress.

To account for the elastic character of the flow, the Weissenberg number, W_e, was introduced as a measure of the amount of recoverable strain in the fluid. Taking into consideration the amplitude and the duration of the deformation, this dimensionless number is defined as the product of the deformation rate, $\dot{\gamma}$, and a characteristic relaxation time of the material, τ:[2,4]

$$W_e = \tau \cdot \dot{\gamma} \tag{3.19}$$

Whether a viscoelastic material behaves as a viscous liquid or an elastic solid also depends on the relation between the time scale of the deformation process and the time required for the system to respond to stress or deformation. The most frequently quoted example to illustrate this behaviour is the children's toy Silly Putty, which is a viscoelastic liquid silicone. It bounces and shows brittle fracture when given a sharp blow, like any solid, but also flows as a liquid if pulled slowly (Figure 3.9). Precisely, if the duration of stress application, Δt, is sufficiently shorter than the relaxation time of the material, τ, the latter responds elastically. This relaxation time is an intrinsic characteristic of the material and defines how quickly the energy of the deformation is dissipated or, in other word, the time interval over which the material is able to store the deformation energy. For example, τ is typically 10^{-12} s for water in the liquid state, but can be of the order of 10^{-6} s for lubricating oils, and may be as high as a few seconds for polymer melts. On the other hand, if the stress is applied over long period ($\Delta t >> \tau$), the material ultimately appears to be viscous, with the idea that everything flows, including the mountains! Indeed, these effects can be seen in geological strata, where rock has flowed to relieve the stresses imposed by geological events.[2,3,7,10]

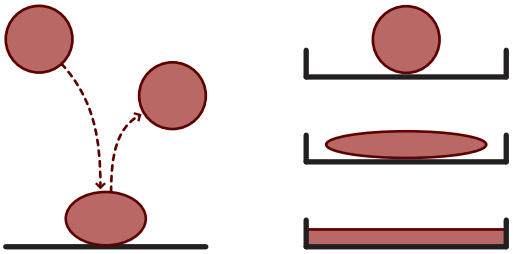

(a) $\Delta t << \tau$ (b) $\Delta t >> \tau$

Figure 3.9 – Viscoelastic response of liquid silicone illustrating the importance of time scaling in rheology.

If, at first glance, there is no apparent connection between *rheology* and *theology*, the clairvoyant Deborah is reported to have declared, in the fifth chapter of the Book of Judges in the Old Testament: "The

mountains flowed before the Lord . . . ".[11] On the basis of this reference, Reiner, one of the founders of the modern science of rheology, introduced the Deborah number, D_e, to achieve the scaling of time in rheology. This dimensionless number is defined as the ratio of the characteristic relaxation time of the material to the time scale of the solicitation process:[2,4]

$$D_e = \frac{\tau}{\Delta t} \tag{3.20}$$

The time τ is infinite for a Hookean elastic solid and zero for a Newtonian viscous fluid. For viscoelastic materials, high Deborah numbers correspond to solid-like behaviour and low Deborah numbers to liquid-like behaviour. A material can therefore appear solid-like either because having a very long characteristic time or because the deformation process is relatively fast (Table 3.3). Thus, even mobile liquids with short relaxation time like water can behave like elastic solids in an ultra-fast deformation process.[2] In the daily life, it is possible to feel this sensation when hitting a pool of water with an open hand, or after missing a dive of a fairly substantial height.

Table 3.3 – Time scales typically involved in familiar processes and related applications.[2]

Process	Stress duration [s]	Application
Sedimentation	10^3 – 10^6	Medicines, paints
Levelling	10^1 – 10^2	Paints, printing inks
Draining	10^{-1} – 10^1	Painting, coating
Extrusion	10^{-3} – 10^0	Polymers
Mixing/stirring	10^{-3} – 10^{-1}	Manufacturing liquids
Pipe flow	10^{-3} – 10^0	Pumping
Brushing	10^{-4} – 10^{-3}	Brush painting
Spraying	10^{-5} – 10^{-3}	Spray-drying, painting
High speed coating	10^{-6} – 10^{-4}	Paper
Lubrication	10^{-7} – 10^{-3}	Gasoline engines

3.5.1 Viscoelastic models

Given the coexistence of viscous and elastic response, most mathematical theories of linear viscoelasticity are based on a superposition principle. Precisely, viscoelasticity is described by combining the two elementary models that are the ideal elastic Hookean solid and the ideal viscous Newtonian fluid.[2] As a reminder, those ideal behaviours are respectively based on the following equations:

$$\sigma(t) = G \cdot \gamma(t) \quad \text{et} \quad \sigma(t) = \eta \cdot \dot{\gamma}(t) \tag{3.21}$$

Generally, these two rheological behaviours are schematically materialized by simple mechanical model elements. On one hand, the elasticity of viscoelastic materials is represented by a coil spring that obeys the Hooke's law (Figure 3.10 (a)). Thus, the response of the spring can be described by an elasticity modulus, G. On the other hand, the viscosity of viscoelastic materials is schematized by a dashpot consisting of a cup filled with a Newtonian oil of given viscosity, η, with a piston placed in the oil (Figure 3.10 (b)).[4,9]

(a) Spring (b) Dashpot

Figure 3.10 – Diagrammatic representations of ideal rheological behaviours: (a) the Hookean spring (a) and the Newtonian dashpot (b).

A combination of these one-dimensional mechanical models of springs and dashpots will display viscoelasticity that can describe seemingly complex experimental behaviours. Usually, the interest is on small strains where these two simple elements display the property of linear viscoelasticity. Under those conditions, the piston remains in the oil and the spring recoils completely once stress is released. Also, it is possible to consider situations in which the piston is pulled free from the oil or where the spring stretches too far and becomes permanently deformed. Whereas more complicated in essence, such non-linear viscoelastic responses became of increasing interest over the past few years.[4]

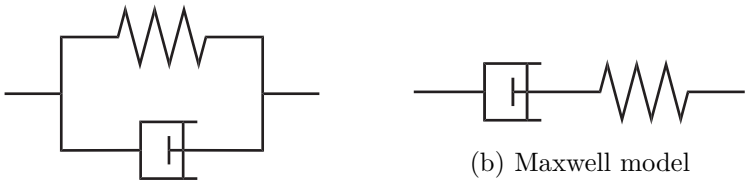

(a) Kelvin–Voigt model

(b) Maxwell model

Figure 3.11 – Simplest models describing viscoelasticity.

The two simplest arrangements so that the overall system behaves analogously to a viscoelastic material are in parallel or in series. The Kelvin model results from a parallel combination of a spring and a dashpot (Figure 3.11 (a)). After sudden imposition of a stress, the spring will eventually reach a steady-state strain, but the dashpot will retard the growth of the strain. Hence, this model is usually used in considering creep experiments, the higher the viscosity, the slower will be the response. In this configuration, the extension of the spring is however at all times equal to the extension in the dashpot. In addition, the total stress is equal to the sum of the stresses in each element:[2,4,9]

$$\sigma(t) = G \cdot \gamma(t) + \eta \cdot \dot{\gamma}(t) \quad \text{or} \quad \frac{\sigma(t)}{\eta} = \xi \cdot \gamma(t) + \dot{\gamma}(t) \tag{3.22}$$

where the parameter ξ defines the relaxation rate of the Kelvin–Voigt element:

$$\xi = \frac{G}{\eta} \tag{3.23}$$

Because of this arrangement, the Voigt element represents in the simplest possible form a viscoelastic solid. Complementary, the connection of a spring in series with a dashpot, which constitutes a Maxwell element (Figure 3.11 (b)), defines the simplest viscoelastic liquid. On one hand, the elastic component deforms instantaneously and relaxes immediately upon stress release. On the other hand, the viscous component grows with time as long as the stress is applied. While not suitable for creep, the Maxwell model accurately predicts stress relaxation for most polymers. Due to the arrangement of model elements in series, the strain

rates linearly add:[2,4,9]

$$\dot{\gamma}(t) = \frac{\dot{\sigma}(t)}{G} + \frac{\sigma(t)}{\eta} \quad \text{or} \quad \eta \cdot \dot{\gamma}(t) = \tau \cdot \dot{\sigma}(t) + \sigma(t) \tag{3.24}$$

where the parameter τ defines the relaxation time of the Maxwell element:

$$\tau = \frac{\eta}{G} \tag{3.25}$$

When a Maxwell element is put under a constant strain, the stress gradually relaxes with time (Figure 3.12). At times very short compared to the relaxation time of the Maxwell element ($t << \tau$), the latter behaves as a spring alone. As a result, the stress immediately follows the strain and increases to a maximum value. At times considerably longer than the relaxation time of the Maxwell element ($t >> \tau$), the model behaves as a dashpot alone and the stress decays exponentially to zero. At intermediate times ($t \approx \tau$), the response involves both the spring and the dashpot.[2,4,9]

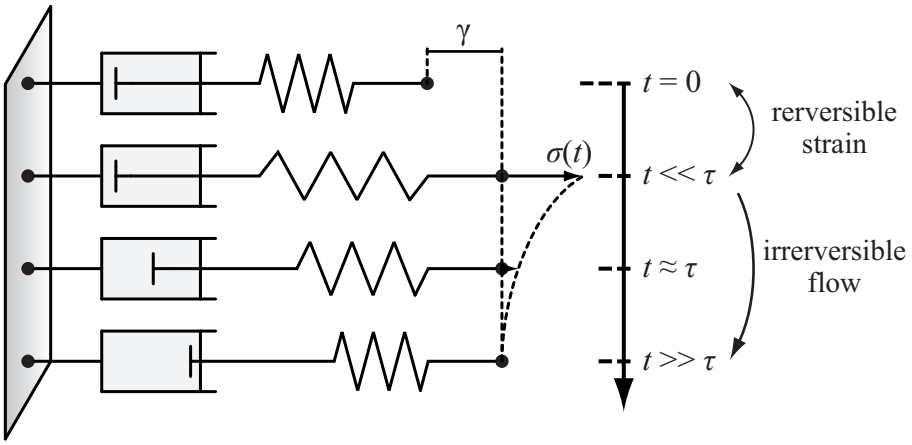

Figure 3.12 – Stress relaxation in a Maxwell element under constant stain.

A consequence of the arrangement of the spring and the dashpot in series, the Maxwell element allows complete relaxation of any applied

strain. The energy initially stored in the spring, which represents its elastic response, decreases with time until fully dissipated in the viscous flow. The latter takes place immediately after the application of the stress, which decreases exponentially with the spring recovery. The viscous response of the dashpot element is thus intimately related to the spring extension, and reaches a maximum when the time scale coincides with the characteristic relaxation time of the whole system. [2,4,9]

The response of both the Maxwell and Kelvin–Voigt models to several kinds of deformation experiments are much simpler than those of real systems. Indeed, these models exhibit only one transition under all conditions whereas real systems, such as polymers, show multiple major transitions. Also, many actual systems imply a distribution of interparticle spaces and particle–particle interactions, which gives a range of relaxation times with accompanying elastic and viscous contributions. While providing qualitative guidance, both Maxwell and Kelvin–Voigt models hence do not provide good quantitative representations of the observed viscoelastic behaviour of real materials. [2,4,9]

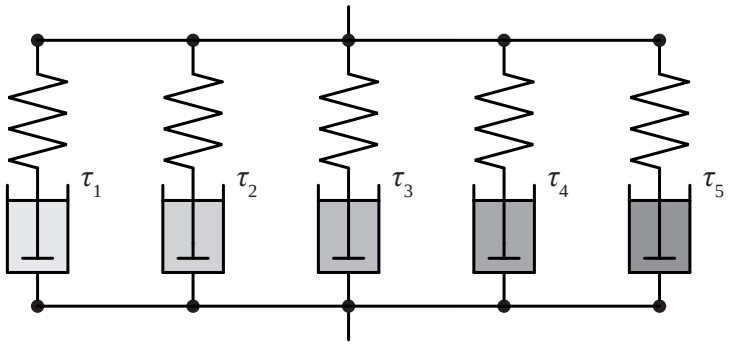

Figure 3.13 – Generalized Maxwell model for viscoelasticity.

To predict the rheological response of real materials to all the possible deformations and time scales, more complicated models have been envisaged. The adopted approach however assumes that the material can be described by a combination of springs and dashpots, added together to give an overall material response. Irrespective of their complexity, those models can be thus reduced to combinations of Maxwell and Voigt elements. In particular, the generalized Maxwell model has a finite or enumerable number of Maxwell elements, each with a different relaxation time (Figure 3.13). In turn, this enables to model a distribu-

tion of molecular interactions with their characteristic relaxation times, each being replaced by a single Maxwell element. In addition, the overall relaxation of the system is obtained by summing all these processes together. [2,4,9]

3.5.2 Oscillation response

When an oscillating stress is applied to a viscoelastic material, a strain is produced in response after an initial start-up period. In practice, this situation is usually encountered in rotational rheometers operating classically with either plate–plate, cone–plate, or concentric cylinder geometry (Figure 3.1). Since the stress has an alternating value with time, the strain also oscillates with time. In particular, a sinusoidal stress applied to a material produces a sinusoidal strain oscillating at the same frequency, f, or angular frequency, $\omega = 2\pi f$. The amplitude of the deformation is proportional to that of the stress, but lags behind the stress curve by some angle, δ, between 0 and 90 °, depending on the elastic/viscous characteristics of the material (Figure 3.14). [3,4,10]

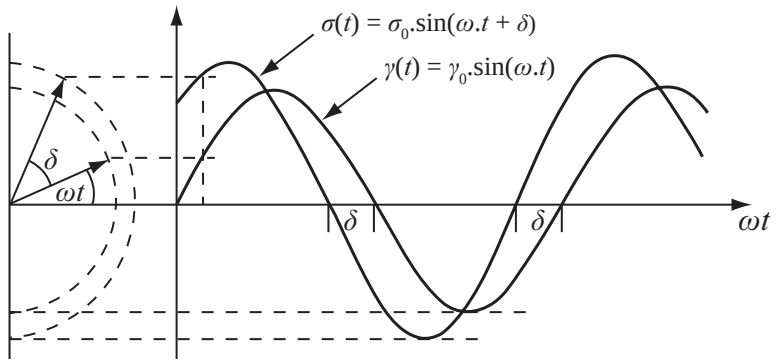

Figure 3.14 – Phase between oscillating strain resulting from the application of oscillating stress to a viscoelastic material.

Normally, the analysis of these systems is performed using the frequency as the variable. The classical procedure starts from the expansion of the stress into two components, one being in phase with the strain, the other 90 ° out of phase: [10]

$$\sigma(t) = \sigma_0 \cdot \sin(\omega t + \delta) = \sigma_0 \cdot \cos(\delta) \cdot \sin(\omega t) + \sigma_0 \cdot \sin(\delta) \cdot \cos(\omega t) \quad (3.26)$$

The relationship between stress and strain in this dynamic case can be thus defined by writing:

$$\sigma(t) = \gamma_0 \cdot \left[G' \cdot \sin(\omega t) + G'' \cdot \cos(\omega t)\right] \quad (3.27)$$

where the parameters G' and G'' are respectively called dynamic storage and loss modulus:[10]

$$G' = \frac{\sigma_0}{\gamma_0} \cdot \cos(\delta) \quad \text{and} \quad G'' = \frac{\sigma_0}{\gamma_0} \cdot \sin(\delta) \quad (3.28)$$

Concretely, the storage modulus gives a measure of the elastic component of the material. At the molecular level, G' is associated with the energy stored in elastic deformation. On the opposite, the loss modulus is associated with viscous dissipation of mechanical energy. The ratio of G'' and G' gives another measure of damping, the dissipation factor or loss tangent, which is the ratio of dissipated energy to stored energy:[3]

$$\tan(\delta) = \frac{G''}{G'} \quad (3.29)$$

In practice, measuring the phase lag between an applied sinusoidal stress and the resulting strain constitutes the first experimental approach to obtain information about the viscoelastic behaviour of a material. For a material dominated by elasticity, δ will be close to $0\,^\circ$. If the viscous effect dominates, δ will be close to $90\,^\circ$.[3,4,10]

In parallel, probing the response of materials as a function of frequency enables to reach experimental information about relaxation processes occurring on the deformation time scale, $t = 1/f$. In this respect, the high-frequency response ($f >> 1/\tau$) of a single Maxwell element is characterised by the invariance and inverse dependence of respectively the storage and loss modulus with the oscillation frequency (Figure 3.15). On the other hand, the low-frequency response ($f << 1/\tau$) of the same element is characterised by the first and second order dependency of moduli with the oscillation frequency.[4]

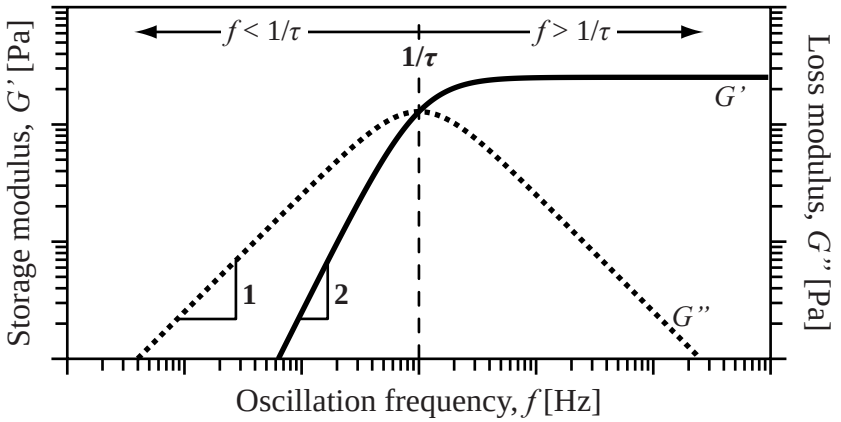

Figure 3.15 – Frequency dependence of dynamic moduli in a Maxwell element.

3.5.3 Polymer viscoelasticity

Viscoelastic effects are much more pronounced in polymers than in metals or ceramics. Because of their long chemical structure, polymers cohere as solids even when discrete chain sections undergo Brownian diffusional motions. Their properties are also much more sensitive to temperature than those of other materials. Changes of molecular orientation with deformation cause dramatic variation in properties and a much greater degree of anisotropy than is observed in other materials. [10]

Deformation of polymers involves distortion of the weak van der Waals bonds between neighbouring chain segments and rotation of covalent bonds. These changes are thus strongly dependent on the nature of the functional groups on the polymer. They result in stretching of flexible macromolecular chains (Figure 3.16 (a)), which is the basic physical mechanism responsible for the elastic response of polymer. Indeed, conformational changes caused by the applied force reduce the number of allowed configurations, which lowers the entropy of the system. This entropy change is the origin of the restoring force of the Gaussian chain. The latter therefore acts like a Hookean spring having an associated entropic elasticity (Figure 3.16 (b)). [8,12,13]

When polymers are stressed by mechanical forces, chain segments tend to orient in the force field. Under momentary deformation, the polymeric material deforms elastically and responds solid-like. To a cer-

tain extend, the Gaussian chains are indeed able to store the deformation energy and to use it in order to recover their initial conformation once the strain is released. Under a prolonged stress, the chains may align in the strain field and lose their initial arrangement, resulting in creep, *i.e.*, permanent deformation. [7,10]

(a) Flexible thread model

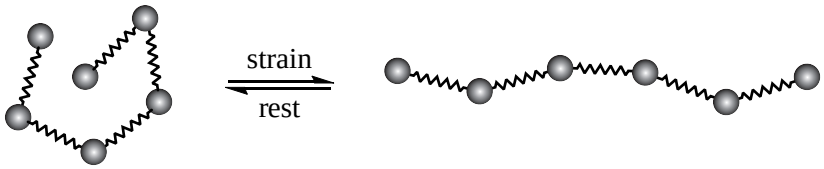

(b) Bead–spring model

Figure 3.16 – Stretching of a Gaussian polymer chain according to different models.

Time dependency of the mechanical response of polymeric materials results in variations of the elastic modulus as a function of loading duration. As schematized in Figure 3.17, different regions of viscoelastic behaviour can be identified that consist of distinct plateaus separated by temporal transitions. Those transitions reflect the material's propensity for mobility, which can be described in terms of either free volume changes or relaxation times. Whereas elasticity is usually the result of bond stretching, stress relaxation results from the motion of atoms or molecules inside of the material. [3,7,8]

In all substances, the local motions dramatically slow down with falling temperatures and inversely. Therefore, a strong temperature dependence of the elastic modulus accompanies the time dependency, as shown in Figure 3.17. Investigating the variation of mechanical properties of polymers with time can only be achieved if the temperature of the measurements is known. Also, the elastic moduli obtained at different temperatures can be compared if the time considered for the

experiment is the same. Practically, it is however difficult to measure the viscoelastic response of a polymer over the full time or temperature range. Fortunately, comparison of isochrone and isothermal measurements of the elastic modulus revealed a time–temperature equivalence. Precisely, it is the logarithm of time that is locally equivalent to temperature. Assuming that no chemical or physical ageing occurs, this empirical equivalence can be thus utilized to develop accelerated testing methods. [7,10,12,14]

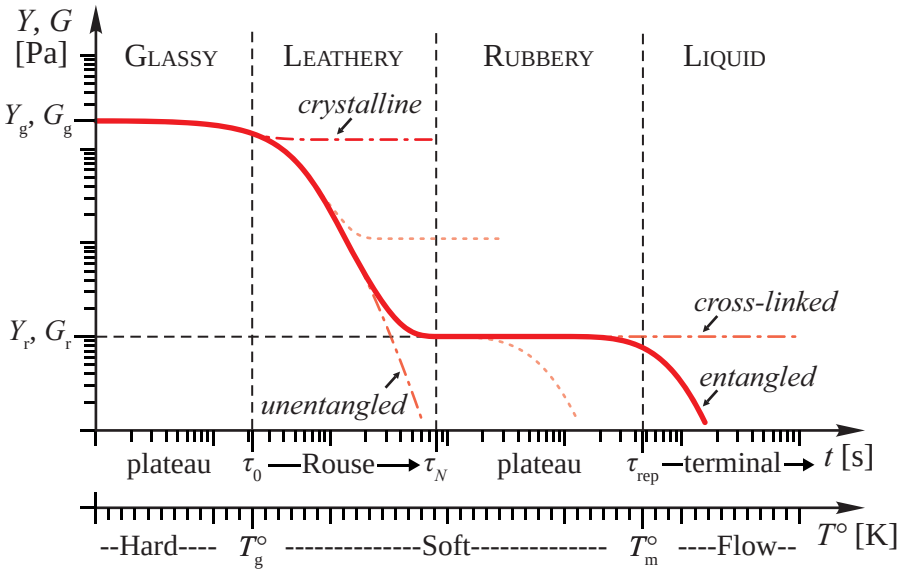

Figure 3.17 – Generic representation showing the temporal and thermal dependency of elastic modulus for purely crystalline, amorphous unentangled, entangled and cross-linked polymers.

Classically, the polymer molecule is treated as a collection of mobile segments that have some degree of free movement (Figure 3.18). For a polymer segment to move from one equilibrium position to another, enough free volume must nevertheless be available. Accordingly, the ability of a polymer segment to move in various directions increases as its free volume increases. In addition, the chain segment must have enough energy to break loose from its neighbours and move into the hole. Finally, because macromolecules consist of a large number of connected segments, they do not relax independently of one another. The motion of a particular segment depends to some degree on that of its neighbours.

Thus, the rearranging movement of one polymer segment is only possible if a certain number, N, of neighbours is also moved. [3,8,14,15]

The number of times per second that a segment of a polymer chain translated from one lattice site to another defines the segmental jump frequency. The latter strongly depends on the nature and composition of the polymer but also varies along the chain. Intuitively, the jump frequency for a side-group not attached rigidly to the main chain will be different from the jump frequency of the chain backbone. Also, a polymer segment near a chain end will, on average, have a higher jump frequency than the usual polymer segment. When this frequency is large, a polymer segment can move easily under the action of an external force, characterizing soft material with high tendency to flow. Indeed, the latter will rearrange quickly and assume its new equilibrium strain soon after the stress is applied. On the other hand, if the jump frequency is extremely low, the molecules will appear to be frozen in place, and the substance will act like a hard, brittle material with high tendency to restore its initial shape. Inversely, it will require a very long time for the material to contract to its new equilibrium strain. [3,8,15]

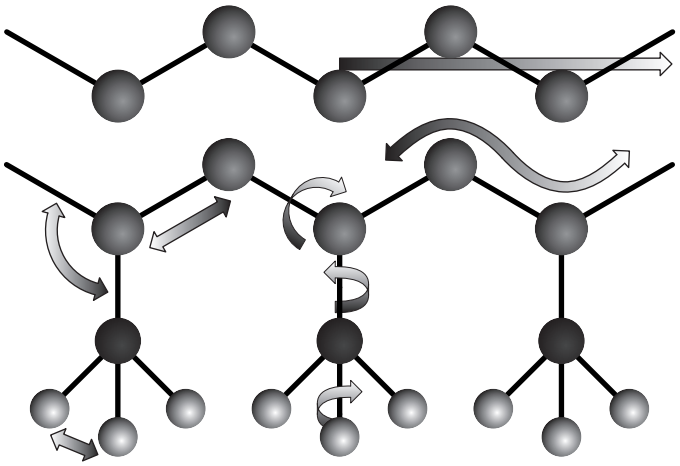

Figure 3.18 – Schematic representation showing different motions of a polymer chain: stretching, bending, rotating and slipping.

Consisting of a large number of atoms, a macromolecule has a very large number of degrees of freedom (Figure 3.18). As a consequence, the polymer chain dynamics covers a very broad range of motional rates.

A general rule is that the slower the mode of motion, the larger the involved domain of the chain. Of course, the lengths and angles of the chemical bonds connecting the atoms may distort, moving the atoms to new positions of greater internal energy. This bond bending and stretching are small motions and occur very quickly, requiring only picoseconds. As the free volume increases as a result of bond motions, side-chain and adjacent atoms in the main chain begin to have enough space to move and the material starts to develop some toughness. Theoretically, these local bond vibrations and motions of small groups of atoms are respectively ascribed to γ- and β-relaxations of the material, which lower its elastic response. However, those transitions are difficult to achieve in practice as they involve extremely short time scales and low activation energy barriers. [3,8,10,15]

The vibrational motions of the chemical bonds and atoms excluded, polymer chain dynamics range from the local segmental motions, with a frequency of around $10^9\,\mathrm{s}^{-1}$, to the slow movement of the whole chain over a distance of the whole-chain size scale. For a polymer of common molecular weight, the characteristic rate of those movements can be easily as slow as $10^{-5}\,\mathrm{s}^{-1}$. Those short to large scale motions occurring in the amorphous portion of the material are described by the Rouse bead–spring model (Figure 3.16 (b)). This model relies on diffusive motions arising from subjecting each bead of the Gaussian chain to thermal fluctuation forces, *i.e.*, Brownian motions. In this respect, a linear polymer chain is considered as relaxed as soon as an extremity has diffused to the other one. [3,8]

Rouse motions constitute the main relaxation mechanism, called α-relaxation, in semi-crystalline and amorphous polymers. For entangled and cross-linked polymers, this relaxation marks the transition between the glassy and rubbery state of the mater, as illustrated in Figure 3.17. In this glassy region, thermal energy is insufficient to surmount the potential barriers for rotational and translational motions of segments of the polymer molecules. The macromolecular chains are essentially "frozen" in fixed positions on the sites of a disordered quasi-lattice with their segments vibrating around these fixed positions. Because mainly elastic bond deformations occur in this vitreous state, polymers behave as rigid solids with relatively high modulus, called the glassy modulus, which is on the order of Gigapascals. [3,7,9,10]

With increasing free volume and/or temperature, the segmental mo-

tions amplify until the thermal energy becomes roughly comparable to the potential barriers to segment rotation and translation. In this region, the polymer is at the glass transition temperature, T_g°, where short-range diffusional motions begin. Segments are free to jump from one lattice site to another; the brittle glass becomes a resilient leather. Factors that enhance mobility, such as absorbed diluent or plasticizer, expansive stress states, and lack of bulky molecular groups, tend all to hurry the glass transition. For a given polymer, the value of T_g° is also very dependent on the degree of polymerization up to a critical value (Figure 3.19). Above this value, the glass transition temperature typically becomes independent of molecular weight. [3,7,9,10]

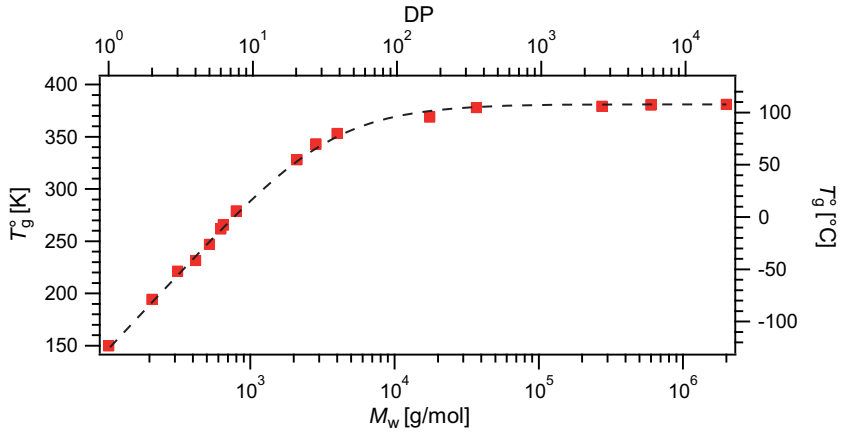

Figure 3.19 – Evolution of the glass transition temperature of polystyrene with chain length. [16]

Above the glass transition, the material stiffness drops dramatically, by perhaps two orders of magnitude, to reach a plateau value called rubbery modulus, with the exception of very low molecular weight oils (Figure 3.17). If the short-range diffusional motions of polymer segments occur above the glass transition, the complete chain relaxation resulting from the diffusion of the entire macromolecule is indeed delayed. It is the presence of strong local interactions between neighbouring chains that usually restrict the long-range cooperative motions of chains. In the case of the cross-linked network, these local interactions consist of chemical primary bonds, whereas they are entanglements in the case of linear polymers. [3,7,9,10,15]

In a polymer network, cross-links keep the chain strands from moving away from their relative positions over a distance larger than the strand size itself. Therefore, the chains do not flow with the deformation and are able to recover their conformations once the stress is released. In other words, nothing happens after the glass transition because the cross-links prevent the chains from slipping past each other, at least until the sample begins to burn and degrade. In contrast to this behaviour, un-cross-linked polymers finally undergo permanent molecular flow, whose characteristic time scale depends on molecular weight. Under prolonged loading, local physical interactions are indeed not sufficient to prevent large-scale translational motions, also called reptation, of oriented polymer chains. Above the terminal region, the mechanical stress is released and the material cannot recover its original shape. [3,8]

3.6 Summary

In this chapter, rheology was defined as the science that studies the deformation and flow of the matter. Following a mathematical approach, the ideal behaviours of Hookean solids and Newtonian fluids were characterized by their response to mechanical stress, which defines properties such as elasticity and viscosity. The intermediate category of viscoelastic materials, *i.e.*, those which exhibit both elastic and viscous behaviour, was then discussed with emphasis on polymers. Their response to mechanical stress was rationalized on the basis of simple viscoelastic models. Finally, the rheological behaviour of polymers was described by relating the distinct relaxation modes to the local, segmental, and long range motions of the chains.

Bibliography

[1] Gooch, J. W. *Encyclopedic dictionary of polymers*; Springer: New York, 2007; pp xxviii, 1237.
[2] Barnes, H. A.; Hutton, J. F.; Walters, K. *An introduction to rheology*; Elsevier: Amsterdam, 1989; pp ix, 199.
[3] Mark, H. F. *Encyclopedia of polymer science and technology*, concise 3rd ed. ed.; Wiley: Hoboken ; Chichester, 2007; pp xxv, 1462.
[4] Goodwin, J. W.; Hughes, R. W. *Rheology for chemists: An introduction*; Royal Society of Chemistry: Cambridge, 2000; pp x, 290.

[5] Han, C. D. *Rheology and processing of polymeric materials*; Oxford University Press: Oxford, 2007; p 2 v.
[6] Walters, K. *Rheometry*; Chapman and Hall: London, 1975; pp x, 278.
[7] Brinson, H. F.; Brinson, L. C. *Polymer engineering science and viscoelasticity: An introduction*; Springer: New York, 2008; pp xvi, 446.
[8] Lin, Y.-H. *Polymer viscoelasticity: Basics, molecular theories and experiments*; World Scientific: London, 2003; pp xii, 251.
[9] Aklonis, J. J.; MacKnight, W. J. *Introduction to polymer viscoelasticity*, 3rd ed.; Wiley: Hoboken, 2005; p 316.
[10] Gargallo, L. *Physicochemical behavior and supramolecular organization of polymers*, 1st ed.; Springer: New York, 2009; pp xiv, 240.
[11] Lias, J. J. *The book of Judges*; Cambridge University Press: Cambridge, 1896; p 220.
[12] Hosford, W. F. *Mechanical behavior of materials*; Cambridge University Press: Cambridge ; New York, 2005; pp xx, 425.
[13] Larson, R. G. *Constitutive equations for polymer melts and solutions*; Butterworths series in chemical engineering; Butterworths: Boston, 1988; pp xvi, 364.
[14] Donth, E.-J. *The glass transition: Relaxation dynamics in liquids and disordered materials*; Springer Ser. Mater. Sci.; Springer: Berlin ; New York, 2001; pp xvii, 418.
[15] Bueche, F. *Physical properties of polymers*; Wiley-Interscience: Huntington, 1962; pp x, 354.
[16] Claudy, P.; Letoffe, J.; Camberlain, Y.; Pascault, J. *Polym. Bull.* **1983**, *9*, 208–215.

Part II

Objectives and strategy

CHAPTER 4

CONTEXT AND AMBITIONS: IN QUEST FOR SMART HEALABLE MATERIALS

Abstract

Smart and healable materials undoubtedly constitute future technological developments that already impact our everyday life. In this context, the goal of this thesis is to access novel polymeric materials with unprecedented control over their structure, organization and dynamics.

4.1 The quest for smart healable materials

Since polymeric materials constitute the technological driving force of the 20th century, the quest for implementing self-healing properties into polymers is sustained. Despite the usually huge amount of intellectual and hand- or machine-driven efforts put in their fabrication, most modern materials are indeed still subject to mechanical destruction as well as chemical degradation, restricting their use. Nevertheless, a short look at superficial injuries in animal or even plant organisms has made the possibilities of self-repair and properties restoration obvious. Since the early 2000's, three conceptual approaches have been thus developed toward self-healing polymer materials, each having advantages and limitations: capsule-based, vascular, and intrinsic healing systems (Figure 4.1). [1,2]

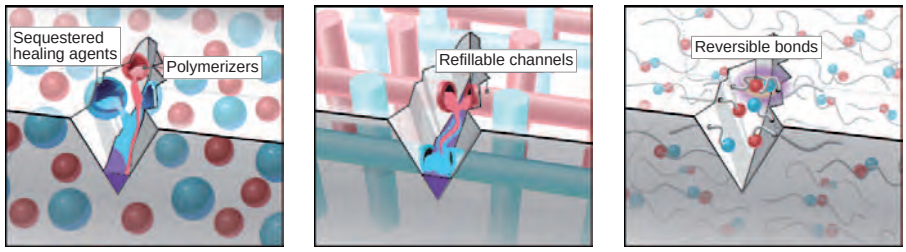

(a) Capsule-based (b) Vascular (c) Intrinsic

Figure 4.1 – Different approaches to self-healing. [1]

Capsule-based self-healing materials sequester the healing agent in discrete capsules (Figure 4.1 (a)). When ruptured, capsules release healing agents in damaged regions and material repairs autonomously, *i.e.*, without external intervention. Unfortunately, micro-capsules are finite, which limit the number of local healing events. Taking the circulatory system as source of inspiration, vascular methods rely on a network of channels to deliver healing agent to the damaged site (Figure 4.1 (b)). The connectivity of breached area allows large amounts of agent to be transported, and hence multiple local healing events. Nevertheless, the complexity of vascular networks presents a daunting challenge for material chemists. Finally, intrinsic systems exploit the reversible nature of physical or certain chemical bonds to incorporate healing abilities directly into the material (Figure 4.1 (c)). While multiple healing events

are possible, these materials usually rely on chain mobility or melting of phases to occurs, which require some external energy. [1,2]

In parallel to the quest for self-healing, "smart" materials, *i.e.*, whose properties can be significantly changed in a controlled fashion by external triggers, are experiencing an unprecedented development over the last few years. As a mirror in modern society, the practical demand for "smart" devices has overwhelmed all other forms of computing and communications in a very short time (Figure 4.2). They consist in smart phones, TVs, glasses, watches, bands (*etc.*) that can operate to some extent interactively and autonomously to fulfill individual requirement. Analogously, "smart" materials have been designed to support a range of properties pertaining to be used in various environments (Figure 4.3). At the basis of those materials lie intelligent (macro-)molecules having the capability to adapt their conformational structures and/or properties in response to external stimuli such as stress, temperature, moisture, pH, redox, electric or magnetic fields... [3,4]

Figure 4.2 – The world of smart devices.

Many complex issues of physico-chemical principles inherent to smart and healable materials are interlinked, prompting the need to under-

stand the underlying processes. Indeed, only materials able to sense the damaging force, thus showing inherent "smartness", can transform it into autonomous healing events. The interlocked design of smart and healable materials is therefore a multidisciplinary process requiring knowledge of their structure, dynamics, and organization, as well as a thorough understanding of physico-chemical mechanisms lying beyond them. Thus, reliably testing, understanding, and further controlling the mechanical properties of smart healable polymers constitute a crucial aspect to meet specific requirements of any field of application. In this continuity, controlling the properties of designed materials in a wide range contributes to broaden their field of application, in a sustainable future with both economic and environmental challenges. [2]

Nano-carrier *Nano-machine* *Molecular motor*

(a) Molecular design

Photochromism *Electrochromism* *Thermochromism*

(b) Stimuli-responsiveness

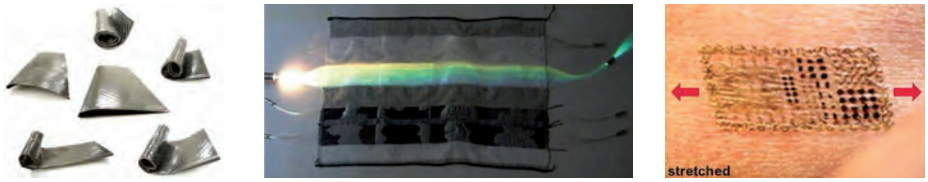

Shape-memory *Textile* *Skin-electronic*

(c) Improved functionality

Figure 4.3 – Smart materials: design, responsiveness and functionality.

4.2 Aims of the present project

With the concern of approaching applied materials, the fundamental goal of this thesis is to gain control over the structure, organization and dynamics of polymeric systems by exploiting a combination of classical macromolecular architectures and supramolecular interactions. The creation of structurally defined materials will be possible by applying the concept of hierarchical self-assembly, *i.e.*, the spontaneous non-covalent organization of molecules and macromolecules over distinct multiple levels (Figure 4.4), in which the assembly processes gradually decrease in strength.[5,6] In turn, the hierarchical structure of the assemblies will lead to a parallel hierarchy of dynamic processes, capable of adjustments in response to a wide variety of stimuli including temperature, chemical environment, and mechanical stress.

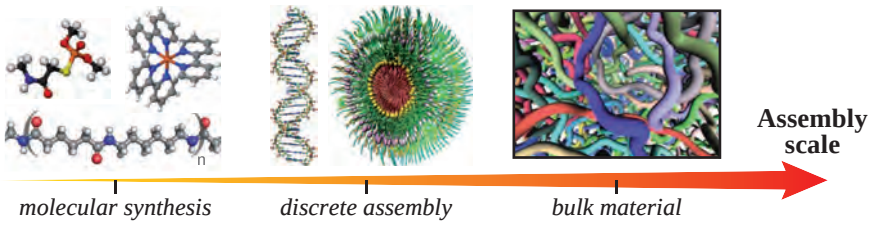

Figure 4.4 – Hierarchical self-assembly across scales.

The designed materials are intended to be tunable and flexible in terms of both structure and properties. To achieve that goal and further impart stimuli-responsiveness, a precise control over the architecture and functionality of macromolecular species constituting the self-assembled materials is required. These building blocks will be then organized over multiple dynamic levels of assembly, providing fine tuning over intermolecular forces involved in the assembly processes. Finally, the rheological behaviour of the accordingly obtained materials will be thoroughly characterized in order to establish relationships between their structure, dynamics and mechanics. In particular, the present work aims at studying in details the dynamic mechanical response of these systems to various external stimuli.

The proposed thesis is thus a highly inter-disciplinary project that combines polymer synthesis, macromolecular engineering, supramolecular assembly, structural characterization, and rheological measurements.

In regards to prior art, the novelty of the approach precisely relies on the hierarchical assembly of stimuli-responsive block copolymers into supramolecular soft materials. By defining a new strategy for designing novel materials and exploring their potential in regard to contemporary needs, this thesis offers exciting new opportunities for stimuli-responsive structures exhibiting reversible tunable properties, with potential applications in material sciences.

Bibliography

[1] Blaiszik, B. J.; Kramer, S. L. B.; Olugebefola, S. C.; Moore, J. S.; Sottos, N. R.; White, S. R. *Annu. Rev. Mater. Res.* **2010**, *40*, 179–211.
[2] Binder, W. H. *Self-healing polymers: From principles to applications*; Wiley-VCH, 2013; pp xix, 425.
[3] Addington, D. M.; Schodek, D. L. *Smart materials and new technologies: For the architecture and design professions*; Architectural Press: Amsterdam ; Boston, 2005; pp xi, 241.
[4] Dai, L. *Intelligent macromolecules for smart devices*; Engineering materials and processes; Springer: New York, 2003; pp xvi, 496.
[5] Ikkala, O.; ten Brinke, G. *Chem. Commun.* **2004**, *40*, 2131–2137.
[6] Elemans, J.; Rowan, A.; Nolte, R. *J. Mater. Chem.* **2003**, *13*, 2661–2670.

CHAPTER 5

DESIGN STRATEGY TOWARD SMART MATERIALS WITH TUNABLE PROPERTIES

Abstract

In this chapter, a theoretical approach is developed to address the goal of this thesis project, drawing the design guidelines of model supramolecular polymer networks. A detailed strategic plan is provided, delimiting three main tasks: the synthesis of macromolecular building blocks, their self-assembly into supramolecular gels, and the characterization of their rheological response.

5.1 Prior theoretical approach

In order to design materials with self-healing properties, a reversible bonding system is required, which establishes a dynamic binding equilibrium. Therefore, the presence of non-covalent linkages such as hydrogen bonds, π–π-stacking, metal–ligand complexes or attracting ions is a crucial element in any hypothetical material. Among those secondary forces, coordination bonds are particularly attractive since those interactions are relatively strong and give access to a wide library of organic ligands, along with appropriated metal ions including nearly half the periodic table.[1] In supramolecular architectures, metal–ligand association can be further combined with many other non-covalent binding interactions, in an orthogonal way.[2,3] Finally, significant changes in the structure, kinetic and thermodynamic stability of the resulting assemblies can be readily achieved depending on the metal–ligand pair.[4,5]

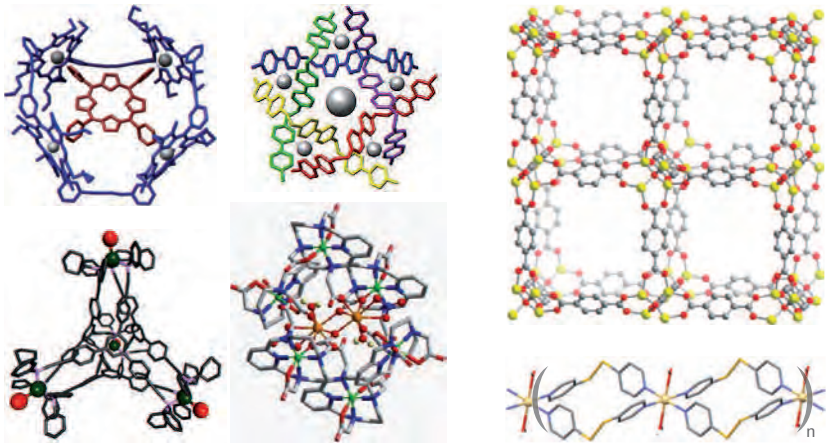

(a) Discrete structures (b) Extended structures

Figure 5.1 – Some examples of supramolecular coordination structures.

Superstructures constructed from coordination bonds include various architectures, ranging from discrete two- and three-dimensional motifs[6–8] to polymeric structures such as coordination polymers[9–12] or metal–organic frameworks (Figure 5.1).[13–15] However, the latter usually fragment into small building blocks upon dissolution and suffer the

loss of their polymeric nature. Indeed, most properties of polymer materials require a continuous covalent bonding between monomer units. To avoid the lack of traditional polymer-like properties, the coordination motif should be thus introduced into a covalent macromolecular architecture.

In the recent years, telechelic star polymers, *i.e.*, bearing a functional group at each arm extremity, have risen as promising precursors of supramolecular materials with model structure.[16–19] Indeed, they allow network formation with close to regular spacing of the cross-links, assuming that the different arms of the star are of comparable lengths. However, varying the functionality of such systems typically requires a control over the number of star branches (Figure 5.2), which can be synthetically challenging or restricted. In particular, reaching high degree of functionality is generally constrained by enhanced steric hindrance in multi-arm star shell.[20]

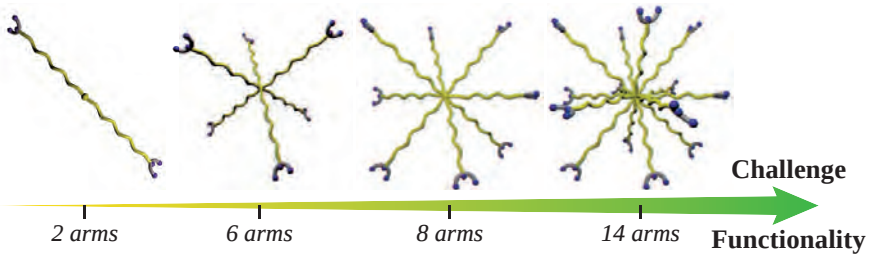

Figure 5.2 – Functionality of star-like telechelic building block.

To circumvent the major drawback of classical synthetic strategies, "arm-first" approaches can be employed in the synthesis of star-like polymers. With living or controlled polymerization techniques as tools, this strategy involves the growth of the linear polymer arms capable of joining their extremities to form a multi-arm star.[21,22] In a practical point of view, this strategy has the advantage of precisely controlling the arm length, and enabling synthesis of miktoarm star polymers, containing arms of mixed sizes or chemical identities.[22,23]

In the "arm-first" synthesis of star polymers, the formation of the multi-arm structure is usually achieved by reaction of cross-linkable units located at one chain extremity.[21,22] A more conceptual approach developed in this work takes advantage of the self-assembly behaviour of

block copolymers into core–corona micelles (Figure 5.3). Unlike conventional star polymer, block copolymer micelles are dynamic entities whose stability depends on the strength of the association. Following this idea, the size, morphology and functionality of the self-assembled aggregates can be further controlled according to the length of the different block constituting the copolymer, along with the conditions employed during the self-assembly process. In addition, it provides the system with additional degree of complexity and versatility, that can be used to fine tune the properties and dynamics of the self-assembled material. Finally, this intermediate level of assembly can be targeted by appropriate stimuli, addressing either the core or the corona of the micellar objects.

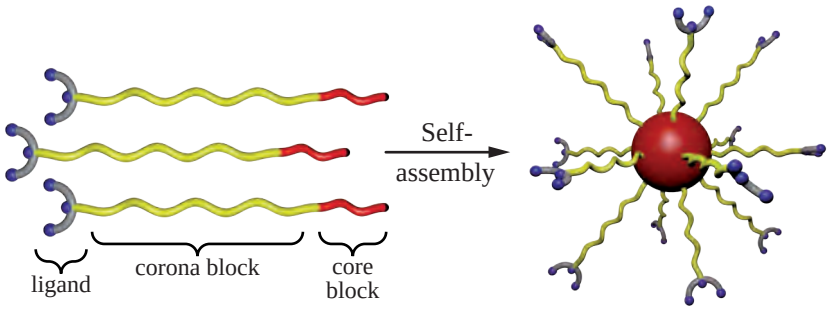

Figure 5.3 – Using self-assembly of block copolymers toward functionalized star-like architectures.

Decorated with coordination motifs at the end of each coronal chains, the micellar nano-objects illustrated in Figure 5.3 would constitute formidable precursors for three-dimensional assemblies. Assuming the coordination of two or more ligands around a metal centre, adding metal cations to the system would trigger the formation of active metallo-bridges between micellar nano-structures. Above a certain percolation threshold, the formation of an inter-connected network of micelles is expected, reaching the final level of organization schematized in Figure 5.4. This non-covalent network may uniformly extend over the whole volume of liquid media, which structurally defines supramolecular polymer gels. Due to their highly complex structure and organization, such materials are suited to serve as ideal systems for studying dynamics and thus self-healing properties. In addition, the surrounding environment of the network is a perfect media for transmission of numerous stimuli, such as light, pH or redox.

In the present strategy, an evident way to further impart responsiveness over the multiple hierarchical levels consists in incorporating stimuli-responsive polymer sequences directly in the self-assembled network. Practically, this can be easily achieved prior any self-assembly process, *i.e.*, during the synthesis of the macromolecular building blocks depicted in Figure 5.3. In this respect, stimuli-sensitive polymer sequences can be used as core-forming blocks to control the self-assembly into micelles. In addition, other smart sequences can be employed as corona-forming blocks, offering the possibility to modulate the conformation of chains bridging micellar cores. In parallel, the stability of metal–ligand junction can be addressed by appropriate stimuli, such as competitive species.

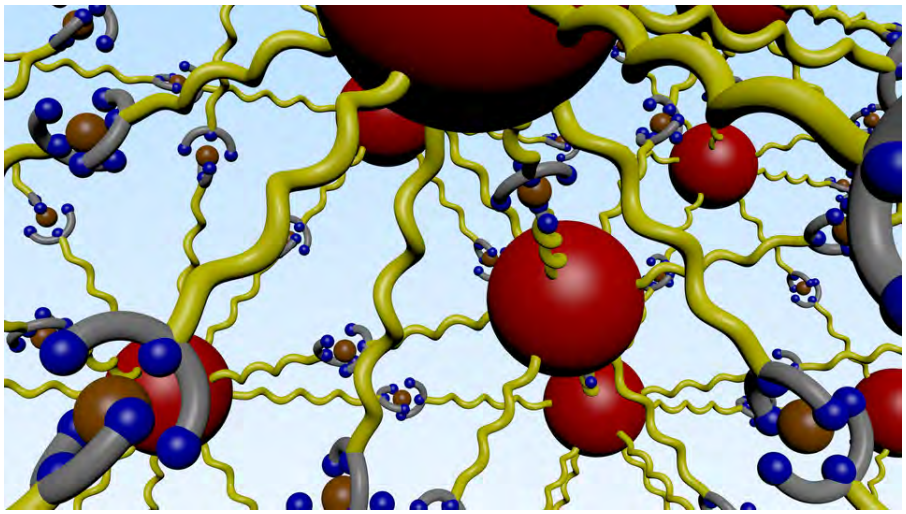

Figure 5.4 – Inner structural view of a metallo-supramolecular network of micelles.

5.2 Detailed strategic plan

The present research project can be subdivided into a number of individual, although interconnected, tasks that are developed in the following chapters. The latter are summarized in Figure 5.5 in the form of a diagram showing graphically the material implementation from the molecular to macroscopic scale.

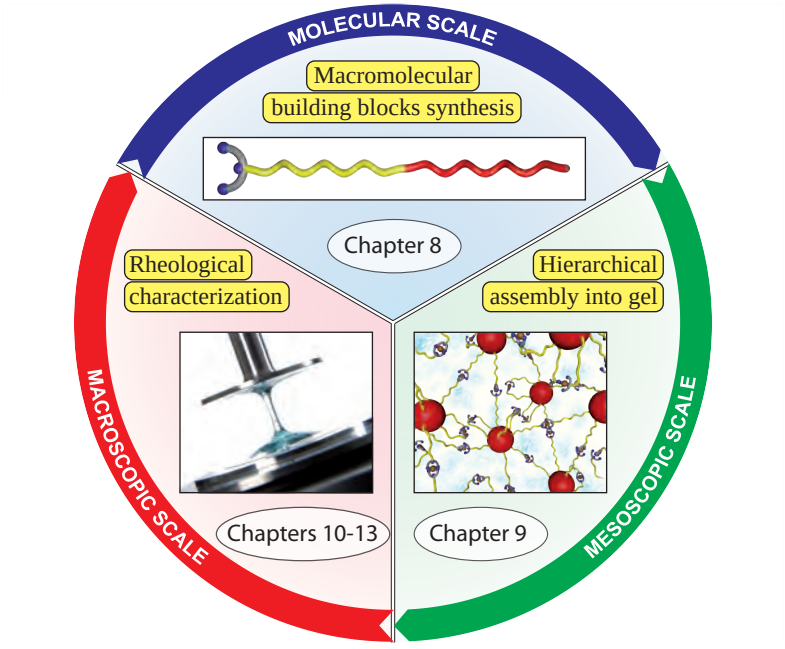

Figure 5.5 – Overall strategy of the present project.

5.2.1 Building block synthesis

To really engineer complex supramolecular architectures with macromolecules in exploitable quantities, several points have to be taken into account. First, the supramolecular building units should offer a high binding affinity. Then, the association strength of the resulting non-covalent interactions should be tunable over a wide range. In addition, the supramolecular unit has to be accessible commercially, or via short synthetic procedures. Finally, functional groups should be easily introduced to allow further chemistries. In this respect, the 2,2':6',2"-terpyridine (tpy) has been selected as a coordination motif fulfilling all these requirements.[24] Beside its high binding affinity for transition metal ions,[25,26] interesting luminescence properties may further result from the binding with lanthanide ions.[27,28]

To introduce the coordination motif in the architecture of macromolecular chains, two main strategies can be envisaged that consist in either the post-modification of pre-synthesized polymers, or the use of functional reactants during the polymerization process.[29] If both ap-

proaches present advantages and drawbacks, the second is more versatile in nature, offering better control over the number and position of incorporated functional groups. Following this strategy, a synthetic route toward block copolymers having a functional terminus is proposed, using modified (macro-)initiators to ensure the incorporation of the terpyridine moiety, as illustrated in Figure 5.6.

The building of structurally defined materials with reliable properties implies that block copolymers can be synthesized with well-defined molecular characteristic features, motivating the use of living or controlled polymerization techniques. Among them, reversible addition–fragmentation chain transfer polymerization is particularly attractive given the wide range of polymerizable monomers, the mild synthetic conditions, and its compatibility with various functional groups, including chelating ligands.[30,31] Therefore, this controlled radical polymerization technique opens the way toward well-defined macromolecular architectures containing two or more responsive components.[32]

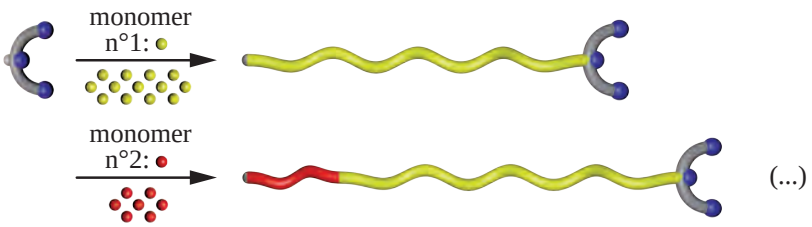

Figure 5.6 – Multi-step synthesis of functional block copolymers.

In practice, numerous monomeric units can be reasonably considered in the frame of this project, including styrenes, (meth-)acrylates, and (meth-)acrylamides. From those, three well-studied candidates are selected to afford the macromolecular building blocks shown in Figure 5.7, each having specific characteristics: polystyrene (PS), poly(*N*-isopropylacrylamide) (PNIPAAm), and poly(2-(dimethylamino)ethyl methacrylate) (PDMAEMA). While the first leads to strong association in water, the two others develop a specific response to variations in temperature and pH.[33,34] In addition, the degree of polymerization of the different blocks can be readily controlled during their synthesis.

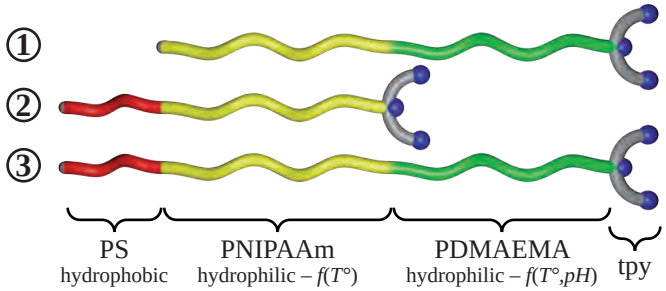

Figure 5.7 – Various macromolecular building blocks having terpyridine terminus.

5.2.2 Hierarchical assembly

This task consists first in studying the micellization of the prepared diblock and triblock copolymers. The accordingly obtained micelles indeed represent the first level of self-assembly in the context of the hierarchically-organized materials that will be further investigated in the project (Figure 5.8). Micellization can be achieved by dissolution of the block copolymers in a selective solvent for the corona-forming blocks. Moreover, the solvating media should be able to solubilize metal salts involved in the second level of self-assembly. Therefore, water appears as an appropriate choice, being a non-solvent for polystyrene but able to solubilize PNIPAAm and PDMAEMA blocks depending on pH and temperature. In case of PNIPAAm-*b*-PDMAEMA-tpy, micellization will be triggered in water by changing temperature and pH. The PNIPAAm-*b*-PDMAEMA-tpy is indeed a typical double hydrophilic copolymer that contains two water soluble polymer blocks at room temperature and in the complete pH range. Increasing the temperature above the LCST of the PNIPAAm blocks will result in the formation of micelles containing a PNIPAAm core and PDMAEMA coronal chains.

In practice, light scattering techniques will constitute essential tools to characterize the formation of micellar nano-structures form both diblock and triblock copolymers. Notably, dynamic light scattering (DLS) will allow measuring the hydrodynamic radius of the micelles and its variation with the nature and length of constituting blocks. In complement, microscopy techniques will be used for direct imaging of micellar objects at the nanometre scale, probing their dimension and morphology. Additionally, the present project aims at studying in details the response

of these systems towards the application of an external stimulus.

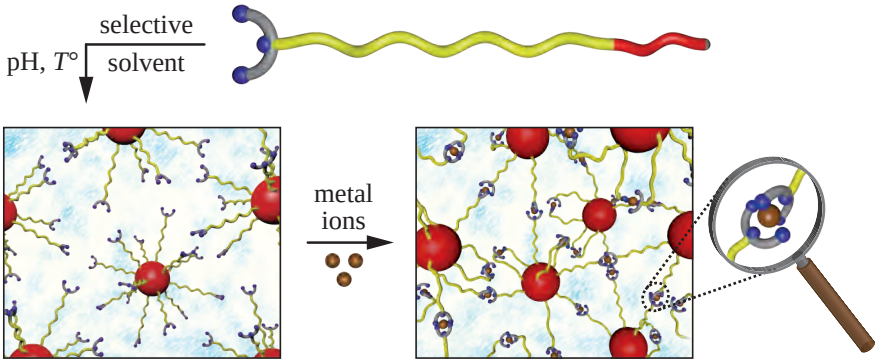

Figure 5.8 – Hierarchical assembly of ligand end-functionalized block copolymers into supramolecular gels.

The various building blocks shown in Figure 5.7 are expected to provide us with a wide landscape of properties for the final materials. The latter will be obtained by adding transition metal ions to concentrated micellar solution, creating reversible association. Indeed, block copolymer micelles with coordination moieties located at the extremity of coronal chains will be self-assembled to create an additional level of organization, as illustrated in Figure 5.8. Special emphasis will be placed on the formation of gels whose properties will be modulated by the micelle concentration, the choice of the metal ion and the metal-ligand ratio.

By combining stimuli-responsive polymer blocks with metal–ligand bonds, multi-responsive systems will be designed, creating materials with enhanced control over their properties. On one hand, using stimuli-sensitive coronal block will allow us to control the swelling of the supramolecular gel by changing the pH or temperature of the surrounding media. On the other hand, stimuli-responsive properties could also be imparted to the core-forming block(s), leading to the assembly, disassembly or strengthening of micellar cores upon application of the stimulus.

5.2.3 Rheological characterization

Generally speaking, associating polymers, *i.e.*, macromolecules containing short chemical sequences interacting with each other, constitute a fascinating class of materials because of their rich rheological

behaviour.[35–37] Their rheology is mainly dictated by the nature and intrinsic stabilities of the transient associations, which confer strength and dynamics to the self-assembled network.[38,39] Accordingly, the richness of our model system is expected to be reflected in the complexity of its hierarchical organization. Indeed, the latter may adopt numerous configurations shown in Figure 5.9, that can be presumably controlled depending on the characteristics of the associating blocks and the conditions for their self-assembly.

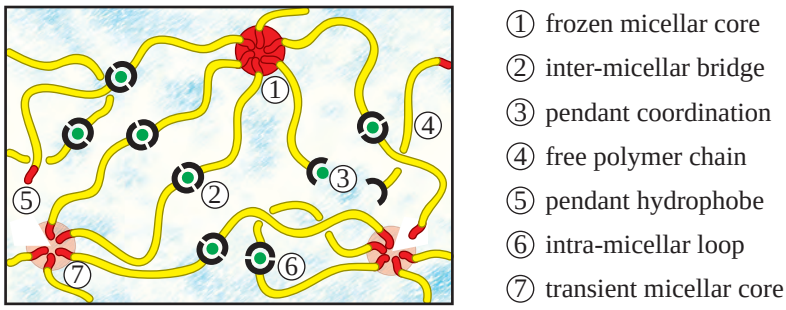

Figure 5.9 – Richness of network configurations in metallo-supramolecular micellar gels.

As the heart of this project, the synthesized materials will be thus thoroughly characterized to unravel their rheological response. The variety of block copolymers and resulting micellar structures achievable through the proposed synthetic routes being truly enormous, viscoelastic characteristics are expected to vary by orders of magnitude, ranging from low viscous solutions to highly elastic gels. Therefore, the main characterization technique will be based on rotational rheometry, using plate–plate geometry modified with a solvent trap to prevent evaporation.

The primary characterization method will be oscillatory frequency sweep tests performed in the linear regime. This will allow isolating the contribution of the metallo-bridges between the micellar cores to the whole dynamic response of the system. The strength of metal–ligand interactions and degree of segregation of micellar cores, *i.e.*, glassy or rubbery, will be varied in order to understand their influence on gel formation and the rheological behaviour of micellar suspensions. To this end, copolymers with standardized composition and molecular weight will be used, keeping also the temperature and the concentration con-

stant.

The amplitude of the viscoelastic response of the investigated material will be controlled by playing on the subtle balance between intra- and inter-micellar associations. In this respect, increasing the volume fraction of solvent within the system should reduce the occurrence of inter-micellar associations. In parallel, the concentration of metal–ligand complexes only can be reduced by dilution with non-functionalized copolymers of identical composition and molecular weight. Finally, the application of external stimuli that decrease the solvent quality for the coronal chains will be tested as an additional control parameter to tune the micellar interaction.

Of particular interest will be the investigation of the respective influence of stimuli (temperature, pH, *etc.*) on structure and dynamics of the synthesized supramolecular gels. Furthermore, the effect of the phase transitions of responsive block copolymer segments on the dynamic mechanical properties of the materials will be investigated. Among stimuli, a particular attention will be paid to mechanical stress, with the possibility to achieve reversible breaking of non-covalent junctions structuring the transient network. Therefore, the rheological characterization will extend into the non-linear regime, with large amplitude oscillatory shear and start-up flows, providing further insight into the structure and its stability.

Bibliography

[1] Lawrance, G. *Introduction to coordination chemistry*; Wiley: Chichester, 2009; pp xiii, 290.
[2] Li, S.-L.; Xiao, T.; Lin, C.; Wang, L. *Chem. Soc. Rev.* **2012**, *41*, 5950–5968.
[3] Hu, X.-Y.; Xiao, T.; Lin, C.; Huang, F.; Wang, L. *Acc. Chem. Res.* **2014**, *47*, 2041–2051.
[4] Goshe, A. J.; Steele, I. M.; Ceccarelli, C.; Rheingold, A. L.; Bosnich, B. *Proc. Natl. Acad. Sci. U. S. A.* **2002**, *99*, 4823–4829.
[5] Van Leeuwen, H. *Electroanalysis* **2001**, *13*, 826–830.
[6] Chakrabarty, R.; Mukherjee, P. S.; Stang, P. J. *Chem. Rev.* **2011**, *111*, 6810–6918.
[7] Swiegers, G.; Malefetse, T. *Chem. Rev.* **2000**, *100*, 3483–3537.
[8] Smulders, M. M.; Riddell, I. A.; Browne, C.; Nitschke, J. R. *Chem. Soc. Rev.* **2013**, *42*, 1728–1754.

[9] Nguyen, P.; Gómez-Elipe, P.; Manners, I. *Chem. Rev.* **1999**, *99*, 1515–1548.
[10] Williams, K. A.; Boydston, A. J.; Bielawski, C. W. *Chem. Soc. Rev.* **2007**, *36*, 729–744.
[11] Archer, R. D. *Inorganic and organometallic polymers*; Wiley: New York, 2001; p 264.
[12] Archer, R. D. *Coord. Chem. Rev.* **1993**, *128*, 49–68.
[13] James, S. L. *Chem. Soc. Rev.* **2003**, *32*, 276–288.
[14] Kitagawa, S.; Kitaura, R.; Noro, S. *Angew. Chem. Int. Ed.* **2004**, *43*, 2334–2375.
[15] Rowsell, J.; Yaghi, O. *Microporous Mesoporous Mater.* **2004**, *73*, 3–14.
[16] Rossow, T.; Seiffert, S. *Polym. Chem.* **2014**, *5*, 3018–3029.
[17] Rossow, T.; Habicht, A.; Seiffert, S. *Macromolecules* **2014**, *47*, 6473–6482.
[18] Ueki, T.; Takasaki, Y.; Bundo, K.; Ueno, T.; Sakai, T.; Akagi, Y.; Yoshida, R. *Soft Matter* **2014**, *10*, 1349–1355.
[19] Asoh, T.-A.; Yoshitake, H.; Takano, Y.; Kikuchi, A. *Macromol. Chem. Phys.* **2013**, *214*, 2534–2539.
[20] Wang, R.; Geven, M.; Dijkstra, P. J.; Martens, P.; Karperien, M. *Soft Matter* **2014**, *10*, 7328–7336.
[21] Liu, P.; Landry, E.; Ye, Z.; Joly, H.; Wang, W.-J.; Li, B.-G. *Macromolecules* **2011**, *44*, 4125–4139.
[22] Gao, H.; Matyjaszewski, K. *J. Am. Chem. Soc.* **2007**, *129*, 11828–11834.
[23] Khanna, K.; Varshney, S.; Kakkar, A. *Polym. Chem.* **2010**, *1*, 1171–1185.
[24] Schubert, U.; Hofmeier, H.; Newkome, G. R. *Modern terpyridine chemistry*; Wiley-VCH: Weinheim, 2006; pp viii, 229.
[25] Holyer, R. H.; Hubbard, C. D.; Kettle, S. F. A.; Wilkins, R. G. *Inorg. Chem.* **1966**, *5*, 622–625.
[26] Hogg, R.; Wilkins, R. *J. Chem. Soc.* **1962**, 341–350.
[27] Kotova, O.; Daly, R.; dos Santos, C.; Boese, M.; Kruger, P.; Boland, J.; Gunnlaugsson, T. *Angew. Chem. Int. Ed.* **2012**, *51*, 7208–7212.
[28] Han, F.; Higuchi, M.; Ikeda, T.; Negishi, Y.; Tsukuda, T.; Kurth, D. *J. Mater. Chem.* **2008**, *18*, 4555–4560.
[29] Lohmeijer, B. G. G.; Schubert, U. S. *J. Polym. Sci., Part A: Polym. Chem.* **2003**, *41*, 1413–1427.
[30] Moad, G.; Chiefari, J.; Krstina, J.; Mayadunne, R.; Postma, A.; Rizzardo, E.; Thang, S. *Polym. Int.* **2000**, *49*, 993–1001.
[31] Perrier, S.; Takolpuckdee, P. *J. Polym. Sci., Part A: Polym. Chem.* **2005**, *43*, 5347–5393.
[32] Smith, A. E.; Xu, X. W.; Mccormick, C. L. *Prog. Polym. Sci.* **2010**, *35*, 45–93.
[33] Roy, D.; Brooks, W. L. A.; Sumerlin, B. S. *Chem. Soc. Rev.* **2013**, *42*, 7214–7243.
[34] Dai, S.; Ravi, P.; Tam, K. C. *Soft Matter* **2008**, *4*, 435–449.
[35] Leibler, L.; Rubinstein, M.; Colby, R. *Macromolecules* **1991**, *24*, 4701–

4707.
[36] Rubinstein, M.; Semenov, A. *Macromolecules* **2001**, *34*, 1058–1068.
[37] Vaccaro, A.; Marrucci, G. *J. Non-Newtonian Fluid Mech.* **2000**, *92*, 261–273.
[38] Rubinstein, M.; Dobrynin, A. *Trends Polym. Sci.* **1997**, *5*, 181–186.
[39] Winnik, M.; Yekta, A. *Curr. Opin. Colloid Interface Sci.* **1997**, *2*, 424–436.

Part III

State of the art

CHAPTER 6

BUILDING METALLO-SUPRAMOLECULAR POLYMER GELS – A LITERATURE REVIEW

Abstract

Through an in depth literature review, this chapter aims to situate the proposed strategy within the context of polymeric networks that are held together by metal–ligand coordination bonds. At first, the concept of the so-called metallo-supramolecular polymer gels (MSPGs) is briefly introduced. Then, the different routes towards MSPGs are described, with relevant examples from the literature. Doing so, a particular accent is put on the stimuli-responsiveness that confers the metallo-assembly to this class of supramolecular materials.

6.1 Structural definitions and concepts

6.1.1 Metallo-supramolecular polymers

When entering the field of supramolecular chemistry, the terms "coordination polymer"[1–5] or "metallo-polymer"[6–8] are commonly used to designate macromolecular assemblies constructed by a supramolecular approach via metal–ligand coordination.[9] In particular, metallo-supramolecular polymers (MSPs) are recognized as a subclass of metal-containing polymers[10–14] in which the coordination bond is dynamic and reversible.[3,7,9,15]

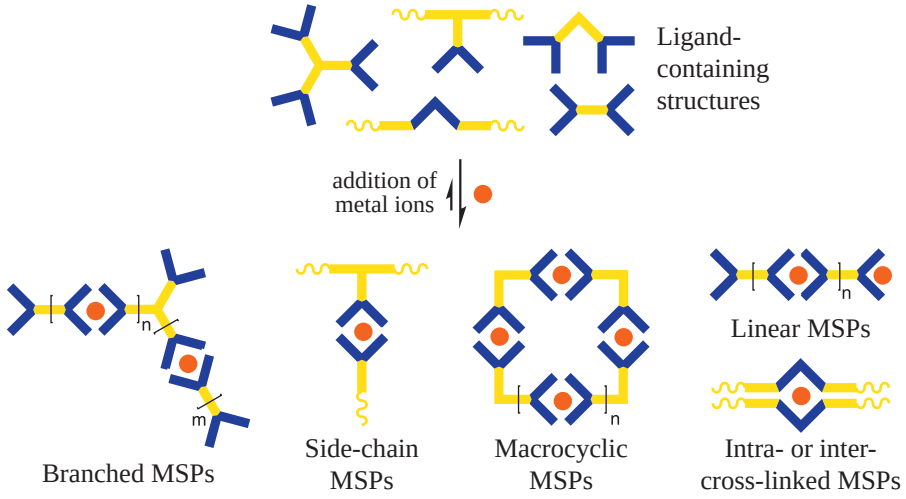

Figure 6.1 – Schematic representations of various metallo-supramolecular polymer structural motifs.[15]

A simple route to MSPs consists in the autonomous assembly of ligand containing structures through the addition of metal cations[2,10,16–22]. The metallo-supramolecular junctions can be incorporated either within the backbone, as part of the side chain, and/or as part of a cross-linking/branching site, opening the access to numerous structural motifs, such as linear,[18–27] side-chain,[28–34] inter-cross-linked,[35–38] or macrocyclic MSPs[39–49] (Figure 6.1).

6.1.2 Dynamic and stability

Not all metallo-polymers show thermo-mechanical reversibility at the metal coordination site. In fact, the coordinative bond can vary more or less continuously from strong linkage, yielding to static or irreversible binding of the metal, to labile and weak interaction, in agreement with dynamic and reversible binding.[50] In case of static metallo-polymers, the binding strength between metal ions and ligands is relatively large while ligand exchange reactions in solution are extremely slow under normal conditions. As a consequence, this class of metallo-polymers displays the characteristics of traditional covalent polymers and can be thus characterized by conventional analytical tools, like ultra-centrifugation or size exclusion chromatography.[51–55]

On the opposite, dynamic metallo-supramolecular interactions result inevitably in a continuous rupture and formation of the polymer chains until a binding equilibrium is reached. Depending on the concentration, reversible metallo-polymers in equilibrium are thus mixtures of linear polymer chains of a given polymerization degree and cyclic oligomer species.[50,56–58] While the degree of supramolecular polymerization is dominated by the complex binding strength, the dynamic of such materials is more dictated by the rate at which ligands exchange.[59–62]

The kinetic lability and thermodynamic stability of MSPs rely mostly on the nature of the metal and ligand pair. While most of the metal–ligand complexes from the first row transition metals are labile,[9] the strength and inertness of the association tend to growth with the second and third row transition metals.[56,63] In addition to transition metal, lanthanoid ions also form kinetically labile but thermodynamically stable complexes in combination with a large library of organic ligands bearing either nitrogen-or oxygen-donor atoms.[64,65] Metal complexes can also take benefit of the chelate effect when used in combination with polydentate ligands, *e.g.*, bipyridine, terpyridine or phenanthroline,[9,14,32,66,67] that can coordinate orders of magnitude more strongly than monodentate ligands.

In conjunction with the intrinsic stability of the metallo-assembly, environmental variables also exert a significant influence on the strength of the binding. Beside the concentration in coordination species, the solvent nature will play a major role on the lability of the metal–ligand complexes.[24,68] At the limit, MSPs that are designed in non-coordinating

solvents will not exhibit any further reversible behaviour. On the opposite, coordinative solvents can dramatically alter the dynamics of metallo-polymers by influencing the dissociation and exchange mechanisms between metal–ligand complexes, triggering fast-equilibration of the supramolecular polymers. Accordingly, coordinating counter-ions will have comparable effects on the dynamic of metallo-supramolecular polymers when acting as competitive species through ligand displacement.[69]

Substituent of the ligand, *e.g.*, the polymer chain itself, may further sensibly affect the kinetic rate constants for formation and dissociation of metallo-complexes through steric[70] or electronic donating/withdrawing[71] effects. Through stretching of polymer chains, mechanical forces were also demonstrated to dramatically affect the dynamics of coordination bonds. Even in organic solvents, they can indeed be reversibly broken when subjected to mechanical stresses like ultra-sonication.[72,73] Last but not least, the temperature constitutes one of the more crucial environmental parameter while playing on the delicate balance between kinetic lability and thermodynamic stability of supramolecular assemblies.[59,74]

6.1.3 Metallo-supramolecular polymer gels

Metallo-supramolecular polymer gels (MSPGs) can be described as a subclass of physical polymer networks,[75,76] swollen in either organic (organogels), ionic (ionogels) or aqueous (hydrogels) solvents, and where linkages between structural components are provided by reversible dynamic coordination bonds. As a structural feature of MSPGs, those coordinative bonds must be present either in the polymeric backbone or as junctions between covalently linked units.

Without distinction, gels that combine labile metal–ligand bonds with other non-covalent interactions in the main-chain can be considered as part of the MSPGs family. On the opposite, fully covalently cross-linked gels with metal complexes on the side-chain[77,78] are regarded as chemical gels. Also, hybrid polymer gels in which covalent cross-links create a permanent scaffold onto which reversible metal–ligand coordinative cross-links are added,[78–84] constitute an intermediate category between physical and chemical gels. Furthermore, metallo-supramolecular polymer networks that do not swell in a certain amount

of solvent [28,85–101] are not to be regarded as gels since they do not incorporate a minimal amount of liquid. Finally, molecular gels, *i.e.*, entangled three-dimensional networks formed by the spontaneous self-assembly of low molecular weight compounds, the so-called "molecular gelator", into fibrous architectures that entrap solvent molecules through surface forces [102–106] that employ metal–ligand coordination as the main driving force are considered apart from their polymeric counterparts since they only involve discrete molecular components.

6.2 Synthetic routes toward MSPGs

Metallo-supramolecular polymer gels have been successfully designed via a multitude of strategies and routes. In practice, they can be classified depending how cross-links are provided through the supramolecular network. Here, three limit categories of MSPGs are distinguished, as illustrated in Figure 6.2. A first category relies on the coordination of ditopic ligands around metal centres that can accommodate at least three ligands (Type I). Another category involves the polyaddition of multitopic ligands with metal ions (Type II). A final category combines the metal–ligand coordination with other supramolecular secondary interactions (Type III).

In MSPGs of type I and II, the formation of a three-dimensional metallo-supramolecular network is conducted by the use of either polyvalent metal ions or multitopic ligand, respectively. In MSPGs of type III, even monotopic ligands can be employed in combination with bivalent metal to yield hybrid supramolecular networks. Following the key concept of hierarchical assembly, where small building blocks are hierarchically organized over two or more levels of assembly [107–114] monotopic ligands can be used as building blocks to build larger multitopic structures that will be then held together by metal–ligand coordination.

Of course, intermediate classes that combine the features or stand between the limits of the three categories of metallo-supramolecular polymer gels are also reported. Most of the time, distinction is easily achieved depending on the type of interaction that ensures cross-linking through the supramolecular network. The following will thus focus on the three aforementioned categories with relevant studies from the literature.

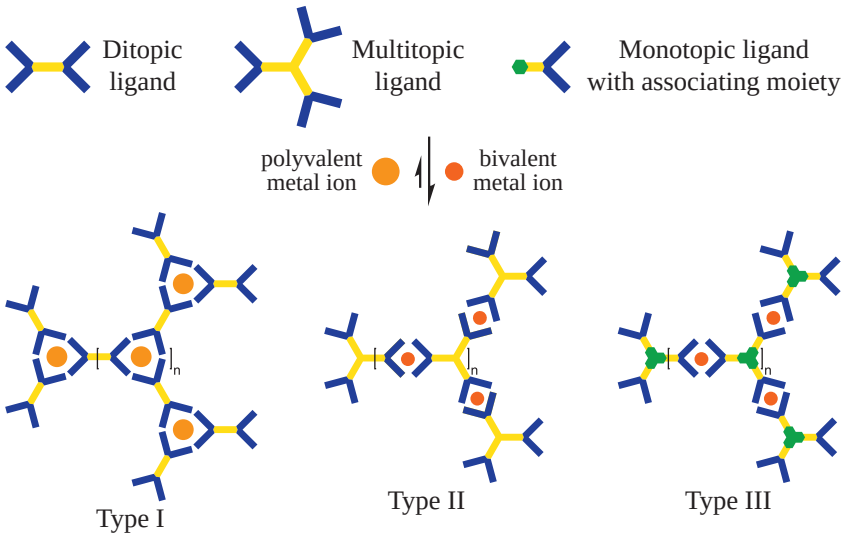

Figure 6.2 – Schematic representation of the different routes to metallo-supramolecular polymer gels.

6.2.1 Metallo-supramolecular polymer gels of type I

Up to now, transition metal ions, as well as lanthanoid ions, have been successfully employed in the elaboration of metallo-supramolecular polymer gels of type I. In combination with appropriate organic ligands, they form associating motifs with a ligand-to-metal stoichiometric ratio larger than 2:1 and, therefore, act as cross-linking points within the network.

6.2.1.1 Transition metal ions as cross-linkers

The use of transition metal ions with ditopic ligands in the formation of stable MSPGs is restricted since their coordination numbers are commonly limited to 6. This approach was however successfully illustrated by the work of Sijbesma and coworkers who prepared ultrasound-responsive reversible coordination networks in chloroform by combining second and third row transition metals with π-acceptor ligands.[115] In their study, diphenylphosphinite telechelic polytetrahydrofuran oligomers were complexed with iridium(I) or rhodium(I) salts in a phosphorous-to-metal stoichiometry of 4:1 to yield MSPGs (Figure 6.3).

Gelation was almost instantaneous for the Rh(I) based gels, but it took approximately 30 min for Ir(I) analogues.

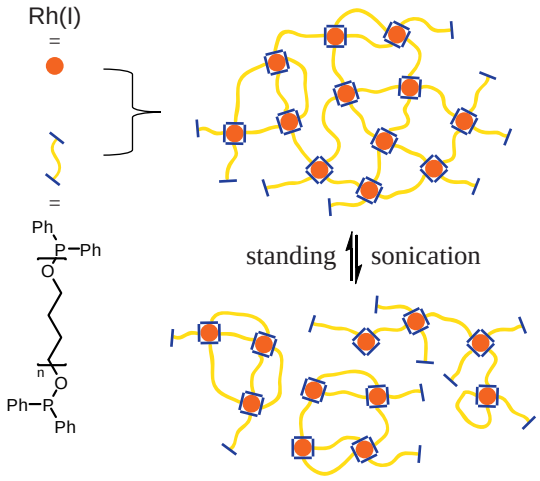

Figure 6.3 – Ultrasound responsive behaviour of MSPGs from diphenylphosphinite telechelic polytetrahydrofurans with rhodium(I) ions.[115]

In the same study,[115] rheological properties of the different metallo-supramolecular gels were compared; Rh(I) gels showed lower modulus than Ir(I) analogues. This dissimilarity was ascribed to the different binding kinetics of Ir(I) and Rh(I) metal ions with diphenylphosphinite ligand. Moving from the second to the third row of the d-block, the rhodium(I) phosphinite complexes are characterized by much faster exchange rates than the iridium(I) phosphinite complexes. The responsive behaviour of MSPGs from diphenylphosphinite telechelic polytetrahydrofurans with Rh(I) ions was demonstrated while sonication resulted in the liquefaction of the gels. Sonication was proposed to lead to ligand exchange, inducing a decrease in the fraction of metal centres in active cross-links, and hence a decrease of the gel fraction (Figure 6.3). Upon standing, the gels recovered at a rate governed by the kinetics of the metal–ligand complexation.

6.2.1.2 Lanthanoid metal ions as cross-linkers

Lanthanoid metal ions are capable of forming strong and dynamic coordination networks. Indeed, their radii are larger than those of transition metal ions, which allow them to coordinate up to three tridentate ligands, thus forming coordination complexes with a ligand-to-metal stoichiometry of 3:1.

In 2004, Vermonden *et al.* reported the formation of hydrosoluble MSPGs using lanthanum(III) and neodymium(III) metal ions and a ditopic oligomeric ligand consisting of flexible oligo(ethylene glycol) spacer end-capped with pyridine-2,6-dicarboxylate tridendate ligands[116,117]. Notably, the use of lanthanoid ions led to solutions with much higher viscosity in comparison with transition metal ions that gave rise to linear metallo-supramolecular polymer chains[58]. The metal–ligand coordination was demonstrated to be reversible with solution viscosities depending on the length of spacer, the oligomer concentration, the temperature, and the oligomer-to-metal ratio.

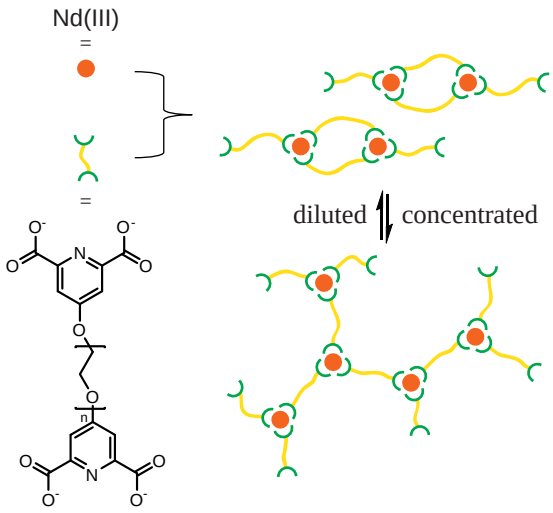

Figure 6.4 – Changes in the structures of MSPGs constructed from ditopic ligand oligomers consisting of an oligo(ethylene glycol) spacer end-capped with tridendate pyridine-2,6-dicarboxylate ligands and Nd(III) metal ions as a function of concentration.[116,117]

Under similar conditions, a comparison of the nuclear magnetic res-

onance spectra and viscosities indicated that the hexa(ethylene glycol) spacer always gives rise to comparatively smaller structures with lanthanoid metal ions than tetra(ethylene glycol). Indeed, long spacers favour the bending of ditopic ligands around a metal centre. As a result, they act as chain stoppers while the ring formations cause the network to stop growing. Even with a short spacer, gelation could only be achieved from concentrated solution. Due to substantial cyclization, the system was assumed to be mainly composed of linear metallo-supramolecular polymer chains (Figure 6.4). The rheological properties of these systems also depend on the ligand-to-metal ratio, which could be ascribed to the formation of different types of ring aggregates. Finally, doping of the gel with transition metal ions inevitably led to its destruction, as only two ligands can coordinate around the metal centre.

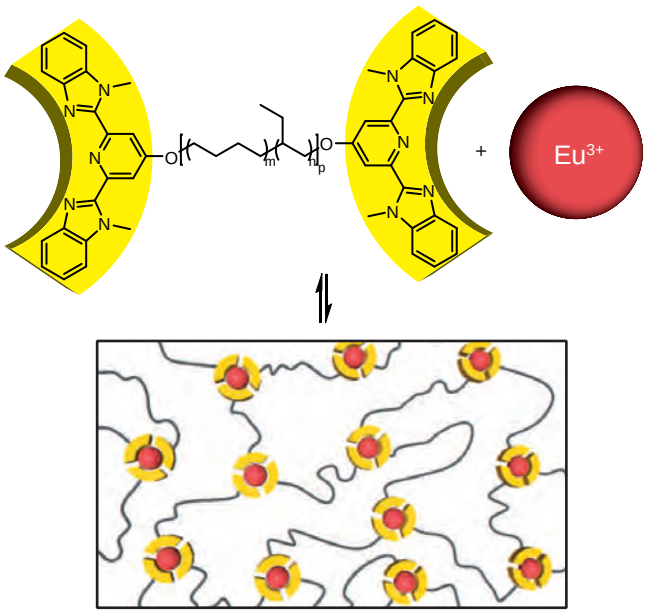

Figure 6.5 – Reversible self-assembly of 2,6-bis(1'-methylbenzimidazolyl)-pyridine end-capped poly(ethylene-co-butylene) and Eu(III) ions into a MSPG. [118]

More recently, Weder *et al.* used the same pyridine-2,6-dicarboxylate ligand as a reference binding motif with the 2,6-bis(1'-methylbenzimidazolyl) pyridine ligand. The first indeed bind much more strongly to europium(III) ions than the second, on which the study was fo-

cused.[118] Precisely, the MSPG studied was a cross-linked network assembled from a europium salt and a telechelic poly(ethylene-*co*-butylene) with 2,6-bis(1'-methylbenzimidazolyl) pyridine ligands at the termini (Figure 6.5), swollen in a mixture of chloroform and acetonitrile. The lanthanoid complexes served both as mechanically responsive binding motifs and as built-in optical probes to quantify the metal complex disassembly process under mechanical strain. Indeed, reversible metal–ligand dissociation occurred upon exposure to ultrasound, which was only possible in case of metallo-supramolecular gels or non-swollen networks. In addition, the influence of the strength of the metal–ligand interactions on the mechano-responsiveness was explored by adjusting the supramolecular motif by the choice of the ligand. Indeed, MSPGs in which the 2,6-bis(1'-methylbenzimidazolyl) pyridine ligands were substituted with more strongly coordinating pyridine-2,6-dicarboxylate ligands did not dissociate upon exposure to ultrasound.

6.2.1.3 Transition and lanthanoid metal ions as cross-linkers

Metallo-supramolecular polymer gels have been also prepared on the basis of ditopic ligand in combination with lanthanoid and transition metal ions together. This approach was first illustrated by Beck and Rowan who combined lanthanoid and transition metal ions with a ditopic oligomer to produce metallo-supramolecular gels that exhibited mechano-, thermo-, and chemo-responses (Figure 6.6), as well as light-emitting properties.[119] In their studies, pyridine bis(imidazolyl) based ditopic ligands were combined in acetonitrile with a small amount of europium(III) or lanthanum(III) ions, as cross-linking components, and cobalt(II) or zinc(II) ions, as linear chain extension binding units (Figure 6.7). All four combinations were tested and exhibited a reversible gel-to-sol transition upon heating. The thermal breakdown of the La(III)–ligand interaction was clearly detected by optical changes upon heating. Furthermore, those gels were also characterized by a pronounced thixotropic behaviour. For example, shaking the Zn(II)/La(III) gel resulted in a free-flowing solution, which thickened again to a jelly-like material upon resting. Since lanthanides are oxophilic, addition of carboxylic acid, such as formic acid, to the Zn(II)/Eu(III) polymer gel dramatically disturbed its mechanical stability.

In another study,[121] Beck and Rowan demonstrated that the nature

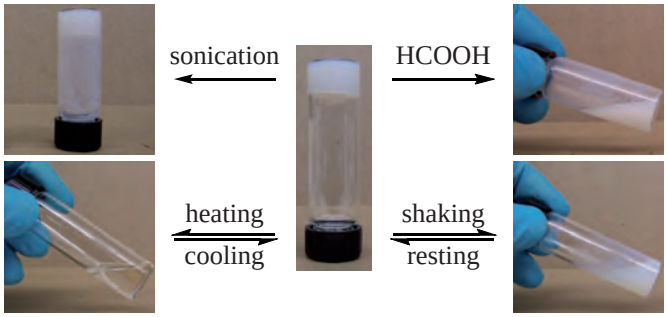

Figure 6.6 – Responsiveness of the acetonitrile swollen Co(II)/La(III) MSPGs prepared by Beck and Rowan.[120]

of the response shown by their systems depends on the metal ion, the counter-ion and the amount of solvent that swells the MSPGs. They investigated in detail the mechanism of response for their supramolecular gels by using a combination of spectroscopic techniques. The proposed thermo-responsive mechanism involved at least a partial decomplexation of the tridentate ligand upon heating from the lanthanide, *i.e.*, the more labile, coordination bonds, which in turn resulted in the breakdown of

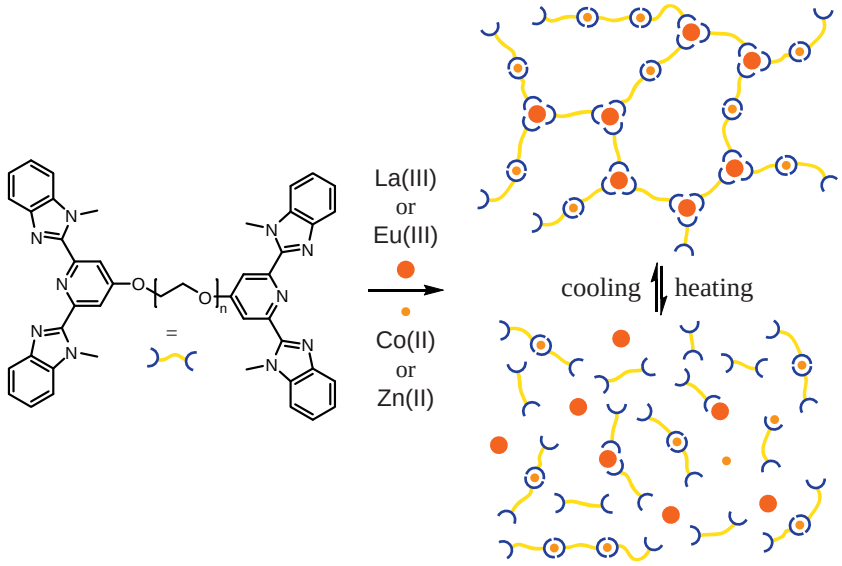

Figure 6.7 – Formation and thermo-response behavior of a MSPG using a combination of lanthanide and transition metal ions mixed with a ditopic oligomer.[119]

the network. At elevated temperature, it appears that the majority of transition metal ions are bound to the ligands, thus resulting in a solution that is mainly a mixture of linear oligomers bound by transition metal ions and lanthanide metal ions bound to none, one or two ligands (Figure 6.7). This emphasizes the use of metal ions with different ligand binding kinetics and strengths in the formation of multi-responsive MSPGs.

6.2.2 Metallo-supramolecular polymer gels of type II

The use of multitopic ligands represents a second approach in the elaboration of MSPGs, in which cross-linking points are ensured by ligands. Nevertheless, using multitopic ligands is not as straightforward as using metal ions that can coordinate numerous ligands. Notably, long spacers are required since they tend to cyclize upon the addition of metal ions. In practice, an unprecedented alternative was found in the use of polymeric ligands, *i.e.*, macromolecular architectures displaying multiple coordination sites along the backbone.

Under specific conditions, polysaccharides,[122–124] cellulose derivatives,[125] and poly(acrylic acid)s[126,127] have been known for a long time to form stable MSPGs in presence of numerous of metal ions. The main drawback of this approach lies in the formation of rather ill-defined systems. Beside linear polymeric ligands, multi-arm star polymers have also proved their applicability in the preparation of metallo-supramolecular networks of type II.

6.2.2.1 Linear polymeric ligands with coordinating groups in the side-chain as cross-linkers

The use of linear polymeric ligands with coordinating groups in the side-chain as cross-linkers was notably illustrated by the work of te Nijenhuis and coworkers. In their studies,[128,129] metallo-supramolecular networks were developed on the basis of partially hydrolysed polyacrylamide that gelated upon the addition of chromium(III) salts. Since amide functionalities were partially converted to coordinating acids, the coordination to Cr(III) ions was shown to be strongly pH-sensitive. While low pH prevented the precipitation of Cr(III) ions of the hydroxide, it protonated the carboxylate groups and made them poor ligands. The narrow

pH region, in which gelation occurred, was reported by dynamic rheological measurements. Under normal conditions, the cross-liking rate was reported to be relatively slow. As a consequence, a dynamic equilibrium was only reached after a long period. Significant acceleration in the process occurred at elevated temperature. Also, addition of a small amount of chromium(II) ions was found to catalyse the gelation. On the other hand, the process could be further slowed down by the addition of citric acid.

Following a similar approach, Tong and coworkers developed redox-sensitive coordination gels from poly(acrylic acid) aqueous solutions and iron(III) metal ions[130]. Indeed, those materials exhibited a reversible gel–sol transition upon switching the redox state of iron ions. In the presence of citrate, ferric ions in the hydrogel were reduced to ferrous ions by sunlight irradiation, which caused dissolution of the gel, as followed by dynamic rheology. The reversibility of the transition was then checked while the poly(acrylic acid) solution was converted back to the supramolecular gel upon oxidation of ferrous to ferric ions for several days, in the dark (Figure 6.8).

(a) Switching gel–sol–gel transition

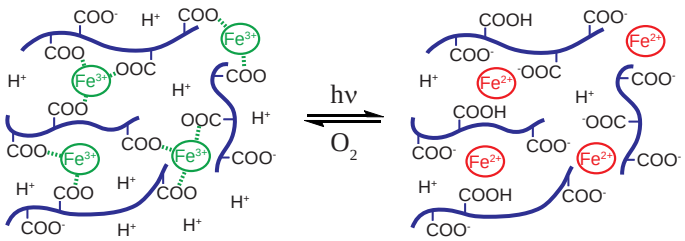

(b) Schematic illustration of the transition

Figure 6.8 – Reversible gel–sol transition triggered in a poly(acrylic acid)–Fe(III) aqueous gel by sunlight and exposure to oxygen.[130]

Beside polymeric ligands bearing oxygen-donor atoms, polymeric lig-

ands bearing nitrogen-donor atoms also constitute a straightforward approach to metallo-supramolecular polymer gels. Among them, polyvinylbipyridine and polyvinylpyridine have been used early by Lewis and Miller to yield non-covalent networks.[131–135]

More recently, Craig *et al.* developed highly tunable cross-linked gels based on polyvinylpyridine as polymeric ligand, ditopic pincers as bridging ligands, and transition metal ions.[136,137] The associating motifs were derived from poly(4-vinylpyridine) and bivalent platinum(II) or palladium(II) pincer complexes (Figure 6.9), and give rise to coordinative networks that swell in organic media like dimethyl sulfoxide. By tuning the dissociation rate of the transient bonding, *i.e.*, how frequently the supramolecular cross-links dissociate, the authors were able to control the dynamic rheological properties of the gels. More precisely, those properties were controlled by properly choosing the metal ion and the structure of the ditopic pincer, without significantly altering their binding constants.

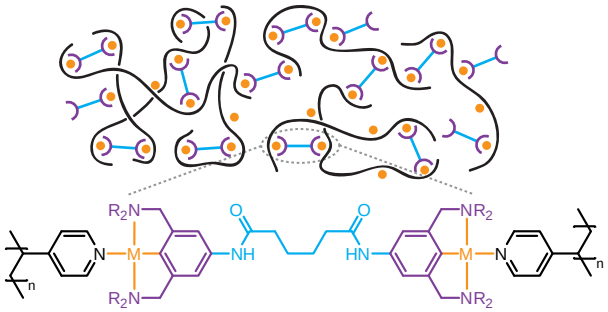

Figure 6.9 – Representation of a MSPG obtained through the coordination of poly(4-vinylpyridine) with bivalent metallo-pincer complexes.[136,137]

The responsive behaviour of the aforementioned MSPGs was further investigated by the same authors in a following study.[138] A critical concentration was first determined for those gels from the abrupt change in viscosity over a narrow cross-linker fraction. The stimuli-responsiveness of the gels was evidenced by adjusting the pH value of the media, or by using competitive coordinating species, such as chloride anions or dimethylaminopyridine ligand. While acids can protonate it, competitive species displaced the vinylpyridine on the polymer backbone, which

decreased the cross-linking degree and weakened the supramolecular network. Notably, the effect of acidification could be reversibly turned off by the addition of a weak base to the system and subsequent reformation of the gel. The chemical-responsive behaviour of the gels was also noted to be more pronounced near the percolation threshold. Mixing bivalent Pt(II) and Pd(II) pincer complexes, *i.e.*, different cross-linkers, with poly(4-vinylpyridine) generated MSPGs rather characterized by a strong to weak gel shift than a defined gel–sol transition. When the concentration of both metallo-pincer complexes exceeded the percolation threshold, the rheological properties of the gel were controlled by the kinetically slower Pt(II) cross-linker. Once the concentration of "active" cross-linker drops below its individual percolation threshold, *e.g.*, by adding the appropriate amount of competitive ligand, but still allows the total amount of cross-linking units to exceed the percolation threshold, the gel properties were dictated by the kinetically faster Pd(II) metallo-pincer.

The formation of coordination complexes between the nitrogen lone pair on poly(4-vinylpyridine) and metal ions was also included in the design strategy of Matsushita and coworkers.[139] Specifically, they reported on the preparation of thermo-reversible supramolecular polymer gels in a hydrophobic ionic liquid by mixing poly(4-vinylpyridine)-*b*-poly(ethyl acrylate)-*b*-poly(4-vinylpyridine) triblock copolymer and zinc chloride as metal salt. Practically, the formation of coordination bonds between zinc(II) and pyridine groups on poly(4-vinylpyridine) blocks was confirmed by infra-red spectroscopy. Also, a slow solvent casting was applied using a polar solvent mixture with coordination ability to produce macroscopically homogeneous gels from a mixture of the triblock copolymer, metal ions and ionic liquid. The latter was employed as a non-volatile solvent to carry out measurements at high temperatures with reproducible thermo-responsiveness. The thermo-induced transition between semi-solid gel and liquid-like state was investigated by temperature-ramp oscillatory shear measurements, showing strong dependency on stoichiometry between ligands and metals. Combining the high potential of ion gels with the characteristic thermo-reversibility of MSPGs, such supramolecular ion gels are thus expected to find attractive applications.

6.2.2.2 Linear polymeric ligands with coordinating groups in the main-chain as cross-linkers

Linear macromolecules with coordinating groups in the main-chain constitute another class of polymeric ligands. While the number of chemical functionalities that can coordinate metal ions is virtually unlimited, the diversity of such polymeric ligands is generally limited by their synthetic feasibility. Among them, conjugated polymers attracted attention,[140–144] particularly because of their electro-optical properties.

This was illustrated by the work of Weder *et al.* who were the first to report on elaboration of a π-conjugated organometallic network based on poly(*p*-phenylene ethynylene)s.[142,143] The synthesis of those materials was readily achieved via ligand exchange reactions between styrene ligands of tris-styrene platinum(0) and polymeric ethynylene moieties (Figure 6.10). As expected, the photo-physical properties of the system was markedly influenced by the coordination of poly(*p*-phenylene ethynylene)s to Pt(0). The luminescence was efficiently quenched, and a hypsochromic shift of the absorption peak in the visible region was observed.

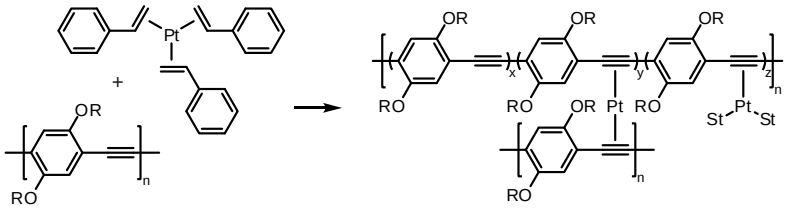

Figure 6.10 – Ligand exchange reaction between tris-styrene Pt(0) complex and poly(*p*-phenylene ethynylene) yielding a conjugated coordination network.[142]

In a following paper,[143] the same authors considered the introduction of auxiliary ligands into the poly(*p*-phenylene ethynylene) backbone and opted to incorporate 2,2'-bipyridine moieties. As consequence, they accessed metallo-supramolecular polymer networks and organogels via addition of first row transition metal ions, such as Cd(II), Zn(II), Ni(II) or Co(II), to those conjugated precursors. As previously, the photophysical properties of the conjugated polymers were markedly influenced by the coordination of metal ions. While complexes with group 12 ions

were emissive, other transition metals exhibited a strong tendency for the formation of metal-to-ligand charge transfer complexes with the polymeric ligand.

More recently, Nitschke and coworkers designed a luminescent metallo-supramolecular polymer that underwent a sol–gel transition as the temperature increased, in contrast with most MSPGs, which do so upon cooling.[144] In their study, a linear conjugated polymeric ligand was first synthesized in DMSO through the polycondensation of bifunctional aldehyde and amine around copper(I) templates. This synthesis was performed in presence of bulky trioctylphosphine ancillary ligands so that the polymer solution underwent a sol-to-gel transition as the temperature rises (Figure 6.11). Although enthalpically unfavourable, the sol–gel transition was nevertheless entropically supported at high temperatures. Indeed, the creation of Cu(I) complex cross-links was associated with the formation of sterically congested Cu(I)–trioctylphosphine complexes in equilibrium with free trioctylphosphine ligands (Figure 6.11). The metallo-supramolecular polymer also exhibited thermo-chromism and photoluminescence, where both the emission and absorption processes showed temperature dependence in terms of colour and intensity. As the temperature increased, the material became more sensitive to degradation under atmospheric oxygen, which frustrated attempts at investigating the rheological properties of the polymer gel.

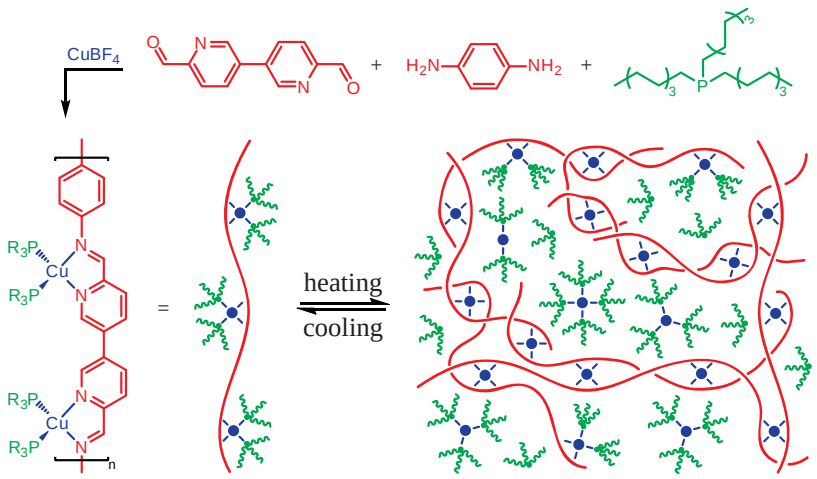

Figure 6.11 – Preparation of conjugated metallo-supramolecular polymer and its sol–gel transition when temperature rises.[144]

In the aforementioned approaches, the metal coordination sites that constitute part of the polymer backbone were built during the polymerization process itself. The versatility of those synthetic strategies has been further illustrated by Meudtner and Hecht who synthesized poly[(triazol-4-yl-1,3-pyridine)-*alt*-(triazol-1-yl-1,3-phenylene)]s via step-growth polymerization, by taking advantage of the copper(I)-catalysed azide–alkyne cycloaddition (CuAAC) "click" reaction.[145] The resulting polymer chains incorporated 2,6-bis(1,2,3-triazolyl)pyridine units in the main-chain and were able of chelating numerous transition metals, thus inducing coordination cross-links and effective gelation of polymer solutions in organic solvents (Figure 6.12). Furthermore, the bridging coordination complexes also opened the way of imparting various functionalities, *i.e.*, magnetic and emissive, for the design of new materials.

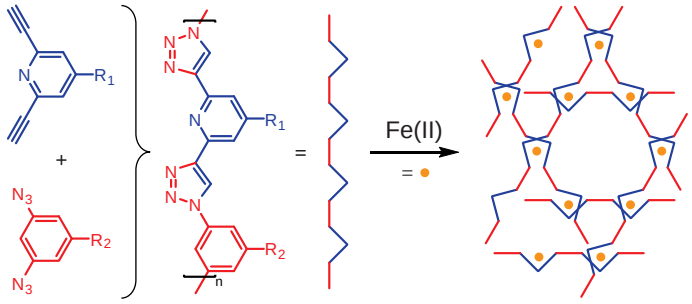

Figure 6.12 – Preparation of hetero-aromatic polymers via CuAAC and the formation of metallo-supramolecular polymer gel trough addition of transition metal ions.[145]

Another precursor for MSPGs has been successfully designed by Wang et al. taking advantage of the CuAAC. In their work,[146] a hierarchical pathway to fabricate supramolecular polymer network via heterometallic coordination-driven self-assembly strategy was investigated. Specifically, terpyridine ligands were attached on both sides of a homoditopic monomer synthesized through CuAAC, with the concomitant formation of embedded 1,2,3-triazole ligand. As a first level of assembly, a linear supramolecular polymer was formed by chain extension of the homoditopic monomer upon addition of metal ions such as iron(II). Subsequently, the 1,2,3-triazole moieties, incorporated into the middle site of the monomeric units, were able to form a disubstituted palladium(II) complex, thereby inducing the cross-linking of the linear species as il-

lustrated in Figure 6.13. Moreover, triggered by competitive ligands, the MSPG was reversibly disassembled, thereby demonstrating the possibility to operate the two kinds of metal–ligand recognition motifs separately.

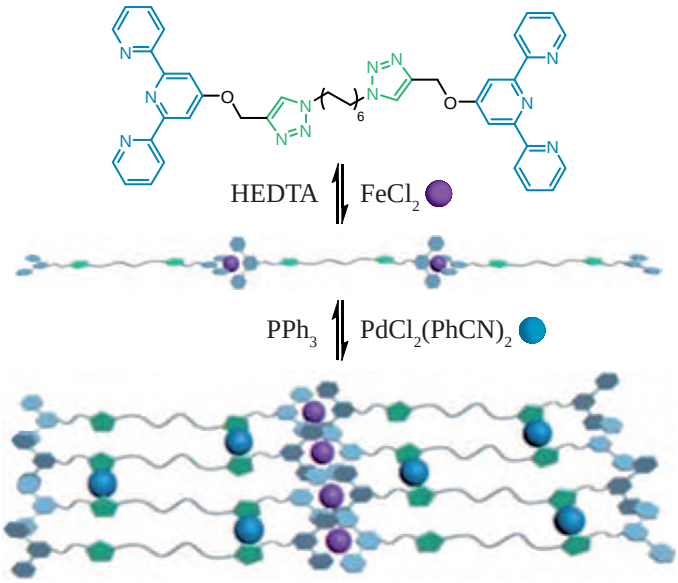

Figure 6.13 – Reversible formation of a MSPG formed by an orthogonal combination of metal–ligand coordinations.[146]

6.2.2.3 Linear polymers modified with coordinating groups as cross-linkers

So far, polymeric ligands have proved their applicability in the elaboration of MSPGs of type II. In the abovementioned studies, coordination sites were either initially present as side-chain or in the main-chain, or created during the polymerization process itself. Unfortunately, not all macromolecules carry proper coordination sites either as side-chain or in the main-chain. Thus, alternatives have been explored in parallel. They generally involve the post-modification of macromolecular chains with binding moieties or coupling those synthons with monomeric units that can be polymerized to yield polymeric ligands.

The first alternative was demonstrated early by the work of Chujo *et*

al. who reported the formation of metallo-supramolecular gels from polyoxazoline showing pendant 2,2'-bipyridyl groups in combination with different transition metal ions.[147–149] Experimentally, the pendant ligands were attached to partially hydrolysed poly(*N*-acetylethylenimine) polymer chains via peptidic coupling. The supramolecular cross-linking and swelling of the bipyridine branched polymers was then triggered by the addition of iron(II), nickel(II), cobalt(III) or ruthenium(II) metal ions. However, only the treatment with Fe(II) and Ru(II) salts gave rise to stable polymer gels at room temperature. In addition to high stability constants for the coordination of metal ions to the bipyridine ligands, the stability of the hydrogel was also pointed to be a consequence of the kinetic inertness of the resulting coordination cross-links. More precisely, the dynamic stabilities of the polymer gels were related to the ligand exchange rates between the bipyridine complexes.[150,151] With time, the inter-molecular metal–ligand complexes that initially drive the construction of a three-dimensional network can be exchanged to entropically favourable intra-molecular complexes, which lead to soluble coordination polymer chains. Finally, the thermodynamic and kinetic stabilities of the bipyridine–metal complexes, and hence the stability of the coordination hydrogels, were markedly affected by environmental parameters such as solvent, redox, pH and temperature. As an example, heating of the gels accelerated the ligand exchange reactions, resulting in the thermal cleavage of the coordination bonds. Besides, the swelling degree and stability of the hydrogels were found to be dependent on the amount of functional groups in the gel.

More recently, a versatile approach for the elaboration of MSPGs has been developed by Schubert *et al.* who modified poly(pentafluorostyrene) chains via selective grafting by a functionalized metallo-supramolecular motif.[152] More specifically, coordination sites were grafted onto the activated polymeric backbone via nucleophilic substitution with amine-functionalized terpyridine synthons. Then, the formation of supramolecular cross-links and hence gelation of the terpyridine-grafted copolymer solution was triggered by the addition of transition metal ions. This behaviour was consistent with the one observed in a previous study for polymethacrylate copolymers with pendant terpyridine groups.[153] The only notable difference was related to the synthesis of the terpyridine-functionalized copolymers. Indeed, a ligand-modified methacrylate was copolymerized with methyl methacrylate by radical copolymerization to yield polymethacrylates with binding sites in the side chains. Viscosity

and UV titration experiments were used to monitor in detail the complexation reaction following the addition of various transition metal ions. Varied behaviours were observed depending on the metal ions and their capacity to form stable bis-complexes with terpyridine ligands. Furthermore, a high concentration in terpyridine ligands was found to favour inter-molecular bridging instead of intra-molecular complexation. Finally, addition of strong competitive ligand completely reversed the formation of terpyridine bis-complexes, clearly evidencing the responsive properties of the metallo-supramolecular gels.

In 2014, Wang and coworkers developed a straightforward method to incorporate a mussel-inspired adhesive moiety into synthetic polymers toward adhesive gels.[154] The mussel adhesive moiety was successfully incorporated into a urethane backbone through a new facile approach using step growth polymerization based on hexamethylene diisocyanate as a hard segment, poly(ethylene glycol) as a soft segment, and lysine-dopamine as a chain extender. Upon addition of iron(III), the gelation of aqueous solutions of mussel mimetic polyurethane can be triggered by pH adjustment to form adhesive hydrogels because of the rapid conversion of Fe(III)–dopamine mono-complexes to bis- and/or tris-complexes. Combining the chemistry of marine adhesive proteins with the flexibility, facile synthesis, and low cost of polyurethanes, those MSPGs show great potential in many applications like, *e.g.*, biomedical material and tissue engineering.

6.2.2.4 Multi-arm star polymeric ligands as cross-linkers

The applicability of telechelic multi-arm star polymers in the preparation of MSPGs has been recently demonstrated, even when use in combination with linear ditopic ligands (Figure 6.14).[87] In 2009, Kimura and coworkers post-functionalized commercial four-arm star poly(ethylene glycol) with terpyridine termini.[155] The accordingly obtained tetrachelic star poly(ethylene glycol) then allowed the formation of metallo-supramolecular polymer gels through the addition of transition metal ions. Finally, addition of ammonia as competitive coordination species led to the collapse of the metallo-supramolecular gels, illustrating the responsiveness of these materials.

Star-shaped poly(ethylene glycol)s (PEG) end-capped with terpyridine moieties have been further used by Seiffert *et al.* as precursors of

model networks that have the potential to exhibit close to regular topologies, approaching ideality.[156,157] Terpyridine moieties were coordinated to different transition metal ions in various media, ranging from apolar organic solvents to water, thereby allowing MSPGs of greatly varying strengths of transient cross-links to be prepared. In parallel, the polymer network mesh size was controlled by the molecular weight of the arms of the star precursor. The high regularity of the network was generally demonstrated by static light scattering, revealing just minor network inhomogeneities in some gels. However, some metal ions induced clustering of the metal–ligand complexes, thereby leading to non-negligible structural heterogeneity. In counterpart, the mechanical strength and resistance to relaxation was greater for those gels, indicating clustering to be a mechanism of reinforcement.

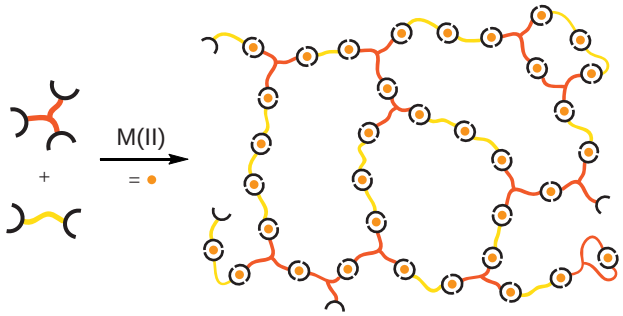

Figure 6.14 – Metallo-supramolecular network formed by the addition of transition metal ions to a mixture of star-like tritopic and linear ditopic ligands.[87]

In parallel, three-arm terpyridine-terminated low-molecular-weight PEGs were employed by Kikuchi and coworkers to prepare self-healable redox-responsive hydrogels under mild conditions.[158] The gelation of the star-shaped precursor solution in presence of cobalt(II) ions occured by aerobic oxidation at ambient temperature, as illustrated in Figure 6.15. As a consequence, this preparation method allows controlling the configuration, shape, elasticity, and handling of the resulting hydrogels. Interestingly, the cured hydrogels can be converted into solutions upon the addition of a reducer. In turn, gelation of the solution was achieved by exposure to air due to the consumption of the reducer.

At the same time, metallo-assemblies obtained from 8-arm PEGs

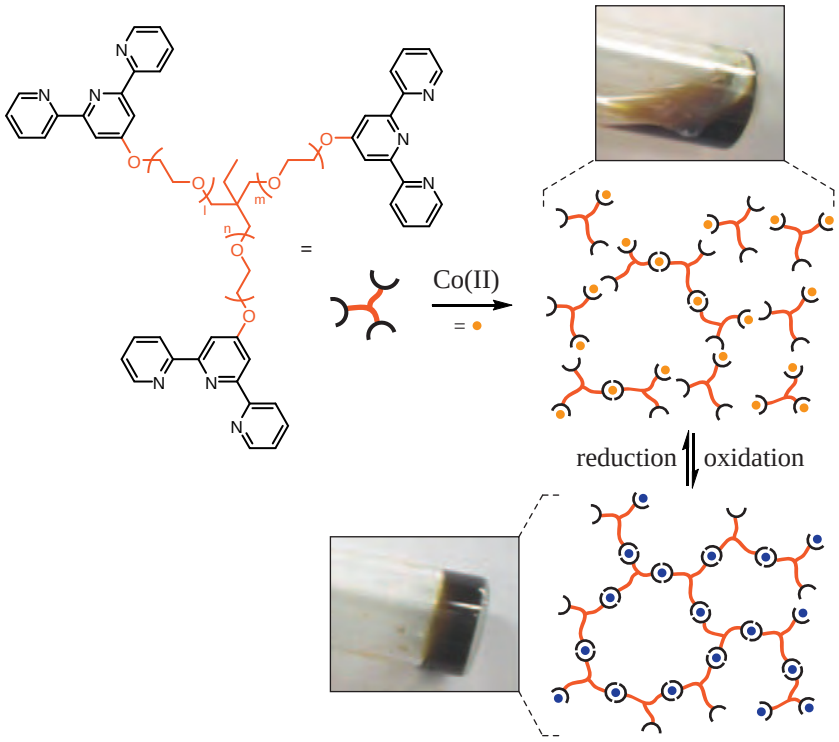

Figure 6.15 – Redox-responsiveness of a MSPG prepared from tritopic terpyridine end-capped star-shaped poly(ethylene oxide)s and cobalt metal ions.[158]

partially substituted with terpyridine end-groups and various transition metal ions were studied at high concentrations by Karperien and coworkers.[159] Hence, they demonstrated that the assembly behaviour in those systems was largely dependent on the dissociation rate constants of the metal–ligand complexes. In this respect, hydrogels formed with kinetically stable cross-links were elastic, and showed minor changes with temperature between 5 and 60 °C. On the other hand, thermo-reversible hydrogels with relatively viscous response were prepared with metal ions providing more labile complexes in combination with the considered ligand.

The effect of the topology of PEG precursor on the metal-induced gelation in those systems was further investigated by Yoshida and coworkers.[160] To this end, a series of PEGs with different numbers of branches (linear, 4-arms, and 8-arms) functionalized with terpyridine ligands as

terminal groups were prepared. The different ligands were used in combination with ruthenium ions as the latter forms mono-terpyridine complexes when oxidized, whereas bis-complexes are obtained when reduced. Accordingly, the three different polymers existed as solutions when ruthenium was in the oxidized state. In contrast, gels were obtained when the metal centre was reduced except when linear PEGs were used as the backbone. Indeed, the formation of three-dimensional polymer networks through metal–ligand coordination was only possible with multi-arm polymer precursors. By increasing the number of star branches, the number of cross-linking points necessary for gelation was reduced, as predicted from the tree-like structure theory.

Inspired by nature, Holten-Andersen *et al.* elaborated self-healing supramolecular gels based on four-arm star PEGs modified with catechol ligands and iron(III) ions.[161,162] The control of inter-molecular cross-linking was achieved through the protonation of catechol hydroxyl groups, which in turn affects the stoichiometry of Fe(III)–catechol complexes. While the solubility of ferric ions is relatively low at anything but acidic media, the formation of bis- and tris-complexes requires pH to be above neutral. To prevent the precipitation of hydroxide, cross-linking reaction was initiated from iron(III) mono-complexes under acidic conditions, and the pH was increased. The dominance of mono-, bis- and tris-complexes at different pH ranges was established by UV-visible absorption spectroscopy. The obtained metallo-supramolecular gel was shown to exhibit autonomous healing properties and dissipates more energy at low deformation rates in comparison to covalent ones. Moreover, the dynamic rheological properties of the gel were readily controlled by properly setting the final pH value, which accordingly affects the average lifetime of the iron(III)–catechol cross-links. Lastly, the chemo-responsiveness of the gel was demonstrated upon exposure to a solution of ethylenediamine tetraacetic acid, as strong iron(III) chelating agent.

Two years later, the same authors extended their work on metal–catechol based MSPGs by using the same catechol modified four-arm star PEG in combination with different metal ions (Figure 6.16).[163] In their comparison, vanadium(III) appeared to induce tris-coordination at pH 8 whereas iron(III) induced bis-coordination under the same condition. This difference in the stoichiometry of the association resulted in higher stability of the vanadium–catechol bridged networks compared to the iron–catechol analogue, therefore showing significantly more

solid-like properties. Although spectroscopy data suggested that aluminium(III) ions did not induce strong coordination bonding with catechol units, the aluminium-based polymer hydrogels were significantly more elastic than the pristine material. Hence, the non-transition metal character of trivalent aluminium ions was believed to induce weaker non-coordinative interactions of perhaps more purely electrostatic nature.

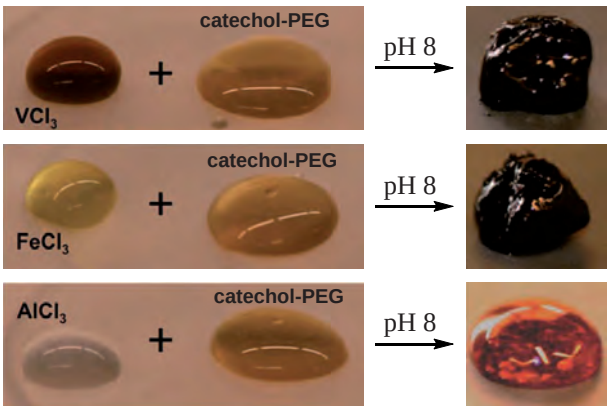

Figure 6.16 – Formation of MSPGs from catechol-modified four-arm star poly(ethylene glycol) in combination with trivalent vanadium(III), iron(III) and aluminum(III) ions.[163]

Concomitantly, a platform based on a 4-arm PEG was employed by Waite *et al.* to explore the utility of the parent catechol and derivatives, 4-nitrocatechol and 3-hydroxy-4-pyridinonone, as structural cross-linking agents.[164] Gelation in those systems was triggered by the addition of Fe(III) and other bio-relevant metal ions with high affinity for this class of chelators. The mechanical properties of the hydrogels were demonstrated to be highly dependent on preparation conditions, pH and choice of metal ion. In this regard, 3-hydroxy-4-pyridinonone moiety was shown to be particularly attractive as a chelating functionality in this architecture. In their presence, a robust gelation with Fe(III) occurred at physiological pH and was found to be largely resistant to oxidative degradation, allowing potential application as injectable gelling agents with excellent encapsulation. Also, 3-hydroxy-4-pyridinonone was shown to be a versatile metal binding species, capable of gelation at physiological pH with Al(III) and Ga(III), and at higher pH with Cu(II) metal ions.

Beside terpyridine and catechol derivatives, other ligands have also demonstrated their applicability in the elaboration of MSPGs from multitopic star polymer precursors. In their work,[165] Aoyagi and his coworkers prepared rapid self-healable and biocompatible hydrogels using the ability of phosphate compounds to form complexes with selective metal ions. To this end, a phosphate-terminated four-arm star PEG was synthesized via a substitution reaction of the hydroxyl end groups using phosphoryl chloride. Then, a variety of metal ions were examined to produce supramolecular network structures from those precursors. Especially, the gels rapidly formed upon addition of trivalent metal ions having relatively small ionic radii, appropriate coulomb potential values and water substitution rates (Figure 6.17). Reversible binding and gel–sol transition have also been demonstrated by switching the redox states of certain metal ions. Also, the rheological properties were finely tuned by the choice of metal ions, chain lengths, and temperature. Learning from biological systems, the proposed phosphate–metal ion based hydrogels could become an attractive candidate for various environmental and biomedical applications.

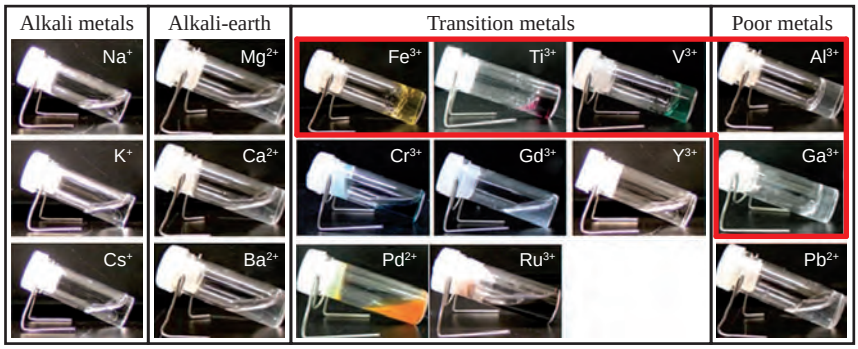

Figure 6.17 – Photographs of 4-arm phosphate end-capped poly(ethylene glycol) aqueous solutions in the presence of various metal ions.[165]

6.2.3 Metallo-supramolecular polymer gels of type III

A final category of metallo-supramolecular polymer gels combine labile metal–ligand coordination with other secondary interactions including but not limited to, hydrogen bonding,[166–168] host–guest complexa-

tion,[169,170] or solvophobic effects.[171–175] Classically, these non-covalent interactions are either combined via orthogonal, cooperative or hierarchical self-assembly so that they confer further strength to the resulting supramolecular network or just allow its construction.

6.2.3.1 Combination with hydrogen bonds

The orthogonal combination of hydrogen bonds with coordinative links in supramolecular gels was remarkably illustrated by Weck and coworkers.[166,168] In their studies, side-chain functionalized copolymers containing both coordination sites and hydrogen bonding units have been synthesized by ring-opening metathesis copolymerization. The coordination motif was exclusively based on palladium(II) metallo-pincer complexes through coordination with a pyridine moiety. On the other hand, the hydrogen bonding motifs for reversible cross-linking were either based on diaminopyridine or cyanuric acid residues. These polymers were then selectively and reversibly cross-linked upon the addition of small molecules as cross-linking agents, involving either metal–ligand coordination, hydrogen bonds or the combination of both interactions (Figure 6.18). Furthermore, the rheological properties and responsive behaviour of the supramolecular networks were modulated depending on the cross-linking strategy. While dramatic changes in the viscosity were observed when coordination motifs were employed for cross-linking, the viscosities of the solutions only poorly increased for cross-linked polymers through hydrogen bonding. In contrast, the coordination cross-linking resulted in a polymer network that was chemically reversible, through addition of ligand displacement agents, whereas the hydrogen cross-linked network mainly exhibited thermo-responsive behaviour. Since the different interactions were fully orthogonal, multi-responsive gels that showed both chemo- and thermo-responsiveness were readily obtained using both hydrogen bonding and metal–ligand coordination as cross-linking.

Another approach was followed by Weng and coworkers who studied multi-responsive supramolecular gels constructed via orthogonal hydrogen bonding interaction and metal–ligand coordination[176]. To this end, macromonomers bearing tridentate 2,6-bis(1,2,3-trizol-4-yl)pyridine ligand unit were synthesized via CuAAC “click” chemistry in the middle of two ureidopyrimidinone motifs linked to the central coordination

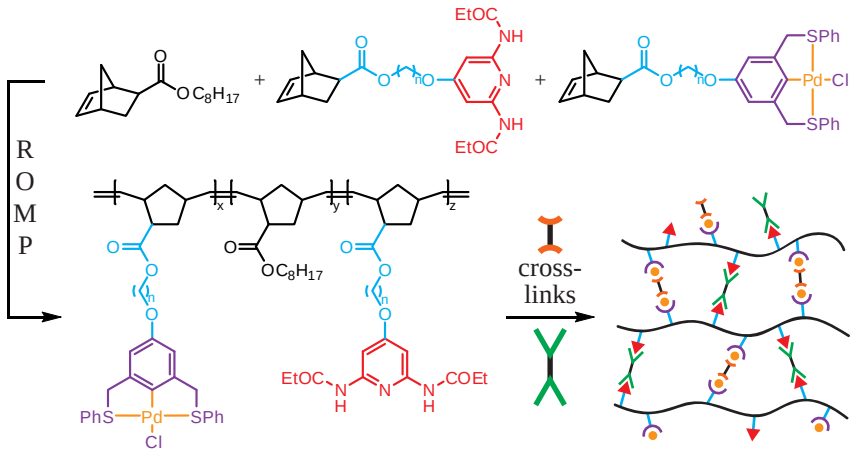

Figure 6.18 – Synthesis of side-chain functionalized copolymer displaying both metal coordination and hydrogen bond sites and its orthogonal reticulation via addition of ditopic cross-linking agents. [168]

unit via poly(ethylene oxide) of various lengths. Their gelation in the presence of europium(III) ions were study in aprotic solvent, which allows quadruple hydrogen bonding between the ureidopyrimidinone units (Figure 6.19). Gels exhibited multi-responsive properties, including photo-luminescence, mechano-responsiveness, self-healing abilities, and thermo-repsonsive and chemo-responsive properties. The different gela-

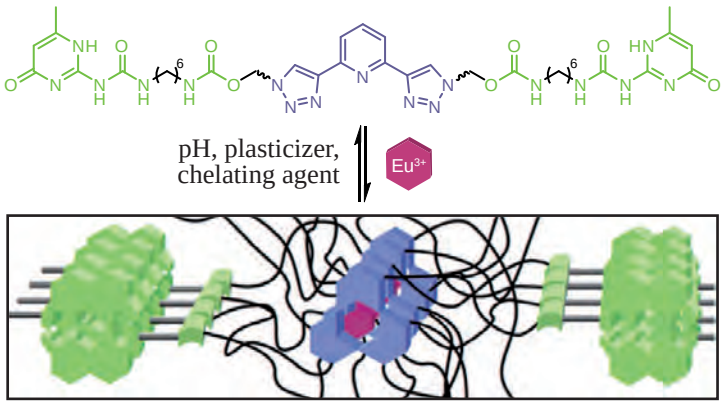

Figure 6.19 – Responsive self-assembly of a MSPG occurring via the formation of ureidopyrimidinone dimers and metal–ligand coordination phase. [176]

tion abilities and multi-responsive properties were shown to result from difference in linker lengths and the introduction of orthogonal metal–ligand coordination and hydrogen bonding interactions.

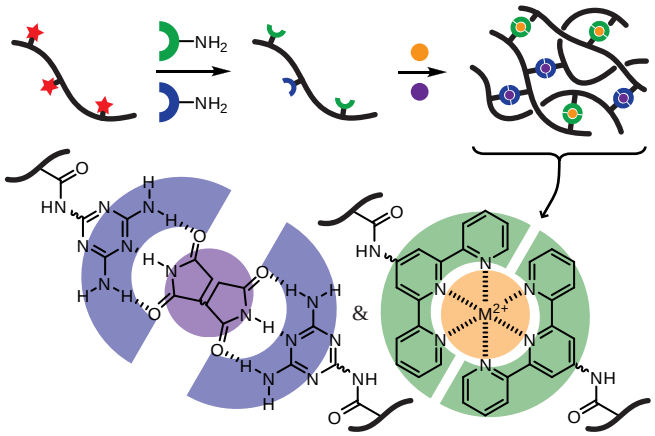

Figure 6.20 – Elaboration of MSPGs combining metal–ligand coordination with H-bonding formed from a common precursor polymer.[177]

At the same time, a modular construction kit for supramolecular polymer gels incorporating metal complexation and hydrogen bonding has been developed by Seiffert and its collaborators.[177] Following a strategy by Whitesides *et al.*,[178] they prepared linear polymers by simple radical copolymerization, that can be functionalized with a variety of side-groups for supramolecular cross-linking, by either H-bonding or metal complexation (Figure 6.20). These precursors consisted in linear chains of methacryl-succinimidyl modified poly(*N*-isopropylacrylamide) that can be readily derived by replacing their electrophilic units by nucleophilic amine-functionalized derivatives. The resulting polymers were then cross-linked by addition of low molecular weight linkers that are complementary to the motifs on the polymer. The multiple hydrogen bonding motifs used were based on diaminotriazine and maleimide, cyanuric acid and Hamilton wedges, or diaminotriazine and cyanuric acid pais, while the metal complexation was based on terpyridine and different metal salts (Figure 6.20). Taking advantage of the good solubility of the polymer backbone in a variety of solvents allowed these networks to be studied in various media with unprecedented flexibility and consistency. Hence, this approach created hybrid MSPGs of varying rheologi-

cal responses, from low viscous liquids to highly elastic gels, each showing consistent and quantitative mutual correspondence between mechanical characteristics and binding strength of the constituent inter-chain cross-linking.

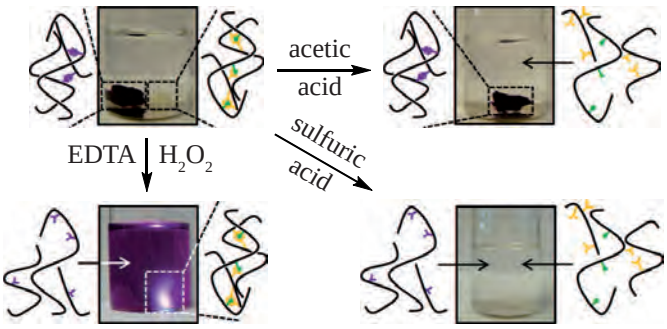

Figure 6.21 – Orthogonal de-cross-linking of multi-responsive supramolecular hydrogels constituted by orthogonal cross-linking of precursor polymers by H-bonding and metal coordination.[179]

In another paper,[179] a similar supramolecular toolkit based on linear polyglycerol functionalized with orthogonal transient cross-linkable side groups was developed by the same group. To this end, strain-promoted azide–alkyne cycloaddition was employed to functionalize the polymer backbone with diaminotriazine and cyanurate moieties that form a multipoint H-bonded array, along with terpyridine ligands that form bis-complexes with transition metal ions. This strategy allowed preparing supramolecular gels in mild conditions in water via hydrogen bonding, metal complexation, or both. These transient cross-links were sensitive to external stimuli such as variation of pH or the presence of competing ligands. As illustrated in Figure 6.21, the multi-responsive hydrogels responded to the different stimuli by partial or complete de-cross-linking in an orthogonal fashion.

6.2.3.2 Combination with host–guest complexation

The orthogonal combination of host–guest complexation and metal–ligand coordination into supramolecular polymer gels was notably illustrated by the studies of Huang and coworkers.[169,170] In their approach, ditopic oligomers containing 1,2,3-triazole groups comprised be-

tween an ammonium guest and a complementary crown ether host were synthesized and hierarchically organized over two levels of assembly (Figure 6.22). The self-assembly into supramolecular polymers was accomplished in acetonitrile through host–guest complexation and was demonstrated to be dependent on oligomer concentration, temperature and association constants. Indeed, all those parameters were exerting a notable influence on the reversible equilibrium between linear polymer chains and cyclic oligomeric species. Above a critical gel concentration, the conversion from the linear supramolecular polymer to a cross-linked supramolecular gel was achieved by forming bis-complexes between 1,2,3-triazole units and Pd(II) ions, as confirmed by rheology measurements. As expected, the accordingly obtained supramolecular gels displayed fully reversible chemo- and thermo-induced gel–sol transitions (Figure 6.23). As an example, destruction and reconstruction of the supramolecular networks were respectively achieved by subsequent additions of competitive coordination species and the metal cross-linker. In the case of dialkylammonium, further control was allowed by varying the pH, *i.e.*, the protonation of the ammonium salt, or by the addition and removal of potassium ions that can form more stable complexes with crown ethers.

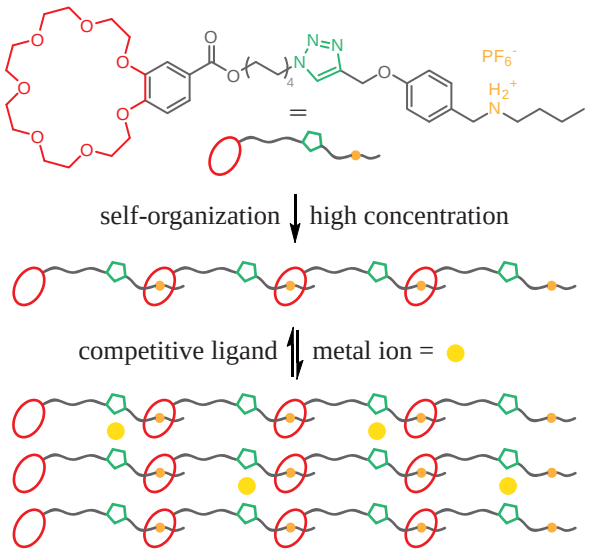

Figure 6.22 – Schematic representation of the hierarchical assembly of a supramolecular polymer gel combining host–guest and metal–ligand interactions.[169]

One year later, the same authors further proposed an alternative approach based on the orthogonal self-assembly of two homoditopic monomers and a metallic cross-linker.[180] The complementary building blocks comprised of bis(benzo-21-crown-7)-based monomer and bis(dialkylammonium salt)-based monomer that further contained two 1,2,3-triazole groups acting as ligands. Practically, a self-assembled linear supramolecular polymer was first obtained when dissolving both homoditopic monomers in acetonitrile. Then, $[PdCl_2(PhCN)_2]$ was added to construct a cross-linked supramolecular polymer network. The obtained materials were not only transparent and free-standing but exhibit reversible gel–sol transitions in response to multiple stimuli. Moreover, the MSPGs showed excellent viscoelastic properties and were moulded into free-standing, shape-persistent objects exhibiting self-healing properties. These unique features were due to the dynamically reversible host–guest complexation and the good mechanical properties of the cross-linked network, making them promising intelligent materials.

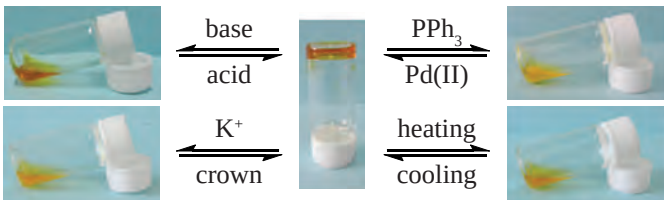

Figure 6.23 – Reversible gel–sol transitions triggered in a supramolecular polymer gel combining host–guest and metal–ligand interactions.[169]

In a collaboration with P. Stang, Huang and coworkers further demonstrated their implication in the development of supramolecular gels unifying metal–ligand bonds with the host–guest chemistry of crown ethers. In their study,[181] a highly directional dipyridyl ligand donor fashioned with a benzo-21-crown-7 moiety was prepared. In presence of a complementary organo-platinum(II) complex acceptor, the latter underwent coordination-driven self-assembly to yield metallo-hexagons. At high concentrations, this macrocyclic precursor was then extended into a supramolecular polymer network upon the formation of [2]-pseudorotaxane linkages with a bis-ammonium salt. The gel that resulted from this supramolecular polymer network exhibited dynamic properties, *i.e.*, thermo- and cation-induced reversible gel–sol transitions. In addition,

they constitute promising candidates for applications in the field of catalysis as their design method preserves internal metallo-cyclic cavities in the resulting network.

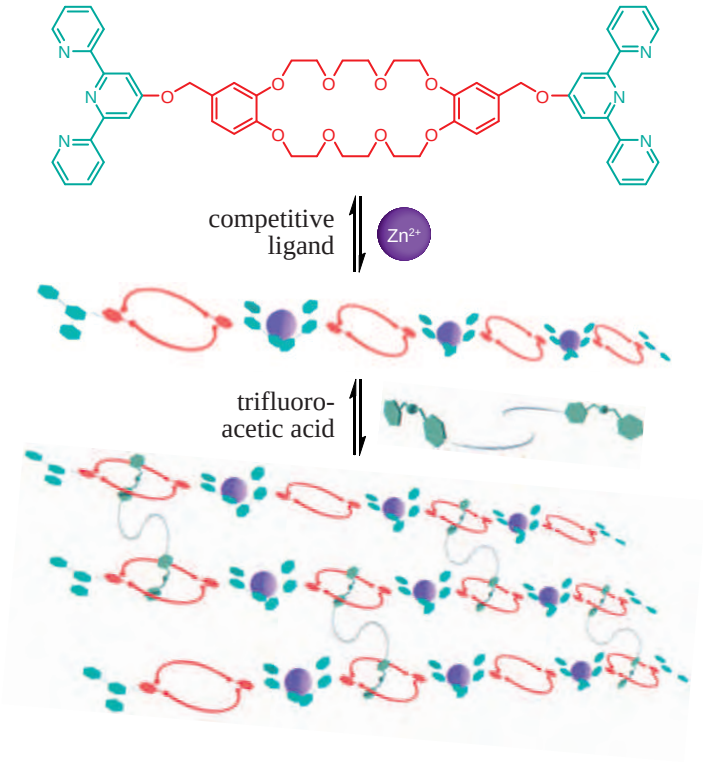

Figure 6.24 – Schematic representation of the reversible formation of a supramolecular polymer gel formed by metal–ligand and host–guest interactions.[182]

The possibility of combining metal–ligand and crown ether-based host–guest interactions has also inspired Yin *et al.* in the construction of stimuli-responsive supramolecular polymer networks.[182,183] In a first paper,[182] they reported the synthesis of a low molecular weight monomeric building block by linking dibenzo-24-crown-8 with two terpyridine units. Thanks to its coordination motifs, this monomer can form linear supramolecular polymers after the addition of zinc(II) triflate. By the continuous addition of a bis-ammonium cross-linker, a supramolecular polymer network was obtained, as shown in Figure 6.24.

Interestingly, the conversion between the linear supramolecular polymer and the supramolecular polymer network can be triggered via pH changes. Indeed, this variable allows controlling the destruction and reconstruction of the interactions between the dibenzo-24-crown-8 and the dibenzylammonium salts. Moreover, the linear supramolecular polymer can also be converted back into monomeric species by the addition of 1,4,7,10-tetraazacyclododecane as a competitive ligand, which destroy the interactions between zinc(II) ion and terpyridine.

In a second paper,[183] the same group further added a level of complexity to their system by introducing a third non-covalent association. Hence, a multi-responsive supramolecular polymer gel was presented on the basis of the host–guest interactions between dibenzo-24-crown-8 and dibenzylammonium salts, and metal–ligand coordination between terpyridine and $Zn(OTf)_2$ and between 1,2,3-triazole and $PdCl_2(PhCN)_2$. The topological structure of the network was easily regulated from monomer to main-chain supramolecular polymer and then to the supramolecular networks by different stimuli, as studied by various characterization methods including proton nuclear magnetic resonance, UV-visible spectroscopy, and rheological measurements. Furthermore, the gel not only showed responsiveness to heat, pH, and competitive ligands but also exhibited self-healing abilities due to the presence of reversible non-covalent interactions in the architecture of the swollen network.

6.2.3.3 Combination with hydrophobic interaction

In 2009, Gohy *et al.* successfully reported a straightforward strategy merging into hierarchical levels the metal–ligand interaction and the self-assembly behaviour of amphiphilic block copolymers.[171] Ligand end-functionalized diblock copolymers were first synthesized by nitroxide mediated polymerization, in the presence of an alkoxyamine bearing a terpyridine moiety. The first level of hierarchical assembly was accomplished by the dissolution of the functionalized diblock copolymers in a selective solvent for one of the block. In practice, the accordingly obtained micelles were constituted of a polystyrene core surrounded by poly(*tert*-butylacrylate) coronal chains bearing a terpyridine ligand at their extremity. The second level of hierarchical assembly was then achieved by addition of transition metal ions. In the dilute regime, the

addition of metal ions was known to result exclusively in intra-micellar complexations and hence flower-like micelles.[184]. However, metallo-supramolecular micellar gels were readily obtained when transition metal ions were added to more concentrated micellar solutions. Notably, the mechanical properties of the supramolecular gels were easily tuned depending on the metal ion that was added to the solution. Finally, the chemo- and mechano-responsive behaviour of those materials were reported while the addition of a strong competitive ligand or large amplitude oscillations weakened the supramolecular network.[171,185]

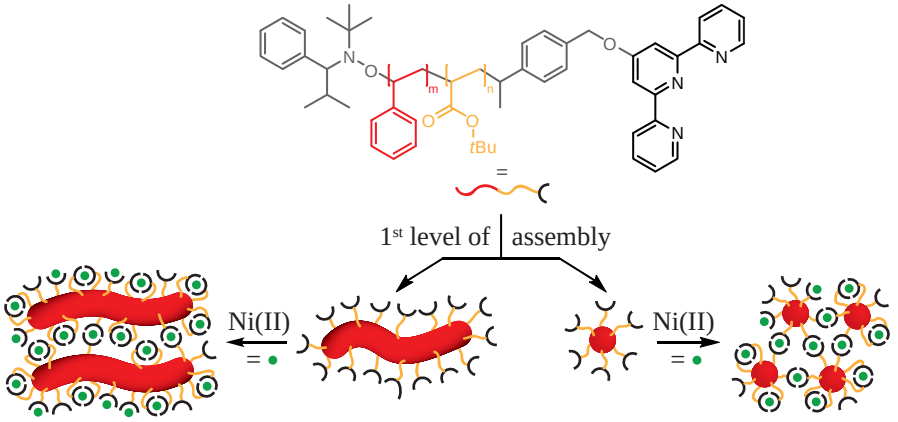

Figure 6.25 – Hierarchical assembly of ligand end-functionalized diblock copolymers into two different micellar gels.[172]

In a next study,[172] the effect of the softness and morphology of the micellar cores on the rheological properties of those coordination micellar gels were investigated. By varying the conditions during the direct dissolution of the diblock copolymers, *i.e.*, temperature and presence of a co-solvent, either spherical or cylindrical micelles with glassy or plasticized cores were firstly obtained (Figure 6.25). Then, supramolecular gels were obtained upon the subsequent addition of nickel(II) metal ions to the concentrated micellar solutions. Not surprisingly, comparatively strong micellar gels were obtained from cylindrical micelles displaying a glassy elongated polystyrene core that acted as a strong constitutive element of these networks. On the opposite, relatively soft micellar gels were prepared from spherical micelles when prepared in presence of toluene as a co-solvent. Additionally, the density of metal cross-linking was readily tuned depending on the environmental conditions during

the addition of transition metal ions, allowing further control over the rheological properties of the hierarchically assembled materials.

In another comparative study,[174] Gohy and coworkers brought into light the contribution of hydrophobic core to the gelation properties of MSPGs involving a combination of hydrophobic and multiple coordinative interactions. To achieve that goal, a water soluble poly(triethylene glycol methylether methacrylate) homopolymer having terpyridine repeating units randomly incorporated as side chain ligands was synthesized by reversible addition-fragmentation chain transfer polymerization. Using this homopolymer as macromolecular chain transfer agent, an amphiphilic block copolymer was derived that incorporated a relatively short polystyrene sequence as second hydrophobic block. Upon addition of nickel(II) ions to a concentrated aqueous solution, both homo- and copolymer were susceptible to gelation. Under comparable conditions, the critical gelation concentration was however dramatically reduced for the copolymer compared to the homopolymer. The effect of the hydrophobic segment was explained by the capability of the block copolymer to form micellar aggregates, which provides additional cross-linking points within the supramolecular network.

Recently, the supramolecular gelation of pyridine end-functionalized poly(ethylene glycol-*b*-lactide) multi-arm star block copolymers has been reported by Feijen and coworkers.[173] In diluted aqueous solutions, these polymers self-organize into micelles and aggregates. Above a critical gel concentration, they were shown to form thermo-reversible, physically cross-linked hydrogels in the absence of metal ions. When transition metal ions like Co(II), Cu(II), or Mn(II) were present, the aggregate dimensions enlarged, which in turn affected the gelation and thermo-reversible behaviour of those materials. The effective interaction between pyridine ligands and transition metal ions was confirmed by oscillatory rheological measurements. Indeed, they formed together coordination complexes with higher storage modulus than in NaCl solutions at similar concentrations. Above the critical gel concentration, the thermo-induced gel–sol transition shifted to higher temperatures due to the formation of additional cross-links from inter-molecular coordination complexes between metal ions and pyridine ligands (Figure 6.26). Compared with gels prepared in the absence of transition metal ions, hydrogels stabilized by metal–ligand coordination showed higher resistance against dissolution and degradation in physiologic conditions, even

at very low metal concentration, which encouraged their use in environmental and biomedical applications.

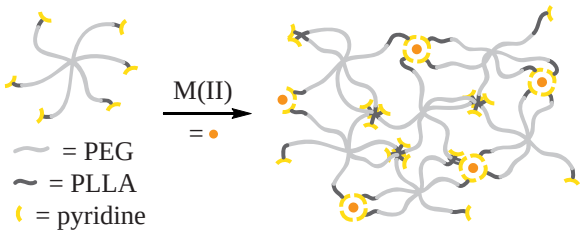

Figure 6.26 – Formation a water-swollen gel from ligands end-functionalized multi-arm star block copolymer in the presence of transition metal ions.[173]

6.3 Summary

Through an in depth literature survey, this chapter summarized progresses achieved to date in the elaboration of metallo-supramolecular polymer gels. These particular materials were described as a subclass of swollen polymer networks where linkages between structural components are provided by dynamic coordination bonds. The three different routes towards metallo-supramolecular polymer gels were reviewed and classified depending on how cross-links were formed through the networks. Doing so, a particular accent was put on the stimuli-responsiveness that the metal–ligand assembly confers to this class of supramolecular materials.

Bibliography

[1] Batten, S. R.; Neville, S. M.; Turner, D. R. *Coordination polymers: Design, analysis and application*; Royal Society of Chemistry: Cambridge, 2009; pp xiii, 424.
[2] Nguyen, P.; Gómez-Elipe, P.; Manners, I. *Chem. Rev.* **1999**, *99*, 1515–1548.
[3] Friese, V.; Kurth, D. *Coord. Chem. Rev.* **2008**, *252*, 199–211.
[4] Friese, V.; Kurth, D. *Curr. Opin. Colloid Interface Sci.* **2009**, *14*, 81–93.
[5] Chen, C.; Suslick, K. *Coord. Chem. Rev.* **1993**, *128*, 293–322.

[6] Whittell, G.; Manners, I. *Adv. Mater.* **2007**, *19*, 3439–3468.
[7] Whittell, G. R.; Hager, M. D.; Schubert, U. S.; Manners, I. *Nat. Mater.* **2011**, *10*, 176–188.
[8] Li, H.; Wu, L. *Soft Matter* **2014**, *10*, 9038–9053.
[9] Dobrawa, R.; Wurthner, F. *J. Polym. Sci., Part A: Polym. Chem.* **2005**, *43*, 4981–4995.
[10] Abd-El-Aziz, A.; Shipman, P.; Boden, B.; McNeil, W. *Prog. Polym. Sci.* **2010**, *35*, 714–836.
[11] Manners, I. *Synthetic metal-containing polymers*; Wiley-VCH: Weinheim, 2004; pp xiii, 275.
[12] Abd-El-Aziz, A.; Manners, I. *Frontiers in transition metal-containing polymers*; Wiley-Interscience: Hoboken, 2007; pp x, 533.
[13] Rehahn, M. *Acta Polym.* **1998**, *49*, 201–224.
[14] Schubert, U. S.; Eschbaumer, C. *Angew. Chem. Int. Ed.* **2002**, *41*, 2893–2926.
[15] McKenzie, B. M.; Rowan, S. J. *Molecular Recognition and Polymers*; John Wiley & Sons: Hoboken, 2008; pp 157–178.
[16] Williams, K. A.; Boydston, A. J.; Bielawski, C. W. *Chem. Soc. Rev.* **2007**, *36*, 729–744.
[17] Knapp, R.; Schott, A.; Rehahn, M. *Macromolecules* **1996**, *29*, 478–480.
[18] Schmatloch, S.; Van den Berg, A. M. J.; Hofmeier, H.; Schubert, U. S. *Des. Monomers Polym.* **2004**, *7*, 191–201.
[19] Schmatloch, S.; Gonzalez, M. F.; Schubert, U. S. *Macromol. Rapid Commun.* **2002**, *23*, 957–961.
[20] Chiper, M.; Meier, M. A. R.; Kranenburg, J. M.; Schubert, U. S. *Macromol. Chem. Phys.* **2007**, *208*, 679–689.
[21] Schmatloch, S.; van den Berg, A. M. J.; Alexeev, A. S.; Hofmeier, H.; Schubert, U. S. *Macromolecules* **2003**, *36*, 9943–9949.
[22] Chiper, M.; Hoogenboom, R.; Schubert, U. S. *Macromol. Rapid Commun.* **2009**, *30*, 565–578.
[23] Han, F.; Higuchi, M.; Kurth, D. *Adv. Mater.* **2007**, *19*, 3928–3931.
[24] Velten, U.; Rehahn, M. *Chem. Commun.* **1996**, *32*, 2639–2640.
[25] Dobrawa, R.; Lysetska, M.; Ballester, P.; Grüne, M.; Würthner, F. *Macromolecules* **2005**, *38*, 1315–1325.
[26] Chiper, M.; Meier, M. A. R.; Wouters, D.; Hoeppener, S.; Fustin, C.-A.; Gohy, J.-F.; Schubert, U. S. *Macromolecules* **2008**, *41*, 2771–2777.
[27] Iyer, P.; Beck, J.; Weder, C.; Rowan, S. *Chem. Commun.* **2005**, *41*, 319–321.
[28] Bustamante, E. A. S.; Galyametdinov, Y. G.; Griesar, K.; Schuhmacher, E.; Haase, W. *Macromol. Chem. Phys.* **1998**, *199*, 1337–1342.
[29] Aamer, K.; de Jeu, W.; Tew, G. *Macromolecules* **2008**, *41*, 2022–2029.
[30] Shunmugam, R.; Tew, G. *Macromol. Rapid Commun.* **2008**, *29*, 1355–1362.
[31] Maier, A.; Rabindranath, A.; Tieke, B. *Adv. Mater.* **2009**, *21*, 959–963.

[32] Shunmugam, R.; Gabriel, G.; Aamer, K.; Tew, G. *Macromol. Rapid Commun.* **2010**, *31*, 784–793.
[33] Calzia, K.; Tew, G. *Macromolecules* **2002**, *35*, 6090–6093.
[34] Shunmugam, R.; Tew, G. *Polym. Adv. Technol.* **2008**, *19*, 596–601.
[35] Kramer, R.; Lehn, J. M.; Marquis-Rigault, A. *Proc. Natl. Acad. Sci. U. S. A.* **1993**, *90*, 5394.
[36] Johnson, R.; Fraser, C. *Macromolecules* **2004**, *37*, 2718–2727.
[37] Pal, R.; Higuchi, M.; Kurth, D. *Org. Lett.* **2009**, *11*, 3562–3565.
[38] Pfeil, A.; Lehn, J. M. *J. Chem. Soc., Chem. Commun.* **1992**, *28*, 838–840.
[39] van Veggel, F.; Verboom, W.; Reinhoudt, D. *Chem. Rev.* **1994**, *94*, 279–299.
[40] Zangrando, E.; Casanova, M.; Alessio, E. *Chem. Rev.* **2008**, *108*, 4979.
[41] Constable, E. C.; Harris, K.; Housecroft, C. E.; Neuburger, M. *Dalton Trans.* **2011**, *40*, 1524–1534.
[42] Wang, P.; Moorefield, C.; Newkome, G. *Angew. Chem. Int. Ed.* **2005**, *44*, 1679–1683.
[43] Zhao, B.; Li, H.; Shen, Q.; Zhang, Y.; Yao, Y.; Lu, C. *Organometallics* **2006**, *25*, 1824–1827.
[44] Troff, R. W.; Hovorka, R.; Weilandt, T.; Lutzen, A.; Cetina, M.; Nieger, M.; Lentz, D.; Rissanen, K.; Schalley, C. A. *Dalton Trans.* **2012**, *41*, 8410–8420.
[45] Andres, P. R.; Schubert, U. S. *Synthesis* **2004**, 1229–1238.
[46] Seeber, G.; Kariuki, B.; Cronin, L. *Chem. Commun.* **2002**, *38*, 2912–2913.
[47] Ni, Z.; Tao, J.; Wernsdorfer, W.; Cui, A.; Kou, H. *Dalton Trans.* **2009**, 2788–2794.
[48] Smith, C.; Constable, E.; Housecroft, C.; Kariuki, B. *Chem. Commun.* **2002**, *38*, 2068–2069.
[49] Brusilowskij, B.; Dzyuba, E. V.; Troff, R. W.; Schalley, C. A. *Chem. Commun.* **2011**, *47*, 1830–1832.
[50] Yan, Y.; de Keizer, A.; Stuart, M.; Besseling, N. *Adv. Polym. Sci.* **2011**, *242*, 91–115.
[51] Meier, M.; Hofmeier, H.; Abeln, C.; Tziatzios, C.; Rasa, M.; Schubert, D.; Schubert, U. *E-Polymers* **2006**, 1–7.
[52] Rasa, M.; Lohmeijer, B. G. G.; Hofmeier, H.; Thijs, H. M. L.; Schubert, D.; Schubert, U. S.; Tziatzios, C. *Macromol. Chem. Phys.* **2006**, *207*, 2029–2041.
[53] Ott, C.; Wouters, D.; Thijs, H. M. L.; Schubert, U. S. *J. Inorg. Organomet. Polym. Mater.* **2007**, *17*, 241–249.
[54] Heller, M.; Schubert, U. S. *Macromol. Rapid Commun.* **2002**, *23*, 411–415.
[55] Ott, C.; Kranenburg, J. M.; Guerrero-Sanchez, C.; Hoeppener, S.; Wouters, D.; Schubert, U. S. *Macromolecules* **2009**, *42*, 2177–2183.
[56] Paulusse, J.; Sijbesma, R. *Chem. Commun.* **2003**, *39*, 1494–1495.

[57] Beck, J.; Ineman, J.; Rowan, S. *Macromolecules* **2005**, *38*, 5060–5068.
[58] Vermonden, T.; van der Gucht, J.; de Waard, P.; Marcelis, A.; Besseling, N.; Sudhölter, E.; Fleer, G.; Stuart, M. *Macromolecules* **2003**, *36*, 7035–7044.
[59] Fox, J. D.; Rowan, S. J. *Macromolecules* **2009**, *42*, 6823–6835.
[60] Kurth, D. G.; Higuchi, M. *Soft Matter* **2006**, *2*, 915–927.
[61] Yount, W.; Juwarker, H.; Craig, S. *J. Am. Chem. Soc.* **2003**, *125*, 15302–15303.
[62] Seiffert, S.; Sprakel, J. *Chem. Soc. Rev.* **2012**, *41*, 909–930.
[63] Paulusse, J.; Huijbers, J.; Sijbesma, R. *Macromolecules* **2005**, *38*, 6290–6298.
[64] Bünzli, J.-C. G.; Piguet, C. *Chem. Rev.* **2002**, *102*, 1897–1928.
[65] Bünzli, J. *Acc. Chem. Res.* **2006**, *39*, 53–61.
[66] Holyer, R. H.; Hubbard, C. D.; Kettle, S. F. A.; Wilkins, R. G. *Inorg. Chem.* **1966**, *5*, 622–625.
[67] Farina, R.; Hogg, R.; Wilkins, R. *Inorg. Chem.* **1968**, *7*, 170–172.
[68] Lahn, B.; Rehahn, M. *E-Polymers* **2002**, 1–33.
[69] Schmatloch, S.; van den Berg, A.; Fijten, M.; Schubert, U. *Macromol. Rapid Commun.* **2004**, *25*, 321–325.
[70] Henderson, I. M.; Hayward, R. C. *Polym. Chem.* **2012**, *3*, 1221–1230.
[71] Ellis, P.; Hogg, R.; Wilkins, R. G. *J. Chem. Soc.* **1959**, 3308–3313.
[72] Paulusse, J.; Huijbers, J.; Sijbesma, R. *Chem. Eur. J.* **2006**, *12*, 4928–4934.
[73] Paulusse, J.; Sijbesma, R. *Angew. Chem.* **2004**, *116*, 4560–4562.
[74] Brunsveld, L.; Folmer, B. J. B.; Meijer, E. W.; Sijbesma, R. P. *Chem. Rev.* **2001**, *101*, 4071–4097.
[75] te Nijenhuis, K. *Thermoreversible networks: Viscoelastic properties and structure of gels*; Springer: New York, 1997; pp xx, 267.
[76] te Nijenhuis, K. *Polym. Bull.* **2007**, *58*, 27–42.
[77] Suzuki, D.; Sakai, T.; Yoshida, R. *Angew. Chem.* **2008**, *120*, 931–934.
[78] Schubert, U. S.; Alexeev, A.; Andres, P. R. *Macromol. Mater. Eng.* **2003**, *288*, 852–860.
[79] Kersey, F. R.; Loveless, D. M.; Craig, S. L. *J. R. Soc. Interface* **2007**, *4*, 373–380.
[80] Hofmeier, H.; El-ghayoury, A.; Schubert, U. S. *E-Polymers* **2003**, 1–13.
[81] El-ghayoury, A.; Hofmeier, H.; de Ruiter, B.; Schubert, U. S. *Macromolecules* **2003**, *36*, 3955–3959.
[82] Fiore, G.; Klinkenberg, J.; Pfister, A.; Fraser, C. *Biomacromolecules* **2008**, *10*, 128–133.
[83] Lee, B. P.; Konst, S. *Adv. Mater.* **2014**, *26*, 3415–3419.
[84] Xu, H.; Nishida, J.; Wu, H.; Higaki, Y.; Otsuka, H.; Ohta, N.; Takahara, A. *Soft Matter* **2013**, *9*, 1967–1974.
[85] Sievers, T.; Vergin, A.; Möhwald, H.; Kurth, D. *Langmuir* **2007**, *23*, 12179–12184.

[86] Kokil, A.; Shiyanovskaya, I.; Singer, K.; Weder, C. *J. Am. Chem. Soc.* **2002**, *124*, 9978–9979.
[87] Schmatloch, S.; Schubert, U. S. *Macromol. Symp.* **2003**, *199*, 483–497.
[88] Meier, M. A. R.; Schubert, U. S. *J. Polym. Sci., Part A: Polym. Chem.* **2003**, *41*, 2964–2973.
[89] Knapton, D.; Rowan, S.; Weder, C. *Macromolecules* **2006**, *39*, 651–657.
[90] Kumpfer, J.; Jin, J.; Rowan, S. *J. Mater. Chem.* **2010**, *20*, 145–151.
[91] Kumpfer, J. R.; Wie, J. J.; Swanson, J. P.; Beyer, F. L.; Mackay, M. E.; Rowant, S. J. *Macromolecules* **2012**, *45*, 473–480.
[92] Welterlich, I.; Tieke, B. *Macromolecules* **2011**, *44*, 4194–4203.
[93] Bode, S.; Zedler, L.; Schacher, F. H.; Dietzek, B.; Schmitt, M.; Popp, J.; Hager, M. D.; Schubert, U. S. *Adv. Mater.* **2013**, *25*, 1634–1638.
[94] Coulibaly, S.; Roulin, A.; Balog, S.; Biyani, M. V.; Foster, E. J.; Rowan, S. J.; Fiore, G. L.; Weder, C. *Macromolecules* **2013**, *47*, 152–160.
[95] Hong, G.; Zhang, H.; Lin, Y.; Chen, Y.; Xu, Y.; Weng, W.; Xia, H. *Macromolecules* **2013**, *46*, 8649–8656.
[96] Jackson, A. C.; Beyer, F. L.; Price, S. C.; Rinderspacher, B. C.; Lambeth, R. H. *Macromolecules* **2013**, *46*, 5416–5422.
[97] Yuan, J.; Zhang, H.; Hong, G.; Chen, Y.; Chen, G.; Xu, Y.; Weng, W. *J. Mater. Chem. B* **2013**, *1*, 4809–4818.
[98] Jackson, A. C.; Walck, S. D.; Strawhecker, K. E.; Butler, B. G.; Lambeth, R. H.; Beyer, F. L. *Macromolecules* **2014**, *47*, 4144–4150.
[99] Wang, Z.; Fan, W.; Tong, R.; Lu, X.; Xia, H. *RSC Advances* **2014**, *4*, 25486–25493.
[100] Yang, B.; Zhang, H.; Peng, H.; Xu, Y.; Wu, B.; Weng, W.; Li, L. *Polym. Chem.* **2014**, *5*, 1945–1953.
[101] Kumpfer, J. R.; Rowan, S. J. *ACS Macro Lett.* **2012**, *1*, 882–887.
[102] Weiss, R. G.; Terech, P. *Molecular gels: Materials with self-assembled fibrillar networks*; Springer: Dordrecht, 2006; pp xv, 978.
[103] Terech, P.; Weiss, R. G. *Chem. Rev.* **1997**, *97*, 3133–3160.
[104] Abdallah, D.; Weiss, R. *Adv. Mater.* **2000**, *12*, 1237–1247.
[105] Estroff, L. A.; Hamilton, A. D. *Chem. Rev.* **2004**, *104*, 1201–1218.
[106] George, M.; Weiss, R. G. *Acc. Chem. Res.* **2006**, *39*, 489–497.
[107] Lin, Y.; Mao, C. *Front. Mater. Sci.* **2011**, *5*, 247–265.
[108] Whitesides, G. M.; Grzybowski, B. *Science* **2002**, *295*, 2418–2421.
[109] Palmer, L. C.; Stupp, S. I. *Acc. Chem. Res.* **2008**, *41*, 1674–1684.
[110] Yan, Y.; Huang, J. B. *Coord. Chem. Rev.* **2010**, *254*, 1072–1080.
[111] Yao, H. B.; Fang, H. Y.; Wang, X. H.; Yu, S. H. *Chem. Soc. Rev.* **2011**, *40*, 3764–3785.
[112] Elemans, J.; Rowan, A.; Nolte, R. *J. Mater. Chem.* **2003**, *13*, 2661–2670.
[113] Ikkala, O.; ten Brinke, G. *Chem. Commun.* **2004**, *40*, 2131–2137.
[114] Choi, I. S.; Bowden, N.; Whitesides, G. M. *Angew. Chem. Int. Ed.* **1999**, *38*, 3078–3081.

[115] Paulusse, J. M.; van Beek, D. J.; Sijbesma, R. P. *J. Am. Chem. Soc.* **2007**, *129*, 2392–2397.
[116] Vermonden, T.; van Steenbergen, M.; Besseling, N.; Marcelis, A.; Hennink, W.; Sudhölter, E.; Stuart, M. *J. Am. Chem. Soc.* **2004**, *126*, 15802–15808.
[117] Vermonden, T.; de Vos, W.; Marcelis, A.; Sudhölter, E. *Eur. J. Inorg. Chem.* **2004**, *2004*, 2847–2852.
[118] Balkenende, D. W. R.; Coulibaly, S.; Balog, S.; Simon, Y. C.; Fiore, G. L.; Weder, C. *J. Am. Chem. Soc.* **2014**, *136*, 10493–10498.
[119] Beck, J. B.; Rowan, S. J. *J. Am. Chem. Soc.* **2003**, *125*, 13922–13923.
[120] Weng, W. G.; Beck, J. B.; Jamieson, A. M.; Rowan, S. J. *J. Am. Chem. Soc.* **2006**, *128*, 11663–11672.
[121] Rowan, S.; Beck, J. *Faraday Discuss.* **2005**, *128*, 43–53.
[122] Pezron, E.; Leibler, L.; Ricard, A.; Audebert, R. *Macromolecules* **1988**, *21*, 1126–1131.
[123] Pezron, E.; Ricard, A.; Lafuma, F.; Audebert, R. *Macromolecules* **1988**, *21*, 1121–1125.
[124] Zasadzinski, J.; Chu, A.; Prud'Homme, R. *Macromolecules* **1986**, *19*, 2960–2964.
[125] Kamide, K.; Yasuda, K.; Okajima, K. *Polym. J.* **1988**, *20*, 259–268.
[126] Yokoi, H.; Kawata, S.; Iwaizumi, M. *J. Am. Chem. Soc.* **1986**, *108*, 3358–3361.
[127] Yokoi, H.; Kawata, S.; Iwaizumi, M. *J. Am. Chem. Soc.* **1986**, *108*, 3361–3365.
[128] te Nijenhuis, K. *Macromol. Symp.* **2001**, *171*, 189–200.
[129] te Nijenhuis, K.; Mensert, A.; Zitha, P. *Rheol. Acta* **2003**, *42*, 132–141.
[130] Peng, F.; Li, G.; Liu, X.; Wu, S.; Tong, Z. *J. Am. Chem. Soc.* **2008**, *130*, 16166–16167.
[131] Lewis, A.; Miller, J. *J. Chem. Soc., Chem. Commun.* **1992**, *28*, 1029–1030.
[132] Lewis, A.; Miller, J. *Polymer* **1993**, *34*, 2453–2457.
[133] Lewis, A.; Miller, J. *J. Mater. Chem.* **1993**, *3*, 897–902.
[134] Lewis, A.; Miller, J. *J. Mater. Chem.* **1994**, *4*, 729–734.
[135] Lewis, A.; Miller, J. *Polymer* **1995**, *36*, 331–339.
[136] Yount, W. C.; Loveless, D. M.; Craig, S. L. *J. Am. Chem. Soc.* **2005**, *127*, 14488–14496.
[137] Yount, W. C.; Loveless, D. M.; Craig, S. L. *Angew. Chem. Int. Ed.* **2005**, *44*, 2746–2748.
[138] Loveless, D. M.; Jeon, S. L.; Craig, S. L. *J. Mater. Chem.* **2007**, *17*, 56–61.
[139] Noro, A.; Matsushima, S.; He, X.; Hayashi, M.; Matsushita, Y. *Macromolecules* **2013**, *46*, 8304–8310.
[140] Wright, M. *Macromolecules* **1989**, *22*, 3256–3259.
[141] Hirao, T.; Yamaguchi, S.; Fukuhara, S. *Tetrahedron Lett.* **1999**, *40*, 3009–

3012.
[142] Kokil, A.; Huber, C.; Caseri, W.; Weder, C. *Macromol. Chem. Phys.* **2003**, *204*, 40–45.
[143] Kokil, A.; Yao, P.; Weder, C. *Macromolecules* **2005**, *38*, 3800–3807.
[144] de Hatten, X.; Bell, N.; Yufa, N.; Christmann, G.; Nitschke, J. R. *J. Am. Chem. Soc.* **2011**, *133*, 3158–3164.
[145] Meudtner, R. M.; Hecht, S. *Macromol. Rapid Commun.* **2008**, *29*, 347–351.
[146] Tian, Y.-K.; Chen, L.; Tian, Y.-J.; Wang, X.-Y.; Wang, F. *Polym. Chem.* **2013**, *4*, 453–457.
[147] Chujo, Y.; Sada, K.; Saegusa, T. *Macromolecules* **1993**, *26*, 6315–6319.
[148] Chujo, Y.; Sada, K.; Saegusa, T. *Polym. J.* **1993**, *25*, 599–608.
[149] Chujo, Y.; Sada, K.; Saegusa, T. *Macromolecules* **1993**, *26*, 6320–6323.
[150] Basolo, F.; Hayes, J.; Neumann, H. *J. Am. Chem. Soc.* **1953**, *75*, 5102–5106.
[151] Basolo, F.; Hayes, J.; Neumann, H. *J. Am. Chem. Soc.* **1954**, *76*, 3807–3809.
[152] Ott, C.; Ulbricht, C.; Hoogenboom, R.; Schubert, U. S. *Macromol. Rapid Commun.* **2012**, *33*, 556–561.
[153] Hofmeier, H.; Schubert, U. S. *Macromol. Chem. Phys.* **2003**, *204*, 1391–1397.
[154] Sun, P.; Wang, J.; Yao, X.; Peng, Y.; Tu, X.; Du, P.; Zheng, Z.; Wang, X. *ACS Appl. Mater. Interfaces* **2014**, *6*, 12495–12504.
[155] Kimura, M.; Nakagawa, Y.; Adachi, N.; Tatewaki, Y.; Fukawa, T.; Shirai, H. *Chem. Lett.* **2009**, *38*, 382–383.
[156] Rossow, T.; Habicht, A.; Seiffert, S. *Macromolecules* **2014**, *47*, 6473–6482.
[157] Rossow, T.; Seiffert, S. *Polym. Chem.* **2014**, *5*, 3018–3029.
[158] Asoh, T.-A.; Yoshitake, H.; Takano, Y.; Kikuchi, A. *Macromol. Chem. Phys.* **2013**, *214*, 2534–2539.
[159] Wang, R.; Geven, M.; Dijkstra, P. J.; Martens, P.; Karperien, M. *Soft Matter* **2014**, *10*, 7328–7336.
[160] Ueki, T.; Takasaki, Y.; Bundo, K.; Ueno, T.; Sakai, T.; Akagi, Y.; Yoshida, R. *Soft Matter* **2014**, *10*, 1349–1355.
[161] Holten-Andersen, N.; Harrington, M.; Birkedal, H.; Lee, B.; Messersmith, P.; Lee, K.; Waite, J. *Proc. Natl. Acad. Sci. U. S. A.* **2011**, *108*, 2651–2655.
[162] Barrett, D.; Fullenkamp, D.; He, L.; Holten-Andersen, N.; Lee, K.; Messersmith, P. *Adv. Funct. Mater.* **2012**, *23*, 1111–1119.
[163] Holten-Andersen, N.; Jaishankar, A.; Harrington, M. J.; Fullenkamp, D. E.; DiMarco, G.; He, L.; McKinley, G. H.; Messersmith, P. B.; Lee, K. Y. C. *J. Mater. Chem. B* **2014**, *2*, 2467–2472.
[164] Menyo, M. S.; Hawker, C. J.; Waite, J. H. *Soft Matter* **2013**, *9*, 10314–10323.

[165] Sato, T.; Ebara, M.; Tanaka, S.; Asoh, T.-A.; Kikuchi, A.; Aoyagi, T. *Phys. Chem. Chem. Phys.* **2013**, *15*, 10628–10635.
[166] Nair, K. P.; Breedveld, V.; Weck, M. *Macromolecules* **2011**, *44*, 3346–3357.
[167] Ghoussoub, A.; Lehn, J. M. *Chem. Commun.* **2005**, *41*, 5763–5765.
[168] Pollino, J.; Nair, K.; Stubbs, L.; Adams, J.; Weck, M. *Tetrahedron* **2004**, *60*, 7205–7215.
[169] Yan, X.; Xu, D.; Chi, X.; Chen, J.; Dong, S.; Ding, X.; Yu, Y.; Huang, F. *Adv. Mater.* **2012**, *24*, 362–369.
[170] Wang, F.; Zhang, J. Q.; Ding, X.; Dong, S. Y.; Liu, M.; Zheng, B.; Li, S. J.; Wu, L.; Yu, Y. H.; Gibson, H. W.; Huang, F. H. *Angew. Chem. Int. Ed.* **2010**, *49*, 1090–1094.
[171] Guillet, P.; Mugemana, C.; Stadler, F. J.; Schubert, U. S.; Fustin, C.-A.; Bailly, C.; Gohy, J.-F. *Soft Matter* **2009**, *5*, 3409–3411.
[172] Brassinne, J.; Mugemana, C.; Guillet, P.; Bertrand, O.; Auhl, D.; Bailly, C.; Fustin, C.-A.; Gohy, J.-F. *Soft Matter* **2012**, *8*, 4499–4506.
[173] Buwalda, S. J.; Dijkstra, P. J.; Feijen, J. *J. Polym. Sci., Part A: Polym. Chem.* **2012**, *50*, 1783–1791.
[174] Jochum, F. D.; Brassinne, J.; Fustin, C.-A.; Gohy, J.-F. *Soft Matter* **2013**, *9*, 2314–2320.
[175] Bharatiya, B.; Fustin, C.-A.; Gohy, J.-F. *Macromol. Chem. Phys.* **2012**, *213*, 2253–2260.
[176] Weng, W.; Fang, X.; Zhang, H.; Peng, H.; Lin, Y.; Chen, Y. *Eur. Polym. J.* **2013**, *49*, 4062–4071.
[177] Rossow, T.; Hackelbusch, S.; van Assenbergh, P.; Seiffert, S. *Polym. Chem.* **2013**, *4*, 2515–2527.
[178] Pollak, A.; Blumenfeld, H.; Wax, M.; Baughn, R. L.; Whitesides, G. M. *J. Am. Chem. Soc.* **1980**, *102*, 6324–6336.
[179] Hackelbusch, S.; Rossow, T.; Becker, H.; Seiffert, S. *Macromolecules* **2014**, *47*, 4028–4036.
[180] Yan, X.; Xu, D.; Chen, J.; Zhang, M.; Hu, B.; Yu, Y.; Huang, F. *Polym. Chem.* **2013**, *4*, 3312–3322.
[181] Yan, X.; Cook, T. R.; Pollock, J. B.; Wei, P.; Zhang, Y.; Yu, Y.; Huang, F.; Stang, P. J. *J. Am. Chem. Soc.* **2014**, *136*, 4460–4463.
[182] Zhan, J.; Li, Q.; Hu, Q.; Wu, Q.; Li, C.; Qiu, H.; Zhang, M.; Yin, S. *Chem. Commun.* **2014**, *50*, 722–724.
[183] Zhan, J.; Zhang, M.; Zhou, M.; Liu, B.; Chen, D.; Liu, Y.; Chen, Q.; Qiu, H.; Yin, S. *Macromol. Rapid Commun.* **2014**, *35*, 1424–1429.
[184] Guillet, P.; Fustin, C.-A.; Mugemana, C.; Ott, C.; Schubert, U. S.; Gohy, J.-F. *Soft Matter* **2008**, *4*, 2278–2282.
[185] Mugemana, C.; Joset, A.; Guillet, P.; Appavou, M.-S.; De Souza, N.; Fustin, C.-A.; Leyh, B.; Gohy, J.-F. *Macromol. Chem. Phys.* **2013**, *214*, 1699–1709.

CHAPTER 7

RHEOLOGY OF METALLO-SUPRAMOLECULAR POLYMER GELS – A LITERATURE REVIEW

Abstract

An analysis of the rheology of metallo-supramolecular polymer gels is herein developed through a comprehensive literature review. At first, the concept of polymer gel is described in a rheological point of view toward its metallo-supramolecular derivation. Then, the rheology of MSPGs is addressed in detail, with pertinent scientific advances in the recent years. In this respect, linear, i.e.*, network cross-linking density and dynamics, and non-linear rheological properties are tackled separately.*

7.1 Rheological definitions and concepts

Arising from the key concepts of metallo-supramolecular chemistry [1,2] and theory of gelation, [3–5] rheological features of metallo-supramolecular polymer gels are barely identified in the literature. In this section, the term "polymer gels" is briefly reminded before formulating a coherent rheology as to what defines MSPGs.

7.1.1 Concept of polymer gels

Usually, the term "gel" refers to soft or hard jelly-like materials. While they are mostly liquid, they exhibit solid-like behaviour and do not flow generally when exposed to stress. They can be of colloidal or polymer nature and swell to a certain finite extent, in aqueous or organic solvents. As highlighted by Keller, [6] reasons why they can attract attention, even as confined to the field of polymer science, are as varied as the types of junctions which can lead to gels (Figure 7.1). However, the concept of "gel" has been used so indiscriminately that a unique definition has become a matter of discussion. In most of the cases, scientific definitions suffer from a lack of accuracy because they do not include exceptions. By instance, the Dictionary of Polymers states "a polymer gel consists of a three dimensional cross-linked network and swells in a solvent, but does not dissolve even in a good solvent". [7] While non-swollen molecular networks, like rubbers, are properly excluded, this definition is clearly limited to chemically, *i.e.*, covalently, cross-linked gels and eliminates physical gels, made by secondary molecular forces.

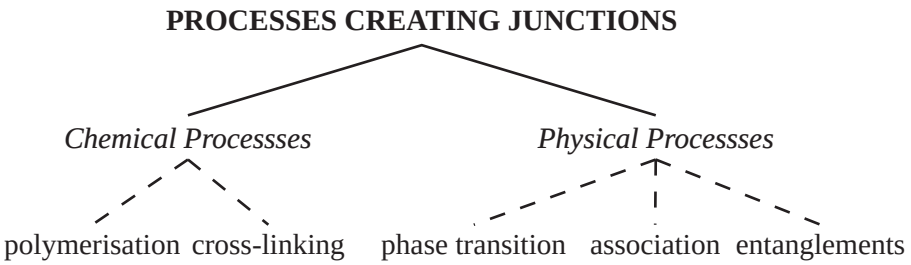

Figure 7.1 – Chart displaying the different sources of junction which can lead to networks and gels. [6]

As pointed by Lloyd in 1926,[8] gels are much easier to recognize than to define, and even recognition is confused by the fact that the limits between gel and sol are not precise. Twenty-three years after, the best available definition referred to a gel as "a two-component system of a semi-solid nature, rich in liquid"[9] or "a coherent system which exhibits mechanical properties of a solid, where both the dispersed component and the dispersion medium extend themselves continuously throughout the whole system"[10]. Later, uncertainties in defining gels were perceived in descriptions emphasizing "a substantially diluted system which exhibits no steady state flow".[11–13]

With the Flory–Stockmayer gelation theory,[3–5] structural criteria, such as the formation of an infinite network, or a three-dimensional structure, featuring properties such as coherence and connectedness, were included in the definition of a gel. In rheological studies, Burchard and Ross-Murphy pointed that gels are, or can be coaxed to be, viscoelastic solids, *i.e.*, they possess a plateau in the real part of the complex modulus extending over an appreciable window of frequencies.[14] Later, those experimental definitions were extended by Almdal and coworkers, who stated that "a gel is a soft, solid or solid-like material, which consists of two or more components, one of which is a liquid, present in substantial quantity"[15]. In particular, solid-like gels are characterized by the absence of an equilibrium modulus, a storage modulus, $G'(\omega)$, which exhibits a pronounced plateau and a loss modulus, $G''(\omega)$, which is considerably smaller in the plateau region.[15]

More recently, the afore-mentioned statement was critically revised by Rogovina and coworkers. Indeed, they pointed that this definition still includes undefined terms, like "soft" and "substantial quantity". Furthermore, they noted that only physical gels are characterized by the absence of an equilibrium modulus since the equilibrium modulus of elasticity is always attained in chemical gels.[16,17] In fact, an equilibrium modulus is observed in physical gels as well, at stresses only below the first yield point.[18] After a brief review of the current status of knowledge in the area of polymer gels, a revised definition was thus proposed by Rogovina and coworkers: "a gel is a solid composed of at least two components, one of which (the polymer) forms a three-dimensional network by virtue of covalent or non-covalent bonding (chemical and physical gels, respectively) in the medium of the other component (the liquid), wherein the minimum amount of the liquid is sufficient for en-

suring the elastic properties of the gel, although it may exceed tens to hundreds of times the amount of the polymer".[19]

Over time, many tentative definitions have been thus proposed to define what polymer gels are. In general, working hypotheses are based on both rheological behaviours and structural features. While most of them are still subject to debate, a more philosophical definition states that "a gel is a gel, as long as one cannot prove that it is not a gel".[20]

7.1.2 Toward metallo-supramolecular polymer gels

In a rheological point of view, MSPGs should exhibit an equilibrium modulus under stress at least below the yield point.[21–25] Viscous and elastic behaviours are recognizable under weak applied stresses, *i.e.*, in the viscoelastic linear regime, and contribute respectively to the elastic storage modulus, G', and the viscous loss modulus, G''. However, under high stress/strain, supramolecular gels display a non-linear behaviour and begin to flow. They are said to be plastic and have an associated yield strain/stress or plasticity threshold beyond which the material flows.[26] At the limit of yielding, different behaviours can be observed depending on the type of interactions structuring the material but also on the relationship between the experiment and material relaxation timescales: strain thinning (decrease in both moduli), strain hardening (increase in both moduli), weak or strong strain overshoot (increase in elastic only, or both moduli, followed by decrease).[27–29]

Since they swell in a minimal amount of solvent, supramolecular gels are characterized by a pronounced thixotropic behaviour,[30–36] *i.e.*, they undergo an isothermal reversible gel–sol (solid–liquid) transition under mechanical stress.[21–25,37–40] While the reversibility of the gel–sol transition is a direct consequence of the reversibility of the metal–ligand interaction, flowing of the material is more a time dependent process that reflects the characteristic time scales of the material.

Whereas stress relaxation in commodity polymers is usually determined by the reptation of covalent polymer chains, the dissociation and association of non–covalent junctions play a much more prominent role in the case of supramolecular analogues.[41–44] In that field, significant advances were made by Craig and coworkers who proposed to define a supramolecular polymer network as corresponding to "the conditions

under which the relaxation of the network is dominated by the dissociation kinetics of cross-linkers", as characterized through linear oscillatory frequency sweep rheology.[45]

Experimentally, the conditions defined by Craig *et al.* are verified when the relaxation time of the supramolecular network is proportional to the lifetime of the cross-linkers. Although attractive, this definition has to be extended to include supramolecular polymer gels that combine labile metal–ligand bonds with other non-covalent interactions or chain entanglement. Indeed, dissipation of mechanical constrains in such systems may involve multiple relaxation mechanisms that reflect their structural complexity. Considering those extra transient associations can considerably influence the dynamics of the physical polymeric networks since its creation results from a combination of associative bonds. Also, the mechanism that governs the relaxation of the stressed materials may sensibly vary depending on environmental constrains, such as the amplitude of solicitation.

To summarize, metallo-supramolecular polymer gels can be thus structurally defined as polymer networks that present coordinative bonds, either in the polymeric backbone or as junctions between their building units. They unambiguously swell in a minimal amount of liquid so that their rheology is characterized by an equilibrium modulus, at stresses at least below the first yield point. Above, mechanical forces induce the reversible flow of physically cross-linked entities, whose dissociation allows stress relaxation of the material.

7.2 Dynamic linear response of MSPGs

Since the appearance of supramolecular polymers gels, attempts have been made to describe their rheological behaviour by adapting existing theories on concentrated entangled polymer solutions. Indeed, in contrast to their classical counterparts, supramolecular polymers exhibit associating moieties that can reversibly bind to each other in a dynamic way, which impart additional levels of complexity in the description of those materials.

The incorporation of the dynamics of those interactions into well-established models opens up the way of predicting the rheological behaviour of supramolecular polymer gels constructed from the non-covalent

association of covalently joined oligo- or polymeric precursors. Active contributions in this field have been made by the groups of Tanaka,[46–51] Semenov–Rubinstein,[52–61] or Jongschaap–Wientjes,[62–64] with theoretical approaches based on transient networks, sticky Rouse or sticky reptation models, without distinction between the different types of association processes.

7.2.1 Network cross-linking density

As a general feature of MSPGs, it can be assumed that the equilibrium modulus is determined by the inter-molecularly bonded metallo-linkers in the semi-dilute unentangled regime, whereas it may be determined by both the inter-molecularly bonded metallo-linkers and entanglements between polymer chains in semi-dilute and concentrated entangled regimes. In turn, the number density of elastically active cross-links units contribute tremendously to the final mechanical properties of MSPGs. In the dilute regime, one can assume that those elastically effective cross-links rely mostly on inter-molecular metallo-bridges since intra-molecular links result in loops. However, loops can concatenate when concentration rises and thus bring their own contribution to the elasticity of the material.

A clear distinction between the contribution of inter- and concatenated intra-molecular links is however difficult to achieve, even for covalent networks.[65,66] However, investigations are currently devoted to a better understanding and control over the number density of elastically active cross-links and thus over the properties of MSPGs. On an enthalpic point of view, intra-molecular metallo-links are as well favoured as inter-molecular ones since both involve the formation of coordinative bonds that are characterized by the same binding strength. However, the formation of elastically effective cross-link may be entropically driven, despite the fact that dynamic supramolecular systems will always reorganize to reach the most thermodynamically favourable state.[67]

Abrupt changes in the mechanical properties of supramolecular gels are obviously reported around the percolation threshold, or gel point, since the formation of a continuous network requires a minimum number of chemical/physical cross-links between their components. For MSPGs, the onset of percolation, defined by the density of cross-linking, will depend on the concentration of both metallo-linkers and oligo- or polymeric

species that will self-assembled in their presence.[45,68,69]

As noted by Craig *et al.*,[45,70] a distinction can be made between four states for the metallo-linkers: free, dangling, intra-molecularly bound, and inter-molecularly bound linkers (Figure 7.2). Of those, only inter-molecular bound metallo-linkers are elastically active, *i.e.*, they contribute to the network modulus. If a metallo-linker dissociates, it changes temporarily to the dangling state, from which it can bind again to an available residue elsewhere, as characterized by the sticky Rouse or sticky reptation models of associative polymer networks.[52,60] In practice, the number of elastically active metallo-linkers can be significantly reduced by addition of chain stoppers or in the presence of strong coordinating solvents, counter-ions, or competitive ligands, which can induce a gel-to-sol transition within the material.[23,38,40,69,71–74]

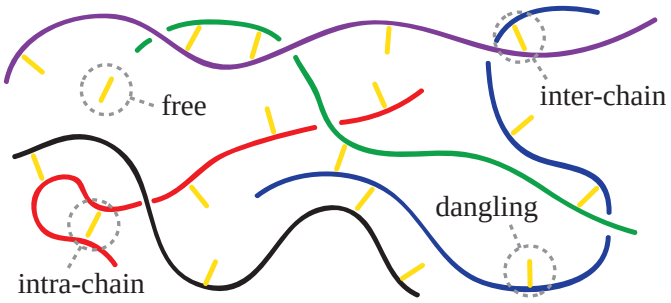

Figure 7.2 – Schematic representation of a metallo-supramolecular network showing the different states of cross-linkers.[45,60]

Experimentally, it is also often found that there are simple scaling relations between concentrations of the components that constitute the MSPGs and their rheological characteristics.[38,44,45,69] Scaling law relationships of the elastic modulus, relaxation time, and zero-shear viscosity with the concentration of oligomer were notably reported by Vermonden *et al.* when they studied the linear rheology of reversible neodymium(III) coordination polymers in aqueous solutions[38]. On the basis of their results, it was found that either cross-linked networks or linear chains were formed in solution, depending on the spacer length between the metallo-supramolecular cross-links. This was explained by the thermodynamically-driven formation of ring-like structures consisting of two oligomer molecules and two metal ions (Figure 6.4). For the linear supramolecular polymer chains, the scaling law was in good agree-

ment with the predictions of Cates' model that describes the dynamics of linear equilibrium polymers.[75] In fact, this indicated at least that the networks had only few cross-links and could be described as linear equilibrium polymers. For the cross-linked supramolecular polymer network, the results were not consistent with the Cates' model, although a good scaling law relationship between zero-shear viscosity and concentration of polymer was still observed.

In another extensive study,[45] Xu and Craig examined the linear rheological properties of networks formed by adding Pd(II) metallo-pincers to poly(4-vinylpyridine) solution in DMSO (Figure 6.9). The scaling law relationships between the zero shear viscosity of the networks versus the concentration of poly(4-vinylpyridine) solutions, the concentration of cross-linkers, and the apparent number density of elastically active chains were experimentally determined and compared to the theoretical expectations of the sticky Rouse or sticky reptation models.[60] Both qualitative and quantitative differences in behaviour were observed with the statement that the sticky Rouse and sticky reptation models were not able to fully describe the experimentally determined scaling law relationships. The lifetime of the physical entanglements between polymer chains, *i.e.*, the Rouse relaxation time, was much smaller than the lifetime of formation and breakage of metallo-supramolecular cross-links. Experimentally, this was correlated to the frequency at which the plateau value of the modulus was characterized. Indeed, this frequency was faster than the rate of dissociation of cross-linkers but much slower than the rate of physical disentanglement between polymer chains, which indicated that the relaxation of the network was dominated by the dissociation kinetics of metallo-supramolecular bonds and not by the disentanglement kinetics. However, when the Rouse relaxation time gets closer to the lifetime of the metallo-supramolecular bonds, it was assumed that physical entanglements between polymer chains should also contribute to the value of the plateau modulus in the semi-dilute entangled regime. Accordingly, the concentration and/or lifetime of metallo-linkers were found to have an influence on the lifetime of physical entanglements between polymer chains, resulting in a renormalized lifetime of physical entanglements between polymer chains.

Beside the concentration dependence of the rheological properties, temperature also plays an important role since it will influence the dynamics of MSPGs. The evolution of both storage and loss moduli as a

function of the temperature was reported by Vermonden and coworkers.[38] While an elastic behaviour clearly characterized the rheological properties of their MSPGs at low temperature, the viscous component progressively tends to dominate the material when temperature rises, meaning that the sample loses its elastic properties and becomes a liquid (Figure 7.3). It was assumed that, at high temperatures, the mobility of the molecules increased but also that the complexation constants between metal ions and ligands decreased, leading to smaller chains and eventually single molecules. Upon cooling, the storage and loss moduli returned immediately to the same level as before the sample was heated, demonstrating the reversibility of the system. Also, increasing the temperature led to a decrease in the relaxation time which was inversely proportional to an increase in the metal–ligand bond dissociating rate. Using the information of the relaxation time (or the rate constant), an overall activation energy for reptation and breaking that matched a reversible system was obtained from the Arrhenius plot.

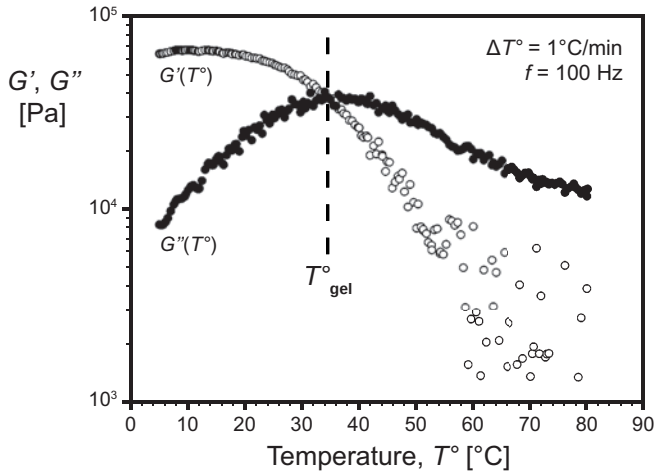

Figure 7.3 – Evolution of storage and loss moduli with temperature for a water soluble neodymium(III) coordination polymer.[38]

As reported in literature, increasing the functionality of the metal centre, *i.e.*, the number of ligand that can be accommodated around the metal cations, also potentially affects the number density of active crosslinks in a positive way. In this respect, playing on the balance between bivalent and multivalent metal ions, when used in combination, can be

considered as a straightforward approach to tune the rheological properties of MSPGs. This methodology was recently illustrated by the work of Weng *et al.*[25] who fine-tuned the gelation and properties of MSPGs based on "click" polymeric ligands by the careful selection of metal ions and their combinations. Zinc(II) containing gels were less elastic and more viscous than the gels containing only europium(III) (Figure 7.4), which is consistent with their different binding characteristics. Indeed, Zn(II) metal ions bind to 2,6-bis(1,2,3-triazol-4-yl)pyridines ligand in a 1:2 ratio while Eu(III) metal ions bind in a 1:3 ratio.

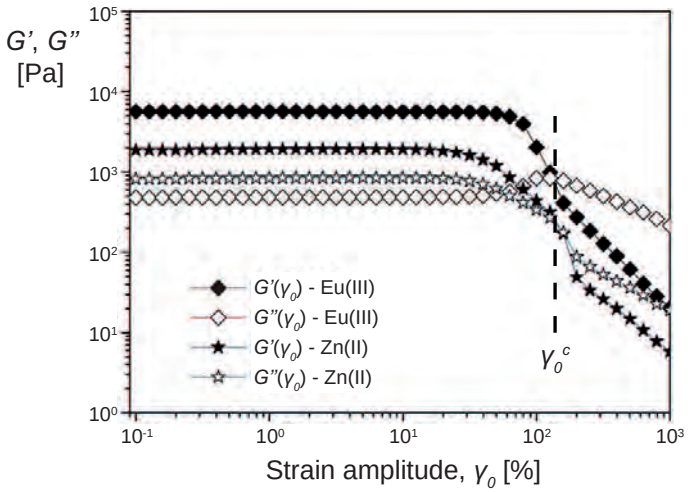

Figure 7.4 – Evolution of storage and loss moduli as a function of the strain amplitude for MSPGs based on "click" polymeric ligand and different metal ions.[25]

Switching from one metallo-linker to another, *e.g.*, by varying the nature of the metal ion, will also affect the strength of the coordinative bond and hence the mechanical properties of the MSPGs. In their studies, Gohy and *et al.* also compared between concentrated terpyridine end-functionalized polystyrene-*b*-poly(tert-butylacrylate) micellar solution charged with half an equivalent of zinc(II), nickel(II) and iron(II) ions.[72] For the Fe(II) and Ni(II) samples, a hard gel withstanding the tube inversion test was rapidly formed in about one minute. This translated into a large increase of the storage and loss moduli compared to the metal-free sample. For both ions, the gels were dominated by elasticity.

On the other hand, no gelling occurred for the sample containing Zn(II) ions, evidencing an essentially Newtonian behaviour that was characterized by a weak but measurable elasticity. The different behaviours were related to the strength of the formed complexes. Indeed zinc(II) forms relatively weak complexes with terpyridines, while iron(II) and nickel(II) are known to form much stronger complexes.[76]

7.2.2 Network dynamics

The dynamics of supramolecular polymer networks is thus governed by two different characteristic time scales. One is the time scale of formation and breakage of supramolecular inter-chain cross-links, while the other is the time scale for the relaxation of chains or chain segments as captured by classical polymer physics.[42]

Practically, this statement was illustrated by the work of Gohy *et al.* on MSPGs constructed from side-chain terpyridine-functionalized copolymers. In their study,[77] the dynamic mechanical properties of the non-covalent network were investigated by oscillatory shear rheology. In particular, the evolution of both moduli as a function of the oscillation frequency was rationalized in the context of a multi-element generalized Maxwell model described by two main relaxation modes. On short time scale, polymer strands were able to relax via diffusive Rouse process, occurring essentially by Brownian motion. This relaxation process was practically evidenced by the parallel frequency scaling of storage and loss moduli achieved in the high frequency regime (Figure 7.5), which was attributed to the local motions of chain segments away from metal–ligand bridges. This motion was however restricted around the non-covalent associations acting as sticky points between chains. Over long time scales, detachment of linear polymer chains from the percolation structure allowed their diffusion within the network, causing stress relaxation and flow of the material.

The rheological properties of supramolecular polymer networks in the linear viscoelastic regime are mostly dictated by the nature of the different constitutive elements and binding motifs between them. In case of supramolecular polymer gels, the presence of solvent will play an additional role by affecting the kinetics and thermodynamic stabilities as well as the subtle balance between intra- and inter-molecular cross-links between the associating species. While most organic solvents do

not play an active role in the breaking and recombination of metallo-supramolecular species, coordinating solvent, on the other hand, will stabilize free or partially bound metallo-linkers, resulting by instance in comparatively shorter relaxation times.[38] In this respect, better understanding of the rheological properties of MSPGs requires extensive studies focusing on the influences of the different environmental parameters affecting the stability and density of coordinative bonds tethering the polymer network.

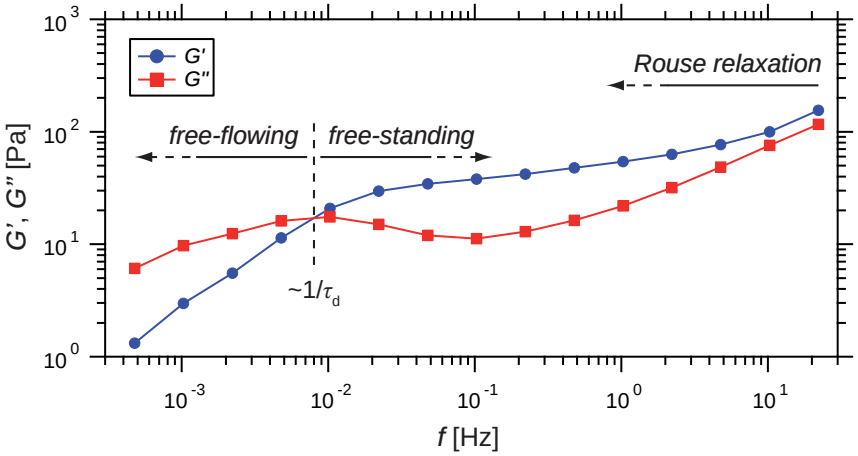

Figure 7.5 – Dynamic frequency sweep showing the fast and slow relaxation modes in a metallo-supramolecular hydrogel constructed from side-chain terpyridine functionalized copolymers.[77]

In practice, tuning the viscoelasticity of MSPGs can be experimentally achieved by choosing the appropriate metal–ligand pair. Nevertheless, attempts to relate the cross-linking strength and dissociation rate to the material properties are usually impaired by the circumstance that an independent control over the thermodynamic and kinetics of such systems is not easy to achieve. As pointed by Chujo *et al.*, the kinetic inertness of metal–ligand cross-links can also contribute to the stability and hence to the mechanical properties of coordination polymer gels, in addition to the required high stability constants for the complexation of metal ions by ligands.[78–80] In order to relate the molecular time scales of the metallo-supramolecular association and dissociation to the viscoelastic properties of the MSPGs, independent control over the cross-linking kinetics and thermodynamics is thus required.

This problem was successfully addressed by Craig *et al.* by utilizing the aforementioned poly(4-vinylpyridine) metallo-pincers supramolecular system in which the exchange rates could be varied by simple steric effects at the metal centre of square planar Pd(II) and Pt(II) complexes, without significantly changing the binding constant.[43,81] Indeed, ligand exchange at this metal centre generally occurs through an associative mechanism, in which the attacking nucleophile associates to the metal centre prior to the departure of the original ligand[44]. Steric effects in the spectator ligands of the complex therefore profoundly affect the rate of ligand exchange while having little effect on the stability of the complex.

By controlling the dissociation rate of the transient cross-links, a precise and predictable control over the dynamic viscosity and the elastic storage modulus was achieved. As an example, addition of the more dynamically labile Pd(II) metallo-linker to a poly(4-vinylpyridine) solution resulted in a viscous material, whereas the corresponding supramolecular network formed with the slower exchanging Pt(II) metallo-linker exhibited a gel-like behaviour. Further studies on these materials and their more thermodynamically and kinetically stable Pt(II) analogues demonstrated that the decomplexation rate of the metal binding motif (and not the binding constant) was responsible for the observed change in viscosity, suggesting that "slower" binding kinetics means "stronger" materials. This statement was related to the low frequency of dissociation when using a strong coordinating metal. In networks formed from multiple types of cross-linkers, the mechanical properties directly reflect the dynamics of the individual cross-linking components, rather than an averaged, cooperative behaviour of the contributing species, as probed in frequency-dependent dynamic measurements (Figure 7.6). At low frequency, the rheological properties were determined by the slower cross-linkers since the faster components dissociate and relax rapidly on the time scale of the slower component dissociation. As the frequency of oscillation increased, the slower cross-links were effectively "intact" on the time scale of the measurement, and the dynamics that dominated the rheological properties of the network was those that involve the faster components.

To further understand the impact of the type, strength, and degree of supramolecular chain cross-linking on the structure, dynamics, and properties of MSPGs, Seiffert *et al.* used a modular toolkit to form

non-covalent networks that exhibited greatly varying strength of transient chain cross-linking.[82,83] By deriving all supramolecular networks from the same common precursor polymer (Figure 6.20), the impact of the microscopic chain dynamics on the network mechanics was studied with high consistency. Precisely, MSPGs that are transiently cross-linked through either triple or sextuple hydrogen bonds or through tridentate transition metal complexes were compared in different media. In all cases, the strength of supramolecular association determined the mechanical properties of the resulting supramolecular gels, with good quantitative mutual correspondence. In parallel, probing the diffusive mobility of fluorescently tagged chains revealed that the concentration dependence of the tracer-chain diffusivity was in agreement with theoretical predictions derived from the "sticky reptation" model by Rubinstein and Semenov, provided the chain association is stronger than a certain threshold. At weaker chain association, classical semi-dilute solution type chain dynamics was contrastingly recovered, delimiting the applicability of the Rubinstein–Semenov model.

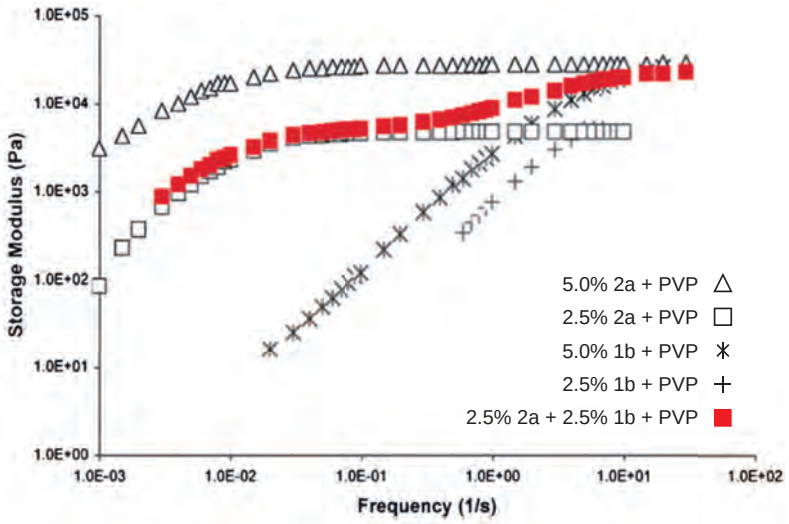

Figure 7.6 – Frequency sweep for different networks prepared from metallo-pincer complexes with poly(4-vinylpyridine) in DMSO.[43]

The same authors further studied the macroscopic relaxation along with the microscopic chain dynamics of MSPGs formed from highly regular star-shaped precursors that were end-capped with terpyridine.[84]

Precisely, the macroscopic mechanics of these model networks were studied by shear rheology, as a function of their different supramolecular cross-linking strength. In addition, the microscopic dynamics and mobilities of the star-shaped polymer were investigated by dynamic light scattering and fluorescence photo-bleaching recovery experiments with samples that contain fluorescently labelled building blocks (Figure 7.7). These complementary investigations revealed that, whereas in a long-term average the networks exhibited percolated connectivity, temporal detachment of one of the arms allowed for their relocation within the networks, entailing relaxation and flow on long time scales. In both micro- and macro-studies, such relaxation occurred on time scales of tens or hundreds of seconds, depending on the strength and stoichiometric ratio of transient associations. In fluorescence study, the relaxation of star polymers having one of their arms labelled was nevertheless found to be faster because of the lack of one connection site as compared to unlabelled counterparts, thereby causing an intrinsic network defect in their close vicinity that facilitated their microscopic relocation.

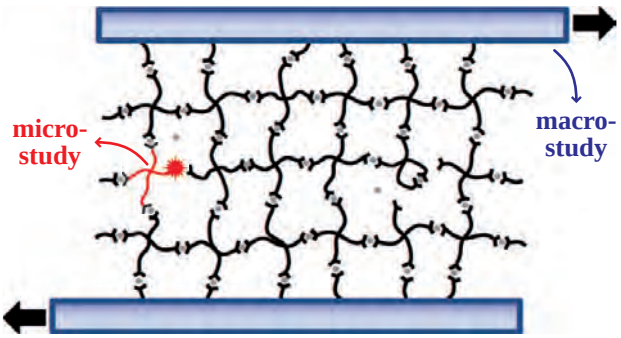

Figure 7.7 – Assessment of macro- and micro-dynamics of a model supramolecular network, respectively observed via shear rheology and fluorescence photo-bleaching recovery. [84]

7.3 Dynamic non-linear response

In parallel, many experimental studies have been focused on the non-linear behaviour of metallo-supramolecular polymer gels. Indeed, they are known to undergo an isothermal gel–sol transition under the yield point, due to the breaking down of the supramolecular network, when

probed at high mechanical deformation, and then to recover when stress or strain decreases below a certain value. The strain/stress amplitudes, at which the transition between the linear and non-linear viscoelastic regimes is observed, are reported as the yield strain/stress and can define together the yield point or yield strength. At a given concentration, those critical parameters are mostly dictated by the structure of the polymer network and the characteristics of the metallo-supramolecular bonding.

At the onset of network destructuring, MSPGs can exhibit shear thinning or shear thickening, which may depend on experimental conditions. In this field, Craig and *et al.* observed both shear thinning and shear thickening on metallo-pincer cross-linked poly(4-vinylpyridine) networks that differed only in the lifetime of the reversible cross-links.[70,85] The shear thinning behaviour, which was observed for samples that had a fast dissociation rate, was attributed to shear induced disentanglement of rapidly associating and dissociating network chains. Thus, the average time that a cross-linker remained detached was too short to permit the local relaxation of polymer chain segments that was necessary for a net conversion of elastically inactive to elastically active metallo-linkers. By contrast, the shear thickening behaviour, which was observed for cross-linkers that had a slower dissociation rate, was attributed to network reorganization under shear, which led to shear-induced network homogenization, and hence, network reinforcement. This hypothesis was supported by the observation that shear thickening was substantially enhanced above a critical shear rate, which directly relates to the lifetime of the metallo-linkers.

In a following study,[86] the same mechanisms have been associated to the strain hardening and strain softening of those gels under large amplitude oscillation shear. In semi-dilute unentangled solutions of poly(4-vinylpyridine), above a critical scanning frequency, strain hardening of both storage moduli and loss moduli was observed. This was attributed primarily to an increase in the number of elastically active chains, as opposed to non-Gaussian stretching of the polymer chains which became apparent only at strains near the network rupture. In the semi-dilute entangled regime, however, strain softening was observed for samples with faster metallo-linkers, whereas strain hardening was observed in contrast for samples with slower metallo-linkers. The divergent strain behaviours of samples were ascribed to the same mechanism previously

reported for the purely shear thinning/thickening behaviour of networks. As a consequence, these observations have painted a picture in which strain softening and shear thinning arise from the same set of molecular mechanisms, conceptually uniting the two non-linear responses for MSPGs.

Mechanisms and kinetics involved in the recovery process of MSPGs, after exposition to a large amplitude stress/strain, have also attracted attention over the last years.[22,23,25,39,72] Indeed, characterizing the rate at which such materials will recover, once broken apart, is of great interest since they are promising for a variety of applications in respect to their self-healing properties.

The recovery of metallo-supramolecular gels formed via sequential binding of a ditopic ligand with lanthanum(III) and zinc(II) metal ions has been notably studied in details by Rowan and coworkers.[22,23] Dynamic controlled stress sweep on those systems revealed a shear-responsive behaviour with a well-defined yield point at which it forms a Newtonian sol. While the gel responded mostly elastically at low shear stresses, the storage modulus dropped dramatically when higher shear stresses were applied. Upon removal of the stress, the gel reformed almost instantaneously, albeit with a smaller modulus, which gradually increased over time towards its original value. At this point, reassembly appeared to be a three-step process. After initial formation of a loose gel, the storage modulus remained essentially constant but the yield stress and strain increased linearly. Subsequently, the storage modulus increased strongly and the yield strain decreased. A possible interpretation was that the initial loose network was formed primarily via 2:1 ligand–La(III) or ligand–Zn(II) complex formation, with many dangling chain ends. In that case, the final phase was thought to involve conversion of the 2:1 La(III) complexes into 3:1 cross-linking sites and/or the formation 2:1 Zn(II) complexes which tied up the loose chain ends. An alternative suggested mechanism involved the metal ion induced self-assembly of the ditopic oligomer into hierarchical cross-linked species that subsequently formed the gel upon aggregation.

Later, Rowan *et al.* moved a step forward in understanding the mechanism of gelation and stimuli-response of their metallo-supramolecular polymers gels.[23,39] Microscopic examination and X-ray diffraction analysis revealed that the material was composed of spherulitic particles which aggregated to yield sample-spanning phases responsible for gela-

tion. Those globular particles were found to be fragile and very sensitive to mechanical perturbation, resulting in thixotropic behaviours that were highly dependent on formation history. For example, the crystalline particles formed by slow cooling were large and their sizes were dependent on the precise thermal history. As the amount of mechanical stress was increased, the globular particles were broken into progressively smaller particles, accompanied by an increase in the strength of the resulting gel once the stress was removed. In particular, gels formed by quenching in a sonication bath, which produces a finely-divided globular morphology, exhibited the highest strength. This was attributed to the increase in the strength of inter-particle interaction through an increase in surface contacts. The responsive nature of the gels was tailored by the metal ion salts used to form the gels. For example, gels containing lanthanide salts with non-coordinating counter-ions exhibited a lower yield stress than gels made with lanthanide salts that have competitive binding counter-ions, or gels made from transition metal ions alone.

7.4 Summary

An analysis of the rheology of metallo-supramolecular polymer gels was herein developed through a comprehensive literature review. At first, the concept of polymer gel was described before identifying the characteristic rheological features of metallo-supramolecular polymer gels. Then, the linear rheology of MSPGs was addressed in detail, with pertinent scientific advances over the past 2 decades. Doing so, the cross-linking density of MSPGs was related to the number of elastically active chain associations in transient networks, which depends on several factors including, *e.g.*, concentration and temperature. Also, the dynamic of MSPGs was correlated to the dissociation lifetime of transient cross-linkers and the time scale for the relaxation of chain segments. Finally, the non-linear response of MSPGs was discussed by showing the importance of the relationship between the solicitation time scale and the lifetime of cross-linkers.

Bibliography

[1] Constable, E. C. *Chem. Ind.* **1994**, 56–59.

[2] Constable, E. *Pure Appl. Chem.* **1996**, *68*, 253–260.
[3] Flory, P. *J. Am. Chem. Soc.* **1941**, *63*, 3083–3090.
[4] Flory, P. *J. Phys. Chem.* **1942**, *46*, 132–140.
[5] Stockmayer, W. *J. Chem. Phys.* **1944**, *12*, 125–131.
[6] Keller, A. *Faraday Discuss.* **1995**, *101*, 1–49.
[7] Nishinari, K. *Prog. Colloid Polym. Sci.* **2009**, *136*, 87–94.
[8] Alexander, J. *Colloid chemistry*; Chemical Catalog: New York, 1926.
[9] Alexander, A.; Johnson, P.; Rideal, E. *Colloid science*; Clarendon Press: Oxford, 1949; Vol. 1.
[10] Kruyt, H. R. *Colloid science: Reversible systems*; Elsevier: New York, 1949; p 753.
[11] Ferry, J. D. *Viscoelastic properties of polymers*; Wiley: New York, 1961; p 482.
[12] Ferry, J. D. *Viscoelastic properties of polymers*, 2nd ed.; Wiley: New York, 1970; pp xxi, 671.
[13] Ferry, J. D. *Viscoelastic properties of polymers*, 3rd ed.; Wiley: New York, 1980; pp xxiv, 641.
[14] Burchard, W.; Ross-Murphy, S. *Physical networks: Polymers and gels*; Elsevier: New York, 1990; pp xviii, 417.
[15] Almdal, K.; Dyre, J.; Hvidt, S.; Kramer, O. *Polym. Gels Networks* **1993**, *1*, 5–17.
[16] Glikman, S. A. *Introduction to physical chemistry of high polymers*; Saratovskogo universiteta: Saratov, 1959; p 378.
[17] Dickinson, E.; Lorient, D. *Food macromolecules and colloids*; Royal Society of Chemistry: Cambridge, 1995; Vol. 156.
[18] Grigor'Eva, V. A.; Rogovina, L. Z.; Slonimskii, G. L. *Vysokomol. Soedin., Ser. A* **1975**, *17*, 2045.
[19] Rogovina, L. Z.; Vasil'ev, V. G.; Braudo, E. E. *Polym. Sci. Ser. C Sel. Top.* **2008**, *50*, 85–92.
[20] te Nijenhuis, K. *Thermoreversible networks: Viscoelastic properties and structure of gels*; Springer: New York, 1997; pp xx, 267.
[21] Lee, H.; Kang, S.; Lee, J.; Jung, J. *Soft Matter* **2012**, *8*, 2950–2955.
[22] Zhao, Y.; Beck, J.; Rowan, S.; Jamieson, A. *Macromolecules* **2004**, *37*, 3529–3531.
[23] Weng, W. G.; Beck, J. B.; Jamieson, A. M.; Rowan, S. J. *J. Am. Chem. Soc.* **2006**, *128*, 11663–11672.
[24] Batabyal, S.; Leong, W.; Vittal, J. *Langmuir* **2010**, *26*, 7464–7468.
[25] Yuan, J.; Fang, X.; Zhang, L.; Hong, G.; Lin, Y.; Zheng, Q.; Xu, Y.; Ruan, Y.; Weng, W.; Xia, H.; Chen, G. *J. Mater. Chem.* **2012**, *22*, 11515–11522.
[26] Piepenbrock, M. O. M.; Lloyd, G. O.; Clarke, N.; Steed, J. W. *Chem. Rev.* **2010**, *110*, 1960–2004.
[27] Kim, S. H.; Sim, H. G.; Ahn, K. H.; Lee, S. J. *Korea-Aust. Rheol. J.* **2002**, *14*, 49–55.

[28] Sim, H.; Ahn, K.; Lee, S. *J. Non-Newtonian Fluid Mech.* **2003**, *112*, 237–250.
[29] Hyun, K.; Kim, S.; Ahn, K.; Lee, S. *J. Non-Newtonian Fluid Mech.* **2002**, *107*, 51–65.
[30] Goodeve, C. *Trans. Faraday Soc.* **1939**, *35*, 342–358.
[31] Mewis, J. *J. Non-Newtonian Fluid Mech.* **1979**, *6*, 1–20.
[32] Barnes, H. *J. Non-Newtonian Fluid Mech.* **1997**, *70*, 1–33.
[33] Mewis, J.; Wagner, N. *Adv. Colloid Interface Sci.* **2009**, *147*, 214–227.
[34] Møller, P.; Mewis, J.; Bonn, D. *Soft Matter* **2006**, *2*, 274–283.
[35] Dullaert, K.; Mewis, J. *J. Rheol.* **2005**, *49*, 1213.
[36] Dullaert, K.; Mewis, J. *J. Non-Newtonian Fluid Mech.* **2006**, *139*, 21–30.
[37] Beck, J. B.; Rowan, S. J. *J. Am. Chem. Soc.* **2003**, *125*, 13922–13923.
[38] Vermonden, T.; van Steenbergen, M.; Besseling, N.; Marcelis, A.; Hennink, W.; Sudhölter, E.; Stuart, M. *J. Am. Chem. Soc.* **2004**, *126*, 15802–15808.
[39] Weng, W. G.; Jamieson, A.; Rowan, S. *Tetrahedron* **2007**, *63*, 7419–7431.
[40] Holten-Andersen, N.; Harrington, M.; Birkedal, H.; Lee, B.; Messersmith, P.; Lee, K.; Waite, J. *Proc. Natl. Acad. Sci. U. S. A.* **2011**, *108*, 2651–2655.
[41] Kersey, F. R.; Loveless, D. M.; Craig, S. L. *J. R. Soc. Interface* **2007**, *4*, 373–380.
[42] Seiffert, S.; Sprakel, J. *Chem. Soc. Rev.* **2012**, *41*, 909–930.
[43] Loveless, D.; Jeon, S.; Craig, S. *Macromolecules* **2005**, *38*, 10171–10177.
[44] Yount, W. C.; Loveless, D. M.; Craig, S. L. *J. Am. Chem. Soc.* **2005**, *127*, 14488–14496.
[45] Xu, D.; Craig, S. L. *Macromolecules* **2011**, *44*, 5465–5472.
[46] Tanaka, F. *J. Non-Cryst. Solids* **2002**, *307*, 688–697.
[47] Tanaka, F.; Edwards, S. F. *Macromolecules* **1992**, *25*, 1516–1523.
[48] Tanaka, F.; Edwards, S. F. *J. Non-Newtonian Fluid Mech.* **1992**, *43*, 247–271.
[49] Tanaka, F.; Edwards, S. F. *J. Non-Newtonian Fluid Mech.* **1992**, *43*, 273–288.
[50] Tanaka, F. *Physica A* **1998**, *257*, 245–255.
[51] Tanaka, F. *Polym. J.* **2002**, *34*, 479–509.
[52] Leibler, L.; Rubinstein, M.; Colby, R. *Macromolecules* **1991**, *24*, 4701–4707.
[53] Semenov, A.; Joanny, J.; Khokhlov, A. *Macromolecules* **1995**, *28*, 1066–1075.
[54] Semenov, A.; Nyrkova, I.; Cates, M. *Macromolecules* **1995**, *28*, 7879–7885.
[55] Rubinstein, M.; Dobrynin, A. *Trends Polym. Sci.* **1997**, *5*, 181–186.
[56] Semenov, A.; Rubinstein, M. *Eur. Phys. J. B* **1998**, *1*, 87–94.
[57] Semenov, A.; Rubinstein, M. *Macromolecules* **1998**, *31*, 1373–1385.
[58] Rubinstein, M.; Semenov, A. *Macromolecules* **1998**, *31*, 1386–1397.
[59] Rubinstein, M.; Dobrynin, A. V. *Curr. Opin. Colloid Interface Sci.* **1999**,

4, 83–87.
[60] Rubinstein, M.; Semenov, A. *Macromolecules* **2001**, *34*, 1058–1068.
[61] Semenov, A.; Rubinstein, M. *Macromolecules* **2002**, *35*, 4821–4837.
[62] Jongschaap, R.; Wientjes, R.; Duits, M.; Mellema, J. *Macromolecules* **2001**, *34*, 1031–1038.
[63] Wientjes, R.; Duits, M.; Jongschaap, R.; Mellema, J. *Macromolecules* **2000**, *33*, 9594–9605.
[64] Wientjes, R.; Duits, M.; Bakker, J.; Jongschaap, R.; Mellema, J. *Macromolecules* **2001**, *34*, 6014–6023.
[65] Balazs, A. *Nature* **2013**, *493*, 172–173.
[66] Zhou, H.; Woo, J.; Cok, A.; Wang, M.; Olsen, B.; Johnson, J. *Proc. Natl. Acad. Sci. U. S. A.* **2012**, *109*, 19119–19124.
[67] Brassinne, J.; Mugemana, C.; Guillet, P.; Bertrand, O.; Auhl, D.; Bailly, C.; Fustin, C.-A.; Gohy, J.-F. *Soft Matter* **2012**, *8*, 4499–4506.
[68] te Nijenhuis, K.; Mensert, A.; Zitha, P. *Rheol. Acta* **2003**, *42*, 132–141.
[69] Loveless, D. M.; Jeon, S. L.; Craig, S. L. *J. Mater. Chem.* **2007**, *17*, 56–61.
[70] Xu, D. H.; Hawk, L. L.; Loveless, D. M.; Jeon, S. L.; Craig, S. L. *Macromolecules* **2010**, *43*, 3556–3565.
[71] Yan, X.; Wang, F.; Zheng, B.; Huang, F. *Chem. Soc. Rev.* **2012**, *41*, 6042–6065.
[72] Guillet, P.; Mugemana, C.; Stadler, F. J.; Schubert, U. S.; Fustin, C.-A.; Bailly, C.; Gohy, J.-F. *Soft Matter* **2009**, *5*, 3409–3411.
[73] Ghoussoub, A.; Lehn, J. M. *Chem. Commun.* **2005**, *41*, 5763–5765.
[74] Ott, C.; Ulbricht, C.; Hoogenboom, R.; Schubert, U. S. *Macromol. Rapid Commun.* **2012**, *33*, 556–561.
[75] Cates, M. *Macromolecules* **1987**, *20*, 2289–2296.
[76] Holyer, R. H.; Hubbard, C. D.; Kettle, S. F. A.; Wilkins, R. G. *Inorg. Chem.* **1966**, *5*, 622–625.
[77] Brassinne, J.; Jochum, F.; Fustin, C.-A.; Gohy, J.-F. *Int. J. Mol. Sci.* **2015**, *16*, 990–1007.
[78] Chujo, Y.; Sada, K.; Saegusa, T. *Macromolecules* **1993**, *26*, 6315–6319.
[79] Chujo, Y.; Sada, K.; Saegusa, T. *Polym. J.* **1993**, *25*, 599–608.
[80] Chujo, Y.; Sada, K.; Saegusa, T. *Macromolecules* **1993**, *26*, 6320–6323.
[81] Yount, W. C.; Loveless, D. M.; Craig, S. L. *Angew. Chem. Int. Ed.* **2005**, *44*, 2746–2748.
[82] Rossow, T.; Hackelbusch, S.; van Assenbergh, P.; Seiffert, S. *Polym. Chem.* **2013**, *4*, 2515–2527.
[83] Hackelbusch, S.; Rossow, T.; van Assenbergh, P.; Seiffert, S. *Macromolecules* **2013**, *46*, 6273–6286.
[84] Rossow, T.; Habicht, A.; Seiffert, S. *Macromolecules* **2014**, *47*, 6473–6482.
[85] Xu, D. H.; Craig, S. L. *J. Phys. Chem. Lett.* **2010**, *1*, 1683–1686.
[86] Xu, D.; Craig, S. L. *Macromolecules* **2011**, *44*, 7478–7488.

Part IV

Results and discussion

CHAPTER 8

SYNTHESIS OF FUNCTIONAL MACROMOLECULAR BUILDING BLOCKS

Abstract

The synthesis of functional block copolymers constituting the basic building blocks for self-assembled materials is herein described. At first, two chain transfer agents are modified with a terpyridine ligand via classical coupling methods. Those control agents are then used to mediate the sequential RAFT copolymerization of selected monomers. At each step, the control over the polymerization process is evidenced by spectroscopic and chromatographic techniques, affording materials with tailored composition and functionality. Following this strategy, a library of well-defined smart block copolymers is obtained, targeting the formation of self-assembled hydrogels with controlled and tunable rheological properties.

8.1 Overview

In this chapter, the synthesis of ligand end-functionalized macromolecular building blocks is described. The latter are composed of two or three different monomer units that have been selected for their ability to afford polymer sequences of desired characteristics (Figure 8.1). In this respect, polystyrene (PS) constitutes a well-studied hydrocarbon polymer of highly hydrophobic nature. Due to the strong interaction between phenyl groups, this hard and rigid sequence is commonly encountered in the field of associative polymers, generally leading to glass-like aggregates.[1,2] However, the glassy character of the aggregates decreases with the length of associating segments,[3] and the presence of plasticizers including co-solvents.[4]

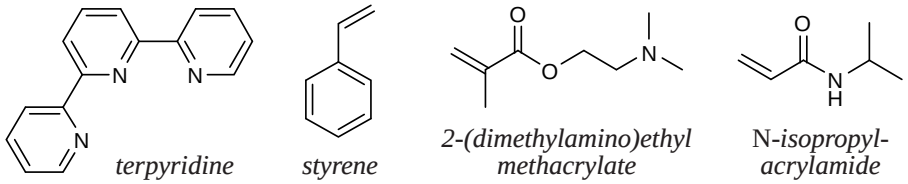

Figure 8.1 – Structures of monomers and ligand used in the synthesis of functional building blocks.

In the field of stimuli-responsive materials, thermo-sensitive poly(*N*-isopropylacrylamide) (PNIPAAm) is a widely used polymer that undergoes a sharp coil-to-globule phase transition in aqueous solution upon heating.[5] Practically, the lower critical solution temperature (LCST) is generally reported around 32 °C,[6] but is affected by hydrophobic or hydrophilic comonomers,[7,8] as well as the presence of salts[9,10] or surfactants.[11,12] Interestingly, the versatility of PNIPAAm has led to its utilization in gels, membranes, sensors, thin films, tissue engineering, and drug delivery.[13]

Despite the fact that an overwhelming majority of reported studies on environmentally sensitive polymers are based on PNIPAAm, a wide range of other thermo-responsive polymers have demonstrated their applicability in the preparation of smart materials.[14] Among them, poly(2-(dimethylamino)ethyl methacrylate) (PDMAEMA) is particularly attractive since it further shows pH-responsiveness. By raising the hydrophilic nature of PDMAEMA through protonation of tertiary amino-

groups ($pK_{a,app} \approx 6$ for the protonated polybase),[15] the overall hydrogen bonding ability of the macromolecules as well as their electrostatic repellency are indeed increased, which leads to higher transition temperatures. Hence, the reported cloud point temperature of PDMAEMA ranges from 30 °C to more than 80 °C in aqueous solution, depending on molecular weight, pH and concentration.[15–18]

The synthesis of block copolymers bearing a chelating ligand at one extremity is sequentially achieved via controlled radical polymerization, as illustrated in Figure 8.2. To this aim, a direct approach is followed employing initiators or control agents modified with the ligand of interest, which is terpyridine (tpy). Being one of the most prominent representatives of its family, this *N*-heteroaromatic ligand is employed in the construction of specific, stable metal complexes with unique properties that can be further tuned by the choice of the metal ion and/or structural modifications.[19,20] Additionally, well-designed supramolecular (co)polymer architectures have been realized, based on the metal–terpyridine connectivity, showing self-healing or responsive abilities, as well as additional functional properties.[21–24]

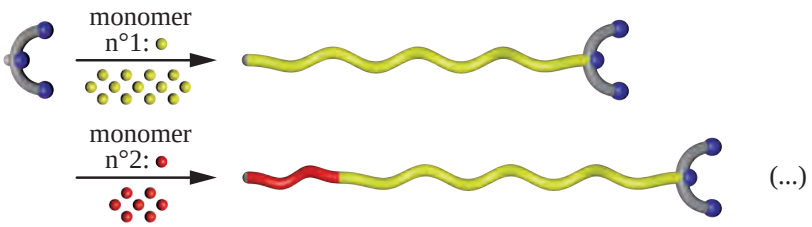

Figure 8.2 – Multi-step synthesis of a functional block copolymer.

Even if its applicability in the synthesis of ligand end-functionalized (co)polymers has been demonstrated in the past,[25] nitroxide-mediated radical polymerization lacks of versatility due to the limited number of monomers that can be polymerized in a control manner.[26] Transition metal-mediated atom transfer radical polymerization is more versatile in essence, because of its compatibility with various functional groups. However, the presence of coordinative moieties, especially strong chelating ligands, generally interferes with the chain growth process due to competition with the ligands for coordination sites of the catalyst or the formation of less active complexes, leading to a large decrease in polymerization rate and increase in dispersity.[27]

With the absence of transition metal as catalyst, reversible addition–fragmentation chain transfer, or simply RAFT, process offers a suitable alternative to other controlled radical polymerization techniques. Even if RAFT process may lack in the incorporation of α-group, this technique covers close to all the monomer classes that can undergo radical polymerization and can be performed in a large range of solvents. [28,29] However, each particular RAFT control agent is only suitable for a limited set of monomers and typically requires a multi-step synthetic procedure and subsequent purification. [30] As detailed in the following, the terpyridine ligand will be introduced into the macromolecular architecture via the use of modified chain transfer agents (CTA). The latter are thus synthesized prior to sequential controlled radical copolymerizations of selected monomers.

8.2 Synthesis of modified chain transfer agents

To prepared functional block copolymers via RAFT, selection of appropriate chain transfer agents for the targeted monomer is of prime importance (Figure 8.3). Indeed, a delicate balance between the rates of degenerative transfer and radical propagation is required so as to ensure that the dormant species are orders of magnitude greater in concentration than the active species, but the exchange between the two forms is rapid. Thus, the reactivity of the RAFT agent must be tailored to match the reactivity and stability of the propagating radical formed from a given monomer. [31]

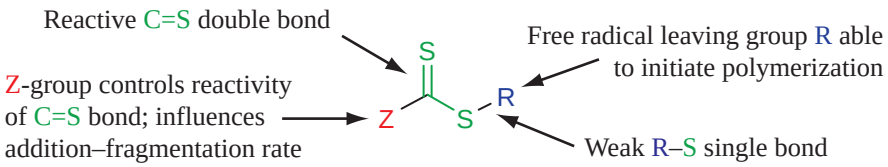

Figure 8.3 – General structure of a RAFT agent, with the impact of substituents.

Polymerizable monomers by RAFT can be divided into two general classes that reflect their ability to react in a free radical process. On one hand, the less activated monomers contain a vinylic group that is adjacent to an electron rich atom, such as oxygen or nitrogen (vinyl

esters, vinylamides). On the other hand, the more activated monomers contain a vinylic group that is conjugated to a neighboring functionality such as, *e.g.*, a carbonyl group (acrylamide, methacrylate, *etc.*), or an aromatic ring (styrenes). Due to the enhanced electronic stabilization, this second category of monomers indeed produces more-stabilized, less reactive radicals. [32]

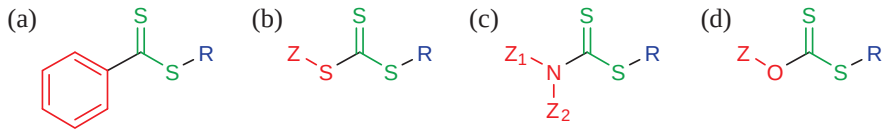

Figure 8.4 – Four classes of RAFT agents: (a) dithiobenzoates, (b) trithiocarbonates, (c) dithiocarbamates, and (d) xanthates.

To control the polymerization of 2-(dimethylamino)ethyl methacrylate, *N*-isopropylacrylamide and styrene monomers, the use of active RAFT agents such as dithioesters, typically dithiobenzoates, or trithiocarbonates is thus encouraged (Figure 8.4). Indeed, they provide a high rate of reversible chain transfer via addition–fragmentation with respect to propagation, allowing for rapid equilibration of growing polymer chains. [32] While showing extremely high chain transfer efficiency, dithiobenzoates are however prone to hydrolysis and may cause polymerization retardation under high concentrations. On the opposite, trithiocarbonates are more hydrolytically stable and cause less retardation but have a more moderate effect on the fragmentation equilibrium. [33]

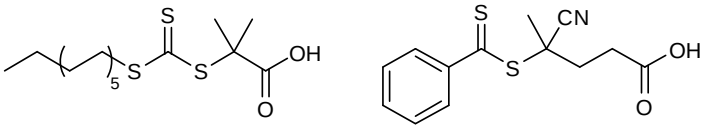

(a) DDMAT (b) CPAD

Figure 8.5 – Structures of two selected RAFT agents.

The specifically selected chain transfer agents must meet certain requirements. At first, they must be accessible commercially, or via short synthetic procedures. In addition, they should be stable and incorporate a functional group capable of undergoing post-modification to attach the terpyridine ligand. Among others, *S*-dodecyl-*S'*-(α, α'-dimethyl-α''-

acetic acid) trithiocarbonate (DDMAT) and 4-cyano-4-(phenylcarbonothioylthio)pentanoic acid (CPAD) thus rise as potential RAFT agents that can be used within the frame of this project (Figure 8.5). Indeed, they possess a carboxylic acid function that can be efficiently coupled with suitable terpyridine derivatives.

8.2.1 Synthesis of DDMAT

DDMAT is synthesized following a procedure described by Lai and coworkers (Figure 8.1).[34] Precisely, one equivalent of alkyl mercaptan and carbon disulfide are first reacted in presence of hydroxide ions, followed by alkylation with chloroform and acetone in a phase transfer catalyzed (PTC) reaction. After acidification, the desired product is isolated from the bis-dodecyl trithiocarbonate side-product, and purified by recrystallization. The high purity and functionality of the synthesized RAFT agent is attested by ^{13}C and ^{1}H nuclear magnetic resonance (NMR) spectroscopy.

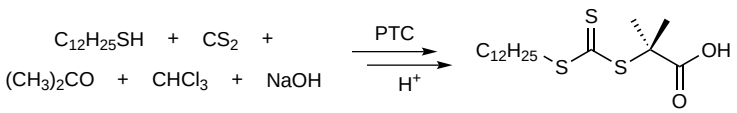

Scheme 8.1 – Synthesis of trithiocarbonate RAFT agent.

8.2.2 Synthesis of amino-terpyridine derivative

An amine functionalized terpyridine derivative is synthesized to allow its further coupling with the carboxylic acid of the RAFT agents. Precisely, amino-pentanol is reacted with chloro-terpyridine according to a procedure described elsewhere.[35] The reaction is performed under basic conditions, *i.e.*, suspension of caustic potash flakes in dimethyl sulfoxide, to yield the desired product (Figure 8.2). Its structure was identified by ^{13}C and ^{1}H NMR spectroscopy. Notably, the efficiency of the reaction is ascertained by a marked downfield shift of the NMR signal of protons initially adjacent to the hydroxyl group, after addition of amino-pentanol onto chloro-terpyridine.

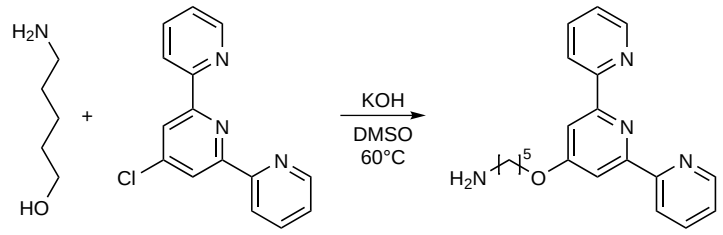

Scheme 8.2 – Synthesis of the amino-terpyridine derivative.

8.2.3 Coupling

As the final step of our convergent strategy, both synthesized DDMAT and commercially available CPAD are coupled with amino-terpyridine derivative to afford ligand-functionalized chain transfer agents. The formation of amide, from the corresponding carboxylic acid by condensation with the primary amine, is mediated by the presence of carbodiimide, following standard method of peptide synthesis (Figure 8.6).[36] Mechanistically, coupling is achieved after activation of carboxyl group

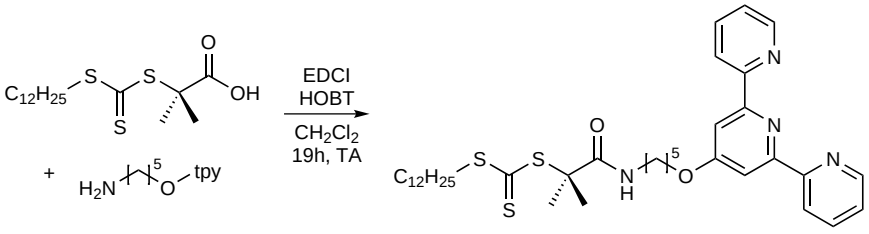

(a) Synthesis of DDMAT-tpy

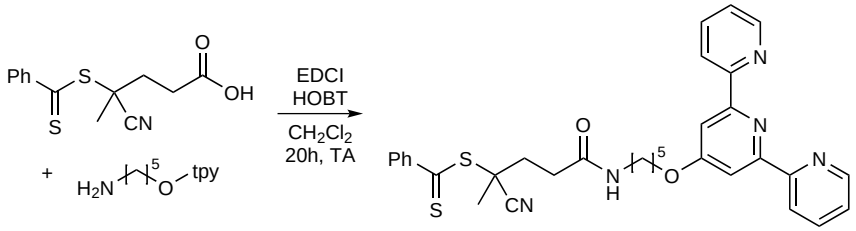

(b) Synthesis of CPAD-tpy

Figure 8.6 – Peptide coupling toward terpyridine-modified chain transfer agents.

with 1-hydroxybenzotriazole/*N*-(3-dimethyl-aminopropyl)-*N'*-ethylcarbodiimide hydrochloride salt (HOBT/EDCI), in dichloromethane (DCM) as solvent. This reaction is catalytic in HOBT but stoichiometric in EDCI, which is converted to the corresponding derived urea.

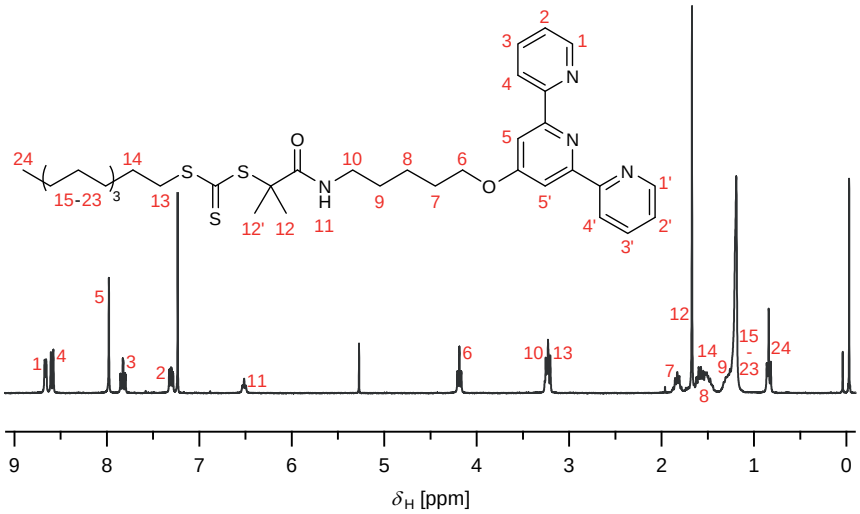

(a) ^{1}H-NMR spectrum of DDMAT-tpy

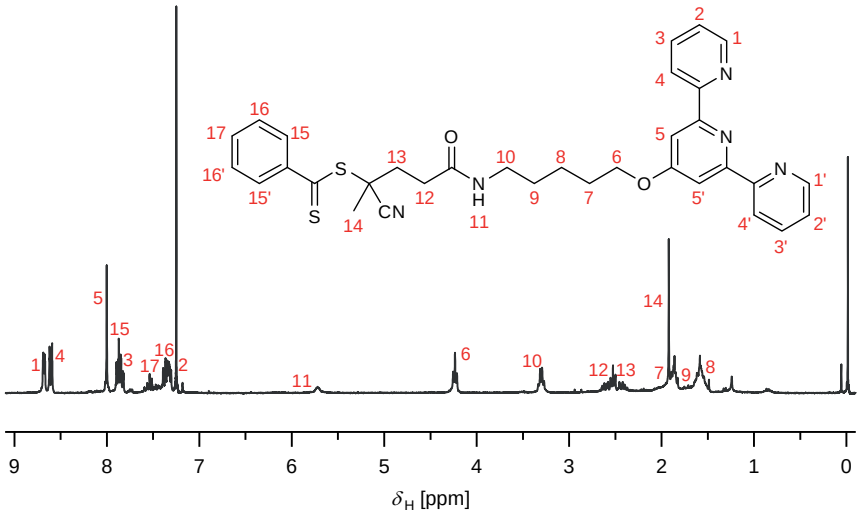

(b) ^{1}H-NMR spetrum of CPAD-tpy

Figure 8.7 – ^{1}H-NMR spectra of terpyridine-modified chain transfer agents in deuterated chloroform.

The characterization of both terpyridine-modified chain transfer agents is carried out using mass spectrometry and NMR spectroscopy, attesting efficient coupling as illustrated in Figure 8.7. In particular, the presence of a peak at a chemical shift (δ_H) around 6 ppm in ^{1}H-NMR, corresponding to the amide proton, along with the downfield shift of the peak of adjacent aliphatic protons, from 2.75 ppm to 3.30 ppm after coupling, constitute the most direct evidences of reaction efficiency.

8.3 Synthesis of functional block copolymers

The most common and simplest method for the preparation of block copolymers using RAFT is through sequential copolymerization of two or more monomers (Figure 8.2), with purification undertaken before each monomer addition. The homopolymer formed from an initial RAFT process acts as a macro-CTA for a second polymerization step, resulting in the formation of the block copolymer. Ideally, the Z-group of the initial CTA must adequately control the polymerization of each monomers that constitute the block copolymer.[32]

To develop reaction conditions for each polymerization, the influence of three stoichiometric ratios are taken into account and finely tuned to achieved control over the RAFT process:[32]

- [M]/[CTA]: As the amount of CTA determines the number of chains formed, the relative ratio of monomer to RAFT agent theoretically determines their average degree of polymerization that would be obtained in the absence of termination or chain transfer.
- [CTA]/[I]: The molar ratio of RAFT agent to initiator influences the functionality at both polymer ends, *i.e.*, the number of R-derived to initiator-derived chains at the α-end, and the number of thiocarbonylthio-functional dormant chains to dead chains, and hence the degree of control over the polymerization.
- [M]/[I]: The ratio between monomer and initiator strongly influences the rate of polymerization, as with conventional radical polymerization.

Along with tuning reaction conditions in terms of ratio between monomer, CTA, and initiator, the absolute concentration of each species

in solution is adjusted to control the polymerization of the different monomers in a reasonable time constrains.[32] If a control over molar mass and dispersity constitutes the primary goal, any adjustment in polymerization conditions may also influences the functionality of chain-ends, which in turn impact the degree of functionalization with the terpyridine ligand. Hence, potential issues with maintaining high end-group fidelity are addressed by NMR and ultraviolet–visible spectroscopic titration. Of course, total functionalization of the copolymer chains can be achieved using terpyridine functionalized radical initiators. However, this approach is not considered here given the high degrees of functionalization that are already attained in RAFT polymerization.

8.3.1 Synthesis of PNIPAAm-tpy

The synthesis of PS-*b*-PNIPAAm-tpy diblock copolymers is achieved by sequential RAFT copolymerization of *N*-isopropylacrylamide and styrene, with the help of A. M. Stevens, on the basis of anterior work developed by Dr. S. Piogé.[37] To this aim, the terpyridine-modified DDMAT is selected as RAFT agent for its particular stability towards hydrolysis and the possibility to copolymerize acrylamide and styrene monomers in a controlled manner.[38] As a first step, the polymerization of NIPAAm is conducted in solution in *N,N*-dimethylformamide (DMF), as a good solvent for all involved species including the growing polymer, as illustrated in Scheme 8.3.

In addition, a radical species must also be introduced into the reaction mixture to initiate polymerization. In this respect, commercially available 2,2'-azobis(isobutyronitrile) (AIBN) is used as source of primary radicals. By thermally decomposing, it generates two equivalents of radical species. In practice, only a portion of these species are actually active in the initiation of the polymerization process, while the others undergo secondary reactions. The fraction of the radicals produced in the homolytic cleavage that initiate polymer chains defines the initiator efficiency (ϑ),[39] which can be evaluated around 0.6 under the present conditions.[40,41]

During the initialization step, a fast balance pre-equilibrium is established between initiating radical species via degenerative transfer. As a result, the homopolymerization of poly(*N*-isopropylacrylamide) is partially initiated by primary radicals generated by the thermal decompo-

sition of AIBN, and partially initiated by the R-residue originated from transfer reaction to the RAFT agent. Therefore, a minimum amount of free radical initiator is used relative to chain transfer agent (ratio of 5:1) in order to ensure high degree of chain-end functionalization. In practice, this amount is however sufficient to initiate the polymerization process and to ensure acceptable polymerization kinetics.

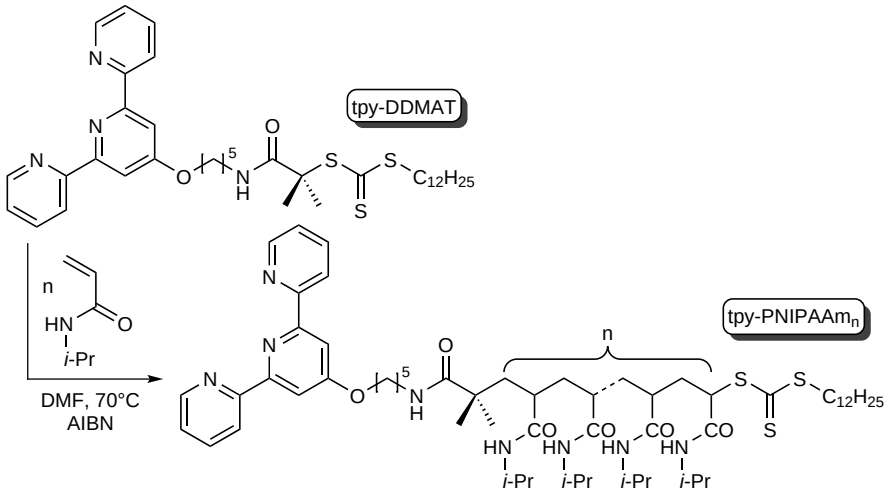

Scheme 8.3 – Synthesis of PNIPAAm-tpy homopolymers.

The initial ratio between NIPAAm monomer and functional RAFT agent is set to 500:1, allowing the preparation of different homopolymers with targeted molar mass. In practice, the monomer conversion, c, is intentionally limited by rapid cooling of the reaction mixture at predetermined time. In this way, the probability of side reactions, including chain termination, is reduced which otherwise classically increases with the degree of monomer conversion. In practice, this conversion is quantitatively evaluated by ^{1}H-NMR spectroscopy of the crude reaction mixture, from the ratio between the peak area (I_{X}) of vinyl proton of unreacted NIPAAm monomers to that of the characteristic *i*-propyl proton of growing PNIPAAm (Figure 8.8), according to:

$$c(t) = \frac{[\mathrm{PNIPAAm}]_t}{[\mathrm{PNIPAAm}]_t + [\mathrm{NIPAAm}]_t} = \frac{I_{\mathrm{H_{a'}}}(t)}{I_{\mathrm{H_{a'}}}(t) + I_{\mathrm{H_a}}(t)} \tag{8.1}$$

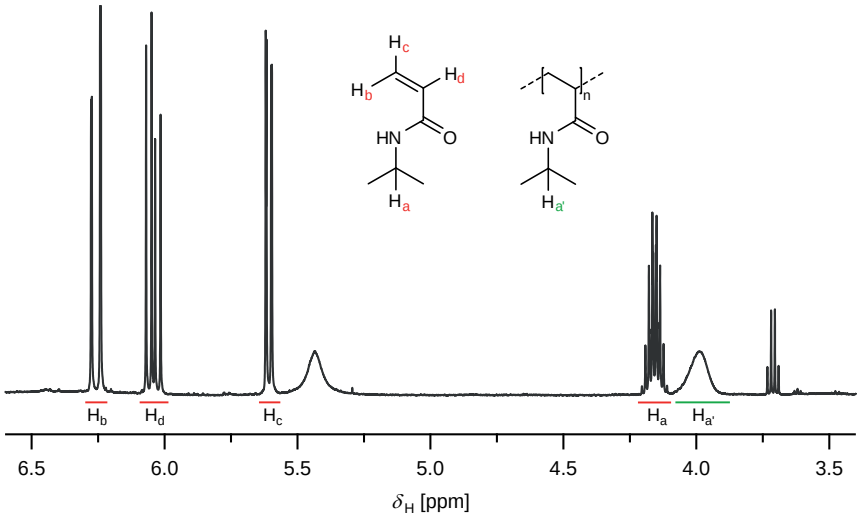

Figure 8.8 – ^{1}H-NMR spectrum of a crude PNIPAAm-tpy polymerization mixture in deuterated chloroform.

By varying the polymerization time, PNIPAAm-tpy homopolymers with different chain lengths are readily synthesized, as reported in Table 8.1. Practically, the number average degree of polymerization, DP, of the synthesized polymer can be evaluated from the monomer conversion and the ratio of engaged monomers to the total number of chains produced. Since the number of initiator-derived chains is low in comparison to CTA-derived chains, the contribution of primary radicals generated by the decomposition of the initiator is generally neglected, giving the more commonly used expression for the theoretical degree of polymerization:[32]

$$\mathrm{DP} = c(t) \cdot \frac{[\mathrm{NIPAAm}]_0}{[\mathrm{CTA}]_0 + 2\vartheta \cdot [\mathrm{AIBN}]_0} \approx c(t) \cdot \frac{[\mathrm{NIPAAm}]_0}{[\mathrm{CTA}]_0} \tag{8.2}$$

With the knowledge of molar masses of the monomer and of the chain control agent, the theoretical molar mass, $\bar{M}_n$, of the different PNIPAAm-tpy homopolymers can be expressed as a function of the monomer conversion:[32]

$$\bar{M}_n \approx M_{\mathrm{CTA}} + \mathrm{DP} \cdot M_{\mathrm{NIPAAm}} \tag{8.3}$$

Table 8.1 – Characteristics of PNIPAAm-tpy homopolymers.

Formula entry	$DP_{PNIPAAm}$ (NMR)	$\bar{M}_n$ (NMR) [g/mol]	$\bar{M}_n{}^a$ (SEC) [g/mol]	$Đ$ (SEC)
$PNIPAAm_{235}$-tpy	235 ± 25	27,200	35,200	1.16
$PNIPAAm_{270}$-tpy	270 ± 30	31,400	36,100	1.22
$PNIPAAm_{300}$-tpy	300 ± 35	34,900	39,200	1.25

[a] Determined with respect to polystyrene standards.

In parallel, absolute molar masses can be further accessed by chain end titration via ^{1}H-NMR spectroscopy of the pure homopolymers. The latter are obtained by double precipitation of the crude reaction mixtures in a solvent that is selective for the unreacted monomers, and subsequent drying of the polymer. In addition, nuclear magnetic resonance spectroscopy of the purified PNIPAAm-tpy provides a first quantitative verification of the presence of terpyridine end-group into the macromolecular architecture (Figure 8.9). Given the relative precision of NMR in the estimation of chain-end groups, the quantitative determination of terpyridine is further addressed by UV-visible titration in a following section.

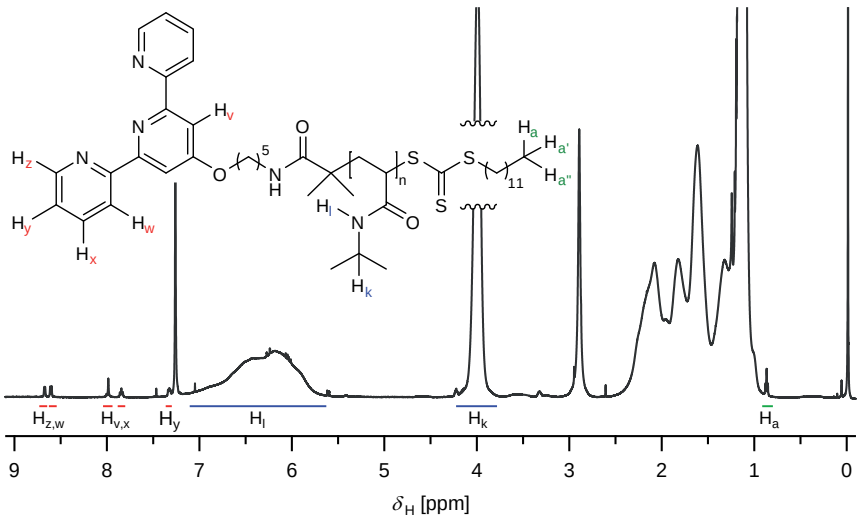

Figure 8.9 – ^{1}H-NMR spectrum of PNIPAAm-tpy homopolymer in deuterated chloroform.

Finally, molar mass distributions of synthesized PNIPAAm-tpy are revealed by size exclusion chromatography (SEC) analyses. In this conventional polymer characterization technique, the polymers in solution are indeed separated based on their molecular size, which can be determined by the retention time. Referring to known standard samples, *e.g.*, polystyrene, molecular mass distribution can be deduced.

As illustrated in Figure 8.10, a decent control over the polymerization process is attested by narrow and symmetrical distributions. As a further indication, calculated dispersities remain relatively low ($Đ < 1.3$) at all conversion levels. In addition, the logical rise in molar masses with polymerization time is clearly evidenced by the shift of SEC traces to lower elution times. Although meaningless, molar masses are determined with respect to polystyrene standards in order to account for this increase (Table 8.1).

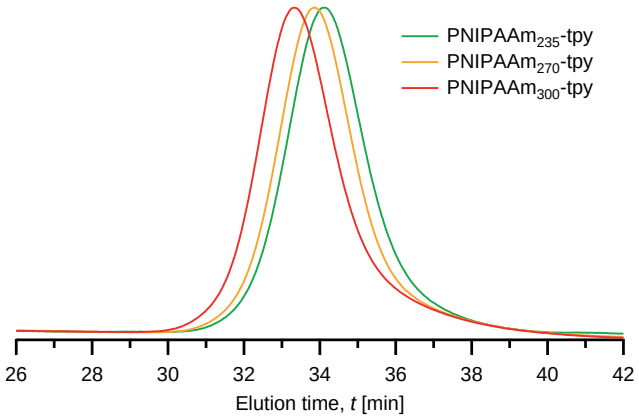

Figure 8.10 – SEC elugrams of PNIPAAm-tpy homopolymers of varying chain length (c = 36, 56, 60 %).

8.3.2 Synthesis of PS-*b*-PNIPAAm-tpy

In a second step, the controlled radical polymerization of styrene monomer is conducted in presence of the synthesized PNIPAAm-based macromolecular chain transfer agents. In a sense, this sequential copolymerization constitutes the ultimate test of "livingness", as it demonstrates the ability to quantitatively chain-extend homopolymers to yield

block copolymers. Such a polymerization is conducted in dry DMF at 90 °C using AIBN as source of primary radicals, as described in Scheme 8.4.

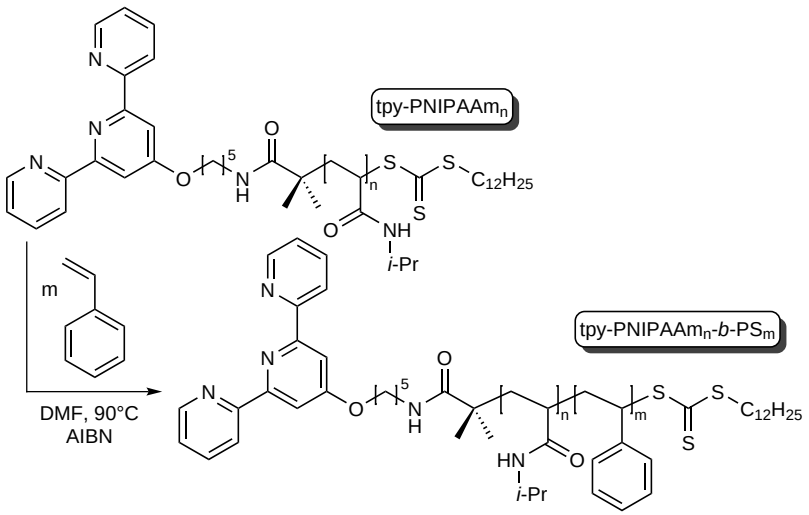

Scheme 8.4 – Synthesis of PS-*b*-PNIPAAm-tpy copolymers.

The initial ratio between styrene monomers, macro-RAFT agent and AIBN is set to 1000:5:1 in order to ensure control over the polymerization process. In this regard, the large excess of engaged monomer allows stopping the polymerization process at low conversions. For the reasons explained above, a minimal amount of free radical initiator is also used relative to the macro-CTA. In addition to the chain extension of PNIPAAm-tpy, a small proportion of chains is directly initiated by free radicals originating from the decomposition of AIBN. The initiator-derived homopolystyrene chains are however removed during the purification process, along with residual monomers, thus affording pure PS-*b*-PNIPAAm-tpy diblock copolymers.

The composition of the obtained diblock copolymers is determined by ^{1}H-NMR spectroscopy, which further attests the presence of terpyridine ligand in the architecture of the chain (Figure 8.11). The ratios between peak areas of terpyridine protons and terminal methyl group protons are in good agreement with a nearly quantitative incorporation of the ligand, which is further addressed in a following section. At the other chain end,

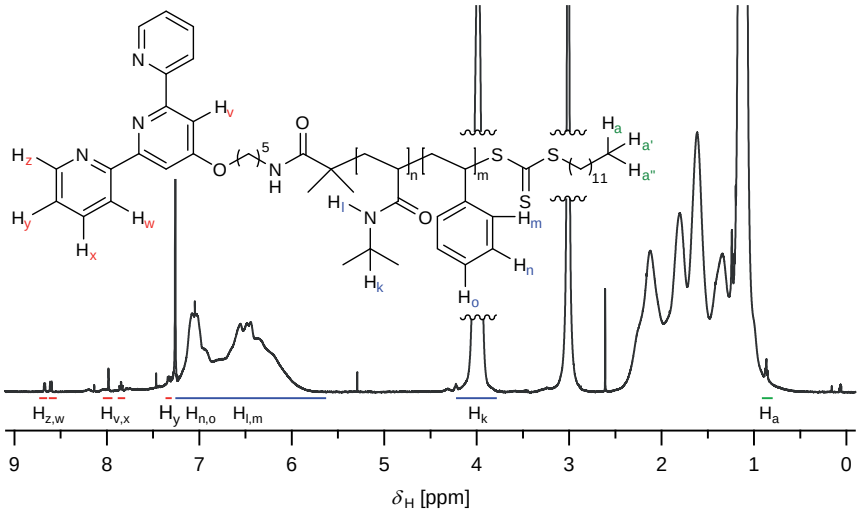

Figure 8.11 – ^{1}H-NMR spectrum of PS-*b*-PNIPAAm-tpy copolymer in deuterated chloroform.

the length of PS segment is readily varied depending on the degree of monomer conversion. Practically, the size of this block is kept short in order to result in sticky association in a selective solvent (Table 8.2).

Table 8.2 – Characteristics of PS-*b*-PNIPAAm-tpy copolymers.

Formula entry	DP_{PS} (NMR)	$\bar{M}_n$ (NMR) [g/mol]	$\bar{M}_n$ [a] (SEC) [g/mol]	$Đ$ (SEC)
PS_4-*b*-$PNIPAAm_{235}$-tpy	4 ± 1	27,500	35,500	1.19
PS_{15}-*b*-$PNIPAAm_{235}$-tpy	15 ± 2	28,700	35,900	1.23
PS_{22}-*b*-$PNIPAAm_{235}$-tpy	22 ± 2	29,500	36,900	1.20
PS_{27}-*b*-$PNIPAAm_{235}$-tpy	27 ± 3	30,000	36,500	1.28
PS_{35}-*b*-$PNIPAAm_{235}$-tpy	35 ± 3	30,800	39,600	1.28
PS_{27}-*b*-$PNIPAAm_{300}$-tpy	27 ± 3	37,700	41,500	1.32

[a] Determined with respect to polystyrene standards.

The ability of PNIPAAm-tpy macro-CTAs to quantitatively chain-extend to afford PS-*b*-PNIPAAm-tpy diblock copolymers is further evidenced by size exclusion chromatography. Even for short PS segments, clear shifts of SEC traces to lower elution times are observed (Fig-

ure 8.12), indicating an increase in molar masses after copolymerization. Moreover, SEC analysis reveals narrow molar mass distributions, attesting that well-defined block copolymers are successfully obtained.

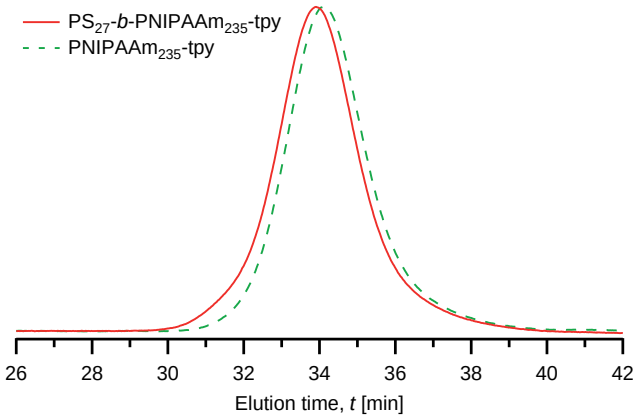

Figure 8.12 – SEC elugrams of PNIPAAm-tpy homopolymer and derived PS-*b*-PNIPAAm-tpy copolymer.

8.3.3 Synthesis of PDMAEMA-tpy

The synthesis of PNIPAAm-*b*-PDMAEMA-tpy diblock and PS-*b*-PNIPAAm-*b*-PDMAEMA-tpy triblock copolymers is achieved by sequential RAFT controlled radical polymerization. In this respect, the terpyridine-modified dithiobenzoate is selected as chain transfer agent due to its compatibility with various functional monomers,[32] affording the possibility to sequentially copolymerize methacrylate with acrylamide and further styrene monomers.[42,43]

At first, the polymerization of 2-(dimethylamino)ethyl methacrylate (DMAEMA) is conducted in 1,4-dioxane (DIO) as solvent, in the presence of CPAD-tpy and AIBN as source of primary radicals (Scheme 8.5). Polymerization kinetics is monitored by extracting aliquots using degassed syringes at predetermined time intervals. Hence, this technique affords PDMAEMA-tpy homopolymers whose chain length can be readily controlled with polymerization time, as reported in Table 8.3.

In practice, monomer conversions are evaluated by ^{1}H-NMR spectroscopy of the crude reaction mixtures, from the ratio between the

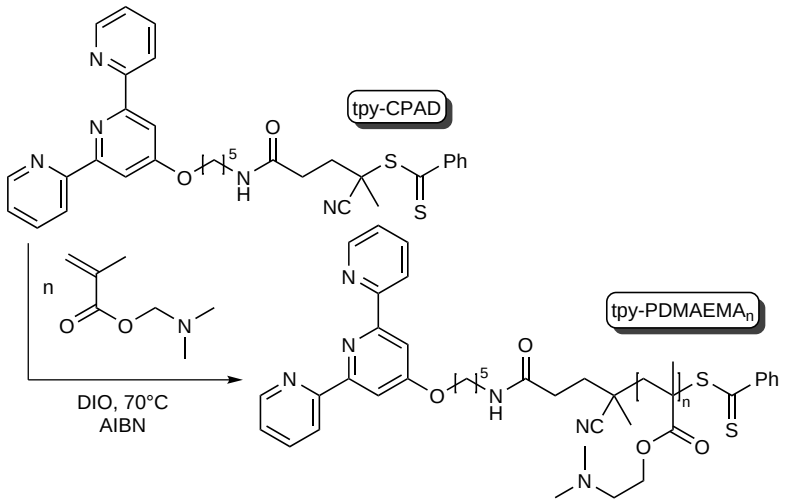

Scheme 8.5 – Synthesis of PDMAEMA-tpy homopolymers.

peak area of vinyl proton of DMAEMA at 5.50 or 6.05 ppm and that of the aliphatic ester proton of PDMAEMA at 4.00 ppm (Figure 8.13 (a)). In parallel, absolute molar masses are determined by analysis of the pure PDMAEMA-tpy homopolymers via end-group titration. Precisely, the number-average degrees of polymerization of chains are calculated from the ratio between the peak area of the aliphatic ester proton of PDMAEMA at 4.00 ppm and that of terpyridine protons at 8.70, 8.60 or 8.00 ppm (Figure 8.13 (b)).

Table 8.3 – Characteristics of PDMAEMA-tpy homopolymers.

Formula entry	$DP_{PNIPAAm}$ (NMR)	$\bar{M}_n$ (NMR) [g/mol]	$\bar{M}_n$ [a] (SEC) [g/mol]	$Đ$ (SEC)
$PDMAEMA_{40}$-tpy	40 ± 4	6850	10,950	1.27
$PDMAEMA_{80}$-tpy	80 ± 8	13,300	18,900	1.21
$PDMAEMA_{125}$-tpy	125 ± 13	20,100	26,900	1.20
$PDMAEMA_{160}$-tpy	160 ± 15	25,600	33,100	1.23
$PDMAEMA_{205}$-tpy	205 ± 20	33,000	41,100	1.28

[a] Determined with respect to polystyrene standards.

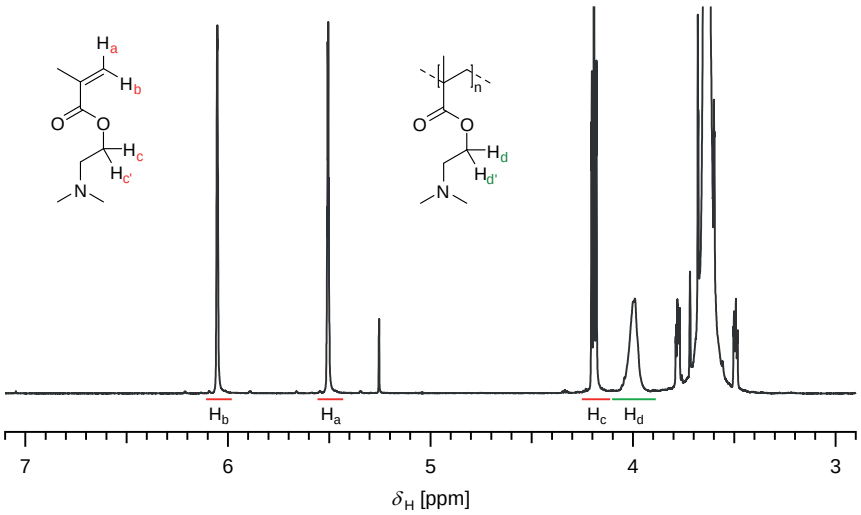

(a) ^{1}H-NMR spectrum of crude PDMAEMA-tpy

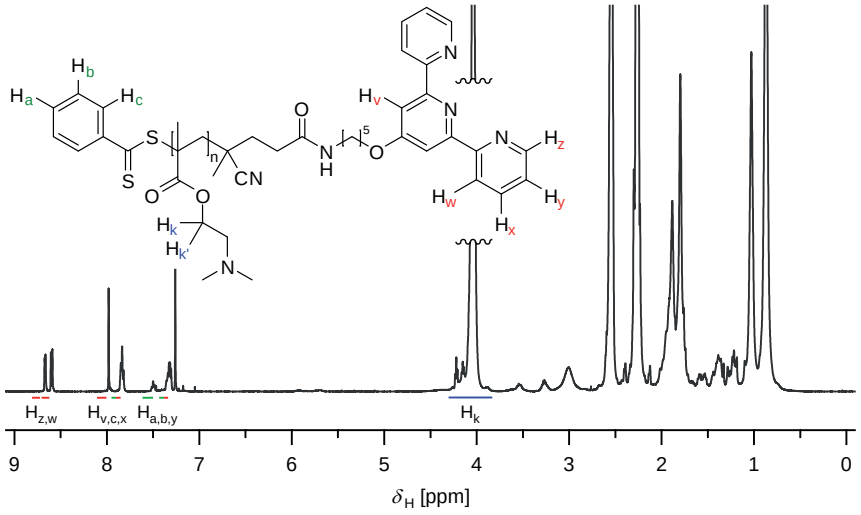

(b) ^{1}H-NMR spectrum of pure PDMAEMA-tpy

Figure 8.13 – ^{1}H-NMR spectrum of (a) a crude PDMAEMA-tpy polymerization mixture and (b) pure PDMAEMA-tpy homopolymer in deuterated chloroform.

As shown in Figure 8.14, the evolution of number average degree of polymerization with polymerization time is in good agreement with monomer conversion. The plot of number average degree of polymer-

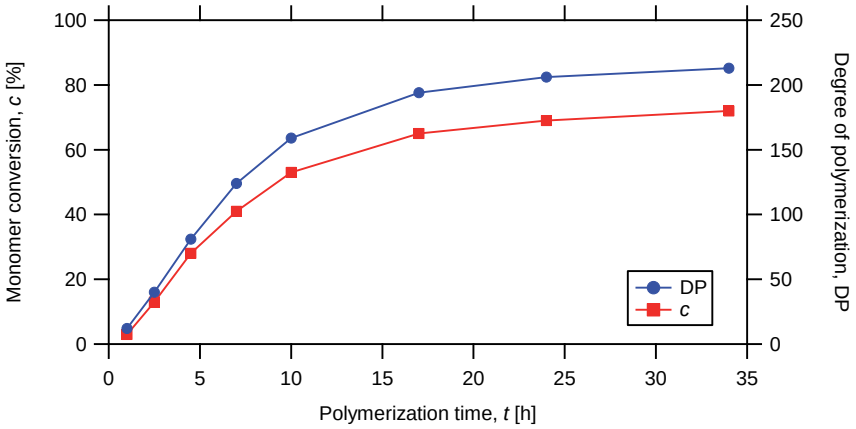

Figure 8.14 – Evolution of DMAEMA monomer conversion and degree of polymerization of PDMAEMA-tpy with polymerization time.

ization versus monomer conversion is further found to be linear (Figure 8.15), and therefore indicates a control over the polymerization of DMAEMA. Also, the presence of characteristic peaks of the aromatic protons of dithiobenzoate is noted in the ^{1}H-NMR spectrum (Figure 8.13 (b)), which attests the living character of the polymerization. However, the degree of monomer conversion reaches a maximum value of about 75 % after 2 days, which can be due to repeated sampling.

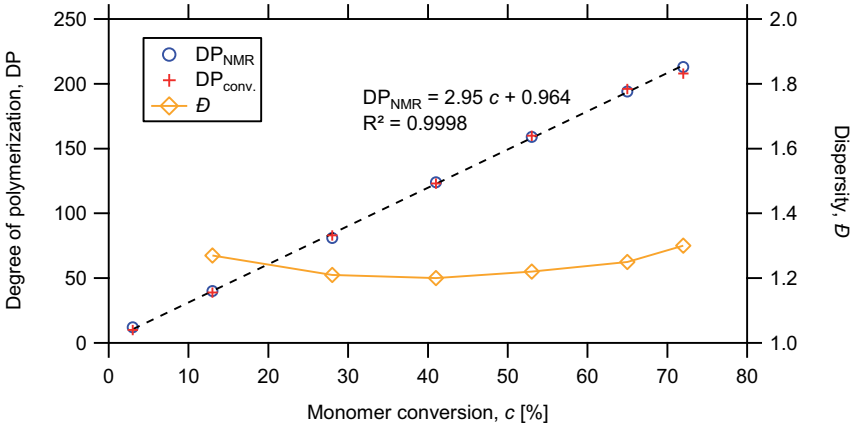

Figure 8.15 – Evolution of degree of polymerization and dispersity of PDMAEMA-tpy with DMAEMA monomer conversion.

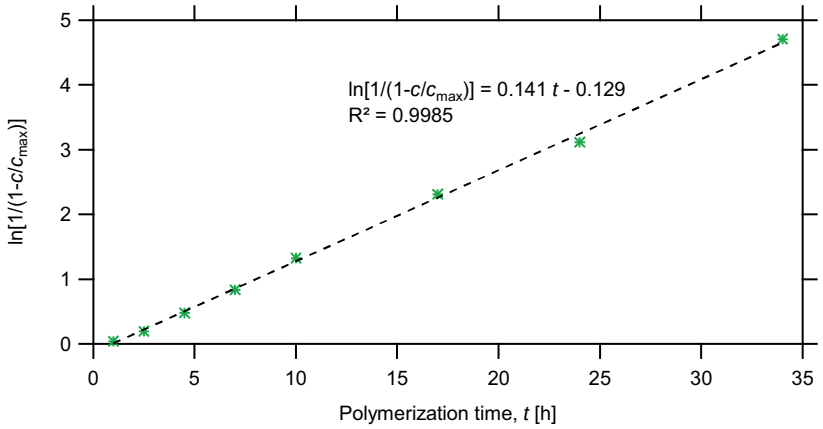

Figure 8.16 – Pseudo-first order for the polymerization of DMAEMA in presence of AIBN and CPAD-tpy.

As noticed in Figure 8.14, the polymerization process shows an induction period of about 30 minutes, *i.e.*, virtually no activity can be observed in the initial phase of the polymerization. Such an induction period is classically observed in RAFT, especially when dithiobenzoates are used as chain transfer agents, and might be ascribed to the pre-equilibrium that takes place in the early stage of the polymerization.[44] After the induction period, the first-order time-conversion plot shows a linear relationship with only slight deviations towards the end of the polymerization (Figure 8.16), which is in agreement with a constant

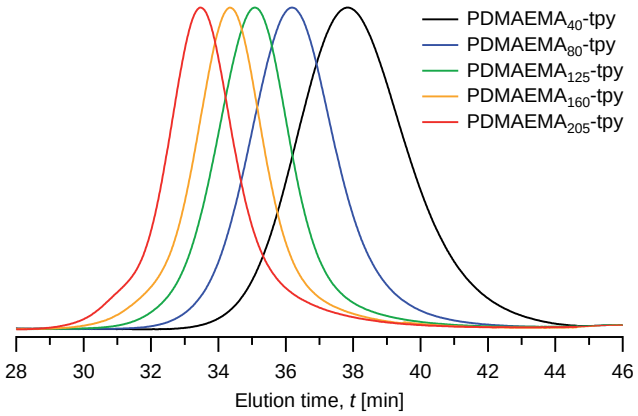

Figure 8.17 – SEC elugrams of PDMAEMA-tpy homopolymers of varying chain length (c = 13, 28, 41, 53, 72 %).

concentration in active species. The plot is constructed by taking into account the limited monomer conversion, which redefines the logarithm of the monomer concentration.

In parallel, size exclusion chromatography analysis on PDMAEMA-tpy reveals narrow symmetrical molar mass distributions. In addition, low dispersities ($Đ < 1.3$) are obtained at all conversion levels, attesting to the decent control over the polymerization process. As shown in Figure 8.17, the increase in molar masses with polymerization time was clearly evidenced by the shift of SEC traces to lower elution times. To account for this increase, molar masses are determined with respect to polystyrene standards and reported in Table 8.3.

8.3.4 Synthesis of PNIPAAm-*b*-PDMAEMA-tpy

In a second step, the controlled radical polymerization of *N*-isopropylacrylamide (NIPAAm) is investigated in presence of PDMAEMA-based macro-CTA. As described in Scheme 8.6, this polymerization is conducted in dry dioxane at 70 °C using AIBN as source of primary radicals.

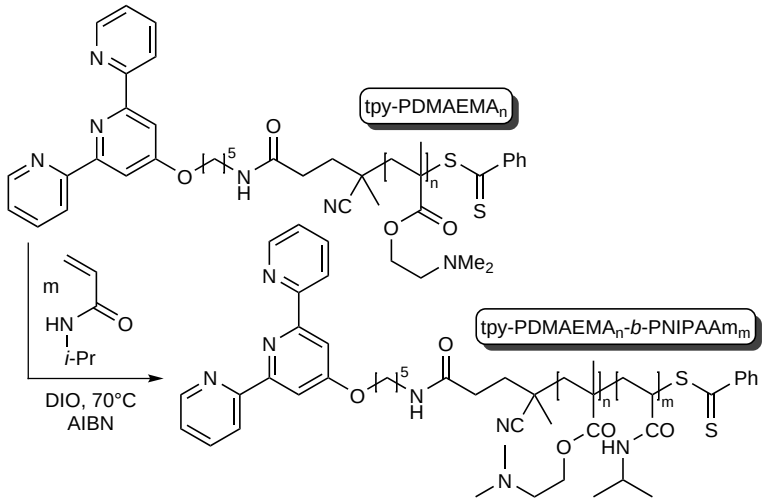

Scheme 8.6 – Synthesis of PNIPAAm-*b*-PDMAEMA-tpy copolymers.

The initial ratio between NIPAAm monomers, PDMAEMA-tpy macro-CTA and AIBN is set in order to ensure control over the polymerization

process. During the reaction, monomer conversion is monitored by ^{1}H-NMR spectroscopy of the crude reaction by following the disappearance of the peak of vinyl proton of NIPAAm at 6.25 or 6.05 ppm, with respect

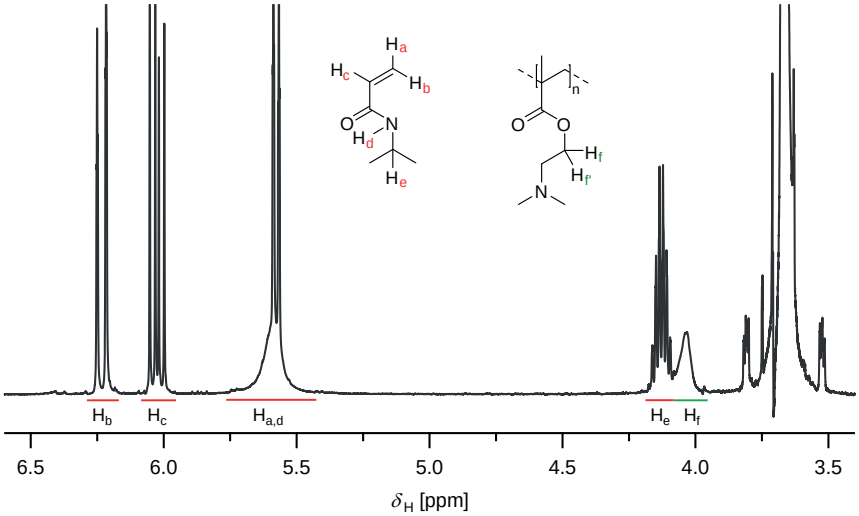

(a) ^{1}H-NMR spectrum at initial reaction time

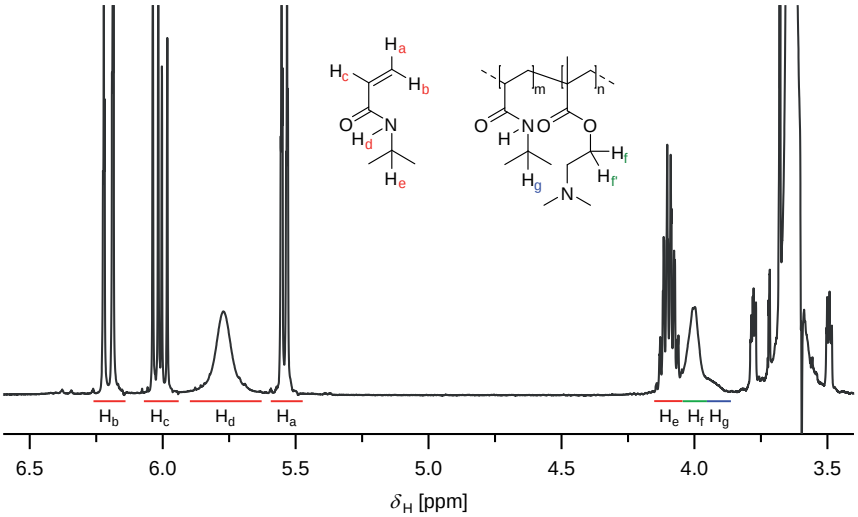

(b) ^{1}H-NMR spectrum after partial monomer conversion

Figure 8.18 – ^{1}H-NMR monitoring of the polymerization of NIPAAm monomers from PDMAEMA-tpy macro-CTA in deuterated chloroform.

to that of isopropyl/aliphatic ester protons in the 3.85–4.20 ppm range (Figure 8.18).

In parallel, absolute molecular weights can be determined by ^{1}H-NMR spectroscopy of the pure PNIPAAm-*b*-PDMAEMA-tpy copolymers either via end-group titration or in relative with PDMAEMA proton peak areas. For sake of accuracy, the number average degrees of polymerization of the PNIPAAm block are evaluated from the ratio between the peak area of the isopropyl/aliphatic ester protons of PNIPAAm-*b*-PDMAEMA-tpy at 4.00 ppm and that of the aliphatic protons of PDMAEMA block at 2.55 ppm. Also, the characteristic peaks of the aromatic protons of dithiobenzoate present in the ^{1}H-NMR spectrum attest the living character of the polymerization.

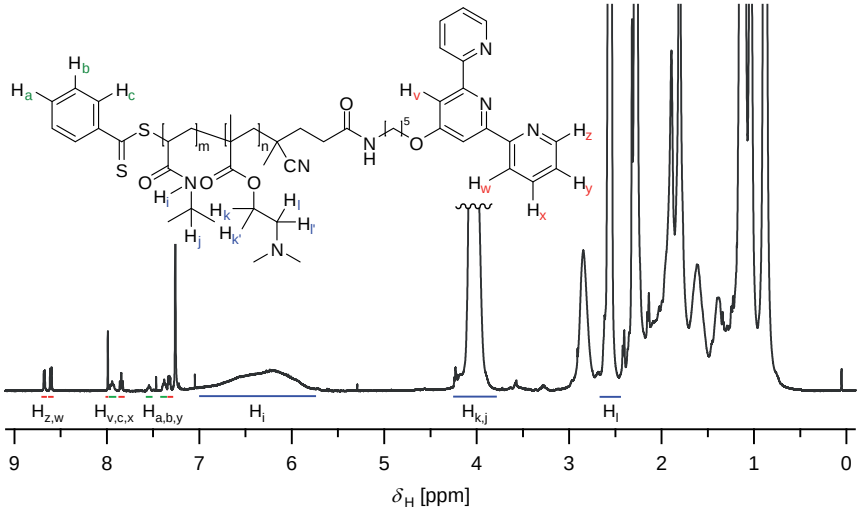

Figure 8.19 – ^{1}H-NMR spectrum of PNIPAAm-*b*-PDMAEMA-tpy copolymer in deuterated chloroform.

By varying the polymerization time, the composition of the different blocks can be easily adjusted toward a majority of PNIPAAm or PDMAEMA. As the length of the second block is increased, a shift of SEC traces is observed toward lower elution times, indicating an increase in molar masses after copolymerization (Figure 8.20). As the length of the PNIPAAm segment is increased, broadening of the SEC elugram is observed which can be due to repeated sampling or ascribed to a modest control of the polymerization process.

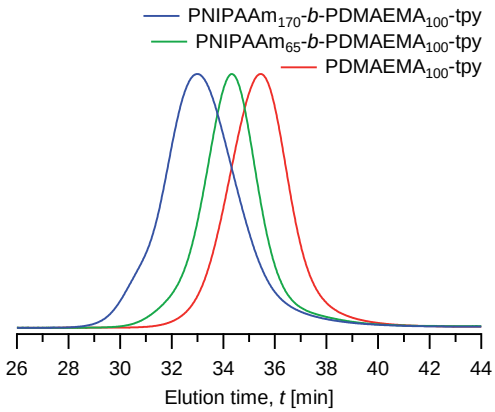

Figure 8.20 – SEC elugrams of PNIPAAm-tpy homopolymer and derived PNIPAAm-*b*-PDMAEMA-tpy copolymers (c = 0, 12, 34 %).

8.3.5 Synthesis of PS-*b*-PNIPAAm-*b*-PDMAEMA-tpy

The possibility to obtain a triblock copolymer composed of a short polystyrene block linked to a poly(*N*-isopropylacrylamide) block and a third poly(2-(dimethylamino)ethyl methacrylate) block (PS-*b*-PNIPAAm-*b*-PDMAEMA) is promising. Indeed, this copolymer is designed to

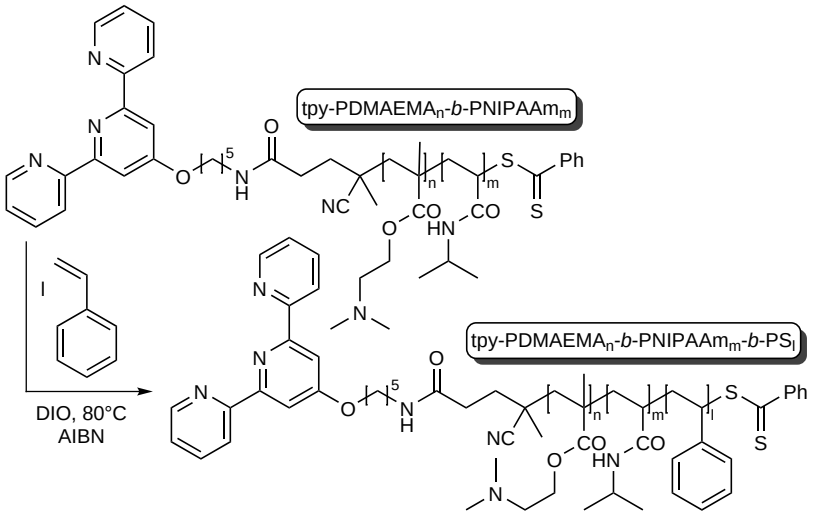

Scheme 8.7 – Synthesis of PS-*b*-PNIPAAm-*b*-PDMAEMA-tpy copolymers.

produce self-assembled hydrogels that would combine the association strength of polystyrene stickers with the stimuli-responsiveness of both PNIPAAm and PDMAEMA blocks.

To achieve this goal, styrene is polymerized in presence of PNIPAAm-*b*-PDMAEMA-tpy as macro-CTA, and AIBN as source of primary radicals (Scheme 8.7). In order to ensure control over the polymerization process, the initial ratio between styrene, macro-CTA and AIBN is set to 3000:7.5:1. In practice, the reaction is conducted at 80 °C in dry dioxane, and stopped at a predetermined time interval to afford a PS-*b*-PNIPAAm-*b*-PDMAEMA-tpy triblock copolymers of given characteristic lengths.

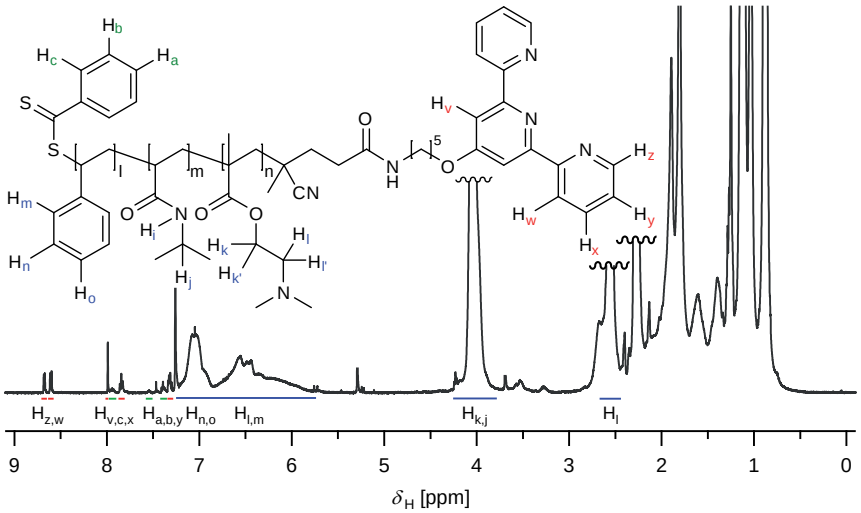

Figure 8.21 – ^{1}H-NMR spectrum of PS-*b*-PNIPAAm-*b*-PDMAEMA-tpy copolymer in deuterated chloroform.

The synthesized triblock copolymers are purified by precipitation of the crude reaction mixture, followed by isolation of the precipitate, and subsequent drying. The compositions of the accordingly obtained materials are assessed by ^{1}H-NMR spectroscopy, as illustrated in Figure 8.21. At first, the NMR spectrum analysis reveals characteristic broad signals of polystyrene and further attests the presence of terpyridine ligand in the chain architecture. In addition, the length of the polystyrene block can be estimated from the ratio between the peak area of PS aro-

matic protons and isopropyl/aliphatic ester protons of the PNIPAAm and PDMAEMA block around 4.00 ppm.

As illustrated in Figure 8.22, the chain extension of PNIPAAm-*b*-PDMAEMA-tpy macro-CTA into PS-*b*-PNIPAAm-*b*-PDMAEMA-tpy triblock copolymers is further evidenced by size exclusion chromatography. This analysis indeed shows a significant shift of the SEC trace to lower elution times after polymerization of the third block, indicating an increase in molar masses. Last but not least, the SEC analysis reveals still narrow molar mass distributions, attesting control over the polymerization process.

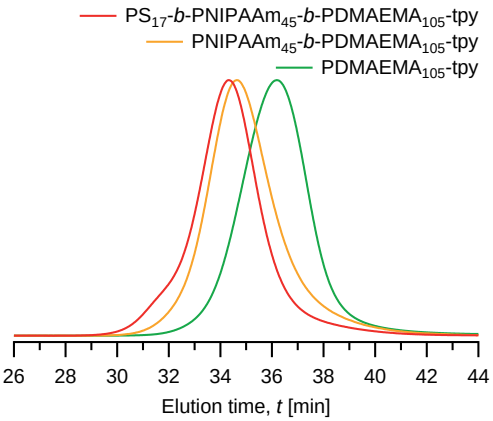

Figure 8.22 – SEC elugrams of PDMAEMA-tpy homopolymer and derived PNIPAAm-*b*-PDMAEMA-tpy diblock and PS-*b*-PNIPAAm-*b*-PDMAEMA-tpy triblock copolymer.

8.4 Titration of terpyridine end-groups

As mentioned above, RAFT polymerization relies on a radical source to initiate the chain growth process. In turn, this may decrease α-end functionality as part of the chains are directly initiated by the primary radicals originating from thermal decomposition of the conventional initiator. In other words, part of the macromolecular chains have therefore no terpyridine ligand at their extremity.

The proportion of chains directly initiated by primary radicals is in-

timately related to the amount of engaged conventional initiator and can be thus roughly estimated. Due to low initiation efficiency, the ratio of CTA- to initiator-derived chains is however greater than that of the initial molar ratio between engaged CTA and conventional initiator. Hence, experimental quantification of the chain-end functionality is essential.

Given the relative precision of ^{1}H-NMR spectroscopy in the quantitative determination of chain-end groups, the degree of functionalization of synthesized block copolymers is further evaluated by UV-visible titration with metal cations. Indeed, the terpyridine ligand is known to form stable coordination complexes in combination with numerous transition metal ions.[19,45,46] In particular, the iron(II)–terpyridine bis-complex is particularly stable and gives rise to a strong absorption in the visible region. However, one should note that both techniques are based on the determination of terpyridine end-groups but lack in determining the number of chains that are directly initiated by the primary radicals originating from the thermal decomposition of AIBN. To directly access the degrees of chain functionalization, an absolute determination of the number average molar mass of each samples would be required via, *e.g.*, size exclusion chromatography with multi-angle light scattering detector, osmometry or tonometry.

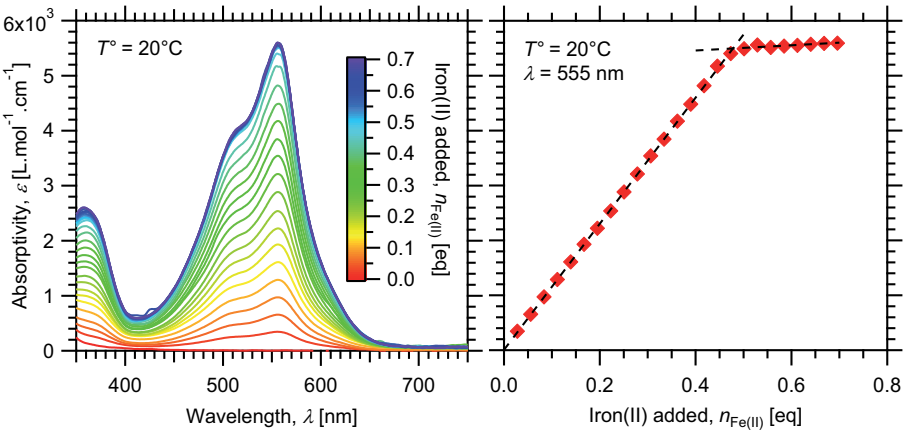

Figure 8.23 – UV-Vis titration of terpyridine end-groups in a PS-*b*-PNIPAAm-tpy copolymer by Fe(II) (left) and evolution of molar absorptivity at 555 nm during the addition of titrant (right).

In UV-Vis experiments, the different block copolymers are dissolved in water at a given concentration around 0.25 mmol/L, and titrated by stepwise addition of aqueous solution of iron(II) chloride stabilized against oxidation by the presence of 0.5 mM ascorbic acid. Indeed, this well-known reducing agent prevents the oxidation of iron(II) into iron(III) ions by lowering the oxidation potential of the media.

As illustrated in Figure 8.23, the formation of Fe(II) bis-terpyridine complexes is evidenced by the strong metal-to-ligand charge-transfer band found around the wavelength (λ) of 555 nm, which gives a characteristic purple colour to the solution. Those transitions arise from the charge transfer of a primarily metal-localized electron from the 3d orbital into the lowest unoccupied molecular orbital of the terpyridine ligand.[47,48]

In case of PS-*b*-PNIPAAm-tpy copolymers, the maximum absorption (ε) is obtained close to the calculated equivalence point (using the molar masses evaluated from ^{1}H-NMR spectroscopy), indicating around 95 % functionality (Figure 8.23). Slightly lower functionalization degrees are obtained for PNIPAAm-*b*-PDMAEMA-tpy copolymers, suggesting that around 90 % of the chains are end-capped with the terpyridine ligand.

The obtained degrees of functionalization are coherent with the conditions employed during the RAFT process, taking into account the reduced initiator efficiency. Furthermore, no significant variations in the degree of functionalization are obtained among related samples. Logically, the latter are prepared under identical conditions and only vary in the length of the constituting blocks.

Once incorporated during the crucial initiation process, the α-end is strongly anchored to the growing polymer chain, which is not the case of the thiocarbonylthio group involved in the addition–fragmentation equilibrium. As monomer conversion increases, the probability of losing the living nature of the chain-end indeed increased accordingly. At the other end, the terpyridine α-group is more reliably preserved, at least under the mild conditions employed during each block synthesis, resulting in the obtained high degrees of functionalization.

8.5 Summary

The main focus of this chapter was the synthesis of smart linear block copolymers bearing a terpyridine ligand at the chain-end. The latter were readily obtained via sequential radical copolymerization controlled by reversible addition–fragmentation chain transfer process. To this aim, two control agents, comprising a trithiocarbonate and a dithiobenzoate, were modified with the ligand of interest via a classical coupling method used in peptide synthesis. Then, the ability of those RAFT agents to control the polymerization of styrene, *N*-isopropylacrylamide, and 2-(dimethylamino)ethyl methacrylate) was successfully demonstrated.

Following this strategy, a library of well-defined functional block copolymers was obtained, as characterized by ^{1}H-NMR spectroscopy, size exclusion chromatography, and UV-Vis titration spectroscopy. They consist in PS-*b*-PNIPAAm-tpy diblock, PNIPAAm-*b*-PDMAEMA-tpy diblock, and PS-*b*-PNIPAAm-*b*-PDMAEMA-tpy triblock copolymers of varying block lengths. Practically, their chemical compositions were determined by proton nuclear magnetic resonance spectroscopy, while size exclusion chromatography revealed narrow molar mass distributions.

Of primary importance, the nearly-quantitative presence of terpyridine ligand at the chain-end was verified by UV-visible titration spectroscopy. In addition, the possibility to form metal–terpyridine bis-complexes was evidenced by the stoichiometry at the equivalence point of the titration. Given the range of accessible macromolecular building blocks, these results definitively pave the way towards the formation of self-assembled hydrogels with controlled and tunable rheological properties.

8.6 Experimental part

Materials

All chemicals are purchased from Acros or Aldrich and are of highest purity grade. All chemicals are used as received unless otherwise specified. 2,2'-Azobis(isobutyronitrile) is recrystallized from diethyl ether. 2-(Dimethylamino)ethyl methacrylate is dried and vacuum-distilled over

calcium hydride. *N*-isopropylacrylamide is recrystallized from *n*-hexane and dried overnight in a vacuum oven at 35°C prior to use. Styrene is passed through a short column filled with activated basic aluminum oxide (Brockmann I) before use or vacuum-distilled over calcium hydride. *N,N*-dimethylformamide, 1,4-dioxane, and dichloromethane are distilled over calcium hydride and stored under molecular sieve (4 Å) and argon atmosphere. Dimethyl sulfoxide is vacuum-distilled over calcium hydride and stored under molecular sieve (3 Å) and argon atmosphere. Iron(II) chloride salt is dried prior to use and weighted under argon atmosphere.

Instrumentation

All ^{1}H and ^{13}C nuclear magnetic resonance spectra are recorded on a Bruker 300 MHz Avance II spectrometer in deuterated solvents containing tetramethylsilane as an internal standard. Chemical shifts are reported in parts per million downfield from the internal standard. Size exclusion chromatography is performed in *N,N*-dimethylformamide containing 2.5 mM NH_4PF_6 to determine molar mass distributions with respect to polystyrene standards. The measurements are carried out on a system composed of two PSS Gram columns (100 Å and 1000 Å) connected to a Waters 410 differential refractive index (DRI) detector operating at 0.5 mL/min flow rate and a temperature of 35 °C. UV-visible spectra are recorded on a Varian Cary 50 Conc. spectrophotometer equipped with a Varian Cary thermostat. The measurements are performed in a 1 cm quartz cell.

Synthesis of DDMAT

1-Dodecanethiol (4.8 mL, 20 mmol), aliquat 336 – tricaprylylmethylammonium chloride – (0.36 mL) and acetone (12 mL) are introduced in a bicol (100 mL). The mixture is left to stir at 10 °C under argon atmosphere during 5 minutes. An 50 %wt/vol aqueous solution of NaOH (1.1 mL, 13.8 mmol) is then slowly added. The solution is stirred at 10 °C under argon atmosphere during 15 minutes. Carbon disulfide (1.2 mL, 20 mmol), dissolved in of acetone (2.5 mL), is then slowly added under argon atmosphere. The solution is left to stir at 10 °C during 10 minutes. Chloroform (2.4 mL, 30 mmol) is next added. A 50 %wt/vol aqueous solution of NaOH (5.3 mL, 66.3 mmol) is then slowly added. The solution

is finally left to stir during at least 10 hours, at 10 ℃ and under argon atmosphere.

The reaction mixture is diluted in of water (30 mL) and carefully concentrated under low pressure to remove the acetone. A concentrated aqueous solution of HCl is then added to reach pH 3. The solid is filtrated and dissolved in isopropanol (100 mL). The insoluble *S*,*S*-bis(1-dodecyl) trithiocarbonate side product is filtrated, washed with isopropanol (30 mL). The remaining solution is subsequently concentrated under vacuum. The obtained red solid is finally crystallized from *n*-hexane (15 mL). The yellow solid is subsequently filtrated, washed several times with cooled *n*-hexane, and dried overnight in a vacuum oven at 35 ℃ to give 38 % yield.

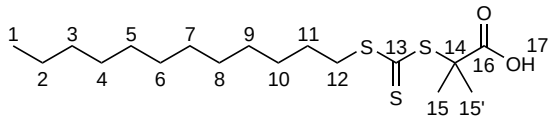

^{1}H-NMR (300 MHz, $CDCl_3$) δ_H: 3.30 (t, 2H, H_{12}), 1.74 (s, 6H, $H_{15,15'}$), 1.69 (q, 2H, H_{11}), 1.44–1.26 (m, 18H, $H_{2\text{-}10}$), 0.90 (t, 3H, H_1).

^{13}C-NMR (75 MHz, $CDCl_3$) δ_C: 220.8 (C_{13}), 178.9 (C_{16}), 55.6 (C_{14}), 37.1 (C_{12}), 31.9 (C_{11}), 29.7 (C_3), 29.6–29.4 ($C_{5\text{-}8}$), 29.1–29.0 ($C_{4,9}$), 27.8 (C_{10}), 25.2 (C_{15}), 22.7 (C_2), 14.2 (C_1)

Synthesis of 4'-(1-aminopentyloxy)-2,2';6',2"-terpyridine

5-Amino-1-pentanol (441 mg, 4.28 mmol) is dissolved in a suspension of potassium hydroxide (1.552 g, 27.65 mmol) in dry DSMO (21 mL) and stirred at 60 ℃ for 30 minutes under argon atmosphere. Small quantities of 4-chloro-2,2':6',2"-terpyridine (891 mg, 3.33 mmol) are then gradually added and the reaction mixture is stirred overnight at 60 ℃. After cooling down to room temperature, the reaction mixture is poured into a 50-times excess of cold distilled water. The yellow precipitate is filtered, subsequently washed with distilled water (3×250 mL) and diethyl ether (3×250 mL), and dried under vacuum to give 40 % yield.

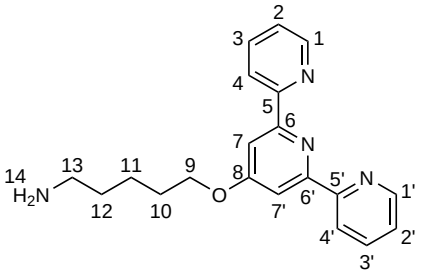

^{1}H-NMR (300 MHz, $CDCl_3$) δ_H: 8.69 (d, 2H, $H_{1,1'}$), 8.61 (d, 2H, $H_{4,4'}$), 8.00 (s, 2H, $H_{7,7'}$), 7.85 (td, 2H, $H_{3,3'}$), 7.33 (dd, 2H, $H_{2,2'}$), 4.24 (t, 2H, H_9), 2.75 (t, 2H, H_{13}), 1.88 (q, 2H, H_{10}), 1.63 (s, 2H, H_{14}), 1.56 (q, 2H, H_{11}), 1.54 (q, 2H, H_{12}).

^{13}C-NMR (75 MHz, $CDCl_3$) δ_C: 167.3 (C_8), 157.1 ($C_{5,5'}$), 156.2 ($C_{7,7'}$), 149.3 ($C_{1,1'}$), 136.8 ($C_{3,3'}$), 123.8 ($C_{4,4'}$), 121.4 ($C_{2,2'}$), 107.4 ($C_{7,7'}$), 68.0 (C_9), 42.1 (C_{13}), 33.3 (C_{12}), 28.9 (C_{10}), 23.4 (C_{11}).

Synthesis of DDMAT-tpy

Hydroxybenzotriazole hydrate (165 mg, 1.08 mmol) and L-(3-dimethylaminopropyl)-3-ethyl carbodiimide hydrochloride (230 mg, 1.20 mmol) are dissolved in a DCM (6 mL) – DMF (0.7 mL) mixture at 0 °C. Afterwards, *S*-dodecyl-*S*′-(α, α'-dimethyl-α''-acetic acid) trithiocarbonate (120.6 mg, 0.43 mmol) is added and the solution is stirred for 30 minutes. 4'-(1-Aminopentyloxy)-2,2';6',2"-terpyridine (407 mg, 1.22 mmol) is added and the reaction mixture is stirred for 19 hours. Then, the mixture is diluted with DCM (100 mL) and consecutively washed with 3×100 mL of sodium carbonate aqueous solution (100 g/L), 3×100 mL of citric acid aqueous solution (100 g/L), and 3×100 mL of distilled water. The organic phase is finally separated, dried over magnesium sulfate, filtered on sintered glass and concentrated under low pressure to give a yellow solid with 90 % yield.

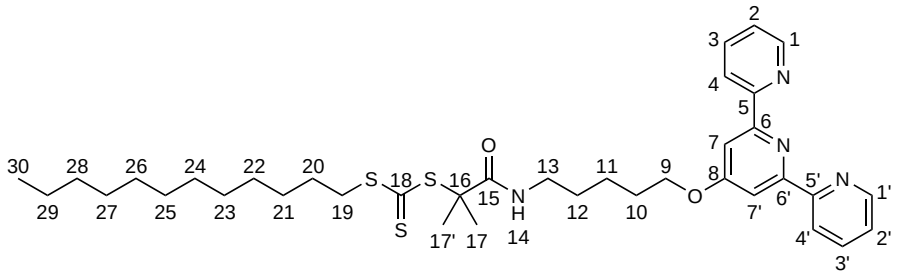

^{1}H-NMR (300 MHz, $CDCl_3$) δ_H: 8.69 (d, 2H, $H_{1,1'}$), 8.61 (d, 2H, $H_{4,4'}$), 8.01 (s, 2H, $H_{7,7'}$), 7.85 (td, 2H, $H_{3,3'}$), 7.33 (dd, 2H, $H_{2,2'}$), 6.55 (br, 1H, H_{14}), 4.24 (t, 2H, H_9), 3.29 (q, 2H, H_{13}), 3.28 (t, 2H, H_{19}), 1.88 (q, 2H, H_{10}), 1.73 (s, 6H, $H_{17,17'}$), 1.69 (q, 2H, H_{20}), 1.59 (q, 2H, H_{12}), 1.57 (q, 2H, H_{17}), 1.44–1.26 (m, 18H, $H_{2\text{-}10}$), 0.90 (t, 3H, H_{30}).

^{13}C-NMR (75 MHz, $CDCl_3$) δ_C: 220.1 (C_{18}), 172.4 (C_{15}), 167.5 (C_8), 157.1 ($C_{5,5'}$), 156.1 ($C_{6,6'}$), 149.3 ($C_{1,1'}$), 137.1 ($C_{3,3'}$), 124.1 ($C_{2,2'}$), 121.6 ($C_{4,4'}$), 107.6 ($C_{7,7'}$), 68.1 (C_9), 52.3 (C_{16}), 40.2 (C_{13}), 37.1 (C_{19}), 31.9 (C_{20}), 29.6 (C_{28}), 29.5–29.3 ($C_{23\text{-}26}$), 29.1–28.7 ($C_{9,10,12,27}$), 27.7 (C_{21}), 26.0 ($C_{15,15'}$), 23.5 (C_{11}), 22.7 (C_{29}), 14.1 (C_{30}).

Synthesis of CPAD-tpy

Hydroxybenzotriazole hydrate (66 mg, 0.43 mmol) and L-(3-dimethylaminopropyl)-3-ethyl carbodiimide hydrochloride (82.5 mg, 0.43 mmol) are dissolved in a DCM (9.1 mL) – DMF (0.255 mL) mixture at 0 °C. Afterwards, 4-cyano-4-(phenylcarbonothioylthio)pentanoic acid (120.6 mg, 0.43 mmol) is added and the solution is stirred at 0 °C for 45 minutes. 4'-(1-Aminopentyloxy)-2,2';6',2"-terpyridine (143.7 mg, 0.43 mmol) is added and the reaction mixture is stirred for 22 hours. Then, the mixture is diluted with DCM (50 mL) and consecutively washed with 3×50 mL of sodium carbonate aqueous solution (100 g/L), 3×50 mL of citric acid aqueous solution (100 g/L), and 3×50 mL of distilled water. The organic phase is finally separated, dried over magnesium sulfate, filtered on sintered glass and concentrated under low pressure to give a red solid with 86 % yield.

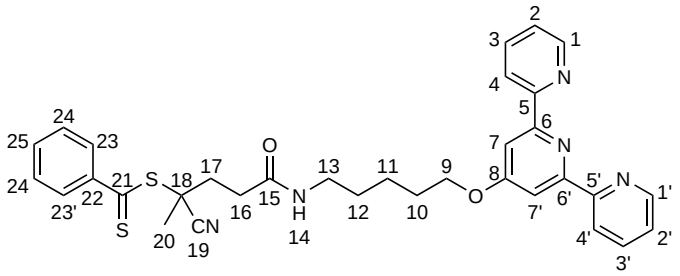

^{1}H-NMR (300 MHz, $CDCl_3$) δ_H: 8.69 (d, 2H, $H_{1,1'}$), 8.61 (d, 2H, $H_{4,4'}$), 8.01 (s, 2H, $H_{7,7'}$), 7.91 (t, 2H, $H_{23,23'}$), 7.85 (td, 2H, $H_{3,3'}$), 7.56 (t, 1H, H_{25}), 7.38 (t, 2H, $H_{24,24'}$), 7.33 (dd, 2H, $H_{2,2'}$), 5.70 (br, 1H, H_{14}), 4.24 (t, 2H, H_9), 3.31 (q, 2H, H_{13}), 2.54 (t, 2H, H_{16}), 2.52 (m, 2H, H_{17}), 1.94 (s, 3H, H_{20}), 1.88 (q, 2H, H_{10}), 1.78 (q, 2H, H_{12}), 1.70 (q, 2H, H_{11}).

^{13}C-NMR (75 MHz, $CDCl_3$) δ_C: 222.8 (C_{21}), 170.5 (C_{15}), 167.5 (C_8), 157.1 ($C_{5,5'}$), 156.1 ($C_{6,6'}$), 149.3 ($C_{1,1'}$), 144.7 (C_{22}), 137.1 ($C_{3,3'}$), 133.2 (C_{25}), 128.7 ($C_{24,24'}$), 126.9 ($C_{23,23'}$), 124.1 ($C_{2,2'}$), 121.6 ($C_{4,4'}$), 118.9 (C_{19}), 107.6 ($C_{7,7'}$), 68.1 (C_9), 46.3 (C_{18}), 39.8 (C_{13}), 34.4 (C_{16}), 32.1 (C_{17}), 29.4 (C_{10}), 28.8 (C_{12}), 24.4 (C_{20}), 23.6 (C_{11}).

MS (ESI) m/z: $[M + Na]^+$ calculated for $C_{33}H_{33}N_5O_2S_2$, 618.20; found, 618.05.

Typical synthesis of PNIPAAm-tpy

NIPAAm (5 g, 44 mmol), DDMAT-tpy (59 mg, 87 µmol) and AIBN (2.85 mg, 17 µmol) are dissolved with dry DMF (10 mL) in a Schlenk tube (50 mL) equipped with a magnetic stirrer. Five freeze–pump–thaw cycles are applied to degas the solution. The reaction tube is then filled with argon, sealed and placed in a pre-heated oil bath at 70 °C. After 60 minutes, the polymerization is stopped by placing the Schlenk tube into liquid nitrogen and the solvent is removed under low pressure at 35 °C. The crude product is dissolved in a minimum amount of DCM and purified by precipitation (two times) into cold diethyl ether. A white solid is finally recovered by filtration and dried in a vacuum oven at 35 °C.

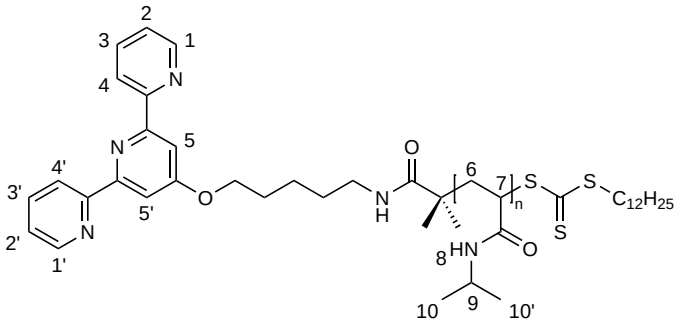

^{1}H-NMR (300 MHz, $CDCl_3$) δ_H: 8.67 (d, 2H, $H_{1,1'}$), 8.61 (d, 2H, $H_{4,4'}$), 7.99 (s, 2H, $H_{5,5'}$), 7.84 (td, 2H, $H_{3,3'}$), 7.32 (dd, 2H, $H_{2,2'}$), 6.35 (br, 300H, H_8), 3.99 (br, 300H, H_9), 2.00 (br, 300H, H_7), 1.60 (br, 600H, H_6), 1.15 (br, 1800H, $H_{10,10'}$).

$\bar{M}_n$(NMR) = 34,900 g/mol, $\bar{M}_n$(SEC) = 39,200 g/mol, $\bar{M}_w$(SEC) = 48,900 g/mol, $Đ$(SEC) = 1.25.

Typical synthesis of PS-*b*-PNIPAAm-tpy

Styrene (563 µL, 4.9 mmol), PNIPAAm-tpy (857 mg, 24.5 µmol), AIBN (0.81 mg, 4.9 µmol) are dissolved with dry DMF (3.94 mL) and dry anisole (280 µL) in a Schlenk tube (25 mL) equipped with a magnetic stirrer. Five freeze–pump–thaw cycles are applied to degas the solution. The reaction tube is filled with argon, sealed and placed in a pre-heated oil bath at 90 °C. After 10 hours, the polymerization is stopped by placing the Schlenk tube into liquid nitrogen and the solvents are removed under low pressure at 35 °C. The crude product is dissolved in a minimum amount of DCM and purified by precipitation (two times) into cold diethyl ether. A white powder is finally recovered by filtration and dried in a vacuum oven at 35 °C.

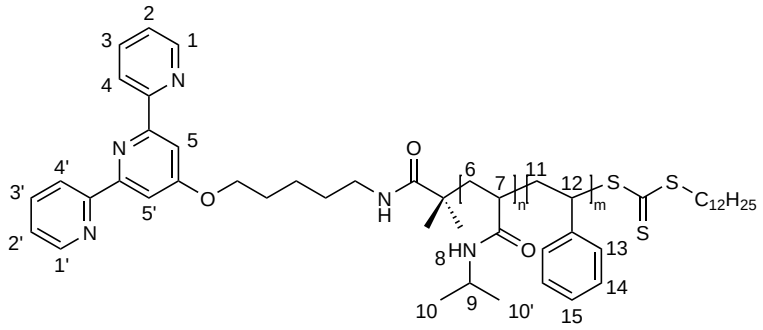

^{1}H-NMR (300 MHz, $CDCl_3$) δ_H: 8.67 (d, 2H, $H_{1,1'}$), 8.61 (d, 2H, $H_{4,4'}$), 7.99 (s, 2H, $H_{5,5'}$), 7.84 (td, 2H, $H_{3,3'}$), 7.32 (dd, 2H, $H_{2,2'}$), 7.05 (br, 54H, $H_{14,14'}$), 6.95 (br, 27H, H_{15}), 6.50 (br, 54H, $H_{13,13'}$), 6.35 (br, 300H, H_8), 3.99 (br, 300H, H_9), 2.00 (br, 327H, $H_{7,12}$), 1.60 (br, 654H, $H_{6,11}$), 1.15 (br, 1800H, $H_{10,10'}$).

$\bar{M}_n$(NMR) = 37,700 g/mol, $\bar{M}_n$(SEC) = 41,500 g/mol, $\bar{M}_w$(SEC) = 54,700 g/mol, $Đ$(SEC) = 1.32.

Typical synthesis of PDMAEMA-tpy

CPAD-tpy (23.8 mg, 40 µmol), DMAEMA (2.02 mL, 12.0 mmol) and AIBN (1.31 mg, 8 µmol) are dissolved in 1,4-dioxane (5.545 mL). The solution is degassed three times by freeze–pump–thaw, filled with argon and stirred in a preheated paraffin oil bath at 70 °C. At predetermined time intervals, samples are withdrawn from the reaction mixture using a degassed syringe and precipitated twice into a 20-times excess of cold *n*-hexane. The precipitate is isolated by centrifugation at 2000 rpm and dried under vacuum at room temperature to afford a red semi-solid.

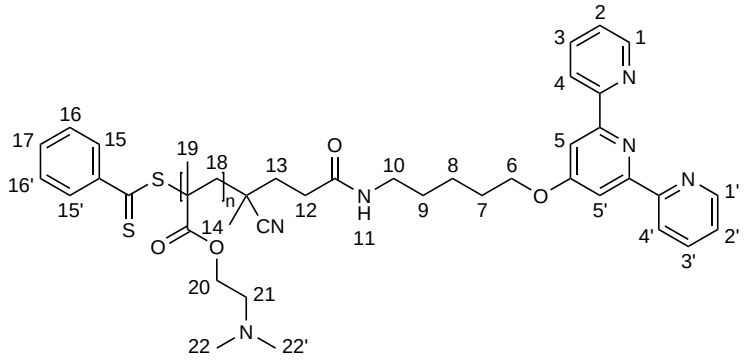

^{1}H-NMR (300 MHz, $CDCl_3$) δ_H: 8.69 (d, 2H, $H_{1,1'}$), 8.61 (d, 2H, $H_{4,4'}$), 8.01 (s, 2H, $H_{5,5'}$), 7.91 (t, 2H, $H_{15,15'}$), 7.85 (td, 2H, $H_{3,3'}$), 7.56 (t, 1H, H_{17}), 7.38 (t, 2H, $H_{16,16'}$), 7.33 (dd, 2H, $H_{2,2'}$), 5.70 (br, 1H, H_{11}), 4.24 (t, 2H, H_6), 4.07 (br, 2nH, H_{20}), 3.31 (q, 2H, H_{10}), 2.54 (t, 2H, H_{12}), 2.53 (br, 2nH, H_{21}), 2.52 (m, 2H, H_{13}), 2.26 (br, 6nH, $H_{22,22'}$), 1.88 (q, 2H, H_7), 1.88–1.80 (br, 2nH, H_{18}), 1.03–0.87 (br, 3nH, H_{19}), 1.78 (q, 2H, H_9), 1.70 (q, 2H, H_8), 0.88 (s, 3H, H_{14}).

Typical synthesis of PNIPAAm-*b*-PDMAEMA-tpy

PDMAEMA-tpy (197.0 mg, 12 µmol), NIPAAm (489.0 mg, 4.3 mmol) and AIBN (0.36 mg, 2.2 µmol) are dissolved in 1,4-dioxane (2.069 mL). The solution is degassed three times by freeze–pump–thaw, filled with argon and stirred in a preheated paraffin oil bath at 70 °C. At predetermined time intervals, samples are withdrawn from the reaction mixture using a degassed syringe and precipitated five times into a 10-times excess of *n*-hexane. The precipitate is isolated by centrifugation at 2000 rpm and dried under vacuum at room temperature to afford a pale red solid.

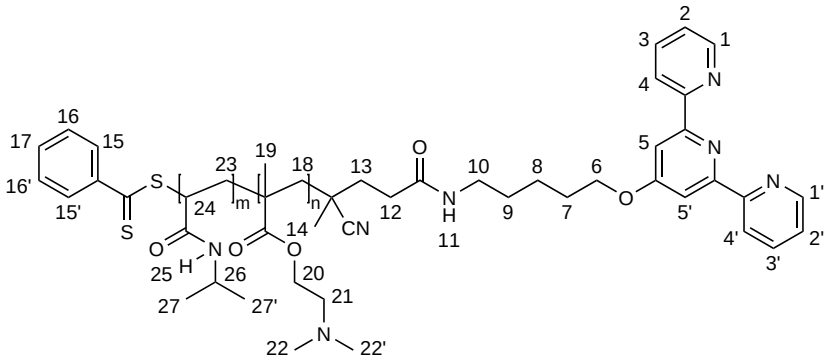

^{1}H-NMR (300 MHz, $CDCl_3$) δ_H: 8.69 (d, 2H, $H_{1,1'}$), 8.61 (d, 2H, $H_{4,4'}$), 8.01 (s, 2H, $H_{5,5'}$), 7.91 (d, 2H, $H_{15,15'}$), 7.85 (td, 2H, $H_{3,3'}$), 7.56 (tt, 1H, H_{17}), 7.38 (t, 2H, $H_{16,16'}$), 7.33 (dd, 2H, $H_{2,2'}$), 6.30 (br, mH, H_{25}), 5.70 (br, 1H, H_{11}), 4.24 (t, 2H, H_6)), 4.07 (br, 2nH, H_{20}), 3.99 (br, mH, H_{26}), 3.31 (q, 2H, H_{10}), 2.54 (t, 2H, H_{12}), 2.53 (br, 2nH, H_{21}), 2.52 (m, 2H, H_{13}), 2.26 (br, 6nH, $H_{22,22'}$), 2.08 (br, mH, H_{24}), 1.88 (q, 2H, H_7), 1.88–1.80 (br, 2nH, H_{18}), 1.82–1.62–1.33 (br, 2mH, H_{23}), 1.12 (br, 6mH, $H_{27,27'}$), 1.03-0.87 (br, 3nH, H_{19}), 1.78 (q, 2H, H_9), 1.70 (q, 2H, H_8), 0.88 (s, 3H, H_{14}).

Typical synthesis of PS-*b*-PNIPAAm-*b*-PDMAEMA-tpy

PNIPAAm-*b*-PDMAEMA-tpy (200.1 mg, 8 µmol), styrene (368 µL, 3.2 mmol) and AIBN (0.175 mg, 1.05 µmol) are dissolved in 1,4-dioxane (1.549 mL). The solution is degassed three times by freeze–pump–thaw, filled with argon and stirred in a preheated paraffin oil bath at 80 °C. At predetermined time intervals, samples are withdrawn from the reaction mixture using a degassed syringe and precipitated three times into a 10-times excess of *n*-hexane. The precipitate is isolated by centrifugation at 2000 rpm and dried under vacuum at room temperature to afford a pale red solid.

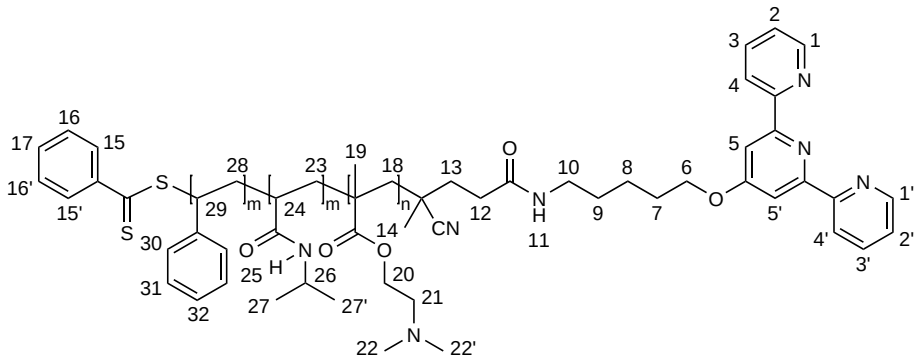

^{1}H-NMR (300 MHz, $CDCl_3$) δ_H: 8.69 (d, 2H, $H_{1,1'}$), 8.61 (d, 2H, $H_{4,4'}$), 8.01 (s, 2H, $H_{5,5'}$), 7.91 (d, 2H, $H_{15,15'}$), 7.85 (td, 2H, $H_{3,3'}$), 7.56 (tt, 1H, H_{17}), 7.38 (t, 2H, $H_{16,16'}$), 7.33 (dd, 2H, $H_{2,2'}$), 7.05 (br, 2lH, $H_{31,31'}$), 6.95 (br, lH, H_{15}), 6.50 (br, 2lH, $H_{30,30'}$), 6.30 (br, mH, H_{25}), 5.70 (br, 1H, H_{11}), 4.24 (t, 2H, H_6), 4.07 (br, 2nH, H_{20}), 3.99 (br, mH, H_{26}), 3.31 (q, 2H, H_{10}), 2.54 (t, 2H, H_{12}), 2.53 (br, 2nH, H_{21}), 2.52 (m, 2H, H_{13}), 2.30–1.70 (br, lH, H_{29}), 2.26 (br, 6nH, $H_{22,22'}$), 2.08 (br, mH, H_{24}), 1.88 (q, 2H, H_7), 1.88–1.80 (br, 2nH, H_{18}), 1.82–1.62–1.33 (br, 2mH, H_{23}), 1.12 (br, 6mH, $H_{27,27'}$), 1.03-0.87 (br, 3nH, H_{19}), 1.78 (q, 2H, H_9), 1.70 (q, 2H, H_8), 1.90–1.30 (br, 2lH, H_{28}), 0.88 (s, 3H, H_{14}).

UV-Vis titration of terpyridine end-groups

Terpyridine-functionalized polymers are dissolved in 1 mL of degassed ultra-pure water, at a given concentration around 0.25 mmol/L. This solution is then titrated by stepwise addition of a 0.125 mmol/L aqueous solution of iron(II) chloride stabilized against oxidation by the presence of 0.5 mmol/L ascorbic acid.

Bibliography

[1] Tsitsilianis, C.; Iliopoulos, I.; Ducouret, G. *Macromolecules* **2000**, *33*, 2936–2943.

[2] Miasnikova, A.; Laschewsky, A.; De Paoli, G.; Papadakis, C.; Muuller-Buschbaum, P.; Funari, S. S. *Langmuir* **2012**, *28*, 4479–4490.

[3] Claudy, P.; Letoffe, J.; Camberlain, Y.; Pascault, J. *Polym. Bull.* **1983**, *9*, 208–215.
[4] Tsitsilianis, C.; Aubry, T.; Iliopoulos, I.; Norvez, S. *Macromolecules* **2010**, *43*, 7779–7784.
[5] Ono, Y.; Shikata, T. *J. Am. Chem. Soc.* **2006**, *128*, 10030–10031.
[6] Heskins, M.; Guillet, J. *J. Macromol. Sci., Chem.* **1968**, *2*, 1441–1455.
[7] Yoshida, R.; Sakai, K.; Okano, T.; Sakurai, Y. *J. Biomater. Sci., Polym. Ed.* **1995**, *6*, 585–598.
[8] Zhang, H.-F.; Zhong, H.; Zhang, L.-L.; Chen, S.-B.; Zhao, Y.-J.; Zhu, Y.-L.; Wang, J.-T. *Carbohydr. Polym.* **2010**, *79*, 131–136.
[9] Inomata, H.; Goto, S.; Otake, K.; Saito, S. *Langmuir* **1992**, *8*, 687–690.
[10] Annaka, M.; Motokawa, K.; Sasaki, S.; Nakahira, T.; Kawasaki, H.; Maeda, H.; Amo, Y.; Tominaga, Y. *J. Chem. Phys.* **2000**, *113*, 5980–5985.
[11] Kokufuta, E.; Zhang, Y.; Tanaka, T.; Mamada, A. *Macromolecules* **1993**, *26*, 1053–1059.
[12] Inomata, H.; Goto, S.; Saito, S. *Langmuir* **1992**, *8*, 1030–1031.
[13] Schild, H. *Prog. Polym. Sci.* **1992**, *17*, 163–249.
[14] Roy, D.; Brooks, W. L. A.; Sumerlin, B. S. *Chem. Soc. Rev.* **2013**, *42*, 7214–7243.
[15] Plamper, F. A.; Ruppel, M.; Schmalz, A.; Borisov, O.; Ballauff, M.; Muller, A. H. E. *Macromolecules* **2007**, *40*, 8361–8366.
[16] Li, F.-M.; Chen, S.-J.; Du, F.-S.; Wu, Z.-Q.; Li, Z.-C. *ACS Symp. Ser.* **1999**, *726*, 266–276.
[17] Liu, Q.; Yu, Z.; Ni, P. *Colloid Polym. Sci.* **2004**, *282*, 387–393.
[18] Butun, V.; Armes, S.; Billingham, N. *Polymer* **2001**, *42*, 5993–6008.
[19] Schubert, U.; Hofmeier, H.; Newkome, G. R. *Modern terpyridine chemistry*; Wiley-VCH: Weinheim, 2006; pp viii, 229.
[20] Schubert, U.; Winter, A.; Newkome, G. R. *Terpyridine-based materials: For catalytic, optoelectronic and life science applications*; Wiley-VCH: Weinheim, 2011; pp xix, 522.
[21] Shunmugam, R.; Gabriel, G.; Aamer, K.; Tew, G. *Macromol. Rapid Commun.* **2010**, *31*, 784–793.
[22] Schwarz, G.; Haßlauer, I.; Kurth, D. G. *Adv. Colloid Interface Sci.* **2014**, *207*, 107–120.
[23] Schubert, U. S.; Eschbaumer, C. *Angew. Chem. Int. Ed.* **2002**, *41*, 2893–2926.
[24] Gao, Y.; Rajwar, D.; Grimsdale, A. C. *Macromol. Rapid Commun.* **2014**, *35*, 1727–1740.
[25] Ott, C.; Lohmeijer, B. G. G.; Wouters, D.; Schubert, U. S. *Macromol. Chem. Phys.* **2006**, *207*, 1439–1449.
[26] Grubbs, R. B. *Polym. Rev.* **2011**, *51*, 104–137.
[27] Matyjaszewski, K.; Xia, J. H. *Chem. Rev.* **2001**, *101*, 2921–2990.
[28] Moad, G.; Chiefari, J.; Krstina, J.; Mayadunne, R.; Postma, A.; Rizzardo, E.; Thang, S. *Polym. Int.* **2000**, *49*, 993–1001.

[29] Perrier, S.; Takolpuckdee, P. *J. Polym. Sci., Part A: Polym. Chem.* **2005**, *43*, 5347–5393.
[30] Moad, G.; Rizzardo, E.; Thang, S. H. *Aust. J. Chem.* **2009**, *62*, 1402–1472.
[31] Barner-Kowollik, C. *Handbook of RAFT polymerization*; Wiley-VCH: Weinheim, 2008; pp xi, 543.
[32] Keddie, D. J. *Chem. Soc. Rev.* **2014**, *43*, 496–505.
[33] Muller, A. H. E.; Matyjaszewski, K. *Controlled and living polymerizations: Methods and materials*; Wiley-VCH: Weinheim, 2009; pp xxi, 612.
[34] Lai, J. T.; Filla, D.; Shea, R. *Macromolecules* **2002**, *35*, 6754–6756.
[35] Schubert, U. S.; Eschbaumer, C.; Hien, O.; Andres, P. R. *Tetrahedron Lett.* **2001**, *42*, 4705–4707.
[36] Chan, L. C.; Cox, B. G. *J. Org. Chem.* **2007**, *72*, 8863–8869.
[37] Piogé, S.; Fustin, C.-A.; Gohy, J.-F. *Macromol. Rapid Commun.* **2012**, *33*, 534–539.
[38] Ke, X.-X.; Wang, L.; Xu, J.-T.; Du, B.-Y.; Tu, Y.-F.; Fan, Z.-Q. *Soft Matter* **2014**, *10*, 5201–5211.
[39] Odian, G. *Principles of polymerization*, 4th ed.; Wiley: Hoboken, 2004; pp xxi, 812.
[40] Van Hook, J.; Tobolsky, A. *J. Polym. Sci.* **1958**, *33*, 429–445.
[41] Hammond, G. S.; Sen, J. N.; Boozer, C. E. *J. Am. Chem. Soc.* **1955**, *77*, 3244–3248.
[42] Liu, L.; Wu, C.; Zhang, J.; Zhang, M.; Liu, Y.; Wang, X.; Fu, G. *J. Polym. Sci., Part A: Polym. Chem.* **2008**, *46*, 3294–3305.
[43] Nuopponen, M.; Ojala, J.; Tenhu, H. *Polymer* **2004**, *45*, 3643–3650.
[44] Barner-Kowollik, C.; Buback, M.; Charleux, B.; Coote, M. L.; Drache, M.; Fukuda, T.; Goto, A.; Klumperman, B.; Lowe, A. B.; Mcleary, J. B. *J. Polym. Sci., Part A: Polym. Chem.* **2006**, *44*, 5809–5831.
[45] Holyer, R. H.; Hubbard, C. D.; Kettle, S. F. A.; Wilkins, R. G. *Inorg. Chem.* **1966**, *5*, 622–625.
[46] Hogg, R.; Wilkins, R. *J. Chem. Soc.* **1962**, 341–350.
[47] Harzmann, G. D.; Neuburger, M.; Mayor, M. *Eur. J. Inorg. Chem.* **2013**, *2013*, 3334–3347.
[48] Chiper, M.; Hoogenboom, R.; Schubert, U. S. *Eur. Polym. J.* **2010**, *46*, 260–269.

CHAPTER 9

HIERARCHICAL ASSEMBLY OF BUILDING BLOCKS INTO SUPRAMOLECULAR GELS

Abstract

Through this chapter, the synthesized macromolecular building blocks are hierarchically assembled into supramolecular hydrogels. At first, micellization of the segmented copolymers is tested by direct dissolution in aqueous media and followed by light scattering and imaging techniques. In this frame, the response developed by the different systems to the application of proper stimuli, e.g., *pH and/or temperature, is investigated in the dilute regime. In parallel, the possibility to establish metal–ligand bridges between two individual copolymer chains is demonstrated by means of size exclusion chromatography. Finally, supramolecular hydrogels are elaborated from concentrated block copolymer solutions, via addition of different transition metal ions, and their thermal behaviour is investigated by calorimetry.*

9.1 Overview

Having synthesized a library of functional macromolecular building blocks, efforts can be directed towards obtaining nano-structured matter based on phase separation and metal coordination. As pointed by Ikkala and ten Brinke,[1,2] the self-assembly of polymeric molecules at different length scales leads to structural hierarchies. This hierarchical assembly offers rich possibilities to control the self-organization processes into specific supramolecular architectures, producing functional materials that combine several properties and may respond to external conditions.

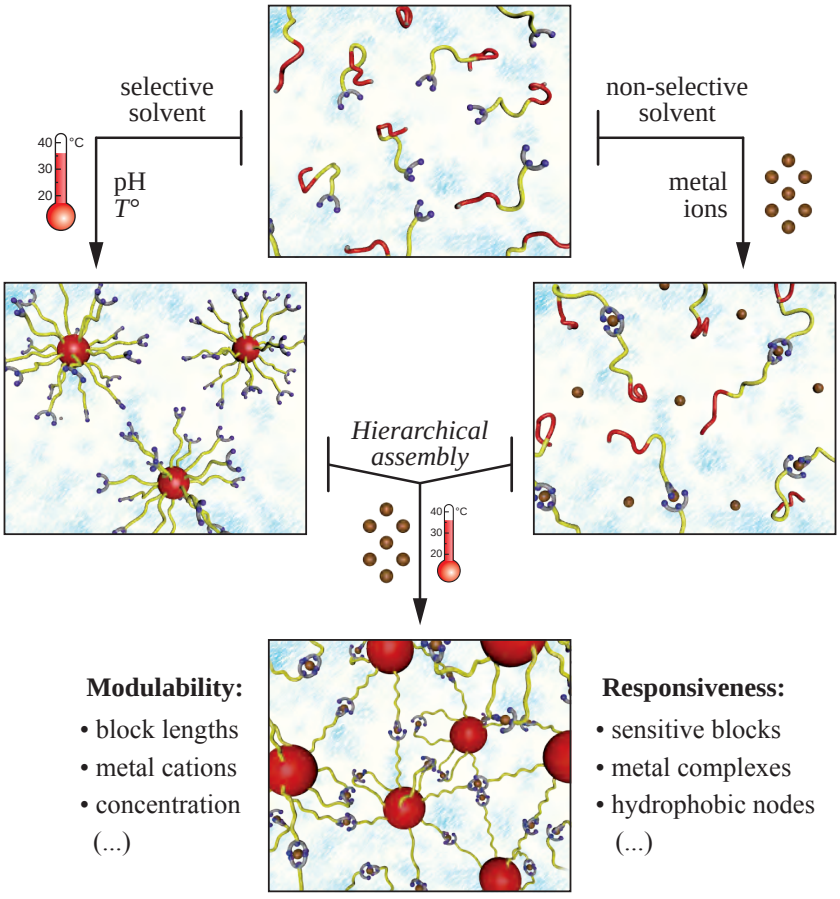

Figure 9.1 – Multiple self-assemblies of ligand end-capped block copolymers towards supramolecular materials.

Here, complexation of terpyridine end-capped block copolymers using metal–ligand coordination leads to symmetrical multi-segmented supramacromolecules. On the other hand, self-assembly at an order of magnitude larger length scale is provided by micellization of block copolymers, potentially triggered by the application of proper stimuli like, *e.g.*, pH and/or temperature. Finally, the combination of the latter two concepts leads to a parallel hierarchy in the form of supramolecular polymer networks, as illustrated in Figure 9.1.

Unless kinetically frozen, a self-assembly process is essentially a thermodynamic equilibrium. Therefore, capturing the transient nature of self-assembled nano-structures or supramolecular materials remains challenging.[3] In practice, this can be achieved through dynamic measurements,[4] which is the matter of the next chapters focusing extensively on the rheological properties of the hierarchically assembled materials. In the present chapter, the aim is to bring into light the different assembly processes and the possibility to influence them via environmental changes.

Although they may clearly influence each others, the analysis of solution self-assembly processes can be tackled individually, at least in a first approach. In the literature, various methods for characterizing the supramolecular organization of macromolecules can be found, including light scattering, mass spectrometry, nuclear magnetic resonance spectroscopy, microscopy techniques, thermal analysis, and computational estimations.[3,5] Practically, each characterization method has clear merits and drawbacks, providing only partial information about the self-assembled nano-materials. Therefore, the combination of carefully selected techniques is usually required to obtain convincing conclusions, without necessarily encompassing the full set of characterization tests.

9.2 Metal-induced self-assembly

Terpyridine ligand is well-known to form stable coordination complexes in combination with numerous transition metal ions.[6,7] This connectivity is here at the basis of the self-assembly of block copolymers into multi-segmented metallo-supramolecular copolymers (Figure 9.2). In the literature, various studies investigate the formation of small metal–terpyridine complexes, focusing on thermo-gravimetric,[8] calorimetric,[9]

spectrometric,[10] spectroscopic[11] and kinetic aspects.[12,13] With the incorporation of the ligand into macromolecular architectures, classical polymer characterization techniques can be further explored, including, *e.g.*, size exclusion chromatography.[14,15]

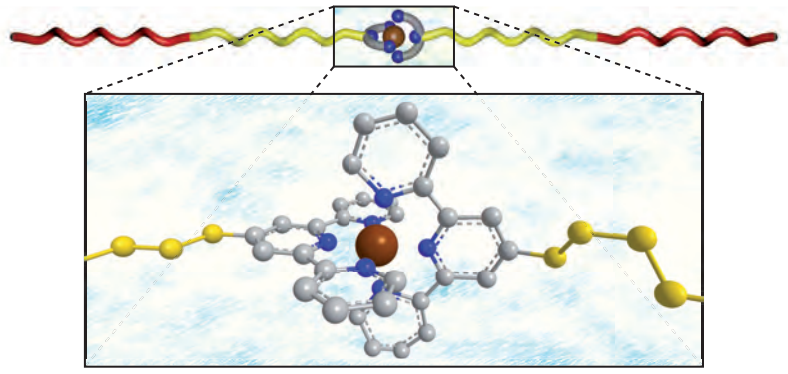

Figure 9.2 – Molecular view of the metal bis-terpyridine junction between segmented copolymers.

Due to the dynamic nature of non-covalent polymers, changes of solvent, concentration, or temperature, may always influence their original molecular organization, which makes conventional characterization difficult. Hence, freezing the supramolecular polymers by physical or chemical approaches before characterization is usually considered. For example, ruthenium(II) ions are commonly used in combination with terpyridine ligands to form very stable complexes, thereby offering the possibility of investigating the obtained species by classical methods.[16] Being one of the rarest metals on Earth, ruthenium and its derivatives are rather expensive and further highly toxic and carcinogenic, which restrict their use. As alternative, other first raw transition metal ions also form stable bis-terpyridine complexes with controlled dissociation and association rates,[12,13] therefore constituting the basis of this study.

The kinetic and thermodynamic equilibrium parameters for the formation and dissociation of terpyridine mono- and bis-complexes with various transition metal ions are given in Table 9.1. However, it should be noted that those values are reported for 2,2':6',2"-terpyridine model complexes, therefore being here sensibly affected by the substituent on the ligand, *i.e.*, the polymer chain itself, through steric and electronic effects.[17,18]

Table 9.1 – Kinetic and thermodynamic equilibrium parameters for the formation and dissociation of terpyridine mono- and bis-complexes with various transition metal ions.[12,13]

Ion	k_1 [$M^{-1}{\cdot}s^{-1}$]	k_{-1} [s^{-1}]	K_1 [M^{-1}]	k_2 [$M^{-1}{\cdot}s^{-1}$]	k_{-2} [s^{-1}]	K_2 [M^{-1}]	β [M^{-2}]
Ni^{II}	$10^{3.1}$	$10^{-7.6}$	$10^{10.7}$	$10^{5.3}$	$10^{-5.8}$	$10^{11.1}$	$10^{21.8}$
Fe^{II}	$10^{4.9}$	$10^{-2.2}$	$10^{7.1}$	$10^{7.0}$	$10^{-6.8}$	$10^{13.8}$	$10^{20.9}$
Co^{II}	$10^{4.4}$	$10^{-4.0}$	$10^{8.4}$	$10^{6.7}$	$10^{-3.2}$	$10^{9.9}$	$10^{18.3}$
Zn^{II}	$10^{6.1}$	$10^{0.1}$	$10^{6.0}$	-	"fast"	$10^{5.2}$	$10^{11.2}$

Values reported in water, at 25 °C.

As addressed above, the formation of iron(II)–terpyridine complexes can be easily followed by UV-visible spectroscopy because of their high absorption coefficient.[11,15] The experiment consists in the stepwise addition of aqueous solution of iron(II) chloride to a solution of terpyridine end-capped block copolymer dissolved in water. To prevent the oxidation of iron(II) into iron(III) ions, the oxidation potential of the media is reduced by the presence of ascorbic acid.

As illustrated in Figure 9.3 for a PNIPAAm-*b*-PDMAEMA-tpy diblock copolymer, an intense absorption in the visible light region increases with the addition of the titrant, the colour of the complex being intense purple. Interestingly, the maximum absorption is obtained close to the calculated equivalence point, indicating full complexation of all terpyridine units. Furthermore, over-titration of the chelating macroligand does not result in any further significant increase of the metal-to-ligand-charge-transfer band detected in the region between 500 and 600 nm, demonstrating that the formed iron(II)–terpyridine complexes are stable.

With the formation of metallo-supramolecular polymeric complexes, a shift in the average molar mass of the system is expected. To verify such hypothesis, size exclusion chromatography (SEC) usually constitutes one of the most used characterization tools in polymer science. However, in the case of reversible bonding based on weak metal–ligand interactions, *e.g.*, zinc(II) or cobalt(II) bis-terpyridine complexes, the comparably low binding strength of such systems in solution leads to fragmentation during the SEC separation.[15] For this reason, the SEC method is suitable for the evaluation of metallo-supramolecular block

copolymers based on metal ions with high binding strength.

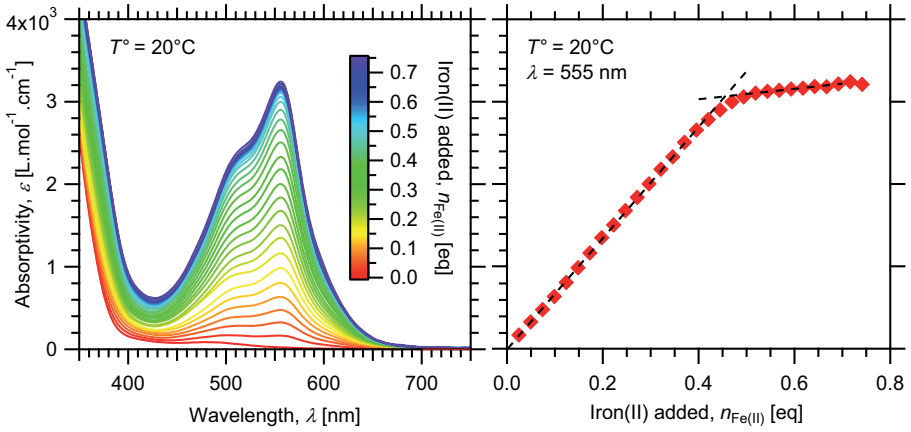

(a) UV-Vis titration (left) and evolution of molar absorptivity (right)

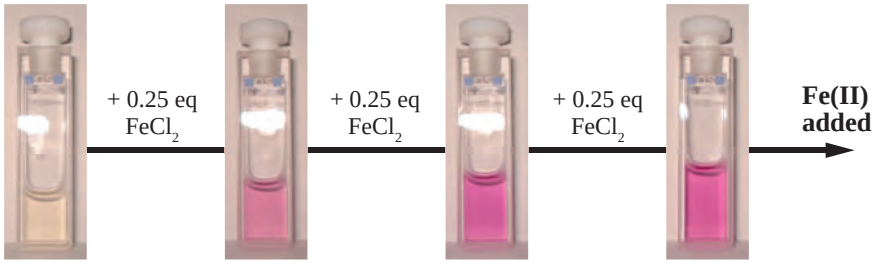

(b) Color change of the solution upon addition of Fe(II) ions

Figure 9.3 – Monitoring the formation of iron(II)–terpyridine bis-complexes between PNIPAAm-*b*-PDMAEMA-tpy macro-ligand.

As demonstrated by Schubert and coworkers,[16] the analysis of supramolecular polymers containing coordination complexes is not trivial and special attention has to be paid to the conditions applied for size exclusion chromatography. Indeed, standard conditions, *i.e.*, eluent, flow rate and temperature, often result in uninterpretable results due to interactions of the investigated polymers with the column material.[16] To screen out non-specific column interactions and avoid fragmentation of the polymeric complexes, ammonium hexafluorophosphate salt is added to dimethylformamide, an unusual but well suited solvent for SEC, offering the possibility to successfully analyse the fragile compounds.

At the start of our investigation, the formation of metallo-supramo-

lecular complexes between the different synthesized block copolymers and iron(II) was considered, as illustrated in Figure 9.4. Based on a qualitative observation of the chromatograms, the presence of both uncomplexed and complexed species is attested by SEC, the equilibrium being in favour of the complex formation. Focusing on uncomplexed chains, a non-ideal behaviour is also observed in the form of peak tailing/broadening and delayed elution times, which is probably due to sticking to the stationary phase.

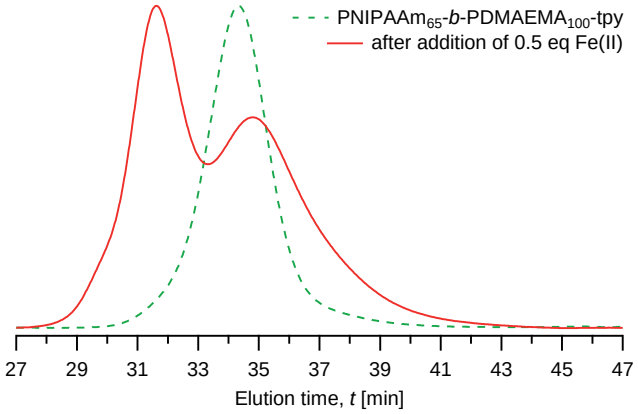

Figure 9.4 – SEC elugrams of a PNIPAAm-*b*-PDMAEMA-tpy copolymer and its iron(II) bis-complex.

Taking into account that the overall binding constant (β) for Ni(II) ions with terpyridine is slightly higher than for Fe(II) ions, the complexation equilibrium is supposed to be shifted to the bis-complexed form. In addition, the possibility of oxidizing Fe(II) to Fe(III) ions is much higher compared to other transition metal ions, lowering the stability of bis-complexes. As illustrated in Figure 9.5, these assumptions are verified by the nearly quantitative coupling of chains upon addition of half an equivalent of Ni(II) ions (with respect to the terpyridine content). Only residual signals of uncomplexed polymer are observed, which might be ascribed to the small fraction of non-functionalized chains derived from primary radicals generated during the RAFT polymerization. In addition, the proportion of linked chains can be interestingly tuned according to the metal-to-ligand ratio, until the 2:1 terpyridine:metal ion stoichiometry is reached.

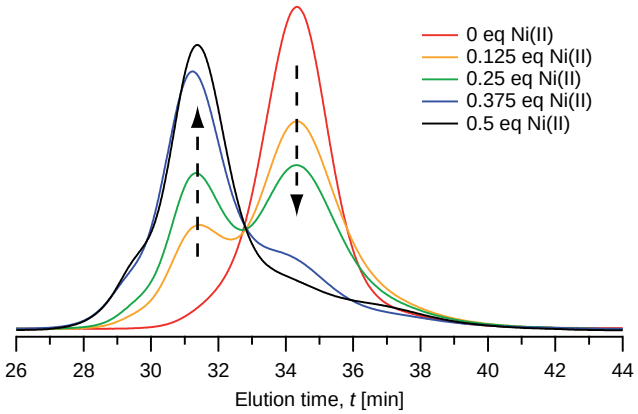

Figure 9.5 – Evolution of molar mass distribution of a PNIPAAm-*b*-PDMAEMA-tpy copolymer with the addition of Ni(II) ions.

9.3 Self-assembly into micelles

When dissolved in a block-selective solvent, segmented copolymers form micelles constituted by a core formed by the insoluble blocks surrounded by a corona composed by the soluble blocks.[19–26] The dimensions and morphology of the accordingly obtained micelles vary depending on molecular and solution parameters.[19,21,23,27] The former one include the nature and length of each block, along with the architecture of the chain.

As the length of the glassy hydrophobic polystyrene segment in the synthesized block copolymer, *i.e.*, PS-*b*-PNIPAAm-tpy diblocks and PS-*b*-PNIPAAm-*b*-PDMAEMA-tpy triblocks, has been deliberately kept short, a direct way to prepare micellar solution can be applied. Precisely, it consists in directly dissolving the bulk sample in aqueous media. Even if it can lead to the formation of larger aggregates, this dissolution method overcomes the limitations encountered for the preparation of concentrated solutions of block copolymers with long core-forming blocks.

The direct dissolution method is further recommended in the case of PNIPAAm-*b*-PDMAEMA-tpy double hydrophilic block copolymers, as both block are water-soluble under ambient conditions. Depending on the applied stimulus, these systems can be assembled or disassembled

upon application of the stimulus. In addition, the unimer–micelle equilibrium can be reversibly tuned by changing pH and/or temperature.

In this project, the self-assembly of the different synthesized block copolymers into micelles is mainly investigated via the analysis of the scattered and transmitted light from their solutions. In this regard, dynamic light scattering (DLS) constitutes one of the most accessible technique for determining the size distribution profile of small particles in suspension or polymers in solution.[28–30] The basic principle of DLS consists in illuminating a solution of particles subjected to Brownian motion with a radiation and to detect the intensity of light scattered by the sample (Figure 9.6). Data are collected as a function of time at a given angle of observation with respect to the incident radiation, thereby providing information about the particle dynamics.

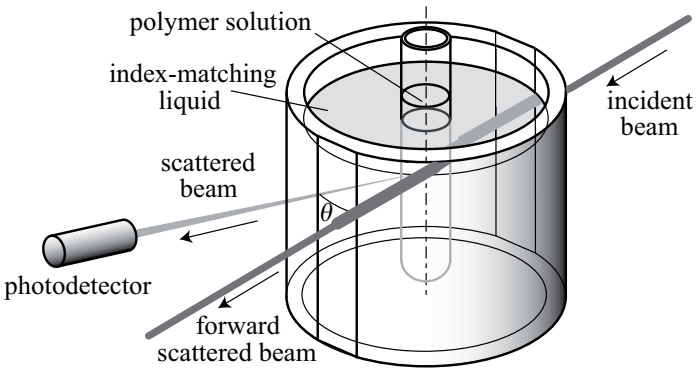

Figure 9.6 – Schematic of the geometry around a sample cell in a light-scattering measurement system.

The infinitesimal fluctuations in scattered intensity due to interference is self-correlated and leads to the characterization of the particle size through hydrodynamic models. Precisely, the diffusion coefficient, D, of Brownian particles in solution is related to their hydrodynamic radius, R_h, by the Stokes–Einstein equation, where k_B is Boltzmann's constant, T° the absolute temperature and η the dynamic viscosity of the media:[30,31]

$$R_h = \frac{k_B T^\circ}{6\pi\eta D} \tag{9.1}$$

As a general rule, small particles move comparatively faster than slow-diffusing bigger analogues, thereby making the relative analysis possible. When present together in the solution, a CONTIN analysis of the DLS signal can be employed to reveal the multimodal distribution of sizes, which is frequently observed with polymer assemblies. Since the contribution to the scattered light intensity is proportional to the sixth power of the scatterer size, the scattering of huge particles rapidly dominates the signal even if they are present in very small amounts.[5,29] In this regard, all solvents are filtered in order to remove dust prior any measurement.

In solution, polymer assemblies may adopt various conformations, each being characterized by a particular DLS signature, that further depends on time and environmental constraints. In this frame, periodic measurements of a sample provides information about how the particles aggregate over time, which results in populations with larger hydrodynamic radius. At the limit, macroscopic phase separation within the system is accompanied by a pronounced decrease in the intensity of transmitted light (Figure 9.7), which is captured by classical turbidimetry. Indeed, DLS instruments are generally designed to measure scattered light intensity only, loosing the information on transmitted light. Therefore, the transmission of light passing through the different samples is recorded in parallel via UV-visible absorption spectroscopy.

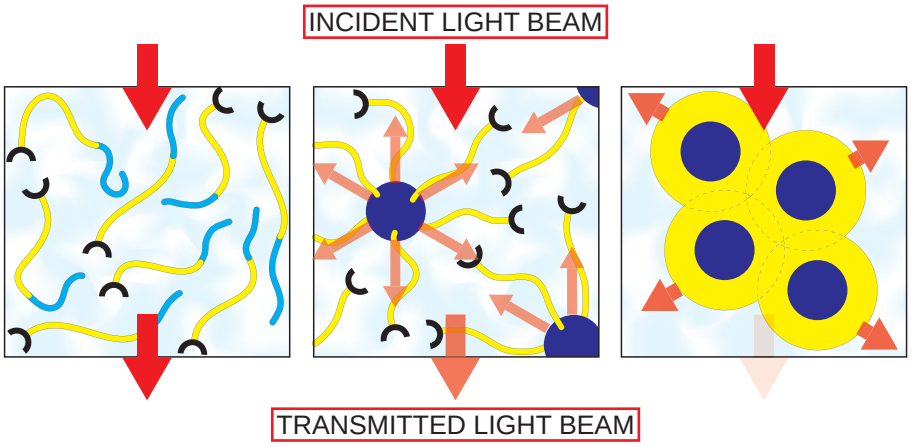

Figure 9.7 – Schematic of scattering and transmission of light by a solution of block copolymer in different media. From left to right: non-selective solvent, selective solvent, non-solvent.

As a valuable complement to scattering and transmission data, microscopy techniques are used to directly image individual particles. Typically, measurements are conducted after removing the sample from its natural state in solution and deposition onto a substrate or a support. Even if drying samples can cause changes in particle dimensions or even destruction of the particles, dry state analysis are largely prevalent in the literature. Indeed, special apparatus keeping the particles solvated are still not widely accessible and can limit imaging resolution. [5]

Among the different experimental tools, scanning microscopes use a probe that scans each point of the object serially in order to form a nano-scale representation. [32,33] In this regard, atomic force microscopy (AFM) constitutes the most commonly used technique where images are formed by dragging or tapping a sharp tip across the surface. Due to convolution effects, the AFM resolution in the x direction is limited by the size of the tip, which is on the order of 5 nm (Figure 9.8). On the other hand, the z-resolution in AFM is extremely high, most instruments being capable of atomic resolution. [34] In turn, this feature promotes the use of AFM in the analysis of nano-particles that flatten once dried onto a substrate, like star-like micelles, which otherwise give weak contrast in electron microscopes.

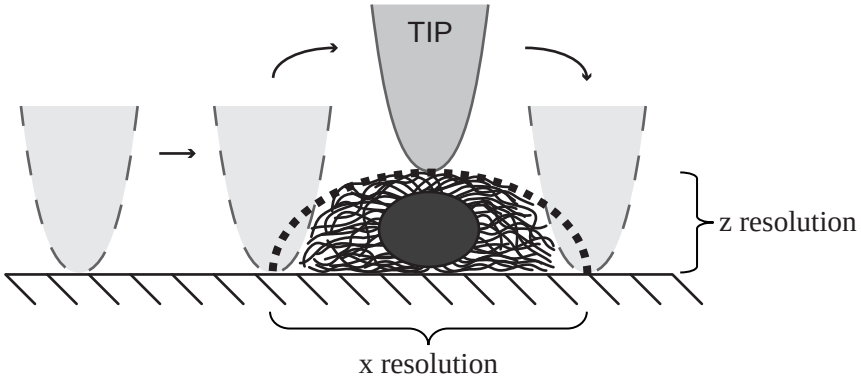

Figure 9.8 – Schematic of an AFM tip measuring a micelle deposited onto a surface, indicating how the x resolution is limited due to tip convolution effects.

In the following, the self-assembly and thermo-response of the different block copolymers that have been synthesized in the frame of this

project are tackled independently. Indeed, their respective compositions allow them to display quite distinct solution behaviours, notably in response to heat and pH. In addition, the effect of the presence of metal ions in solution is investigated on the thermal response of the different systems.

9.3.1 Self-assembly of PS-*b*-PNIPAAm-tpy copolymers

Herein, the self-assembly into micelles and the thermal response of the different PS-*b*-PNIPAAm-tpy copolymers is experimented in the dilute regime. Thanks to their hydrophilc-to-hydrophobic balance, micellization is achieved by direct dissolution of the diblock copolymers in MilliQ water, at concentrations around 1 g/L. In practice, the sealed reaction vessels are placed in a fridge and shaken from time to time until forming homogenous solutions.

Given the solubility of the inner block under ambient and low temperature conditions, micelles made of a PS core and thermo-sensitive PNIPAAm coronal chains, bearing terpyridine moiety at their extremity are thus obtained (Figure 9.9). Since the synthesized associating copolymers features a corona-forming block much longer than the core-forming block, *ca.*, only a few tens of repeating styrene units against a few hundreds for PNIPAAm block, "star-like" micelles only are expected to be formed in each cases.

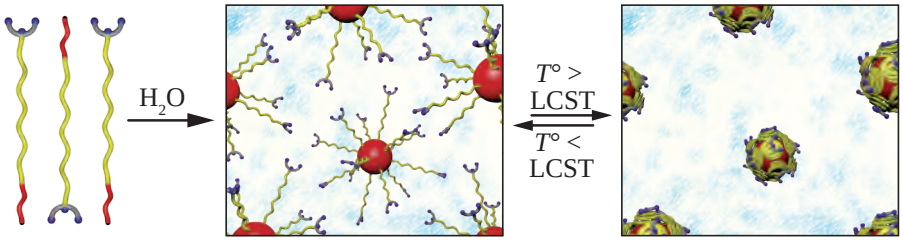

Figure 9.9 – Self-assembly of the PS-*b*-PNIPAAm-tpy copolymers in aqueous media, showing the thermo-shrinking of PNIPAAm coronal chains upon heating.

Given the stimuli-responsiveness of poly(*N*-isopropylacrylamide), the solution behaviour of PS-*b*-PNIPAAm-tpy copolymers should be highly dependent on temperature of the media. Precisely, the collapse of coro-

nal chains is expected above the lower critical solution temperature of the PNIPAAm sequence, which is schematically represented in Figure 9.9.

9.3.1.1 Effect of block length

Practically, dynamic light scattering allows determining the apparent hydrodynamic radius and size distribution histograms of the formed micellar aggregates. For all synthesized PS-*b*-PNIPAAm-tpy copolymers, CONTIN analysis of DLS data indicates mainly the formation of rather well-defined micelles, with an average $R_{h,app}$ of a few tens of nanometres. Importantly, almost no dependence of the DLS signal as function of the scattered angle is noted in the investigated concentration range (0.1 to 2 g/L), which is in agreement with the formation of spherical micelles.

In some cases, a small proportion of isolated unimers chains as well as larger aggregates are also evidenced by the presence of additional

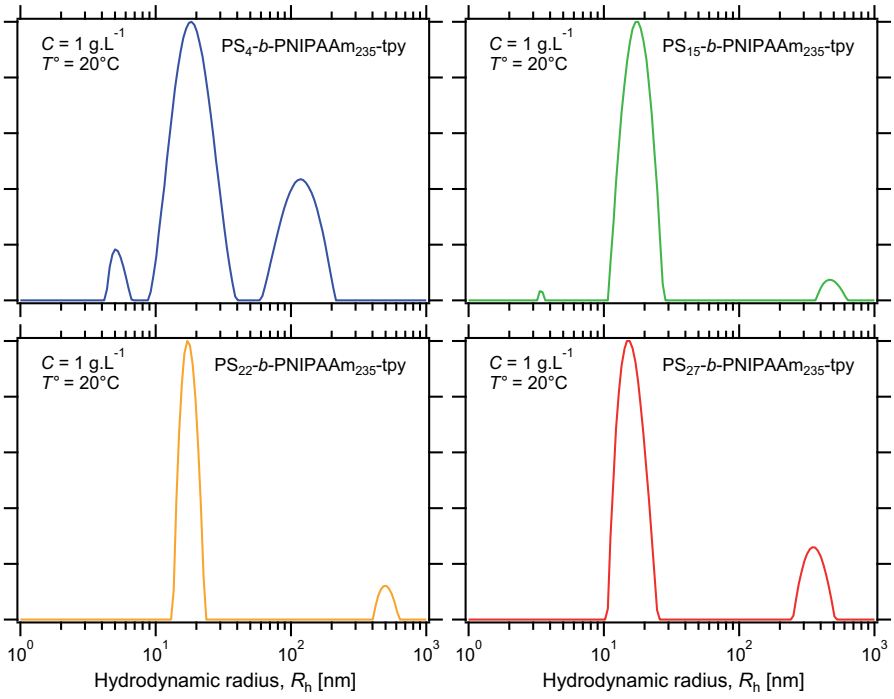

Figure 9.10 – Size distribution histograms of micelles prepared from different PS-*b*-PNIPAAm-tpy copolymers, in aqueous solution.

populations, respectively around a few and a few hundreds of nanometres (Figure 9.10). On one hand, the presence of unimer chains is a good indicator of dynamic exchange between micelles in solution, which in turn favours the formation of equilibrium nano-structures. On the other hand, the larger aggregates having a significant contribution to the overall scattering intensity can be considered to make up a negligible concentration in solution for the reason discussed above.

As illustrated in Figure 9.10, the presence of free copolymer chains in solution is clearly evidenced for short hydrophobic segments, while large aggregates have a higher tendency to form when increasing the length of the insoluble block. Interestingly, varying the size of the polystyrene segment has only a weak impact on the radius of micelles, which is mainly dictated by the size of the PNIPAAm block. This statement is rationalized by the theory of Daoud and Cotton, predicting the core size of classical "star-like" micelles should only scale as the 0.6^{th} power of the degree of polymerization of the insoluble block.[35,36]

If only insignificant variations are obtained as a function of the insoluble block length, the size of micelles relies more on the length of the hydrophilic outer block. Indeed, the poly(*N*-isopropylacrylamide) segments adopt a stretched coil conformation in order to form the corona of micellar nano-structures.[37] Accordingly, the average hydrodynamic radii of micelles prepared here are found to increase by around 10 nm when varying the polymerization degree of the PNIPAAm block from 235 to 300 (Figure 9.11).

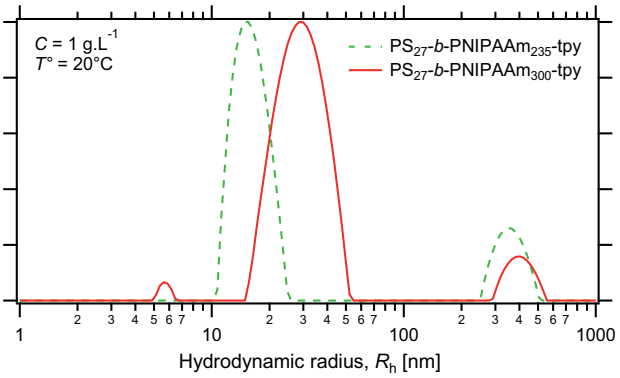

Figure 9.11 – Size distribution histograms of micelles prepared from different PS-*b*-PNIPAAm-tpy copolymers, in aqueous solution.

9.3.1.2 Effect of metal ions

The impact of transition metal ions on the self-assembly of PS-*b*-PNIPAAm-tpy copolymers in solution is investigated by adding half an equivalent of Ni(II) as its chlorinated salt to the micellar solution, with respect to the amount of terpyridine groups. According to the previous work, only flower-like micelles originating from intra-micellar bridging are formed in the dilute regime.[38–40] Under those conditions, the mean distance between nano-objects in solution indeed largely prevents the formation of inter-micellar bridges via metal–ligand coordination.

As illustrated in Figure 9.12, dynamic light scattering measurements on solutions containing Ni(II) salts essentially shows the same results as the micellar solution with no metal ions added. Only slight increases in the size of the micelles are observed, which are in accordance with anterior results obtained on analogous systems.[41] In the given example of the PS_{27}-*b*-$PNIPAAm_{300}$-tpy copolymer, CONTIN analysis reveals the formation of micelles with an average $R_{h,app}$ of 30.8 nm in the presence of metal ions, against 28.4 nm in the absence of metal ions. In essence, this observation can be rationalized by the swelling of micellar corona due to charged metal–terpyridine bis-complexes at the extremity of their coronal chains.

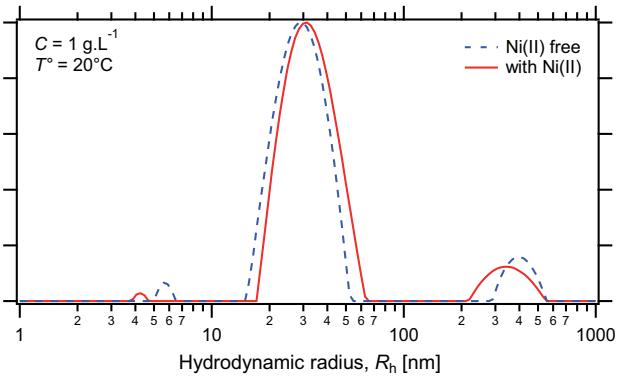

Figure 9.12 – Size distribution histogram of PS_{27}-*b*-$PNIPAAm_{300}$-tpy micelles in aqueous solution, in the absence and presence of half an equivalent of Ni(II) ions.

9.3.1.3 Effect of temperature

The thermal dependence of the size of micellar nano-structures is further tested in the absence and presence of half an equivalent of transition metal ions, respective to the terpyridine content. Precisely, the phase transition of PNIPAAm coronal chains is monitored by dynamic light scattering by following the evolution of the apparent hydrodynamic radius as a function of temperature, which is illustrated in Figure 9.13.

Below a critical temperature matching the limit of solubility of PNIPAAm chains, micelles are found to decrease in size upon heating, while their size is always slightly higher in the presence of Ni(II) ions. Above this critical solution temperature, collapsed micelles tend to combine to form larger aggregates, which is captured by DLS as an dramatic increase in the size of aggregates in solution. Ultimately macroscopic phase separation occurs within the system, thereby resulting in cloudy solutions (Figure 9.13).

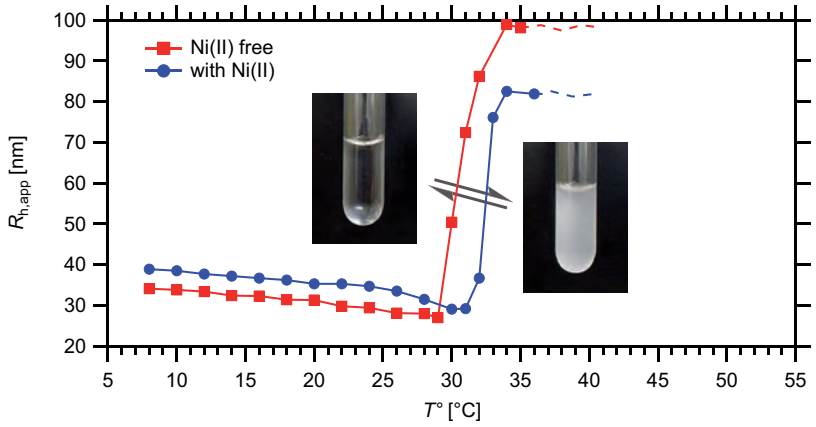

Figure 9.13 – Thermal evolution of the apparent hydrodynamic radius of PS_{27}-*b*-$PNIPAAm_{300}$-tpy nano-structures in aqueous solution, in the absence and presence of half an equivalent of Ni(II) ions.

As further noted in Figure 9.13, the onset of collapsing increases from 29 for the uncomplexed micelles to about 32 °C in presence of metal ions. This observation is consistent with the solution behaviour reported by Schubert *et al.* for PNIPAAm-tpy homopolymer chains when compared to their metallo-supramolecular complexes.[42] Besides, the same authors

already performed detailed characterization and LCST investigations on these particular systems, demonstrating that the cloud point is sensibly influenced by the type of metal cations and counter ions utilized.

9.3.2 Self-assembly of PNIPAAm-*b*-PDMAEMA-tpy copolymers

In this section, the focus is on the thermo-induced self-assembly of PNIPAAm-*b*-PDMAEMA-tpy copolymers in aqueous solution, at various pH. To this aim, different solutions are prepared by dissolution of the double hydrophilic copolymers in ultrapure water, at selected pH of 3, 6 and 9, which respectively afford total, partial and no protonation of the amine functions of the PDMAEMA block (Figure 9.14).[43] Then, those solutions are analysed by dynamic light scattering for size determination and turbidimetry for cloud point measurements. In addition, atomic force microscopy is used for imaging the self-assembled nano-structures formed in solution.

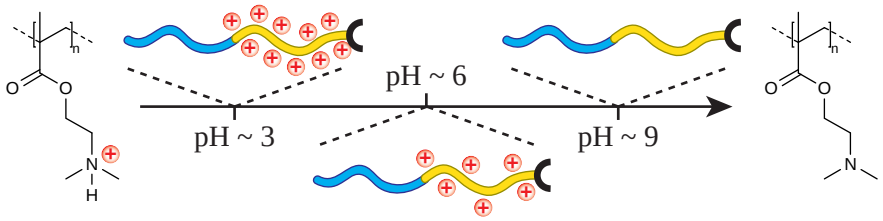

Figure 9.14 – Schematic of the ionization degree of PDMAEMA block in a PNIPAAm-*b*-PDMAEMA-tpy copolymers as a function of the pH.

9.3.2.1 Effect of temperature and pH

The intensity of scattered light (I_s) from a solution being proportional to particle size, the aggregation of PNIPAAm-*b*-PDMAEMA-tpy copolymers into micelles is monitored by the evolution of the normalized scattered light intensity (I_s/I_0, I_0 being the intensity of the light source) with temperature. On the other hand, the phase separation of the entire copolymer chains from the initially homogeneous solution is evaluated

by turbidimetry measurements via absorption spectroscopy (Figure 9.7). Since both PNIPAAm and PDMAEMA blocks are characterized by a LCST-type behaviour, a complex effect of the temperature on the system is expected to be monitored. Moreover, the ionization degree of the PDMAEMA block is expected to influence the phase transition temperature not only of PDMAEMA but also of the neighbouring PNIPAAm block (Figure 9.15).

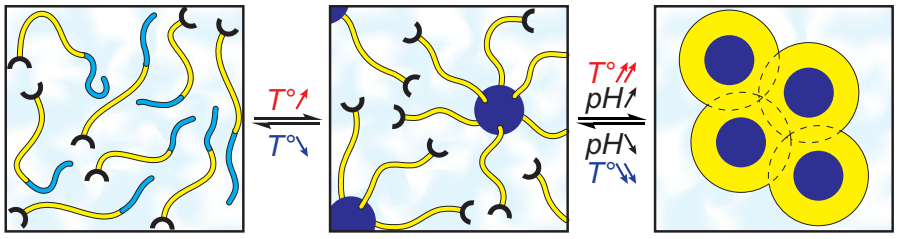

Figure 9.15 – Self-assembly behaviour of PNIPAAm-*b*-PDMAEMA-tpy double hydrophilic diblock copolymers in aqueous solution in response to heat and pH.

As shown in Figure 9.16, the relative intensities of light scattered by aqueous solutions of a selected PNIPAAm-*b*-PDMAEMA-tpy copolymer at pH 9, 6 and 3 undergo sharp increases around 28, 33 and 40 °C respectively, which is attributed to the aggregation of the PNIPAAm blocks. Indeed, this results in the formation of micellar objects made of a PNIPAAm core surrounded by a soluble PDMAEMA corona, as illustrated in Figure 9.15. In this picture, low pH increases the overall solubility of the copolymer by protonation of the PDMAEMA block, thus delaying the thermo-induced aggregation of the PNIPAAm block, and inversely.[44] Nevertheless, no information about the collapse of the PDMAEMA blocks can be deduced at this stage. According to this PNIPAAm core – PDMAEMA corona model, a collapse of the PDMAEMA block should result in the aggregation of the primary micelles into large aggregates (Figure 9.15), which would increase the turbidity of the solution and ultimately lead to precipitation.

As an indication of the collapse transition of the PDMAEMA block, expected around 35 and 50 °C at pH 9 and 6 respectively,[45] an increase in the turbidity of the same solution is monitored upon temperature rises (Figure 9.16). This increase is clearly marked at pH 9 and closely follows the aggregation of PNIPAAm blocks. Under those conditions,

the weak polybase block is formally deprotonated, which decreases its water solubility and hence forces the copolymer to phase separate. Decreasing the pH of the solution essentially delays the phase separation toward higher temperatures, which is ultimately not observed at pH 3 anymore. Also, the increase in turbidity becomes less pronounced and disappears as the pH is reduced from 9 to 6 and further to 3.

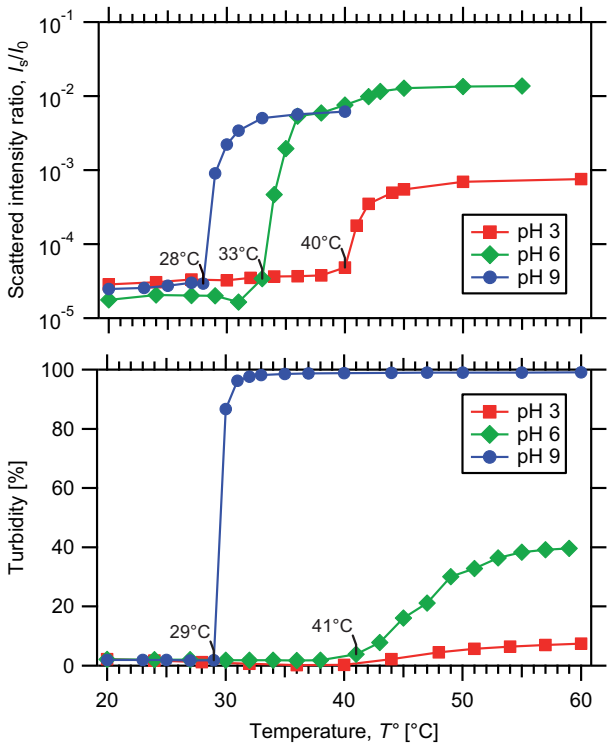

Figure 9.16 – Thermal dependence of the relative proportion of scattered and transmitted light by an aqueous solution of PNIPAAm$_{65}$-*b*-PDMAEMA$_{100}$-tpy diblock copolymer, at different pH.

Combining DLS and turbidimetry experiments suggests the following picture for the aggregation of the selected PNIPAAm$_{65}$-*b*-PDMAEMA$_{100}$-tpy diblock copolymer (numbers in subscript indicate the average degree of polymerization) as a function of pH and temperature: At pH 9, micelles are formed at 28 °C but since the phase separation temperatures of both blocks are reached more or less concomitantly they aggregate into larger structures due to the lack of stabilizing soluble block. At pH

6, micelles with a PNIPAAm core and a PDMAEMA corona are formed at 33 ℃, a further increase in temperature inducing the formation of aggregates due to the desolvation of PDMAEMA. At pH 3, the phase transition of PNIPAAm is shifted towards 41 ℃ because of the presence of a charged hydrophilic PDMAEMA block, the resulting micelles being weakly affected by a further increase of the temperature due to the presence of a polyelectrolyte-like corona.

In complement, information about size distributions of samples at different pH and temperatures is obtained by the CONTIN analysis of intensity autocorrelation functions (Figures 9.17, 9.18 and 9.19). In each cases, the obtained histograms are in good agreement with results derived from the scattered/transmitted light analysis, namely the presence of unimers below both phase transition temperatures, and formation of micellar nano-structures and higher aggregates due to the collapse of PNIPAAm and then PDMAEMA blocks.

At a pH of 6, the distribution of hydrodynamic radii essentially reveals the presence of isolated polymer chains with a size of a few nanometres as long as the temperature of the media is maintained below 32 ℃ (Figure 9.17). This population is apparently accompanied by larger aggregates that could in fact arise from slow diffusion modes of the polyelectrolyte. As the temperature crosses the phase transition temperature of PNIPAAm estimated from the increase in intensity of scattered light by the solution, nano-objects with a size of a few tens of nanometres become apparent. The latter can be reasonably ascribed to the formation of micellar structures made of a PNIPAAm core surrounded by soluble PDMAEMA coronal chains.

However, the size distribution histograms are systematically spoiled by the presence of a dominating population, around 100 nm in hydrodynamic radius, which could arise from a strong polyelectrolyte effect likely due to the quaternized PDMAEMA block. A plausible aggregation via inter-micellar interactions between terpyridine pendant groups is also not excluded. Indeed, the latter may interact with each other via the formation of hydrophobic domains or by pi–pi stacking. Above the phase transition temperature of PDMAEMA evaluated by absorbance spectroscopy, a population centred around 300 nm in radius and with a relatively narrow size distribution is mainly observed, along with a few micellar nano-objects.

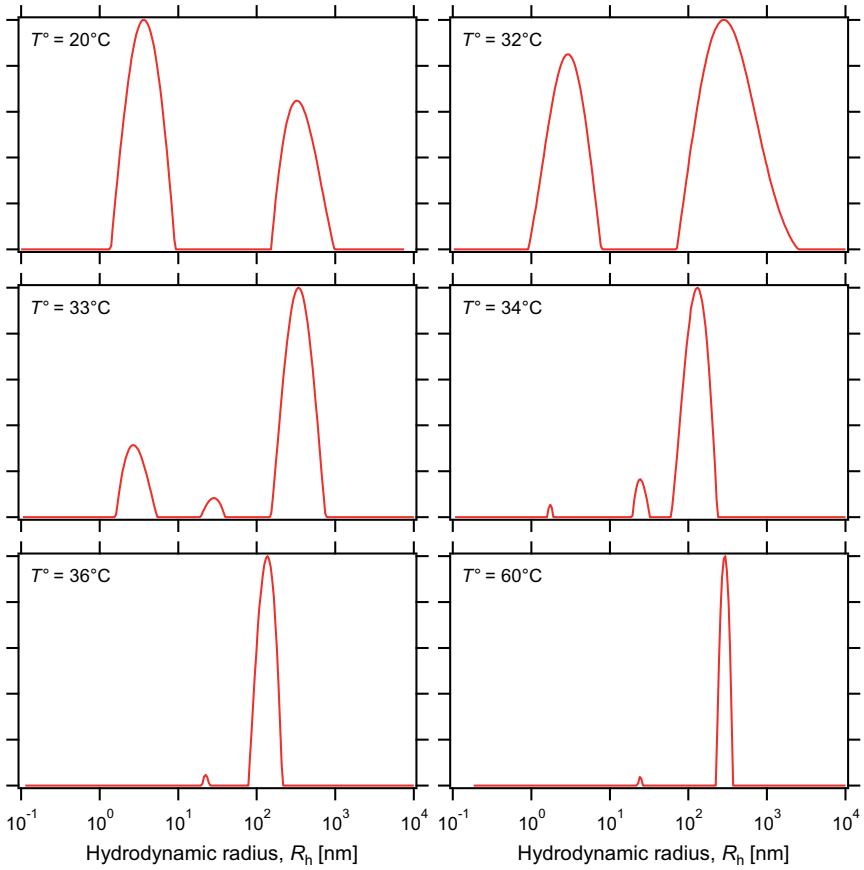

Figure 9.17 – Size distribution histograms of $PNIPAAm_{65}$-*b*-$PDMAEMA_{100}$-tpy copolymer and its aggregates in aqueous solution at pH 6.

A similar story happens at pH 3 that is the presence of unimer chains below the phase transition temperature of PNIPAAm, followed by the advent of micellar nano-structures above (Figure 9.18). The thermo-induced collapse of the PNIPAAm blocks, and hence the onset of formation of micellar nano-structures, is however shifted to higher temperature, *i.e.*, around 40 °C. Also, isolated chains remain apparent at high temperature, which might be due to their lower tendency to aggregate due to the presence of positive charges along the protonated PDMAEMA block. The same stabilization prevents the collapse of PDMAEMA chains so that micelles are observed even at 60 °C. Under such acidic conditions, the presence of a dominating population centred at 100 nm

in radius is more than presumably related to the strong polyelectrolyte effect of the quaternized PDMAEMA block.

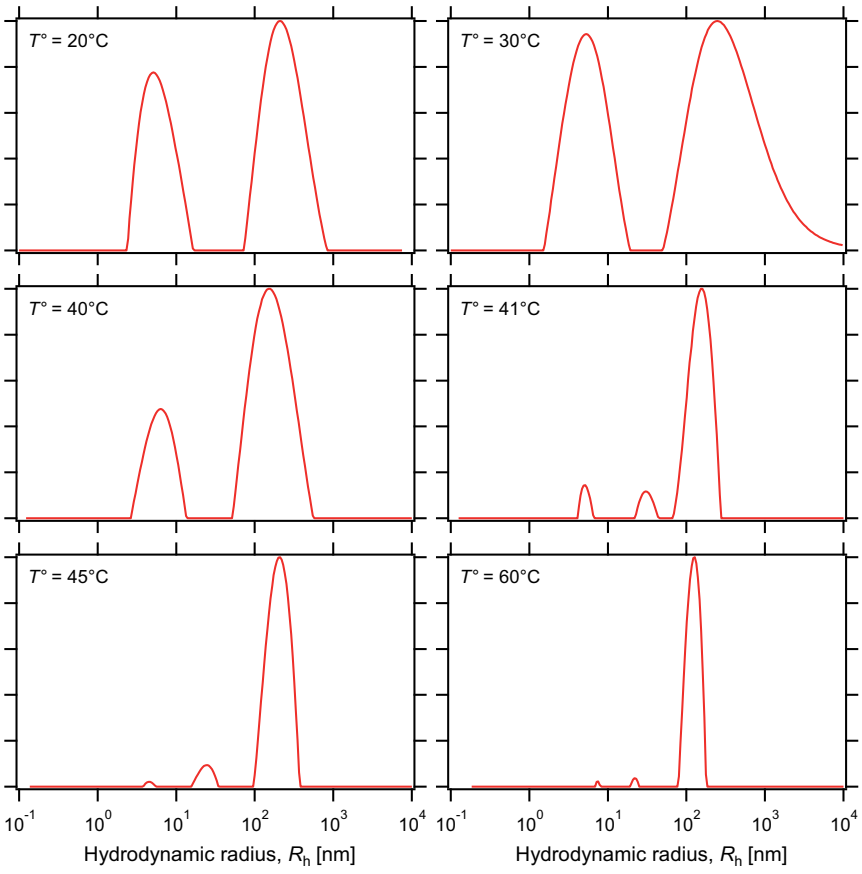

Figure 9.18 – Size distribution histograms of PNIPAAm$_{65}$-*b*-PDMAEMA$_{100}$-tpy copolymer and its aggregates in aqueous solution at pH 3.

Finally, at a pH of 9, the decreased hydrophilicity of the deprotonated PDMAEMA block severely weakens the solubility of the entire copolymer. As a consequence, the collapse of PNIPAAm block is observed as the temperature is increased above 28 °C, closely followed by the phase separation of the entire block copolymer (Figure 9.19). According to dynamic light scattering measurements, micellar aggregates would only be observed, if any, in a narrow temperature window around 29 °C. Be-

low, unimer chains of a few nanometre size are clearly distinguished. Above, large micro-particles, whose size is probably underestimated due to multiple light diffusion process, are only observed.

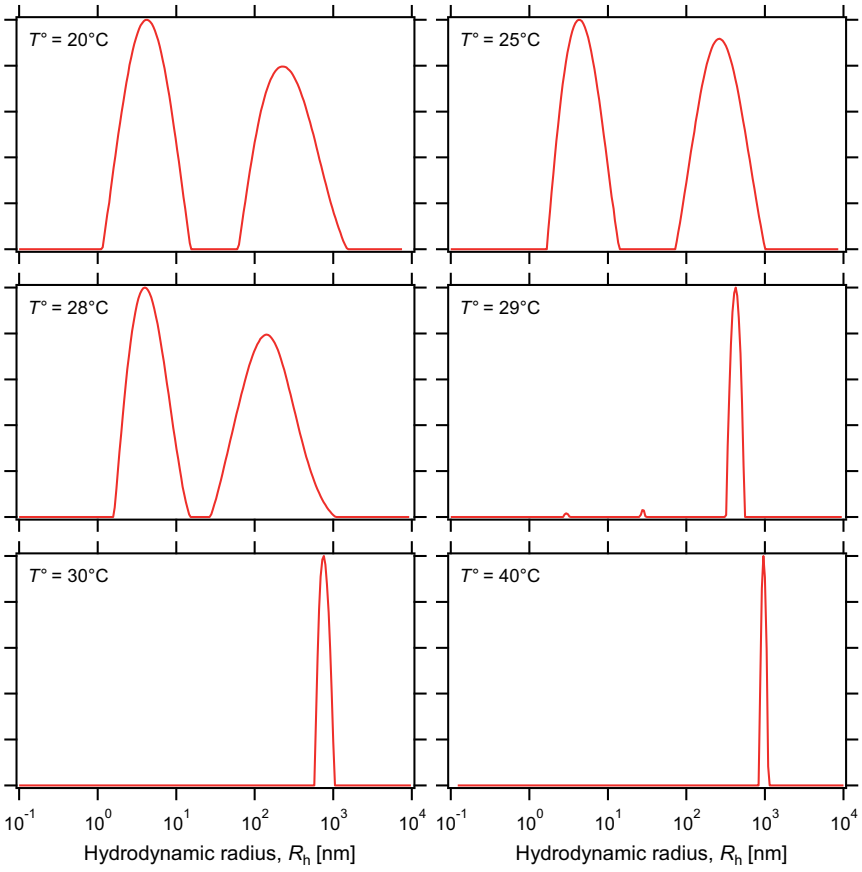

Figure 9.19 – Size distribution histograms of PNIPAAm$_{65}$-*b*-PDMAEMA$_{100}$-tpy copolymer and its aggregates in aqueous solution at pH 9.

9.3.2.2 AFM imaging

To avoid any ambiguous interpretation of DLS data, micellar nanostructures and higher aggregates are imaged by atomic force microscopy after spin-coating of the preheated block copolymer solutions onto silicon

wafers. Measurements are conducted mainly on solutions of the selected PNIPAAm$_{65}$-*b*-PDMAEMA$_{100}$-tpy block copolymer, with the help of Elio Poggi.

As illustrated by Figure 9.20 (a), spherical objects of a few tens of nanometres are distinguished at pH 6 when the solution is preheated at 35 °C, which presumably corresponds to micellar objects. Taking into account flattening of self-assembled nano-objects on the surface (as evidenced by height contrast images) and further overestimation due to tip convolution effects, their sizes are in reasonable agreement with results obtained from the CONTIN analysis of DLS data. However, almost no higher aggregates are detected when probing the surface of the silicon wafer.

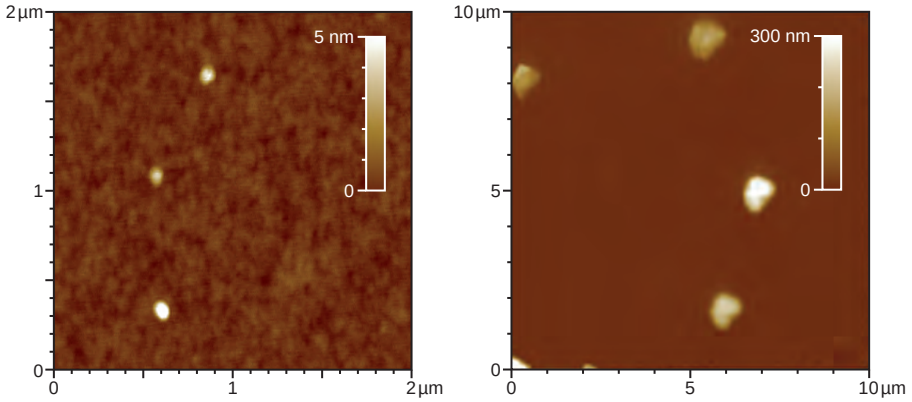

(a) Temperature of 35 °C (b) Temperature of 60 °C

Figure 9.20 – AFM height contrast images of PNIPAAm$_{65}$-*b*-PDMAEMA$_{100}$-tpy aggregates formed at pH 6 and different temperatures, deposited onto a silicon wafer.

On the other hand, large objects (around 350 nm in radius) are mainly observed form the block copolymer solution preheated at 60 °C, as illustrated by Figure 9.20 (b). In agreement with absorption spectroscopy measurements, this observation further supports the aggregation of micelles under these conditions, which is likely due to the change in water affinity of the PDMAEMA block.

9.3.2.3 Effect of metal ions

Lastly, the effect of adding metal ions on the thermo-induced assembly of PNIPAAm-*b*-PDMAEMA-tpy block copolymers is investigated by DLS and turbidimetry measurements. As observed by Chiper *et al.*[42] and confirmed by Piogé and coworkers,[38] the presence of a charged complex in a copolymer architecture may sensibly delays the thermo-induced phase transition of the constituting blocks. Practically, the intensities of scattered and transmitted light by the block copolymer solutions are thus monitored as a function of temperature, at different pH.

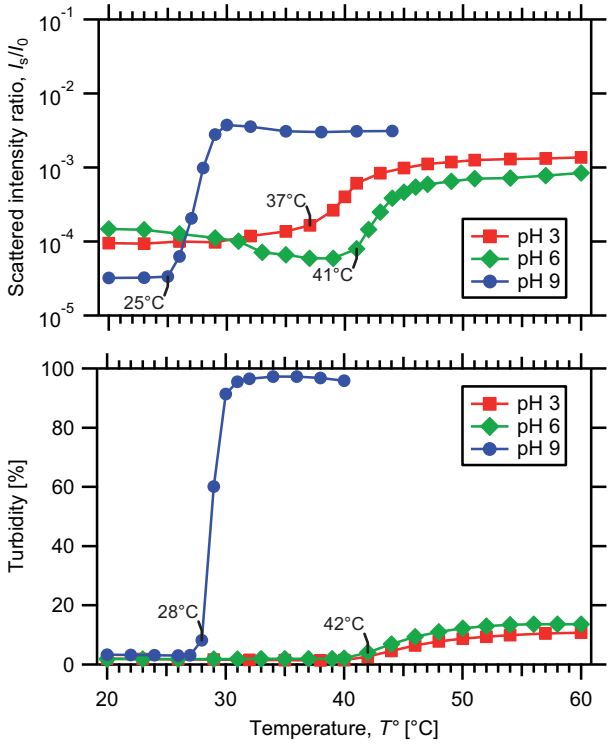

Figure 9.21 – Thermal dependence of the relative proportion of scattered and transmitted light by an aqueous solution of $PNIPAAm_{65}$-*b*-$PDMAEMA_{100}$-tpy diblock copolymer mixed with 0.5 eq of $NiCl_2$ salt, at different pH.

As shown in Figure 9.21, the relative intensities of light scattered by aqueous solutions of the selected $PNIPAAm_{65}$-*b*-$PDMAEMA_{100}$-tpy

containing 0.5 eq of nickel(II) salt undergo gradual increases as temperature rises. The onsets of the presumably thermo-induced aggregation of the PNIPAAm blocks are found around 25, 41 and 37 °C when the pH of the solution is respectively adjusted at 9, 6 and 3.

As an indication of the collapse transition of the PDMAEMA block, an increase in turbidity of the same solution is monitored upon temperature rises (Figure 9.21). This increase is clearly marked at pH 9 and follows the aggregation of PNIPAAm blocks observed in DLS measurements. A diminution in pH of the solution — from 9 to 6 and further to 3 — dramatically enhances the stability of PNIPAAm-*b*-PDMAEMA-tpy micelles toward aggregation. Their lower tendency to aggregate and thus phase separate may be ascribed to the presence of both charged metal–ligand complexes and quaternized ammonium groups in the micellar corona. Hence, only slight increases in the turbidity of those solutions are observed upon heating, which can be closely correlated to the evolution of scattered light intensities due to micellization.

The presence of $NiCl_2$ has thus a particularly marked effect at pH 6 where the onset of thermo-induced micellization was shifted from 33 °C, without metal added, to 41 °C, in presence of metal ions. Also, the increase in turbidity of the same solution with the collapse of PDMAEMA blocks was also less pronounced in presence of nickel salt. Hence, it was concluded that the charged metal–terpyridine bis-complexes in the micellar corona impeded the formation of large micellar clusters and hence the precipitation of micelles.

At pH 3 and 9, the presence of metal ions has only a weak impact on the thermo-response of the PNIPAAm-*b*-PDMAEMA-tpy copolymer chains in solution. In fact, only broadening of the phase transitions over the temperature range is mainly achieved, so that the onsets of the latter are observed at even slightly lower temperatures. At pH 9, it is assumed that the presence of the charged complex has no significant weight to counterbalance the macroscopic phase separation of the entire copolymer chains. On the other hand, the same complex does not add extra weight in delaying the thermo-induced micellization of copolymer chains at pH 3, which is in fact largely dominated by protonation of the PDMAEMA block.

9.3.3 Self-assembly of PS-*b*-PNIPAAm-*b*-PDMAEMA-tpy copolymers

Last but not least, the thermo-responsive phase behaviour of PS-*b*-PNIPAAm-*b*-PDMAEMA-tpy triblock copolymers in aqueous solution is investigated. Structurally speaking, the only major difference compared to PNIPAAm-*b*-PDMAEMA-tpy diblock precursors lies in the presence of a short hydrophobic segment at the chain end. Nevertheless, this additional block should force the copolymer chains to aggregate into micelles even below the critical solution temperature of poly(*N*-isopropylacrylamide). Above, the partial collapse of coronal chains would result in the formation of three-layer micelles with a hydrophobic PS core, a collapsed PNIPAAm shell, and a PDMAEMA corona, as schematized in Figure 9.22.

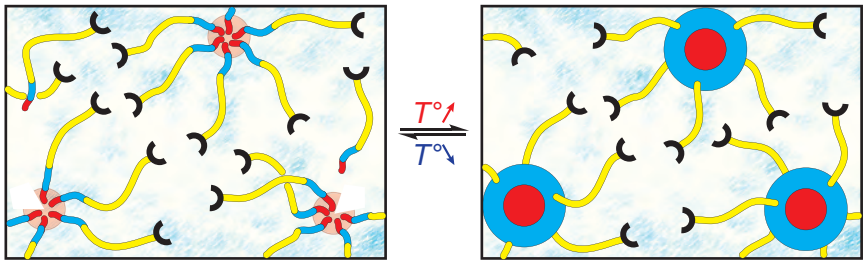

Figure 9.22 – Self-assembly behaviour of PS-*b*-PNIPAAm-*b*-PDMAEMA-tpy triblock copolymers in aqueous solution at different temperatures.

To verify those assumptions, dynamic light scattering measurements are performed on aqueous solution of PS-*b*-PNIPAAm-*b*-PDMAEMA-tpy triblock copolymers at different temperatures. As expected, micellar objects with hydrodynamic radius of a dozen nanometres are apparent at ambient temperature, even for short hydrophobic segment (Figure 9.23). This observation can be reasonably attributed to the high incompatibility of polystyrene with aqueous media. However, the presence of isolated unimer chains in solution, as revealed by CONTIN analysis of the DLS signal, suggests a dynamic exchange of free chains between micellar objects, which is particularly marked for triblock copolymers containing short PS segment (Figure 9.23).[46]

Upon temperature rises, the presumably weak aggregation of tri-

block copolymer chains in solution strengthens due to the collapse of PNIPAAm block onto PS cores (Figure 9.22). As an indication of the partial collapse of coronal chains, the size of micellar objects in solution is found to decrease when crossing the critical solubility temperature of around 35 °C. In DLS, the phase transition of PNIPAAm is further accompanied by an exaltation of slow diffusion modes of the polyelectrolyte micelles, as already observed for PNIPAAm-*b*-PDMAEMA-tpy diblock precursors (Figure 9.17). Compared to the situation observed at room temperature where transient micelles are formed, the enhanced cohesion of core–shell–corona particles is thought to favour their diffusion as a whole as they are less prone to disaggregation.

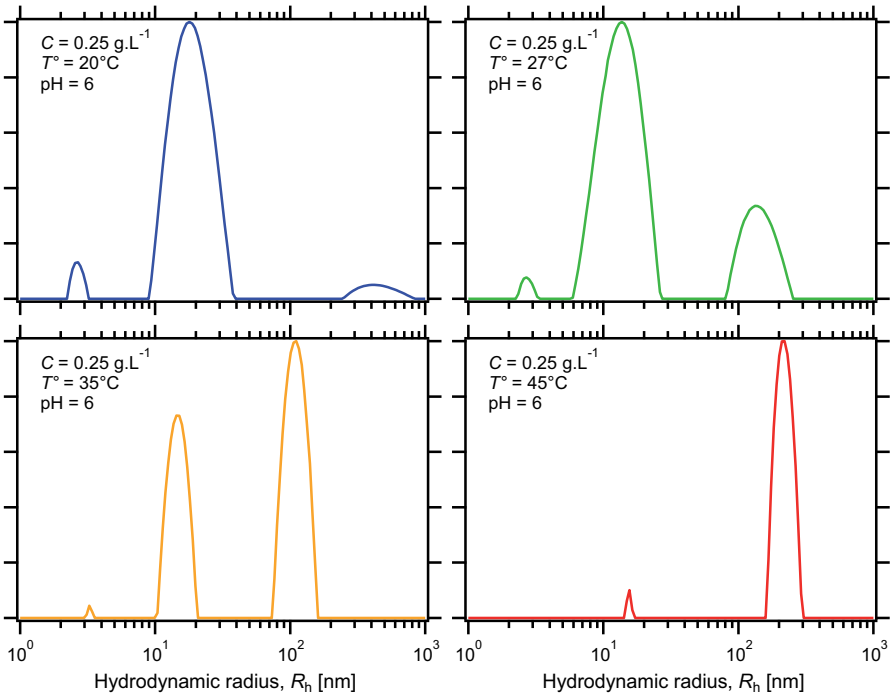

Figure 9.23 – Size distribution histograms of micelles prepared from PS_8-*b*-$PNIPAAm_{75}$-*b*-$PDMAEMA_{105}$-tpy copolymers, in aqueous solution at different temperatures.

9.4 Hierarchical assembly into gels

In this final section, combining the self-assembly behaviour of block copolymer in solution with metal–ligand coordination is used to engineer hierarchically organized materials (Figure 9.24). The first level of assembly, *i.e.*, the formation of micelles, is achieved upon direct dissolution of the block copolymers in ultra-pure water, and application of proper stimuli in case of induced micellization. All studied block copolymers are found to be easily dispersible in water at low to room temperature. At this point, free-flowing concentrated solutions are obtained and no gelation occurred, which can be explained by the lack of entanglement between coronal chains of neighbouring micelles.

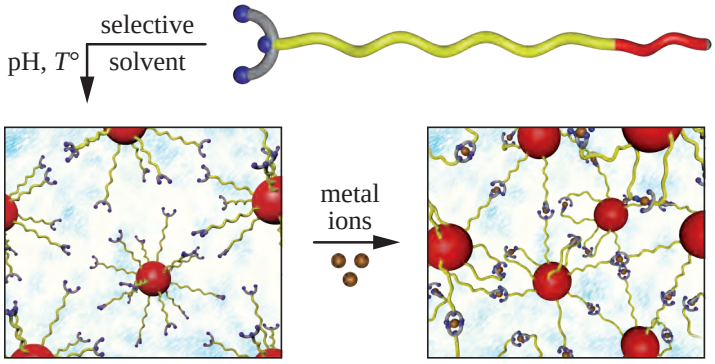

Figure 9.24 – Hierarchical assembly of ligand end-functionalized block copolymers into supramolecular gels.

As a second level of assembly, half an equivalent of selected transition metal ions, as their chloride salts, are added to the concentrated micellar solutions, with respect to the terpyridine content. In this regard, four cations are readily selected for their distinct affinity for terpyridine ligand (Table 9.1): nickel(II), iron(II), cobalt(II) and zinc(II).[12,13] In combination, they may form metal–ligand bis-complexes providing effective bridges between hydrophobic nodes, towards the formation of supramolecular polymer networks (Figure 9.24). To drive the formation of metallo-bridges at the expense of intra-micellar loops, concentration of copolymers in samples is kept in the semi-dilute regime, *i.e.*, between 3 to 20 %w/v.

9.4.1 Visual characterization

In practice, the formation of a percolated network structure, *i.e.*, a gel, can be evidenced by the inverted-tube test. As shown in Figure 9.25, the initially free-flowing concentrated solutions of PS-*b*-PNIPAAm-tpy copolymers indeed turn into free-standing supramolecular gels upon the addition of metal ions, which occur within seconds to minutes. Additionally, the hypothetical formation of metal–terpyridine bis-complexes between copolymer chains is strongly supported by the colour change arising from the addition of the metal ions, which gives characteristic purple colour, in case of iron(II), and yellow–orange colour, in case of cobalt(II).

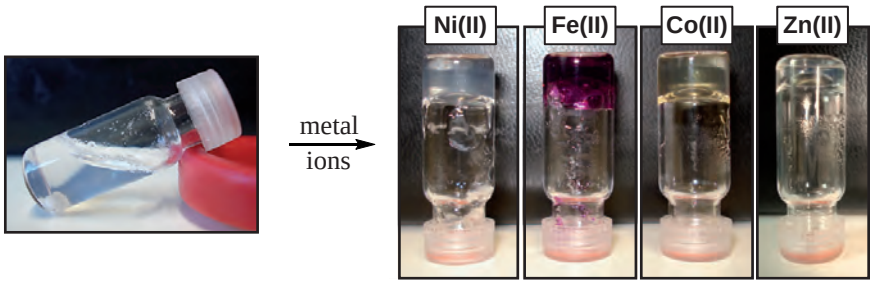

Figure 9.25 – Pictures of supramolecular hydrogels obtained from PS_{27}-*b*-$PNIPAAm_{300}$-tpy solutions upon the addition of different transition metal ions.

The thermo-responsiveness of PS-*b*-PNIPAAm-tpy hydrogels is visually evidenced by immersing samples in a heated water bath. Above a critical temperature around 32 °C, a mesoscopic phase separation is observed, the gel becoming cloudy as shown in Figure 9.26 (b), which is in agreement with DLS results obtained for those systems. Surprisingly, no macroscopic phase separation arising from the deswelling and subsequent shrinkage of the gel occurred, as compared to metal-free micellar solutions (Figure 9.26 (a)). Indeed, poly(*N*-isopropylacrylamide) hydrogels are commonly characterized by a sharp volume change upon heating,[47,48] unless stabilized by the presence of hydrophilic groups.[49] Hence, it is assumed that the positively charged metal–terpyridine junctions ensure here a certain hydration of the gel and further prevent its collapse, mainly because of the inherent electrostatic repulsions between charged complexes. Also, the possibility of having kinetically trapped

systems above the LSCT of PNIPAAm chains is not excluded to explain the absence of macroscopic phase separation, which may occur on long time scales.

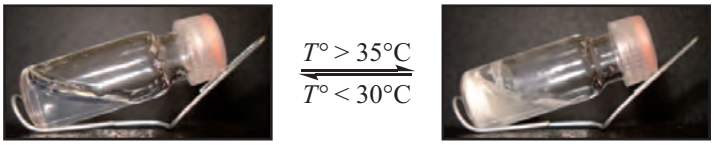

(a) Free-flowing micellar solution

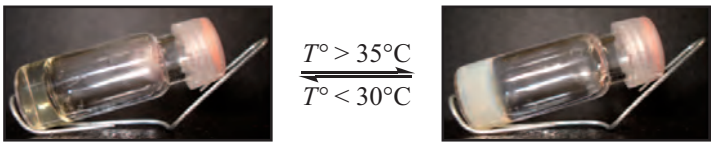

(b) Co(II)-based supramolecular hydrogel

Figure 9.26 – Pictures showing the responsiveness of a solution of PS_{27}-*b*-$PNIPAAm_{300}$-tpy copolymer and a hydrogel prepared from PS_{27}-*b*-$PNIPAAm_{300}$-tpy copolymer and Co(II) ions.

Having both constituting blocks soluble at room temperature, the behaviour of PNIPAAm-*b*-PDMAEMA-tpy double hydrophilic block copolymers is rather distinct from PS-*b*-PNIPAAm-tpy analogues. Indeed, solutions of the first diblock copolymers do not gel after addition of transition metal ions, at least when prepared under ambient temperature conditions. In agreement with the DLS study in the dilute regime, the formation of free-standing hydrogels is only achieved when heating the copolymer solutions above the solubility limit of PNIPAAm, leading to aggregation into network nodes (Figure 9.27 (a)).

Under neutral or acidic conditions, no phase separation can be observed within the solubility limit of PDMAEMA block, the hydrogels remaining transparent upon temperature rise (Figure 9.27 (b)), which is compatible with the formation of micelle-like nano-structures. Under basic conditions, however, a phase separation is observed when the PNIPAAm-*b*-PDMAEMA-tpy solutions are heated above a critical temperature of around 35 °C (Figure 9.28), which is in agreement with results obtained by DLS on dilute solutions. Furthermore, no gelation occurs during heating, meaning that the formation of a supramolecular network can be efficiently inhibited depending on pH of the media.

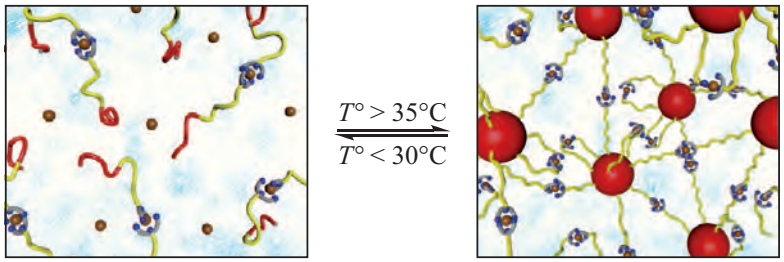

(a) Schematic showing the thermo-induced assembly

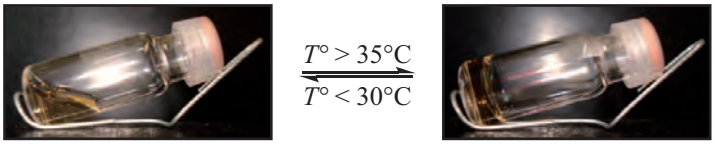

(b) Pictures showing the thermo-induced gelation

Figure 9.27 – Schematic and pictures showing the thermo-induced gelation of a solution of PNIPAAm$_{75}$-*b*-PDMAEMA$_{105}$-tpy copolymer in presence of Ni(II) ions, at pH 6.

The third and last system investigated here, *i.e.*, gels based on PS-*b*-PNIPAAm-*b*-PDMAEMA-tpy triblock copolymers, constitutes an intermediate category between the two afore-discussed diblock copolymers. On one hand, free-standing supramolecular hydrogels can be already obtained at room temperature thanks to the segregation of hydrophobic polystyrene segments. Their aggregation indeed provides branching points within the supramolecular network. But unlike PS-*b*-PNIPAAm-tpy systems, the PDMAEMA segment in the triblock architecture ensures swelling of the gel phase in a temperature range that may largely exceed the upper solubility limit of PNIPAAm block. Hence, no phase separation is visually observed when heating PS-*b*-PNIPAAm-*b*-PDMAEMA-tpy based hydrogels above 35 °C, at least under acidic and

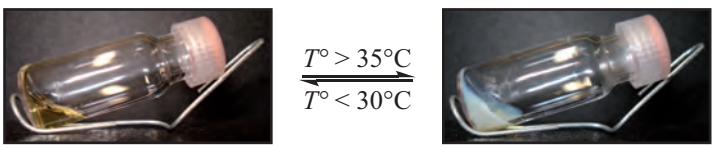

Figure 9.28 – Pictures showing the thermo-induced phase separation of a solution of PNIPAAm$_{45}$-*b*-PDMAEMA$_{105}$-tpy copolymer in presence of Ni(II) ions, at pH 9.

neutral pH conditions.

9.4.2 Thermal analysis

To further provide insight into the temperature triggered transitions in supramolecular hydrogels, differential scanning calorimetry (DSC) is used as thermo-analytic method, with the grateful help of Jean-Pierre Bourgeois. This technique measures the difference in heat flow required to increase the temperature of a sample and a reference as a function of temperature.[50] When the sample undergoes a physical or chemical transformation, more or less heat is needed for the latter in regard to the reference so that both are maintained at the same temperature throughout the experiment. Whether less or more heat must flow to the sample depends on whether the process is exothermic or endothermic.

In this point of view, the phase separation considered here is effectively a controlled event driven by the breaking of H-bonds between water molecules and, *e.g.*, PNIPAAm amide groups.[51] An endothermic peak can be thus monitored when metallo-supramolecular gels or solutions undergo a phase transition phenomenon because more heat is required to the sample to increase its temperature relative to the reference. On the opposite, less heat is required to increase the sample temperature when the latter undergoes the reverse exothermic processes.[52] The result of DSC measurements is therefore a thermogram showing the evolution of heat flow versus temperature or time.[50]

9.4.2.1 Thermal analysis of PS-*b*-PNIPAAm-tpy gels

At first, DSC measurements are carried out on self-assembled hydrogels prepared from PS-*b*-PNIPAAm-tpy copolymers exhibiting different block lengths, in combination with various transition metal ions. In agreement with the turbidity observations (Figure 9.26 (b)), DSC measurements performed between 20 and 45 °C indicate that all samples undergo a phase transition upon temperature rises (Figure 9.29).

This phenomenon is rationally attributed to the coil-to-globule transition of PNIPAAm chains from a swollen hydrated state to a shrunken dehydrated state.[53,54] Below the critical solubility temperature, hydrogen bonds between water molecules and hydrophilic groups ensure

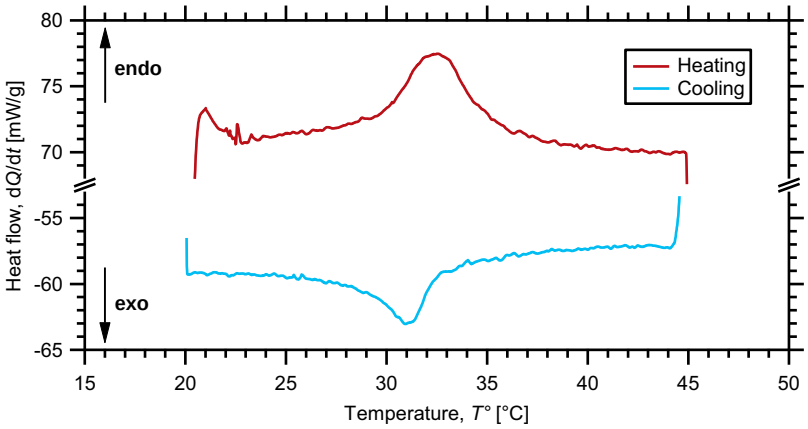

Figure 9.29 – DSC thermogram of a 5 %w/v hydrogel prepared from PS_{27}-*b*-$PNIPAAm_{300}$-tpy copolymer and Co(II) ions.

a good solubility of the hydrogel. When the temperature is increased above the critical solubility temperature, the PNIPAAm chains change from hydrophilic to hydrophobic, causing a phase separation of the gel matrix.

Practically, the heat-induced phase transitions of the investigated hydrogels are identified as endotherms in thermograms, while the reversibility of the processes has been checked upon cooling (Figure 9.29). The onsets of thermal transitions, T°_{onset}, are determined from the intersection of the baseline and the leading edge of endotherms. On the other hand, the phase separation temperatures are taken from measurements as that centred at the transition, T°_{peak}, *i.e.*, as the maximum of the endotherms.

As listed in Table 9.2, all phase transitions are observed in a temperature range between 31.5 and 32.5 °C, which is consistent with the reported value for the critical solution temperature of PNIPAAm.[55] Hence, varying the composition of the diblock copolymers, or the nature of added metal ions, only weakly affect the collapse of PNIPAAm chains. The transition temperature upon cooling was however 1.5 to 2 °C lower that in the heating process, clearly indicating a hysteresis. This particular phenomenon is usually attributed to intra-molecular hydrogen bondings between poly(*N*-isopropylacrylamide) chains in the collapsed state.[56–58]

In addition, DSC measurements permit the determination of the

Table 9.2 – Phase transition temperatures and enthalpies for 5 %w/v hydrogels prepared from different PS-*b*-PNIPAAm-tpy copolymers in combination with various transition metal ions.

Sample composition		Heating			Cooling	
Copolymer	Ion	T°_{onset} [°C]	T°_{peak} [°C]	ΔH^{a} [kJ/ mol]	T°_{onset} [°C]	T°_{peak} [°C]
PS_{15}-*b*-$PNIPAAm_{235}$-tpy	Ni^{II}	30.2	32.1	4.8	31.8	31.1
PS_{22}-*b*-$PNIPAAm_{235}$-tpy	Ni^{II}	28.9	31.7	5.3	31.4	30.5
PS_{27}-*b*-$PNIPAAm_{235}$-tpy	Ni^{II}	30.2	32.4	5.3	32.2	31.2
PS_{35}-*b*-$PNIPAAm_{235}$-tpy	Ni^{II}	29.9	32.6	5.6	32.5	31.1
PS_{27}-*b*-$PNIPAAm_{300}$-tpy	Ni^{II}	29.9	32.4	4.7	32.0	30.6
PS_{27}-*b*-$PNIPAAm_{300}$-tpy	Fe^{II}	30.6	31.9	4.6	31.9	30.2
PS_{27}-*b*-$PNIPAAm_{300}$-tpy	Co^{II}	29.5	32.6	4.7	32.6	30.9
PS_{27}-*b*-$PNIPAAm_{300}$-tpy	Zn^{II}	29.3	32.2	5.1	31.5	30.0

[a] Value of enthalpy change of per mole of PNIPAAm repeating units.

thermodynamic data of the thermal processes. Precisely, the enthalpy changes associated to phase transition, ΔH, are evaluated for each sample from the peak area of the endotherms. For comparison between samples, results are normalized per mole of PNIPAAm repeating units in the associating copolymer chains. As summarized in Table 9.2, all enthalpy changes are found around 5 kJ/mol, which is close but slightly lower than the values of 5.8 to 6.3 kJ/mol reported in the literature for PNIPAAm homopolymers.[57,59,60] This slight deviation suggests that the PNIPAAm chains, and thus the gel scaffold, remain at least partially hydrated, which is in agreement with visual observations showing mesoscopic but not macroscopic phase separation upon heating.

9.4.2.2 Thermal analysis of PNIPAAm-*b*-PDMAEMA-tpy solutions

Differential scanning calorimetry is further conducted on concentrated solutions of PNIPAAm-*b*-PDMAEMA-tpy diblock copolymers with different block lengths, in presence of half an equivalent of transition metal ions. In practice, measurements are performed in presence of half an equivalent of transition metal ions, in a temperature range that

covers the thermal transitions of both blocks. However, only a unique endotherm can be detected upon heating in the range of 30, − 35 °C. Depending on pH conditions, this endotherm can be attributed to the phase transition of the PNIPAAm blocks, resulting in gelation (Figure 9.27 (b)), or the simultaneous collapse of both blocks, resulting in phase separation (Figure 9.28). In addition to pH, the concentration in associating copolymers and the nature of metal ions are varied between samples.

From the main results summarized in Table 9.3, transition metal ions are found to only have insignificant effects on the gelation temperature of PNIPAAm-*b*-PDMAEMA-tpy solutions. In reality, their thermal signature is more significantly affected by the length of the PNIPAAm segment in the copolymer architecture. By increasing the fraction of PNIPAAm, a slight shift in the endotherm peak to lower temperature is indeed observed at a pH of 6, which is compatible with the lowered influence of the partially quaternized PDMAEMA block.[61,62]

Table 9.3 – Phase transition temperatures and enthalpies for hydrogels prepared from different PNIPAAm-*b*-PDMAEMA-tpy copolymers in combination with various transition metal ions, at different pH and concentrations.

Copolymer	Ion	pH	C [%]	T°_{peak} [°C]	ΔH^a [kJ/ mol]
$PNIPAAm_{45}$-*b*-$PDMAEMA_{105}$-tpy	Ni^{II}	3	20	29.3	2.9
$PNIPAAm_{45}$-*b*-$PDMAEMA_{105}$-tpy	Ni^{II}	9	20	34.2	5.2
$PNIPAAm_{45}$-*b*-$PDMAEMA_{105}$-tpy	Ni^{II}	6	20	34.4	3.4
$PNIPAAm_{75}$-*b*-$PDMAEMA_{105}$-tpy	Ni^{II}	6	20	32.3	3.6
$PNIPAAm_{75}$-*b*-$PDMAEMA_{105}$-tpy	Co^{II}	6	20	32.1	3.4
$PNIPAAm_{75}$-*b*-$PDMAEMA_{105}$-tpy	Zn^{II}	6	20	32.4	3.4
$PNIPAAm_{45}$-*b*-$PDMAEMA_{105}$-tpy	Ni^{II}	6	5	40.2	3.4
$PNIPAAm_{75}$-*b*-$PDMAEMA_{105}$-tpy	Ni^{II}	6	5	39.7	3.4

[a] Value of enthalpy change of per mole of PNIPAAm repeating units.

The most pronounced variations in thermal properties are however induced by concentration changes in associating copolymer solutions. At low concentrations and close to neutral pH, the endotherms in DSC are

centred around 40 °C, which closely correlates to the dilute solution behaviour of PNIPAAm-*b*-PDMAEMA-tpy chains captured by DLS (Figure 9.21). On the other hand, the entire thermogram is shifted by more than 15 °C to lower temperatures when the concentration in copolymers is increased to 20 %w/v. This observation can be explained by the polymer chain association in concentrated aqueous solutions which is easier than that in diluted one. Hence, the strong confinement and difference in polarity between the two blocks may force the latter to adopt a pre-organized configuration in solution, thus promoting the phase separation.

As reported in Table 9.3, the enthalpy changes associated to the phase transition are much lower than expected from the theoretical value of around 6 kJ/mol relative to the number of PNIPAAm units.[57,59,60] As suggested by other studies,[62] this observation can be mainly attributed to the influence of the hydrophilic PDMAEMA block in the molecular architecture of the chains. Interestingly, this hypothesis further explains the effect of pH on the ΔH associated with the collapse of the PNIPAAm segment. In this respect, lowering the pH leads to the protonation and thus an increased hydrophilicity of the PDMAEMA block, which results in a loss of transition enthalpy. On the other hand, the switch in behaviour of the PDMAEMA block under basic conditions results in a more complete dehydration of the PNIPAAm block upon temperature rise.

Last but not least, DSC measurements show that the solution behaviour of PNIPAAm-*b*-PDMAEMA-tpy chains is also subjected to pH changes (Figure 9.30). As discussed above, lowering the pH of the medium protonates the amine function of PDMAEMA, rendering this thermo-sensitive block more hydrophilic (Figure 9.14). Hence, an increase in the critical micellization temperature is expected under acidic condition, which is not verified at high concentration (Table 9.3). Nevertheless, the opposite shift in transition temperature can be explained by the high degree of quaternization of the PDMAEMA block, which competes with PNIPAAm by strongly complexing water molecules in this concentration regime. In the literature, this situation is also encountered in presence of large amount of salt in solution, resulting in destabilizing salting effects on the solubility of PNIPAAm chain segments.[63–66] In more dilute solutions, the same competition is less pronounced and deviations from the solution behaviour revealed by DLS is consequently

reduced.

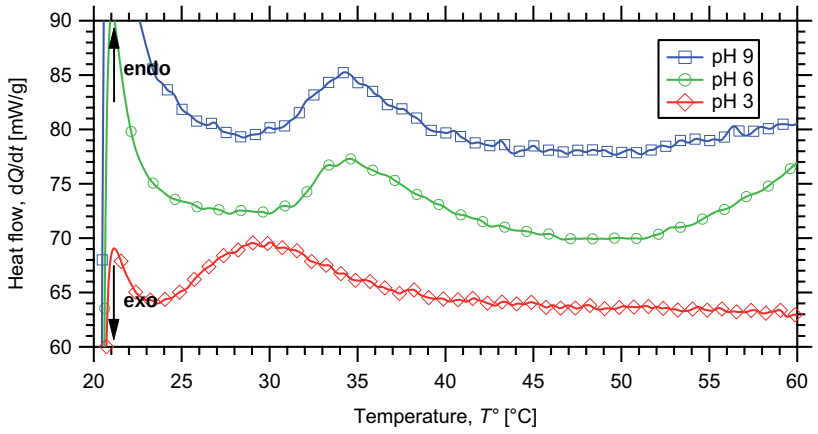

Figure 9.30 – DSC thermogram of 20 %w/v hydrogels prepared from PNIPAAm$_{45}$-*b*-PDMAEMA$_{105}$-tpy copolymer and Ni(II) ions, at different pH.

9.5 Summary

Through this chapter, the possibility to form metallo-supramolecular micellar networks with distinctive features was demonstrated. To this aim, the three synthesized block copolymers, *i.e.*, PS-*b*-PNIPAAm-tpy, PNIPAAm-*b*-PDMAEMA-tpy, and PS-*b*-PNIPAAm-*b*-PDMAEMA-tpy, were used as precursors of self-assembled hydrogels. Prior to the elaboration of the supramolecular materials, the self-assembly behaviour of each associating copolymers was separately investigated in dilute aqueous solution, via a combination of selected analytical techniques.

At first, the metal induced assembly of macro-ligand into metallo-supramolecular multi-segmented copolymers was explored by absorption spectroscopy and size exclusion chromatography. The first analytical method indicated quantitative binding of all terpyridine units when following the appearance of metal-to-ligand-charge-transfer band upon complexation with metal ions. In parallel, the formation of bis-complexes was accompanied by a two-times increase in size exclusion chromatography, which clearly demonstrated the potential of the ligand-

functionalized copolymers to act as building blocks for supramolecular chemistry.

The self-assembly of terpyridine end-capped block copolymers into micelles was then studied in dilute aqueous media. In this regard, a direct dissolution method was followed, leading to the formation of rather well-defined micelles from PS-*b*-PNIPAAm-tpy and PS-*b*-PNIPAAm-*b*-PDMAEMA-tpy copolymers. Through a combination of light scattering and transmission techniques, the thermo-induced collapse of PNIPAAm block in those architectures was monitored around the theoretical value of 32 °C.

In case of double hydrophilic PNIPAAm-*b*-PDMAEMA-tpy block copolymers, the micellization was triggered by heat and further controlled via pH changes. In this respect, protonation of the PDMAEMA block was found to delay the thermo-induced collapse transitions of both blocks. In addition, the presence of charged metal–ligand complexes in the micellar corona also lowered the tendency for thermo-responsive blocks to aggregate.

Finally, combining the self-assembly behaviour of block copolymer in solution with metal–ligand coordination successfully led to the formation of supramolecular gel-like materials. By means of differential scanning calorimetry, light was shed on the thermo-responsiveness of prepared hydrogels, which was further supported by visual observations. Interestingly, results obtained were in accordance with light scattering and transmission data, thereby enhancing the comprehension of phase transition phenomena occurring in the gel phase.

9.6 Experimental part

Materials

Terpyridine end-capped block copolymers are synthesized via sequential reversible addition–fragmentation chain transfer control radical copolymerization, as reported in the previous chapter. Nickel(II), iron(II), cobalt(II) and zinc(II) chlorides salts are dried, kept in a glove box, and weighted under argon atmosphere.

Instrumentation

Dynamic light scattering experiments are performed on a Malvern CGS-3 apparatus equipped with a He–Ne laser with a wavelength of 632.8 nm and a thermostat. The size distribution histograms of the self-assembled nano-structures are obtained by the CONTIN method. Size exclusion chromatography is performed in *N,N*-dimethylformamide containing 2.5 mM NH_4PF_6 to determine molar mass distributions with respect to polystyrene standards. The measurements are carried out on a system composed of two PSS Gram columns (100 Å and 1000 Å) connected to a Waters 410 differential refractive index (DRI) detector operating at 0.5 mL/min flow rate and a temperature of 35 °C. UV-visible spectra are recorded on a Varian Cary 50 Conc spectrophotometer equipped with a Varian Cary thermostat. The measurements are performed in a 1 cm quartz cell. Differential scanning calorimetry measurements are performed on a Mettler Toledo 821 calorimeter. Samples are placed in a sealed aluminium capsule (40 μL) in order to avoid water evaporation. The DSC instrument is calibrated using an indium standard. Sample are initially heated at 1 °C/min under static air atmosphere, followed by cooling at the same rate immediately after heating. Atomic force microscopy measurements are performed on a Digital Instruments Nanoscope V scanning force microscope in tapping mode using NCL cantilevers (Si, 48 N/m, 300 kHz, Nanosensors). The silicon wafers are cleaned by sonication in acetone followed by immersion in a piranha solution (H_2SO_4 98 % (70 %v/v) and H_2SO_4 35 % (30 %v/v) for 90 minutes and thoroughly rinsed with ultrapure water. Volumes of 75 μL of preheated block copolymer solutions are spin-coated on dried silicon wafers at 2000 rpm for 40 s. Samples are further dried in vacuum at 35 °C overnight, prior to any measurement.

Preparation of supramolecular gels

Hydrogels are prepared by dissolving mixing given amounts of block copolymer with Milli-Q water. The sealed reaction vessels are placed in a fridge and shaken periodically to form homogeneous concentrated solutions after a few days. When necessary, the pH of the media is adjusted by addition of hydrochloric acid aqueous solution of a given molarity. The gels are then readily obtained by adding the stoichiometric amount of half an equivalent of transition metal ions (with respect to the ter-

pyridine content) dissolved in a defined amount of Milli-Q water to each concentrated solutions. Lastly, the reaction vessels are placed again in the fridge over three days to ensure homogeneous gelation and stabilization of the gels. The final concentration of copolymers in samples varied in the semi-diluted regime, from 3 to 20 %w/v.

UV-Vis titration of terpyridine end-groups

Terpyridine-functionalized polymers are dissolved in 1 mL of degassed ultra-pure water, at a given concentration around 0.25 mmol/L. This solution is then titrated by stepwise addition of a 0.125 mmol/L aqueous solution of iron(II) chloride stabilized against oxidation by the presence of 0.5 mmol/L ascorbic acid.

Bibliography

[1] Ikkala, O.; ten Brinke, G. *Chem. Commun.* **2004**, *40*, 2131–2137.
[2] Ikkala, O.; ten Brinke, G. *Science* **2002**, *295*, 2407–2409.
[3] Liu, Y.; Wang, Z.; Zhang, X. *Chem. Soc. Rev.* **2012**, *41*, 5922–5932.
[4] Piepenbrock, M. O. M.; Lloyd, G. O.; Clarke, N.; Steed, J. W. *Chem. Rev.* **2010**, *110*, 1960–2004.
[5] Patterson, J. P.; Robin, M. P.; Chassenieux, C.; Colombani, O.; O'Reilly, R. K. *Chem. Soc. Rev.* **2014**, *43*, 2412–2425.
[6] Schubert, U.; Hofmeier, H.; Newkome, G. R. *Modern terpyridine chemistry*; Wiley-VCH: Weinheim, 2006; pp viii, 229.
[7] Schubert, U.; Winter, A.; Newkome, G. R. *Terpyridine-based materials: For catalytic, optoelectronic and life science applications*; Wiley-VCH: Weinheim, 2011; pp xix, 522.
[8] Schubert, U. S.; Eschbaumer, C.; An, Q. R.; Salditt, T. *J. Inclusion Phenom. Macrocyclic Chem.* **1999**, *35*, 35–43.
[9] Kim, K.-Y.; Nancollas, G. H. *J. Phys. Chem.* **1977**, *81*, 948–952.
[10] Meier, M. A. R.; Lohmeijer, B. G. G.; Schubert, U. S. *J. Mass Spectrom.* **2003**, *38*, 510–516.
[11] Harzmann, G. D.; Neuburger, M.; Mayor, M. *Eur. J. Inorg. Chem.* **2013**, *2013*, 3334–3347.
[12] Hogg, R.; Wilkins, R. *J. Chem. Soc.* **1962**, 341–350.
[13] Holyer, R. H.; Hubbard, C. D.; Kettle, S. F. A.; Wilkins, R. G. *Inorg. Chem.* **1966**, *5*, 622–625.
[14] Chiper, M.; Meier, M. A. R.; Kranenburg, J. M.; Schubert, U. S. *Macromol. Chem. Phys.* **2007**, *208*, 679–689.

[15] Chiper, M.; Hoogenboom, R.; Schubert, U. S. *Eur. Polym. J.* **2010**, *46*, 260–269.
[16] Meier, M. A. R.; Lohmeijer, B. G. G.; Schubert, U. S. *Macromol. Rapid Commun.* **2003**, *24*, 852–857.
[17] Henderson, I. M.; Hayward, R. C. *Polym. Chem.* **2012**, *3*, 1221–1230.
[18] Ellis, P.; Hogg, R.; Wilkins, R. G. *J. Chem. Soc.* **1959**, 3308–3313.
[19] Lazzari, M.; Liu, G.; Lecommandoux, S. *Block copolymers in nanoscience*; Wiley-VCH: Weinheim, 2006; pp xix, 428.
[20] Abetz, V. *Block copolymers. Vol. 1*; Springer: Berlin ; London, 2005; pp x, 238.
[21] Abetz, V. *Block copolymers. Vol. 2*; Springer: Berlin ; London, 2005; pp x, 249.
[22] Hamley, I. W. *Developments in block copolymer science and technology*; Wiley: Chichester, 2004; pp ix, 367.
[23] Forster, S.; Plantenberg, T. *Angew. Chem. Int. Ed.* **2002**, *41*, 689–714.
[24] Rodriguez-Hernandez, J.; Checot, F.; Gnanou, Y.; Lecommandoux, S. *Prog. Polym. Sci.* **2005**, *30*, 691–724.
[25] Mai, Y.; Eisenberg, A. *Chem. Soc. Rev.* **2012**, *41*, 5969–5985.
[26] Riess, G. *Prog. Polym. Sci.* **2003**, *28*, 1107–1170.
[27] Lee, Y. S. *Self-assembly and nanotechnology: A force balance approach*; Wiley-Blackwell: Oxford, 2008; pp xvi, 344.
[28] Goldburg, W. *American Journal of Physics* **1999**, *67*, 1152–1160.
[29] Schärtl, W. *Light scattering from polymer solutions and nanoparticle dispersions*; Springer Laboratory Manuals in Polymer Science; Springer: Berlin ; New York, 2007; pp xiv, 191.
[30] Cebe, P.; Hsiao, B. S.; Lohse, D. J. *Scattering from polymers: Characterization by X-rays, neutrons, and light*; ACS Symp. Ser.; American Chemical Society: Washington, 1999; pp xii, 558.
[31] Teraoka, I. *Polymer solutions: An introduction to physical properties*; Wiley: New York, 2002; pp xv, 338.
[32] Bowen, W. R.; Hilal, N. *Atomic force microscopy in process engineering: Introduction to AFM for improved processes and products*; Butterworth-Heinemann: Amsterdam ; London, 2009; pp xvi, 283.
[33] Bhushan, B. *Scanning probe microscopy in nanoscience and nanotechnology*; Springer: Berlin ; London, 2010; pp xxx, 956.
[34] Giessibl, F. J. *Rev. Mod. Phys.* **2003**, *75*, 949–983.
[35] Daoud, M.; Cotton, J. *J. Phys.* **1982**, *43*, 531–538.
[36] Halperin, A. *Macromolecules* **1987**, *20*, 2943–2946.
[37] Cogan, K. A.; Capel, M.; Gast, A. P. *Macromolecules* **1991**, *24*, 6512–6520.
[38] Piogé, S.; Fustin, C.-A.; Gohy, J.-F. *Macromol. Rapid Commun.* **2012**, *33*, 534–539.
[39] Guillet, P.; Fustin, C.-A.; Mugemana, C.; Ott, C.; Schubert, U. S.; Gohy, J.-F. *Soft Matter* **2008**, *4*, 2278–2282.

[40] Chiper, M.; Hoeppener, S.; Schubert, U. S.; Fustin, C.-A.; Gohy, J.-F. *Macromol. Chem. Phys.* **2010**, *211*, 2323–2330.
[41] Jochum, F. D.; Brassinne, J.; Fustin, C.-A.; Gohy, J.-F. *Soft Matter* **2013**, *9*, 2314–2320.
[42] Chiper, M.; Fournier, D.; Hoogenboom, R.; Schubert, U. S. *Macromol. Rapid Commun.* **2008**, *29*, 1640–1647.
[43] Plamper, F. A.; Ruppel, M.; Schmalz, A.; Borisov, O.; Ballauff, M.; Muller, A. H. E. *Macromolecules* **2007**, *40*, 8361–8366.
[44] Chung, J.; Yokoyama, M.; Aoyagi, T.; Sakurai, Y.; Okano, T. *J. Controlled Release* **1998**, *53*, 119–130.
[45] Fournier, D.; Hoogenboom, R.; Thijs, H. M.; Paulus, R. M.; Schubert, U. S. *Macromolecules* **2007**, *40*, 915–920.
[46] Nicolai, T.; Colombani, O.; Chassenieux, C. *Soft Matter* **2010**, *6*, 3111–3118.
[47] Park, T. G.; Hoffman, A. S. *J. Appl. Polym. Sci.* **1994**, *52*, 85–89.
[48] Suzuki, A.; Yoshikawa, S.; Bai, G. *J. Chem. Phys.* **1999**, *111*, 360–367.
[49] Chen, H.; Li, W.; Zhao, H.; Gao, J.; Zhang, Q. *J. Colloid Interface Sci.* **2006**, *298*, 991–995.
[50] Menczel, J. D.; Judovits, L.; Prime, R. B.; Bair, H. E.; Reading, M.; Swier, S. *Thermal Analysis of Polymers*; Wiley: Hoboken, 2008; pp 7–239.
[51] Ahmed, Z.; Gooding, E. A.; Pimenov, K. V.; Wang, L.; Asher, S. A. *J. Phys. Chem. B* **2009**, *113*, 4248–4256.
[52] Yu, G.; Yan, X.; Han, C.; Huang, F. *Chem. Soc. Rev.* **2013**, *42*, 6697–6722.
[53] Hirokawa, Y.; Tanaka, T. *J. Chem. Phys.* **1984**, *81*, 6379–6380.
[54] Otake, K.; Inomata, H.; Konno, M.; Saito, S. *Macromolecules* **1990**, *23*, 283–289.
[55] Heskins, M.; Guillet, J. *J. Macromol. Sci., Chem.* **1968**, *2*, 1441–1455.
[56] Wu, C.; Wang, X. *Phys. Rev. Lett.* **1998**, *80*, 4092–4094.
[57] Ding, Y.; Ye, X.; Zhang, G. *Macromolecules* **2005**, *38*, 904–908.
[58] Cheng, H.; Shen, L.; Wu, C. *Macromolecules* **2006**, *39*, 2325–2329.
[59] Schild, H. G.; Tirrell, D. A. *J. Phys. Chem.* **1990**, *94*, 4352–4356.
[60] Schild, H. *Prog. Polym. Sci.* **1992**, *17*, 163–249.
[61] Lee, K. K.; Jung, J. C.; Jhon, M. S. *Polym. Bull.* **1998**, *40*, 455–460.
[62] Tang, X.; Liang, X.; Yang, Q.; Fan, X.; Shen, Z.; Zhou, Q. *J. Polym. Sci., Part A: Polym. Chem.* **2009**, *47*, 4420–4427.
[63] Cacace, M.; Landau, E.; Ramsden, J. *Q. Rev. Biophys.* **1997**, *30*, 241–277.
[64] Lopez-Leon, T.; Fernandez-Nieves, A. *Phys. Rev. E: Stat., Nonlinear, Soft Matter Phys.* **2007**, *75*, 011801.
[65] Zhang, Y.; Cremer, P. S. *Curr. Opin. Chem. Biol.* **2006**, *10*, 658–663.
[66] Zhang, Y.; Furyk, S.; Bergbreiter, D. E.; Cremer, P. S. *J. Am. Chem. Soc.* **2005**, *127*, 14505–14510.

CHAPTER 10

ON THE DYNAMICS OF METALLO-SUPRAMOLECULAR MICELLAR GELS

Abstract

One of the most important aspect of supramolecular gels lies in the control over their dynamic mechanical properties. Indeed, the transient nature of the self-assembled network allows its relaxation on time scales that exceed the lifetime of the non-covalent associations. Control over dynamics is herein achieved by varying the length of segments that aggregate to form hydrophobic nodes, as well as the nature of bridging metal complexes.

10.1 Overview

In the fascinating field of supramolecular polymer networks and gels, rheology is perhaps the most critical defining feature.[1–4] Unlike permanent analogues, supramolecular networks consist in macromolecules connected together by transient interactions. As a result, they exhibit properties that are not encountered in classical, covalently jointed networks, such as stimuli-responsiveness, self-healing, and shape-memory.[5–7]

To promote their use as high-performance materials, a fundamental physico-chemical characterization is a key step. However, even if notable efforts have been placed on the derivation of such knowledge, a comprehensive picture of the structure, self-organization and dynamics associated to transient polymer networks is still far from complete. In this field of research, a particular emphasis is put on the manifestation of the cross-link dissociation dynamics in the macroscopic relaxation of supramolecular networks.[3,4,8–11]

Due to the interplay of supramolecular chemistry and polymer physics, the viscoelastic behaviour of supramolecular polymer networks is extremely rich and complex. However, carrying out tensile measurements on supramolecular gels can be difficult because they tend to have little stiffness or toughness and they may not maintain their shape for a long time. To quantitatively assess useful information about the structure and dynamics of these astonishing materials, rotational rheometry is the obvious choice, as it studies the deformation and flow of matter under the influence of an applied shear stress.

10.2 Rotational rheometry

Practically, samples are loaded into a gap between two specifically designed flat plates and a shear stress, σ, is applied by a low inertia motor moving one plate relative to the other. In turn, the resulting shear strain, γ, is measured using a high precision position encoder under controlled atmosphere and temperature (Figure 10.1). If the material resists to the deformation induced by a weak stress, then it is a solid. If the material eventually flows, then it behaves as a liquid.

Supramolecular gels belong to intermediate classes of behaviour that

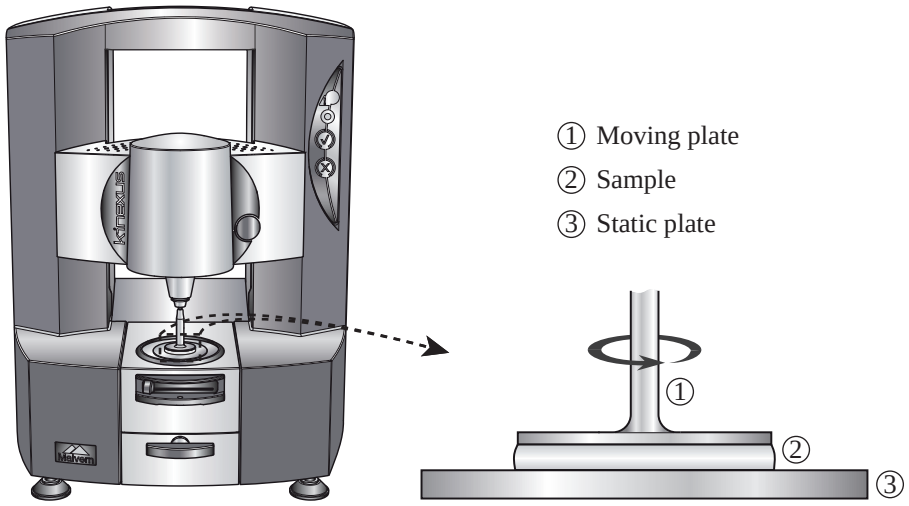

Figure 10.1 – Schematic view of a Malvern Kinexus rotational shear rheometer and a plate–plate geometry.

fall between the limits of solid and liquid. Due to diffusion of molecules in the amorphous gel phase, they indeed exhibit some of both characteristics, which further depends on the time scale and amplitude of strain. As long as the amount of deformation is proportional to applied force, the material is said to be elastic. However, when the deformation rate is proportional to the stress, the material is said to be viscous. [2,12]

In a rheometry experiment, the two plates are moved back and forth relative to one another, shearing the gel sample. The induced oscillating movement is decomposed into an in- and out-of-phase component, which gives the elastic and viscous contributions of the response. Those contributions are respectively measured by the elastic storage modulus, G', and the viscous loss modulus, G'', both having units of Pascals. For purely elastic materials, the stress and strain are in phase, in contrast with purely viscous materials for which the strain follows stress by a 90° phase lag. For viscoelastic materials, the behaviour is somewhere in between and the strain lag, δ, is not zero but is less than 90°. [2,12]

Typically, two common rheological experiments are used by chemists to probe supramolecular gel behaviours. The linear viscoelastic response (LVR) is determined at a fixed small stress or strain amplitude, where elastic and viscous behaviours are recognizable. When increasing shear forces on sample, non-linear behaviour (NLVR) of gels is probed. In-

deed, they are plastic and have an associated plasticity threshold beyond which the material flows (Figure 10.2 (a)). Below critical values of shear amplitude, defined by yield stress, σ^c, and yield strain, γ^c, the storage modulus remains constant. Above, it decreases rapidly, suggesting that the network collapses as a consequence of the application of force.[2,12]

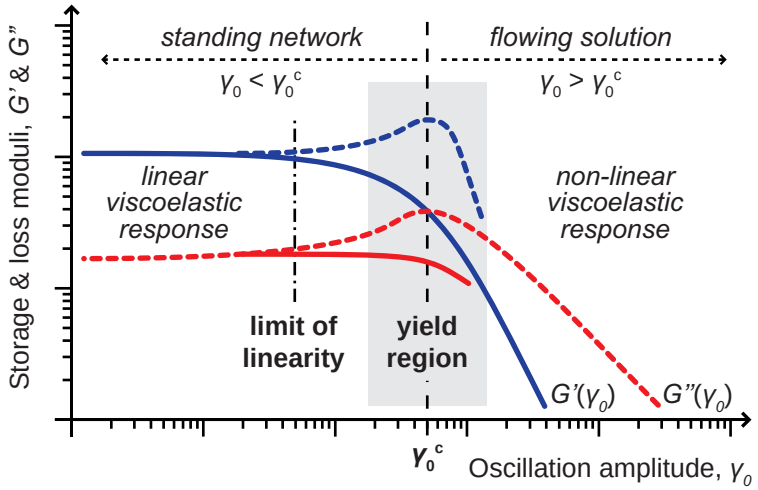

(a) Amplitude strain sweep showing different possible non-linear responses.

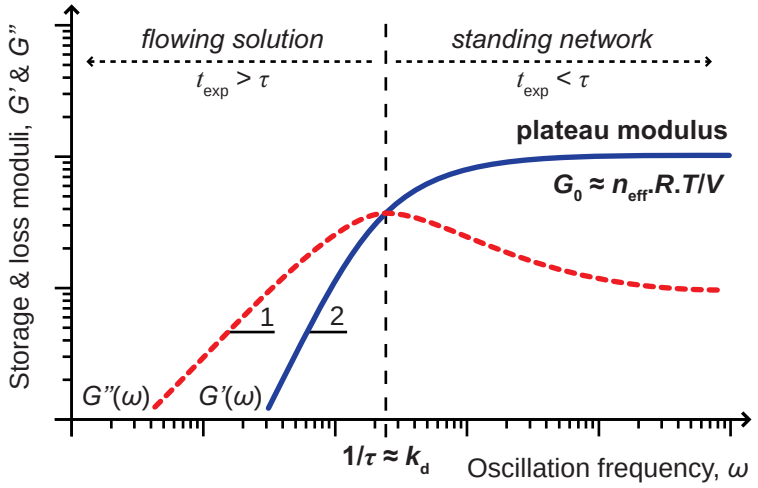

(b) Oscillation frequency sweep showing terminal Maxwell mode.

Figure 10.2 – Theoretical behaviour of supramolecular polymer gels under dynamic rheological measurements.

In parallel, varying the frequency of the oscillatory shear allows capturing the time scale of stress relaxation in supramolecular networks, τ. On short experimental time scale ($t_{exp} < \tau$), motions of the supramolecular network are restricted around the non-covalent associations acting as sticky points between chains.[13–16] Stress on sample is thus mainly stored in elastic distortion and entropic stretching of polymer chains. When increasing the oscillation time scale ($t_{exp} > \tau$), inter-chain cross-links dissociate, thereby allowing chain segments to diffuse through the solvating media. An onset of material flow is thus observed when lowering oscillation frequency, as evidenced by a characteristic decrease in storage and loss moduli (Figure 10.2 (b)). In turn, the time scale of network relaxation evidenced by the modulus cross-over can be related to the dissociation rate of physical cross-links.[1]

10.3 Prior consideration

Above the percolation threshold, the characteristic features, *i.e.*, lability and strength, of the reversible associations largely dictate the viscoelastic response of associating polymer networks. In line, Tenhu *et al.* pointed out the effect of hydrophobic sticker length on the rheological properties of aqueous solutions of telechelic star copolymers.[17] Increasing the length of the non-soluble segments, *i.e.*, the strength of hydrophobic interactions, leads to more elastic networks. On the other hand, more labile, shorter, hydrophobic segments provide "strong" gels with long linear responses. In parallel, Craig and coworkers demonstrated the importance of the lifetime of transient associations on the relaxation of supramolecular networks.[11,18,19] Indeed, they correlated macroscopic relaxation times of materials with molecular dissociation rates, *i.e.*, exchange kinetics, of metallo-pincers responsible for cross-linking.[8,9]

The first chapter devoted to the rheological characterization of the engineered materials mainly focuses on their viscoelastic response. The emphasis is logically put on the dynamics of the self-assembled material, which is associated to the transient associations structuring the supramolecular network (Figure 10.3). Unless kinetically frozen, those associations are indeed involved in an association–dissociation equilibrium responsible for strain release. Accordingly, the length of associating segments in the copolymer architecture and the nature of metal–ligand

bridges between hydrophobic domains is varied in order to shed light onto their influence on material rheology.

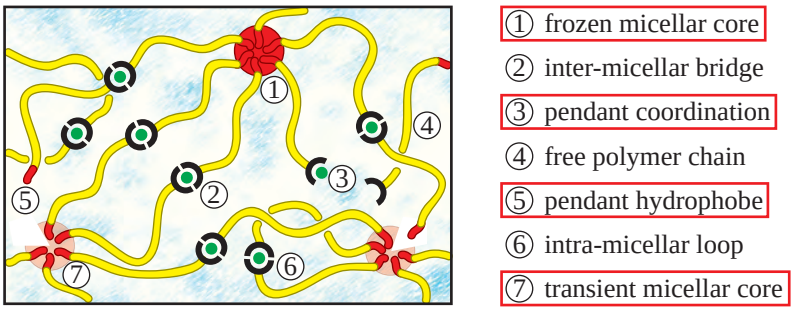

Figure 10.3 – Richness of network configurations in metallo-supramolecular micellar gels, with focus on the dynamics.

In this study, terpyridine end-capped polystyrene-*block*-poly(*N*-isopropylacrylamide) copolymers are used as simple building blocks to generate model networks. Regardless of structural imperfections such as loops, those hetero-telechelic copolymers, *i.e.*, they possess different associating groups at each end, indeed generate homogeneous polymer networks with close to regular monodisperse mesh sizes. In the following, the rheological characterization of supramolecular hydrogels prepared from PS-*b*-PNIPAAm-tpy copolymers is hence presented while varying the afore-mentioned parameters. Then, having a global view on the viscoelastic behaviour of those unique materials, a discussion is oriented toward the interpretation of rheological data.

In the following, many descriptions are derived from the analysis of the linear rheological data, *i.e.*, modulus amplitudes and the phases between stress and strain. However, these familiar material functions used to quantify the linear behaviour do not always result in a simple physical picture or rigorous interpretation of the non-linear experimental output. Indeed, many inhomogeneous flows in the measuring geometries like, *e.g.*, shear banding,[20,21] wall slip,[22] elastic instability,[23,24] and secondary flows,[25] are susceptible to occur especially under large amplitude of deformation. In addition to imperfect mechanical excitation, these non-linear phenomena can violate the mathematical assumptions describing the stress and strain inputs.[26] Being aware of these inherent limitations, direct interpretations of both linear and non-linear moduli are however proposed in the present and following chapters, but would

clearly require a deeper analysis of the raw stress–strain data.

10.4 Rheological characterization

10.4.1 Low strain mechanical response

The dynamic mechanical properties of associating polymer hydrogels combining hydrophobic and coordinative interactions are first investigated under low-strain conditions. In this respect, an oscillatory frequency sweep is carried out by recording the evolution of dynamic moduli for a self-assembled hydrogel prepared from PS_{27}-*b*-$PNIPAAm_{235}$-tpy diblock copolymer (numbers in subscript indicate the average degree of polymerization) and nickel(II) ions.

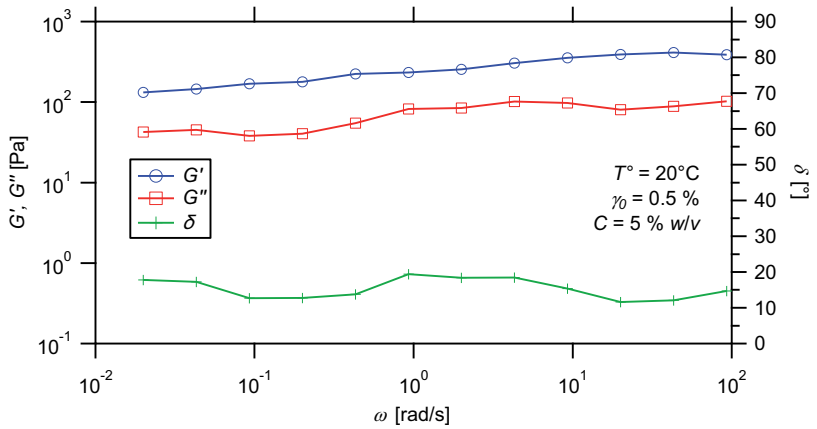

Figure 10.4 – Frequency sweep on hydrogel prepared from PS_{27}-*b*-$PNIPAAm_{235}$-tpy copolymer and Ni(II) ions under low-strain condition.

As illustrated in Figure 10.4, the low-strain, or linear, viscoelastic response of the investigated hydrogel is characterized by an equilibrium in both storage and loss moduli that extends over frequency decades. In addition, the elastic response is nearly one order of magnitude higher than the viscous counterpart, at least in the investigated frequency range. In a rheological point of view, these features are the trademark of “hard”, nearly-covalently cross-linked hydrogels. In this picture, the

metal–ligand complexes provide efficient bridges between strong micellar cores made of long polystyrene stickers.

10.4.2 Medium-to-high strain mechanical response

The dynamic mechanical properties of associating polymer hydrogels are then investigated under higher amplitude of deformation. At first, oscillatory frequency sweeps were carried out on the hydrogel prepared from the PS_{27}-*b*-$PNIPAAm_{235}$-tpy copolymer and Ni(II) ions, at different amplitudes of deformation. In addition, oscillatory strain sweeps are carried out on the same material by following the evolution of dynamic moduli under increasing and decreasing strain amplitude in order to provide further information about the viscoelastic response of the gel under high-strain conditions.

10.4.2.1 Oscillatory frequency sweep

The influence of shear amplitude on the rheological properties of supramolecular hydrogels is investigated by running frequency sweeps at various amplitudes of deformation (Figure 10.5). At low strain, nearly parallel moduli are achieved over the investigated frequency range, resulting in an almost frequency-independent phase angle. Notably, the storage modulus remains nearly constant and higher than the loss modulus, so that the material is exclusively characterized by a solid-like behaviour.

With increasing strain amplitude, both moduli progressively decrease at low frequency, forming a second plateau (Figure 10.5). At high frequency, the first plateau is still observed for both moduli, while G' remains nearly one order of magnitude higher than G''. For fast oscillations, the largest part of the deformation energy is thus still stored in entropic distortions of the supramolecular network. Below a certain frequency of oscillation, the elastic modulus starts to drop while the viscous modulus goes through a local maximum, so that both moduli cross each other at the crossover frequency.

In practice, this transition reveals a first stress relaxation time scale, τ_1, for the associating polymer gel that is a signature of a transient hydrophobic network.[27–30] Although the material is dominated by elastic-

ity before the modulus crossover, a liquid-like behaviour tends to govern the sample at low oscillation frequencies.

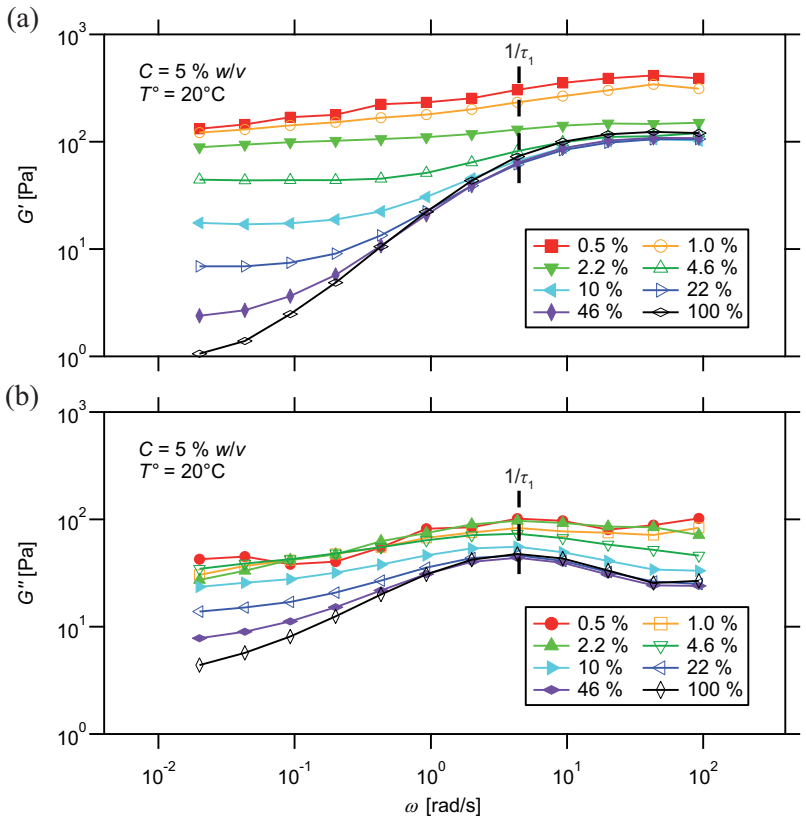

Figure 10.5 – Frequency dependence of (a) elastic and (b) viscous moduli for a hydrogel prepared from PS_{27}-*b*-$PNIPAAm_{235}$-tpy copolymer and Ni(II) ions, at different strain amplitudes.

However, a second plateau in modulus is achieved at low frequency, evidencing a slower relaxation process associated with a longer time scale, τ_2. Interestingly, the plateau values for moduli at low-frequency follow an exponential decrease with strain amplitude when the latter exceeds the first yield point (Figure 10.6). At 100 % strain, the low-frequency viscous and elastic moduli respectively suffer from a one and two orders of magnitude decrease, while values for high-frequency moduli are only slightly smaller than observed at low strain. In parallel, no significant strain-dependence is observed for the first stress relaxation

time (τ_1) of the supramolecular network under shear.

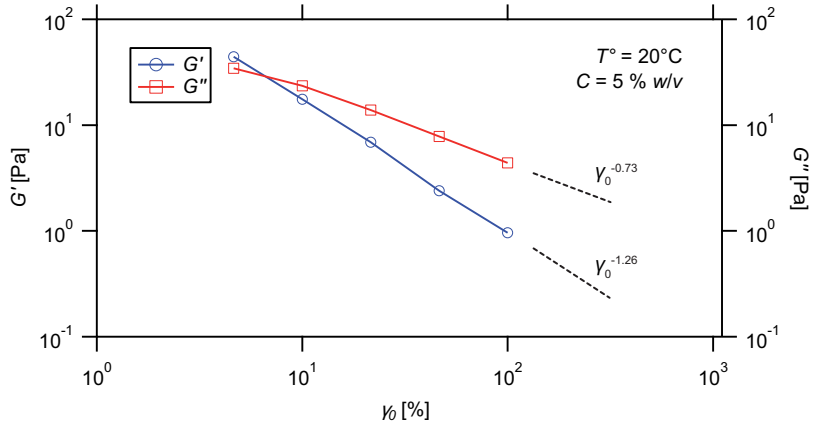

Figure 10.6 – Strain dependence of low-frequency plateau dynamic moduli for a hydrogel prepared from PS_{27}-*b*-$PNIPAAm_{235}$-tpy copolymer and Ni(II) ions, under increasing strain.

10.4.2.2 Oscillatory strain sweep

Under increasing strain amplitude, supramolecular hydrogels prepared from the PS_{27}-*b*-$PNIPAAm_{235}$-tpy copolymer are characterized by an outstanding "two-step" gel-to-sol transition. In contrast to other supramolecular gels, which only display a single gel–sol transition, they indeed transit through distinct viscoelastic regimes, as shown in Figure 10.7.

In the literature, multiple yielding has been widely reported for colloidal glasses [31,32] or congested micellar phases. [33,34] However, to the best of our knowledge, such behaviour has been only observed once for semi-diluted solutions of associating polymers, without further investigation. Precisely, observations were made by Tsitsilianis *et al.* when studying the influence of addition of plasticizer on the rheological properties of a reversible hydrogel composed of triblock copolymers of ionized poly(acrylic acid) end-capped with short PS blocks. [35]

At low strain amplitudes, the rheological behaviour of the experienced hydrogels is expressed by a first plateau in loss and storage moduli (Figure 10.7), which corresponds to the first linear viscoelastic regime (1st

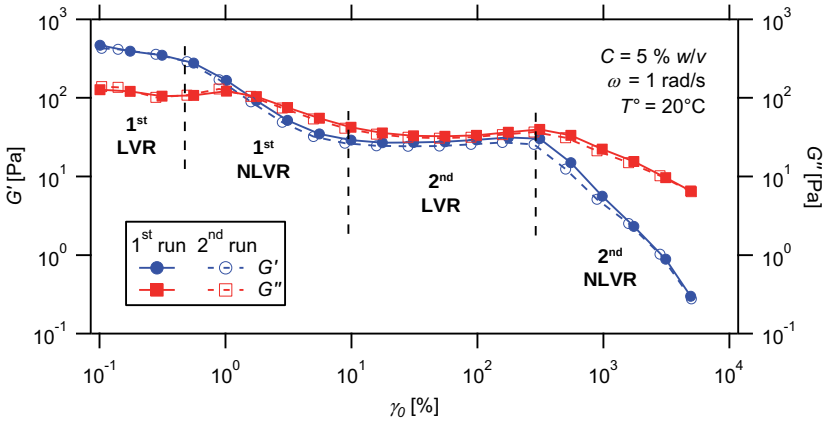

Figure 10.7 – Strain dependence of dynamic moduli for a hydrogel prepared from PS_{27}-*b*-$PNIPAAm_{235}$-tpy copolymer and Ni(II) ions: 1st run under increasing strain, 2nd run under decreasing strain.

LVR). Under those conditions, strain on the sample increases linearly with stress amplitude (Figure 10.8) while elasticity dominates over viscous effects. At larger deformation, a first transition is observed from a "hard" to a comparatively "soft" gel, where elastic and viscous moduli cross each other before reaching a plateau, corresponding to the second linear viscoelastic regime (2nd LVR).

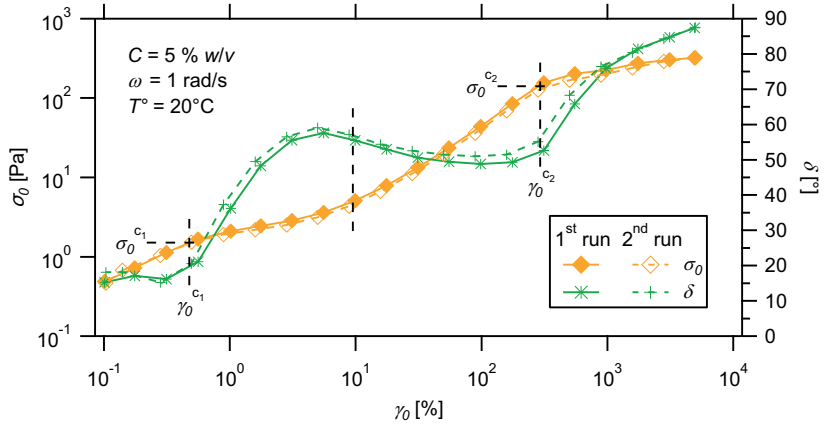

Figure 10.8 – Stress–strain relationship for a hydrogel prepared from PS_{27}-*b*-$PNIPAAm_{235}$-tpy copolymer and Ni(II) ions: 1st run under increasing strain, 2nd run under decreasing strain.

At the transition between the first and second plateau in moduli, the strain–stress relationship largely deviates, which corresponds to the first non-linear viscoelastic regime (1st NLVR). As shown in Figure 10.8, the linearity is however recovered at the onset of the 2nd linear region. In this regime, the linearity of the viscoelastic response is further checked from the Lissajous patterns. The latter describe the angular displacement of one plate relative to the other, θ, as a function of the applied torque, T, showing no higher harmonic contribution to the raw stress–strain signal (Figure 10.9). Instead, a symmetric elliptic pattern clearly indicates a single-harmonic, elastic strain response of the gel, at least before yielding.

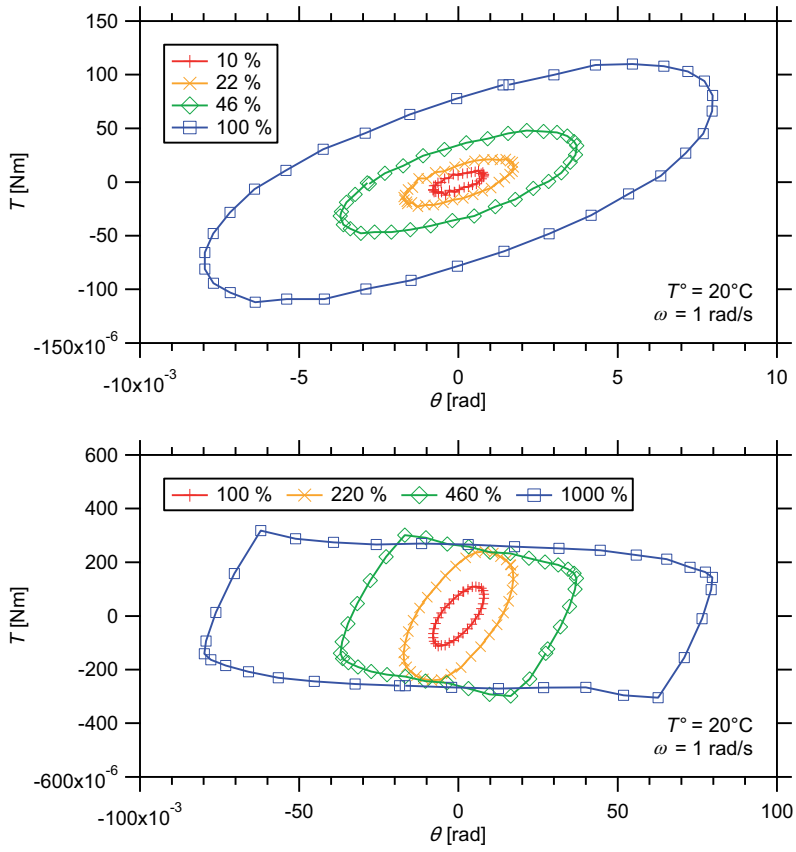

Figure 10.9 – Lissajous patterns obtained for a hydrogel prepared from PS_{27}-*b*-$PNIPAAm_{235}$-tpy copolymer and Ni(II) ions, at various strain amplitudes.

Under large amplitude oscillatory shear, strain softening is finally observed, both moduli decreasing characteristically beyond the second yield point. As revealed by the analysis of stress–strain curves (Figure 10.8), this terminal flow corresponds to the 2nd non-linear viscoelastic regime. Accordingly, the Lissajous pattern is progressively distorted from ellipsoid to an asymmetric rounded parallelogram (Figure 10.9), evidencing plastic flows within the material.[36] As illustrated in Figure 10.7, the reversibility of the transition is also checked, both moduli recovering their original values under decreasing strain. Only a slight hysteresis is observed when coming back to small deformations, evidencing efficient and autonomous healing of gels.

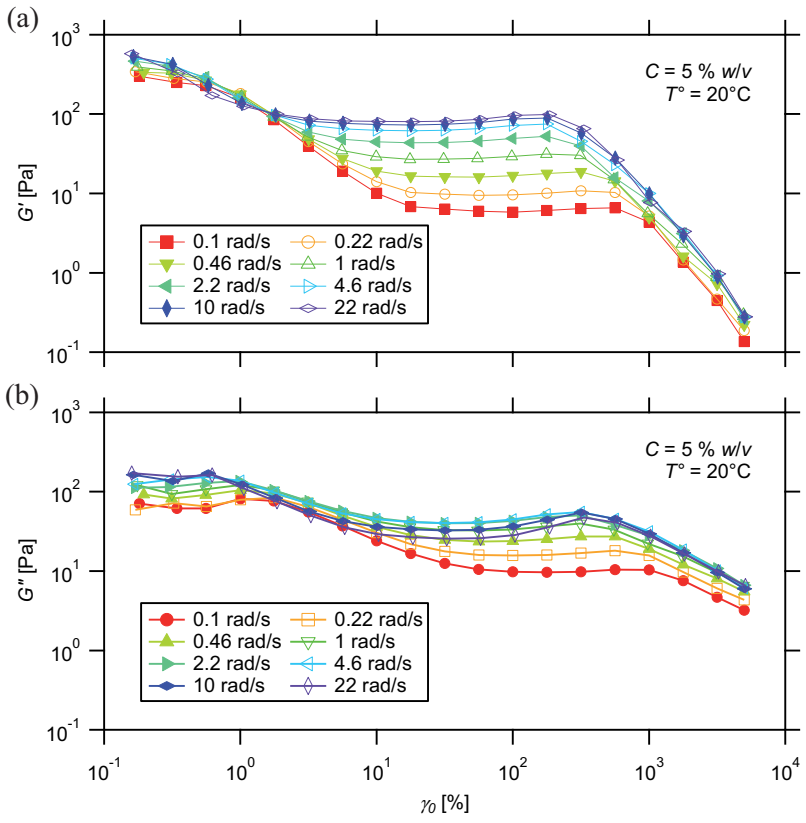

Figure 10.10 – Strain dependence of (a) elastic and (b) viscous moduli for a hydrogel prepared from PS_{27}-*b*-$PNIPAAm_{235}$-tpy copolymer and Ni(II) ions, at different oscillation frequencies.

When increasing the frequency at which strain sweeps are performed, a gradual transition is observed in the viscoelastic behaviour of the

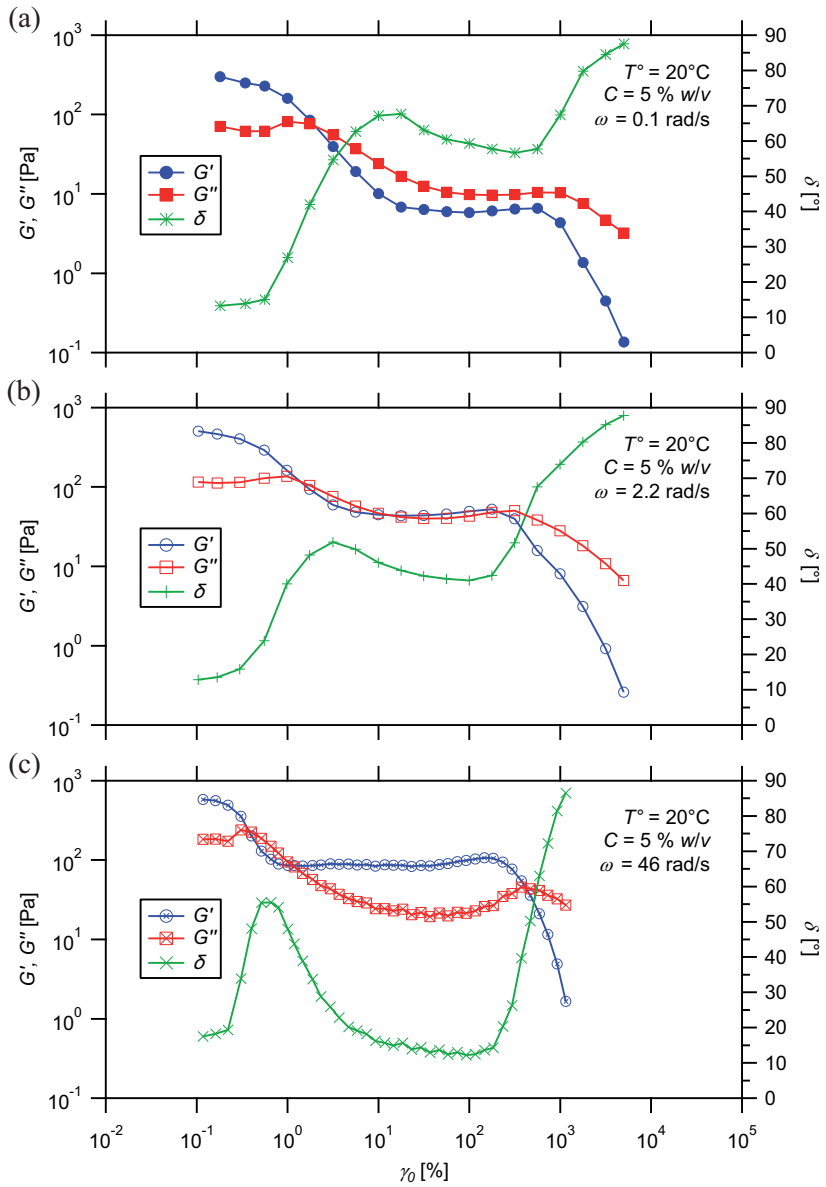

Figure 10.11 – Strain dependence of dynamic moduli for a hydrogel prepared from PS_{27}-*b*-$PNIPAAm_{235}$-tpy copolymer and Ni(II) ions, at selected oscillation frequencies.

supramolecular gels (Figure 10.10). A pronounced influence is noted at intermediate strains, *i.e.*, in the second linear viscoelastic regime, in agreement with results from frequency sweeps. In accordance also, the first plateau value for elastic modulus is almost frequency-independent whereas the second strongly depends on the frequency at which the material is stressed. More precisely, the elastic modulus values at the second plateau gradually increase with an increasing oscillation frequency.

At high frequency, the viscoelastic response of the material is dominated by elasticity so that it still behaves like a "hard" gel. Under those conditions, the ratio between G' and G'', and hence the phase angle, δ, are comparable between the first and second plateau region (Figure 10.11 (a)). At the transition between the two LVRs, dynamic moduli cross each other so that the first yield point is clearly seen when following the evolution of stress against strain amplitude (Figure 10.12). In the region of the first relaxation frequency, the viscoelastic response corresponds to a "soft" gel while the viscous and elastic components are almost equivalent in values (Figure 10.11 (b)). At lower frequency, samples finally show an essentially viscous response in the 2$^{\text{nd}}$ LVR, which is characteristic of "soft" gels too (Figure 10.11 (c)).

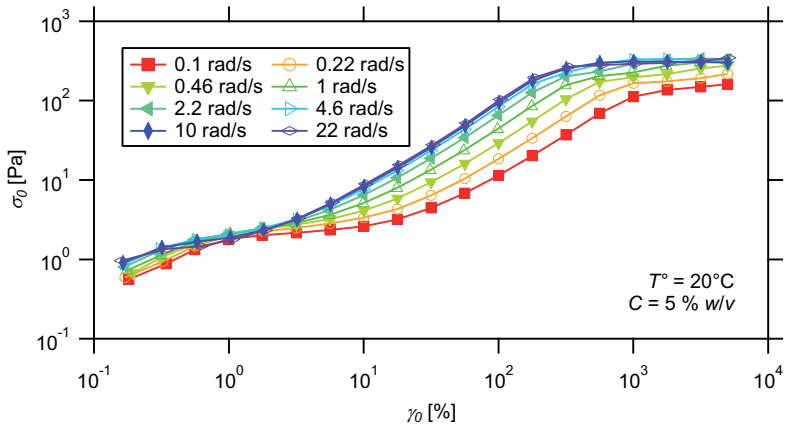

Figure 10.12 – Stress–strain relationship for a hydrogel prepared from PS_{27}-*b*-$PNIPAAm_{235}$-tpy copolymer and Ni(II) ions, at different oscillation frequencies.

Critical or yield strain, γ_0^c, and stress, σ_0^c, determined at the transition between linear and non-linear regions are also found to be highly

frequency-dependent. For both yield points, transitions are observed at lower strain when the oscillatory frequency is high (Figure 10.12). As summarized in Figure 10.13, the frequency dependence of yield strains is characterized by an exponential decrease that is even more pronounced for the second yield point. At very low frequency, supramolecular hydrogels can theoretically withstand infinite deformation. Indeed, their dynamic structure reorganizes over long time scale, which dissipates mechanical strain. At elevated frequency, yield strains stabilize around values that should correspond to the largest extent to which the network can be stretched without altering its structure.

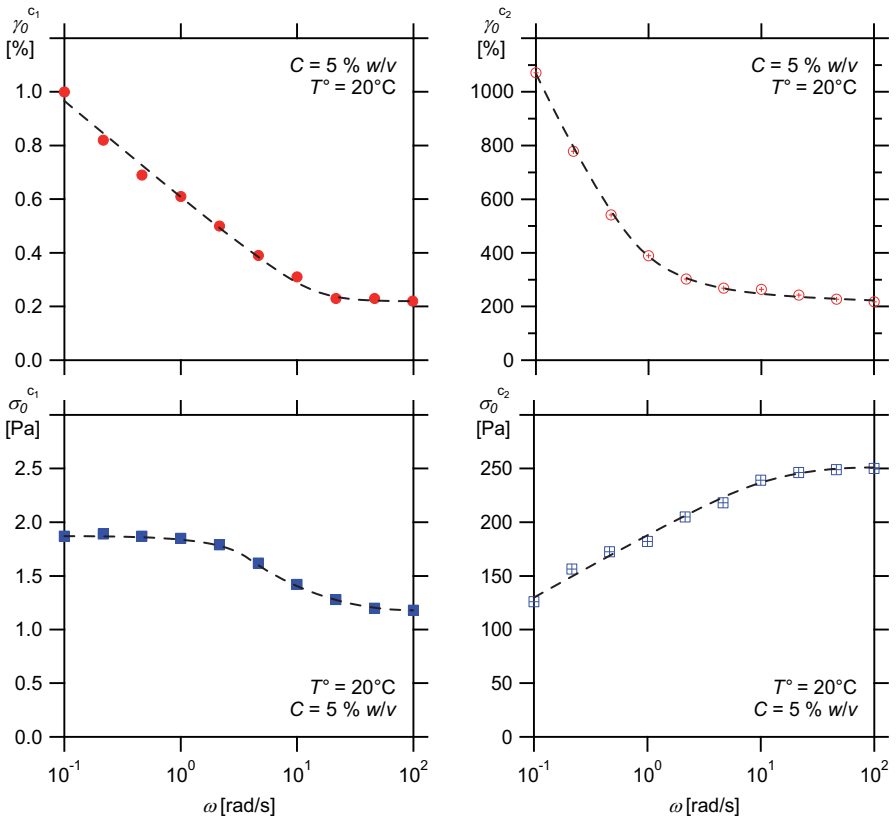

Figure 10.13 – Frequency dependences of the first (left) and second (right) yield strain (top) and stress (bottom) for a hydrogel prepared from PS_{27}-*b*-$PNIPAAm_{235}$-tpy copolymer and Ni(II) ions.

In parallel, yield stress values should increase up to a plateau, which

is related to the mechanical strength of the non-covalent junctions structuring the material. Indeed, these junctions are fully stressed at high oscillation frequency, *i.e.*, when mechanical stress is not dissipated through relaxation of the network. In practice, this situation is only verified for the second yield point. Indeed, the frequency-dependence of the first yield point follows a sigmoidal trend, while low and high frequency regimes are respectively characterized by a high and low plateau value. Moreover, the curve inflection point is located at a frequency corresponding to the first relaxation time, τ_1, of the associating network.

Last but not least, significant changes in the large amplitude oscillatory shear behaviour of supramolecular gels are observed when varying oscillation frequency (Figure 10.10). Below the crossover frequency, strain softening is only observed at the transition between the first and second LVR, as well as at the limit of network rupture. Above, a clear increase in the viscous response of the gels followed by strain softening is evidenced at both yield points. This frequency-dependent behaviour has been already observed for similar systems and further related to the apparent lifetime of the supramolecular interactions tethering the network.[19] However, the complexity of rheological phenomena occurring in this region will only be discussed in a following chapter.

10.4.3 Influence of hydrophobe length

In order to investigate the influence of the length of the hydrophobic segment, different associating copolymers are synthesized as reported in a previous chapter. Concretely, the length of the hydrophobic segment is varied from a few units to a few tens of units, against few hundreds of units for the water-soluble block. The main characteristics of the associating copolymers can be found in Table 8.2.

Upon addition of transition metal ions, nearly all copolymer solutions form gels within minutes. Only associating copolymers exhibiting a very short polystyrene block of a few units do not induce gelation, evidencing the critical contribution of hydrophobic cores on the gelation process itself, and hence on the mechanical properties of the gels. Accordingly, it is assumed that ten hydrophobic units constitute here the critical length mandatory for the formation of elastically active junctions within the network. Below, the hydrophobic interaction between segments might be too weak to ensure the formation of supramolecular hydrogels.

10.4.3.1 Oscillatory frequency sweep

Above the critical length, varying the size of the hydrophobic segment tremendously affects the dynamic rheological properties of the supramolecular hydrogels. Experimentally, a first influence is evidenced from frequency sweep measurements on supramolecular hydrogels from associating copolymers having polystyrene blocks of different lengths (Figure 10.14). Precisely, the size of PS segment is varied during the copolymer synthesis from 15 to 35 repeating units, against 235 for the PNIPAAm block that is kept constant.

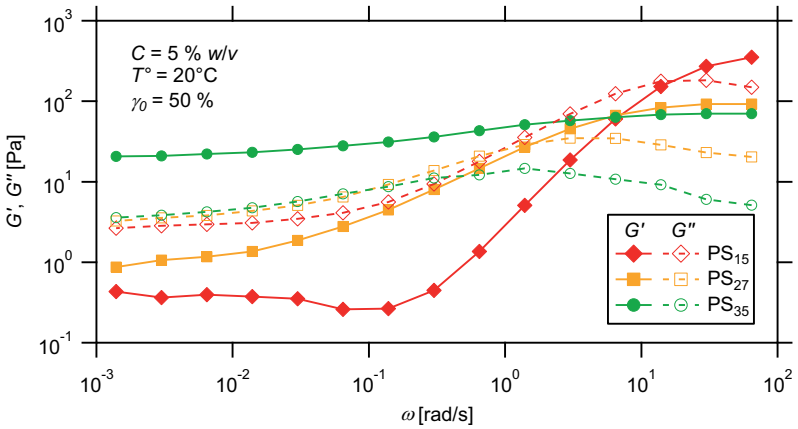

Figure 10.14 – Frequency dependence of (a) elastic and (b) viscous moduli for hydrogels prepared from PS_m-*b*-$PNIPAAm_{235}$-tpy copolymers and Ni(II) ions, while increasing the PS segment length.

To a certain extend, associating polymer gels prepared from PS-*b*-PNIPAAm-tpy copolymers show pronounced dynamics in the high-frequency range, at least when stressed above the first yield point. As shown in Figure 10.14, storage and loss modulus curves generally cross each other at a frequency slightly below the first relaxation frequency of the material, and reach a low-frequency plateau. However, such response can be only achieved as long as the hydrophobic segment does not exceed a few tens of repeating units, for a soluble block of a few hundreds. Indeed, hydrogels made of associating copolymers exhibiting a long PS block are exclusively characterized by nearly parallel moduli over a large frequency range when probed under oscillation shear. In essence, this rheological behaviour is correlated to the one observed for

supramolecular gels at stresses below the first yield point (Figure 10.4). In turn, this highlights a straight relationship between the behaviour, transient or frozen, that tends to dominate the materials under shear and the stability of micellar cores that is further related to the length of polystyrene stickers.

While the low-frequency plateau in elastic modulus shows a clear dependency on the PS segment length, the dynamic viscous modulus reaches a consistent value for the different samples at low oscillatory frequency (Figure 10.14). In the high-frequency region, a decrease in both storage and loss moduli is observed as the size of the hydrophobic sticker increases. Instinctively, larger micellar cores would facilitate the formation of loops because the larger core size lowers the entropy penalty for polymer chains to loop back to the same core.[37] As a consequence, the number of elastically active chains within the network, and hence the high-frequency plateau moduli, are found to drop as the length of the polystyrene segment increases.

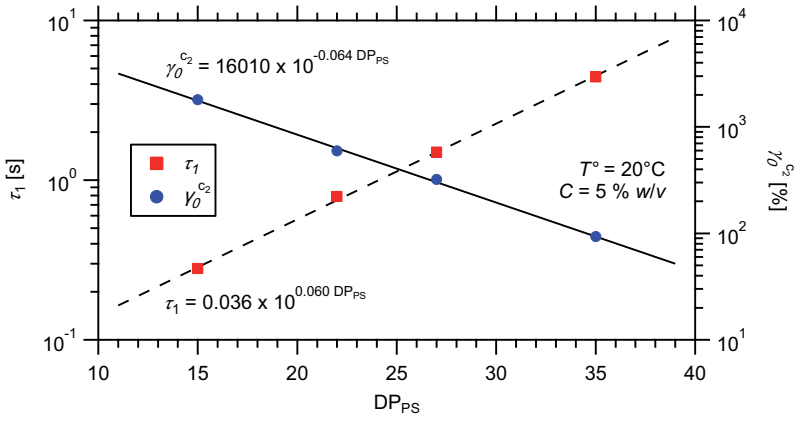

Figure 10.15 – First relaxation time and second yield strain at a frequency of 1 rad/s of supramolecular hydrogels prepared from PS_m-*b*-$PNIPAAm_{235}$-tpy copolymers and Ni(II) ions, while increasing the hydrophobic segment length.

In parallel, the first relaxation time of the networks, τ_1, when stressed within the limit of the second LVR, is found to increase with the size of the hydrophobic stickers (Figure 10.15). Indeed, this relaxation time is identified as the local maximum in G'', which shifts to lower frequency when increasing the size of the PS segment (Figure 10.14). This

statement further evidences the role of micellar cores in the considered relaxation process. Moreover, the relationship highlighted between the first stress relaxation time of the gels and the length of the PS segment is consistent with the literature on transient hydrophobic networks. [29]

10.4.3.2 Oscillatory strain sweep

In parallel, the effects of the hydrophobic segment length on the mechanical properties of the gels are investigated by strain sweep experiments. In practice, different viscoelastic responses are achieved depending on the length of the hydrophobic block, so that distinct situations can be discussed.

As illustrated in Figure 10.7, supramolecular gels from associating copolymers exhibiting a PS block of 27 repeating units are characterized by a "hard" to "soft" gel transition under increasing strain. However, the first yield is believed to shift to lower strains when decreasing the length of the hydrophobic segment. Hence, the aforementioned transition is difficult to detect experimentally for copolymers exhibiting PS blocks of only 22 repeating units (Figure 10.16 (a)). Beyond the first yield point, the viscoelastic response of such materials is dominated by viscosity, at least in the low frequency range, which is characteristic of "soft" gels. In agreement with a decreasing strength of hydrophobic interactions, shortening the length of PS segments leads to less elastic networks.

As the size of the hydrophobic segment is increased, the first yield point is progressively shifted to measurable values, which is encountered for PS_{27}-*b*-$PNIPAAm_{235}$-tpy based hydrogels (Figure 10.7). Ultimately, the first yield point merges with the second when the hydrophobic segment length exceeds a critical value and gels behave as "hard" materials exclusively. In this regime, the viscoelastic response of those hydrogels is indeed dominated by elasticity as long as strain on the sample does not exceed the yield point (Figure 10.16 (b)). Above, a unique gel–sol transition followed by strain softening is observed.

When probed at a given frequency, the stiffness of the supramolecular gels is correlated to the length of the PS block, *i.e.*, the stability of the hydrophobic association (Figure 10.15). Precisely, the yield strain is found to decrease when increasing the length of the PS segment, as also observed by Tenhu and coworkers for associative star copolymers in

aqueous solutions.[17]

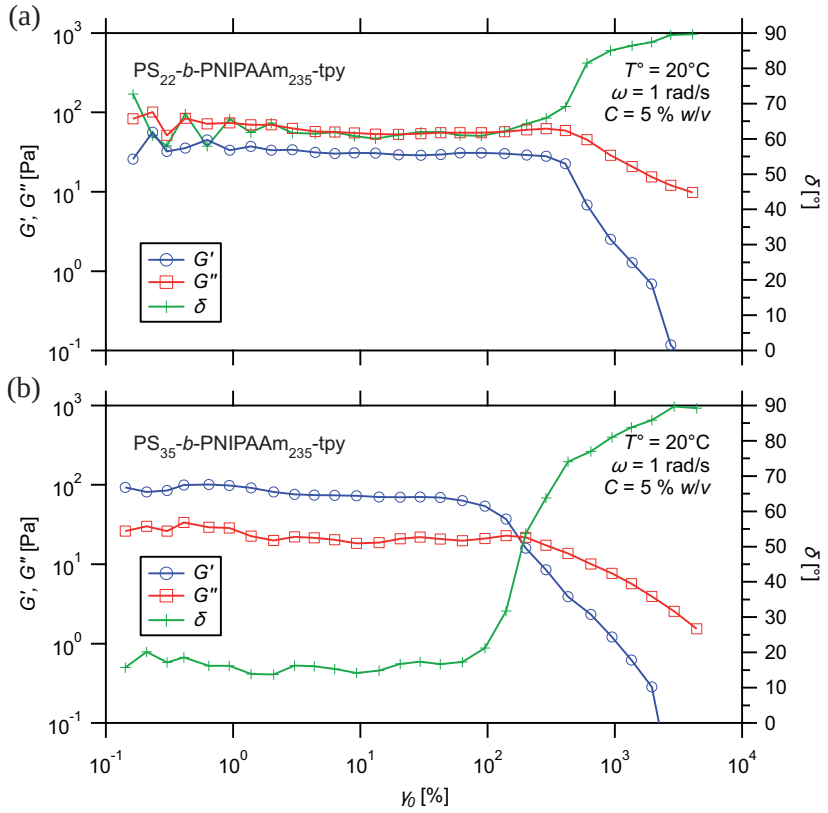

Figure 10.16 – Strain dependence of dynamic moduli for hydrogels prepared from (a) PS_{22}-*b*-$PNIPAAm_{235}$-tpy or (b) PS_{35}-*b*-$PNIPAAm_{235}$-tpy copolymer and Ni(II) ions.

10.4.4 Influence of metal ion

In order to investigate the influence of first row transition metal ions on the rheological properties of supramolecular hydrogels, different samples are prepared from a given associating copolymer solution. Precisely, half an equivalent of Fe(II), Ni(II), Co(II) or Zn(II) ions are added to each micellar solutions, with respect to the terpyridine content. By varying the nature of metal–terpyridine bis-complexes bridging the hydrophobic cores, a fine tuning over the mechanical properties and stress

relaxation of the sheared materials is achieved.

10.4.4.1 Oscillatory frequency sweep

At first, frequency sweeps are performed on gels at stresses that match the second linear viscoelastic regime. As observed from Figures 10.17 and 10.18, the metal ion nature itself has actually a small impact on the first relaxation mode that dictates the high-frequency dynamics of associating networks under shear. Indeed, no significant changes are observed in the apparent relaxation time, τ_1, associated to this process while switching from one transition metal to another. In addition, com-

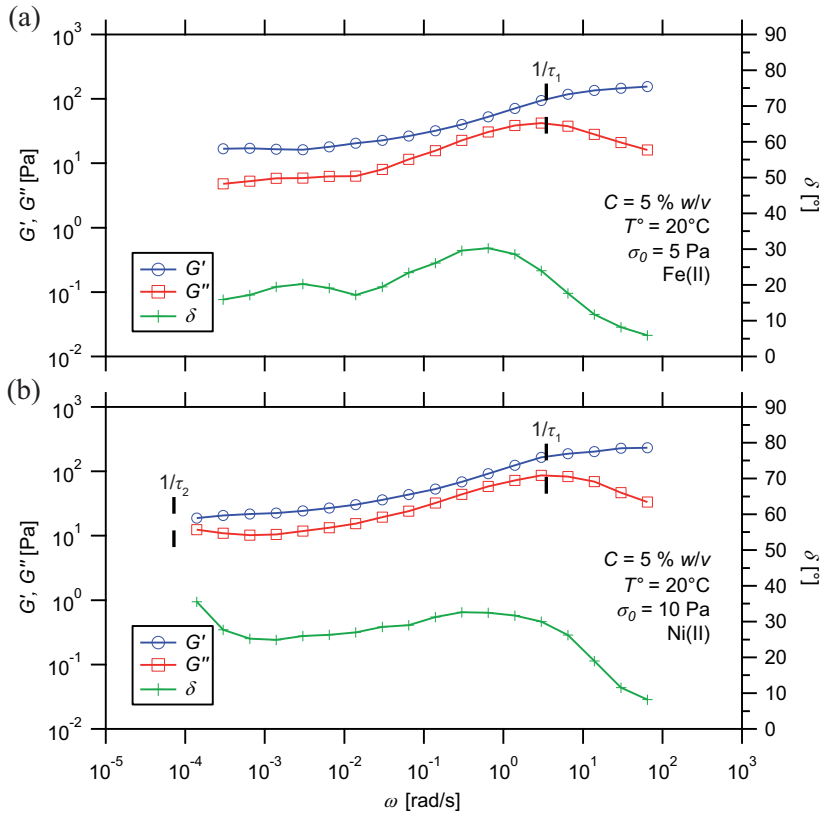

Figure 10.17 – Frequency dependence of dynamic moduli for hydrogels prepared from PS_{27}-*b*-$PNIPAAm_{300}$-tpy copolymer and (a) Fe(II) or (b) Ni(II) ions.

parison of the viscoelastic properties of gels in the high-frequency range only indicates no significant influence of the metal ion.

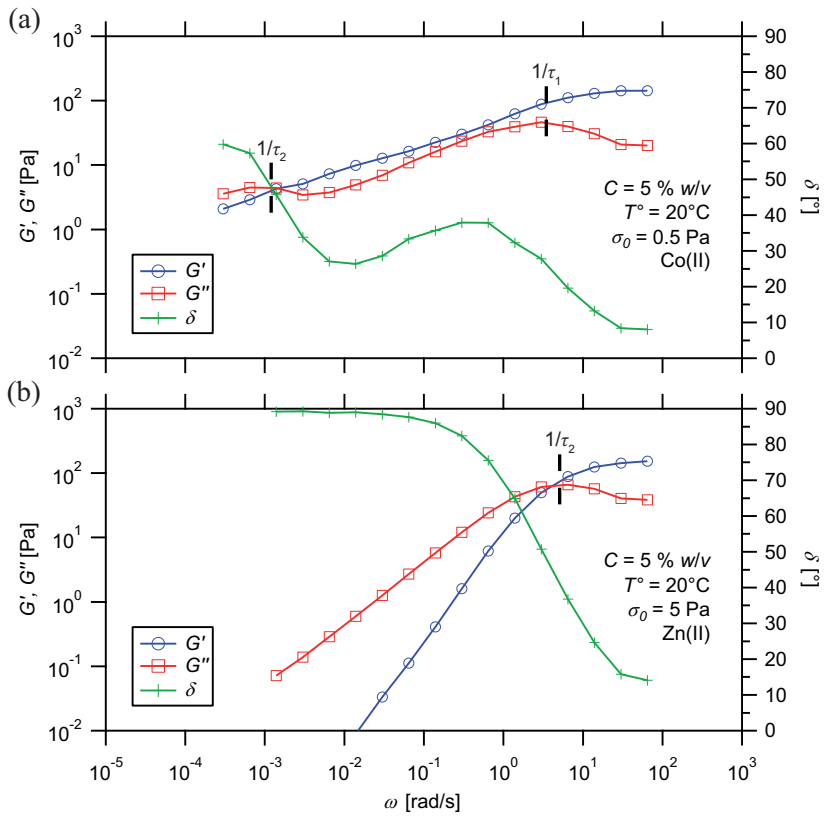

Figure 10.18 – Frequency dependence of dynamic moduli for hydrogels prepared from PS_{27}-*b*-$PNIPAAm_{300}$-tpy copolymer and (a) Co(II) or (b) Zn(II) ions.

As shown in Figures 10.17 and 10.18, the viscoelastic response of gels in the low-frequency range is more deeply affected by the nature of the metallo-bridges between hydrophobic nodes. In the case of nickel(II) and iron(II) ions, the low-frequency plateau modulus spans over a large range of frequencies, evidencing an extremely long relaxation time, τ_2, that is difficult to detect experimentally but noticeable in the case of Ni(II). The associated relaxation mode was more clearly observed in the case of cobalt(II), while storage and loss modulus curves cross each other at relatively low oscillation frequency. Finally, only one single relaxation

time is apparently observed when zinc(II) ions are used.

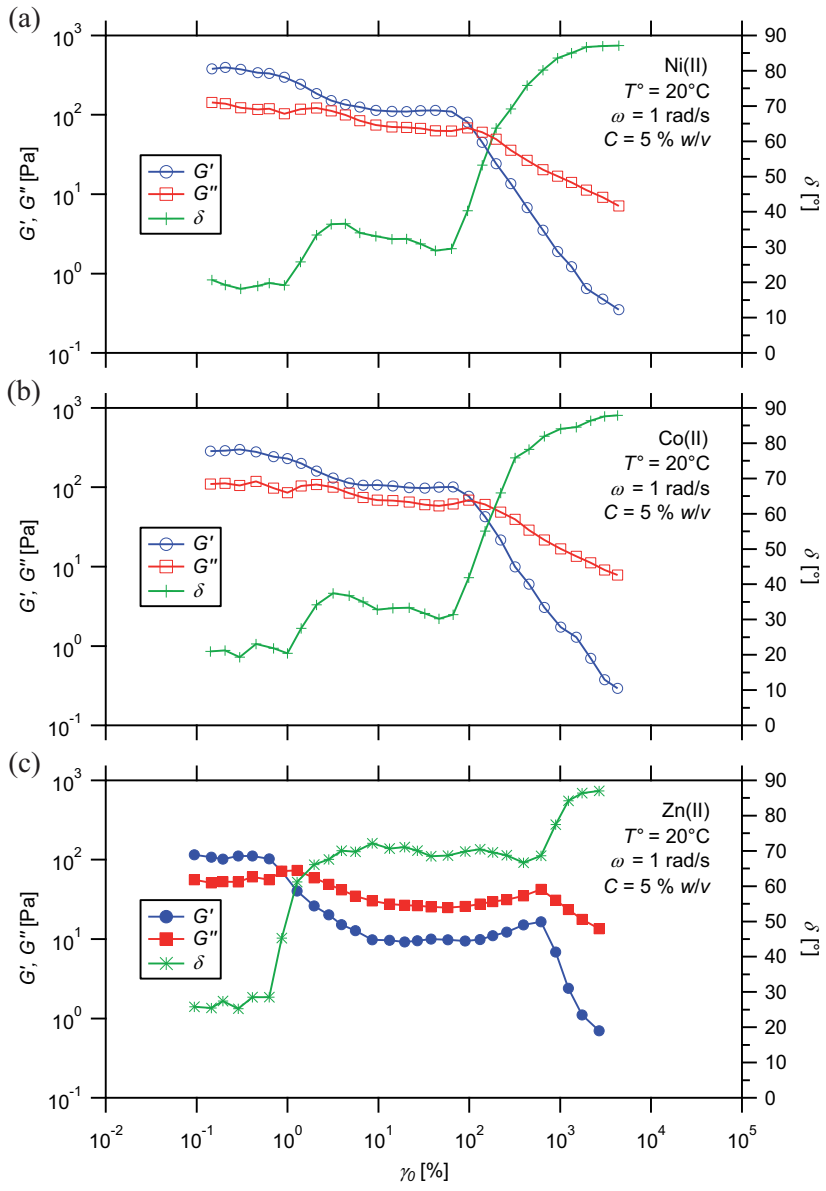

Figure 10.19 – Strain dependence of dynamic moduli for hydrogels prepared from PS_{27}-*b*-$PNIPAAm_{300}$-tpy copolymer and (a) Ni(II), (b) Co(II) or (c) Zn(II) ions.

10.4.4.2 Oscillatory strain sweep

The influence of transition metal ions on the rheological properties of the gels is studied in parallel by strain sweep measurements. In practice, only a small effect on the viscoelastic response of the gels is observed under increasing strain at a frequency of 1 rad/s when using Fe(II), Ni(II) or Co(II) ions indifferently, as illustrated in Figures 10.19 (a) and (b). Indeed, comparable viscoelastic responses characterize the different supramolecular networks under oscillatory shear, at least at frequencies that span over the low-frequency plateau modulus.

Only hydrogels prepared from copolymers in combination with Zn(II) ions exhibit a distinct rheological behaviour (Figure 10.19 (c)). While showing a slightly lower viscoelastic response at low deformation, those supramolecular gels drastically differ from their analogues above the first yield strain. Indeed, viscous effects clearly dominate over elasticity in the second plateau region, which is a signature of relatively "soft" gels. In return, those networks withstand higher deformation and hence are comparatively more flexible under low-frequency oscillatory shear than networks based on Fe(II), Ni(II) or Co(II) ions.

10.5 Interpretation of rheological data

From a physical point of view, transient networks are here formed through the self-assembly of linear water-soluble polymers bearing a different associating unit at each extremity: a short polystyrene block as hydrophobic segment, and a terpyridine ligand as coordination motif (Figure 10.20). As a general rule, stress relaxation in such multicomponent associative polymer networks is largely dictated by the exchange kinetics of the fast-dissociating cross-linker.[38] Once the latter detaches from a junction, the polymer segments indeed become pendant and thus elastically inactive. Hence, the viscoelastic response of hetero-telechelic associating polymer solutions is comparable to that observed for solutions of homo-telechelic associating polymers involving the fastest cross-linker. These solutions behave as Maxwell fluids with a well-defined relaxation time, well separated from the faster internal modes characteristic of the conformational relaxation of the chains.[27–30] In the present work, the stabilities of both cross-links tethering the networks can be readily tuned depending on the metal ion and the length of the

hydrophobic segment. Under proper conditions, this versatility allows the elaboration of supramolecular hydrogels whose viscoelastic response reflects the discrete contribution from each individual transient interaction.

The first contribution to the network formation arises from the self-assembly of the amphiphilic copolymer in aqueous solutions.[39–41] The micellization process is characterized by the aggregation of a given number of polymer chains. Those aggregated copolymer chains are in equilibrium with free chains in solution, called unimers, allowing stress relaxation within micellar networks via detachment of a hydrophobic segment from a micelle and subsequent exchange with an other through diffusion in the media (Figure 10.20).[29,42]

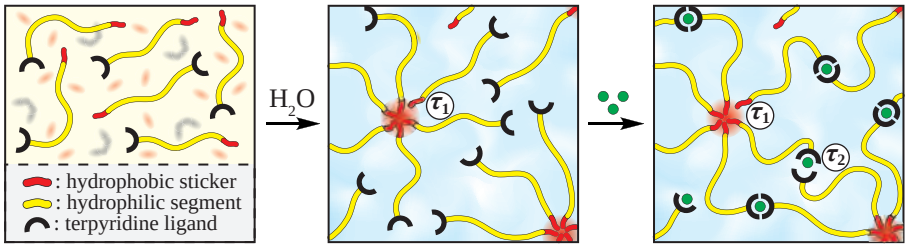

Figure 10.20 – Hierarchical assembly of hetero-telechelic associating copolymers into a transient coordination micellar gel with two orthogonal dynamic processes.

Relaxation rates for micellar networks are dictated by the dynamics of the transient association, *i.e.*, the rate at which unimers dissociate from micelles, which in turn is affected by the hydrophilic–hydrophobic balance in a given amphiphilic block copolymer.[29,42] In this respect, short hydrophobic stickers easily detach themselves from micellar cores while longer segments give rise to more stable, ultimately frozen, aggregates.[43] Experimentally, this can be correlated to the viscoelastic response of gels prepared from associating polymers having polystyrene segments of different lengths (Figure 10.14). While short stickers lead to the formation of transient micelles and hence to supramolecular hydrogels, nearly-covalent networks can be obtained with long hydrophobic segments.

The second contribution is obtained by adding half an equivalent of various transition metal ions to the micellar solutions, which results

in gelation. Indeed, terpyridine ligands coordinate to metal ions and hence form stable bis-complexes bridging the hydrophobic micellar cores (Figure 10.20). Those transient junctions can also lead to mechanical stress relaxation within the supramolecular network, via an activated dissociation mechanism. In contrast to hydrophobic junctions, only two terpyridine ligands can be coordinated around a transition metal ion. In this respect, metallo-supramolecular networks inevitably lose their integrity when ligand dissociation from the metal complex. Besides, the thermodynamic and kinetic stabilities of terpyridine bis-complexes can be readily varied depending on the choice of the transition metal ion, which is reported in Table 9.1.

The rate at which supramolecular hydrogels relax stress under shear and hence dissipate mechanical energy depends on the relationship between the experiment time scale and the different relaxation times of the material itself. When supramolecular junctions are stressed at rates that largely exceed their characteristic dissociation rates, they are virtually "intact" and thus stress on sample is transferred to the structural components of the network, *i.e.*, the polymer chains. On the other hand, the majority of the deformation energy is dissipated when supramolecular networks are stressed over long periods. Practically, the proportion of the deformation energy that is stored in entropic distortions of the network is measured by the storage modulus, G'. In complement, the loss modulus, G'', measures the proportion of the deformation energy that is dissipated due to relaxations that occur on the deformation time scale.

In practice, the different trends observed as a function of oscillation frequency can be rationalized in the context of a multi-element generalized Maxwell model described by at least two relaxation rates, τ_1, τ_2. The latter can be ascribed to the different relaxation processes of the supramolecular material under shear, as schematized in Figure 10.20. In turn, the associated time scales might be correlated to the lifetime of transient hydrophobic and coordinative interactions structuring the network.

From the dependence of τ_1 with the length of the hydrophobic sticker (Figure 10.15), the related relaxation process is attributed to the exchange of chains between micellar cores. In this respect, short polystyrene blocks give rise to relatively weak transient associations that allow the material to relax mechanical stress on a very short time scale. As the

length of PS segments is increased, the strength of the hydrophobic association accordingly rises towards glassy nano-domains, which in turn prevent stress release. Hence, the material is able to carry mechanical stress and store the deformation energy via stretching of polymeric chains, on short as long time scales (Figure 10.14).

Logically, the second relaxation mode (τ_2) is attributed to the exchange of ligands around the different metal centres. Accordingly, the frequencies that mark the end of the low-frequency plateau modulus, when achievable experimentally (Figures 10.17 and 10.18), are in good agreement with dissociation rates, k_{-2}, reported for metal–terpyridine bis-complexes (Table 9.1).[44,45] In this respect, Fe(II) and Zn(II) ions respectively yield the slowest and fastest dissociating cross-linkers, while Ni(II) and Co(II) constitute intermediate cases.

The viscoelastic response of associative gels under oscillatory shear is also profoundly affected by the amplitude at which the material is stressed. This remarkable mechano-responsiveness is illustrated for hydrogels prepared from associating copolymers having a medium size hydrophobic segment, *i.e.*, of around 27 repeating units (Figure 10.7). For small oscillations, the majority of stress-bearing cross-links are mechanically unaltered and the deformation energy is mostly stored in entropic stretching of the polymeric chains. Under those conditions, the material displays a solid-like behaviour, with G' dominating G'' over short and long time scales, indicating that the hydrogel is highly structured (Figure 10.4). In theory, this observation can be rationalized by taking into account the relative stability of micellar assembly that prevents the escape of hydrophobes and hence relaxation of the gels. As a result, the number of elastically active chains, *i.e.*, chains that contribute to the elasticity of the transient network, does not fall down when the latter is slightly stressed over a period exceeding the first apparent relaxation time (Figure 10.4).

Increasing strain amplitude above the first yield point disrupts the integrity of micellar structures, which causes a drop in both dynamic moduli (Figure 10.7). As a consequence, an outstanding transition from a “hard”, highly elastic, hydrogel to a “soft”, more viscous, material is achieved. While the first behaves as if chemically cross-linked, the second presents a dynamic nature that is characteristic of transient micellar gels. In other words, this “hard”-to-“soft” gel transition is accompanied by a dynamization of the initially frozen network, and hence is attributed

to the stress-induced plastic flow of latent polystyrene segments within glassy micellar cores (Figure 10.21 (c)).[46]

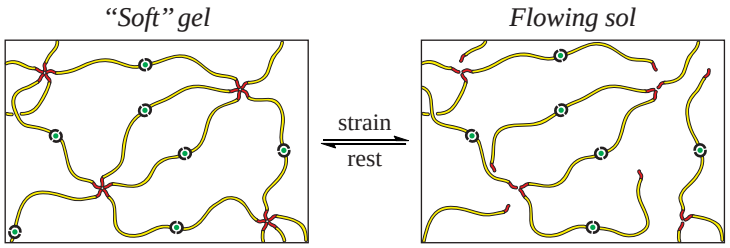

(a) Associating copolymers with short hydrophobic bloc

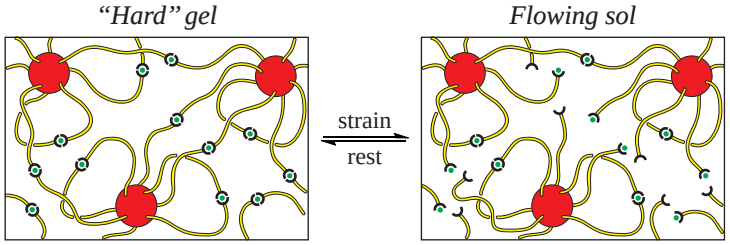

(b) Associating copolymers with long hydrophobic bloc

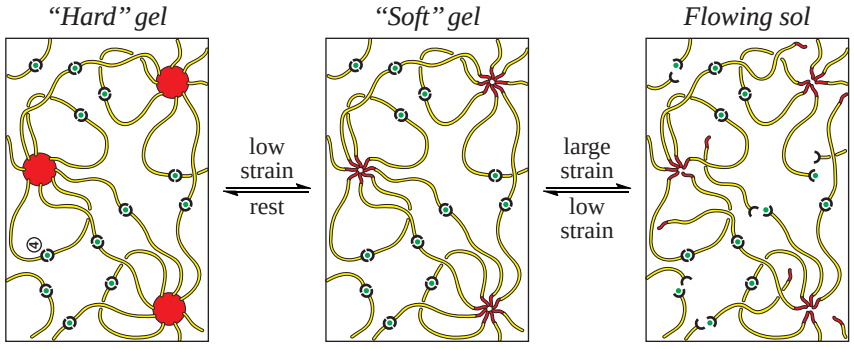

(c) Associating copolymers with intermediate hydrophobic bloc

Figure 10.21 – Effect of strain on supramolecular networks elaborated from associating polymers bearing a coordinating moiety and a hydrophobic segment, as a function of its size.

The extent to which the micellar networks can be mechanically stressed without altering their glassy equilibrium mostly depends on the strength of the hydrophobic interactions. In this respect, long PS stickers give

rise to strong glassy hydrophobic cores that retain their structural integrity, even under high-strain conditions (Figure 10.21 (b)). Hence, a single gel-to-sol transition is achieved in those systems when the strain on the sample exceeds the onset of network breaking (Figure 10.16 (b)). On the opposite, short PS stickers would give rise to less stable aggregates, resulting in a continuous rupture and formation of the transient hydrophobic cores (Figure 10.21 (a)). Even under low-strain conditions, such micellar gels have indeed a natural tendency to flow when mechanically constrained (Figure 10.16 (a)). If achievable, the transition between the first and second viscoelastic region would be thus difficult to detect experimentally. Hence, a liquid-like behaviour exclusively characterizes those samples in the low-frequency regime.

Above the first yield strain, γ_0^{c1}, the number of remaining active crosslinks largely depends on the time scale under which the material is stressed. At frequencies higher than the exchange rate of associating copolymer between hydrophobic cores, the latter appear "intact", which gives rise to a highly elastic response (Figure 10.10). Under those conditions, the ratios between stored and dissipated energy, and hence the phase angle, are thus comparable between the first and second linear viscoelastic regimes, as further illustrated in Figure 10.11 (c). However, the plateau modulus in the second LVR is comparatively lower due to the stress induced plasticization of the hydrophobic cores. The effect of this phenomenon on the mechanical properties of the gels is even more clearly appreciated in oscillatory frequency sweeps, especially when following the evolution of the high-frequency plateau modulus with an increasing strain (Figure 10.5). In addition, the number of elastically active chains, and hence the high-frequency plateau moduli, drops as the length of the polystyrene sticker increases (Figure 10.14). As mentioned above, larger micellar cores would facilitate the formation of loops because the larger core size lowers the entropy penalty for polymer chains to loop back to the same core (Figure 10.21 (b)).[37]

In the low-frequency regime, longer hydrophobic segments enhance the stability of the mechanically perturbed micellar aggregates and thus favour elastically effective junctions between them (Figure 10.14). Intuitively, metal–ligand junctions between hydrophobic cores are only effective if the latter remain at least partially intact. On the other hand, a polymer chain becomes pendant and hence elastically inactive if it dissociates from a micellar core, regardless of the association state

of the metal–ligand junction. Active metallo-bridges are thus favoured when long hydrophobic stickers, that give rise to glassy micellar cores, are used. In addition, the proportion of elastically active chains between micellar cores will further depend on the stress on the sample when medium size stickers are used (Figure 10.5). While active metallo-bridges between glassy polystyrene cores are promoted below the first yield strain, their proportion falls down as the detachment of hydrophobic segments is induced by mechanical forces.

Beside the inherent stability of micellar cores, the kinetic lability of metal–ligand complexes between them will determine the viscoelastic response that dominates the material in the low-frequency regime. In fact, hydrophobic cores are structurally restrictive only if they dissociate much faster than the coordinative junctions themselves. Under the present conditions, this situation is practically achieved for most of the transition metal ions, which have therefore only a weak influence on the viscoelastic response of the gels. Here, only Zn(II) ions form, in combination with the terpyridine ligand, metallo-bridges that dissociate at least as fast as the micellar cores, and thus dictate the viscoelastic response of the gels above the first yield point (Figure 10.19).

As illustrated in Figure 10.7, supramolecular hydrogels finally lose their viscoelastic properties under large strain oscillations, meaning that the transient network is mechanically broken. Under these conditions, the classical gel-to-sol transition observed for swollen supramolecular networks is ultimately achieved. Together with the applied stress, the mechanical strength of the physical networks will determine the behaviour, semi-solid or viscous-like, that dominates the material under shear. In fact, the deformation range in which the material responds linearly hangs on how efficiently mechanical energy is dissipated through reversible breaking of the cross-links and diffusion of polymer chains through the media.

Accordingly, the maximum deformation that the networks can withstand under shear is mainly dictated by the faster dissociating cross-linker, that is the hydrophobic cores, except in the case of fast-dissociating Zn(II) complexes. Hence, the second yield strain, $\gamma_0^{c_2}$, dramatically drops while increasing the length of the PS sticker (Figure 10.15). In parallel, fine tuning is achieved depending on the dynamic properties of the metal–ligand junctions bridging the hydrophobic cores, excluding the particular case of Zn(II) complexes. Indeed, values for second

yield strain increase slightly when switching from very to moderately slow-dissociating complexes (Figure 10.19).

Finally, the ability of transient networks to relax stress further depends on how effective are the cross-linkers on the experiment time scale (Figure 10.13). In the low-frequency range, the deformation energy is largely dissipated though the dissociation of transient cross-links and subsequent exchange of polymer chains. As a result, supramolecular hydrogels withstand larger deformations due to the viscous flow that occurs over long time scale. In the high-frequency range, even fast-dissociating cross-linkers are effectively "intact", limiting the extent of relaxation that can occur upon dissociation. At the limit, the mechanical strength of the physical network is solely governed by the nature and composition of the constitutive polymer chains. On short time scales, their ability to deform elastically through entropic distortions ultimately determines the deformation range in which they respond linearly to applied stress.

10.6 Summary

This chapter provides new insights in the comprehension of the rheological behaviour of associating polymer solutions. Precisely, transient networks were formed through the self-assembly of linear water-soluble polymers bearing a short hydrophobic segment and a coordinating motif. While the first aggregated into micellar nano-structures, the second provided efficient bridges between them, when placed in presence of transition metal ions. Depending on the stability of the associations and mechanical constrains, the viscoelastic response of the accordingly obtained materials was varied from that of chemically cross-linked hydrogels to the one of transient networks.

The dynamics of the investigated materials reflected the discrete contribution from each individual supramolecular junction, being largely dictated by the fast-dissociating cross-linker (τ_1) and fine-tuned by the slow-dissociating cross-linker (τ_2). Accordingly, the dynamic exchange of transient associations constituted the most decisive variable, allowing unprecedented control over the strength and viscoelastic response of the materials under shear. Since the exchange processes occurred at rates determined by the dissociation of cross-linkers, they were thus controlled by the length of the hydrophobic sticker and by the choice of the metal

ion (Figure 10.22).

Depending on the solicitation time scale, t_{exp}, each individual transient cross-link tethering the network appeared either inert or labile. As a result, hydrogels essentially showed an elastic response to shear when stressed at elevated frequencies, as schematized in Figure 10.22. On the contrary, a more viscous-like behaviour tended to dominate samples in the low-frequency regime due to the drop in the number of elastically active junctions.

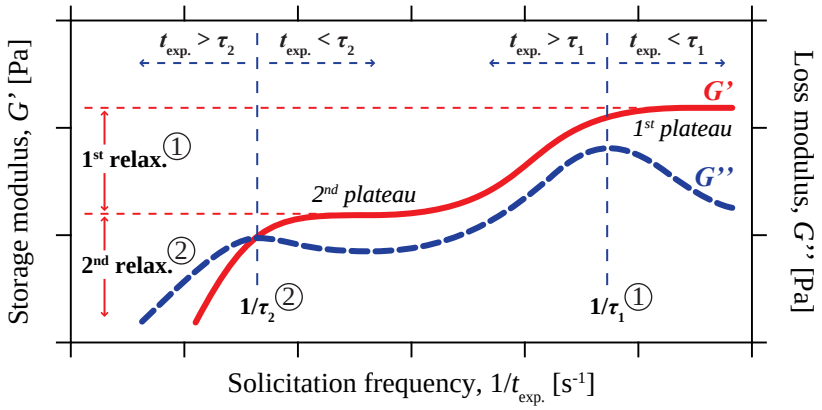

① Control with the hydrophobe length ② Control with the nature of metal ion

Figure 10.22 – Dynamic mechanical response of transient network constructed from associating polymers bearing a coordinating moiety and a hydrophobic segment.

Regarding strain magnitude, the integrity of the transient junctions was also more or less intensely affected by mechanical forces. At low strain, strong structural cross-links were only weakly altered by mechanical stress and fully contributed to the elasticity of the network. At moderate shear strain amplitude, the same junctions started being altered by mechanical force. As a consequence, the proportion of elastically active polymer chains fell down but reached a second dynamic equilibrium, which depends on stress on samples. Finally, large amplitude oscillatory shear strongly overwhelmed stress-bearing junctions within the network, resulting in the Newtonian flow of the material.

Via fine tuning over the associating copolymer architecture, hydrogels that exhibited a remarkable “two-step” gel–sol transition were pre-

pared. Under shear, the structure of such network was first modestly, then deeply disrupted by mechanical stress. While the "hard" network essentially behaved solid-like, the dynamic nature of the "soft" equivalent allowed additional conversion of the mechanical work into chemical energy. In turn, the material further relaxed stress through a single or multiple relaxation modes that occurred on the experiment time scale. However, our study demonstrated that it is the existence of distinct mechanisms of energy conversion, rather than multiple relaxation modes, that allows discrete linear responses and multi-step yielding.

10.7 Experimental part

Materials

Terpyridine end-capped block copolymers are synthesized via sequential reversible addition–fragmentation chain transfer control radical copolymerization, as reported in a previous chapter. Nickel(II), iron(II), cobalt(II) and zinc(II) chloride salts are dried, kept in a glove box, and weighted under argon atmosphere.

Instrumentation

Shear rheological experiments are performed on a Kinexus Ultra (Malvern Instrument) rheometer equipped with a heat exchanger and modified with a solvent trap. Measurements are carried out at given temperatures, using a 20 mm plate–plate geometry, in a water saturated atmosphere in order to minimize evaporation of the solvent. The gap is adjusted between 50 and 250 µm so that the geometry is completely filled. Normal forces are checked to be relaxed prior any measurement.

Preparation of supramolecular gels

Hydrogels are prepared by mixing given amounts of block copolymer with Milli-Q water. The sealed reaction vessels are placed in a fridge and shaken periodically to form homogeneous concentrated solutions after a few days. The gels are then readily obtained by adding the

stoichiometric amount of half an equivalent of transition metal ions (with respect to the terpyridine content) dissolved in defined amounts of Milli-Q water to each concentrated solutions. Lastly, the reaction vessels are placed again in the fridge over three days to ensure homogeneous gelation and stabilization of the gels. The final concentration of copolymers in samples is 5 %w/v.

Loading and testing protocol

Around 50 µL of gel is loaded onto the stationary bottom plate of the rheometer preheated at 20 °C. By stepwise lowering the gap between the two plates, the sample is compressed and forced to spread over the geometry so that the gap is completely filled. Equilibration of the sample is followed by monitoring the evolution of normal force, storage and loss moduli with time, under small amplitude oscillatory shear. Rheological tests are started when both moduli reach constant values and normal force has relaxed to < 0.05 N.

Bibliography

[1] Seiffert, S.; Sprakel, J. *Chem. Soc. Rev.* **2012**, *41*, 909–930.
[2] Yu, G.; Yan, X.; Han, C.; Huang, F. *Chem. Soc. Rev.* **2013**, *42*, 6697–6722.
[3] Hackelbusch, S.; Rossow, T.; van Assenbergh, P.; Seiffert, S. *Macromolecules* **2013**, *46*, 6273–6286.
[4] Rossow, T.; Habicht, A.; Seiffert, S. *Macromolecules* **2014**, *47*, 6473–6482.
[5] Wei, Z.; Yang, J. H.; Zhou, J.; Xu, F.; Zrinyi, M.; Dussault, P. H.; Osada, Y.; Chen, Y. M. *Chem. Soc. Rev.* **2014**, *43*, 8114–8131.
[6] Appel, E. A.; del Barrio, J.; Loh, X. J.; Scherman, O. A. *Chem. Soc. Rev.* **2012**, *41*, 6195–6214.
[7] Noro, A.; Hayashi, M.; Matsushita, Y. *Soft Matter* **2012**, *8*, 2416–2429.
[8] Loveless, D.; Jeon, S.; Craig, S. *Macromolecules* **2005**, *38*, 10171–10177.
[9] Yount, W. C.; Loveless, D. M.; Craig, S. L. *J. Am. Chem. Soc.* **2005**, *127*, 14488–14496.
[10] Loveless, D. M.; Jeon, S. L.; Craig, S. L. *J. Mater. Chem.* **2007**, *17*, 56–61.
[11] Xu, D. H.; Craig, S. L. *J. Phys. Chem. Lett.* **2010**, *1*, 1683–1686.
[12] Piepenbrock, M. O. M.; Lloyd, G. O.; Clarke, N.; Steed, J. W. *Chem. Rev.* **2010**, *110*, 1960–2004.
[13] Rubinstein, M.; Semenov, A. *Macromolecules* **2001**, *34*, 1058–1068.
[14] Jongschaap, R.; Wientjes, R.; Duits, M.; Mellema, J. *Macromolecules* **2001**, *34*, 1031–1038.

[15] Rubinstein, M.; Dobrynin, A. V. *Curr. Opin. Colloid Interface Sci.* **1999**, *4*, 83–87.
[16] Tanaka, F.; Edwards, S. F. *J. Non-Newtonian Fluid Mech.* **1992**, *43*, 247–271.
[17] Hietala, S.; Strandman, S.; Jarvi, P.; Torkkeli, M.; Jankova, K.; Hvilsted, S.; Tenhu, H. *Macromolecules* **2009**, *42*, 1726–1732.
[18] Xu, D. H.; Hawk, L. L.; Loveless, D. M.; Jeon, S. L.; Craig, S. L. *Macromolecules* **2010**, *43*, 3556–3565.
[19] Xu, D.; Craig, S. L. *Macromolecules* **2011**, *44*, 7478–7488.
[20] Tapadia, P.; Ravindranath, S.; Wang, S.-Q. *Phys. Rev. Lett.* **2006**, *96*, 196001.
[21] Olmsted, P. D. *Rheol. Acta* **2008**, *47*, 283–300.
[22] Graham, M. D. *J. Rheol.* **1995**, *39*, 697–712.
[23] Larson, R. G. *Rheol. Acta* **1992**, *31*, 213–263.
[24] Groisman, A.; Steinberg, V. *Nature* **2000**, *405*, 53–55.
[25] Atalık, K.; Keunings, R. *J. Non-Newtonian Fluid Mech.* **2004**, *122*, 107–116.
[26] Hyun, K.; Wilhelm, M.; Klein, C. O.; Cho, K. S.; Nam, J. G.; Ahn, K. H.; Lee, S. J.; Ewoldt, R. H.; McKinley, G. H. *Prog. Polym. Sci.* **2011**, *36*, 1697–1753.
[27] Kujawa, P.; Watanabe, H.; Tanaka, F.; Winnik, F. M. *Eur. Phys. J. E* **2005**, *17*, 129–137.
[28] Pham, Q.; Russel, W.; Thibeault, J.; Lau, W. *Macromolecules* **1999**, *32*, 5139–5146.
[29] Annable, T.; Buscall, R.; Ettelaie, R. *Colloids Surf., A* **1996**, *112*, 97–116.
[30] Regalado, E. J.; Selb, J.; Candau, F. *Macromolecules* **1999**, *32*, 8580–8588.
[31] Koumakis, N.; Petekidis, G. *Soft Matter* **2011**, *7*, 2456–2470.
[32] Pham, K.; Petekidis, G.; Vlassopoulos, D.; Egelhaaf, S.; Poon, W.; Pusey, P. *J. Rheol.* **2008**, *52*, 649–676.
[33] Linemann, R.; Läuger, J.; Schmidt, G.; Kratzat, K.; Richtering, W. *Rheol. Acta* **1995**, *34*, 440–449.
[34] Eiser, E.; Molino, F.; Porte, G.; Diat, O. *Phys. Rev. E: Stat., Nonlinear, Soft Matter Phys.* **2000**, *61*, 6759–6764.
[35] Tsitsilianis, C.; Aubry, T.; Iliopoulos, I.; Norvez, S. *Macromolecules* **2010**, *43*, 7779–7784.
[36] Rogers, S. A.; Erwin, B. M.; Vlassopoulos, D.; Cloitre, M. *J. Rheol.* **2011**, *55*, 435–458.
[37] O'Lenick, T. G.; Jin, N.; Woodcock, J. W.; Zhao, B. *J. Phys. Chem. B* **2011**, *115*, 2870–2881.
[38] Rufier, C.; Collet, A.; Viguier, M.; Oberdisse, J.; Mora, S. *Macromolecules* **2008**, *41*, 5854–5862.
[39] Gohy, J.-F. *Adv. Polym. Sci.* **2005**, *190*, 65–136.
[40] Riess, G. *Prog. Polym. Sci.* **2003**, *28*, 1107–1170.
[41] Rodriguez-Hernandez, J.; Checot, F.; Gnanou, Y.; Lecommandoux, S.

Prog. Polym. Sci. **2005**, *30*, 691–724.
[42] Annable, T.; Buscall, R.; Ettelaie, R.; Whittlestone, D. *J. Rheol.* **1993**, *37*, 695–726.
[43] Nicolai, T.; Colombani, O.; Chassenieux, C. *Soft Matter* **2010**, *6*, 3111–3118.
[44] Hogg, R.; Wilkins, R. *J. Chem. Soc.* **1962**, 341–350.
[45] Holyer, R. H.; Hubbard, C. D.; Kettle, S. F. A.; Wilkins, R. G. *Inorg. Chem.* **1966**, *5*, 622–625.
[46] Argon, A. S.; Bessonov, M. *Polym. Eng. Sci.* **1977**, *17*, 174–182.

CHAPTER 11

CROSS-LINK DENSITY OF METALLO-SUPRAMOLECULAR MICELLAR GELS

Abstract

This chapter aims to control the magnitude of the viscoelastic response of supramolecular hydrogels built through the hierarchical assembly of hetero-telechelic copolymers. The influence of different variables, i.e.*, the temperature, the length of the associating copolymer, and its overall or effective concentration, on the rheological properties of those materials is investigated and discussed in term of cross-link density. In this respect, two distinct regimes are distinguished that correspond to the well percolated network, with a high cross-linking density, and the weakly percolated network, with a low cross-linking density.*

11.1 Overview

In the previous chapter, the rheological properties of associating hydrogels combining both transient hydrophobic and coordinative interactions were investigated, using polystyrene-*block*-poly(*N*-isopropylacrylamide) associating copolymers as model systems. When these materials were stressed under oscillatory shear, two distinct relaxation modes were distinguished, denoted τ_1 and τ_2. The main relaxation process was identified as corresponding to the fast exchange of hydrophobic stickers between micellar nano-structures (τ_1). On the other hand, a second relaxation, that matches the dissociation of the coordinative bridges between hydrophobic nodes, dictated the terminal flow of the materials when achievable experimentally (τ_2).

Besides dynamics, controlling the cross-link density of the transient network is of primary importance for tuning the macroscopic mechanical properties of supramolecular materials. [1] Increasing network density leads to an increase in the storage and loss moduli of the gel and can be accomplished by either increasing the concentration of cross-linkers, or by reducing the fraction of mechanically inactive cross-links. The latter consist of dangling chains and loops in the network, which do not contribute to the mechanical properties (Figure 11.1).

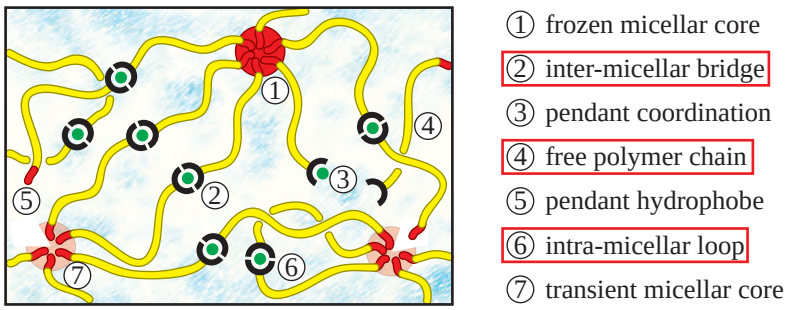

Figure 11.1 – Richness of network configurations in metallo-supramolecular micellar gels, with focus on the cross-link density.

In rheology, much of the fundamental knowledge related to polymer networks is built on the assumption of an ideal network structure. In such architectures, every polymer strand forms connections to other

strands, strengthening the resulting material. On the other hand, real networks invariably possess topological imperfections that negatively affect mechanical properties.[2] After decades of effort, quantification of the fraction of primary loops and dangling chains in end-linked materials was only achieved via site-selective network disassembly.[3] However, this method can only be applied for permanent networks since supramolecular analogues will always rearrange upon disassembly.

In physical networks, cross-links inevitably change to the dangling state at a rate that is correlated to the lifetime of the transient association.[4–6] Due to the reversibility of the association, a sticker can bind again to the same partner, resulting in no change, or to an available residue elsewhere, resulting in stress relaxation. In turn, the generated dynamic equilibrium dictates the number of dangling chains in the system.[7–9] Hence, such imperfections can be minimized when strong associations are formed between functional groups, which is here achieved with long hydrophobic stickers and slow-dissociating metal complexes. Accordingly, the probability to find free unbounded chains in the system is very low since the latter have a high tendency to associate to the supramolecular network, at least via one sticky end.

The simplest but also more investigated topological network imperfections thus consist in primary loops that form when a flexible polymer strand closes on itself without connecting to other chains (Figure 11.1).[2] In the case of both ends of a linker connecting the same network node, it provides no contribution to the modulus of the system. Indeed, such a chain is tied to the network at only one point and is thus not stressed by the applied mechanical force. In this continuity, only stress-carrying connections made between two different network nodes contribute to the macroscopic properties, *i.e.*, the modulus of the network.

11.2 Rheological characterization

In this chapter, we extend the rheological study on the behaviour of supramolecular hydrogels formed from PS-*b*-PNIPAAm-tpy associating copolymers, as model systems, in the semi-diluted non-entangled regime. The focus is on different parameters affecting the magnitude of the elastic and viscous responses of the gels under shear, like concentration. The results obtained are qualitatively interpreted in the context of transient

network theories. Although more quantitative data about the number of elastically active chains can be derived from rheology, such a detailed analysis is not provided here but could extend the discussion on results.

Among the investigated variables, a special interest is paid to temperature. Indeed, this factor contrastingly affects the viscoelastic response of gels in the low- and high-frequency regimes, at least in the investigated temperature range. Indeed, experiments are here performed within the limit of solubility of PNIPAAm chains, taking into account that the latter undergo a shrinking-type volume phase transition above 32 °C.[10,11]

11.2.1 Influence of the concentration

The concentration in associating copolymers is known to play a crucial role for the rheological properties of coordination micellar gels. In the diluted regime, telechelic polymer chains in solution lead mainly to flower-like micelles, resulting in no gelation.[12,13] Above the critical gel concentration, the flowers form a reversible network through multiple inter-micellar bridges. Increasing further the concentration in associating copolymer would enhance the formation of bridges between micellar cores, resulting into a net increase in the density of elastically active chains.[14] Practically, the viscoelastic response of the present hydrogels is measured as a function of oscillation frequency and strain amplitude at different concentrations in the semi-diluted non-entangled regime.

11.2.1.1 Oscillatory frequency sweep

At first, frequency sweeps are performed on hydrogels under shear amplitudes that ensure a linear response (Figures 11.2 and 11.3). The investigated materials consist first in a PS_{27}-*b*-$PNIPAAm_{300}$-tpy copolymer (numbers in subscript refer to the average degree of polymerization of each block) dissolved in Milli-Q water in presence of Ni(II) ions, to reach final concentrations of 3, 4, 5, 7 and 10 %w/v.

From those experiments, a significant impact of the concentration in associating polymer is evidenced on the apparent relaxation time scale of the network, τ_1. The latter is derived from the local maximum in loss modulus, G'', and shifts to lower frequency as the concentration increases (Figures 11.2 and 11.3). This concentration dependence is attributed to

the existence of super-bridges within the system, *i.e.*, strings of bridged micelles through which stress is transmitted.[9,15,16] As the concentration rises, a decrease in the length of those super-chains, which are further incorporated into the percolation structures of the network, leads to an increase in the measured relaxation time (τ_1).[17,18] As shown in Figure 11.4, this increase is particularly noticeable in the low concentration range, *i.e.*, from 3 to 5 %w/v, and becomes less appreciable at higher polymer contents.

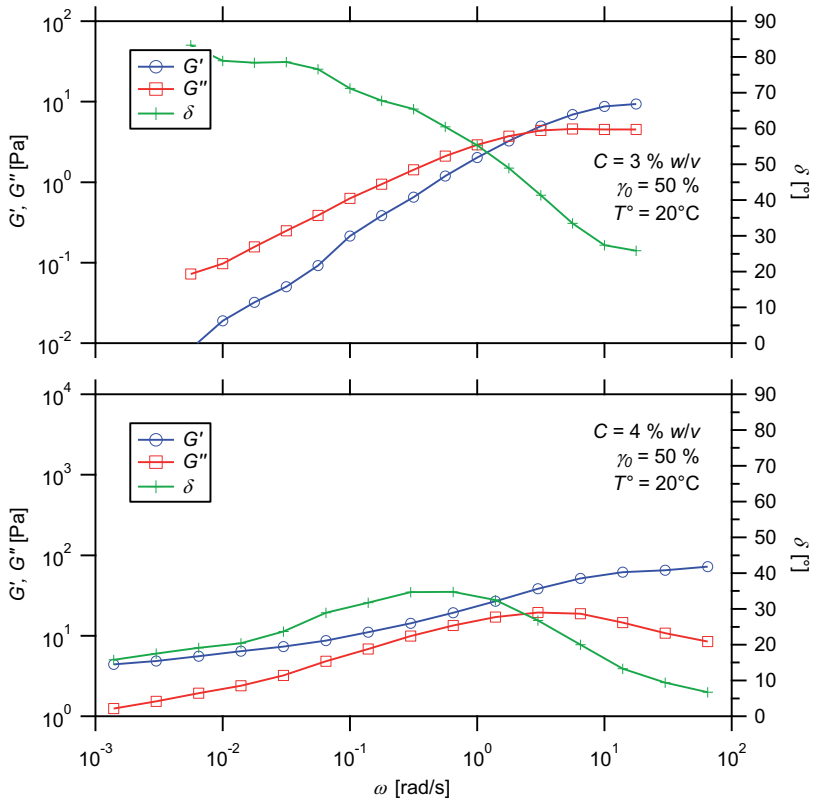

Figure 11.2 – Frequency dependence of dynamic moduli for hydrogels prepared from the PS_{27}-*b*-$PNIPAAm_{300}$-tpy copolymer and Ni(II) ions, at different concentrations.

As the concentration in hetero-telechelic polymer is reduced from 10 to 5 %w/v, both moduli are gradually shifted to lower values by nearly one order of magnitude (Figure 11.3). This shift occurs in the low- as well

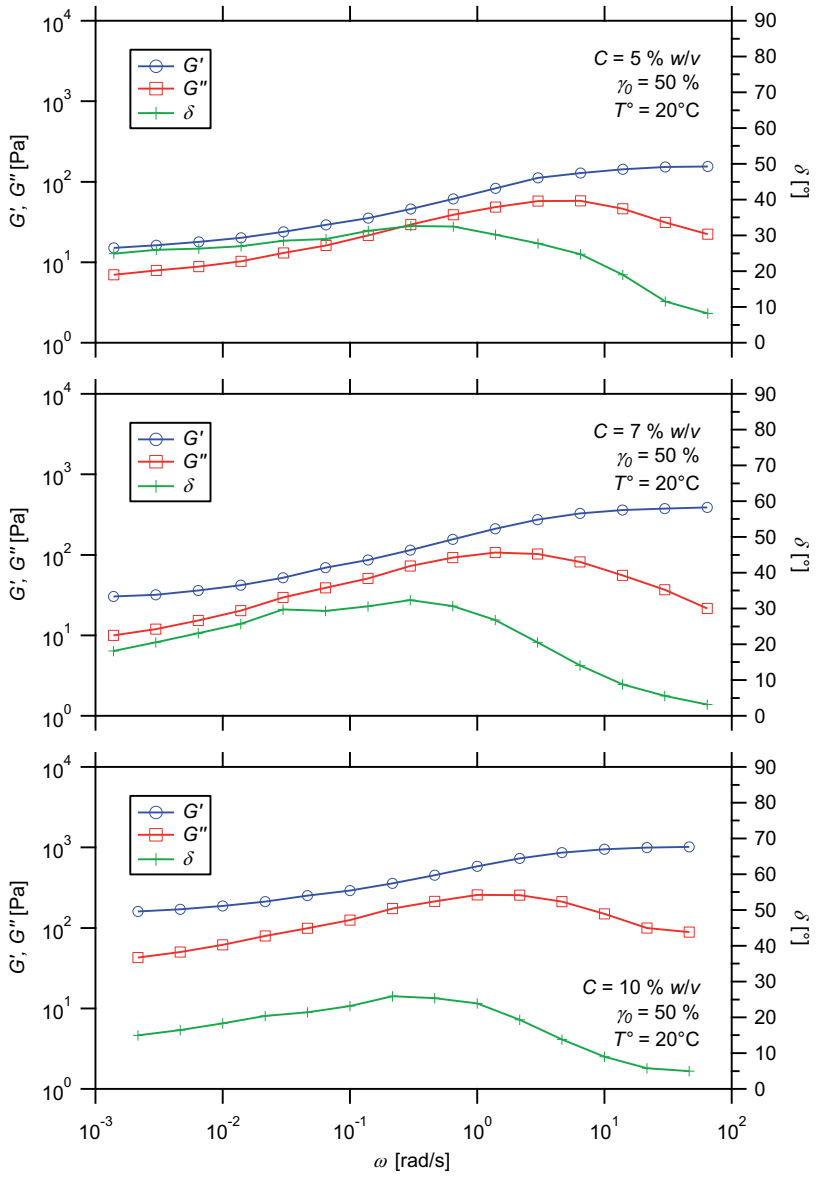

Figure 11.3 – Frequency dependence of dynamic moduli for hydrogels prepared from PS_{27}-*b*-$PNIPAAm_{300}$-tpy copolymer and Ni(II) ions, at different concentrations.

as in the high-frequency regime so that the general behaviour observed as function of the oscillation frequency remains essentially unchanged.

In this concentration range, the dependence of the viscoelastic properties thus tends to satisfy the classical scaling law relationships reported in the context of self-associating polymer gels (Figure 11.4).[19] In this respect, decreasing the density of mechanically active polymer strands within the network leads to a less elastic response to shear stress. These observations can be rationalized by taking into account the subsequent decrease in the proportion of mechanically active chains upon a drop in the total amount of associating polymers in the solution.

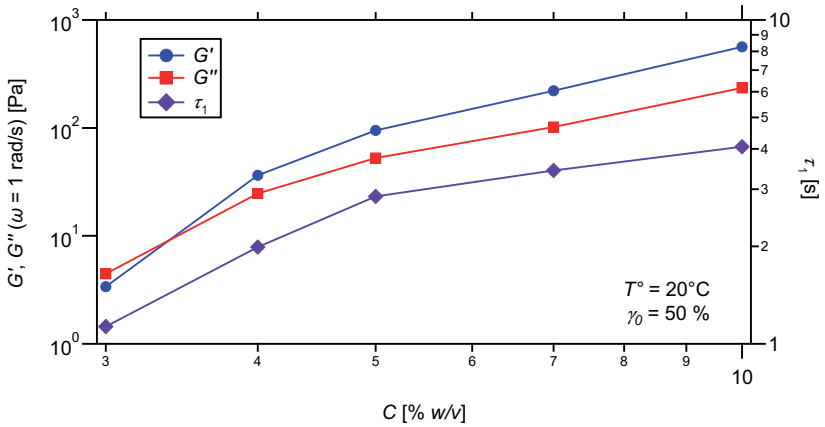

Figure 11.4 – Concentration dependence of the first relaxation time and dynamic moduli for hydrogels prepared from PS_{27}-*b*-$PNIPAAm_{300}$-tpy copolymer and Ni(II) ions.

Further decreasing the amount of associating copolymers is accompanied by an abrupt transition in the rheological behaviour of the material. As shown in Figure 11.2, the 3 %w/v hydrogel is characterized by a comparatively weak elastic response in the high-frequency plateau region, which is the signature of a soft material. As the oscillatory frequency is lowered, the dynamic moduli cross each other and further decline significantly while a low-frequency plateau becomes difficult to achieve experimentally. Hence, the 3 %w/v gel essentially presents the rheological features of a weak transient micellar gel, with a single relaxation mode (τ_1) reflecting the exchange of stress-carrying chains between hydrophobic cores. These observations can be rationalized by taking into account the change in network topology with concentration.[15] As the amount of associating copolymer decreases, the average distance between micellar aggregates increases so that the penalty for stretching the water-soluble

block to bridge aggregates via metal–ligand complexes becomes more severe.[20,21] As a result, the loop-to-bridge ratio increases within the network, leading to a pronounced decrease in the elastic response of the gel, which is particularly marked at low concentration.

According to the dependence of the rheological properties of the gels, two distinct regimes can be thus distinguished, which are the low- and high-concentration regimes. On one hand, the viscoelastic response of concentrated solutions shows a relatively weak, scalable dependence on concentration. On the other hand, the same dependency is more pronounced at low concentration, where the dynamic response of the gels markedly deviates from the simple scaling law.

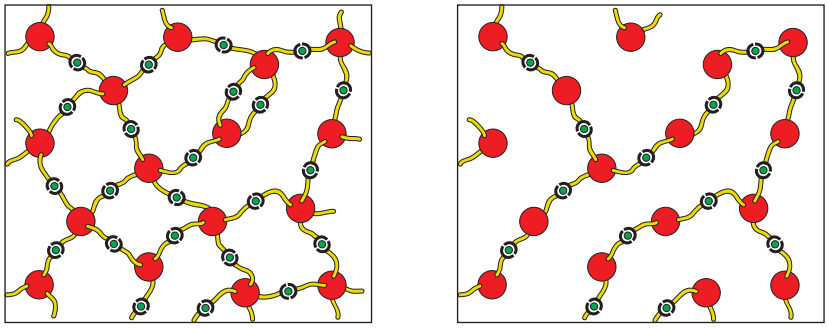

(a) Densely connected (b) Sparsely connected

Figure 11.5 – Schematics of coordination micellar networks with distinct cross-link densities.

The existence of distinct concentration regimes is in agreement with the theory proposed by Watanabe *et al.* in order to explain the concentration dependence of the rheological properties of telechelic associative polymer solutions.[22,23] Developed on the basis of experimental results obtained for aqueous solutions of hydrophobic ethoxylated urethanes, their model takes into account the effects of the average number of elastically active chains per micellar core. In the high-concentration regime, densely connected networks are formed since the number of bridging chains per core is rather large (Figure 11.5 (a)). On the opposite, only sparse, weakly percolated networks can be achieved at low polymer content. In such conditions, most of the hydrophobic cores indeed link only two bridging chains and cannot be considered as elastically active nodes

(Figure 11.5 (b)). As a consequence, the resulting network is mainly formed by super-bridged structures whereas the apparent proportion of stress-carrying chains within the system dramatically falls down.

11.2.1.2 Oscillatory strain sweep

The effect of the concentration in associating copolymer on the rheological properties of the PS-*b*-PNIPAAm-tpy hydrogels is further investigated by performing strain sweep experiments (Figure 11.6). Practically, the oscillation frequency is kept constant around the stress relaxation frequency of the material while the strain is gradually increased. Due

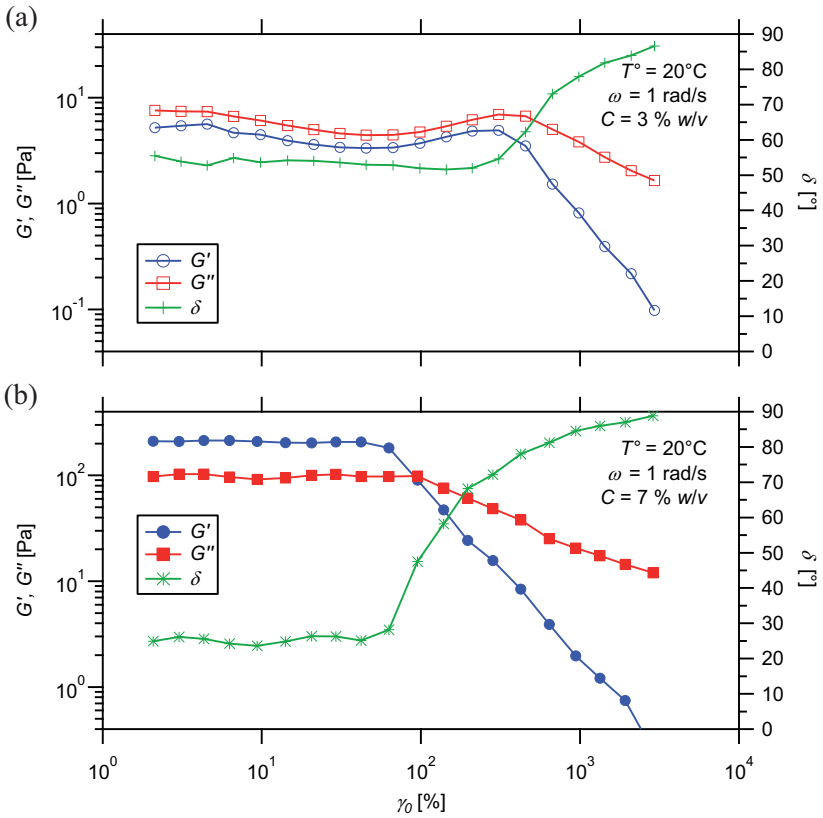

Figure 11.6 – Strain dependence of dynamic moduli for hydrogels prepared from PS_{27}-*b*-$PNIPAAm_{300}$-tpy copolymer and Ni(II) ions, at different concentrations.

to the mechanical breakage of transient cross-links, our materials are characterized by a reversible transition from a jelly-like solid to a viscous solution, when stress increases on sample. At low deformation, the materials respond elastically and the strain amplitude on sample increases linearly with the applied stress, which corresponds to the linear viscoelastic regime. At larger deformation, the viscous effects tend to dominate the material, dissipating the mechanical energy due to relaxations that occur on the time scale of the deformation. In this regime, stress on sample becomes almost independent of shear strain, which characterizes the non-linear response of the material.

In accordance with the results obtained from frequency sweeps, increasing the concentration in associating copolymer gives rise to a more pronounced response from the gels to shear. While elasticity dominates over viscous effects at high concentration, both become comparable in the low-concentration regime (Figure 11.6), meaning that the material has a greater tendency to flow. In return, this tendency allows the hydrogels to withstand larger deformations, due to the viscous flow that dissipates mechanical forces on the solicitation time scale. As illustrated in Figure 11.7 (a), the deformation at which yield occurs was found to decreases drastically as the amount of associating copolymers in the system is increased from 3 to 10 %w/v. In the high-concentration regime, the shear yield strain reaches a constant value that reflects the structural features of a densely cross-linked network. In agreement with an increasing cross-linking density of the network, the yield strength of the material is found to gradually rise with the concentration in associating copolymer in the gel (Figure 11.7 (b)).

According to theory of rubber elasticity,[24,25] the maximum degree of stretching of a network is given by the molecular weight, *i.e.*, the length, of the polymer segments between two branching nodes. In a densely connected network (Figure 11.5 (a)), the probability for an active polymer chain to be connected to a branching node at each extremity is high. Therefore, each individual chain is stressed by mechanical forces and inevitably detaches from transient nodes when the imposed deformation exceeds its fully stretched conformation. In a sparsely connected network (Figure 11.5 (b)), chains belong to super-bridge strands that can be further stretched before detaching from a network node. Indeed, each entire super-bridge has to be considered as a single effective chain,[9] which virtually increases the mean length of polymer segments between

two consecutive branching points of the network.

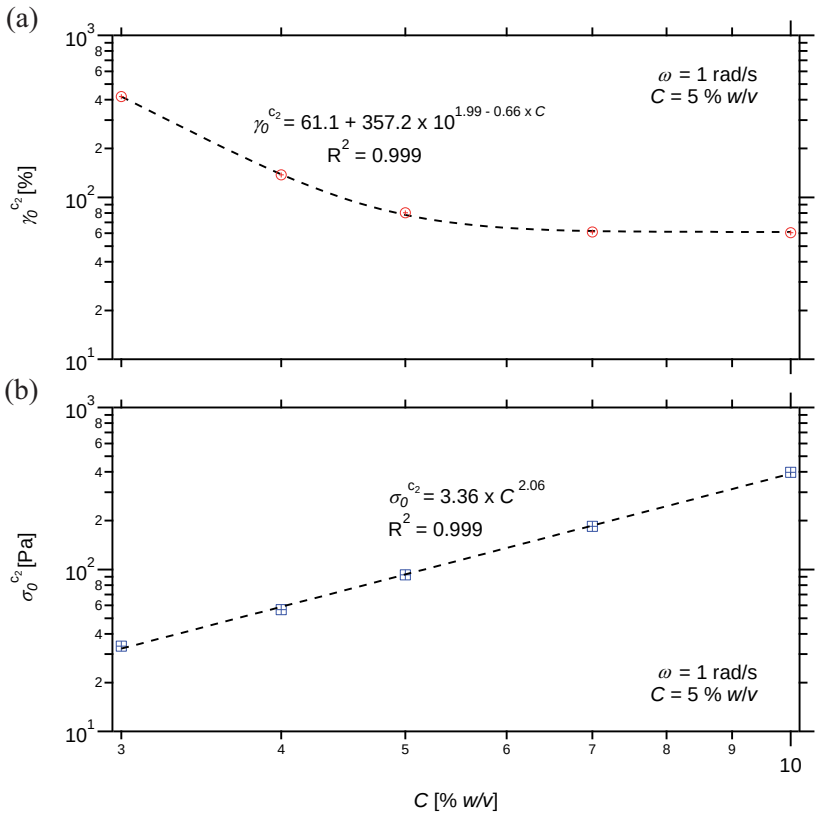

Figure 11.7 – Concentration dependence of (a) yield strain and (b) stress for hydrogels prepared from PS_{27}-*b*-$PNIPAAm_{300}$-tpy copolymer and Ni(II) ions.

In agreement, the rheological behaviour of the gels at the onset of destructuring is found to be markedly affected by the concentration in associating copolymer, as reported in Figure 11.6. At high polymer content, strain softening only is observed, both storage and loss moduli decreasing characteristically when the material is exposed to large amplitude oscillatory shear. In the low-concentration regime, the same material shows early softening as both dynamic moduli reach a local minimum around 40 % deformation, which might be due to weakening of the poorly percolated material. Then, a strong strain overshoot is observed at higher deformation rates, *i.e.*, G' and G'' exhibit strain

hardening followed by strain thinning,[26,27] which is as well observed when coming back to small amplitude deformation.

In agreement with the transient network theory,[28] strain hardening evidences a shear-induced increase of the density of elastically active chains through an increase in the proportion of bridging chains at the expense of intra-micellar loops. As suggested by Tam and coworkers,[18] this increase may be due to the incorporation of free micelles or higher aggregates of finite size into the percolated network, which in turn leads to a net shortening of the super-bridges. As shown in Figure 11.6, this particular shear response starts at a deformation that matches the yield of a correspondingly well-percolated network. As mentioned above, this shear strain marks the onset of chain withdrawal from the branching nodes, evidencing the presence of "normal" bridges and their role in the reorganization of the supramolecular network at lower concentration.

11.2.2 Influence of semi-telechelic

To probe the influence of the overall number of metal–ligand junctions on the rheological response of the gels, our strategy consists in controlling the proportion of ligand-functionalized copolymer within the system. In this respect, a semi-telechelic polystyrene-*block*-poly(*N*-isopropylacrylamide) copolymer has been synthesized according to the experimental conditions used for the synthesis of the PS_{27}-*b*-$PNIPAAm_{300}$-tpy copolymer. In practice, the terpyridine-modified chain transfer agent was simply replaced by the unmodified analogue in order to afford a semi-telechelic copolymer with the corresponding block lengths.

To prepared supramolecular hydrogels, both hetero- and semi-telechelic copolymers are first mixed and dissolved in Milli-Q water according to different proportions. Then, the amount of transition metal ions added to the micellar solutions is adjusted in order to match half an equivalent with respect to the terpyridine content. This strategy has been chosen in order to prevent inherent difficulties that would arise from a decrease of the 1/2 metal ion/ligand ratio. The presence of an excess of ligand-functionalized copolymers would add a higher level of complexity in the analysis of the dynamic viscoelastic response of gels. Indeed, deviating from the stoichiometric 1/2 ratio would change the association equilibrium of the complexes and might moreover induce secondary hydrophobic associations between free terpyridines.[29]

Following our strategy, different gels are elaborated with a total polymer content of 5 %w/v. Precisely, hetero- and semi-telechelic copolymers are mixed in 100:0, 80:20 and 60:40 ratios, which respectively correspond to effective contents in associating chains of 5, 4, and 3 %w/v. Indeed, only telechelic copolymers are involved in the formation of mechanically active chains within the network. On the other hand, semi-telechelic analogues can be regarded as dangling inactive chains and do not contribute to the network elasticity. As usually, the viscoelastic response of the accordingly obtained materials is investigated by performing frequency and amplitude strain sweeps.

11.2.2.1 Oscillatory frequency sweep

Frequency sweeps are first performed by following the evolution of the dynamic response of gels, under decreasing oscillation frequencies. As shown in Figure 11.8, both storage and loss moduli are found to drop as the proportion in hetero-telechelic polymer chains decreases. As mentioned above, this dependence is consistent with a diminution in the number of network forming chains, while the overall polymer content within the gels remains at 5 %w/v. Increasing the proportion of semi-telechelic polymer chains in the system thus results in an apparent dilution of the latter.

Accordingly, apparent low- and high-concentration regimes can be distinguished while varying the fraction in hetero-telechelic associating polymers. As mentioned above, the transition between those two regimes is clearly marked for slow oscillations, while a low-frequency plateau in modulus was more or less difficult to achieve depending on the composition of the system, as shown in Figure 11.8. In parallel, an enhanced formation of super-bridges is evidenced by a distinct shift in the apparent relaxation time characterizing the materials while increasing the content in semi-telechelic polymers.

In contrast with the samples where the overall content in associating copolymer is decreased, the corresponding gels prepared in the presence of semi-telechelic polymers show a more pronounced response to shear. In the investigated frequency range, both elastic and viscous moduli are indeed comparatively higher when the semi-telechelic polymers are added (Figure 11.8). Such a difference in the viscoelastic responses of the materials might be explained by taking into account the presence of

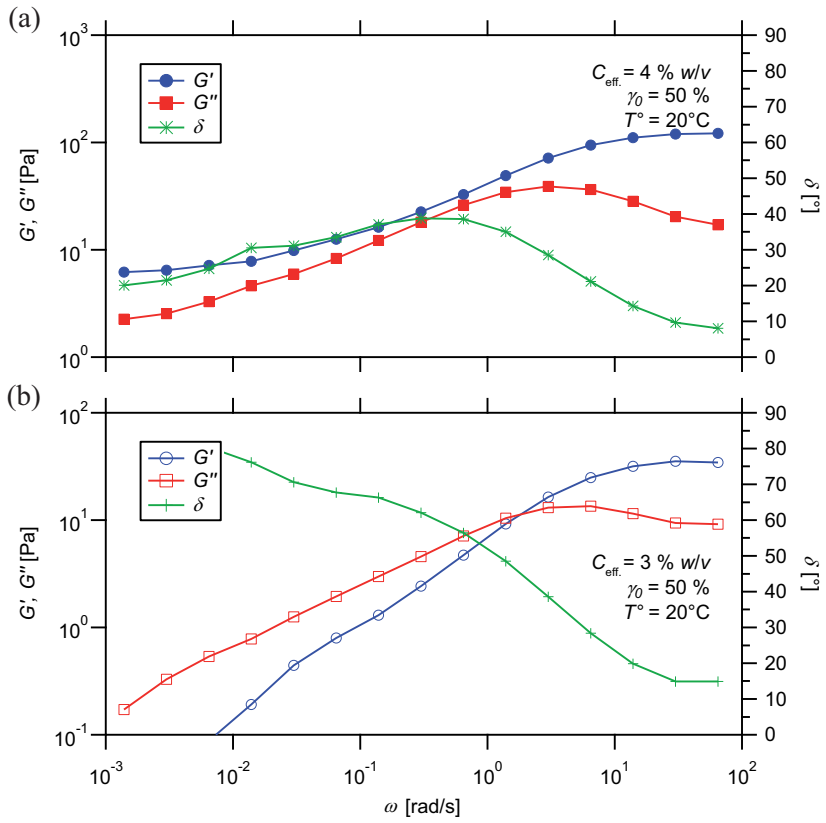

Figure 11.8 – Frequency dependence of dynamic moduli for hydrogels prepared from (a) 80:20 and (b) 60:40 mixture of hetero-telechelic and semi-telechelic copolymers, and Ni(II) ions.

pendant associating chains in the architecture of the network. Indeed, the latter counterbalances the loss in hetero-telechelic copolymers that would arise from a net diminution in the overall content in associating polymer. Hence, the number of micellar nano-structures in solution remains almost unaffected; only their functionality, *i.e.*, the average number of coronal chains terminated by a terpyridine ligand per micelle, is reduced. In turn, this allows the average distance between micellar aggregates to stay constant, which otherwise would increase the tendency of the associating copolymer chains to form mechanically inactive loops. At the same time, pendant uncapped chains might promote the formation of inter-micellar complexes between terpyridine end-functionalized coronal chains at the expense of intra-micellar complexation. Assum-

ing a homogeneous distribution of the semi-telechelics in the micelles, the latter might indeed sterically prevent the bending of the ligand end-capped coronal chains and hence the formation of intra-micellar loops.

11.2.2.2 Oscillatory strain sweep

In parallel, the influence of semi-telechelic copolymer chains on the rheological properties of micellar gels is investigated by amplitude strain sweeps. As shown in Figure 11.9, increasing the fraction of semi-telechelic chains lowers the viscoelastic response of gels, in agreement with the results obtained from frequency sweeps. Moreover, the large amplitude

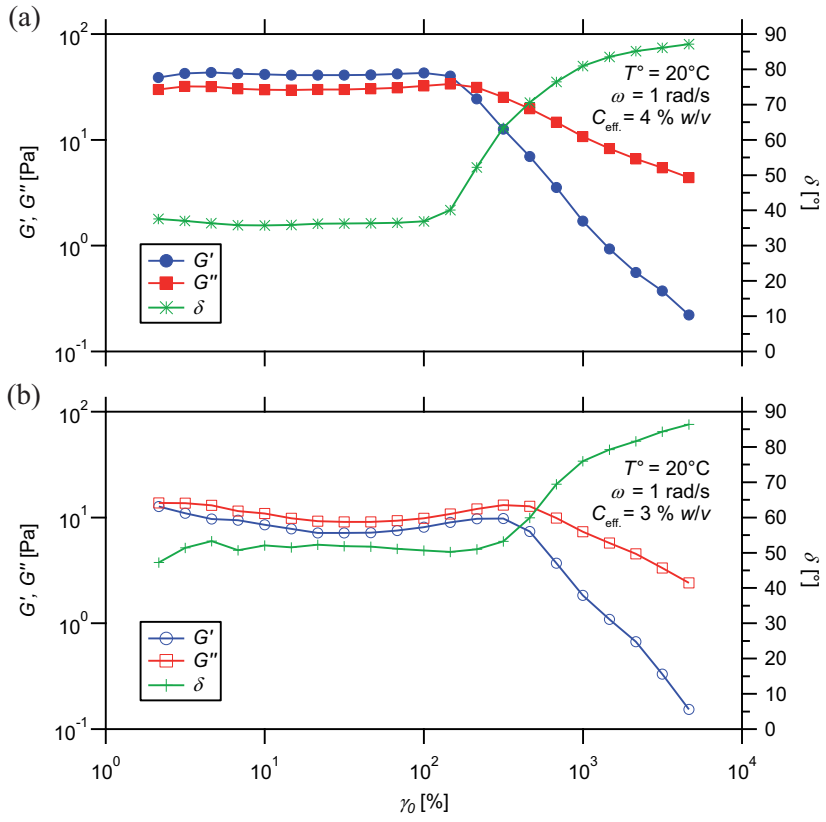

Figure 11.9 – Strain dependence of dynamic moduli for hydrogels prepared from (a) 80:20 and (b) 60:40 mixture of hetero-telechelic and semi-telechelic copolymers, and Ni(II) ions.

oscillatory shear behaviour of the gel is found to be markedly affected by the proportion of hetero-telechelic copolymer chains in the system. At high content, strain softening characterized the sample while both dynamic moduli drop characteristically when strain on samples exceeds the yield point. As the fraction in hetero-telechelic copolymers decreases, strain hardening becomes observable in G' and G'', which evidences a diminution in the cross-linking density of the network via the formation of super-bridges. As addressed above, this variation might be ascribed to a decreased functionality of the structural elements of the network, *i.e.*, the self-assembled micelles, which in turn limit the formation of active bridges between them.

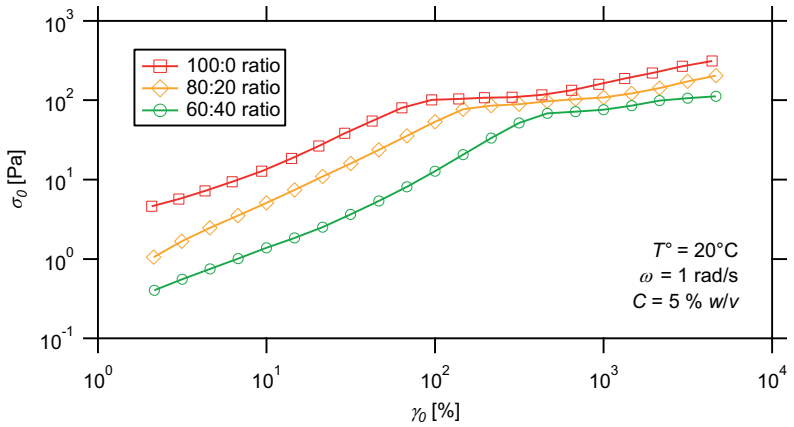

Figure 11.10 – Stress–strain relationships for hydrogels prepared from 100:0, 80:20 and 60:40 mixtures of hetero-telechelic and semi-telechelic copolymers, and Ni(II) ions.

The decrease in the cross-linking density of the self-assembled network is further observable when looking at the stress–strain relationships that describe the materials under shear. When increasing the fraction of semi-telechelics within the system, the yield strain of the accordingly obtained hydrogels dramatically rises, as evidenced by the rightward shift in stress–strain curves (Figure 11.10). As mentioned above, the yield strain of the material is determined by the average distance between transient cross-links, which reflects the cross-linking density of the network.[24,25] At the same time, the stress at which yield occurs is found to decrease significantly with the fraction in hetero-telechelic associating copolymer. The latter marks the end of the linear viscoelastic regime

and is proportional to the number of cross-linking points per unit volume.[30] In this respect, a diminution in the yield stress of the materials under shear further evidences a drop in the number of stress-carrying segments within the network.

11.2.3 Influence of hydrophile length

The influence of the length of the water-soluble segment is investigated by comparing the rheological properties of hydrogels prepared from associating copolymers exhibiting equivalent polystyrene block but different length of the hydrophilic segment. The hydrophilic–hydrophobic balance in the hydrogels is thus varied significantly.

11.2.3.1 Oscillatory frequency sweep

At first, the influence of the length of the hydrophilic segment on the dynamic properties of gels is studied under frequency sweeps. Measurements are conducted on samples prepared from different associating copolymers, *i.e.*, the PS_{27}-*b*-$PNIPAAm_{300}$-tpy and the PS_{27}-*b*-$PNIPAAm_{235}$-tpy, in combination with Ni(II) ions (Figure 11.11).

Experimentally, no significant change in the first relaxation time, τ_1, characterizing the materials under shear is observed while varying the length of the water-soluble segment. As demonstrated in the previous chapter, this relaxation process is attributed to the dissociation and exchange of the associating polymer chains between transient micellar cores. This relaxation mode thus proceeds at a rate that is mainly dictated by the length of the hydrophobic core-forming segment, *i.e.*, the polystyrene sticker, which is kept constant here.

If the relaxation process itself shows a relatively weak dependence on the length of the hydrophilic segment, the magnitude of the viscoelastic response of the materials is more deeply affected. In the high-frequency regime, nearly half a decade decrease is noticeable in the elastic plateau modulus while decreasing the length of the hydrophilic segment. In the low-frequency regime, this decrease is even more pronounced so that a crossover of the dynamic moduli is observed in the case of the PS_{27}-*b*-$PNIPAAm_{235}$-tpy associating copolymer (Figure 11.11).

Both observations indicate an increase in the density of mechanically active chains upon increasing the length of the associating segments. In accordance with an increase in radius of micelles (Figure 9.11), a long hydrophilic block acts in favour of the formation of elastically active bridges between micellar cores. Indeed, the tendency for the associating copolymer chains to loop back in the same hydrophobic core decreases significantly while increasing the length of the soluble chains. [31–34]

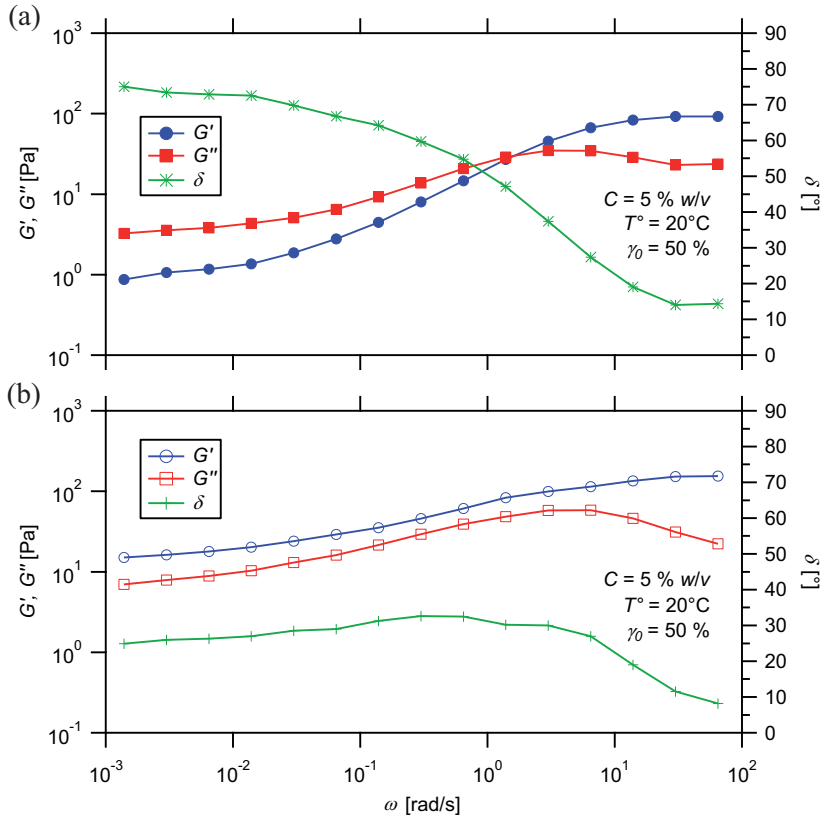

Figure 11.11 – Frequency dependence of dynamic moduli for hydrogels prepared from (a) PS_{27}-*b*-$PNIPAAm_{235}$-tpy or (b) PS_{27}-*b*-$PNIPAAm_{300}$-tpy copolymer and Ni(II) ions.

In the low-frequency regime, the small variation (*ca.* $< 25\%$) of the PNIPAAm length has a more pronounced effect since in this regime the network further relaxes stress through the dissociation of hydrophobes from micellar nodes. Indeed, this relaxation dramatically weakens the

viscoelastic response of the hydrogels. Hence, an additional diminution in the number of bridges between micellar nodes results in a tremendous decrease in the value of the low-frequency plateau modulus.

11.2.3.2 Oscillatory strain sweep

The effect of the hydrophilic block length on the mechanical properties of metallo-supramolecular micellar hydrogels is further investigated by strain sweep experiments. Measurements are conducted on samples prepared from PS_{27}-*b*-$PNIPAAm_{300}$-tpy and PS_{27}-*b*-$PNIPAAm_{235}$-tpy associating copolymers, both in combination with nickel(II) metal ions.

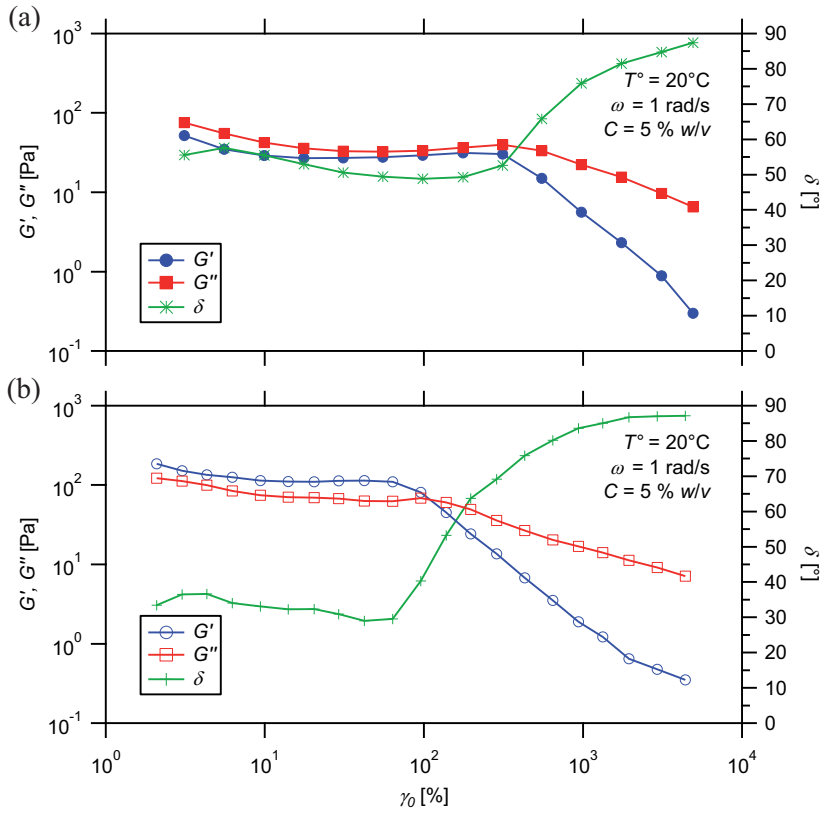

Figure 11.12 – Strain dependence of dynamic moduli for hydrogels prepared from (a) PS_{27}-*b*-$PNIPAAm_{235}$-tpy or (b) PS_{27}-*b*-$PNIPAAm_{300}$-tpy copolymer and Ni(II) ions.

As revealed in Figure 11.12, the viscoelastic response of the materials is deeply affected by the length of the hydrophilic block. The gel prepared from the associating copolymer showing a longer soluble block is characterized by higher values for both elastic and viscous modulus. In addition, the same gel shows a more elastic response to shear strain, which is in accordance with the results obtained from frequency sweep measurements. However, no change in the large amplitude shear behaviour of the gel is observed when varying the length of the PNIPAAm segment. Indeed, strain softening only occurs for the different samples under high strain conditions, both moduli decreasing characteristically above the yield point.

Last but not least, varying the size of the water-soluble block affects the yield strength of the hydrogels in shear. As clearly shown in Figure 11.12, the onset of network destructuring is found to increase drastically when the length of the hydrophilic segment is reduced. This observation provides further evidence of a decrease in the number of elastically active bridges between hydrophobic nodes in the gel.

11.2.4 Influence of temperature

So far, temperature is known to markedly affect the dynamics of transient interactions. Indeed, their dissociation mechanism generally follows an activated process that classically speeds up when temperature rises, as theoretically predicted by the Arrhenius relationship. In the present system, the temperature plays an additional role by determining the quality of water as a solvent for PNIPAAm chains.

As revealed by DLS measurements conducted on PS_{27}-*b*-$PNIPAAm_{300}$-tpy copolymer solution (Figure 9.13), a continuous decrease in the apparent hydrodynamic radius of the micelles is observed upon heating, in the presence as well as in the absence of transition metal ions. In agreement with a previous study,[35] this observation can be rationalized by the progressive deswelling of PNIPAAm coronal chains upon heating, in a temperature range that matches the limit of solubility of the latter. By varying the temperature from 8 to 28 °C, the apparent hydrodynamic radius of micelles in solution is reduced of about 20 %, which is attributed to the deswelling of the thermo-sensitive coronal chains (Figure 9.13).

Having those considerations in mind, the influence of the temper-

ature on the mechanical behaviour of the supramolecular hydrogels is investigated by rotational rheometry. In practice, measurements are conducted within the limit of solubility of the PNIPAAm block, *i.e.*, below its critical solubility temperature, which is about 32 °C.[10,11] Above this temperature, the precipitation of the thermo-sensitive chains forces the gel to phase separate, which is investigated in the next chapter.

11.2.4.1 Oscillatory frequency sweep

The thermal dependence of the dynamic mechanical properties of the associating networks is first investigated by conducting frequency sweeps on gels at various temperatures. Measurements are carried out under strain control for different concentrations by recording the evolution of dynamic moduli under decreasing frequency.

As illustrated in Figure 11.13 for a 5 %w/v gel, a diminution in the apparent relaxation frequency ($1/\tau_1$) is observed upon heating, the local maximum in G'' monotonously shifting to higher frequencies. Indeed, stress relaxation within the material occurs mainly via the dissociation of elastically active transient cross-links and the subsequent motion of the polymer chains. In this respect, providing thermal energy to the system enhances the dissipation of mechanical forces and leads to a decrease in the apparent relaxation time characterizing the material under shear.

When plotted against temperature (Figure 11.14), the apparent relaxation time of the transient networks shows an exponential decrease with a slope that is related to the activation energy, E_a, for this relaxation mode, *i.e.*, the exchange of hydrophobes between micellar nodes. From the temperature dependences of relaxation times, activation energies of around 70 kJ/mol are determined for the breaking and exchange of the polymer chains, which match reversible processes, in agreement with literature values. For example, activation energies of 100 kJ/mol have been reported by Mattice *et al.* for the exchange of unimer chains between oligostyrene-*block*-poly(ethylene oxide) micelles in aqueous solution.[36]

As reported in Table 11.1, the values of activation energies are found to increase with the length of the polystyrene block. Indeed, longer hydrophobes favour the formation of more stable, ultimately frozen micellar cores, which in turn increases the energy barrier to extract a chain

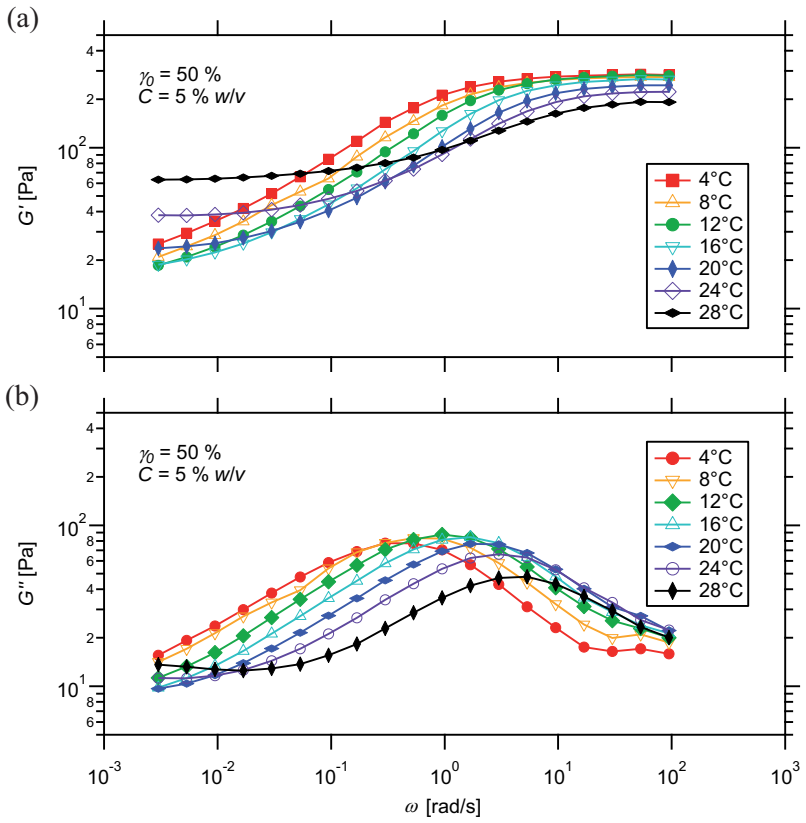

Figure 11.13 – Frequency dependence of (a) elastic and (b) viscous moduli for a hydrogel prepared from PS_{27}-*b*-$PNIPAAm_{300}$-tpy copolymer and Ni(II) ions, at different temperatures.

segment.[37] On the other hand, the activation energies show no dependence on the metal ions forming metallo-bridges between the micelles, which evidences their very small contribution, if any, to this relaxation mode. Last but not least, varying the amount of associative copolymer in the gels reveals an effect of the concentration on the rate at which samples relax stress. This effect was particularly marked when increasing the concentration of copolymer in the solution from 3 to 5 %w/v, which in fact corresponds to the transition between the low- and high-concentration regimes. As reported in Table 11.1, the apparent energy barrier for the extraction of the hydrophobic segment is found to rise as the concentration in associating copolymers decreases in the solution.

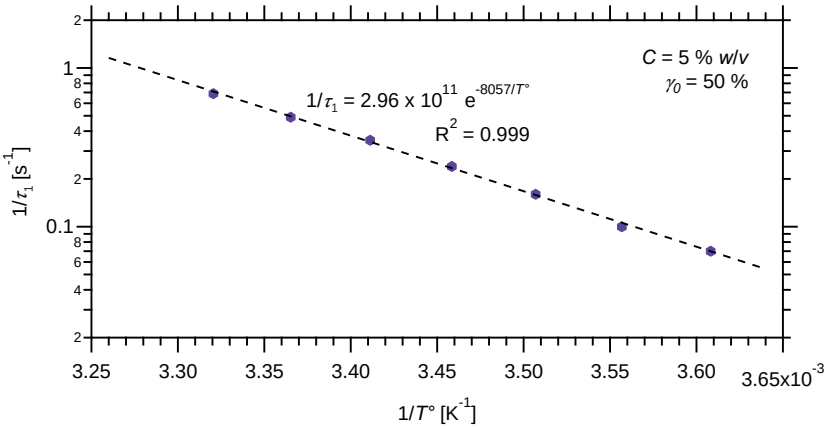

Figure 11.14 – Arrhenius plot of the apparent relaxation rate for hydrogels prepared from the PS_{27}-*b*-$PNIPAAm_{300}$-tpy copolymer and Ni(II) ions.

Above a given temperature, a gradual decrease in the high-frequency plateau elastic modulus might be additionally observed upon heating (Figure 11.13). According to the transient network theory,[28] the assumed value for G' in this regime is expressed as the product of the

Table 11.1 – Kinetic parameters for the apparent relaxation mode of supramolecular hydrogels prepared from different associative copolymers and transition metal ions, at various concentrations.

Associating copolymer	Conc. [%w/v]	Metal ion	$A \times 10^{-10}$ [s^{-1}]	E_a [kJ/mol]
PS_{15}-*b*-$PNIPAAm_{235}$-tpy	5	Ni(II)	11.9	59.2 ± 0.6
PS_{22}-*b*-$PNIPAAm_{235}$-tpy	5	Ni(II)	21.7	63.6 ± 0.4
PS_{27}-*b*-$PNIPAAm_{235}$-tpy	5	Ni(II)	133	69.0 ± 0.4
PS_{35}-*b*-$PNIPAAm_{235}$-tpy	5	Ni(II)	9620	82.5 ± 0.7
PS_{27}-*b*-$PNIPAAm_{300}$-tpy	3	Ni(II)	5000	77.2 ± 0.4
PS_{27}-*b*-$PNIPAAm_{300}$-tpy	5	Ni(II)	98.1	69.8 ± 0.8
PS_{27}-*b*-$PNIPAAm_{300}$-tpy	7	Ni(II)	38.4	68.0 ± 0.9
PS_{27}-*b*-$PNIPAAm_{300}$-tpy	10	Ni(II)	13.4	65.9 ± 0.9
PS_{27}-*b*-$PNIPAAm_{300}$-tpy	5	Fe(II)	89.5	68.8 ± 0.8
PS_{27}-*b*-$PNIPAAm_{300}$-tpy	5	Co(II)	100.5	69.6 ± 0.9

A, pre-exponential factor; E_a, activation energy

number density of elastically active network strands and the stored energy per strand, *i.e.*, the thermal agitation energy. Thus, a decrease in the high-frequency plateau modulus brings here a clear evidence of a net diminution in the number of elastically effective bridges between micelles within the network.

The latter assumption can be rationally explained by taking into account a variation in the swelling degree of the thermo-sensitive chains in this temperature range, as determined by light scattering technique (Figure 9.13). At low temperature, the extended conformation of the associating copolymer chains would largely favour the formation of elastically active bridges between hydrophobic cores.[38] As the temperature rises, the progressive deswelling of PNIPAAm chains triggers the formation of inactive intra-micellar loops at the expense of inter-micellar bridges (Figure 11.15). Indeed, this conformational adaptation avoids the free energy penalty for stretching the PNIPAAm chains in a solvent of decreasing quality in order to bridge two adjacent hydrophobic nodes. In practice, this hypothesis is strongly supported by the aforediscussed results obtained when varying the length of the hydrophilic segment, which show that inter-micellar bridges are favoured for longer associating polymers.

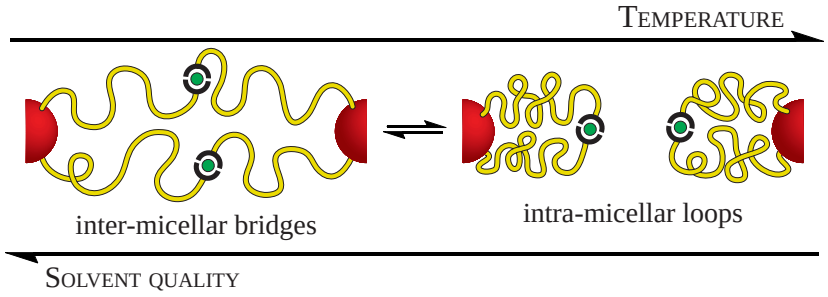

Figure 11.15 – Schematic of the thermo-induced bridge-to-loop conversion in thermo-sensitive coordination micellar gels.

Theoretically, the energy price to pay for stretching the soluble chains between two adjacent PS cores would depend on the average distance between the latter. To test this proposal, the same frequency sweep measurements are conducted on gels at different concentrations to probe the thermal dependence of their viscoelastic response (Figures 11.16 and 11.17). In this respect, decreasing the amount of associating copolymer

in solution would increase the average distance between micellar aggregates and hence accentuate the effect of heating on the number of elastically active chains. In accordance, the diminution in the high-frequency plateau storage modulus is profoundly marked for the gel prepared at a concentration of 3 %w/v (Figure 11.16). On the other hand, the same effect is not observed for the 10 %w/v analogue (Figure 11.17), at least in the investigated temperature range.

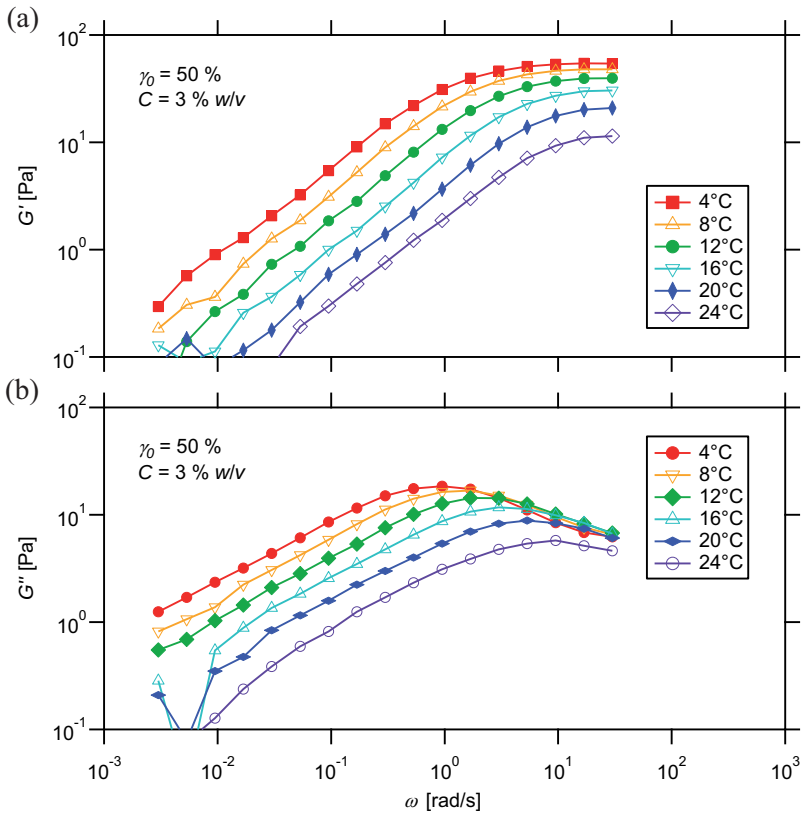

Figure 11.16 – Frequency dependence of (a) elastic and (b) viscous moduli for a 3 %w/v hydrogel prepared from PS_{27}-*b*-$PNIPAAm_{300}$-tpy copolymer and Ni(II) ions, at different temperatures.

As summarized in Figure 11.18, the temperature threshold, above which the thermal-shrinkage of PNIPAAm chains induces a bridge-to-loop conversion within the micellar network and thus a drop in the elastic modulus, shows a clear dependence on the concentration in asso-

ciating copolymer. In the low-concentration regime, the dilution of the system forces the soluble chains to adopt an extended conformation in order to bridge two different polystyrene cores. As a result, this primary conformational stress causes the number density of mechanically active bridges to inevitably drop upon heating. At higher concentrations, the decreasing average distance between micellar cores increases the conformational freedom of active strands which allows them to withstand temperature changes and thus delays the thermally induced bridge-to-loop conversion. In those situations, the threshold for the bridge-to-loop conversion would correspond to the temperature at which the associated gain in conformational entropy counterbalances the energy penalty for stretching the active strand to span the hydrophobic cores.

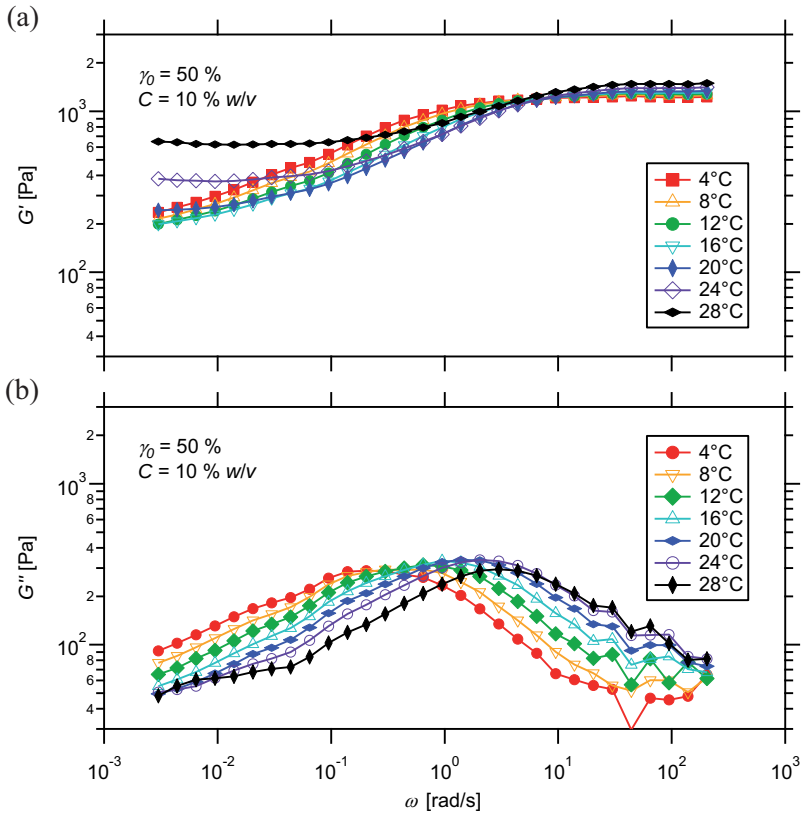

Figure 11.17 – Frequency dependence of (a) elastic and (b) viscous moduli for a 10 %w/v hydrogel prepared from PS_{27}-*b*-$PNIPAAm_{300}$-tpy copolymer and Ni(II) ions, at different temperatures.

As illustrated in Figure 11.13, the low-frequency plateau value for storage modulus is also found to undergo a sharp increase upon warming, so that the transition between the low- and high-frequency regimes becomes less pronounced. In contrast with the high-frequency measurements, the influence of temperature on the elastic response of the gels is visible even at high concentration (Figure 11.17). On the other hand, the same influence is not visible at low concentration since a low-frequency plateau is difficult to achieve in this regime (Figure 11.17). This unique thermo-response of the gels at low frequency can be further rationalized through the progressive deswelling of PNIPAAm chains upon temperature rises, which progressively shields the transient micellar nodes and reinforces them mechanically. The low-frequency viscoelastic response of the materials benefits from this shielding since it limits the stress relaxation that occurs on the time scale of the detachment, and thus the subsequent exchange of associating chains between micellar nodes.

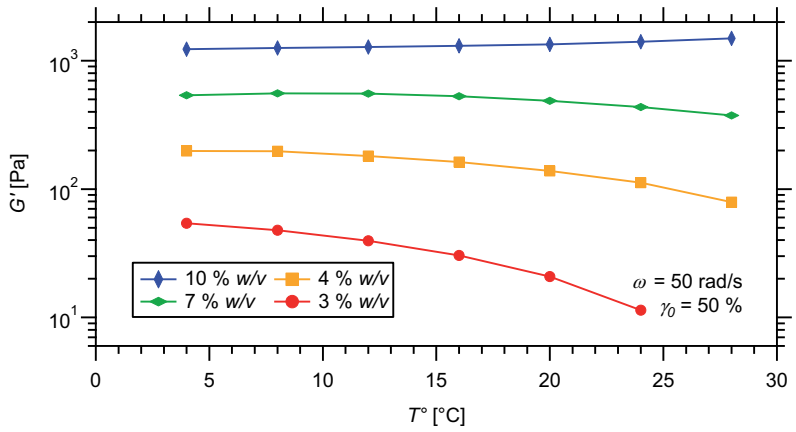

Figure 11.18 – Thermal dependence of the elastic plateau modulus for hydrogels prepared from PS_{27}-*b*-$PNIPAAm_{300}$-tpy copolymer and Ni(II) ions, at different concentrations.

11.2.4.2 Oscillatory strain sweep

The temperature dependence of the viscoelastic response of supramolecular hydrogels is then further investigated by carrying out amplitude sweeps at various temperatures. In agreement with frequency sweep measurements, the thermal response of the present materials is

particularly marked at low concentration. Hence, strain sweep measurements performed on 3 %w/v hydrogels reveal a clear dependence of their viscoelastic properties, both linear storage and loss moduli dramatically falling down as temperature increases (Figure 11.19).

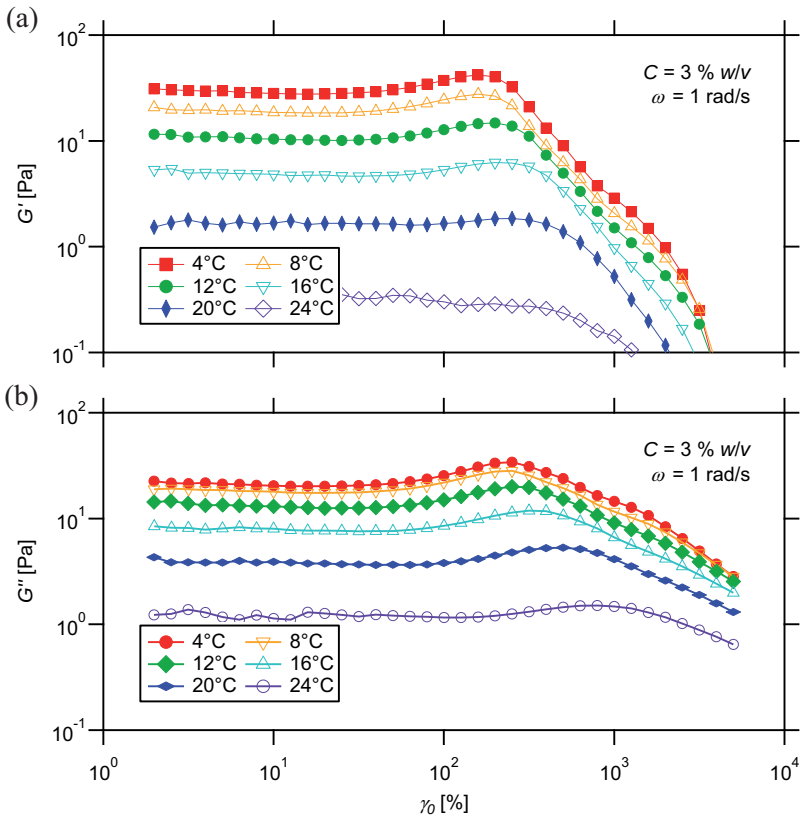

Figure 11.19 – Strain dependence of (a) elastic and (b) viscous moduli for a hydrogel prepared from PS_{27}-*b*-$PNIPAAm_{300}$-tpy copolymer and Ni(II) ions, at different temperatures.

Beyond the linear response of the gels, their non-linear viscoelastic behaviour at the onset of breaking is also found to be markedly affected by thermal changes. At low temperature, both dynamic moduli exhibit strain hardening followed by the Newtonian viscous flow of the material. Upon heating, strain hardening becomes less pronounced, especially in elastic modulus, until strain softening only is achieved under large amplitude oscillatory shear.

Critical shear strains and stresses that mark the limit between supramolecular gels and viscous solutions are also found to be highly temperature dependent. As illustrated in Figure 11.20 (a), the amplitudes of deformation that the transient networks can withstand before destructuring dramatically rise at elevated temperatures. On the other hand, the polymer gels lose their cross-linked structures when subjected to lower stress. The stress at which yield occurs is found to decrease linearly while increasing the temperature (Figure 11.20 (b)).

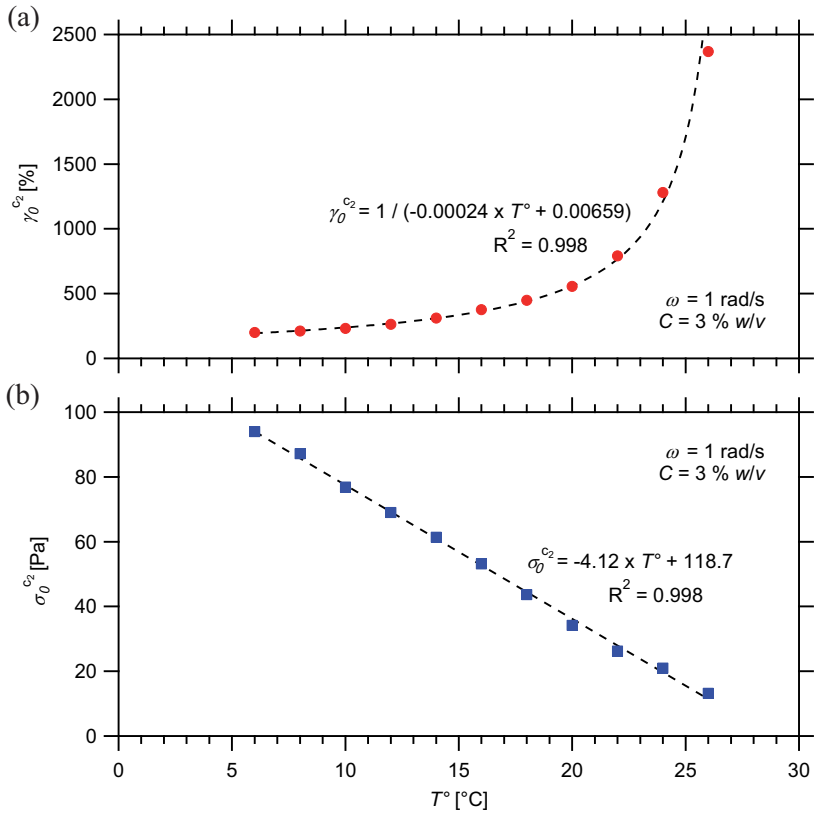

Figure 11.20 – Thermal dependence of (a) yield strain and (b) stress for hydrogels prepared from PS_{27}-*b*-$PNIPAAm_{300}$-tpy copolymer and Ni(II) ions.

Those relationships clearly indicate a decrease in the cross-linking density of the micellar network. As the cross-linking density decreases, the average molecular weight of polymer segments between the branch-

ing nodes indeed rises due to the formation of super-bridges, which in turn dictates the maximum degree of stretching of the network.[24,25] Moreover, the proposed diminution in the number of mechanically active segments is in accordance with the thermally induced conversion of elastically active bridges into intra-micellar loops. Upon heating, the number of stress-bearing junctions thus drops so that the maximum shear stress carried by the material decreases accordingly.

11.3 Summary

This chapter provided further insights in the understanding of the rheological properties of associating polymer gels. Non-covalent networks were formed through the self-assembly of hetero-telechelic linear poly(*N*-isopropylacrylamide)s, as a thermo-sensitive sequence. The latter were functionalized by a terpyridine ligand at one end, and carried a polystyrene sticker at the other extremity. In aqueous solution, they aggregated into transient micellar structures that were bridged together in the presence of transition metal ions.

Depending on the fraction of bridging chains, the hydrophobic cores acted as network nodes or as chain extenders, leading to the formation of super-bridges. Hence, two distinct regimes with specific rheological behaviours were distinguished, which correspond to sparsely and densely connected networks (Figure 11.21). When stressed by shear forces, the first one withstood larger amplitudes of deformation due to the enhanced conformational flexibility, and thus stretching ability, of the super-bridges. On the other hand, an increased cross-linking density of the network allowed the resulting material to carry higher shear stresses. Also, the rheological behaviour of the gels at the onset of yielding was markedly affected by the cross-link density of the latter. While strain softening was only observed for a densely connected network, a strong overshoot characterized the viscoelastic response of weakly percolated analogues.

As illustrated in Figure 11.21, tuning the amplitude of the viscoelastic response of the micellar networks was addressed by controlling the proportion of mechanically active bridges compared to intra-micellar loops. In this chapter, several factors were investigated that are the operating temperature, the length of the associating copolymer, and its overall

or effective concentration. In this respect, decreasing the effective concentration in associating copolymer led to weakly percolated hydrogels that show extended linear responses. In practice, this was achieved by decreasing the overall content in telechelic copolymers or by replacing a proportion of the latter with semi-telechelic copolymers.

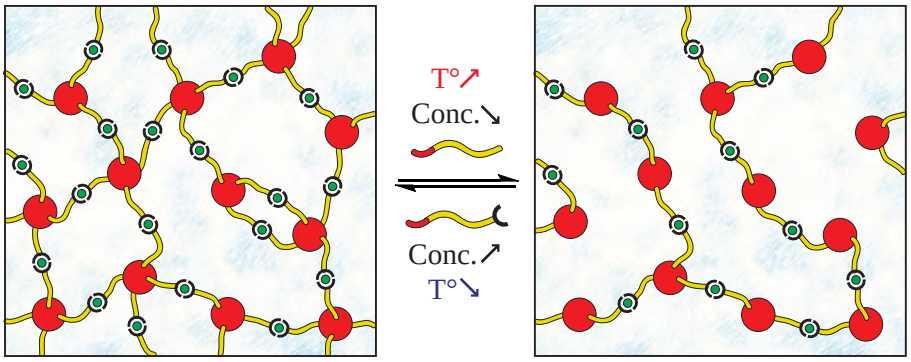

Figure 11.21 – Tuning the cross-link density of transient network constructed from associating polymers bearing a coordinating moiety and a hydrophobic segment.

Additionally, the formation of active bridges between micellar cores was favoured by increasing the length of associating copolymer chains, which was attributed to a lower tendency for looping back in the same hydrophobic core. Due to the thermo-induced volume change of poly(*N*-isopropylacrylamide) segment in aqueous media, the same effect was achieved by changing the external temperature. Precisely, an extended conformation of the associating copolymers was favoured at low temperature, which benefited to the high-frequency response of the gels. On the other hand, the deswelling of thermo-sensitive chains, and partial collapse onto micellar nodes, reduced stress relaxation that occurred through the dynamic exchange of hydrophobic segments, which in turn benefited to the low-frequency viscoelastic response. Along with the other investigated variables, such a unique thermo-response thus allowed an unprecedented control over the rheological properties of the gels in a large range of frequencies.

11.4 Experimental part

Materials

Terpyridine end-capped block copolymers are synthesized via sequential reversible addition–fragmentation chain transfer control radical copolymerization, as reported in a previous chapter. Nickel(II), iron(II) and cobalt(II) chloride salts are dried, kept in a glove box, and weighted under argon atmosphere.

Instrumentation

Shear rheological experiments are performed on a Kinexus Ultra (Malvern Instrument) rheometer equipped with a heat exchanger and modified with a solvent trap. Measurements are carried out at given temperatures, using a 20 mm plate–plate geometry, in a water saturated atmosphere in order to minimize evaporation of the solvent. The gap is adjusted between 50 and 250 µm so that the geometry is completely filled. Normal forces are checked to be relaxed prior any measurement.

Preparation of supramolecular gels

Hydrogels are prepared by mixing given amountst of block copolymer with Milli-Q water. The sealed reaction vessels are placed in a fridge and shaken periodically to form homogeneous concentrated solutions after a few days. The gels are then readily obtained by adding the stoichiometric amount of half an equivalent of transition metal ions (with respect to the terpyridine content) dissolved in defined amountst of Milli-Q water to each concentrated solutions. Lastly, the reaction vessels are placed again in the fridge over three days to ensure homogeneous gelation and stabilization of the gels. The final concentration of copolymers in samples varies in the semi-diluted regime, from 3 to 10 %w/v.

Loading and testing protocol

Around 50 µL of gel is loaded onto the stationary bottom plate of the rheometer preheated at 20 °C. By stepwise lowering the gap between

the two plates, the sample is compressed and forced to spread over the geometry so that the gap is completely filled. Equilibration of the sample is followed by monitoring the evolution of normal force, storage and loss moduli with time, under small amplitude oscillatory shear. Rheological tests are started when both moduli reach constant values and normal force has relaxed to $< 0.05\,\mathrm{N}$.

Bibliography

[1] Koenigs, M. M. E.; Pal, A.; Mortazavi, H.; Pawar, G. M.; Storm, C.; Sijbesma, R. P. *Macromolecules* **2014**, *47*, 2712–2717.
[2] Balazs, A. *Nature* **2013**, *493*, 172–173.
[3] Zhou, H.; Woo, J.; Cok, A.; Wang, M.; Olsen, B.; Johnson, J. *Proc. Natl. Acad. Sci. U. S. A.* **2012**, *109*, 19119–19124.
[4] Xu, D. H.; Hawk, L. L.; Loveless, D. M.; Jeon, S. L.; Craig, S. L. *Macromolecules* **2010**, *43*, 3556–3565.
[5] Xu, D. H.; Craig, S. L. *J. Phys. Chem. Lett.* **2010**, *1*, 1683–1686.
[6] Xu, D.; Craig, S. L. *Macromolecules* **2011**, *44*, 7478–7488.
[7] Semenov, A.; Joanny, J.; Khokhlov, A. *Macromolecules* **1995**, *28*, 1066–1075.
[8] Nguyen-Misra, M.; Mattice, W. L. *Macromolecules* **1995**, *28*, 1444–1457.
[9] Annable, T.; Buscall, R.; Ettelaie, R. *Colloids Surf., A* **1996**, *112*, 97–116.
[10] Hirokawa, Y.; Tanaka, T. *J. Chem. Phys.* **1984**, *81*, 6379–6380.
[11] Otake, K.; Inomata, H.; Konno, M.; Saito, S. *Macromolecules* **1990**, *23*, 283–289.
[12] Guillet, P.; Fustin, C.-A.; Mugemana, C.; Ott, C.; Schubert, U. S.; Gohy, J.-F. *Soft Matter* **2008**, *4*, 2278–2282.
[13] Kujawa, P.; Watanabe, H.; Tanaka, F.; Winnik, F. M. *Eur. Phys. J. E* **2005**, *17*, 129–137.
[14] Tanaka, F.; Koga, T. *Comput. Theor. Polym. Sci.* **2000**, *10*, 259–267.
[15] Annable, T.; Buscall, R.; Ettelaie, R.; Whittlestone, D. *J. Rheol.* **1993**, *37*, 695–726.
[16] Groot, R. D.; Agterof, W. G. *Macromolecules* **1995**, *28*, 6284–6295.
[17] Winnik, M.; Yekta, A. *Curr. Opin. Colloid Interface Sci.* **1997**, *2*, 424–436.
[18] Tam, K.; Jenkins, R.; Winnik, M.; Bassett, D. *Macromolecules* **1998**, *31*, 4149–4159.
[19] Rubinstein, M.; Semenov, A. *Macromolecules* **2001**, *34*, 1058–1068.
[20] Shen, W.; Kornfield, J. A.; Tirrell, D. A. *Soft Matter* **2007**, *3*, 99–107.
[21] Watanabe, H.; Sato, T.; Osaki, K. *Macromolecules* **2000**, *33*, 2545–2550.
[22] Uneyama, T.; Suzuki, S.; Watanabe, H. *Phys. Rev. E: Stat., Nonlinear, Soft Matter Phys.* **2012**, *86*, 031802.

[23] Suzuki, S.; Uneyama, T.; Watanabe, H. *Macromolecules* **2013**, *46*, 3497–3504.
[24] Edwards, S. *Br. Polym. J.* **1977**, *9*, 140–143.
[25] Boué, F.; Vilgis, T. *Colloid Polym. Sci.* **1986**, *264*, 285–291.
[26] Kim, S. H.; Sim, H. G.; Ahn, K. H.; Lee, S. J. *Korea-Aust. Rheol. J.* **2002**, *14*, 49–55.
[27] Sim, H.; Ahn, K.; Lee, S. *J. Non-Newtonian Fluid Mech.* **2003**, *112*, 237–250.
[28] Tanaka, F.; Edwards, S. F. *Macromolecules* **1992**, *25*, 1516–1523.
[29] Chiper, M.; Hoeppener, S.; Schubert, U. S.; Fustin, C.-A.; Gohy, J.-F. *Macromol. Chem. Phys.* **2010**, *211*, 2323–2330.
[30] Treloar, L. R. G. *The physics of rubber elasticity*; Oxford University Press: Oxford, 1975; pp xii, 310.
[31] Sliozberg, Y. R.; Andzelm, J. W.; Brennan, J. K.; Vanlandingham, M. R.; Pryamitsyn, V.; Ganesan, V. *J. Polym. Sci., Part B: Polym. Phys.* **2010**, *48*, 15–25.
[32] Zhou, Z.; Chu, B.; Nace, V. M. *Langmuir* **1996**, *12*, 5016–5021.
[33] Szczubialka, K.; Ishikawa, K.; Morishima, Y. *Langmuir* **2000**, *16*, 2083–2092.
[34] Miasnikova, A.; Laschewsky, A.; De Paoli, G.; Papadakis, C.; Muuller-Buschbaum, P.; Funari, S. S. *Langmuir* **2012**, *28*, 4479–4490.
[35] Piogé, S.; Fustin, C.-A.; Gohy, J.-F. *Macromol. Rapid Commun.* **2012**, *33*, 534–539.
[36] Wang, Y.; Kausch, C.; Chun, M.; Quirk, R.; Mattice, W. *Macromolecules* **1995**, *28*, 904–911.
[37] Zana, R.; Marques, C.; Johner, A. *Adv. Colloid Interface Sci.* **2006**, *123*, 345–351.
[38] Willet, N.; Gohy, J.-F.; Lei, L. C.; Heinrich, M.; Auvray, L.; Varshney, S.; Jerome, R.; Leyh, B. *Angew. Chem. Int. Ed.* **2007**, *46*, 7988–7992.

CHAPTER 12

STIMULI-RESPONSIVENESS OF METALLO-SUPRAMOLECULAR MICELLAR GELS

Abstract

Due to the intrinsic sensitivity of constituting building blocks and the non-covalent interactions between them, supramolecular gels can respond to specific external triggers, e.g., *pH or temperature. These stimuli are here intended to manipulate the rheological behaviour of metallo-supramolecular micellar gels. Thanks to the large panel of synthesized building blocks, a fine control is achieved over numerous structural aspects of the hierarchically assembled materials, including network formation, strength, and dynamics.*

12.1 Overview

The two previous chapters respectively examined the time scale and magnitude of the viscoelastic response of metallo-supramolecular micellar gels. On one hand, control over dynamics was achieved by tuning the strength of transient associations tethering the network through the length of hydrophobic stickers and the nature of metal–ligand complexes. On the other hand, the magnitude of the viscoelastic response was controlled via the network structure, *i.e.*, the proportion of metallo-bridges in regard to elastically inactive loops. In this frame, temperature was already used as an external factor affecting the swelling degree of the soluble block.

In this continuity, the rheological response of metallo-supramolecular micellar gels in reaction to the application of environmental stimuli is herein investigated. The driving force for this chapter is that the strength, or even formation, and dynamics of the non-covalent associations that contribute to the network structure together can be reversibly altered by external stimuli. In material chemistry, this means that the dynamic mechanical properties of the supramolecular hydrogels, *i.e.*, shear modulus, stress relaxation, and yield strength, might be changed in real time or in situ.

Because of the dynamic and reversible nature of non-covalent interactions, supramolecular systems are inherently intelligent and adapt to their environment at the micro-, meso- and macroscopic scales.[1] Hence, examples of self-assemblies that respond to stimuli such as variations in temperature,[2–5] redox,[6–8] irradiation,[9–11] solvation,[12–15] or pH,[16–20] are widely found in the literature.[21–24] Accordingly, these intriguing systems possess a wide range of interesting properties, such as shape-memory[25–27] and self-healing,[28–31] making them unique candidates for “smart” materials.

Further combining supramolecular chemistry and polymer science in an elegant, controllable and fashionable manner, not only lead to traditional polymeric properties, but also impart stimuli-responsiveness mediated by specific polymer–polymer and polymer–solvent interactions.[32] In particular, polymers that undergo a hydrophilic-to-hydrophobic phase transition are of great interest since their solution behaviour can promote the formation, breaking, transformation or stabilization of aggregates in response to, *e.g.*, temperature,[33–38] pH,[39–42] light,[43–46] or redox.[47]

In the frame of this project, thermo- and further pH-sensitive sequences are incorporated into the different copolymer architectures that constitute the building block for supramolecular hydrogels, therefore allowing control over network formation and dynamic mechanical response of the materials.

In the following, the dynamics of non-covalent associations tethering the supramolecular materials, *i.e.*, hydrophobic and coordinative, is first addressed by application of chemical stimuli. Then, responsive polymer sequences that compose the gel scaffold are specifically targeted via environmental changes. As characterization technique, rotational rheometry is used to monitor changes in the viscoelastic response of sheared materials upon stimulation, the focus being mainly on thermo-rheological properties. In this regard, the three different systems, *i.e.*, the PS-*b*-PNIPAAm-tpy, PNIPAAm-*b*-PDMAEMA-tpy and PS-*b*-PNIPAAm-*b*-PDMAEMA-tpy based materials, are tackled to demonstrate the possibility of controlling gel dynamics, formation and viscoelastic response.

12.2 Addressing the network dynamics

In the field of supramolecular polymer gels, combining multiple non-covalent interactions has opened the way to hierarchically assembled materials with a parallel hierarchy of dynamic processes. [48–50] Such systems hence show multi-responsiveness with the possibility of orthogonally targeting each individual association by appropriate stimulus. [17,51–54] However, only binary gel–sol transitions are generally triggered due to the intensity of solicitation, which in return provides facile visualizations of the response. [55–58]

Despite the effort expended so far, the possibility to use stimuli to finely control the dynamic mechanical properties of orthogonally self-organized materials is not clearly demonstrated yet. This finding would however extend our fundamental understanding and technical mastery over supramolecular polymers, which further benefits the field of material sciences. To achieve that goal, hetero-telechelic PS-*b*-PNIPAAm-tpy associating copolymers are selected as macromolecular building units. Indeed, the viscoelastic response of PS-*b*-PNIPAAm-tpy based hydrogels reflects the individual contribution from each transient junction, being readily tuned with the hydrophobe length and the nature of metal

complexes. Hence, such materials constitute formidable model systems to demonstrate the possibility of targeting the molecular dynamics of each transient junctions and evaluate the effect on the macroscopic mechanical properties of the material.

To demonstrate the possibility of orthogonally addressing the dynamic mechanical properties of hetero-telechelic associating polymer networks, two common stimuli have been selected, that are the pH and a plasticizing co-solvent. On one hand, protonation of the terpyridine ligand at low pH should compete with metal–ligand coordination preference. In this frame, Schubert *et al.* already investigated the stability of different bis-terpyridine macro-complexes regarding pH variations. In their study,[59] the possibility to open such complexes by protonation of the macro-ligands was demonstrated under acidic conditions, suggesting that material properties can be tuned accordingly. On the other hand, the presence of plasticizing co-solvent species should dramatically enhance chain mobility in the hydrophobic domains, *i.e.*, the micellar cores. In this context, Tsitsilianis *et al.* reported on the effect of dimethylformamide (DMF) on the rheological properties of ionized hydrogels formed by poly(acrylic acid) end-capped with short polystyrene blocks.[60] Notably, they showed that addition of DMF mainly affects the magnitude and extent of the linear viscoelastic response of the self-assembled materials. However, the associating networks were characterized by long relaxation times that could not be determined within the time of the experiment.

At the basis of this investigation, the selected PS_{27}-*b*-$PNIPAAm_{300}$-tpy block copolymer is dispersed in acidic water solutions or water–DMF mixture to reach a given concentration ranging in the semi-dilute non-entangled regime. To induce gelation, half an equivalent of Ni(II) ions, as their chloride salts, are added to the concentrated micellar solutions, with respect to the terpyridine content. This metal ion was selected so that the dynamics of metal–ligand bonds is of orders of magnitude distinguishable from the one of hydrophobic associations. To probe the dynamic response of the materials, rheological characterization are conducted on the different samples in the form of frequency sweeps at a controlled, small amplitude oscillatory stress.

12.2.1 Addressing the metal–ligand exchange dynamics

In a first series of samples, increasing molar amounts — 0.001, 0.01 and 0.1 M — of hydrochloric acid (HCl) are introduced during gel preparation while keeping the final concentration in associating copolymer constant at 5 %w/v. As shown in Figure 12.1, acidification of the gel media leads to a pronounced decrease in the slow relaxation time characterizing the self-assembled network, τ_2. Indeed, the modulus cross-over that marks the terminal relaxation of the material is gradually shifted by two orders of magnitude to higher frequencies as the concentration in HCl is increased from 0.001 to 0.1 M.

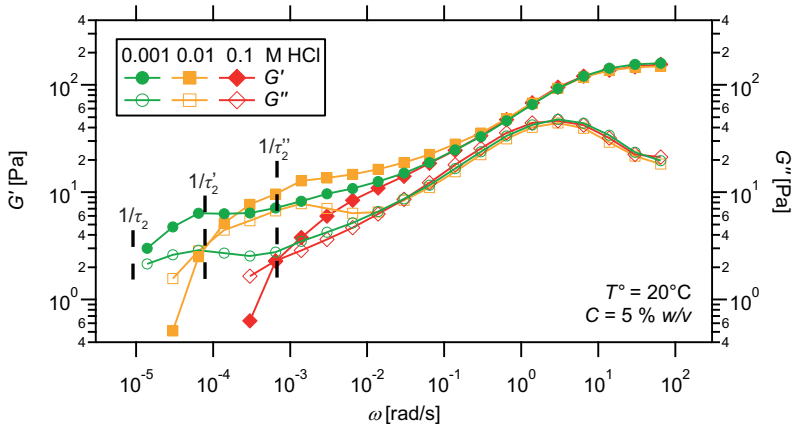

Figure 12.1 – Dynamic mechanical response of hydrogels prepared from PS_{27}-*b*-$PNIPAAm_{300}$-tpy copolymers and Ni(II) ions, with increasing concentrations in HCl.

From a chemical point of view, the pH-dependency of τ_2 can be rationalized by the early determination of rate–pH profile for the dissociation of metal–terpyridine complexes in water by Wilkins and collaborators.[61,62] Through kinetic measurements and theoretical calculations, they indeed demonstrated that medium-to-high acidic conditions open an enhanced dissociation pathway for ligand exchange, via protonation of the pyridine units. In particular, a roughly 100-times increase in the dissociation rates of metal–terpyridine bis-complexes has been reported when increasing the concentration of HCl in the range of 0.001 to 0.1 M,[61,62] which is in extremely good agreement with results shown in Figure 12.1. In addition, the rheological characterization demonstrates

no significant impact on the high frequency response of the associating networks, which attests the specificity of the selected stimuli and thus paves the way towards orthogonal control over material dynamics.

12.2.2 Addressing the hydrophobe exchange dynamics

Following the same approach, a second series of gel samples with increasing amount — 1, 5 and 10 %v/v — of DMF is subsequently prepared, while keeping pH of the media around neutral. As shown in Figure 12.2, the presence of the plasticizing solvent essentially accelerates the fast relaxation of the gels, as evidenced by the shift of the local maximum in G'' toward higher oscillatory frequencies. On the other hand, the dynamics of the sheared materials remains essentially unaltered in the low-frequency regime, therefore attesting the specificity of the plasticizing agent for hydrophobic associations.

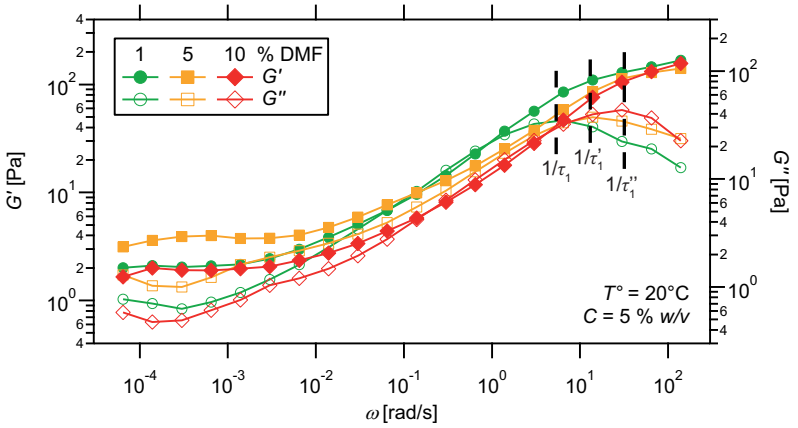

Figure 12.2 – Dynamic mechanical response of hydrogels prepared from PS_{27}-*b*-$PNIPAAm_{300}$-tpy copolymers and Ni(II) ions, with increasing amount in DMF.

As a matter of fact, adding DMF to the gel media should predominantly increase the mobility of the PS stickers, possibly due to preferential absorption by the hydrophobic domains. In turn, the reduced interfacial tension between the hydrophobic stickers and the surrounding media would enhance the detachment of the chain-ends from the network nodes,[63] leading to a decrease of the fast relaxation time, τ_1.

Interestingly, such findings can be correlated to dynamic tensile measurements on lightly modified polystyrenes by Hara *et al.* who demonstrated that exposition to DMF also enhances chain relaxation in the bulk PS materials.[64]

12.3 Controlling the network formation

In the field of associating copolymers, the formation of a percolated structure is often achieved by micellar aggregation. A control over this process can thus be easily gained provided that the copolymer architecture integrates a sequence that undergoes reversible changes in response to a certain external parameter. Such systems are typically composed of linear triblock copolymers or star-shaped block copolymers whose chain-ends become hydrophobic at a certain pH or temperature, thus forming the network junctions.[65] Examples from the vast literature include but are not limited to stimuli-responsive ABA triblock copolymers,[37,38,66,67] ABC triblock terpolymers,[38,42,68–70] star copolymers with segmented BA arm structure.[71,72]

In the library of building blocks synthesized here, the double hydrophilic, stimuli-responsive PNIPAAm-*b*-PDMAEMA-tpy copolymers appear as the best candidates to demonstrate the possibility of controlling supramolecular organization via temperature and pH. By having the PNIPAAm segment water soluble but thermo-responsive, it is possible to produce hydrogels in a stepwise manner, by first forming metallo-supramolecular triblock copolymers, then gels by subsequent thermo-induced block association (Figure 9.1). As supported by visual observations (Figure 9.27), the formation of a three-dimensional micellar network from the metallo-supramolecular triblock copolymer solutions occurs above the LCST of the PNIPAAm block. The gelation process is driven by the association of thermo-responsive PNIPAAm blocks into hydrophobic domains, forming physical cross-links within the supramolecular network, in which the PDMAEMA blocks form bridges among neighbouring micelles.

To investigate the gelation behaviour of PNIPAAm-*b*-PDMAEMA-tpy diblock copolymers, aqueous solutions with concentrations ranging in the semi-dilute non-entangled regime are prepared, followed by the addition of half an equivalent of selected transition metal ions, in the form

of their chloride salts. The pH of the gels is adjusted by addition of HCl during samples preparation to afford total, partial and no protonation of the amine functions of the PDMAEMA block (Figure 9.14). In the following, the thermo-responsive behaviour of PNIPAAm-*b*-PDMAEMA-tpy in solution is investigated systematically by rheology. A particular attention is paid to the effect of pH, length of the associating segments, and nature of added metal ions.

12.3.1 Thermally induced gelation

Oscillatory shear tests are conducted to study the thermo-induced sol–gel transitions of aqueous solutions of PNIPAAm-*b*-PDMAEMA-tpy, around neutral pH conditions. Rheological measurements are first carried out by sweeping the temperature over a range that covers the phase transition of PNIPAAm block, as evaluated by DSC (Table 9.3). In parallel, the formation of a transient metallo-supramolecular network is followed by frequency sweep in the investigated temperature range. In all cases, low stress amplitudes are used to ensure that the measurements are taken in the linear viscoelastic regime.

12.3.1.1 Oscillatory temperature sweep

As first experiment, the evolution of dynamic storage and loss modulus against temperature is monitored as an indication of the sol-to-gel transition. During measurements, the temperature is varied between 20 and 60 °C (1st run), followed by cooling at the same rate immediately after heating (2nd run). Each temperature ramp is performed at a stress amplitude of 10 Pa, a fixed frequency of 1 rad/s, with a heating rate, $\mathrm{d}T^{\circ}/\,\mathrm{d}t$, of 2 °C/min.

As illustrated in Figure 12.3, the viscoelastic response of PNIPAAm-*b*-PDMAEMA-tpy copolymer solutions, even in the presence of strongly chelated metal ions, is relatively weak at temperature below 30 °C. Indeed, the values for both dynamic moduli are relatively low, G'' being two orders of magnitude higher than G', which indicates a free-flowing sol state. On further increasing temperature, the magnitude of both elastic and viscous moduli rises abruptly in the range of 30 and 40 °C, which correlates very closely with DSC measurements (Table 9.3). Above a temperature of 40 °C, plateaus in both moduli tend to establish, without

any further tremendous increase. As the increase in G' is more significant than G'', the elastic response dominates over viscosity in this plateau region, indicating the solid-like behaviour.

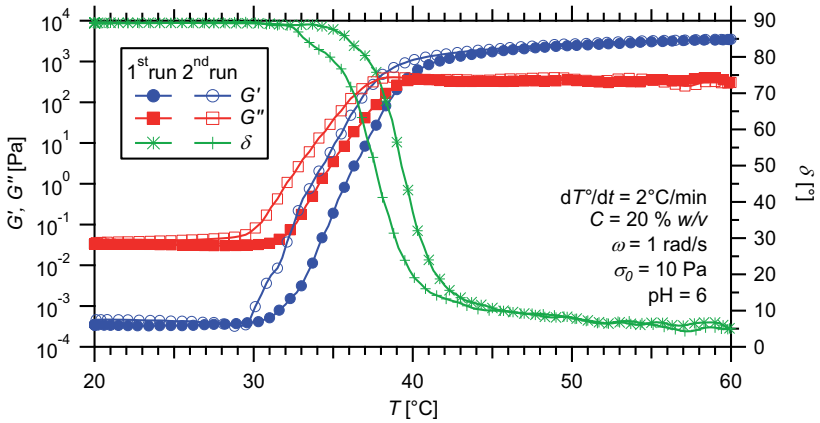

Figure 12.3 – Temperature dependence of dynamic moduli for a hydrogel prepared from PNIPAAm$_{75}$-*b*-PDMAEMA$_{105}$-tpy copolymer and Ni(II) ions: 1st run upon heating, 2nd run upon cooling.

The results obtained from temperature sweeps are in good agreement with visual observations made on the same materials (Figure 9.27 (b)). Indeed, the latter indicated that the initial samples were free-flowing transparent liquids at room temperature, and became free-standing and well-hydrated hydrogels when heated above 35 °C. In addition, the gels formed on heating solutions reverted to sol form on cooling, which is also observed in dynamic temperature sweep measurements (Figure 12.3).

Although the gelation process is fully thermo-reversible, both moduli recovering their initial values upon cooling, the disassembly of the gel phase is significantly shifted to lower temperatures, as also captured by DSC. Being observed in repeated heating and cooling cycles, this phenomenon cannot be seen as an indication of high-temperature fatigue or changes in material properties after first heating. Instead, this hysteresis in the thermal dependence of dynamic moduli is rather a consequence of additional inter-chain hydrogen bonds in the collapsed network nodes.[73–75] The latter reinforce the cross-linking points of the percolated structure, which delay the disaggregation of the network to lower temperatures. In addition, mechanical stress applied to the sample dur-

ing the measurement might also hinder the formation of the structures building the gel when temperature rises.[69]

By combining temperature-dependent rheology with light scattering study on dilute solutions, the sharp transition observed as a function of temperature can be without doubt attributed to the collapse of PNIPAAm blocks. Above the predetermined critical solubility temperature, these segments aggregate into hydrophobic domains that form the network nodes. Although not excluded, a contribution of the partial collapse of PDMAEMA block to the dynamic mechanical properties of the gel is not apparent. Indeed, only a unique sharp transition is observed in the investigated temperature range, which is in accordance with DSC measurements (Figure 9.30).

As a common indicator of the sol-to-gel transition, the cross-over of the storage and loss modulus can be used to evaluate the gelation temperature. The latter indicates the point at which micellar aggregates form a percolating three-dimensional network strong enough to result in an elastic response that is in the order of the viscous loss.[42] In this respect, one should note that the gelation temperature, as measured by rheometry (Figure 12.3), is reached well beyond the onset of the modulus increase. This observation suggests that, in the early stage of the thermal transition, micelles essentially assemble into growing aggregates that are ultimately incorporated into the network structure.

12.3.1.2 Oscillatory frequency sweep

In parallel, the heat-induced transition from viscous PNIPAAm-*b*-PDMAEMA-tpy copolymer solutions to nano-structured elastic hydrogels is investigated by frequency sweep experiments at selected temperatures. Practically, oscillatory tests are promptly performed in the temperature range that covers the thermal transition, with a control over stress amplitude. As illustrated in Figure 12.4, data collected from these measurements further evidence the formation of a well-percolated network upon temperature rise.

At temperatures below the phase transition, the storage modulus is smaller than the viscous modulus in the entire investigated frequency window. Moreover, both moduli exhibit power law dependencies on frequency that are the typical rheological behaviour of a liquid. At 35 °C,

which is centred on the phase transition, G' and G'' increase by around three orders of magnitude. However, different trends can be distinguished in the viscoelastic response of the gelling solution. Although the loss modulus undergoes parallel scaling, the storage modulus indeed clearly deviates from its power law frequency dependence of 2, especially at high frequencies. At 40 °C, which is slightly above but still very close to the gelation temperature, G' becomes higher than G'' and tends to form a plateau in the frequency range of 0.1 to more than 100 rad/s. Well beyond the gelation temperature, both storage and loss moduli are nearly independent of frequency, spanning five orders of magnitude, which is a characteristic of solid-like behaviour.

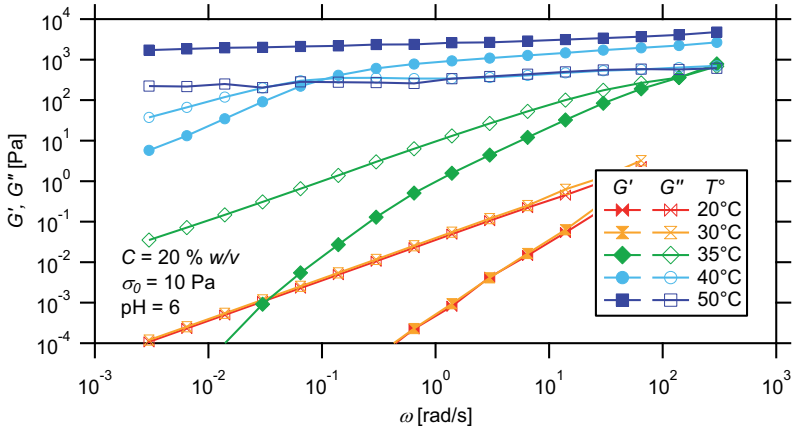

Figure 12.4 – Frequency dependence of dynamic moduli for a hydrogel prepared from PNIPAAm$_{75}$-*b*-PDMAEMA$_{105}$-tpy copolymer and Ni(II) ions, at different temperatures.

To attest the supramolecular nature of the thermo-assembled material, frequency sweeps are further extended in a wider range spreading over the low-frequency region. As shown in Figure 12.5, the pronounced plateau in storage modulus finally ends at low frequencies, where G' drops down before crossing G''. The cross-over between the dynamic moduli marks the onset of material flow, presumably via temporal detachment of metal–ligand bridges between collapsed micellar nodes, which is accelerated at elevated temperature. As a primary evidence, the cross-over frequency, *i.e.*, the rate at which the terminal relaxation of the material occurs, perfectly matches the dissociation kinetics reported by Hogg and Wilkins for nickel(II)–terpyridine bis-complexes at 60 °C,

precisely $k_{-2} = 6 \times 10^{-5}\,\mathrm{s}^{-1}$.[76]

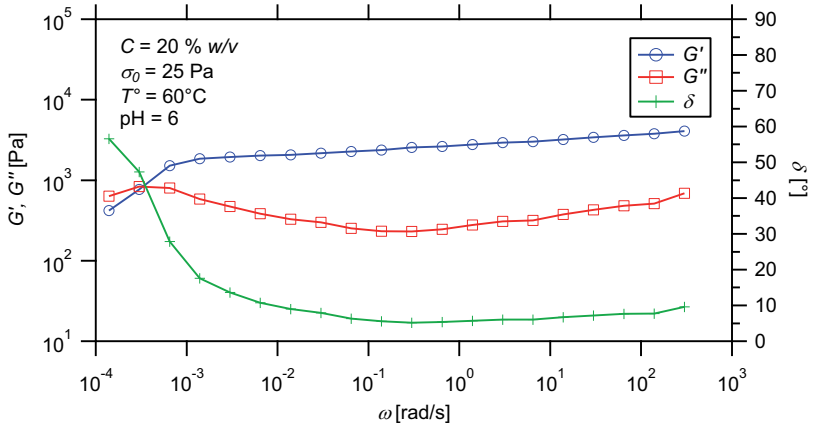

Figure 12.5 – Frequency dependence of dynamic moduli for a hydrogel prepared from PNIPAAm$_{75}$-*b*-PDMAEMA$_{105}$-tpy copolymer and Ni(II) ions, at 60 °C.

12.3.2 Effect of metal ions

In the field of associating polymers, controlling the network formation and dynamics is essentially achieved through the same transient association.[14,77,78] Here, the control over supramolecular network formation and dynamics can be presumably achieved in an orthogonal fashion. Indeed, the gel formation is ensured by the aggregation of PNIPAAm blocks into hydrophobic nodes, whereas the relaxation of the material can be dictated by the fast-dissociating metal–ligand bridges between them.

To test this hypothesis, hydrogels are prepared from PNIPAAm$_{75}$-*b*-PDMAEMA$_{105}$-tpy copolymer solutions in presence of different transition metal salts. In this respect, two metal ions are selected, namely Co(II) and Zn(II), that form relatively labile bis-complexes in combination with the terpyridine ligand.[62,76] As first monitored by temperature sweeps, each flowing solution turns into a supramolecular gel when heated above the LCST of the PNIPAAm block. Then, frequency sweep experiments are performed on gels to estimate the time scale at which relaxations of the percolated networks occur.

12.3.2.1 Oscillatory temperature sweep

As shown in Figure 12.6 in further comparison with Figure 12.3, the nature of metal ions in presence can substantially affects the thermo-induced gelation of PNIPAAm-*b*-PDMAEMA-tpy copolymer solutions. Although results obtained from temperature sweeps for the Zn(II) and Ni(II) containing samples are essentially comparable, the Co(II) containing copolymer solution turns into gel state at significantly lower temperature. In addition, reversing gel-to-sol transformations by cooling samples to room temperature (2nd run) indicate that hysteresis loops are also affected by the nature of metal ions. In this regard, the less and

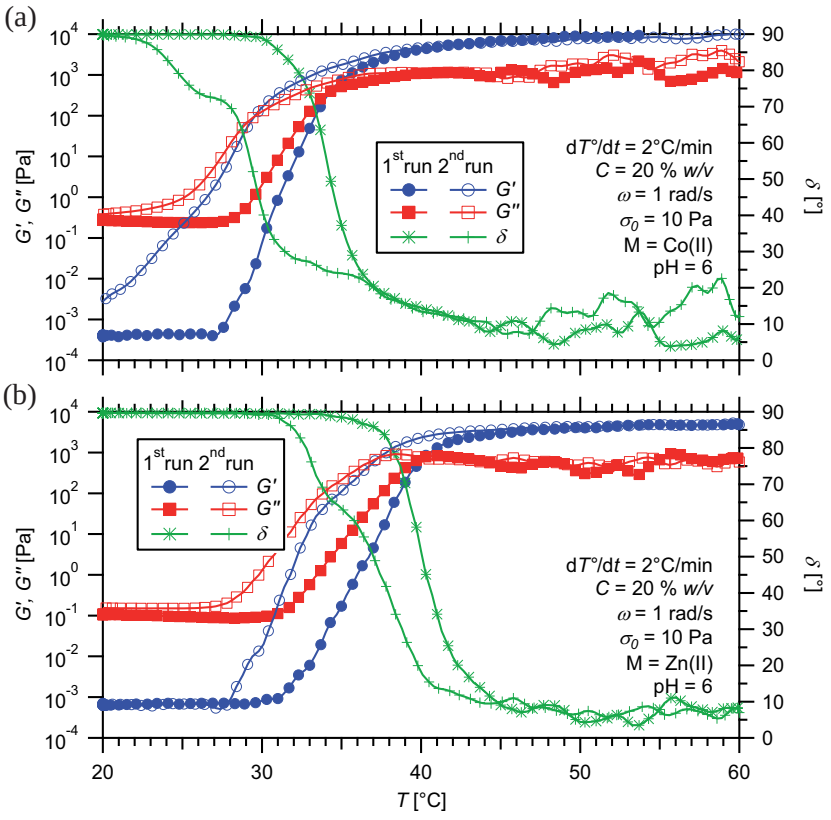

Figure 12.6 – Temperature dependence of dynamic moduli for hydrogels prepared from $PNIPAAm_{75}$-*b*-$PDMAEMA_{105}$-tpy copolymer and (a) Co(II) or (b) Zn(II) ions: 1st run upon heating, 2nd run upon cooling.

more pronounced hysteresis are respectively observed for samples prepared in presence Ni(II) and Co(II), while Zn(II) containing samples constitute the intermediate category.

Depending on the selected metal ions, a control can be thus practically achieved over the transition temperature that defines the limit between viscous copolymer solutions and supramolecular gels. In a theoretical point of view, this experimental conclusion can be presumably rationalized by the interplay of still underinvestigated effects of charged metal–ligand complexes on solvation and hydrophobic forces that direct the formation of micelle. In essence, coordination complexes can indeed have stabilizing or destabilizing salting effects on macromolecules, which modulate adsorption and aggregation phenomena.[79–82] However, further insights into the underlying mechanisms require every system to be studied individually in greater detail.

12.3.2.2 Oscillatory frequency sweep

Alongside temperature sweeps, the dynamic viscoelastic response of Co(II) and Zn(II) containing PNIPAAm-*b*-PDMAEMA-tpy hydrogels is studied as a function of oscillation frequency. Measurements are performed under controlled low shear stress, at a temperature well above the transition region. As shown in Figure 12.7 in relation to Figure 12.4, a shift in the cross-over point of G' and G'' toward higher frequency is observed when switching from Ni(II) to Co(II) and further to Zn(II). Interestingly, this shift is rather modest, *ca.* one and half frequency decades, meaning that the terminal relaxation of the material can be precisely controlled depending on the choice of the metal ions.

Clearly, variations in the terminal relaxation time of PNIPAAm-*b*-PDMAEMA-tpy hydrogels, as a function of metal ions, follows the stability order of metal–terpyridine bis-complexes. In respect to literature data on exchange rates,[62,76] Ni(II) and Zn(II) ions indeed respectively afford the more and less stable complexes in combination with the terpyridine ligand, while Co(II) ions constitute the intermediate case. However, the small adjustments made in the material relaxation time scale are in contrast to the large expected variations in terpyridine bis-complex lifetime, when switching from one metal ion to another. Nevertheless, the apparent dynamics of metallo-supramolecular bonds are known to largely vary depending on substituents on the ligand,[83] as

well as the surrounding environment.[84] Indeed, both factors may lower or rise the activation barrier for complex dissociation by stabilizing or destabilizing the transition state energy relative to that of the bound state. Here, the particularly high ionic strength and congestion of the gels, due to quaternization of the PDMAEMA block, may clearly slow down the dissociation of coordination complexes and subsequent diffusion of dangling chain ends across the medium, which actually dominate the relaxation of the material. Also, a plausible interaction between metal ions or metal–ligand complexes and the tertiary amine groups of the PDMAEMA blocks and metal or metal–ligand complexes is not excluded.[85]

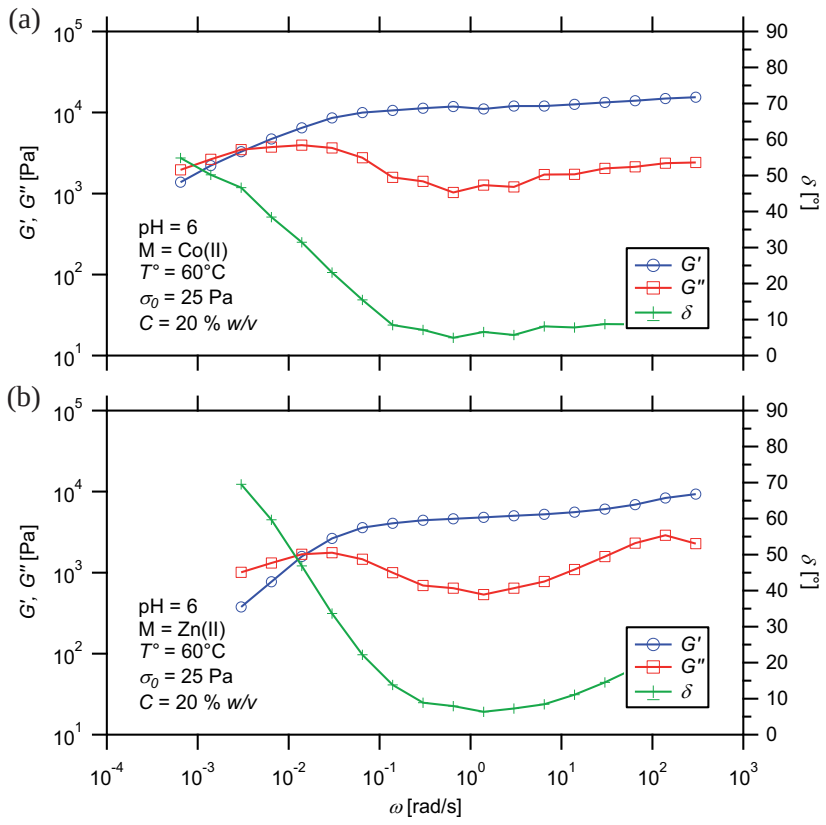

Figure 12.7 – Frequency dependence of dynamic moduli for hydrogels prepared from PNIPAAm$_{75}$-*b*-PDMAEMA$_{105}$-tpy copolymer and (a) Co(II) or (b) Zn(II) ions, at 60 °C.

12.3.3 Effect of block length

To achieve orthogonal control over the formation and dynamics of PNIPAAm-*b*-PDMAEMA-tpy associating polymer networks, it is assumed that metal–ligand associations constitute the fast-dissociating cross-linkers. Ideally, the lifetime of hydrophobic nodes, that are formed by the aggregation of PNIPAAm segments, must exceed by orders of magnitude the stability of coordination bridges between them, otherwise, relaxation of the material might be dominated by the dynamic exchange of the associating segments between the segregated domains.

To ensure the formation of kinetically stable to "frozen" hydrophobic domains, nearly symmetric diblock copolymers are used that feature thermo-sensitive associating segments of several tens of units (Figure 12.5). Decreasing the length of the PNIPAAm block, *e.g.*, from 75 to 45 repeating units, while keeping the length of PDMAEMA block constant, significantly affects the relaxation of the material under shear. As revealed by frequency sweep performed at 60 °C (Figure 12.8), the cross-over of moduli indeed occurs at a higher frequency for the hydrogel prepared from the PNIPAAm-*b*-PDMAEMA-tpy copolymer with a shorter PNIPAAm block. This observation suggests that the dissociation of hydrophobic segments from micellar network nodes becomes the relaxation determining process when the length of the PNIPAAm is

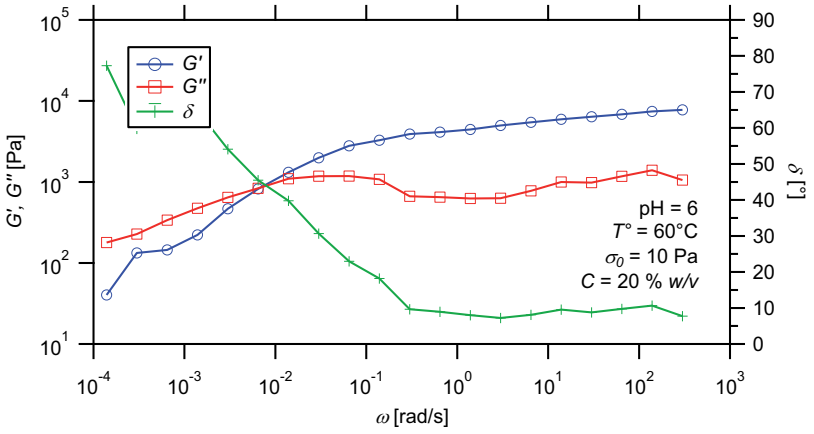

Figure 12.8 – Frequency dependence of dynamic moduli for a hydrogel prepared from $PNIPAAm_{45}$-*b*-$PDMAEMA_{105}$-tpy copolymer and Ni(II) ions, at 60 °C.

reduced.

A closer look at the frequency dependence of both moduli suggests that a second plateau in storage modulus tends to be achieved in the low-frequency regime. This pseudo-plateau rapidly ends when the time scale of the experiment exceeds the lifetime of metal–ligand bonds, as evaluated from Figure 12.5. In this picture, both hydrophobic and coordinative interactions thus contribute to stress relaxation by material creep, similarly to what is observed for PS-*b*-PNIPAAm-tpy systems, the plateau at low frequencies being interpreted as reflecting a remanent network structure.

In accordance with a weaker aggregation of shorter associating segments, temperature sweeps shows a broadened gel-to-sol transition when the length of the PNIPAAm block is reduced to 45 repeating units (Figure 12.9). Although the modulus cross-over is observed at a comparable temperature of 40 °C, the establishment of an equilibrium in moduli is indeed only achieved at much elevated temperatures. Intuitively, the shorter PNIPAAm blocks require a higher degree of dehydration to form a sufficiently mechanically strong three-dimensional network. Once formed, the hydrogel shows essentially the same viscoelastic properties, in terms of both storage and loss modulus, than the one formed with longer associating segments, suggesting that the final structure of the self-assembled network is essentially the same.

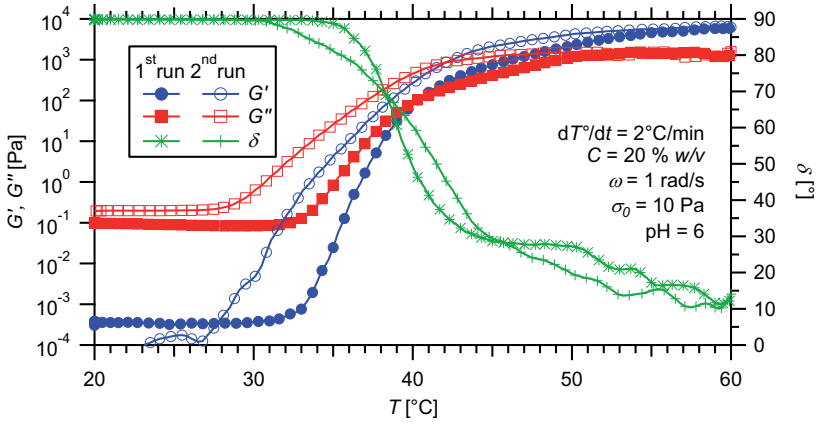

Figure 12.9 – Temperature dependence of dynamic moduli for a hydrogel prepared from $PNIPAAm_{45}$-*b*-$PDMAEMA_{105}$-tpy copolymer and Ni(II) ions: 1st run upon heating, 2nd run upon cooling.

12.3.4 Effect of pH

In the field of associating polymers, it is desirable to have other variables besides temperature to regulate the assembly process. To this end, pH constitutes the most widely used stimuli to modulate or reverse the solvophilicity of thermo-sensitive polymers.[37,40–42,69] In practice, joint thermo- and pH-mediated assembly can be investigated either by fixing temperature and varying pH, or by keeping pH constant and changing temperature. In the following, the second approach is exclusively followed since temperature can be easily controlled in situ during rheological measurements.

12.3.4.1 Oscillatory temperature sweep

As monitored by dynamic temperature sweep measurements (Figure 12.10), dramatically distinct behaviours are encountered depending on the pH of the gel medium. The latter is acidified by addition of HCl during sample preparation, while dissolution of the polybase in pure water directly leads to an alkaline pH of 9. Hence, the difference in the thermo-mechanical responses of the double hydrophilic block copolymer solutions can be discussed in detail as a function of the ionization degree of the PDMAEMA block. Under acidic conditions, virtually all amino groups of PDMAEMA are expected to be protonated and thus positively charged, while the inverse situation is achieved at high pH.

At low pH (Figure 12.10 (a)), the experiment reveals a very gradual and broad sol-to-gel transition upon temperature rise. Such an observation is in contrast with the simplistic conception of the coil-to-globule transition expected for PNIPAAm chains in solution.[86,87] As a matter of fact, the latter is generally assumed to be sharp near the critical solubility temperature, as also evaluated by DSC (Figure 9.30).

In the field of associating copolymer gels, however, the gelation temperature is frequently reported above the critical solubility temperature. Indeed, the gelation requires the formation of a percolated network with sufficient mechanical strength, while the critical solubility temperature is already reached when the thermo-sensitive blocks starts to collapse in solution.[41] Taking into account that a large scale organization of the initially collapsed chain segments is required for the formation of a network, it is understandable that the high degree of ionization of

PDMAEMA blocks sensibly delays the gelation due to impeding electrostatic repulsions in the system. Once established, the self-organized network is supposed to be stable, which accounts for the marked hysteresis observed when cooling the sample back to room temperature (Figure 12.10 (a)).

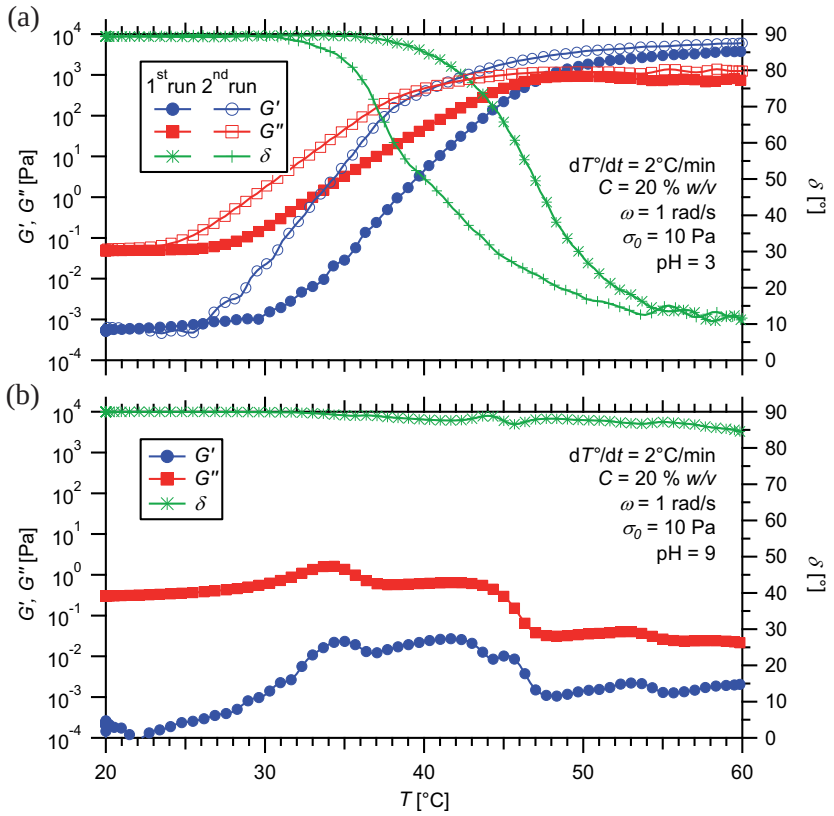

Figure 12.10 – Temperature dependence of dynamic moduli for hydrogels prepared from PNIPAAm$_{45}$-*b*-PDMAEMA$_{105}$-tpy copolymer and Ni(II) ions, at pH of (a) 3 and (b) 9: 1st run upon heating, 2nd run upon cooling.

As indicated by visual observation (Figure 9.28), the formation of a micellar network can be efficiently inhibited at high pH due to the collapse of both blocks, resulting in phase separation instead of gelation. In accordance, temperature sweep performed under even slightly basic conditions, *ca.* pH of 9, shows that a viscous behaviour dominates

in the whole investigated temperature range (Figure 12.10 (b)). Upon heating, a rather stochastic pattern in G' and G'' is observed as a function of temperature, which can emerge naturally from a competition between two antagonistic phenomena, namely the network formation and the phase separation. Although a slight increase in moduli tends to be achieved above 30 °C, it is clear that intra-micellar collapse of the outer PDMAEMA blocks then quickly overtakes the development of significant inter-micellar interactions that are a prerequisite for macroscopic gelation.

12.3.4.2 Oscillatory frequency sweep

As monitored by frequency sweep on the gel at low pH and elevated temperature, the presence of numerous charges along the polymer chain not only contributes to broaden the phase transition, but also affects the dynamics of the material. From Figure 12.5, two plateau in elastic modulus are observed as a function of the oscillation frequency, which is comparable with the situation achieved for the same system but at around neutral pH (Figure 12.5). However, both characteristic relaxations of the metallo-supramolecular micellar network are promoted at low pH, as attested by the half decade increase in the relaxation frequencies.

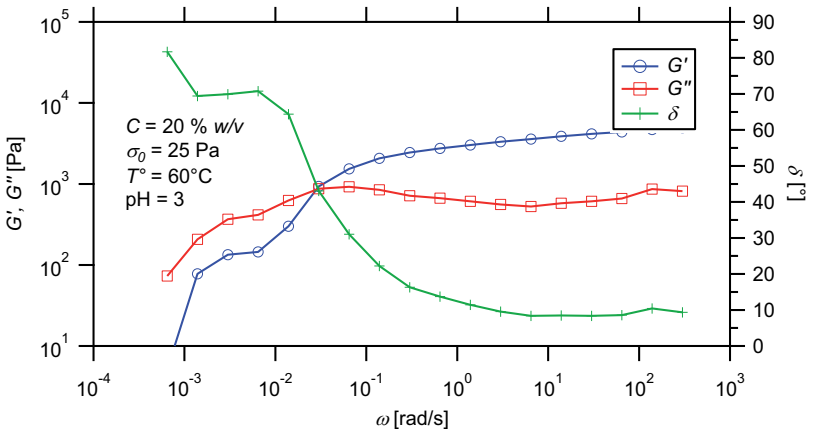

Figure 12.11 – Frequency dependence of dynamic moduli for hydrogels prepared from PNIPAAm$_{45}$-*b*-PDMAEMA$_{105}$-tpy copolymer and Ni(II) ions, at 60 °C and pH 3.

The dependence of the first relaxation time on the degree of protonation of the PDMAEMA coronal block is in agreement with results obtained by Nicolai *et al.* from pH-responsive associative networks in aqueous media. In their study on triblock copolymers with a poly(acrylic acid) central block and random copolymer hydrophobic end blocks,[40] they indeed evidenced a clear variation of the relaxation frequency of the self-assembled materials with the degree of ionization of the hydrophilic middle block. To account for an increase in the cross-over frequency, they assumed that the energy barrier for the escape of an end-block effectively decreases with increasing charge density of the coronal chains, which in turn leads to an enhanced exchange of the associating copolymers.

Due to the high concentration of diblock copolymer in the media, pH of the media is adjusted to about 3 by adding concentrated hydrochloric acid solution. Even if strongly buffered by the presence of the polybase, the acidity of the media further enhances the dissociation of metal–ligand bridges, thus leading to a decrease in the second relaxation time of the thermally assembled network. As already evidenced for PS-*b*-PNIPAAm-tpy analogues, acidic conditions indeed open an enhanced dissociation pathway for the ligand exchange. This alternate mechanistic path is promoted by the protonation of pyridine units at low pH, which directly competes with the coordination of ligands to metal ions.[61,62]

12.3.5 Effect of concentration

As last but not least parameter, the concentration of associating copolymer in solution is varied to reveal the influence of this factor on the thermo-mechanical properties of the supramolecular assemblies. In the above-discussed experiments, the weight fraction of PNIPAAm-*b*-PDMAEMA-tpy diblock copolymers was kept high enough to ensure, in each case, an appreciable response of the sols to shear stress, as well as a linear response from the gels. As demonstrated in the previous chapter, varying the relative amount of associating groups in the gels notably affects their extent of cross-linking, with a pronounced dependency near the critical gelation concentration.

In practice, the effect of dilution on the thermo-induced gelation of an aqueous solution of the selected $PNIPAAm_{45}$-*b*-$PDMAEMA_{105}$-tpy diblock copolymer is first tested by following the evolution of dynamic

moduli during heating-cooling cycles (Figure 12.12). Compared with the situation at higher polymer concentration (Figure 12.9), temperature sweep carried out at 5 %w/v clearly indicates that higher degrees of dehydration and organization of thermo-sensitive blocks are required to form a sufficiently percolated three-dimensional network. Indeed, the onset of increase in G' only occurs at 45 °C. Again, this observation can be closely correlated to DSC measurement on the same system, which points a critical solubility temperature in the range of 40 °C, as reported in Table 9.3.

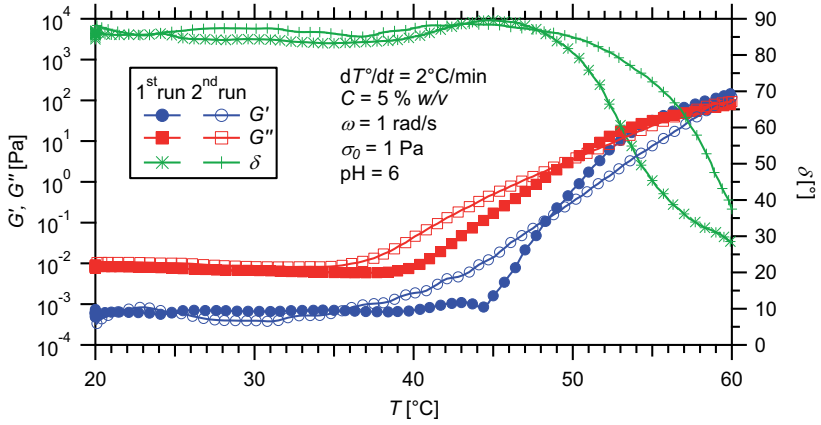

Figure 12.12 – Temperature dependence of dynamic moduli for a 5 %w/v hydrogel prepared from PNIPAAm$_{45}$-*b*-PDMAEMA$_{105}$-tpy copolymer and Ni(II) ions: 1st run upon heating, 2nd run upon cooling.

Above the gelation temperature found at around 50 °C, both moduli tend to reach a plateau equilibrium but remain very close in value (Figure 12.12), which is indicative of a weakly structured gel. The low viscoelastic response of this sparsely percolated network is further highlighted by frequency sweep performed on the gel formed at 60 °C. As graphically depicted in Figure 12.13, the results show a broad relaxation process in the high-frequency range, that might be related to the dissociation of the poorly associated hydrophobic segments. In contrast with measurements at a higher concentration (Figure 12.9), no second plateau modulus can be achieved in the low-frequency region with a low associating copolymer content, which is coherent with the picture draw from the rheological behaviour of PS-*b*-PNIPAAm-tpy associative networks.

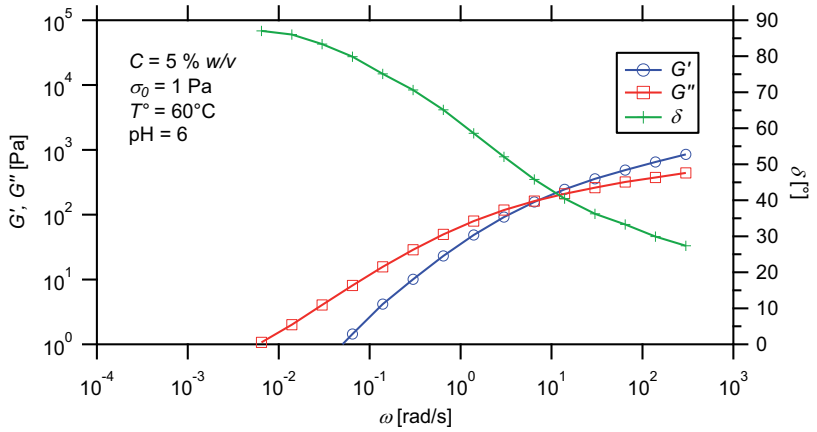

Figure 12.13 – Frequency dependence of dynamic moduli for a 5 %w/v hydrogel prepared from PNIPAAm$_{45}$-*b*-PDMAEMA$_{105}$-tpy copolymer and Ni(II) ions, at 60 °C.

12.4 Tuning the viscoelastic response

Beyond the control of supramolecular network formation, stimuli can also be used to modulate numerous aspects of the viscoelastic response of self-assembled materials, including the strength and dynamics of the assembly. In the field of stimuli-responsive block copolymer gels, this control is generally achieved through adjustments in the network structure via temperature or pH changes.[36,41] Compared with conventional gels, such additional stimuli-response offers greater design flexibility that can be required for many specific applications.

As suggested in the previous chapter, temperature plays an overall role in determining the quality of water as a selective solvent for the PNIPAAm block, thereby controlling the swelling degree of the chains. However, the thermo-responsive behaviour of this well-studied polymer is generally referred as the collapse of the chain, from hydrated coils into hydrophobic globules, above the critical solubility temperature.[88,89] In the following, this change in chain conformation is exploited to finely tune the rheological properties of supramolecular hydrogels prepared from both PS-*b*-PNIPAAm-tpy and PS-*b*-PNIPAAm-*b*-PDMAEMA-tpy block copolymers. Although the heat induced collapse transition of PNIPAAm chains is reported to be extremely sharp,[86,87] the dynamic mechanical response of the different hydrogels are hoped to be precisely,

reversibly, and continuously tuned in a wider temperature range.

12.4.1 Responsiveness of PS-*b*-PNIPAAm-tpy hydrogels

First of all, the thermo-mechanical behaviour of PS-*b*-PNIPAAm-tpy based hydrogels is investigated by rotational rheometry. In a first approach, time sweeps are performed by following the evolution of dynamic storage and loss moduli upon thermal variations. Then, frequency sweeps are performed to probe the dynamic response of the gels, under ambient conditions and around the phase transition temperature determined by DSC (Table 9.2). In practice, those measurements are performed under strain amplitudes that ensure a linear response from the material. Then, the non-linear viscoelastic behaviour of the gels is investigated by amplitude strain sweeps, at a given oscillation frequency. In this respect, a particular attention is paid to the relationship between the applied stress and the resulting deformation, along with the behaviour of the gels at the limit of destructuration.

12.4.1.1 Oscillatory time sweep

Time sweeps are performed on gels by following the evolution of the dynamic moduli at different temperature plateaus, *i.e.*, 20, 30 and 35 °C. Hence, time-dependencies associated to the dynamic processes occurring in the vicinity of the phase transition can be successfully addressed in isotherm regimes, separated by fast temperature ramps in between, with heating/cooling rates of 5 °C/min. In practice, experiments are conducted under small amplitude strain and a fixed oscillation frequency of 1 rad/s. The investigated samples consist in supramolecular hydrogels prepared from PS-*b*-PNIPAAm-tpy copolymers with different block lengths, in combination with various transition metal ions. In the following, the emphasis is first put on the influence of the size of the polystyrene sticker, which dictates the stability of the hydrophobic nodes within the micellar network. Finally, the influence of the nature of metal–ligand bridges between them is discussed.

Below the critical solubility temperature of the PNIPAAm block, the dynamic mechanical response of each hydrogel is characterized by an equilibrium in both moduli. Under those conditions, the invariability of their viscoelastic responses is appreciated during isotherms performed

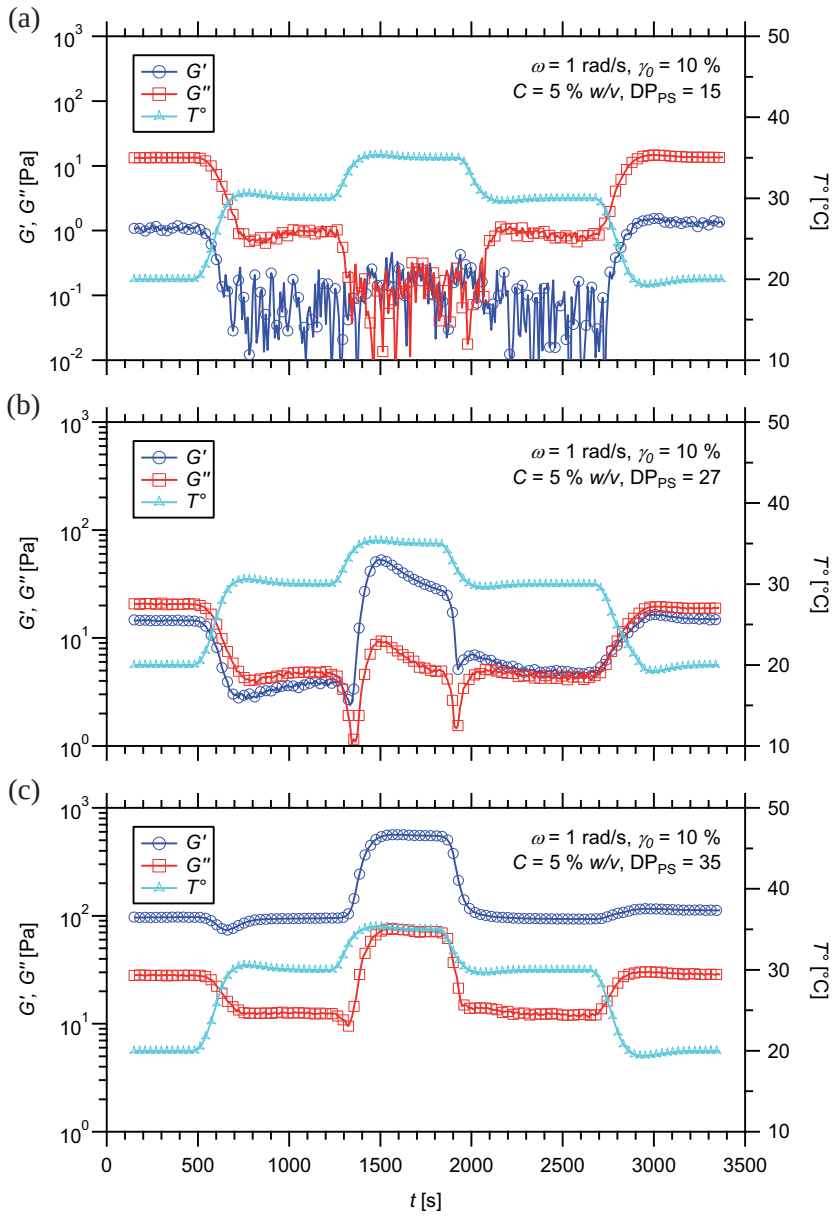

Figure 12.14 – Time dependence of dynamic moduli for hydrogels prepared from PS_m-*b*-$PNIPAAm_{235}$-tpy copolymers with increasing PS segment length and Ni(II) ions, at different temperatures.

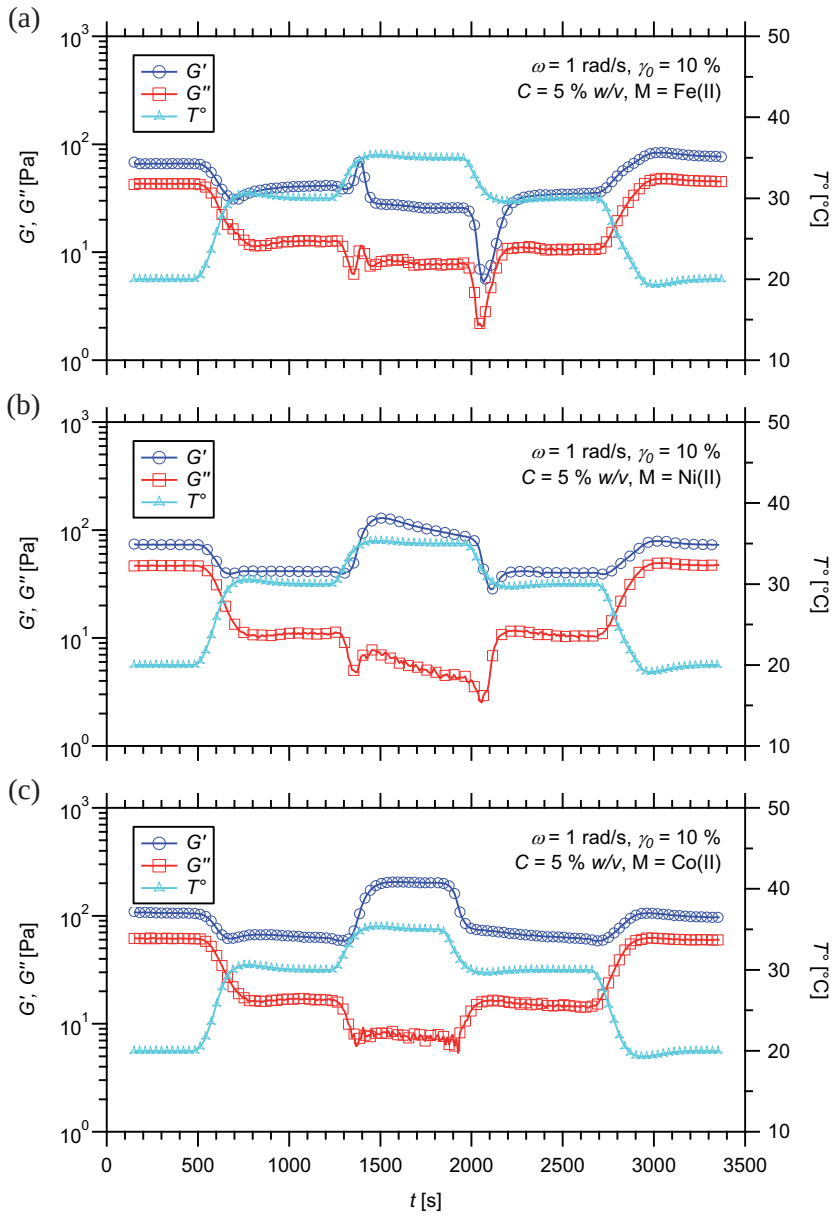

Figure 12.15 – Time dependence of dynamic moduli for hydrogels prepared from PS_{27}-*b*-$PNIPAAm_{300}$-tpy copolymer and various transition metal ions, at different temperatures.

at 20 and 30 °C, as shown in Figure 12.14. Within this temperature range, both moduli nevertheless decline upon heating, which is due to the thermally enhanced relaxation of the materials. As demonstrated in a previous chapter, the dissociation of the transient PS micellar cores indeed intensifies upon temperature rises, thus lowering the viscoelastic responses of the gels.

When the temperature is further increased, a sharp transition in the viscoelastic response of the materials is observed at the vicinity of the phase transition temperature, *ca.* 32 °C. At the early stage of the transition, the response of the gels becomes more pronounced but then declines over time (Figure 12.14). The only exception is given by the hydrogel prepared from the copolymer exhibiting short polystyrene segment. The latter is indeed characterized by a very weak response to shear above the critical solution temperature (Figure 12.14 (a)). For longer associating stickers, the instabilities of the self-assembled gels at 35 °C become appreciable over long time scales, both moduli falling down at a rate that depends on the length of the associating segment. In this respect, long polystyrene stickers give rise to more stable hydrogels that tend to maintain their strong mechanical properties above the phase transition temperature of PNIPAAm (Figure 12.14 (c)).

Essentially, those observations point out a straight relationship between the strength of polystyrene cores and the kinetic stability of the micellar network at 35 °C. Assuming that PS nano-domains act as seeds for the collapse of PNIPAAm chains (Figure 12.16), an increased stability of these domains would indeed prevent the network to lose its integrity above the phase separation temperature. Indeed, the collapsed PNIPAAm chains would preferentially aggregate onto PS cores, thus reinforcing the micellar network whose partial hydration is presumably ensured by the presence of charged metal–ligand complexes. Finally, the reversibility of the phase transition is checked while both moduli recover their original value when coming back to 30 °C, then further to 20 °C.

As illustrated in Figure 12.15, the thermo-mechanical behaviour of the gels also depends on the nature of metallo-bridges tethering the micellar network. When cobalt(II) metal ions are used, no significant evolution in the viscoelastic response of the gel is observed above the critical solution temperature of PNIPAAm (Figure 12.15 (c)). When the same associating copolymer is used in combination with nickel(II) or iron(II) metal ions, a pronounced instability characterizes the accordingly ob-

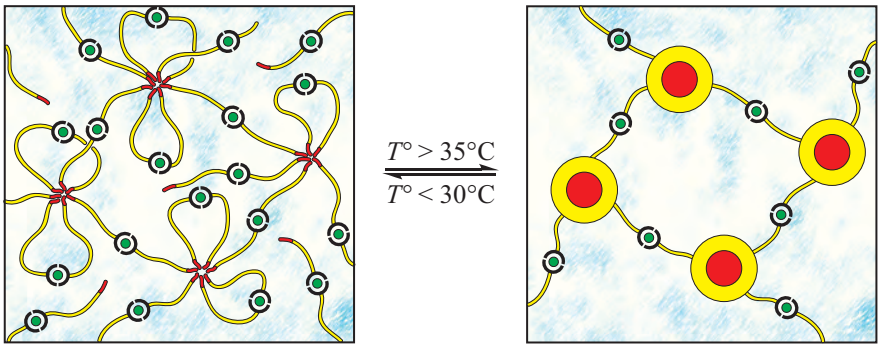

Figure 12.16 – Structural responsiveness of PS-*b*-PNIPAAm-tpy metallo-supramolecular micellar gels.

tained hydrogels above their phase separation temperature. Precisely, a decrease in both dynamic moduli, that is particularly marked for the iron-containing gel, follows the primary heat-induced transition in the viscoelastic response of the material (Figure 12.15 (a) and (b)). To rationalize these observations, it is assumed that the hydration degree of the gel above the LCST of PNIPAAm, which is ensured by the presence of positively charged bis-complexes, strongly depends on the nature of the chelated ions.

12.4.1.2 Oscillatory frequency sweep

As illustrated in Figure 12.17, a drastic change in the rheological behaviour of the gel is noticed in frequency sweeps when the external temperature is increased from 20 °C to 35 °C. Under ambient conditions (Figure 12.17 (a)), the material shows the characteristic features of a transient metallo-supramolecular micellar networks, as described in a previous chapter. At high frequencies, the non-covalent network indeed appears intact since the supramolecular junctions do not dissociate on the experiment time scale. As the time scale of the oscillations increases, the material relaxes stress, both storage and loss modulus curves falling down as the frequency of the oscillations is decreased. In this respect, two relaxation time scales are distinguished at 20 °C that correspond to the dissociation of associating stickers and subsequent exchange of polymer chains between hydrophobic nodes, τ_1, and the dissociation kinetics of the metal–terpyridine bis-complexes tethering the network, τ_2.

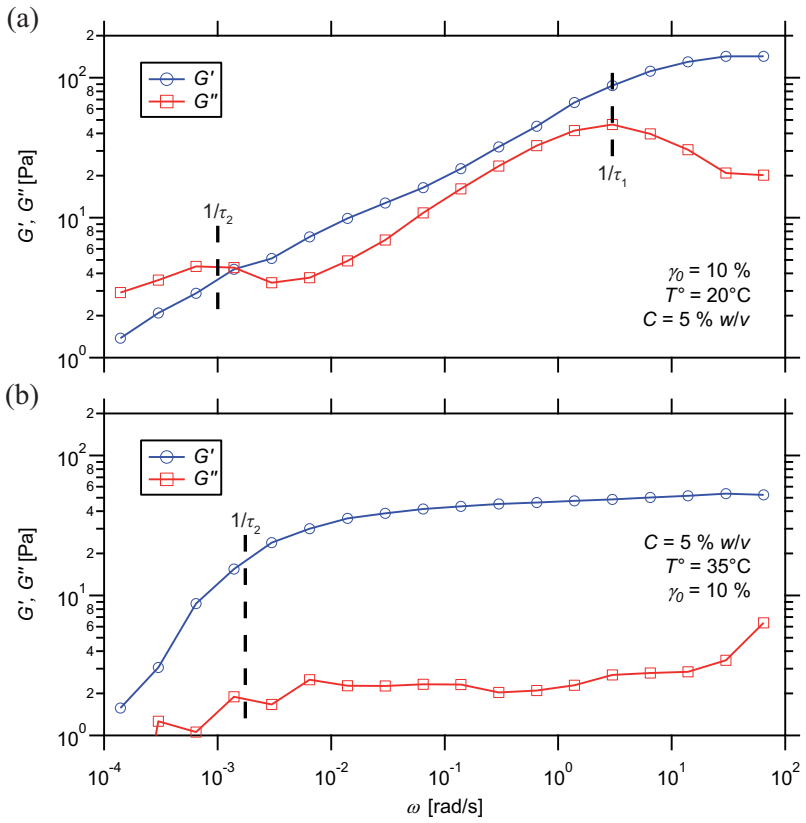

Figure 12.17 – Frequency dependence of dynamic moduli for a hydrogel prepared from PS_{27}-*b*-$PNIPAAm_{300}$-tpy copolymer and Co(II) ions, at (a) 20 °C and (b) 35 °C.

Above the LCST of PNIPAAm, the same materials behave more solid-like, nearly as covalently bound polymer networks. Indeed, elasticity clearly dominates the viscous dissipation over frequency decades. Compared with measurements at 20 °C, only a single relaxation is achieved at 35 °C, on a time scale that matches the one of metal–ligand bridge dissociation, τ_2 (Figure 12.17 (b)). Such an observation suggests that the escape of hydrophobic stickers from micellar cores has been frozen, which in turn would prevent the relaxation of the material over short time scale.

Essentially, these observations might be rationalized by taking into account the partial collapse of the thermo-sensitive chains onto the tran-

sient micellar cores, which results in turn in the shielding of the latter (Figure 12.16). In this picture, the core–shell type structure of the hydrophobic nodes would indeed prevent the network integrity from being mechanically perturbed by shear forces. Also, the presence of remaining metal–ligand bridges between collapsed micellar objects is attested by the terminal flow behaviour of the metallo-supramolecular gel (Figure 12.17 (b)).

12.4.1.3 Oscillatory strain sweep

The change in the rheological properties of the gel in response to heat was finally investigated by performing amplitude strain sweeps on a selected sample prepared from PS_{27}-*b*-$PNIPAAm_{300}$-tpy copolymer, in combination with Co(II) ions. Precisely, the evolution of storage and loss moduli is checked at a given oscillation frequency of 1 rad/s, under increasing amplitudes of deformation (1^{st} run). In addition, the reversibility of the phenomenon occurring under large oscillatory shear is addressed by coming back to small oscillation amplitudes right after the first strain sweep (2^{nd} run).

At low strain, the micellar gel is characterized by a plateau in both moduli, which extends over the linear viscoelastic regime, *i.e.*, the region where stress on the sample increases linearly with the deformation. As shown in previous chapters, the three-dimensional structure of the network is only weakly affected by mechanical forces in this region, and deforms elastically through entropic distortions. Due to its supramolecular character, the gel however exhibits a reversible gel-to-sol transition when stressed above the yield strength. At larger deformations, shear stress becomes almost independent of shear strain, meaning that the supramolecular network is mechanically disrupted, which corresponds to the non-linear regime. In the following, the critical shear strain and stress values, γ_0^c and σ_0^c, that separate the linear from the non-linear regime, are determined from strain–stress curves as the onset of breaking.

In the first experiments, strain sweeps are performed on the associating copolymer hydrogel at room temperature and at the phase transition temperature. From the comparison between Figures 12.18 (a) and 12.19 (a), the plateau values for the storage modulus, at an oscillatory frequency of 1 rad/s, appear to be comparable between 20 and

32 °C. However, the loss modulus was half an order of magnitude lower at 32 °C, lowering the proportion of energy that is dissipated through the irreversible flow of the network.

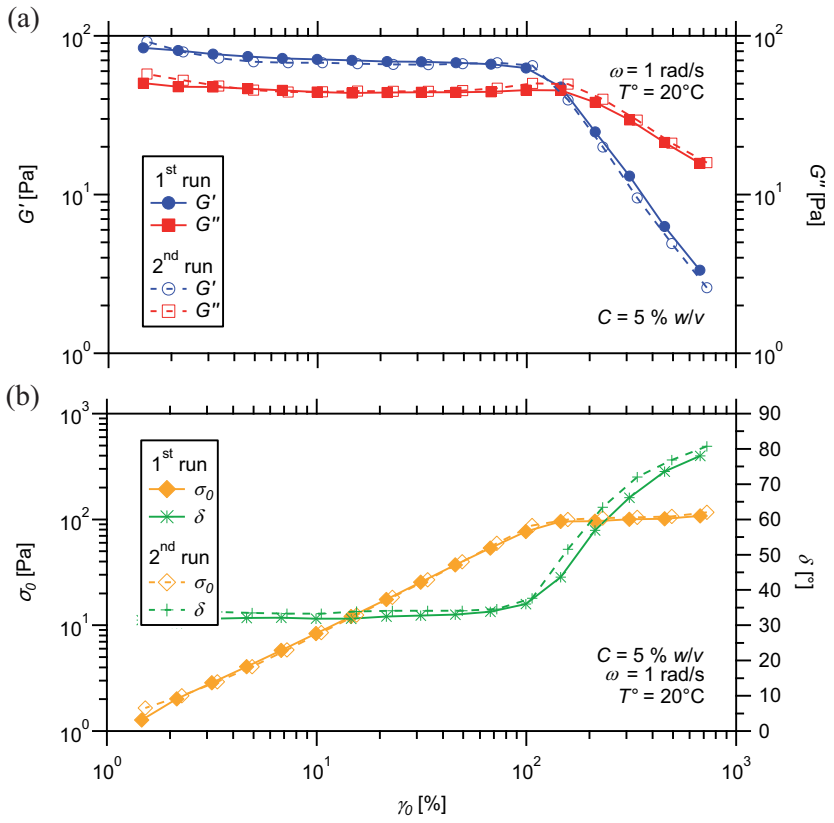

Figure 12.18 – Strain dependence of (a) dynamic moduli and (b) stress amplitude for a hydrogel prepared from PS_{27}-*b*-$PNIPAAm_{300}$-tpy copolymer and Co(II) ions, at 20 °C: 1st run under increasing strain, 2nd run under decreasing strain.

When comparing Figures 12.18 (b) and 12.19 (b), the applied shear strain at which the material yield occurs is found to vary significantly. Precisely, the supramolecular hydrogel withstands larger deformations under ambient conditions (Figure 12.18 (b) — $\gamma_0^c \approx 100\,\%$) than at the phase transition temperature (Figure 12.19 (b) — $\gamma_0^c \approx 50\,\%$). Moreover, the stress–strain curve displays a maximum stress at a temperature of 32 °C (Figure 12.19 (b) — $\sigma_0^{c,max.} \approx 20\,\text{Pa}$), before reaching an equi-

librium stress (Figure 12.19 (b) — $\sigma_0^{c,equi.} \approx 10\,\text{Pa}$) that is one order of magnitude lower than the equilibrium stress at 20 °C (Figure 12.18 (b) — $\sigma_0^{c,equi.} \approx 100\,\text{Pa}$).

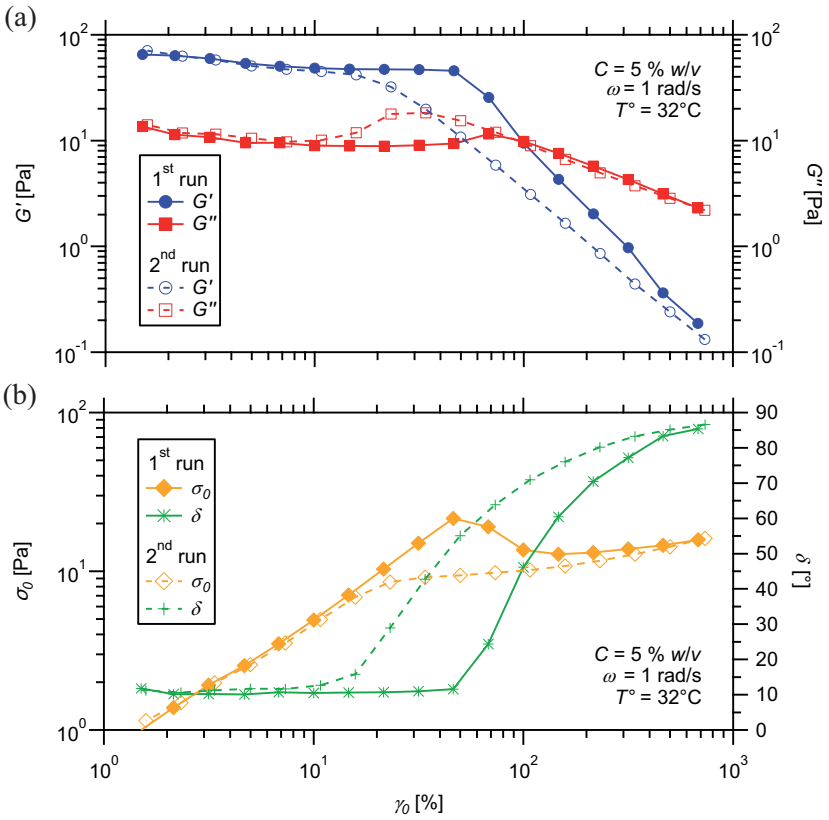

Figure 12.19 – Strain dependence of (a) dynamic moduli and (b) stress amplitude for a hydrogel prepared from PS_{27}-*b*-$PNIPAAm_{300}$-tpy copolymer and Co(II) ions, at 32 °C: 1st run under increasing strain, 2nd run under decreasing strain.

Beyond the limit of destructuring, the storage modulus clearly deviates from the linear to the non-linear viscoelastic regime, and strain softening is finally observed at both 20 °C (Figure 12.18 (a)) and 32 °C (Figure 12.19 (a)). Coming back to small deformations, full healing of the gel is observed at both temperatures, while storage and loss moduli recovered their original values. Compared to the situation achieved at 20 °C, a peculiar hysteresis, that is particularly marked in G', is how-

ever observed at 32 °C during the healing process (Figure 12.19 (b)). This observation suggests that a certain proportion of the mechanical energy, that is reversibly stored in the entropic distortion of the polymeric network, is dissipated during shear-induced flow of the gel. This proportion is known as the hysteresis loss and is given, in respect to the strain energy, by the area under the stress–strain loop. [90]

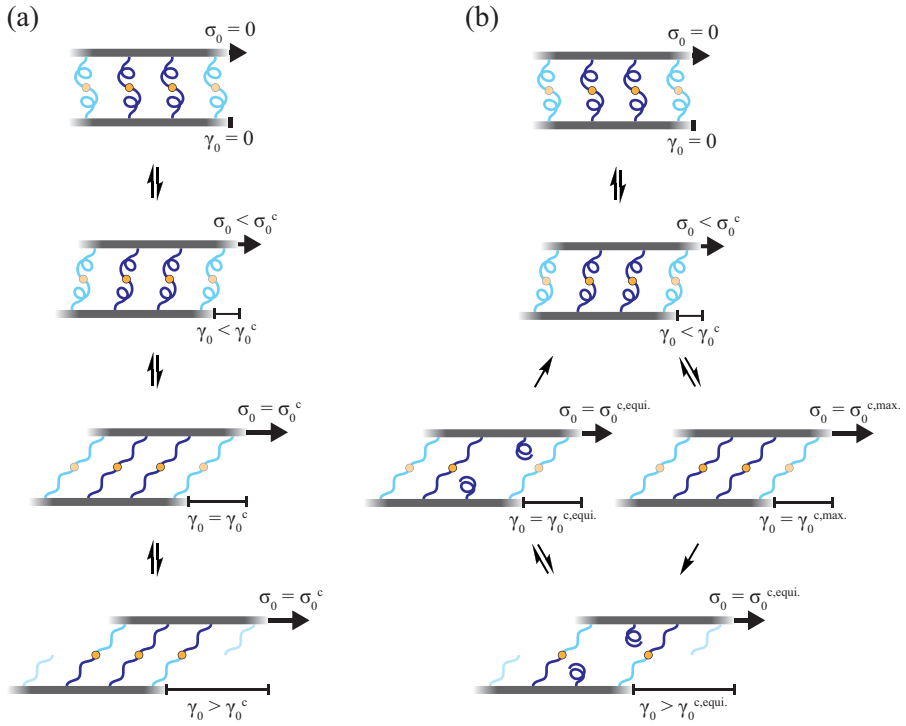

Figure 12.20 – Sketches featuring the behaviour of non-covalently bridged thermo-sensitive polymer chains under shear, (a) below and (b) above the LCST.

In essence, the thermo-rheological response of the investigated hydrogel is consistent with the responsive behaviour of poly(*N*-isopropylacrylamide) chains in aqueous solution. Below the LCST, favourable interactions allow the dissolution of the polymer in water, via hydrogen bonding. Due to micellar organization, PNIPAAm chains adopt in a fairly extended conformation at 20 °C, which in turn allows them to reversibly bind via supramolecular links. Under those conditions, the

release of mechanical stress proceeds via activated dissociation and subsequent exchange of the non-covalent bonds structuring the material, as schematically illustrated in Figure 12.20 (a).

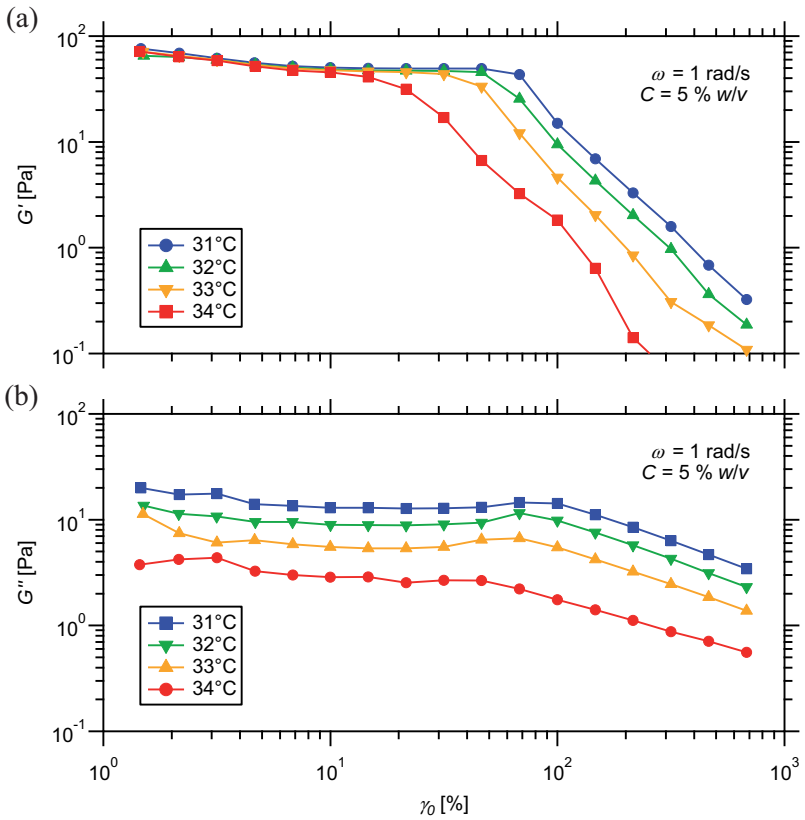

Figure 12.21 – Strain dependence of (a) elastic and (b) viscous moduli for a hydrogel prepared from PS_{27}-*b*-$PNIPAAm_{300}$-tpy copolymer and Co(II) ions, at different temperatures.

During the phase transition, the hydrogen bonds are disrupted and thus the polymer phase separates. From a structural point of view, free macromolecular chains are expected to undergo a coil-to-globule transition. Within the network, mechanical forces can however induce stretching of PNIPAAm chains up to a certain extend that is lowered in the range of the phase transition temperature (Figure 12.19). Exceeding the yield strength of the material then allows stress release and collapse of the polymer chains (Figure 12.20 (b)). Once the network

is mechanically disturbed, a certain proportion of stretched chains thus transits to the globule conformation, which is responsible for the hysteresis loss. At large strain, the conformation of the collapsed chains prevents the reformation of elastically active cross-links. Complete healing of the gel is thus only observed when coming back to small deformations (Figure 12.19), which subsequently allows the reformation of elastically active junctions between polymer strands (Figure 12.20 (b)).

To further illustrate the thermo-sensitivity of the selected materials, their mechanical properties are investigated more deeply in the range of the phase transition temperature. In practice, isothermal amplitude strain sweeps are performed on the gel with an incremental temperature change. As shown in Figure 12.21, the linear storage modulus shows a consistent value all over the transition temperature region, meaning that the number of mechanically active chains tethering the micellar network remains essentially constant. On the other hand, the equilibrium viscous modulus gradually decreases when temperature rises. As the PNIPAAm chains undergo a coil-to-globule transition, the volume fraction of polymer in solution is indeed reduced, as illustrated in Figure 12.16, which lowers the fraction of mechanical energy dissipated through viscous effects.

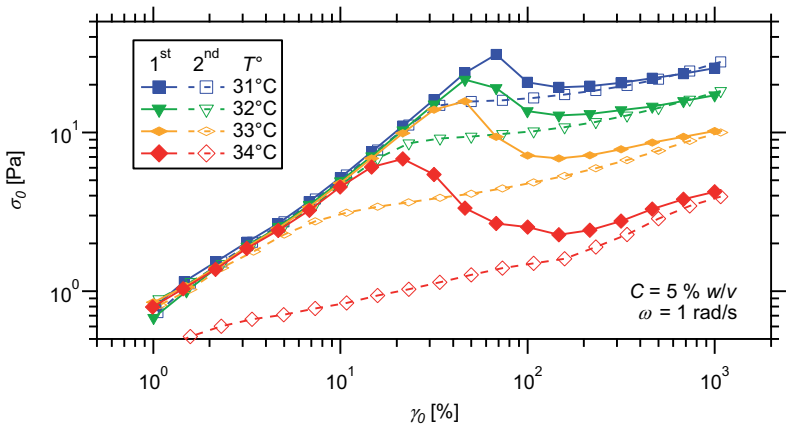

Figure 12.22 – Stress–strain relationship for a hydrogel prepared from PS_{27}-*b*-$PNIPAAm_{300}$-tpy copolymer and Co(II) ions, at different temperatures: 1st run under increasing strain, 2nd run under decreasing strain.

The consistent number of stress carrying chains in the network is further supported by the invariance of the linear strain–stress relationships (Figure 12.22). As noted above, the onset of network breaking is however shifted to lower strain amplitude when the temperature is increased. In the range of the phase transition, the yield strain of the material is progressively reduced by nearly one order of magnitude. Fundamentally, this observation reflects the will of PNIPAAm chains to adopt a globule conformation upon heating. In agreement, the hysteresis loss evaluated from strain–stress curves becomes drastically more pronounced, as shown in Figure 12.23. Along with a decreasing yield strain, the stress value that marks the end of the linear viscoelastic response of the material gradually declines upon heating. On the whole, the phase transition is responsible for a nearly one decade decrease in the yield strength of the material.

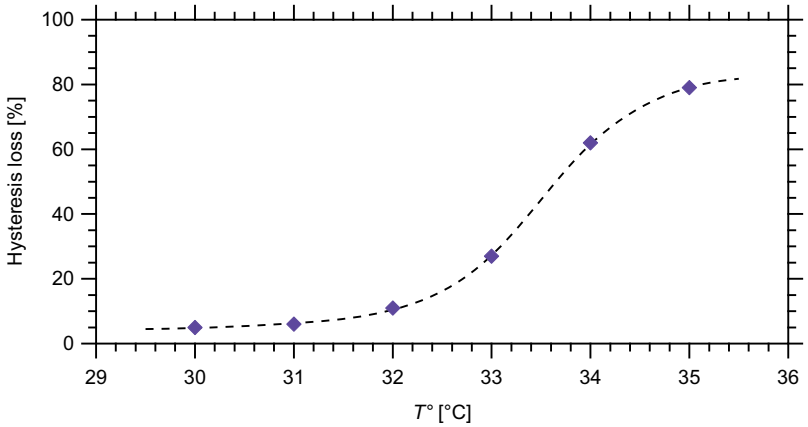

Figure 12.23 – Percentage of hysteresis loss for a hydrogel prepared from PS_{27}-*b*-$PNIPAAm_{300}$-tpy copolymer and Co(II) ions, as a function of the temperature.

12.4.2 Responsiveness of PS-*b*-PNIPAAm-*b*-PDMAEMA-tpy hydrogels

Although synthetically challenging, stimuli-responsive multiblock copolymers produce well-defined physical gels through the triggered or autonomous non-covalent association of one or more blocks. In turn, they provide appealing flexibility for controlling the gel micro-structure and

physical properties through variation of the block lengths and application of proper stimuli.[36,70,91] Accordingly, the use of PS-*b*-PNIPAAm-*b*-PDMAEMA-tpy triblock terpolymers as precursors of supramolecular gels offers here several advantages compared to their diblock counterparts. For example, PS-*b*-PNIPAAm-tpy hydrogels tend to phase separate and thus may lose their integrity when heated above the collapse temperature of the PNIPAAm block. Contrastingly, PNIPAAm-*b*-PDMAEMA-tpy based materials only behave solid-like above the same critical temperature while, for many applications, it would be desirable to also have a gel-like behaviour under ambient conditions instead of a free-flowing solution.

By varying the molecular weight of the different segments constituting the triblock terpolymer chains, their solution behaviour can be continuously varied from the one of PS-*b*-PNIPAAm-tpy to the one of PNIPAAm-*b*-PDMAEMA-tpy diblock copolymers, thus bridging the gap between the two above-discussed systems. In essence, the rheological signature of PS-*b*-PNIPAAm-*b*-PDMAEMA-tpy terpolymer gels can be thus interpreted on the basis of the thermo-mechanical responses of both diblock copolymer counterparts. Despite being the most advanced building blocks synthesized in the frame of this project, they thus only bring a little contribution to the fundamental understanding of the rheology of metallo-supramolecular micellar gels.

12.4.2.1 Analogy with PNIPAAm-*b*-PDMAEMA-tpy solutions

When a very short PS segment is located at the extremity of the chain, the solution behaviour of PS-*b*-PNIPAAm-*b*-PDMAEMA-tpy triblock copolymers is essentially similar to that observed for PNIPAAm-*b*-PDMAEMA-tpy analogues. At room temperature, their solutions indeed behave as Newtonian liquids with characteristic frequency dependences of dynamic moduli, that transit from the sol to the gel state upon heating. However, temperature sweep experiments show that the onset of modulus increase can occur earlier when triblock terpolymers are used in place of double hydrophilic diblock copolymers (Figure 12.24). To account for this early transition, it is strongly believed that the presence of PS segments in the architecture of the chains benefits to the early formation of the micellar network, notably by serving as nucleation sites for hydrophobic domains.

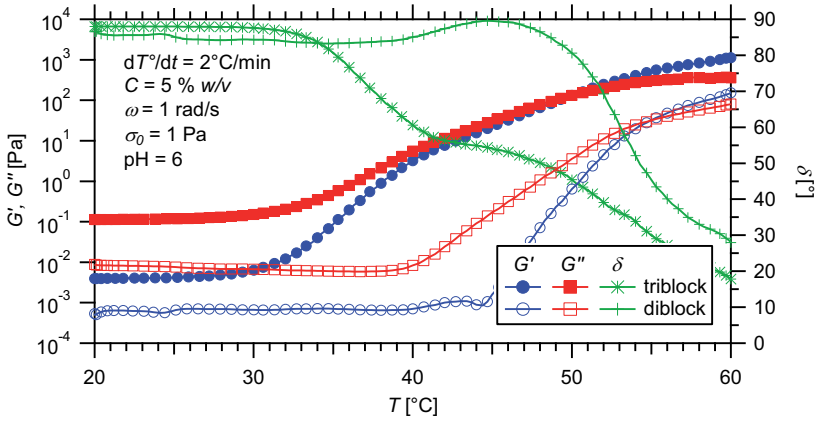

Figure 12.24 – Temperature dependence of dynamic moduli for hydrogels prepared from PNIPAAm$_{75}$-*b*-PDMAEMA$_{105}$-tpy diblock and PS$_4$-*b*-PNIPAAm$_{75}$-*b*-PDMAEMA$_{105}$-tpy triblock copolymers and Ni(II) ions.

As evaluated by the cross-over between G' and G'' in temperature sweeps (Figure 12.24), the gelation temperatures are comparable for each formulation, *i.e.*, involving either the diblock or triblock copolymer. Hence, this observation points at a relatively poor contribution of

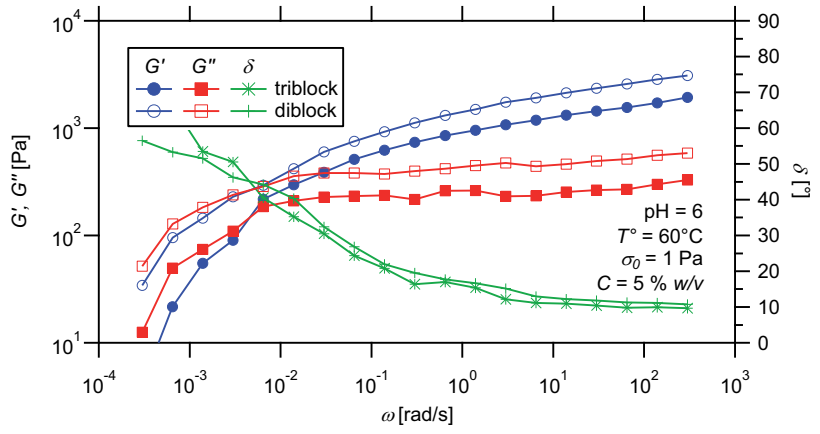

Figure 12.25 – Frequency dependence of dynamic moduli for hydrogels prepared from PNIPAAm$_{75}$-*b*-PDMAEMA$_{105}$-tpy diblock and PS$_4$-*b*-PNIPAAm$_{75}$-*b*-PDMAEMA$_{105}$-tpy triblock copolymers and Ni(II) ions, at 60 °C.

the polystyrene end-group to the growing stability of the micellar nodes. In frequency sweep tests performed after full equilibration of the samples, this negligible contribution results in comparable relaxation times for micellar networks prepared from triblock and diblock copolymers (Figure 12.25).

12.4.2.2 Analogy with PS-*b*-PNIPAAm-tpy hydrogels

When the length of the PS segment is increased, the solution behaviour of PS-*b*-PNIPAAm-*b*-PDMAEMA-tpy triblock terpolymers deviates from the one of PNIPAAm-*b*-PDMAEMA-tpy copolymers to the one of PS-*b*-PNIPAAm-tpy copolymers. Above a critical concentration, free-standing hydrogels are indeed obtained at room temperature, due to the formation of active metallo-bridges among the segregated PS rich domains. Upon heating, the structure of the triblock micellar networks is expected to be further reinforced by the collapse of PNIPAAm segments onto the preformed micellar nodes (Figure 12.26). In contrast to PS-*b*-PNIPAAm-tpy hydrogels, no phase separation is generally observed for triblock copolymer gels at high temperatures. In practice, this situation is precisely achieved as long as the PDMAEMA block ensures a sufficient hydration of the network, which depends on its length relative to the other blocks, as well as environmental parameters, *e.g.*, temperature and pH, as addressed above.

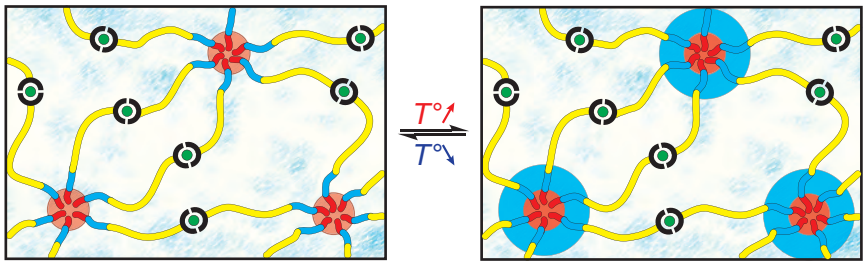

Figure 12.26 – Structural responsiveness of PS-*b*-PNIPAAm-*b*-PDMAEMA-tpy metallo-supramolecular micellar gels.

In the following, oscillatory shear measurements are conducted on PS-*b*-PNIPAAm-*b*-PDMAEMA-tpy hydrogels to elucidate the particular effect of temperature on their rheological behaviour, around neutral

pH. At first, the evolution of dynamic moduli upon thermal variations is followed in the form of temperature sweeps. Then, frequency sweeps are performed under small amplitude oscillatory shear, over a temperature range that covers the phase transition of the PNIPAAm block. Finally, the non-linear viscoelastic response of the gels is investigated by amplitude strain sweeps operating at different temperatures.

12.4.2.3 Oscillatory temperature sweep

Due to an enhanced relaxation of the transient cross-links, supramolecular gels often suffer a loss in their mechanical properties when tested at elevated temperatures.[92] In sharp contrast, PS-*b*-PNIPAAm-*b*-PDMAEMA-tpy hydrogels show a strengthened viscoelastic response to shear, as attested by dynamic temperature sweeps (Figure 12.27). For both G' and G'', the thermal transition forms a continuum extending over almost the entire investigated temperature range, with a net increase that may approach one and a half order of magnitude depending on the length of PS segment with respect to PNIPAAm block.

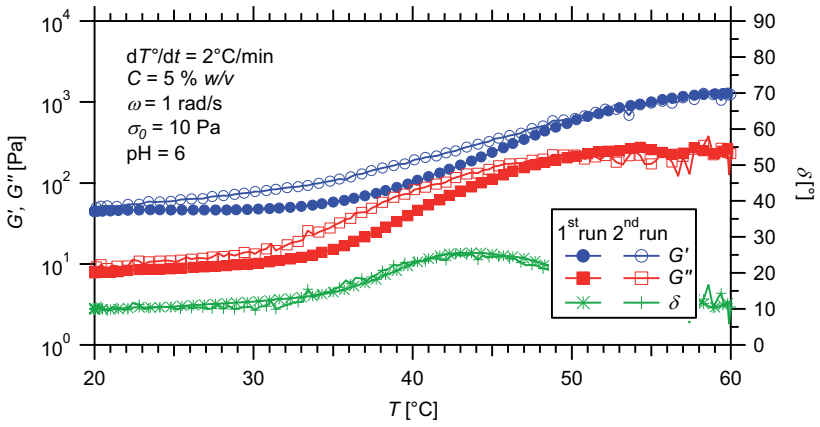

Figure 12.27 – Temperature dependence of dynamic moduli for a hydrogel prepared from PS_{12}-*b*-$PNIPAAm_{75}$-*b*-$PDMAEMA_{105}$-tpy copolymer and Ni(II) ions: 1st run upon heating, 2nd run upon cooling.

Under ambient condition, the gel strength results from the aggregation of PS segments into hydrophobic domains that are further bridged by metal–ligand associations. Above a certain temperature, core-shell-

corona micelles are formed with the PS blocks forming micellar cores and the PNIPAAm segments constituting the shell layer. This temperature-induced transition, centred around 40 °C, stems from the solution behaviour of the thermo-sensitive middle block of the triblock copolymer. When the temperature is raised above the LCST of PNIPAAm segments, they undergo a hydration-to-dehydration that reinforce the network structure, as illustrated in Figure 12.26. Although not clearly evidenced, a plausible additional contribution from the partial collapse of the PDMAEMA block is not a priori excluded at high temperature. Then, decreasing temperature dissolves the PNIPAAm blocks and weakens the network, resulting in the reverse transition with almost no hysteresis.

12.4.2.4 Oscillatory frequency sweep

To get further insight into the thermo-responsive behaviour of PS-*b*-PNIPAAm-*b*-PDMAEMA-tpy triblock copolymer gels, frequency sweeps are conducted using low stress amplitude, at selected temperatures covering the strengthening transition range (Figure 12.28). In agreement with temperature sweep, the plateau dynamic storage modulus, obtained from frequency sweeps, increases by around one and a half order of magnitude upon heating. Under ambient conditions, a rubber-like behaviour is observed for the triblock copolymer gel, as indicated by the weak frequency-dependent plateaus in both moduli over the entire investigated frequency range. During the transition, the increase in modulus is however more pronounced in the high-frequency regime than in the low-frequency region, so that a fast relaxation process becomes apparent, especially around 40 °C. Finally, at higher temperature, both G' and G'' tend to show again much weaker frequency dependencies, which is hampered by the thermally activated terminal relaxation of the material. For better assessment, a frequency sweep in a wider range, *i.e.*, spanning 6 orders in magnitude, is collected at 60 °C where both the plateau behaviour and the terminal flow are observed (Figure 12.29).

As already discussed above, relaxation of mechanical stress in micellar gels proceeds mainly via the exchange of polymer strands between hydrophobic nodes of the network.[93,94] To dissociate from a junction, a chain segment must first overcome an energy barrier before diffusing into the surrounding medium. As demonstrated for PS-*b*-PNIPAAm-

tpy networks, this energy barrier can be dramatically increased by the collapse of PNIPAAm chain segments onto micellar cores. In turn, this suppresses the relaxation of the material via exchange of hydrophobes, thereby benefiting to the low frequency response of the gel only. However, rheological characterization of triblock copolymer gels show that, even in the absence of relaxation processes, both elastic and viscous responses increase significantly upon heating (Figure 12.28).

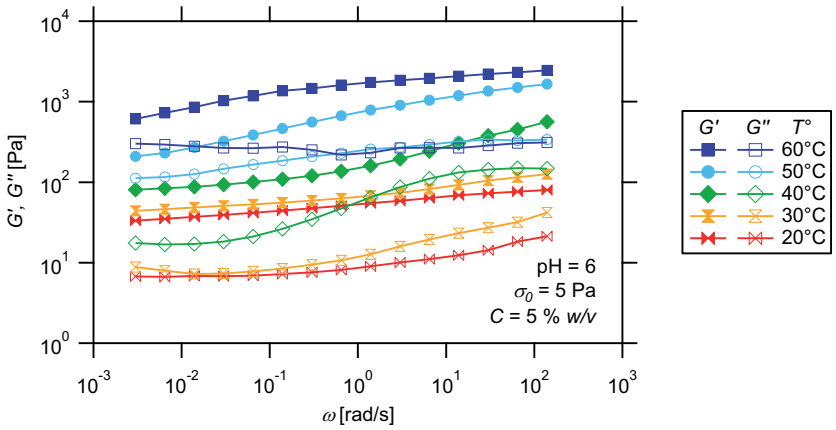

Figure 12.28 – Frequency dependence of dynamic moduli for a hydrogel prepared from PS_{12}-*b*-$PNIPAAm_{75}$-*b*-$PDMAEMA_{105}$-tpy copolymer and Ni(II) ions, at different temperatures.

To explain the thermal transition in moduli, it is hypothesized that the relaxation being observed at intermediate temperatures corresponds to local motions of PNIPAAm segment. At low temperature, relaxation of the chain segments in solution is extremely prompt due to micro-Brownian motions, which do not contribute to the modulus. Being part of the fast relaxation spectrum of the material, these motions are not directly accessible by experiment since they involve extremely short time scales and low activation energy barriers. Upon heating, the collapse of PNIPAAm block onto preformed micellar cores progressively restricts the motions of chain segments in solution. In turn, the decreasing degree of motional freedom, caused by intra- and inter-chain association in the collapsed state, results in a gradual shift of this relaxation mode to lower frequencies. At elevated temperatures, the advanced dehydration of the PNIPAAm block leads to a dramatic increase in conformational rigidity, therefore disabling the motion of PNIPAAm segments as schematized in

Figure 12.26.

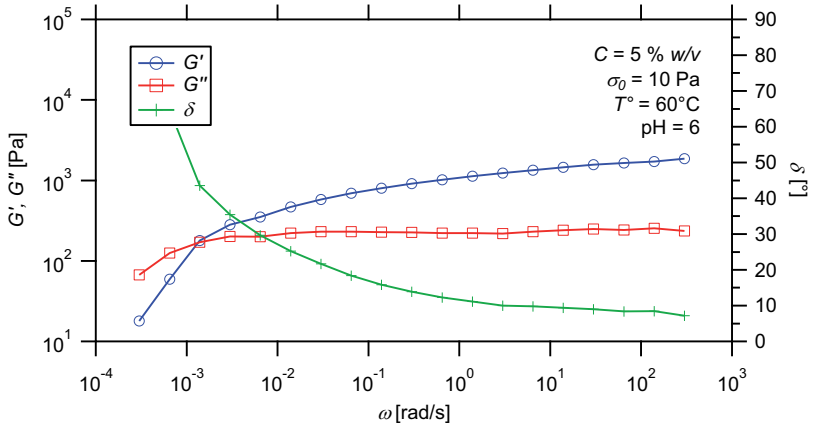

Figure 12.29 – Frequency dependence of dynamic moduli for a hydrogel prepared from PS_{12}-*b*-$PNIPAAm_{75}$-*b*-$PDMAEMA_{105}$-tpy copolymer and Ni(II) ions, at 60 °C.

12.4.2.5 Oscillatory strain sweep

To further look into the gel characteristics, amplitude strain sweeps are conducted on triblock copolymer gels at various temperatures and a given frequency of 1 rad/s. As illustrated in Figure 12.30, the studied materials display long linear viscoelastic response over the whole covered temperature range. Under small amplitude oscillatory shear, moduli indeed remain nearly invariant with respect to strain amplitude, indicating no break up of the network structure. At larger deformations, both moduli drop dramatically with strain on sample, which is highly characteristic of non-linear response.

A first consequence of the collapse of PNIPAAm mid-block onto micellar cores is that hydrogels exhibit stronger stress robustness at higher temperature. Nevertheless, the yield of the materials is observed around comparable strain amplitudes in the nearly entire temperature range. In practice, a significant deviation is only observed at a temperature of 60 °C. Under this condition, a mild dehydration of the network can be expected due to the partial collapse of PDMAEMA chains, which would indeed result in lower stretchability. However, almost no hysteresis loss

can be observed when coming back to small deformations (Figure 12.31), suggesting that triblock copolymer gels remain well hydrated even at high temperatures, at least around neutral pH.

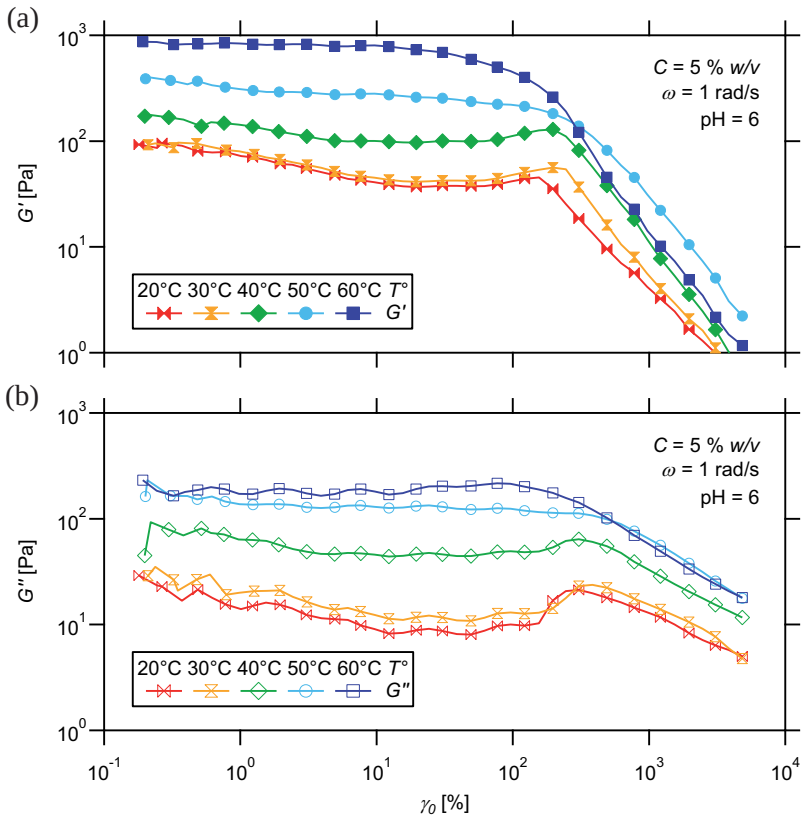

Figure 12.30 – Strain dependence of dynamic moduli for a hydrogel prepared from PS_{12}-*b*-$PNIPAAm_{75}$-*b*-$PDMAEMA_{105}$-tpy copolymer and Ni(II) ions, at different temperatures.

The dynamic strain sweep study also reveals significant thermal variations in the behaviour of the gels at the limit of the linear range (Figure 12.30). At low temperatures, a hardening response to strain, that is particularly marked in the loss modulus, is observed prior yielding. As suggested by Tam and coworkers,[95] such a behaviour may result from the incorporation of finite size aggregates into the percolated hydrogel, which is possible due to reorganization of the weakly associated network structure. As the temperature is increased, the collapse of PNIPAAm

segments onto micellar nodes is thought to reduce the tolerance and flexibility of the same structure against high shear deformation. As a consequence, strain softening is only observed above 40 °C, as shown in Figure 12.30.

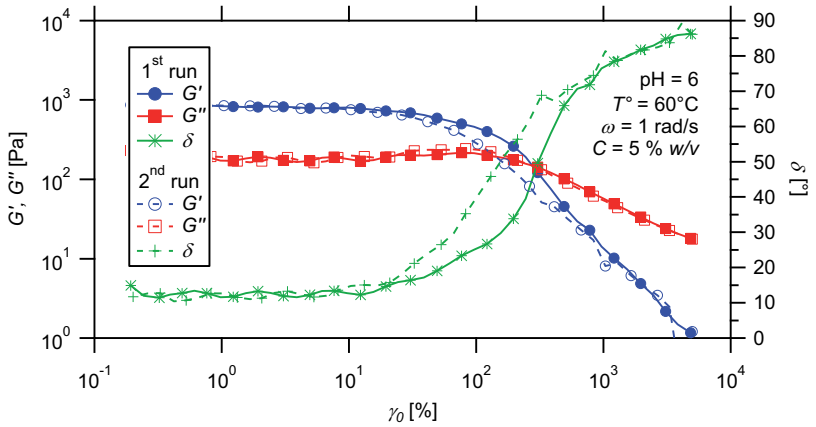

Figure 12.31 – Strain dependence of dynamic moduli for a hydrogel prepared from PS_{12}-*b*-$PNIPAAm_{75}$-*b*-$PDMAEMA_{105}$-tpy copolymer and Ni(II) ions, at 60 °C: 1st run under increasing strain, 2nd run under decreasing strain.

12.5 Summary

This chapter explored the possibility of controlling the formation, strength, and dynamics of metallo-supramolecular micellar networks in response to specific environmental triggers. The latter included temperature, pH, and the presence of co-solvent, thus targeting both non-covalent associations tethering the supramolecular materials and the responsive polymer sequences that compose the gel scaffolds. As characterization technique, rotational rheometry was used to monitor changes in the viscoelastic response of diblock and triblock copolymer based materials upon stimulation.

At first, the dynamics of PS-*b*-PNIPAAm-tpy associating copolymer gels was addressed in an orthogonal and controllable fashion, while keeping their overall viscoelastic response essentially unaltered. On one hand, the protonation of the terpyridine ligands under medium-to-high acidic

conditions was demonstrated to promote the dissociation of the metal–ligand complexes, thus affecting the slow relaxation of the network. On the other hand, solvent-induced plasticization of the hydrophobic associations enhanced the detachment of the chain-ends from the network nodes, leading to a decrease of the fast relaxation time.

Then, the use of external stimuli to trigger the formation of micellar networks was tested on concentrated solutions of PNIPAAm-*b*-PDMAEMA-tpy double hydrophilic diblock copolymers. Beyond the temperature-dependent behaviour of PNIPAAm blocks, rheological measurements showed that micellar aggregation manifests itself as a delayed gelation, at least under neutral or acidic conditions. Besides, the formation of a percolated network was effectively inhibited under basic conditions due to the low solubility of the deprotonated PDMAEMA block at high temperatures. In addition, the gelation temperature range was adjusted depending on several factors including the concentration in diblock copolymer, the pH of the solution, and the nature of metal ions. Interestingly, an independent control over the network formation and dynamics was notably achieved, via proper choice of the metal ions, when long PNIPAAm segments were used. Finally, the reversible nature of the thermo-induced sol–gel transition was verified upon cooling, the micellar network disaggregating into individual chains.

The change in chain conformation of PNIPAAm segment was further exploited to tune the rheological response of hydrogels prepared from PS-*b*-PNIPAAm-tpy diblock copolymers. Below the critical solution temperature of PNIPAAm chain segments, the materials showed the characteristic features of temporary micellar networks. Above the phase transition temperature, the collapse of PNIPAAm chains caused the shielding of transient micellar cores, thus reinforcing them kinetically. As a result, the rheological behaviour of PS-*b*-PNIPAAm-tpy based materials changed from the one of transient micellar gels to the one of dynamically more stable coordination rubbery gels.

Even if a mesoscopic phase separation occurred, the mechanical integrity of PS-*b*-PNIPAAm-tpy hydrogels was however preserved at high temperatures, which was attributed to the presence of charged metal–ligand complexes. When stressed by mechanical forces, the self-assembled materials exhibited a fully reversible gel-to-sol transition, at the collapse temperature of PNIPAAm as well as under ambient conditions. Self-healing of the gels was however marked by a hysteresis at the phase

transition temperature, which was rationally correlated with the conformational behaviour of the thermo-sensitive chains in aqueous solution. In this regard, heating the gels across the phase transition boundaries led to a more pronounced hysteresis, along with a gradual decrease in the yield strength of the materials.

Lastly, the same thermo-rheological study was extended on PS-*b*-PNIPAAm-*b*-PDMAEMA-tpy triblock terpolymer hydrogels. Depending on the length of the PS segment, their behaviour was in fact varied from the one of PNIPAAm-*b*-PDMAEMA-tpy diblock copolymer solutions to the one of PS-*b*-PNIPAAm-tpy diblock copolymer gels. For short polystyrene, the association strength of the terminal sticker was not strong enough to generate a long-lived network, but was sufficient to assist the thermo-induced gelation of the system. For longer PS segments, well-hydrated gels were readily obtained whose frequency- and strain-dependences of their linear viscoelastic moduli were reported as a function of the temperature. Notably, results evidenced that the high degree of freedom of the PNIPAAm segment in the hydrated state allowed partial relaxation of mechanical stress. This wasted contribution to the elastic response was however modulated by the solubility of the middle block at higher temperatures. By ultimately suppressing the segmental relaxation, the collapse of PNIPAAm block also led to stronger hydrophobic associations that are less easily disrupted by mechanical forces. Finally, the response of the gels under large oscillatory shear was sensibly varied across the investigated temperature range. Precisely, an overshoot in both moduli was observed below the collapse transition temperature of PNIPAAm segment, while the same materials exhibit strain thinning only at higher temperatures.

12.6 Experimental part

Materials

Terpyridine end-capped block copolymers are synthesized via sequential reversible addition–fragmentation chain transfer control radical copolymerization, as reported in a previous chapter. Nickel(II), iron(II), cobalt(II) and zinc(II) chloride salts are dried, kept in a glove box, and weighted under argon atmosphere.

Instrumentation

Shear rheological experiments are performed on a Kinexus Ultra (Malvern Instrument) rheometer equipped with a heat exchanger and modified with a solvent trap. Measurements are carried out at given temperatures, using a 20 mm plate–plate geometry, in a water saturated atmosphere in order to minimize evaporation of the solvent. The gap is adjusted between 50 and 250 µm so that the geometry is completely filled. Normal forces are checked to be relaxed prior any measurement.

Preparation of supramolecular gels

Hydrogels are prepared by mixing given amounts of block copolymer with Milli-Q water. The sealed reaction vessels are placed in a fridge and shaken periodically to form homogeneous concentrated solutions after a few days. When required, pH of the solutions is adjusted via addition of hydrochloric acid aqueous solution of a given molarity. In this respect, targeting total, half and no protonation of the amine groups of PDMAEMA respectively lead to pH values of 3, 6 and 9. The gels or precursor solutions are then readily obtained by adding the stoichiometric amount of half an equivalent of transition metal ions (with respect to the terpyridine content) dissolved in defined amounts of Milli-Q water to each concentrated solutions. Lastly, the reaction vessels are placed again in the fridge over three days to ensure homogenization and stabilization of the materials. The final concentration of copolymers in samples varies in the semi-diluted regime, from 5 to 20 %w/v.

Loading and testing protocol

Around 50 µL of gel is loaded onto the stationary bottom plate of the rheometer preheated at 20 °C. By stepwise lowering the gap between the two plates, the sample is compressed and forced to spread over the geometry so that the gap is completely filled. Equilibration of the sample is followed by monitoring the evolution of normal force, storage and loss moduli with time, under small amplitude oscillatory shear. Rheological tests are started when both moduli reach constant values and normal force has relaxed to < 0.05 N.

Bibliography

[1] Yu, G.; Yan, X.; Han, C.; Huang, F. *Chem. Soc. Rev.* **2013**, *42*, 6697–6722.
[2] Beck, J. B.; Rowan, S. J. *J. Am. Chem. Soc.* **2003**, *125*, 13922–13923.
[3] Noro, A.; Matsushima, S.; He, X.; Hayashi, M.; Matsushita, Y. *Macromolecules* **2013**, *46*, 8304–8310.
[4] Yang, C. H.; Wang, M. X.; Haider, H.; Yang, J. H.; Sun, J.-Y.; Chen, Y. M.; Zhou, J.; Suo, Z. *ACS Appl. Mater. Interfaces* **2013**, *5*, 10418–10422.
[5] Chen, D.; Liu, H.; Kobayashi, T.; Yu, H. *J. Mater. Chem.* **2010**, *20*, 3610–3614.
[6] Nakahata, M.; Takashima, Y.; Harada, A. *Angew. Chem. Int. Ed.* **2014**, *53*, 3617–3621.
[7] Miller, A. K.; Li, Z.; Streletzky, K. A.; Jamieson, A. M.; Rowan, S. J. *Polym. Chem.* **2012**, *3*, 3132–3138.
[8] Yan, Q.; Feng, A.; Zhang, H.; Yin, Y.; Yuan, J. *Polym. Chem.* **2013**, *4*, 1216–1220.
[9] Zhou, L.; Li, J.; Luo, Q.; Zhu, J.; Zou, H.; Gao, Y.; Wang, L.; Xu, J.; Dong, Z.; Liu, J. *Soft Matter* **2013**, *9*, 4635–4641.
[10] Zhang, Q.; Qu, D.-H.; Wu, J.; Ma, X.; Wang, Q.; Tian, H. *Langmuir* **2013**, *29*, 5345–5350.
[11] Burnworth, M.; Tang, L. M.; Kumpfer, J. R.; Duncan, A. J.; Beyer, F. L.; Fiore, G. L.; Rowan, S. J.; Weder, C. *Nature* **2011**, *472*, 334–230.
[12] Guo, M.; Pitet, L. M.; Wyss, H. M.; Vos, M.; Dankers, P. Y. W.; Meijer, E. W. *J. Am. Chem. Soc.* **2014**, *136*, 6969–6977.
[13] Qi, Z.; Traulsen, N. L.; Malo de Molina, P.; Schlaich, C.; Gradzielski, M.; Schalley, C. A. *Org. Biomol. Chem.* **2014**, *12*, 503–510.
[14] Rossow, T.; Seiffert, S. *Polym. Chem.* **2014**, *5*, 3018–3029.
[15] Rossow, T.; Hackelbusch, S.; van Assenbergh, P.; Seiffert, S. *Polym. Chem.* **2013**, *4*, 2515–2527.
[16] Zhan, J.; Li, Q.; Hu, Q.; Wu, Q.; Li, C.; Qiu, H.; Zhang, M.; Yin, S. *Chem. Commun.* **2014**, *50*, 722–724.
[17] Hackelbusch, S.; Rossow, T.; Becker, H.; Seiffert, S. *Macromolecules* **2014**, *47*, 4028–4036.
[18] Vatankhah-Varnoosfaderani, M.; GhavamiNejad, A.; Hashmi, S.; Stadler, F. J. *Chem. Commun.* **2013**, *49*, 4685–4687.
[19] Fleischer, M.; Schmuck, C. *Chem. Commun.* **2014**, *50*, 10464–10467.
[20] Yao, X.; Chen, L.; Chen, X.; He, C.; Zhang, J.; Chen, X. *Macromol. Rapid Commun.* **2014**, *35*, 1697–1705.
[21] Segarra-Maset, M. D.; Nebot, V. J.; Miravet, J. F.; Escuder, B. *Chem. Soc. Rev.* **2013**, *42*, 7086–7098.
[22] Yan, X.; Wang, F.; Zheng, B.; Huang, F. *Chem. Soc. Rev.* **2012**, *41*, 6042–6065.
[23] Pasparakis, G.; Vamvakaki, M. *Polym. Chem.* **2011**, *2*, 1234–1248.

[24] Ma, X.; Tian, H. *Acc. Chem. Res.* **2014**, *47*, 1971–1981.
[25] Gulyuz, U.; Okay, O. *Macromolecules* **2014**, *47*, 6889–6899.
[26] Wang, Z.; Fan, W.; Tong, R.; Lu, X.; Xia, H. *RSC Advances* **2014**, *4*, 25486–25493.
[27] Kumpfer, J. R.; Rowan, S. J. *J. Am. Chem. Soc.* **2011**, *133*, 12866–12874.
[28] Wei, Z.; Yang, J. H.; Zhou, J.; Xu, F.; Zrinyi, M.; Dussault, P. H.; Osada, Y.; Chen, Y. M. *Chem. Soc. Rev.* **2014**, *43*, 8114–8131.
[29] Herbst, F.; Döhler, D.; Michael, P.; Binder, W. H. *Macromol. Rapid Commun.* **2013**, *34*, 203–220.
[30] Stukalin, E. B.; Cai, L.-H.; Kumar, N. A.; Leibler, L.; Rubinstein, M. *Macromolecules* **2013**, *46*, 7525–7541.
[31] Yan, L.; Gou, S.; Ye, Z.; Zhang, S.; Ma, L. *Chem. Commun.* **2014**, *50*, 12847–12850.
[32] Vatankhah-Varnoosfaderani, M.; Hashmi, S.; GhavamiNejad, A.; Stadler, F. J. *Polym. Chem.* **2014**, *5*, 512–523.
[33] Roy, D.; Brooks, W. L. A.; Sumerlin, B. S. *Chem. Soc. Rev.* **2013**, *42*, 7214–7243.
[34] Liu, R. X.; Fraylich, M.; Saunders, B. R. *Colloid Polym. Sci.* **2009**, *287*, 627–643.
[35] Miasnikova, A.; Laschewsky, A.; De Paoli, G.; Papadakis, C.; Muuller-Buschbaum, P.; Funari, S. S. *Langmuir* **2012**, *28*, 4479–4490.
[36] He, Y.; Lodge, T. P. *Macromolecules* **2008**, *41*, 167–174.
[37] O'Lenick, T. G.; Jiang, X.; Zhao, B. *Langmuir* **2010**, *26*, 8787–8796.
[38] Li, C.; Buurma, N. J.; Haq, I.; Turner, C.; Armes, S. P.; Castelletto, V.; Hamley, I. W.; Lewis, A. L. *Langmuir* **2005**, *21*, 11026–11033.
[39] Dai, S.; Ravi, P.; Tam, K. C. *Soft Matter* **2008**, *4*, 435–449.
[40] Charbonneau, C.; Chassenieux, C.; Colombani, O.; Nicolai, T. *Macromolecules* **2011**, *44*, 4487–4495.
[41] O'Lenick, T. G.; Jin, N.; Woodcock, J. W.; Zhao, B. *J. Phys. Chem. B* **2011**, *115*, 2870–2881.
[42] Koonar, I.; Zhou, C.; Hillmyer, M. A.; Lodge, T. P.; Siegel, R. A. *Langmuir* **2012**, *28*, 17785–17794.
[43] Huang, Y.; Dong, R.; Zhu, X.; Yan, D. *Soft Matter* **2014**, *10*, 6121–6138.
[44] Gohy, J.-F.; Zhao, Y. *Chem. Soc. Rev.* **2013**, *42*, 7117–7129.
[45] Jochum, F. D.; Theato, P. *Chem. Soc. Rev.* **2013**, *42*, 7468–7483.
[46] Schumers, J.; Fustin, C.; Gohy, J. *Macromol. Rapid Commun.* **2010**, *31*, 1588–1607.
[47] Klaikherd, A.; Nagamani, C.; Thayumanavan, S. *J. Am. Chem. Soc.* **2009**, *131*, 4830–4838.
[48] Loveless, D.; Jeon, S.; Craig, S. *Macromolecules* **2005**, *38*, 10171–10177.
[49] Yount, W. C.; Loveless, D. M.; Craig, S. L. *J. Am. Chem. Soc.* **2005**, *127*, 14488–14496.
[50] Hackelbusch, S.; Rossow, T.; van Assenbergh, P.; Seiffert, S. *Macromolecules* **2013**, *46*, 6273–6286.

[51] Nair, K. P.; Breedveld, V.; Weck, M. *Macromolecules* **2011**, *44*, 3346–3357.
[52] Tian, Y.-K.; Chen, L.; Tian, Y.-J.; Wang, X.-Y.; Wang, F. *Polym. Chem.* **2013**, *4*, 453–457.
[53] Weng, W.; Fang, X.; Zhang, H.; Peng, H.; Lin, Y.; Chen, Y. *Eur. Polym. J.* **2013**, *49*, 4062–4071.
[54] Yan, X.; Xu, D.; Chen, J.; Zhang, M.; Hu, B.; Yu, Y.; Huang, F. *Polym. Chem.* **2013**, *4*, 3312–3322.
[55] Yan, X.; Xu, D.; Chi, X.; Chen, J.; Dong, S.; Ding, X.; Yu, Y.; Huang, F. *Adv. Mater.* **2012**, *24*, 362–369.
[56] Zeng, F.; Han, Y.; Yan, Z.-C.; Liu, C.-Y.; Chen, C.-F. *Polymer* **2013**, *54*, 6929–6935.
[57] Weng, W. G.; Beck, J. B.; Jamieson, A. M.; Rowan, S. J. *J. Am. Chem. Soc.* **2006**, *128*, 11663–11672.
[58] Chen, L.; Tian, Y.; Ding, Y.; Tian, Y.; Wang, F. *Macromolecules* **2012**, *45*, 8412–8419.
[59] Lohmeijer, B. G. G.; Schubert, U. S. *Macromol. Chem. Phys.* **2003**, *204*, 1072–1078.
[60] Tsitsilianis, C.; Aubry, T.; Iliopoulos, I.; Norvez, S. *Macromolecules* **2010**, *43*, 7779–7784.
[61] Farina, R.; Hogg, R.; Wilkins, R. *Inorg. Chem.* **1968**, *7*, 170–172.
[62] Holyer, R. H.; Hubbard, C. D.; Kettle, S. F. A.; Wilkins, R. G. *Inorg. Chem.* **1966**, *5*, 622–625.
[63] Nicolai, T.; Colombani, O.; Chassenieux, C. *Soft Matter* **2010**, *6*, 3111–3118.
[64] Hara, M.; Jar, P.; Sauer, J. *Polymer* **1991**, *32*, 1380–1383.
[65] Tsitsilianis, C. *Soft Matter* **2010**, *6*, 2372–2388.
[66] Bae, S. J.; Joo, M. K.; Jeong, Y.; Kim, S. W.; Lee, W.-K.; Sohn, Y. S.; Jeong, B. *Macromolecules* **2006**, *39*, 4873–4879.
[67] Iddon, P.; Armes, S. *Eur. Polym. J.* **2007**, *43*, 1234–1244.
[68] Zhou, C.; Hillmyer, M. A.; Lodge, T. P. *J. Am. Chem. Soc.* **2012**, *134*, 10365–10368.
[69] Reinicke, S.; Schmelz, J.; Lapp, A.; Karg, M.; Hellweg, T.; Schmalz, H. *Soft Matter* **2009**, *5*, 2648–2657.
[70] Sugihara, S.; Kanaoka, S.; Aoshima, S. *J. Polym. Sci., Part A: Polym. Chem.* **2004**, *42*, 2601–2611.
[71] Lin, H. H.; Cheng, Y. L. *Macromolecules* **2001**, *34*, 3710–3715.
[72] Fechler, N.; Badi, N.; Schade, K.; Pfeifer, S.; Lutz, J.-F. *Macromolecules* **2008**, *42*, 33–36.
[73] Wu, C.; Wang, X. *Phys. Rev. Lett.* **1998**, *80*, 4092–4094.
[74] Ding, Y.; Ye, X.; Zhang, G. *Macromolecules* **2005**, *38*, 904–908.
[75] Cheng, H.; Shen, L.; Wu, C. *Macromolecules* **2006**, *39*, 2325–2329.
[76] Hogg, R.; Wilkins, R. *J. Chem. Soc.* **1962**, 341–350.
[77] Pham Trong, L. C.; Djabourov, M.; Ponton, A. *J. Colloid Interface Sci.*

2008, *328*, 278–287.
[78] Rossow, T.; Habicht, A.; Seiffert, S. *Macromolecules* **2014**, *47*, 6473–6482.
[79] Cacace, M.; Landau, E.; Ramsden, J. *Q. Rev. Biophys.* **1997**, *30*, 241–277.
[80] Lopez-Leon, T.; Fernandez-Nieves, A. *Phys. Rev. E: Stat., Nonlinear, Soft Matter Phys.* **2007**, *75*, 011801.
[81] Zhang, Y.; Cremer, P. S. *Curr. Opin. Chem. Biol.* **2006**, *10*, 658–663.
[82] Zhang, Y.; Furyk, S.; Bergbreiter, D. E.; Cremer, P. S. *J. Am. Chem. Soc.* **2005**, *127*, 14505–14510.
[83] Henderson, I. M.; Hayward, R. C. *Polym. Chem.* **2012**, *3*, 1221–1230.
[84] Henderson, I. M.; Hayward, R. C. *J. Mater. Chem.* **2012**, *22*, 21366–21369.
[85] Rivas, B.; Pereira, E.; Moreno-Villoslada, I. *Prog. Polym. Sci.* **2003**, *28*, 173–208.
[86] Park, T. G.; Hoffman, A. S. *J. Appl. Polym. Sci.* **1994**, *52*, 85–89.
[87] Suzuki, A.; Yoshikawa, S.; Bai, G. *J. Chem. Phys.* **1999**, *111*, 360–367.
[88] Hirokawa, Y.; Tanaka, T. *J. Chem. Phys.* **1984**, *81*, 6379–6380.
[89] Otake, K.; Inomata, H.; Konno, M.; Saito, S. *Macromolecules* **1990**, *23*, 283–289.
[90] Gent, A. *J. Appl. Polym. Sci.* **1974**, *18*, 1397–1406.
[91] Dyakonova, M. A.; Stavrouli, N.; Popescu, M. T.; Kyriakos, K.; Grillo, I.; Philipp, M.; Jaksch, S.; Tsitsilianis, C.; Papadakis, C. M. *Macromolecules* **2014**, *47*, 7561–7572.
[92] Vermonden, T.; van Steenbergen, M.; Besseling, N.; Marcelis, A.; Hennink, W.; Sudhölter, E.; Stuart, M. *J. Am. Chem. Soc.* **2004**, *126*, 15802–15808.
[93] Annable, T.; Buscall, R.; Ettelaie, R. *Colloids Surf., A* **1996**, *112*, 97–116.
[94] Annable, T.; Buscall, R.; Ettelaie, R.; Whittlestone, D. *J. Rheol.* **1993**, *37*, 695–726.
[95] Tam, K.; Jenkins, R.; Winnik, M.; Bassett, D. *Macromolecules* **1998**, *31*, 4149–4159.

CHAPTER 13

LARGE AMPLITUDE SHEAR ON METALLO-SUPRAMOLECULAR MICELLAR GELS

Abstract

A crucial but still not well understood aspect of supramolecular gels is their behaviour under large amplitude oscillatory shear. Under such conditions, the interactions between associating segments are mechanically altered by shear forces, which complexify the analysis of their rheological signature. Based on the viscoelastic response of a hetero-telechelic associating model network over a wide range of frequency and amplitude of deformation, a tentative picture of the non-linear phenomena is proposed involving contributions from both associating stickers.

13.1 Overview

As seen in the previous chapters, the linear viscoelastic response of metallo-supramolecular micellar gels is closely related to the structural characteristics of the transient networks. Hence, their dynamics and cross-linking density are respectively dictated by the nature of non-covalent associations and the fraction of metal–ligand bridges between hydrophobic nodes. However, a still nebulous aspect, but arguably of importance, of supramolecular polymer networks is their complex response when probed at high deformation, which is often referred to non-linear rheology.[1–4] Despite efforts devoted to that field,[5–8] a clear picture on this feature indeed remains elusive.

In some cases, supramolecular polymer networks exhibit shear thinning under continuous shear, or correspondingly strain softening under oscillatory shear, whereas in other cases, they show shear thickening or strain hardening. As reported by many groups,[9–11] mechanically induced dissociation of the physical cross-linkers is clearly implicated in thinning/softening behaviours, which are crucial for numerous applications as they confer injectability to the material.[12] By contrast, thickening/hardening behaviours are generally attributed to network reorganization under shear, which leads to mechano-induced homogenization, and hence reinforcement of the material,[13–15] or to repulsive interaction between the chains that are forced to interpenetrate one another by the shear flow.[16] Although intimately related to the transient nature of non-covalent cross-links, the mechanisms of thinning/softening and thickening/hardening are often not clearly understood. The comprehension of such non-linear phenomena is even further complicated by the fact that these ambiguous behaviours can be observed on the same system depending on the experimental conditions, *e.g.*, concentration or shear rate.[17,18]

Not surprisingly, more complex LAOS behaviours, as various types of shear thinning and shear thickening characteristics, can be observed when increasing complexity of supramolecular polymer networks. As pointed by Craig and coworkers,[19] all these types of shear behaviour can be nevertheless considered as simply different end points of a continuum of shear response, which all indicate a competition between different time scales: the time scale of the solicitation, the time scale at which a transient junction dissociates, and the time scale for network chain

relaxation. For example, if the chain motion occurs faster than the reconnection of an open cross-link, strain-hardening might occurs due to the transformation of intra-molecular to inter-molecular cross-links.

13.2 Rheological characterization

In this chapter, the behaviour of PS-*block*-PNIPAAm-tpy model networks is examined under large amplitude oscillatory shear (LAOS), which is central for the comprehension of complex phenomena occurring around the yield point. Only the terminal flow of materials is considered regardless prior yielding that can be observed, for some particular systems, under medium amplitude oscillatory shear. Depending on the relationship between the solicitation time scale and relaxation times characterizing the material, a weak strain overshoot, *i.e.*, a local increase in the viscous response of gels, followed by strain softening, might be observed at the limit of network rupture. In addition, LAOS experiments allow the probing of the contribution of each of the transient junctions, *i.e.*, coordinative and hydrophobic, to the non-linear response of materials.

Our methodological approach consists in following the viscoelastic response of materials under oscillatory shear while increasing the amplitude of solicitation. To access the transient network dynamics, frequency sweeps are performed within a large range of applied strain, spanning from the linear to the non-linear viscoelastic responses of the material. Hence, the evolution of dynamic moduli was recorded as a function of both oscillation frequency (Figure 13.1) and amplitude (Figure 13.2). In turn, this allows a three-dimensional mapping of the viscoelastic response of the material under shear as illustrated in Figure 13.3. Although LAOS measurements can provide meaningful information,[15] it should be noted that both storage and loss moduli have arguably ambiguous physical meaning in the non-linear region. Unlike in the linear viscoelastic regime, the oscillatory stress is indeed no more expressed as a linear combination of a sine wave and a cosine wave.[1] However, the analysis of the higher harmonic contributions is significantly too specific,[5,20,21] and is therefore not discussed here.

From Figure 13.1 (a), a high- and low-frequency plateau in storage modulus can be distinguished under the limit of small deformations, which is also delimited in Figure 13.3. Those plateaus are separated

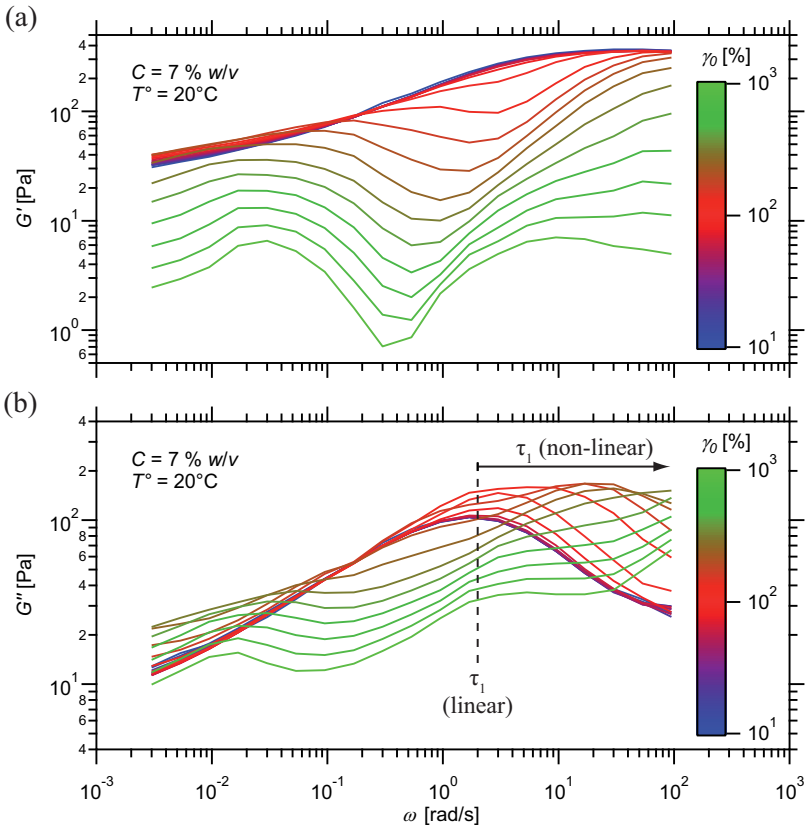

Figure 13.1 – Frequency dependence of (a) elastic and (b) viscous moduli for a hydrogel prepared from PS_{27}-*b*-$PNIPAAm_{300}$-tpy copolymer and Ni(II) ions, at different strain amplitudes.

by a transition region described by the fast relaxation time, τ_1, practically identified in Figure 13.1 (b) as the local maximum in loss modulus. In practice, the structural characteristics, *i.e.*, hydrophobe length and metal ions, of the investigated material are specifically selected to bring into light the two distinct plateau regimes. As a penalty to pay, the choice of nickel(II) metal ions makes the time scale of the terminal relaxation mode, τ_2, difficult to achieve experimentally. As already identified in the previous chapters, this slow relaxation is indeed ascribed to the exchange of ligands around the different metal centres, while the fast mode is attributed to the exchange of hydrophobes between micellar nodes.

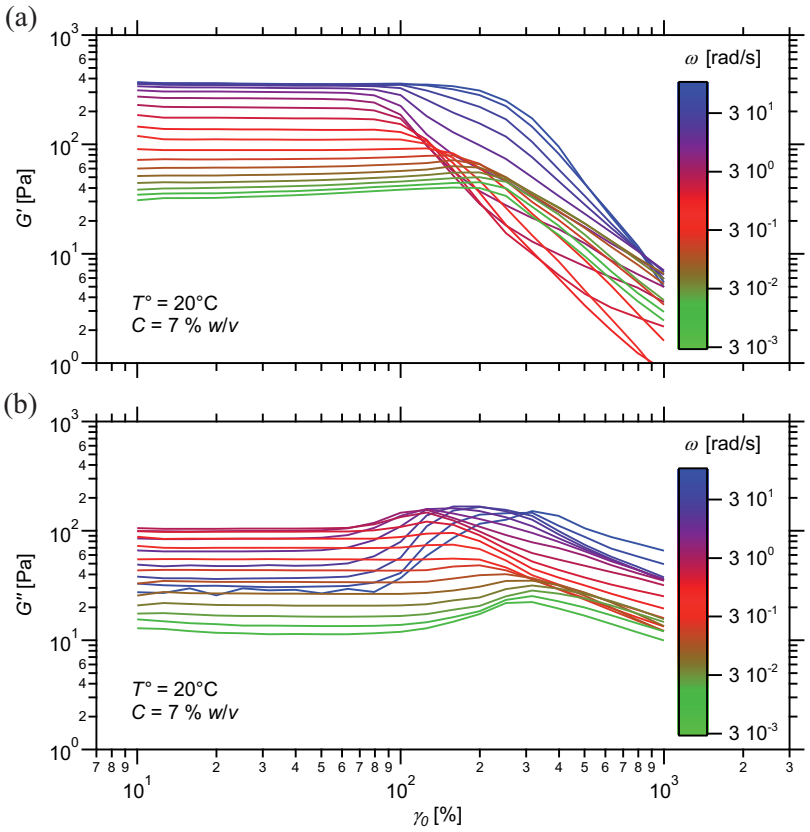

Figure 13.2 – Strain dependence of (a) elastic and (b) viscous moduli for a hydrogel prepared from PS_{27}-*b*-$PNIPAAm_{300}$-tpy copolymer and Ni(II) ions, at different oscillation frequencies.

From the strain-dependence of storage modulus (Figure 13.2 (a)), one can differentiate different viscoelastic regimes depending on the solicitation time scale and strain amplitude on sample. Practically, the frontiers between these different regimes are determined from stress–strain relationships (Figure 13.4) as the limit of linear regions, *i.e.*, where strain amplitude increases linearly with stress amplitude. At low strain ($\gamma_0 < 50\,\%$), dynamic moduli remain constant at a given frequency (Figure 13.2), G' being higher than G'', which means the deformation energy is mostly stored in entropic distortion of network chains. In addition, the frequency-dependence of both dynamic moduli remains constant whatever the strain amplitude on the gel (Figure 13.1). However, as the applied strain exceeds the limits of the linear viscoelastic regime (1st

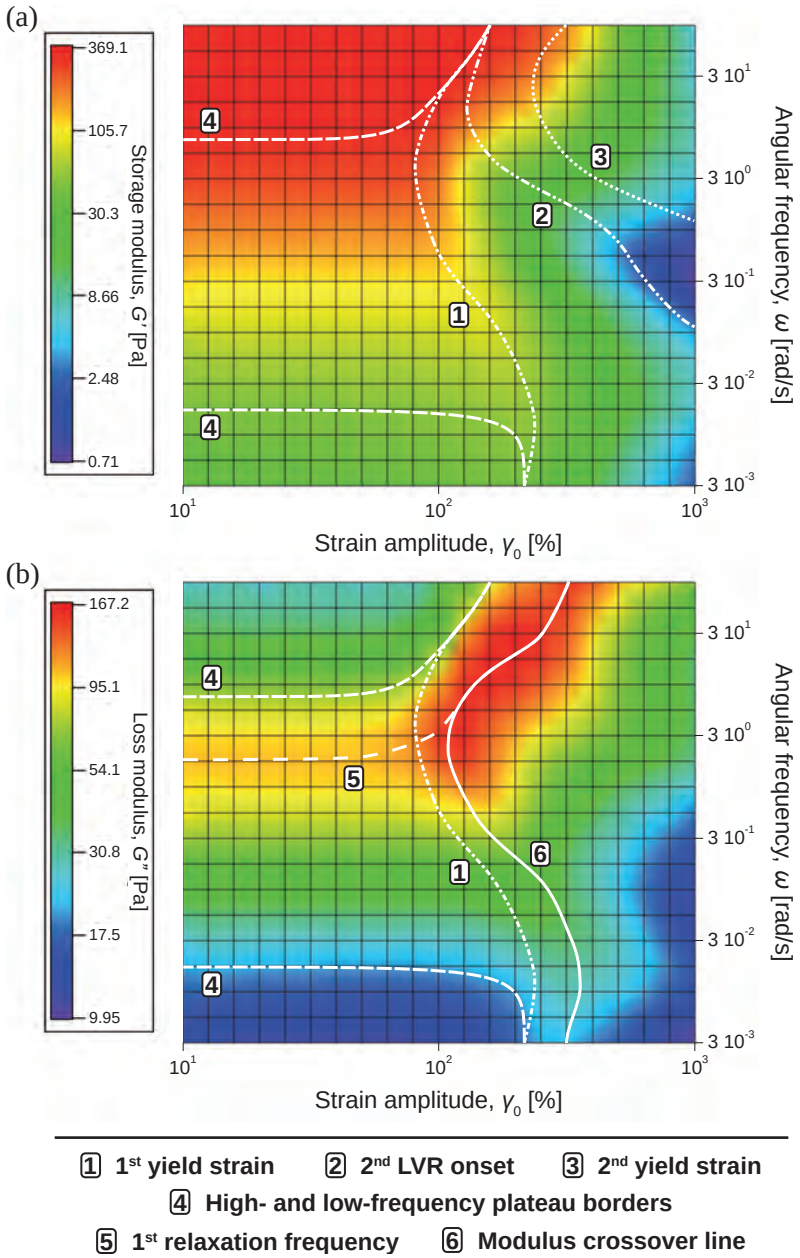

Figure 13.3 – Strain/frequency dependence of (a) elastic and (b) viscous moduli for a hydrogel prepared from PS_{27}-*b*-$PNIPAAm_{300}$-tpy copolymer and Ni(II) ions.

LVR), a deviation toward non-linearity is observed, *i.e.*, stress on sample becomes independent of strain (Figure 13.4).

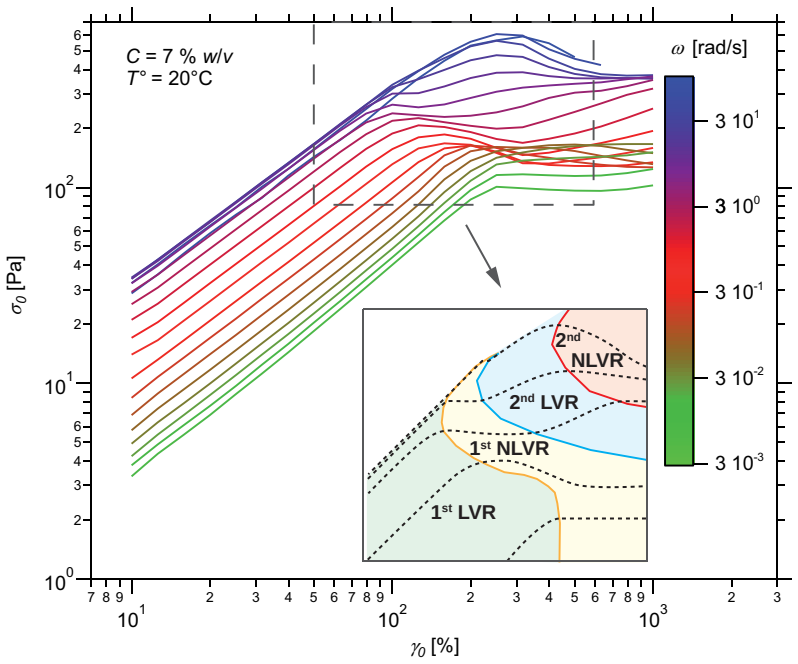

Figure 13.4 – Stress–strain relationship for a hydrogel prepared from PS_{27}-*b*-$PNIPAAm_{300}$-tpy copolymer and Ni(II) ions, revealing distinct viscoelastic regimes.

At the onset of the first non-linear viscoelastic region (1st NLVR), elastically active junctions start being altered by mechanical forces, which in turn affects the balance between the formation and dissociation rates of transient cross-links.[21,22] As further revealed by stress–strain relationships (Figure 13.4), a second LVR followed by non-linearity tends to be achieved under large amplitude oscillations. This terminology denotes the fact that stress on sample locally recovers with strain, which is attributed to further stretching of the associating network. Hence, it is thought that this particular behaviour reflects the structural complexity of the present material and can be rationalized by taking into account the contribution of both hydrophobic cores and metallo-bridges.

In the non-linear regions, the strain energy that is transmitted to stress-bearing junctions promotes the detachment of associating units

and subsequent relaxation of polymer chains, as predicted by Tanaka and Edwards.[23,24] In turn, this results in a large reduction of the number of elastically active chains within the network, as attested by the decrease in elastic modulus under large oscillatory shear (Figure 13.2 (a)). Under those conditions, the frequency at which the material is stressed also affects the magnitude of its elastic response which follows a rather complex pattern (Figure 13.1 (a)). At a given strain amplitude, a minimum in G' can for example be observed in the region intermediate to the high- and low-frequency regimes. The complexity of such nonlinear response is the first indication of a delicate interplay between the strain-promoted destruction and reformation of network junctions, which depends on both solicitation time scale and amplitude.[21,22]

When entering in the 1st NLVR, a drastic decrease is observed in the fast relaxation time, τ_1, characterizing the associating network (Figure 13.5), which is classically reported for hetero-telechelic associating polymer network.[25–28] As observed in Figure 13.1 (b) and further reported in Figure 13.3, this mechanical activation is clearly visualized by the increase in the apparent relaxation frequency of the associating network, practically identified as the local maximum in G''. In other words, the apparent dissociation kinetics of hydrophobic junctions intensifies with strain on sample, evidencing mechanical cleavage of the fast-dissociating hydrophobic cores. When exceeding the 1st limit of lin-

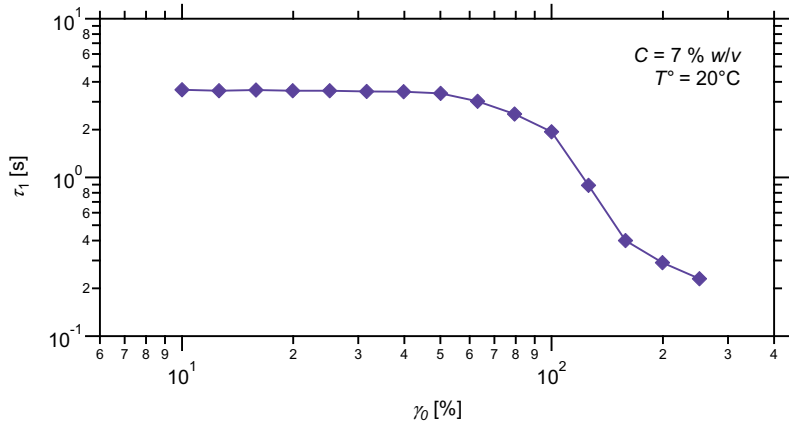

Figure 13.5 – Strain dependence of the first relaxation time for a hydrogel prepared from PS_{27}-*b*-$PNIPAAm_{300}$-tpy copolymer and Ni(II) ions.

earity, the viscous modulus further increases in value (Figure 13.1 (b)), which is principally marked in the high- and low-frequency regimes. According to Ahn and coworkers,[21,22] this increase in G'' suggest that both creation and loss of transient cross-links are enhanced by large amplitude shear. In a rheological point of view, the dissociation of junctions is thus partially counterbalanced by their reattachment to the network, which benefits to the large amplitude elastic response in specific frequency ranges (Figure 13.1 (a)). The loss term being however dominant whatever reformation is mechanically favoured or not, the viscous modulus finally drops when strain is dramatically increases on sample.

Not surprisingly, the response of the material at the onset of the first non-linear viscoelastic regime is found to be highly frequency-dependent. As shown in Figure 13.2 (b), a weak to strong overshoot in G'' might be observed under increasing strain, while strain softening is exclusively observed for G' (Figure 13.2 (a)). Precisely, this particular behaviour occurs at frequencies higher than the characteristic relaxation frequencies of each physical cross-link, and has to be discussed in regard to their dissociation kinetics. Indeed, the relative amount of energy that is dissipated as heat, due to relaxations that occur on the time scale of the deformation, is maximal when the latter coincides with the lifetime of the non-covalent junctions. Despite the apparent intactness of the hydrophobic association in the high-frequency linear regime, the effective loss modulus shows a pronounced overshoot above the limit of linearity (Figure 13.2 (b)), which is due to strain-enhanced detachment of hydrophobes from micellar cores. In addition, a weak strain overshoot in G'' is observed in the low-frequency region as well, evidencing a mechanically promoted cleavage of the slow-dissociating cross-linkers, *i.e.*, metal–ligand bis-complexes.

As evaluated from stress–strain relationships (Figure 13.4) and further reported in Figure 13.3, the onset of the second LVR is found to be highly frequency-dependent so that it has been only observed in the high-frequency region. Below the 1^{st} relaxation frequency, transient micellar cores indeed provide efficient relaxation of mechanical stress, while metallo-bridges remain essentially intact. Since the largest part of the deformation energy is dissipated through the dissociation of hydrophobic cores, the 2^{nd} LVR is not observed except at extremely high strain. Under such conditions, the extra strain energy actually allows the polymer chains to be further stretched until stress-bearing metallo-bridges

become in turn altered by mechanical force, which corresponds to the onset of the second NLVR.

As the oscillation time scale is reduced, *i.e.*, the frequency of oscillation is increased, the balance between stored and lost energy progressively shifts to favour the stretching of polymer chains due to the increasing integrity of micellar cores. This apparent growing strength of the latter is accompanied by a gradual increase in the first yield stress (Figure 13.4). In parallel, the onset of the 2nd LVR is observed at lower strain when increasing the oscillation frequency, as further reported in Figure 13.3. Above the apparent kinetics associated to the fast relaxation mode, both linear viscoelastic regimes tend to merge into a single

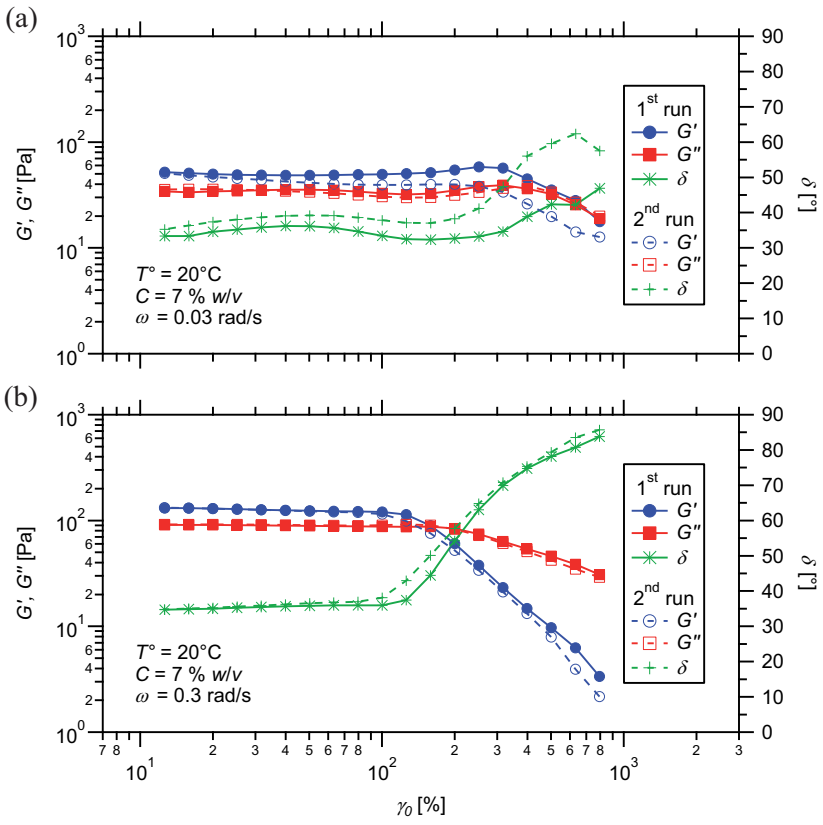

Figure 13.6 – Strain dependence of dynamic moduli for a hydrogel prepared from PS_{27}-*b*-$PNIPAAm_{300}$-tpy copolymer and Ni(II) ions, at selected oscillation frequencies of (a) 0.03 rad/s and (b) 0.3 rad/s.

one (Figure 13.4), suggesting that kinetically "frozen" hydrophobic cores ultimately surpass metal–ligand bis-complexes in strength. Indeed, this allows the cores to withstand the imposed stress, at least until the complexes are mechanically disrupted.

In parallel, the viscoelastic response of the material is studied by performing amplitude strain sweeps at various oscillation frequencies. When the stress on the sample is further reduced, the reversibility of the non-linear phenomena is always observed while both moduli recover their original values, indicating that the global structure after recovery is identical to that of the initial network. As illustrated in Figure 13.6 and 13.7, a significant hysteresis might however be observed when coming back to

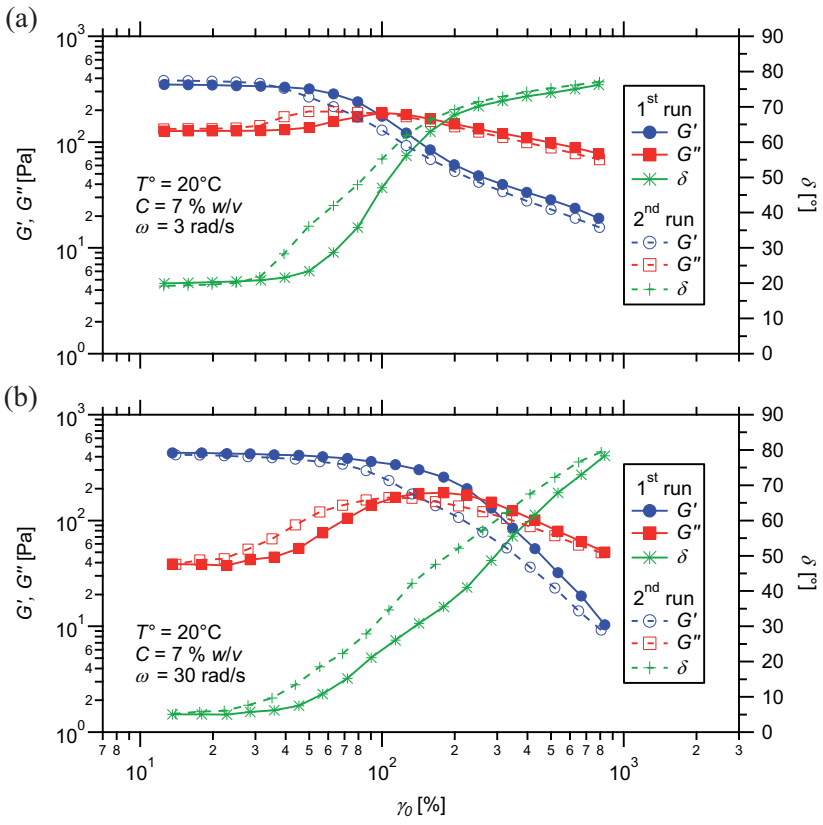

Figure 13.7 – Strain dependence of dynamic moduli for a hydrogel prepared from PS_{27}-*b*-$PNIPAAm_{300}$-tpy copolymer and Ni(II) ions, at selected oscillation frequencies of (a) 3 rad/s and (b) 30 rad/s.

small deformations, which depends on oscillatory shear frequency. The presence of such hysteresis indicates that the LAOS imposed on the gel results in major structural changes and that the relaxation of the perturbed system toward its equilibrium structure is slow.[28] In practice, this situation is achieved when the stress-carrying junctions are constrained at rates that exceed their own dissociation rates.

On short time scales compared to their intrinsic lifetimes, the stress on the sample is indeed fully transmitted to intact, elastically-active junctions, which in turn strongly perturbs the structural equilibrium of the network. Under large amplitude oscillatory shear, the increasing dissociation rates for cross-linkers can thus be viewed as the consequence of the natural tendency for the system to continuously reach an equilibrium structure. In that sense, more frequent dissociations indeed allow faster reorganization of the mechanically constrained material. In the high-frequency regime (Figure 13.7 (b)), both hydrophobic and coordinative cross-links are mechanically altered, resulting in a profound hysteresis in loss and storage modulus. In the low-frequency region, only the metal–ligand complexes are disrupted by mechanical force, which mainly affects the elasticity of the gel (Figure 13.6 (a)). At the transition in between, the presence of transient hydrophobic junctions at those experiment time scales ensures a dynamic equilibrium during the structural reorganization of the gel. Hence, only a weak hysteresis is observed, as illustrated in Figure 13.7 (a).

13.3 Summary

In summary, we have drawn here a tentative picture of the non-linear phenomena occurring in a class of hetero-telechelic associating polymer gels under large amplitude oscillatory shear. The investigated material consisted of a terpyridine end-capped polystyrene-*block*-poly(*N*-isopropylacrylamide) copolymer that self-assembles in aqueous solutions toward coordination micellar gels with complex but defined network structure. In turn, their structural complexity resulted in a rich non-linear response that was discussed by taking into account the contribution of both hydrophobic cores and metallo-bridges between them.

The viscous response of the material showed an overshoot at intermediate strain when solicited at frequencies higher than the lifetime of

the stress-active cross-linker. This particular behaviour was rationalized by taking into account the effect of mechanical forces on the gel. Above the first yield strain, mechanical stress increased the dissociation rate of non-covalent cross-linkers. This acceleration is believed to reflect the tendency of the system to reach its equilibrium under LAOS, which is consistent with the observation of hysteresis for the non-linear phenomena.

Behind our approach, thus lies a fundamental comprehension of the physical-chemistry, especially the mechano-chemistry, of supramolecular soft matter. In this context, our contribution aims to understand the mechanistic conversion of mechanical work in coordination micellar gels. Primarily, the deformation energy is indeed elastically absorbed through entropic distortion of the self-assembled polymer network. Then, the transmission of shear forces to stress-carrying junctions induces a transformation of the mechanical energy into chemical energy, resulting in the activated rupture of non-covalent associations. This bond breaking occurred via a multi-step yielding, thereby delimiting discrete linear and non-linear responses. In turn, this allowed the material to relax stress through a single or multiple relaxation modes that occurred on the deformation time scale and amplitude.

13.4 Experimental part

Materials

Terpyridine end-capped block copolymers are synthesized via sequential reversible addition–fragmentation chain transfer control radical copolymerization, as reported in a previous chapter. Nickel(II) chloride salt is dried, kept in a glove box, and weighted under argon atmosphere.

Instrumentation

Shear rheological experiments are performed on a Kinexus Ultra (Malvern Instrument) rheometer equipped with a heat exchanger and modified with a solvent trap. Measurements are carried out at given temperatures, using a 20 mm plate–plate geometry, in a water saturated atmosphere in order to minimize evaporation of the solvent. The gap

is adjusted between 50 and 250 µm so that the geometry is completely filled. Normal forces are checked to be relaxed prior any measurement.

Preparation of supramolecular gels

Hydrogels are prepared by mixing given amounts of block copolymer with Milli-Q water. The sealed reaction vessels are placed in a fridge and shaken periodically to form homogeneous concentrated solutions after a few days. The gels are then readily obtained by adding the stoichiometric amount of half an equivalent of nickel(II) ions (with respect to the terpyridine content) dissolved in defined amounts of Milli-Q water to each concentrated solutions. Lastly, the reaction vessels are placed again in the fridge over three days to ensure homogeneous gelation and stabilization of the gels. The final concentration of copolymers in samples is 7 %w/v.

Loading and testing protocol

Around 50 µL of gel is loaded onto the stationary bottom plate of the rheometer preheated at 20 °C. By stepwise lowering the gap between the two plates, the sample is compressed and forced to spread over the geometry so that the gap is completely filled. Equilibration of the sample is followed by monitoring the evolution of normal force, storage and loss moduli with time, under small amplitude oscillatory shear. Rheological tests are started when both moduli reach constant values and normal force has relaxed to < 0.05 N.

Bibliography

[1] Hyun, K.; Wilhelm, M.; Klein, C. O.; Cho, K. S.; Nam, J. G.; Ahn, K. H.; Lee, S. J.; Ewoldt, R. H.; McKinley, G. H. *Prog. Polym. Sci.* **2011**, *36*, 1697–1753.
[2] Seiffert, S.; Sprakel, J. *Chem. Soc. Rev.* **2012**, *41*, 909–930.
[3] Appel, E. A.; del Barrio, J.; Loh, X. J.; Scherman, O. A. *Chem. Soc. Rev.* **2012**, *41*, 6195–6214.
[4] Chassenieux, C.; Nicolai, T.; Benyahia, L. *Curr. Opin. Colloid Interface Sci.* **2011**, *16*, 18–26.

[5] Hyun, K.; Nam, J.; Wilhelm, M.; Ahn, K.; Lee, S. *Korea-Aust. Rheol. J.* **2003**, *15*, 97–105.
[6] Vaccaro, A.; Marrucci, G. *J. Non-Newtonian Fluid Mech.* **2000**, *92*, 261–273.
[7] Berret, J.; Séréro, Y.; Winkelman, B.; Calvet, D.; Collet, A.; Viguier, M. *J. Rheol.* **2001**, *45*, 477–492.
[8] Pellens, L.; Gamez Corrales, R.; Mewis, J. *J. Rheol.* **2004**, *48*, 379–393.
[9] Regalado, E. J.; Selb, J.; Candau, F. *Macromolecules* **1999**, *32*, 8580–8588.
[10] Serero, Y.; Jacobsen, V.; Berret, J.-F.; May, R. *Macromolecules* **2000**, *33*, 1841–1847.
[11] Kersey, F.; Yount, W.; Craig, S. *J. Am. Chem. Soc.* **2006**, *128*, 3886–3887.
[12] Guvendiren, M.; Lu, H. D.; Burdick, J. A. *Soft Matter* **2012**, *8*, 260–272.
[13] Indei, T.; Koga, T.; Tanaka, F. *Macromol. Rapid Commun.* **2005**, *26*, 701–706.
[14] Xu, D. H.; Hawk, L. L.; Loveless, D. M.; Jeon, S. L.; Craig, S. L. *Macromolecules* **2010**, *43*, 3556–3565.
[15] Xu, D.; Craig, S. L. *Macromolecules* **2011**, *44*, 7478–7488.
[16] Ianniruberto, G.; Marrucci, G. *Macromolecules* **2015**, *48*, 5439–5449.
[17] Xu, D. H.; Craig, S. L. *J. Phys. Chem. Lett.* **2010**, *1*, 1683–1686.
[18] Suzuki, S.; Uneyama, T.; Inoue, T.; Watanabe, H. *Macromolecules* **2012**, *45*, 888–898.
[19] Xu, D.; Liu, C.-Y.; Craig, S. L. *Macromolecules* **2011**, *44*, 2343–2353.
[20] Hyun, K.; Kim, S.; Ahn, K.; Lee, S. *J. Non-Newtonian Fluid Mech.* **2002**, *107*, 51–65.
[21] Kim, S. H.; Sim, H. G.; Ahn, K. H.; Lee, S. J. *Korea-Aust. Rheol. J.* **2002**, *14*, 49–55.
[22] Sim, H.; Ahn, K.; Lee, S. *J. Non-Newtonian Fluid Mech.* **2003**, *112*, 237–250.
[23] Tanaka, F.; Edwards, S. F. *Macromolecules* **1992**, *25*, 1516–1523.
[24] Tanaka, F.; Edwards, S. F. *J. Non-Newtonian Fluid Mech.* **1992**, *43*, 247–271.
[25] Tirtaatmadja, V.; Tam, K.; Jenkins, R. *Macromolecules* **1997**, *30*, 1426–1433.
[26] Mewis, J.; Kaffashi, B.; Vermant, J.; Butera, R. *Macromolecules* **2001**, *34*, 1376–1383.
[27] Sprakel, J.; Spruijt, E.; Stuart, M.; Besseling, N.; Lettinga, M.; van der Gucht, J. *Soft Matter* **2008**, *4*, 1696–1705.
[28] Tam, K.; Jenkins, R.; Winnik, M.; Bassett, D. *Macromolecules* **1998**, *31*, 4149–4159.

Part V

Concluding remarks

CHAPTER 14

CONCLUSIONS

Through bibliographic searching, material preparation, data collection and analysis, this thesis claims chief attention in the broad field of exact sciences. In this systematic study, the use of metal–ligand interaction in combination with classical macromolecular architectures has proved to be a straightforward approach towards supramolecular multiresponsive polymer materials with control over their structure, organization and dynamics. From this work has risen, in a broad sense, a design strategy that will hopefully guide researchers in the development and characterization of smart healable materials.

Since this thesis merges the fields of macromolecular chemistry, supramolecular assembly and polymer rheology, an overview of the characteristic features of polymers, the tools for their synthesis, and their complex solution behaviour was first presented in the introductory part (Chapter 1). Then, fundamental principles of supramolecular chemistry were introduced, from non-covalent bonds towards self-assembled materials with responsive, adaptive, and self-healing abilities (Chapter 2). Finally, the rheology of soft matter, especially polymers, was described and explained to fall between the two extremes of elastic solids and viscous fluids (Chapter 3).

The motivation for this work arose in the context of challenging technological developments, namely smart and healable materials. In this respect, the goal of this thesis was to access novel polymeric materi-

als with unprecedented control over their dynamic mechanical properties (Chapter 4). To this aim, a design strategy was developed based on the self-assembly behaviour of block copolymers in solution and the bis-coordination of 2,2':6',2"-terpyridine ligands around transition metal ions (Chapter 5).

A state of the art then summarized recent progresses achieved to date in the field of polymer materials that are held together by coordination bonds. At first, the different routes towards so-called metallo-supramolecular polymer gels were reviewed and classified into three main categories depending on how cross-links are formed through the networks (Chapter 6). Then, the linear and non-linear viscoelastic responses of this particular class of materials were addressed with recent advances in the scientific community, highlighting the complexity but richness of their rheology (Chapter 7).

In order to build supramolecular polymer materials, macromolecular building blocks were essential, especially those of well-defined and tailored architecture. In this respect, three libraries of linear associating copolymers were synthesized via radical copolymerization controlled by reversible addition–fragmentation chain transfer (Chapter 8). The first consisted in a series of hetero-telechelic poly(*N*-isopropylacrylamide)s bearing a terpyridine ligand at one extremity, and a short polystyrene sticker at the other end. The second is composed of terpyridine end-capped double hydrophilic poly(*N*-isopropylacrylamide)-*block*-poly(2-(dimethylamino)ethyl methacrylate) copolymers. Finally, the third family is constituted by terpyridine end-functionalized polystyrene-*block*-poly(*N*-isopropylacrylamide)-*block*-poly(2-(dimethylamino)ethyl methacrylate) triblock copolymers.

Each syntheses involved the sequential polymerization of selected comonomers, affording polymer sequences with specific features, *e.g.*, weak affinity for water or thermo-responsiveness. The sequential polymerization processes were conducted in solution and were mediated by chain transfer agents that have been modified with the 2,2':6',2"-terpyridine ligand. Practically, control over the block length, mass distribution and functionality was confirmed by a combination of analytical techniques involving nuclear magnetic resonance spectroscopy, size exclusion chromatography, and end-group titration via UV-Visible absorption spectroscopy.

The synthesized macromolecular building blocks were assembled over distinct levels of hierarchy to yield metallo-supramolecular micellar gels (Chapter 9). In a first approach, the self-assembly of the different functional building blocks was tested in dilute solutions, via a combination of selected analytical techniques. On one hand, the possibility to establish metal–ligand bridges between two individual copolymer chains was demonstrated by means of absorption spectroscopy and size exclusion chromatography, showing efficient coupling. On the other hand, the solution behaviour of the block copolymers was systematically studied as a function of the structure parameters defined by the macromolecular design, namely the nature and length of the blocks, and the environmental variables, *e.g.*, the pH and temperature.

The effective micellization of associating copolymers bearing a hydrophobic sticker at one end, namely PS-*b*-PNIPAAm-*b*-PDMAEMA-tpy and PS-*b*-PNIPAAm-tpy, was confirmed by dynamic light scattering measurements. Indeed, the analysis of the raw signal indicated the presence of well-defined objects of a few tens of nanometres size under ambient condition. The heat-induced collapse transition of PNIPAAm block in those architectures was further monitored around the theoretical value, causing macro-phase separation of PS-*b*-PNIPAAm-tpy solutions. In parallel, the complex solution behaviour of double hydrophilic PNIPAAm-*b*-PDMAEMA-tpy copolymers was rationalized taking into account the responsiveness of each constituting blocks in regard to environmental changes. The micellization and macro-phase separation in those systems was triggered by heat and further controlled via pH changes. In this respect, protonation of the PDMAEMA block was found to delay the thermo-induced collapse transitions of both blocks.

Working in a more concentrated regime, supramolecular hydrogels were successfully prepared from the different associating block copolymers. The first level of organization was reached upon direct dissolution of the block copolymers in aqueous media, resulting in spontaneous or triggered assembly into micellar nano-structures. Utilizing metal–ligand coordination as the driving force for network formation, supramolecular hydrogels were then readily prepared by adding transition metal ions to the concentrated micellar solutions. In the case of PNIPAAm-*b*-PDMAEMA-tpy copolymers, stimuli-induced gelation was reversibly achieved by heating the metal-containing solutions, which further depended on the pH of the media. In complement to visual observations,

light was shed on the thermo-responsiveness of the different hydrogels by means of differential scanning calorimetry.

At the core of this research, the dynamic mechanical properties of metallo-supramolecular micellar gels were investigated in depth using rotational rheometry measurements. Not surprisingly, the structural complexity and hierarchical organisation of the studied materials was accompanied by a relatively rich rheology. At first, the linear response, *i.e.*, dynamics (Chapter 10) and cross-linking density (Chapter 11), of the gels was closely related to the structural characteristics of the transient networks. Their ability to respond to environmental, *i.e.*, pH and temperature, changes was monitored in terms of rheology and rationalized by the solution behaviour of the associating copolymers (Chapter 12). Finally, the rheological characterization was extended into the non-linear regime, probing the large amplitude oscillatory shear response of materials (Chapter 13).

The dynamics of the investigated PS-*b*-PNIPAAm-tpy associating gels, as model networks, reflected the discrete contributions from each transient cross-linkers. A first contribution to the network dynamics arose from the self-assembly of amphiphiles in aqueous solutions. Depending on the hydrophilic–hydrophobic balance, stress relaxation by network rearrangement was enabled via detachment and subsequent exchange of stickers between hydrophobic domains. A second contribution was provided by the coordination bridges between associating nodes. The latter further allowed material relaxation via exchange of ligands around different metal centres, at a rate that matched the lifetime of the terpyridine bis-complexes. Accordingly, an orthogonal control over the dynamics of PS-*b*-PNIPAAm-tpy associating networks was achieved by varying the length of hydrophobic segment and the nature of metal ions.

Depending on the stability of the different associations, the viscoelastic response of the self-assembled materials was varied from that of highly elastic “hard” hydrogels to the one of more viscous “soft” matter. While the first essentially behaved as if chemically cross-linked, the second presented the features characteristic of transient physical gels. Due to enhanced mechanical energy dissipation, the dynamic nature of “soft” hydrogels allowed them to withstand larger deformations compared with “hard” analogues, thus showing an extended linear response. Beyond these findings, hydrogels that exhibited a remarkable “two-step”

gel–sol transition in response to mechanical stress were prepared via fine tuning over the associating copolymer architecture.

The cross-linking density of hierarchically assembled PS-*b*-PNIPAAm-tpy hydrogels was then adjusted by controlling the fraction of elastically active inter-micellar bridges in the system, compared to inactive intra-micellar loops. To achieve that goal, several factors were investigated that are the operating temperature, the length of the associating copolymer, and its overall or effective concentration. Hence, the formation of active bridges was favoured by increasing the length of the NIPAAm inner segment, or its degree of swelling in response to cooling. On the other hand, decreasing the effective concentration in associating copolymers, either by reducing the overall content in telechelics or by replacing a proportion of the latter with semi-telechelics, led to weakly percolated hydrogels.

By varying the fraction of bridging chains, two distinct regimes with specific rheological behaviours were distinguished that correspond to the well percolated networks, with a high cross-linking density, and the weakly percolated networks, with a low cross-linking density. In densely connected hydrogels, the high degree of cross-linking resulted in an increased viscoelastic response, therefore allowing the material to carry higher shear stresses. In sparsely connected networks, the hydrophobic cores acted as chain extenders instead of network nodes, which leads to the formation of super-bridges. In turn, these strings of bridged micelles enhanced stress relaxation and allowed the materials to be stretched to a greater extent.

The stimuli-responsiveness of materials elaborated from the different functional building blocks was investigated by rotational rheometry. Hence, light was shed on the influence of commonly encountered environmental variables, *i.e.*, temperature, pH and co-solvent, on the dynamic mechanical response of the gels. Being of transient nature, the non-covalent junctions structuring the PS-*b*-PNIPAAm-tpy networks, *i.e.*, hydrophobic and coordinative, were targeted by the application of proper stimuli, namely the addition of a co-solvent and variations in pH. In this respect, an orthogonal control was gained over the material relaxation, each stimulus affecting the dynamic exchange of the specifically targeted associations.

External stimuli were then used to trigger the formation of percolated

networks from concentrated solutions of PNIPAAm-*b*-PDMAEMA-tpy copolymers. In this respect, rheological measurements showed that the thermo-induced micellization indeed manifested itself as gelation. However, the formation of a percolated structure was evidenced to be controlled by the supramolecular organization of the network rather than the prior collapse of PNIPAAm segments. Besides, the thermoreversible gelation was readily modulated by the concentration in associating copolymer, the pH of the media, the length of the PNIPAAm block, and the nature of metal ions involved in the assembly process.

The thermo-induced change of PNIPAAm segment conformation was further exploited to tune the magnitude of the viscoelatic response of hydrogels prepared from PS-*b*-PNIPAAm-tpy diblock and PS-*b*-PNIPAAm-*b*-PDMAEMA-tpy triblock copolymers. Above the phase transition temperature, the rheological signature of PS-*b*-PNIPAAm-tpy based materials notably changed from the one of transient micellar gels to the one of coordination rubbery gels. Even if partial hydration of these hydrogels was preserved at high temperatures, the mesoscopic phase separation resulted in lower stretchability and a pronounced hysteresis during the healing process. Due to the presence of a third hydrophilic block, these penalties were overcome in the case of PS-*b*-PNIPAAm-*b*-PDMAEMA-tpy triblock copolymer hydrogels. Indeed, thermo-rheological measurements on these systems showed that the collapse of PNIPAAm blocks onto pre-formed micellar cores only benefits to their rheological properties, *i.e.*, modulus and yield strength.

Finally, a closer but quick look to the non-linear rheology of metallo-supramolecular micellar gels showed the complex behaviour they adopt under large amplitude oscillatory shear. Depending on the relationship between the time scales of solicitation and relaxation of the materials, a local increase in the viscous response of gels might be observed prior strain softening. Although elusive, a tentative picture of the non-linear phenomena was drawn, involving distinct processes of network disassembly that are core disruption and metal–ligand dissociation.

To summarize, the original contribution and significance of this research to the field of exact sciences is threefold. From an applied point of view, this thesis provides a design strategy and guidelines for the elaboration of supramolecular polymer materials with control over their structure, self-organization and dynamics. From a more fundamental point of view, this work has established clear relationships between the structure

and rheological properties of a particular class of self-assembled materials, namely metallo-supramolecular micellar gels. Finally, this thesis offers exciting breakthrough to drive future developments and possible applications in the field of material sciences and engineering.

CHAPTER 15

PERSPECTIVES AND POTENTIAL APPLICATIONS

From this research, it is clear that metallo-supramolecular micellar gels offer a straightforward route to responsive, adaptive and tunable inorganic/organic hybrid materials. Their properties can be tailored by proper selection of transition metal ions and appropriate manipulation of copolymer composition and architecture. Additionally, the hierarchical assembly and resulting behaviour of these smart materials, mainly their linear and non-linear viscoelastic responses, can be influenced by environmental variables, such as temperature and pH. In the following, some recommendations for future work are thus given, followed by possible application for those materials.

15.1 Perspectives

As a matter of fact, terpyrdine ligands constitute formidable coordination motifs for building well-defined supramolecular architectures with control over structure and dynamics. Indeed, the binding strength of metal–terpyridine bis-complexes can be varied by orders of magnitude depending on the chelated ions,[1,2] the substituent groups on the ligand,[3] as well as the surrounding medium.[4] Nevertheless, the cost of terpyridine derivatives limits their use for high-value applications, consequently lowering attractiveness for industry. Therefore, enlarging

the scope of this study with less specific, but economically competitive candidates, such as phosphate or carboxylate ligands,[5–7] would clearly benefit to industrial perspectives including biomedical and environmental applications.

Other metal cations may also offers new possibilities to direct the self-assembly of engineered polymer architectures into supramolecular gels. In particular, lanthanide ions are of primary interest since they form, in combination with terpyridine, associating motifs with a ligand-to-metal stoichiometric ratio of 3:1. In that sense, the coordination complexes not only act as chain extenders but rather provide branching points and connection within the network structure.[8,9] Furthermore, the luminescence properties of lanthanoid containing metallo-gels offer a probe to investigate their assembly and disassembly process and make them attractive for various applications.[10]

The possibility to follow chain motional dynamic or, at a larger scale, material relaxation constitutes an exciting perspective. This challenging task can be tackled by introducing labelled building blocks into the supramolecular architecture.[11,12] However, simultaneous monitoring of microscopic chain dynamics and macroscopic material relaxation would require more sophisticated instrumentation than expected for standard investigation. Equipped with real-time spectroscopy probes, such as fluorescence, UV-Vis, Raman or infra-red, or even coupled with neutron, X-rays or light scattering techniques, advanced rheometers can track changes in molecular structures as a function of deformation and temperature, along with changes of viscoelastic properties.[13,14] In particular, the analysis of the spectroscopic or scattering signal would benefit the comprehension of complex phenomena occurring under large amplitude oscillatory shear or in the vicinity of the phase transitions.

Although useful for a broad class of complex fluids and soft matter, large amplitude oscillatory strain tests further require a deeper analysis of the raw signal, notably via the construction of Lissajous curves.[15] Beyond, the separation of the non-linear signals into a superposition of harmonic contributions can be analysed as spectra in Fourier space with respect to their frequencies, amplitudes and phase angle.[16,17] If strain amplitude and frequency can be varied independently in oscillatory shear rheology, allowing a broad spectrum of conditions to be attained, other methods are needed for quantifying the non-linear response of the materials.[18] Along with Fourier transform rheology, steady shear

flow experiments and orthogonal/parallel superposition rheometry can be considered as powerful tools in the analysis of the non-linear viscoelastic response of the elaborated materials. [19]

Beyond classical to more advanced rheological characterization methods, other techniques have emerged as valuable tools to quantify the mechanical properties of soft matter. Among them, nano-indentation using modified AFM probes has allowed testing the very local mechanical properties of materials, which refer to the mesocopic scale. [20,21] In that sense, such tribological technique therefore fills the scale gap between molecular characterizations and macro-rheological measurements. In parallel, advanced light scattering techniques, such as diffusing wave spectroscopy, have been developed to monitor sub-nanometre displacement of particles trapped within a gel network. Since particle motion is sensitive to the rheology of the local environment, such scattering techniques constitute excellent and reliable tools for studying dynamics in non-ergodic samples. [22] Equipped with fast photon detectors, optical instruments can further measure particle displacements at high frequencies, which overcome one of the most frustrating limitation of mechanical rheometers, *i.e.*, the accessibility to high frequencies. [23]

By lowering the amount of solvent in the investigated systems, the present study can be extended from supramolecular polymer gels to nano-structured bulk materials. Precisely, self-healing multiphase polymers are expected to be developed in which a percolated network is created by dynamic coordination bonds within a soft matrix mechanically anchored to a hard phase. [24,25] In such thermoplastic elastomers, the interplay between the multiple assembly processes is expected to become more complex. [26] For example, the presence of coordination bonds in the soft phase may significantly influence the phase behaviour and thus the self-healing of the hybrid polymer. In addition, ionic coacervation of charged metal–ligand complexes may significantly improve modulus, mechanical stability, creep resistance, and strength of the self-assembled materials. [27,28]

15.2 Applications

Prospects for everyday to advanced applications directly arise from the unique characteristics of supramolecular bonds and polymer se-

quences used in the frame of this project. Along with the reversible nature of non-covalent associations, their response to various physical and chemical stimuli could lead to the development of new multifunctional "smart" materials. Among them, mechano-sensors and soft actuators are especially targeted since the presented hydrogels show a complex rheological response that reflects both the intensity of mechanical constrains and the deformation time scale. Besides, the structural and organizational complexity of those materials can be regarded as a powerful tool, since it allows targeting a large number of constitutive elements in those systems.

The autonomous healing ability and thixotropic properties of the developed hydrogels may find numerous applications including, but not restricted to, passive dampers, shock absorbers, vibration insulators or self-restructuring metal coatings. Indeed, they possess a certain rigidity but are able to dissipate mechanical energy, which is function of stress intensity and duration. For all those perspectives, an advanced control over the rheological properties of the materials is therefore crucial, with the intention of varying them in a wide range, *e.g.*, from viscous liquids to hard solids. Whereas an elastic response confers ductility to the material, a more viscous behaviour allows dissipating mechanical energy when used as insulator, or healing fractures when used as self-repairing coating. In this continuity, the presence of multiple distinct viscoelastic regimes, as a function of solicitation amplitude and frequency, constitutes a valuable feature since it delimits a wide range of mechano-responses that reflect the environmental constrains encountered by the material.

According to their dynamic mechanical response, the investigated materials may find application in numerous fields including medical, engineering and electronic (Figure 15.1). Integrated in the heels of damping shoes, passive shock absorbers damp the shocks on hard grounds while keeping the rigidity that is necessary for a perfect stability. Without protecting the ankles from the impact of landing, the shock wave spreads in the organism and is absorbed by the joints, the knees and the spine, leading to pathologies such as back pain, tendinitis, and muscle tensions. Embedded in the high-rebound head of a golf club or on the frame of a tennis racket, the same material absorbs the excess force applied on them, allowing a comfortable feeling of impact during golf swing or tennis serve. As a consequence, the vibration soother limits the in-

flammation risk at the elbows of the tennis players, or the shoulder pain of the golf players.

Shoe cushioning *Electronic device* *Crash helmet*

(a) Applications in shock absorption

Machine insulation *Electronic component* *Percussion instrument*

(b) Applications in vibration damping

Figure 15.1 – Gel materials as shock absorbers and vibration dampers by RTOM Corporation, Sidas Technologies, and Taica Corporation.

Applied on electronic devices such as computer boards, engine controllers, cameras, smart phones or tablets, anti-vibrators ideally prevent a maximum of damages that may occur during transportation or due to inappropriate use or falling down. In the form of adhesive gel sticks or sheet, the same materials can suppress vibration under precision instruments and testing machines for instant and prolonged damping, which consequently reduces noise during data acquisition. In acoustics, vibration dampers are able to absorb sound waves over a selected frequency range, thereby specifically negating some noise pollution and reducing hearing problems that could result. In studio, the self-assembled hydrogels can stick to the surface of drums, cymbals, and most percussion instruments to diminish the higher overtones, eliminate any unwanted resonance, and therefore obtain the exact sound the situation demands.

To target all of these possible applications, the mechanical properties

of metallo-supramolecular micellar gels must be finely tuned to reach a good balance between robustness and performance. For example, this can be achieved by varying the weight fraction of associating polymers in the gels, or modulating the strength of the non-covalent associations tethering the networks. In addition, reinforcing the properties of supramolecular gels can be considered via the incorporation of mechanically active components like, *e.g.*, nano-tubes, fibres or particles, into the gel scaffolds. Due to physical adsorption of polymers onto nano-particle surfaces, the mechanical performances of these composite gels are indeed generally improved in comparison with those of the corresponding native materials.[29–31]

Given the particular dynamic flexibility of their inner structure, the presented materials integrate fast, autonomous and efficient healing ability, and thus fully recover their initial mechanical properties after high-strain loading. By absorbing potential handling defects, this self-healing ability dramatically simplifies the implementation of these materials in new high performance devices, which in turn increases economic efficiency. By reducing fatigue and postponing failure, this potential to repair damage caused by mechanical usage over time also increases the material lifetime considerably. Last but not least, the adaptiveness of these astonishing materials confers facile processing, handling and recycling, thereby embracing innovation to sustainably feed a future with both economic and environmental challenges!

Bibliography

[1] Hogg, R.; Wilkins, R. *J. Chem. Soc.* **1962**, 341–350.
[2] Holyer, R. H.; Hubbard, C. D.; Kettle, S. F. A.; Wilkins, R. G. *Inorg. Chem.* **1966**, *5*, 622–625.
[3] Henderson, I. M.; Hayward, R. C. *Polym. Chem.* **2012**, *3*, 1221–1230.
[4] Henderson, I. M.; Hayward, R. C. *J. Mater. Chem.* **2012**, *22*, 21366–21369.
[5] Sato, T.; Ebara, M.; Tanaka, S.; Asoh, T.-A.; Kikuchi, A.; Aoyagi, T. *Phys. Chem. Chem. Phys.* **2013**, *15*, 10628–10635.
[6] Furusho, Y.; Endo, T. *J. Polym. Sci., Part A: Polym. Chem.* **2014**, *52*, 1815–1824.
[7] Hayashi, M.; Noro, A.; Matsushita, Y. *J. Polym. Sci., Part B: Polym. Phys.* **2014**, *52*, 755–764.
[8] Vermonden, T.; van Steenbergen, M.; Besseling, N.; Marcelis, A.; Hen-

nink, W.; Sudhölter, E.; Stuart, M. *J. Am. Chem. Soc.* **2004**, *126*, 15802–15808.
[9] Beck, J. B.; Rowan, S. J. *J. Am. Chem. Soc.* **2003**, *125*, 13922–13923.
[10] Balkenende, D. W. R.; Coulibaly, S.; Balog, S.; Simon, Y. C.; Fiore, G. L.; Weder, C. *J. Am. Chem. Soc.* **2014**, *136*, 10493–10498.
[11] Hackelbusch, S.; Rossow, T.; van Assenbergh, P.; Seiffert, S. *Macromolecules* **2013**, *46*, 6273–6286.
[12] Rossow, T.; Habicht, A.; Seiffert, S. *Macromolecules* **2014**, *47*, 6473–6482.
[13] Steeman, P. A. M.; Dias, A. A.; Wienke, D.; Zwartkruis, T. *Macromolecules* **2004**, *37*, 7001–7007.
[14] Polushkin, E.; Alberda van Ekenstein, G.; Ikkala, O.; ten Brinke, G. *Rheol. Acta* **2004**, *43*, 364–372.
[15] Rogers, S. A. *J. Rheol.* **2012**, *56*, 1129–1151.
[16] Wilhelm, M.; Maring, D.; Spiess, H. W. *Rheol. Acta* **1998**, *37*, 399–405.
[17] Wilhelm, M. *Macromol. Mater. Eng.* **2002**, *287*, 83–105.
[18] Hyun, K.; Wilhelm, M.; Klein, C. O.; Cho, K. S.; Nam, J. G.; Ahn, K. H.; Lee, S. J.; Ewoldt, R. H.; McKinley, G. H. *Prog. Polym. Sci.* **2011**, *36*, 1697–1753.
[19] Tirtaatmadja, V.; Tam, K.; Jenkins, R. *Macromolecules* **1997**, *30*, 1426–1433.
[20] Matzelle, T.; Ivanov, D.; Landwehr, D.; Heinrich, L. A.; Herkt-Bruns, C.; Reichelt, R.; Kruse, N. *J. Phys. Chem. B* **2002**, *106*, 2861–2866.
[21] Matzelle, T.; Geuskens, G.; Kruse, N. *Macromolecules* **2003**, *36*, 2926–2931.
[22] Scheffold, F.; Skipetrov, S.; Romer, S.; Schurtenberger, P. *Phys. Rev. E: Stat., Nonlinear, Soft Matter Phys.* **2001**, *63*, 061404.
[23] Mason, T. G.; Weitz, D. *Phys. Rev. Lett.* **1995**, *74*, 1250–1253.
[24] Mozhdehi, D.; Ayala, S.; Cromwell, O. R.; Guan, Z. *J. Am. Chem. Soc.* **2014**, *136*, 16128–16131.
[25] Li, H.; Wei, W.; Xiong, H. *Polymer* **2014**, *55*, 5739–5745.
[26] Herbst, F.; Döhler, D.; Michael, P.; Binder, W. H. *Macromol. Rapid Commun.* **2013**, *34*, 203–220.
[27] Jackson, A. C.; Beyer, F. L.; Price, S. C.; Rinderspacher, B. C.; Lambeth, R. H. *Macromolecules* **2013**, *46*, 5416–5422.
[28] Jackson, A. C.; Walck, S. D.; Strawhecker, K. E.; Butler, B. G.; Lambeth, R. H.; Beyer, F. L. *Macromolecules* **2014**, *47*, 4144–4150.
[29] Guo, M. Y.; Jiang, M.; Pispas, S.; Yu, W.; Zhou, C. X. *Macromolecules* **2008**, *41*, 9744–9749.
[30] Zheng, C.; Huang, Z. *Colloids Surf., A* **2015**, *468*, 327–332.
[31] Gerth, M.; Bohdan, M.; Fokkink, R.; Voets, I.; van der Gucht, J.; Sprakel, J. *Macromol. Rapid Commun.* **2014**, *35*, 2065–2070.

AFTERWORD

Even if this original piece of research might be a droplet in the vast ocean of academic production, it is however a landmark in my personal life and learning trajectory. It marks the end of a long process of anything but individual efforts, thoughts and accomplishments. From this work has risen a line of reasoning that, to a great extent, will guide me about how to work in the context of scientific research, especially when it comes improving intra- and inter-group relations.

This work was accompanied by academic forms of knowledge dissemination including published peer-reviewed papers, as well as poster and oral communications in national and international conferences. In parallel, conducting researches in disciplines closely related to the dissertation subject, either in the form of fruitful collaborations or burgeoning side-projects, constituted an other treasure of my doctoral education. Along the way, I finally had the opportunity to transfer the legacy of knowledge and skills inherited from predecessors to the young generation of talented scientific researchers.

With these words, my hope is that I may have communicated to my readers some of the pleasure of writing this book, whether they are interested in specific or broad aspects of developing new materials with functional, adaptive and tunable properties!

CURRICULUM VITAE

Refereed publications

Gokmen, M. T.; Brassinne, J.; Prasath, R. A.; Du Prez, F. E., *Chem. Commun.* **2011**, *47*, 4652–4654.

Brassinne, J.; Mugemana, C.; Guillet, P.; Bertrand, O.; Auhl, D.; Bailly, C.; Fustin, C.-A. Gohy, J.-F. *Soft Matter* **2012**, *8*, 4499–4506.

Brassinne, J.; Mugemana, C.; Bailly, C.; Fustin, C.-A.; Gohy, J.-F., *Chim. Nouv.* **2012**, *30*, 13–18.

Brassinne, J.; Fustin, C.-A.; Gohy, J.-F., *J. Inorg. Organomet. Polym. Mater.* **2013**, *23*, 24–40.

Jochum, F. D.; Brassinne, J.; Fustin, C.-A.; Gohy, J.-F. *Soft Matter* **2013**, *9*, 2314–2320.

Brassinne, J.; Fustin, C.-A.; Gohy, J.-F., *Mater. Res. Soc. Symp. Proc.* **2013**, *1499*, mrsf12-1499-n02-10.

Ghoos, T.; Brassinne, J.; Fustin, C.-A.; Gohy, J.-F.; Defour, M.; Van den Brande, N.; Van Mele, B.; Lutsen, L.; Vanderzande, D. J.; Maes, W., *Polymer* **2013**, *54*, 6293–6304.

Brassinne, J.; Stevens, A. M.; Van Ruymbeke, E.; Gohy, J.-F.; Fustin, C.-A., *Macromolecules* **2013**, *46*, 9134–9143.

Brassinne, J.; Bourgeois, J.-P.; Fustin, C.-A.; Gohy, J.-F., *Soft Matter*

2014, *10*, 3086–3092.

Ghoos, T.; Van den Brande, N.; Defour, M.; Brassinne, J.; Fustin, C.-A.; Gohy, J.-F.; Hoeppener, S.; Schubert, U. S.; Vanormelingen, W.; Lutsen, L., *Eur. Polym. J.* **2014**, *53*, 206–214.

Rolland, J.; Brassinne, J.; Bourgeois, J.-P.; Poggi, E.; Vlad, A.; Gohy, J.-F., *J. Mater. Chem. A* **2014**, *2*, 11839–11846.

Brassinne, J.; Gohy, J.-F.; Fustin, C.-A., *Macromolecules* **2014**, *47*, 4514–4524.

Gohy, J.-F.; Fustin, C.-A.; Brassinne, J., *Polym. Prepr.* **2014**, *55*, n/a–n/a.

Goldansaz, H.; Voleppe, Q.; Piogé, S.; Fustin, C. A.; Gohy, J. F.; Brassinne, J.; Auhl, D.; van Ruymbeke, E., *Soft Matter* **2015**, *11*, 762–774.

Brassinne, J.; Poggi, E.; Fustin, C.-A.; Gohy, J.-F., *Macromol. Rapid Commun.* **2015**, *36*, 610–615.

Brassinne, J.; Jochum, F.; Fustin, C.-A.; Gohy, J.-F., *Int. J. Mol. Sci.* **2015**, *16*, 990–1007.

Poster and oral communications

Brassinne, J.; Mugemana, C.; Bailly, C.; Fustin, C.-A.; Gohy, J.-F., *Journée Scientifique Annuelle de la SRC* **2011**, *Brussel*, Belgium (oral).

Brassinne, J.; Mugemana, C.; Bailly, C.; Fustin, C.-A.; Gohy, J.-F., *1st Precision Polymer Materials Conference* **2011**, Obernai, France (poster).

Brassinne, J.; Mugemana, C.; Bailly, C.; Fustin, C.-A.; Gohy, J.-F., *Belgian Polymer Group Annual Meeting* **2012**, Blankenberge, Belgium (poster).

Brassinne, J.; Mugemana, C.; Jochum, F. D.; Guillet, P.; Bailly, C.; Fustin, C.-A.; Gohy, J.-F. *Materials Research Society Fall Meeting* **2012**, *Boston*, United States of America (oral).

Brassinne, J.; Stevens, A. M.; Fustin, C.-A.; Gohy, J.-F., *Belgian Polymer Group Annual Meeting* **2013**, Houffalize, Belgium (poster).

Brassinne, J.; Fustin, C.-A.; Gohy, J.-F., *Ph.D. Student's Day* **2013**, Louvain-la-Neuve, Belgium (poster).

Brassinne, J.; Stevens, A. M.; Fustin, C.-A.; Gohy, J.-F., *Precision Polymer Materials Winter School* **2014**, Zakopane, Poland (poster).

Brassinne, J.; Bailly, C.; Fustin, C.-A.; Goldansaz, H.; Gohy, J.-F.; van Ruymbeke, E., *Belgian Polymer Group Annual Meeting* **2014**, Ghent, Belgium (poster).

Brassinne, J.; Fustin, C.-A.; Gohy, J.-F., *Ph.D. Student's Day* **2014**, Louvain-la-Neuve, Belgium (oral).

Brassinne, J.; Fustin, C.-A.; Gohy, J.-F., *Belgian Polymer Group Annual Meeting* **2015**, Houffalize, Belgium (oral).

Brassinne, J.; Bailly, C.; Fustin, C.-A.; Goldansaz, H.; Gohy, J.-F.; van Ruymbeke, E., *Precision Polymer Materials Final Meeting* **2015**, Bordeaux, France (poster).

Brassinne, J.; Bailly, C.; Fustin, C.-A.; Goldansaz, H.; Gohy, J.-F.; van Ruymbeke, E., *Supolen Summer School* **2015**, Anacapri, Italy (poster).

Awards and honors

Award for the best Master thesis in chemistry, *Société Royale de Chimie* **2011**.

Award for the best Master thesis in chemistry, *Solvay* **2011**.

Poster award of the 1st Precision Polymer Materials conference, *European Science Foundation* **2011**.

Poster award of the 20th Belgian Polymer Group Annual Meeting, *Belgian Polymer Group* **2014**.

Best oral presentation award of the Ph.D. Student's Day, *Université catholique de Louvain* **2014**.

Best oral presentation award of the Belgian Polymer Group Annual Meeting, *Belgian Polymer Group* **2015**.